MAGMATISM OF THE EARTH AND RELATED STRATEGIC METAL DEPOSITS

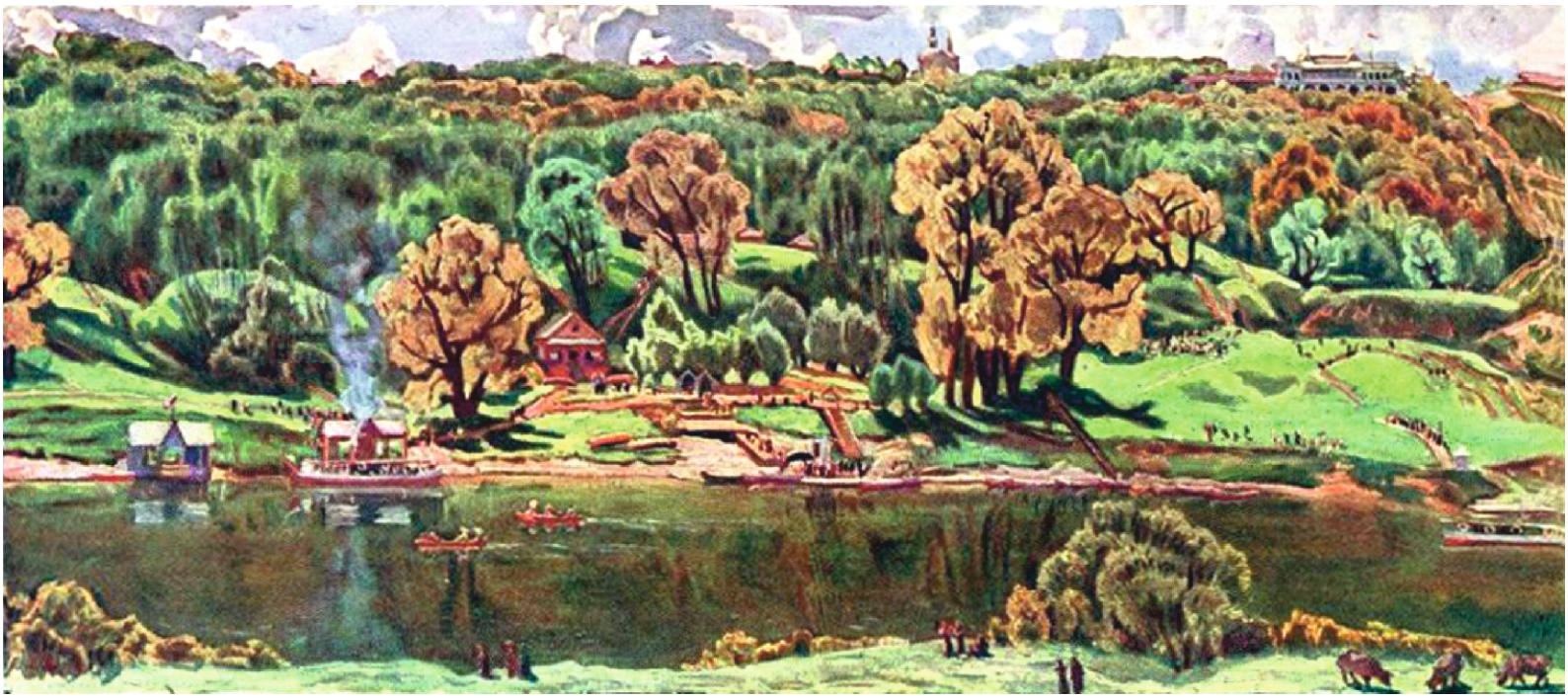

PROCEEDINGS OF XXXV INTERNATIONAL CONFERENCE

MOSCOW, 3-7 SEPTEMBER 2018

ГЕОХИ

VERNADSKY INSTITUTE OF GEOCHEMISTRY
AND ANALYTICAL CHEMISTRY
OF RUSSIAN ACADEMY OF SCIENCES
(GEOKHI RAS)

Magmatism of the Earth and related strategic metal deposits

Proceedings of XXXV International Conference

3-7 September 2018, Moscow

Supported by Russian Foundation for Basic Research grant 18-05-20065

Sponsors:

"Magmatism of the Earth and related strategic metal deposits". Abstracts of XXXV International Conference. Vernadsky Institute of Geochemistry and Anlytical Chemistry of Russian Academy of Sciences (GEOKHI RAS). 3-7 September 2018 / Editors V.N. Ermolaeva, V.A. Zaitsev. – M.: GEOKHI RAS, 2018. 358 p. - ISSN 2618-835X.

The mineral deposits of strategic metals are vulnerable to political and economic changes, and their availability is essential for high-technology, green energy, and other applications. The most of they are related to the deep – seated alkaline magmas.

This book offers a collection of papers presented at the 35th International Conference on Magmatism of the Earth and Related Strategic Metal Deposits held from September 3th to 7th 2018 in Moscow, Russia.

The conference articles are focused on the understanding of the geological processes that produce high concentrations of critical metals in geological systems such as the metal transport in the mantle (possibly from the core-mantle boundary) and crust and enrichment processes, hydrothermal and metasomatic processes leading to the formation of such significant deposits. Papers in this book give a representative overview including mineralogy, geochemistry and origin of strategic metals deposits.

Supported by Russian Foundation for Basic Research (grant 18-05-20065).

ISSN 2618-835X

The cover pictures - Sparrow Hills, May. Konstantin Fedorovich Yuon, 1910.

Content

MODEL OF THE GENESIS OF COLLISIONAL PORPHYRY COPPER DEPOSITS MISHANO-ZANGEZUR ZONE IN THE SOUTH OF THE LESSER CAUCASUS

Abbasov N.A., Huseynova A.N.
Baku State University, puccina2012@yahoo.com

The article deals with the questions of genesis of collision of the copper-molybdenum deposits Mishano-Zangezur zone in the South of the lesser Caucasus. As a result of the studies revealed that copper-porphyry deposits forming the island arc belt Lesser Caucasus ore-magmatic system is associated with two (Megri-Ordubad and Dalidagskiy) various intrusive complexes, in the petrographic composition. Copper-porphyry, gold-copper-molybdenum, copper-molybdenum and gold-polymetallic formation with polymetallic form a genetic series - ore complex paragenetic associated with the Eocene-Miocene intrusive activity in Mishano-Zangezur zone.

In the regionalization schemes based on the principles of plate tectonics, the geodynamic setting and the rotational-shear movements Mischano, Kafan trany and Olborsky plate (M. Rustamov, 2008), with different density of island arc development in postneoliberal stage soldered regional transform faults forming the southern island arc belt lesser Caucausus ore-magmatic system. In all geodynamic constructions intense multi-stage magmatism of postpeace-Miocene in the South of the lesser Caucasus spatial alignment of the subduction zone and distribution of magmatism are also other types of deflections and hail epicontinental Islands of volcanic and tectonic origin, are divided into two sectors, which differ in deep structure, composition, age and Genesis of composing their complexes, controlled by two zones deep faults in Mishano-Zangezur zone (Ismail-zade, 2001) the First Zangezur raising, (Ordubad ore region), second Akerinsky raising (Dalidag ore district).

The intensity of copper mineralization in porphyry Mischano-Zangezur zone, the similarity of the mineral composition of the products of mineralization, and polystageness it significantly complicated to determine their age and a genetic link with certain intrusions. Most common in this area of the ore field associated with discontinuities, intersecting intrusives of igneous rocks, deals a certain position in folded structures, as well a certain position intersecting faults (3). In this regard, within these areas, ore fields include such ore field, which are confined to transverse fractures in areas with branching and mates in different directions. Ore field in the areas of branching and coupling faults of different directions are significant spread in the South of the area. They are characterized by the fact that their localization effect block structure. In General terms, branching and pairing of faults with different directions there are a large number of relatively small too differently oriented faults and cracks between the branches of larger, regional long-lived faults. The result is a kind of frame (block) of more or less dense network of cracks, which creates favorable conditions for the circulation of ore-bearing solutions and the phased deposits of ores. This is especially typical in the South of this zone in the Central and extreme North-Western part of the Ordubad ore region, where the bifurcation of the major regional Ordubad-Dalidag-Gadabay fault is at small angles. Therefore, in Diakhchay and Agurt-Shelalinsky ore fields formed weakened areas are wedge-shaped and the ore bodies have the form of tectonic wedges (Shelale, Diakhchay, Danaly, Muradkhanly). For most ore fields in these areas are often characterized by rather complex shape of ore bodies or intersecting and willing bodies, as we see for example in Goygol-Geydagsky, Agurt-Shalinsky and Teymurchaydagsky ore field on Mischano-Zangezur.

Regional Ordubad-Dalidag-Gadabay deep the rift is a highly important structural elements having a very large ore-controlling value on all distance (Azerbaijan part) lesser Caucausus ore belt. These long-developing fault structures penetrating to the very depths, confined various igneous formations of endogenous deposits, as in Tobacco ore district as well in a number of other ore districts of the lesser Caucasus (Dalidag and Gadabay). In areas where Agurt-Shalalinsky ore field, branching and pairing gaps in different directions are significant spread. They are characterized by the fact that their localization is influenced by the so-called frame (block) structure. In many cases, these sites of branching and pairing gaps in different directions there are a large number of relatively small gaps between the branches of larger gaps. The result is a sort of skeleton of more or less dense network of cracks, which created favorable conditions for the circulation of ore-bearing fluids and deposition of

ores. In many cases, these areas of branching and coupling faults in different directions, as noted above there are a large number of relatively small faults between the branches of larger regional faults of a stretch. In the Northern and North-Eastern part Mischano-Zangezur zone in its physical and mechanical properties very different from the enclosing rocks are favorable for the localization of copper-molybdenum mineralization and is subordinate importance core type. In this case the ore concentration are concentrated in endo-and exocontact zone of Intrusive Kalidascope array, and temporary displays of copper-molybdenum-porphyry ores correspond to the final stage of formation of the granitoid intrusion. Ramazanov, V. G.(9) here notes a clear controlling mineralization from dikes of quartz-diorite porphyry, which are products of the final stage of granitoid magmatism in the Central and southwestern part of the area. While ore veins and dikes are confined to the same system of cracks. Questions of age and genetic relationship of porphyry copper mineralization and associated pyrite-polymetallic and gold-ore and gold porphyry copper-gold ore cannot be considered as finally settled. To resolve questions of age and genetic relationship of mineralization of copper-molybdenum-porphyry deposits is important to understanding the relationship of intrusive rocks, dikes and mineralization, which already many years are the subject of intense debate. Comprehensive studies of intrusive rocks, hydrothermal-metasomatic formations and copper-molybdenum mineralization conducted by a large team of geologists IGEM, Academy of Sciences of the Russian Federation under the leadership of S. V. Efremova (1984), S. A. Pashkov (1975) and others found that copper-molybdenum mineralization in the aftermath of the aplite dikes, torn at the time of formation of the intrusion of the dikes oligoclase quartz-diorite. Some researchers (M.V.Lygin, S.E. Guleva 1953) on the example of the Kadjaransky deposit dikes of Zangezur considered post-ore, the other (M.P. Isaenko, etc. 1975), all the dikes of the Zangezur ore district belong to prior-ore formations. In addition prior-ore dikes of aplite and diorite porphyry composition, allocates and post-ore in relation to the main productive stages of granodiorite-porphyry dykes, which, however, in relation to polymetallic stages are prior-ore.

Interaction with dykes of granodiorite-porphyries, Sh.M. Azizbeyov, T.G. Hadjiyev M.I. Rustamov (1961, 1964), etc. is not installed. Given that the dikes of granodiorite porphyry, and in places the diorite-porphyry cut by quartz-molibden veins and veins and these veins contain fragments observed in the dike and turn intersected quartz-chalcopyrite veins, intruded after the quartz-molybdenite, but the quartz-pyrite-chalcopyrite stage of mineralization. Features of composition and structure, irregular contacts with numerous branching apophyses allowed S.V. Ephraimov (1984), E.A. Mamedov, (1981), S.A. Pashkov (1986) and others assume that composing the dyke material was characterized by large permeability in the host rock due to saturation of the melt volatile, is a product of differential residual lesion and cannot be seen as a manifestation of a new phase of intrusive activity.

The study collected us the actual material on the Ordubad and Dalidag ore district, confirms the conclusion that composing the noted dyke material was characterized by large permeability, which in our opinion can be attributed to other causes, in particular the assimilation of a significant amount of ore minerals molybdenite, chalcopyrite, pyrite of the early stage of mineralization. Therefore it seems not justified to assume that dikes originating the lesion was residual and differential and hence to deny the possibility of the formation of these dikes resulted in a new phase of Intrusive activity. Detailed microscopic study of a large number of polished sections of dyke species shows that both the granodiorite-porphyry and diorite-porphyrites (Geydag-Goygol) is included in the dyke and the dyke itself bear ore mineralization. Are pyrite, chalcopyrite, molybdenite (Diakhchay, Shelale, Goygol), as well as sphalerite, galenite, gold and silver, the quantitative interaction which in diorite-porphyrite and in the dyke variety. In Geydagsky field of quartz syenite-diorites contain considerably more molybdenite than the dikes of granodiorite-porphyry composition, and the latter contains mainly chalcopyrite mineralization with disseminated molybdenite and gold sometimes intersecting polymetallic veins. All this, in our view, confirms the previously stated point of view on duration and phasing of industrial rudoobrazovanie process of Ordubad ore region (1993, 1999, 2003) and in copper-molybdenum deposits of Mischano-Zangezur zone, shown apparently due to the formation of two (Megri-Ordubad and Dalidagsky) various intrusive complexes, in the petrographic composition.

The formation of multi-formational deposits or ore fields, in our opinion, more correct to explain the evolution of the magma chamber, which depending on the tectonic conditions of collision belts, periodically supplying the upper layers of the earth's crust by magma and hydrothermal ore-bearing solutions. In this case, it would be natural to expect more complicated interaction of intrusive rocks, dikes and mineralization. Post-ore stage to the early stage of the breed should be prior-ore for a later phase, but the igneous rocks taken as a whole, if they are associated with ore-hearth, must be prior-ore, for the last stage of ore formation usually distorts and obscures the facts, widely studied on dikes and rocks of the late stage against the early mineralization stage.

It should be noted that the quartz-molybdenite veins and veinlets Geydagskiy deposits relate to an earlier phase of mineralization compared to the gold-polymetallic ore-deposits. According to V.M. Baba-zade, V. G. Ramazanov, A. A. Masimov and N.A.Abbasov copper-molybdenum and gold-polymetallic formation with polymetallic form a genetic series-ore complex paragenetic associated with the Eocene-Miocene Intrusive activity in Mischano-Zangezur zone. It is possible to assume that copper-molybdenum and gold-sulphide mineralization are formed after the implementation of the aplite dikes, granodiorite-porphyry, spessartite and diorite-porphyrite which are genetically associated with magmatic centers and is due to the emergence of a qualitatively distinct, isolated foci, which differ in the ratio of the useful components of Mo, Cu, Au, Ag, Zn, Pb, As, Bi.

In the mineral composition of ores in addition to the main ore-forming minerals of pyrite, chalcopyrite, sphalerite and galenite participate native gold, fahlores, marcasite, bismuthinite, from the gangue minerals quartz, calcium.

Along the veins of the breed intensively sericitizationed and piritizationed, sometimes kaolizationed, carbonizationed and quartzationed. Ore in general, are the result of a multistage process of mineralization. Various researchers (Abbasov, 2003, Azibekov, 1961, Baba-zade, 1999, Pashkov, 1985) are allocated from 6 to 10 stages of mineralization, among which the main ones are productive for metallopeptidase zones of molybdenite-chalcopyrite, quartz-molybdenite-chalcopyrite, quartz-pyrite-chalcopyrite. More than half of the molybdenum deposits associated with quartz-molybdenum stage and fewer with quartz-molybdenite-chalcopyrite. The bulk of the copper associated with quartz-pyrite-chalcopyrite stage, relatively weakly manifested quartz-galenite-sphalerite and quartz-magnetite stage. In the ore zone, showing (as in the region and also in Dalidagsky ore district) zoning of the distribution of mineralization, expressed in the alternation of the relatively high temperature of low-temperature stages as the distance from the main Ordubad (Ordubad ore region) and Qatardash-Dalidasgsky. (Dalidagsky ore district) is a ore-controlling, representing fragments of Ordubad-Dalidag-Gadabay long-lived, cross-cutting lineament structure, copper-molybdenum-porphyry and specialization which are identified everywhere. Mineralization within Kalidascope ore district is localized on segments of fault zones, saturated dykes of granodiorite-porphyry, granodiorite-syenite-granitic composition. In the North-Eastern part Mischano-Zangezur zone of Terter along the transverse fault, the porphyry intrusions, in apical parts, which developed a rich intense fracturing and hydrothermal processing of rocks, was a favorable environment for the placement of copper-molybdenum ores.

On the Eastern part of Mishano-Zangezur zone, posteocene-low-miocene granite-granosyenites formation Dalidagsky pluto spatial and paragenetic associated copper-molybdenum Dalidagsky, SultanGeydarsky, Teymurachadagsky symptoms. In the ore-bearing rocks - granodiorites, granodiorite-porphyries and quartz sienite-diorite widely developed complex series of dykes of granodiorite-porphyries and other vein rocks. However, as the mineralization develops close to them, they can be considered the number one of the search characteristics of the copper-molybdenum ore.

References

Аббасов Н.А. Особенности образование и закономерности размешения медно-молибден-порфировых месторождения Ордубадского рудного района. Авт. на сои. н.с. к.г-м.н. Баку, 2003.

Азизбеков Ш.А. Геология Нахичеванской АССР. Госгеолтехздат,Москва,1961.

Баба-Заде В.М., Рамазанов В.Г., Аббасов Н.А. и др. Минералого-геохимические факторы золотоносности руд медно-порфировых месторождений Ордубадского рудного района. В сбор. БГУ сер. Естественных наук. Баку, 1999 . №3.

Исмаил-Заде А.Д., Мустафаев Г.В., Рустамов М.И. Геология Азербайджана.,т. III. Магматиэм, Баку 2001, 433с.

Пашков Ю.Н.,Ефремова С.В. и др. О месте медного и молибденового оруденения в интрузивном процессе (на примере Каджаранского Cu-Mo месторождения) - В кн.: Магматизм и полезные ископаемые. Москва, Наука, 1975.

Рамазанов В.Г. Медно-порфировая формации Азербайджана. Автор. дисс. на соис. у. ст. доктора г.-м. наук. Тбилиси 1993.

Hedenquist J.W., Arribas A.Jr., Reynolds T.J., 1998, Evolution of an Intrusion-Centered Hydrothermal System: Far Southeast-Lepanto Porphyry and Epithermal Cu-Au Deposits, Philippines, Economic Geology and Bulletin of the society of Economic geology, v. 93, № 4, pp 373-404.

Sillitoe R.H., 2010, Porphyry Copper Systems, Society of Economic Geologists, Inc. Eco-nomic Geology, v. 105, pp. 3–41.

DYKE COMPLEX CHARACTERIZED MEHRI-ORDUBAD GRANITOID INTRUSIVE SITUATED IN THE SOUTH-WEST OF MISKHANA-ZENGAZUR METALLOGENIC ZONE

Abbasov N.A.[1], Safari M.H.[2], Hasanov F.D.[1], Rustamova R.E.[1], Huseynova A.N.[1]

[1]Baku State University

[2]University of Payame Noor, Iran, puccina2012@yahoo.com

Complex structured Mehri-Ordubad granitoid intrusive is situated in the south part of Lesser Caucasus, in the south-west of Miskhana-Zengazur metallogenic zone. Mehri-Ordubad and Delidagh intrusive masses are situated in this zone, which differ from each-other by their geological-structural and petrographic composition and a lot of associated industrial ore and non-metallic minerals are also concentrated in this zone. In terms of metallogeny these deposits are assembled in ancient Azerbaijani lands - Ordubad, Delidagh and Gafan ore regions. Ordubad ore region is separated by Mehri-Ordubad granitoid batholith and the dyke complex with rich petrographic composition characterizing its different phases. The role of dyke complex is valued highly in location and concretion of the endogenic ore deposits in the region. The dyke complex rocks of ore region can be divided into 2 parts according to their petrographic composition: 1) Acidic and medium-acidic dykes - aplites, pegmatites, granodiorite-porphyries, granosyenite-porphyries, coarse-grained granodiorite and granosyenites, syenite-diorites; 2) Main and medium compositional dykes - diabases, gabbro-diabases, quartz diabases, gabbro-diorites, andesite and diorite-porphyries, quartz porphyrites and lamprophyres (spessartites, kersantites, vogesites and minettes). They were formed till pluton and at all stages of pluton. As it is known ore deposits are accompanied by large depth dislocation and when contact plane of ore-bearing intrusives combines with wall rocks and these depth faults, sometimes coincides, mineralization is situated in endo- and exo-contacts of intrusives depending on their shapes. Mineralization concentrates mainly in convenient ore-oriented structures, which are formed in intersections of regional control structures and different directed local fault systems.

Copper-porphyry, gold-bearing copper-porphyry, polymetal, pyrite- polymetal, gold-bearing copper-molybdenum and other native metal-bearing many types of sulphide deposits on the structural blocks, which were formed by Paragachai Goygol-Goydagh, Gapijikh-Goygol ore-oriented faults in north-east direction along Ordubad-Delidagh-Gadabey regional ore controlling depth fault, are situated in complex geological structural Mehri-Ordubad pluton intrusives, mainly in contact stripe of granosyenite and granodiorite-porphyry intrusives. Younger granodiorite-porphyries spread widely in ore regions. Dykes belonging to granodiorite-porphyry intrusive spread widely in all ore areas of the region. Their thicknesses range from 0,4 to 20-23 m, sometimes 45-50 m, extend from several meters to 6-7 km. It extends beyond borders in the west ends of ore region. Studying the formation sequence of magmatic rocks, various dykes, small intrusives and the analysis of their interaction with

mineralization show that placer-vein, copper-molybdenum-porphyry mineralization are related mainly with granodiorite-porphyry body, dykes and dyke-like intrusives. However, there is a variety of opinions among researchers, which leads to the wrong results in the assessment of the ore deposits during search and exploration works. So, when V.T. Pokolova (10) studied ore deposits situated in the south slopes of Lesser Caucasus, she stated in her book "The basis of assessment and prognosis of natural resources" that the majority of copper-molybdenum mineralization is accumulated in porphyry rock bodies, dyke-like intrusive formation and dykes. When V.S. Popov (9) described the origin and geology of copper and molybdenum porphyry deposits, he showed that ore deposits belonging to copper-porphyry formation situated in Miskhana-Zengazur ore zone of Lesser Caucasus is associated with potassium-natrium granitoids, mainly with porphyry dykes. When V.A. Pervago (8) studied Garajan ore deposit in Miskhana-Zengazur ore region, he concerned granodiorite-porphyry dykes to the period of ore formation and before it, at the same time he showed that diorite-porphyry dykes belong to the period of ore formation. When M.P. Isaenko and others (10) studied copper-molybdenum deposits situated in Miskhana-Zengazur ore region, they stated that placer-veinlets, copper-molybdenum mineralization are accompanied by porphyry dykes, mainly granodiorite-porphyry, diorite-porphyry dykes.

When S.V. Yefremova (1983) studied copper-molybdenum ore formation in Miskhana-Zengazur region of Lesser Caucasus, she showed that most of copper-porphyry deposits are mainly related to dyke-like formation and dykes of granodiorite-porphyry and porphyry rocks. But he noted that endogenic ore deposits in Ordubad ore region are associated with relatively young diorite-porphyry, granosyenite, granodiorite-porphyry dykes. According to F.I. Vekilova (1954) copper-molybdenum mineralization is richer in lamprophyre, mainly in granite and aplite dykes in Paraghachai ore area of Ordubad ore region. V.M. Babazdeh, V.G. Ramazanov, A.A. Masimov, N.A. Abbasov (Abbasov, 2000, Babazadeh, 1990) show that copper, copper-molybdenum, copper-porphyry mineralization in Ordubad ore region is associated with small intrusive, but S.M. Suleymanov, E.M. Mammadov (13) stated that they are related to dykes of misdag and pezmere types. When V.M. Babazadeh, V.G. Ramazanov (Babazadeh , 1990) studied spreading peculiarity of alkaline elements in magmatic rocks in Ordubad ore region of Mehri-Ordubad pluton, they noted that the amount of alkaline elements is high in aplite (100 g/t rubidium), andesite-dasite (48 g/t rubidium) and andesite-porphyry (45 g/t rubidium) dykes. S.A. Baktashi (6) correlates copper-porphyry and polymetal mineralization genetically with granite and granosyenite intrusives in Ordubad ore region, shows their paragenetic relation with granodiorite-porphyry, granite-porphyry and lamprophyre dykes. At the same time, he noted that occurrence of native metals is related with contact halo of longitudinal body-like intrusive veins with paragenetic diorite-porphyry composition. Occurring of body-like granodiorite-porphyry intrusive on the surface of ground is observed relatively in wide area in Zangazur pass in Ordubad ore region. Many dykes of body-like intrusive divide and extend for 25-30 km at intervals in Diakhchai, Shalala, Yashillig ore deposits.

We consider that, mainly granodiorite-porphyry, diorite-porphyry dykes play important role in restricted localization of copper-porphyry and related gold ore situated in the north-west and central part of Ordubad ore region and at the same time granodiorite-porphyry dykes in explored part of Mehri-Ordubad pluton are represented by two stages of dyke-formation– granosyenite phase and granodiorite-porphyry phase: granodiorite-porphyry dykes are involved almost in structure of all ore areas of ore region. From this point of view Paragachai, Gapichig, Goygol, Goydagh, Aghyurd, Shalala, Goyhundur, Diyakhchai copper-molybdenum-porphyry, gold-bearing copper-molybdenum deposits play great role in clarifying the relation of dykes with mineralization in ore region. Mainly granodiorite-porphyry, granosyenite-porphyry, diorite-porphyry dykes spread widely in Paraghachai ore area. It should be noted that these dykes are associated closely with copper-molybdenum mineralization in ore-controlling structure. Quartz-molybdenite veins are observed in granodiorite-porphyry and diabase bearing dykes situated within coarse-grained diorite intrusive in Paraghachai deposit. Both rocks are cut by quartz-chalcopyrite and sometimes quartz-carbonate veins and veinlets. Different directed and crossing quartz-chalcopyrite veinlets are accompanied mostly by spreading pyrite in granodiorite-porphyry dykes, also in quartz syenite-diorite in Mundere deposit. Sometimes

quartz-molybdenum veinlets, mainly these dykes intersect with quartz veinlets with many wrong morphological shaped small faults in contact of granodiorite-porphyry dykes with coarse-grained in Mundere area. These features of quartz show that there was local compression and expansion when these veinlets were formed. These quartz veins are rich with placer molybdenum mineralization. A part of copper-molybdenum-porphyry deposits of industrial importance is situated in Goydagh-Goygol ore area of Ordubad ore region. Goydagh, Goygol, Khanadagh, Jajikhli, Gumushdere, Dikyurd, Bashkendchai copper-porphyry, copper-molybdenum, gold-bearing copper-molybdenum ore deposits and occurrences, which are situated in endo- and exo-intersect strip of Sekersu and Goydagh granosyenite intrusives in the transverse structure layer of the ore area, are characterized by "Daykali" tin-lead mineralization occurrence. Interaction of ore masses and dykes in this type of deposit play great role in mineralization. Unlike copper-molybdenum-porphyry deposits and besides dykes of granosyenit and granodiorite-porphyry phases, Middle Eocene aged dykes and dyke-like andesite and andesite-dacites also participate in the structure of polimetal deposits situated not far from the contact halo of intrusives comparatively than copper-molybdenum porphyry deposits mainly in the central and north-west part of the ore region.

As a result it should be noted that dyke complex of Ordubad ore region is divided into acid and basic dykes according to petrographic composition and they were formed till pluton period and at all stages of pluton. Analysis of interaction of mineralization dykes in gold-bearing copper-molybdenum-porphyry deposits in the ore region show that mineralization spread widely in granodiorite-porphyry dykes, mainly in its side part, whereas mineralization weakens a little far away from it and generally ore veinlets wedge to it. This also shows that there has been a certain active tectonic movement between mineralization and granodiorite-porphyries and it witnesses their formation at the same time. Structural network of gold-bearing copper-porphyry and gold copper-porphyry deposits and occurrences situated in ore region is defined by small intrusive complex and dykes system belonging to the last granodiorite-porphyry phase of intrusive activity of the ore region. Moreover, spatial orientation of dyke often defines the orientation of ore masses.

References

Abbasov N.A., Ismailov A.I. Dykes and their role in the formation of endogenous mineralization of Ordubad ore region. 3rd Republican Scientific conference "Natural resources of Azerbaijan, prognosis of potential areas and new methods of research". Baku, Publishing house of BSU, 2000, pp. 57-58.

Babazadeh V.M., Mahmudov A.I., Ramazanov V.G. Copper- and molybdenum-porphyry deposits. Baku, Azerneshr 1990, p. 376.

Bektashi S.A., Hajiyev T.G. and oth. To petrochemistry of granodiorite intrusive of Mehri-Ordubad complex pluton. "Scientific records. ASU, ser. Geo-geographic science." Baku, 1972, #2, pp. 34-40.

Yefermova S.V. Dykes and endogenous mineralization. "Nedra", Moscow, 1983, pp. 191-198.

Pervago V.A. Some features of the metallogeny of the Pacific belt. In the book "The main problems of the metallogeny of the Pacific ore belts". Vladivostok, DNU, USSR Academy of Sciences, 1971, pp. 21-24.

Popov V.S. Geology and genesis of copper and molybdenum-porphyry deposits. Moscow, "Nauka", 1977, pp. 103-108.

Prognosis principles and assessment of mineral deposits. (edited by V.T.Pokolova). Moscow, "Nedra", 1977, V. 1, p. 310.

Isaenko M.P., Movsesov S.A. Complex copper-molybdenum deposits. Moscow. "Nedra" 1974, p. 344.

Suleymanov S.M., Mammadov E.A. Volcanism and metallogeny of the south of Lesser Caucasus. Thematic collection of scientific works of ASU named after S.M.Kirov "Volcanism and associated minerals of Azerbaijan", Baku, 1985, pp. 3-8.

Рамазанов В.Г. Медно-порфировая формации Азербайджана. Автор. дисс. на соис. у. ст. доктора г.-м. наук. Тбилиси 1993

PORPHYRY SYSTEM OF THE BYSTRINSKY CU-AU-FE DEPOSIT, EASTERN TRANSBAIKALIA, RUSSIA: COMPOSITION OF THE PORPHYRY ROCKS AND PARAMETERS OF PROCESSES THAT GENERATED THE ORE-BEARING MAGMAS

***Abramov S.S.*, Kovalenker V.A., Yazykova Yu. I., Kiseleva G.D., Krylova T.L.**

Institute of geology of ore deposits, petrography, mineralogy and geochemistry (IGEM) RAS, Moscow, westabra@yandex.ru

The large (2.2 mln. tones Cu, 250 tonnes Au, 1100 tonnes Ag, and 75 mln. tones Fe; Shevchuk et al., 2010) Bystrinsky Cu–Au–Fe skarn–porphyry deposit (51º32'N, 118º38' E) in the southern part of the Gazimur–Zavodsky area in Transbaikalia, Russia, is constrained to he intersection of the Uryumkan–Budyumkan and Nerzavodsk–Sretensky deep faults. The porphyry-type ore-forming system of this deposit was hosted in the Bystrinsky dome structure of a central volcano. The structure consists of terrigenous–carbonate sedimentary rocks (limestone, sandstone, siltstone, mudstone, and less abundant conglomerate) and magmatic bodies cutting them. The skarn and ore mineralization were produced in genetic relations with the Bystrinsky stock of diorite porphyry, syenodiorite, and granite porphyry, which are classed with the Shakhtaminsky intrusive complex of Middle–Late Jurassic age. The porphyritic rocks make up stocks and dikes of diorite, monzodiorite, quartz monzonite, and granodiorite porphyries. The center of Bystrinsky structure is a phase-1 diorite massif (approximately 3 × 4 km in map view) belonging to the Middle–Late Jurassic Shakhtaminsky magmatic complex. The next, second magmatic phase of the complex resulted in the emplacement of stock-shaped bodies and dikes, which are dominated by granodiorite porphyry. The K–Ar and Ar–Ar phlogopite age (163 ± 3 and 160.8 ± 1.6 Ma, respectively) of the magnesian skarn at the Bystrinsky deposit (Kovalenker et al., 2015) correspond to the emplacement time of the phase-1 plutonic rocks of the Shakhtaminsky Complex (163–159 Ma; Berzina et al., 2014).

According to their petrochemical characteristics, the porphyry rocks belong to the high-K calc–alkaline and shoshonitic series and are very close to porphyritic rocks at the Shakhtaminsky deposit. As the SiO_2 concentration increases (from 52 to 68 wt %), the MgO concentration of the rocks remains high (4–10 wt %), and the Mg# of the rocks increases to 65 mol % in the mafic rocks and 75 mol % in the acid ones. This make intrusive rocks at the deposit similar to adakites in post-subduction systems. Compared to typical adakite, which are high in Sr (rarely less than 400 ppm), the rocks at the Bystrinsky deposit are poorer in this element (50–300 ppm). Similar to typical adakite, these rocks contain low concentrations of Y (2–11 ppm) and Yb (0.5–1.5 ppm), at variable $(La/Yb)_N$, lower mantle-normalized concentrations of elements from LILE to LREE and MREE, and lower concentrations of HFSE (Nb, Ta, and Ti) and HREE. However, although the petrochemistry and geochemistry of these rocks are generally close to those of adakites, the former and porphyry rocks of the Shakhtaminsky Mo porphyry deposit (Berzina et al., 2014) are rich in MgO (up to 10 wt %), which makes these adakite-like rocks similar to high-Mg andesite (Martin et. al., 2005).

The earliest intrusive phases are diorite and diorite porphyry, both found composing stocks and small intrusions. The equigranular varieties are fine-grained and occur in the marginal portions of the intrusive bodies. The porphyritic rocks are found in the central parts of the magmatic bodies, and the equigranular and porphyritic rocks show mutual transitions.

The equigranular diorite possesses a microgabbro texture, with the dominance of plagioclase laths over all other minerals of the rocks. The proportions of the primary magmatic minerals are as follows: *Pl* 40 vol %, *Kfs* 30 vol %, *Ap* + *Bt* 5 vol %. The secondary minerals are carbonate, an opaque mineral (20 vol % together), and ilmenite (5 vol %). The phenocryst minerals of the porphyritic rocks are plagioclase, clinopyroxene, and hornblende. The phenocryst minerals are dominated by plagioclase (50 vol %), with amphibole (40%) and clinopyroxene (10 vol %) found in subordinate amounts. The groundmass of the rocks is completely replaced by mixture of carbonate and chlorite.

The granodiorite consists of the assemblages of phenocryst minerals *Pl* + *Kfs* + *Amph* + *Cpx* + *Bt* and a fine-grained matrix consisting of *Bt* + *Amph* + *Pl* + *Kfs* + *Qtz*. The phenocrysts are dominated by plagioclase (60 vol %) and amphibole (30–40 vol %), and clinopyroxene is preserved as relicts in large

grains of amphibole, which corrodes the clinopyroxene. A noteworthy feature of the granodiorite is that it contains large potassic feldspar phenocrysts, which make up ovoids. The latter show a complicated inner structure because of their long-lasting recrystallization. The potassic-feldspar ovoids host amphibole and plagioclase inclusions, which were captured during crystallization. The compositions of the plagioclase and amphibole are close to those of these minerals in the phenocrysts. The accessory minerals of the granodiorite are titanite, tourmaline, zircon, and apatite.

Although the intrusive rocks are significantly altered by secondary processes, their textures provide a clue for distinguishing the major evolutionary phases. The first minerals to crystallize in the granodiorite and syenodiorite were their phenocryst minerals: these were plagioclase + clinopyroxene in the diorite and plagioclase + potassic feldspar in the granosyentite, which were followed by the crystallization of groundmass minerals and the phenocryst assemblage of *Kfs* + *Pl* + *Bt* + *Amph* + *Qtz* in the granodiorite. The identified equilibrium pairs of plagioclase and feldspars in the syenodiorite and granodiorite make it possible to apply the two-feldspar thermometer (Nekvasil and Burnham, 1987) to estimate the crystallization temperature. In the syenodiorite, Pl_{57} crystallized at 890–870°C at 2 kbar, and Pl_{41} and K–Na *Fsp* crystallized at 870–840°C, 2 kbar. In the granodiorite, oligoclase with K–Na feldspar in ovoids crystallized at 720°C, 1 kbar. The compositions of the groundmass albite and potassic feldspar correspond to crystallization temperatures of 390–410°C, and these minerals were produced by postmagmatic recrystallization.

The composition of the amphibole also provides information on the crystallization conditions of the melt. The *P–T* parameters were calculated using the amphibole–plagioclase geothermometer (Holland and Blundy, 1994) and geobarometer (Anderson and Smith, 1995). The *P–T* parameters were calculated for the following mineral pairs: Pl_{41} + *Hbl* phenocrysts from the diorite porphyry and Pl_{27} + *Hbl* phenocrysts from the granodiorite porphyry. The estimates yield two pressure ranges: 2.3–1.7 kbar for the crystallization of phenocryst minerals in the diorite porphyry and 0.5–0.3 kbar for the crystallization of minerals hosted in phenocrysts in the granodiorite. The temperature ranges of 760–740°C for the diorite and 680–720°C for the granodiorite are 50–100°C lower than estimates of the crystallization temperatures by the two-feldspar thermometer. Higher temperatures and pressures are calculated using the amphibole geothermobarometer (Ridolfi et al. 2009). According to this geothermobarometer, amphibole phenocrysts in the diorite crystallized within a pressure range of 1.23 to 1.8 kbar at temperatures of 870–820°C, and amphibole phenocrysts in the granodiorite crystallized at 0.8–0.5 kbar and 800–730°C. These temperature estimates are closely similar to the crystallization temperatures of feldspar phenocrysts in the diorite porphyry (870-840°C) and granodiorite (720°C). The oxygen fugacity calculated with the geothermobarometer (Ridolfi et al. 2009) shows that crystallization conditions became more oxidizing with the transition from the diorite porphyry to granodiorite and evolved from parameters close to the NNO buffer to NNO + 2.5. The increase in the oxidation potential in the granodiorite led to the crystallization of titanite according to the following schematic reaction: *Hed* + *Ilm* + O_2 = *Tnt* + *Mt* + *Qtz* (Wones, 1989).

The estimates of the intensive parameters of crystallization of the porphyritic rocks led us to suggest that they crystallized at two depth levels. One of them was hypabyssal, under pressures of 2 to 1.5 kbar and corresponded to the crystallization of phenocryst minerals in the diorite and syenodiorite. The crystallization temperatures were 820–870°C. The other level was subvolcanic, corresponded to pressures of 0.9–0.5 kbar, when the granodiorite porphyry and, perhaps, more acid rocks crystallized. The oxygen fugacity in the crystallization products increased from the NNO buffer to NNO + 2–2.5 in the granodiorite.

The data presented above indicate that the porphyritic rocks to which the Bystrinsky skarn–porphyry deposit is related show petro- and geochemical features and crystallization parameters comparable to those of adakite-like rocks at the Shakhtaminsky Mo porphyry deposit (Berzina et al., 2014), which was reportedly produced during the postcollisional evolutionary episode of this territory. Our estimates of the parameters of the oxidized fluid (oxygen fugacity corresponding to NNO + 1–2) and the oxidizing trend from earlier to later intrusive phases in the magmatic system of the deposit are close to those of the well-known Altar Porphyry Cu-Au-Mo-porphyry system (Maydagan at al, 2014). High sulfur concentrations in the accessory apatite of the granodiorite and the high f_{O_2} of the melt

indicate that the melts should have been in equilibrium with fluid containing high sulfur concentrations (Cao et al., 2014).

This study was supported by the Presidium of the Russian Academy of Sciences (Program No. 48, Project No 1.48-6), and, partly, by the Russian Foundation for Basic Research, Project No 18-05-00673.

NEW FINDING PYROCLASTIC ROCK IN THE WESTERN MARGIN OF THE PROTEROZOIC PAKHAL BASIN IN AND AROUND KHAMMAM, TELANGANA, INDIA: EVIDENCE OF ALKALINE MAGMATISM

Adhikary D.[1], Sahoo R.K.[2], Behara K.K.[2]

[1]Geological Survey of India, Eastern Region, Kolkata-700091

[2]Geological Survey of India, State Unit: Andhra Pradesh, Southern Region, Hyderabad-500068, India, debapriya.adhikary@gmail.com

The various parts of Cudappah Igneous Provice (CIP)/Prakasham Alkaline Province (PAP) of the Eastern Dharwar Craton (EDC), southern India is known for the occurrence of alkaline rocks (Chalapati Rao,N.V 2008). Present paper reports new pyroclastic rock in and around Khammam area, Telangana, India . Plug like body of the pyroclastic rock are present in the contact zone between northeastern margin of the EDC and western margin of the proterozoic Pakhal Basin. The pyroclastic rock of the study area has been intruded within granitoids of the EDC but not intruded in the Proterozoic Pakhal Basin. This field evidence indicates that alkaline magmatism was occurring before the Proterozoic sedimentation started. The plug bodies are more or less parallel having a common trend of NNW-SSE. These are of 3-5 m wide and 20-25m in length. Megascopically it consists of euhedral to anhedral crystals of carbonate (Fig. 1). The crystals mainly comprise carbonate which can be observed in the thin sections also (Fig. 2).In the EPMA study it is shown that this carbonate are replaced the original mafic crystal in the rock. In some section pyroxene clast is also present. In this rock some phlogopite mica is also present in the ground mass. More over in the present condition the rock is full of carbonate in both ground mass and phenocrysts part. In the field, it gives effervescence to dilute HCl. From the surface to a depth 1 ft. it is highly limonitised and weathered. Specific gravity of the rock is towards higher range. Geomorphologically it forms a high mound on the surface. In the geochemistry study this rock showed high Ni value.

Fig. 1. Pyroclastic like rock near Sripuram village near Khammam.

Fig. 2. Photomicrograph of Pyroclastic like rock near Sripuram village near Khammam.

References

Chalapathi Rao, N.V. (2008). Precambrian alkaline potassic ultrapotassic, mafic ultramafic magmatism in Peninsular India. Jour. Geol. Soc. India, v.72, pp.57-82.

RARE-METAL MINERALIZATION OF THE TUNGSTIC-TIN DEPOSITS ASSOCIATED WITH LITHIUM-FLUORIC GRANITES IN RUSSIAN FAR EAST

Alekseev V.I.
Saint-Petersburg Mining University, Saint-Petersburg, Russia, alekseev_vi@pers.spmi.ru

Conceptions «rare metals» and «strategic metals» constantly change the maintenance depending on development of prospecting and processing technologies and a conjuncture of the raw market. The modern increase in demand at rare metals and progress of technologies of their treatment dictate necessity of the inventory of their natural sources. Geological-economic types of rare-metal deposits are rather various and are defined by formational type of magmatic complexes and a genetic class of ore-bearing rocks. The productive concern calc-alkali-granite, subalkali-granite, alkali-granite, agpaitic-sienite, alkali-gabbroid and the alkali-ultrabasic intrusive complexes. Abroad rare-metal deposits with one-two main components while in Russia complex deposits prevail are fulfilled. The basic directions of their development are the profound mineralogic-geochemical estimation, complex use and deep processing of raw materials (Solodov, 1985; Bykhovsky, Potanin, 2009; Kremenetsky, Kalish, 2014; Bortnikov et al., 2016; Rare Earth …, 2016).

The large deposits of Russia genetically connected with rare-metal granite – sources of scarce raw materials are especially allocated: tantalum, beryllium, yttrium, the heavy rare earth, rare alkali, hafnium and cryolite. Our attention was involved with the deposits interfaced with subalkaline lithium-fluoric granite among which, along with rare-metal (Li, Rb, Cs, Ta, Nb, Be) objects, tens tungstic-tin deposits with associated rare-metal mineralization of Europe, Asia, Africa and America (Etykinskoe, Spokoyninskoe, Maykul, Karaoba, Zhanchivlan, Baga-Gazryn, Altenberg, Zinovec, Eshassyer, Lost-River, Tin-Amzi, Ichun, Syankhualin, etc.) (Beskin, Marin, 2015) are allocated.

In the Russia Far East are considerably widespread large deposits tungstic-tin ore zwitters with associated rare metals: Voznesenskoe, Pogranichnoe, Pravourmiyskoe, Tigrinoe, Kester, Odinokoe, Polyarnoe, Pyrkakayskoe, etc. It is offered to allocate a new "rare-metal-tin" formation of the deposits connected with Li-F granite, and Far East tin-rare-metal ore belt, stretched from Primorye to Chukotka (Gonevchuk, 2002; Geodinamics…, 2006; Alekseev, 2014). An origin, localisation conditions, the composition and scales of rare-metal ore body the of East Russia demand today serious revision. The decision of the given problem should include studying of rare metals mineral forms in hydrothermal-metasomatic formations, associated with Li-F granites.

As illustration of such approach the new information about associated rare-metal mineralization in metasomatite of Verkhneurmiysky ore claster in Badzhalsky area of Amur River region. Here it is allocated pravourmiyskiy complex of Li-F granites and ongonites and the unique maintained tin deposit – Pravourmiyskoe where as passing rare metals are specified In, Nb, Sc, Y, REE (Bykhovsky, Potanin, 2009; Alekseev, Marin, 2015). The researches area is characterised by multistage development of postmagmatic processes: ore zwitter of acid dissolution stages precede muscovite greisen and biotit-feldspathic metasomatite to an early alkaline stage, on zwitters develop tourmaline and chloritic metasomatite of late alkaline and neutral stages. Products of each stage are characterised by wide facial variability – from calc-alkaline to subalkaline (basically albitic) mineral paragenesis.

In early biotit-feldspathic metasomatites by us are established rare-metal minerals – allanite, monazite, xenotime, zircon and containing rare-metal impurity apatite, ilmenite, thorite, biotite (LREE, Sc, Y, Li, Rb, Cs). On biotite metasomatite are imposed muscovite-quartz greisens in which are met cassiterite, wolframite, molybdenite and muscovite, containing Nb, Ta, Sc, Li. The rare-metal minerals found in tungstic-tin ore zwitters: fergusonite, euxenite, plumbopyrochlore, monazite, xenotime, zircon, hedleyite, beryl. Besides, ore minerals (wolframite, cassiterite, scheelite, sphalerite, native bismuth, rutile) and veined minerals of zwitters (siderophyllite, muscovite, fluorite) contain impurity Nb, Ta, Li, Rb, Cs, Y, HREE, Sc, Te, Se.

In lateore tourmalinite the economic Cu-Sn mineralization is developed and the minerals containing in essential quantity In, Cd, Sc, Nb, Y, HREE are established: roquesite, sakuraiite, monazite, zircon, scheelite, cassiterite, wolframite, chalcopyrite, stannoidite, bornite, native bismuth, pyrite, REE-epidote, fluorite. Postore chloritic metasomatites contain insignificant quantity of minerals

with an impurity of the same rare metals (basically In, Cd, Se, Y, REE): sphalerite, galenite, fluorite, epidote.

Conclusions: 1) Li-F granite in the Far East are accompanied tungstic-tin ore metasomatites with passing complex a rare-metal mineralization (Nb, Ta, Li, Y, all spectrum REE, Be, Rb, Cs, Zr, Hf, In, Sc, Se, Cd); 2) two forms of concentration of rare metals are observed: rare-metal minerals (fergusonite, euxenite, pyrochlore, allanite, zircon, monazite, xenotime, roquesite) and impurity in ore minerals (wolframite, cassiterite, Cu, Sn, Zn sulphides, native bismuth) and in veined minerals (fluorite, micas, epidote); 3) postmagmatic minerals of rare metals inherit accessories composition of Li-F granites and are formed at all stages of postmagmatic process with evolution of composition from lithophylous to chalcophylic elements: LREE, Zr, Be → Nb, Li, W, Y, HREE, Sc → In, Cd, Se.

The formulated conclusions allow to consider, that mineralogical additional appraisal of Far East tin and tungsten deposits associated with Li-F granites, expands prospects of a Russia raw-material base of rare metals.

The research was supported by the Ministry of Education and Science of Russia (basic part of the state task in the scientific sphere № 5.9248.2017/6.7 for 2017-2019).

References

Alekseev V.I. Lithium-fluoric granites of the Far East. National university of mineral resources «Mining». St Petersburg, 2014, 244 p. (in Russian).

Alekseev V.I., Marin Yu.B. Composition and Evolution of Accessory Mineralization of Li–F granites in the Far East As Indicators of Their Ore Potential // Geology of Ore Deposits. 2015. Vol. 57. No. 8. P. 635-644. (in Russian).

Beskin S.M., Marin Yu.B. Complex systematisation tantalic and tantalic- niobic deposits // Zapiski RMO. 2015. No. 3. pp. 45-54. (in Russian).

Bortnikov N.S., Volkov A.V., Galjamov A.L. et al. Mineral resources of high-tech metals in Russia: State of the art and outlook // Geology of ore deposits. 2016. Vol. 58. No. 2. pp. 83-103. (in Russian).

Bykhovsky L.Z., Potanin S.D. Geological-economic types of the rare-metal deposits // Mineral raw materials. A geological-economic series. № 28. M: VIMS, 2009. 157 p. (in Russian).

Geodinamics, magmatism and metallogeny of the Russian East: in 2 books / ed. by A.I. Khanchuk. Vladivostok: Dalnauka, 2006. Book 1. P. 1-572. (in Russian).

Gonevchuk V.G. Tin-bearing magmatic systems of the Far East: magmatism and ore genesis. Vladivostok: Dalnauka, 2002. 298 p. (in Russian).

Kremenetsky A.A., Kalish E.A. Complex rare-metal deposits of Russia and the basic directions of their investment appeal increase // Prospect and protection of mineral resources. 2014. № 9. pp. 3-11. (in Russian).

Rare Earth and Critical Elements in Ore Deposits // Reviews in Economic Geology. 2016. Vol. 18. 365 p.

Solodov N.A. Minerageny of the rare-metal formations. M: Nedra, 1985. 224 p. (in Russian).

GEOCHRONOLOGY AND ISOTOPE GEOCHEMISTRY OF THE KOLA ALKALINE INTRUSIONS, NORTHEASTERN FENNOSCANDIAN SHIELD: WHAT WE CAN DO MORE?

Arzamastsev A.A. [1,2]

[1]*Institute of Precambrian Geology and Geochronology, Saint-Petersburg, Russia*

[2]*Saint-Petersburg State University, arzamas@ipgg.ru*

The Kola Devonian alkaline province in the northeastern Fennoscandian Shield is composed of giant agpaitic syenite plutons, 20 carbonatite intrusions, alkaline volcanics and enormous alkaline dykes. Since 1960s numerous geochronological studies were performed in order to determine the age of Khibina and Lovozero massifs, ultrabasic alkaline intrusions (Kovdor, Afrikanda, Turiy Mys) and to compare the time span of agpaitic and carbonatitic magmatism.

The comprehensive isotope studies performed by U. Kramm, L. Kogarko, V. Kononova (Kramm et al., 1993, 1994) provided the short time span of the Palaeozoic alkaline magmatism in the NE Fennoscandia. During a period of 380 - 360 Ma agpaitic complexes of Khibina and Lovozero were formed simultaneously with numerous carbonatite intrusions of Kovdor, Turiy Mys, Afrikanda, Sokli, etc. The U-Pb age estimates for zircons in ultrabasic rocks and alkaline syenite of the Kurga intrusion which is located in immediate vicinity of the Lovozero complex gave the age of 387+7 Ma (Arzamastsev et al., 1999).

Zircon, the best precise U-Pb geochronometer, is absent in the most of agpaitic and ultrabasic alkaline rocks. This fact inspired geologists to test new geochronological methods in order to decipher the history of the Kola in Devonian. More than 140 age determinations of the Kola alkaline rocks include Rb-Sr and Sm-Nd mineral isochron data, U-Pb baddeleyite and apatite, Lu-Hf data of apatite, *in-situ* LA ICP MS data of perovskite, eudialyte, $^{40}Ar/^{39}Ar$ determinations of biotite, amphibole and feldspar.

Our recent studies of the Kola alkaline rocks include determination of time span of magmatism in Kola part of the Fennoscandian Shield in Paleozoic time.

Studies of tholeiitic magmatism in Kola. Among numerous Proterozoic dykes of the Pechenga, Barents Sea, and Eastern Kola swarms we found dolerites which were formed 380-390 Ma ago, i.e., directly before the main stage of the Paleozoic alkaline magmatism of the Kola province. Based on $^{40}Ar/^{39}Ar$ dating, the biotite and plagioclase fractions from several dykes of the three Barents Coast swarms yielded age of 385 ± 15 Ma. The Rb-Sr and Sm-Nd isotope systematics of the dolerites suggest that their origin from the mantle spinel lherzolite facies. The depleted mantle material from which tholeiite magma was derived shows no evidence for metasomatic event. The relatively short stage of mantle metasomatism directly after the emplacement of tholeiitic magmas was accompanied by significant enrichment of the mantle in HFSE and REE. In contrast to the other LIPs, the Kola province is characterized by systematic plume-lithosphere evolution process expressed in deepening of the level of magma generation, development of mantle metasomatism and accompanying fertilization of mantle materials, and systematic changes in the composition of melts reaching the surface (Arzamastsev et al., 2017).

Determination of time span of alkaline magmatism in Kola. Among the 19 ultrabasic-alkaline massifs of the Kola province, rocks from the Khabozero group were selected for U–Pb age determination and Sr–Nd isotopic analyses using in situ ion probe and laser ablation techniques. The main reason to choose these massifs is that each of them is represented by a single rock type: olivinite (Lesnaya Varaka Massif), pyroxenite (Afrikanda Massif), and foidolite (Ozernaya Varaka Massif). Thus, derivatives of the Khabozero group sequentially intruded through different conduits, and we believe that the absence of later derivatives minimizes resetting of isotopic systems of early differentiates and allows to obtain correct age estimates. Mineral separates of perovskite from the olivinite and pyroxenite exhibit the age of 385–377 Ma. Age estimates for perovskite from the more evolved rocks of the series range from 376 to 367 Ma. The analysis of rare perovskite grains from the rocks of the Khibiny Massif revealed significant differences between the ages of the pyroxenite and xenoliths of ultrabasic alkaline rocks (383 ± 7 Ma) and apatite–nepheline ores (370 ± 3 Ma), which is consistent with geological observations of rock relationships. Together with geological observations, these data allow us to distinguish the following stages of Paleozoic magmatism in the northeastern Fennoscandian Shield.

393–381 Ma. Emplacement of subalkaline dolerite dikes in the distal zone adjacent to the Barents Sea region of the Kola–Kanin monocline.

387±7 Ma. Origination of a series of faults in Late Archean tonalites, trondhjemites, and granodiorites; formation of the Kurga Massif and ultrabasic and subalkaline volcanics in the northeastern part of the future Lovozero ring structure.

388±6 Ma. Formation of a series of ring faults and the origin of the Khibiny caldera at the contact of the Late Archean gneiss complex and the Paleoproterozoic Pechenga–Imandra–Varzuga paleorift rock series; injection of the first portions of melanephelinite magma and formation of framing ring dikes.

380±5 Ma. Emplacement of ultrabasic alkaline melts in the peripheric parts of the Khibiny and Lovozero calderas. Formation of ultrabasic alkaline complexes with carbonatites in the Kovdor Massif, as well as the Turiy Mys, Afrikanda, Lesnaya Varaka, Ozernaya Varaka, Ivanovka, Pesochnyi and other massifs.

373–367 Ma. Formation of the plutonic complexes of agpaitic syenites in the Khibiny and Lovozero calderas. Intrusion of carbonatite and pulaskite stocks in the eastern part of the Khibiny caldera.

377–362 Ma. Several pulses of dyke emplacement and formation of diatremes of alkali picrite, kimberlite, olivine melanephelinite, nephelinite, and phonolite mainly in the framing of the Kandalaksha paleorift.

359±5 Ma. Formation of late microcline–albite veins with ilmenite and zircon in the framing of the Lovozero Massif.

347±8 Ma. Postmagmatic processes in the alkali syenites of the central part of the Lovozero Massif marking the termination of thermal activity in the Khibina and Lovozero calderas.

What we can do more is to test the most abundant minerals titanite and Ca-Ti garnet as geochronometers. The first experience is as follows.

Titanite by SHRIMP. The U-Pb age estimates for titanite fractions in agpaitic syenites and apatite ores of the Khibina and Lovozero massifs was performed using SHRIMP-II (Rodionov et al., 2018 in press). The obtained age of 374.1±3.7 Ma for Khibina agpaitic syenites coincide with the age of apatite mineralization (371.1±4.2 Ma). Age estimation of the Lovozero lujavrite-foyaite-urtite complex is significantly older 380.9±4.5 Ma), whereas the time of titanite mineralization in the Suluai titanite deposit (361.4±3.2 Ma) supports the long-term postmagmatic history of these two giant plutons.

U-Pb age of Ca-garnet. The first successful geochronological studies of Ca-Ti garnets in carbonatites of the Afrikanda massif (Salnikova et al., 2017) inspired for further U-Pb age determinations of garnets from foidolites in the other massifs of the Kola Province. Obtained U-Pb ages for Salmagorsky massif is 377±2 Ma, Sallanlatva 378±3 Ma, Vuorijarvi 373±5 Ma. These data fall the time span of the ultrabasic alkaline intrusions of the Kola Province which were obtained by (Kramm et al., 1993, 1994; Arzamastsev, Wu, 2014 and refs ibid).

Further geochronological investigations of the Kola alkaline magmatism will be focused on age determinations using titanite, perovskite and Ca-garnet.

References

Arzamastsev A.A., Wu Fu-Yuan. U–Pb Geochronology and Sr–Nd Isotopic Systematics of Minerals from the Ultrabasic Alkaline Massifs of the Kola Province. Petrology, 2014, Vol. 22, No. 5, pp. 462–479.

Arzamastsev A. A., Bayanova T. B., Arzamastseva L. V., Balashov Yu. A., and Gogol O. V. Initial Magmatism Related to the Paleozoic Tectono-Magmatic Reactivation in the Northeastern Baltic Shield: The Age and Geochemistry of the Kurga Massif, Kola Peninsula. Geochemistry International, Vol. 37, No. 11, 1999 p. 1025-1035.

Arzamastsev A.A., Vesolovskiy R.V., Travin A.V., Yudin D.S., Belyatsky B.V. Paleozoic Tholeiitic Magmatism of the Kola Province: Spatial Distribution, Age, and Relation to Alkaline Magmatism. Petrology, 2017, Vol. 25, No. 1, pp. 42–65.

Kramm U., Kogarko L.N., Kononova V.A., Vartiainen H. The Kola Alkaline Province of the CIS and Finland: Precise Rb-Sr ages define 380-360 age range for all magmatism. Lithos, 1993, vol.30, p.33-44.

Kramm U., Kogarko L.N. Nd and Sr isotope signatures of the Khibina and Lovozero agpaitic centres, Kola Alkaline Province, Russia// Lithos. 1994. Vol.32. P.225-242.

Rodionov N.V., Lepekhina E.N., Antonov A.V., Kapitonov I.N., Balashova Yu.S., Beluyatsky B.V., Arzamastsev A.A., Sergeev S.A. U-Pb SHRIMP-II geochronology of titanite: Determination of the time of apatite-nepheline mineralization of the Khibina and Lovozero alkaline massifs (Kola peninsula). Geology and Geophysics, 2018, no.8 (in press).

Salnikova E.B., Stifeeva M.V., Chakhmouradian A.R. , Glebovitsky V.A., Reguir E.P. The U–Pb System in Schorlomite from Calcite–Amphobole–Pyroxene Pegmatite of the Afrikanda Complex (Kola Peninsula). Doklady Earth Sciences, 2018, Vol. 478, Part 2, pp. 148–151.

SPATIAL REGULARITIES OF THE LOCATION OF DEPOSITS ASSOCIATED WITH ALKALINE AND BASIC MAGMATISM OF THE 251 MA SIBERIAN AND 259 MA CHINESE LIP PROVINCES

***Asavin A.M.*[1], *Chesalova E.I.*[2]**
[1]*GEOHI RAS, Moscow, aalex06@lnbox.ru*
[2]*SGM RAS, Moscow*

Large igneous provinces – LIP, fix the appearance of extensive and short-lives magmatic outbursts on the Earth. They correspond to the basic and ultrabasic types of magmatism of normal alkalinity and to the ore deposits associated with it. Studies of these provinces have revealed a temporary link with the large ore provinces, located along the border of the LIP volcanic area [Zhang et al., 2008; Dobretsov et al., 2011; Ernst & Jowitt 2013]. The authors link this provinces with the large alkaline provinces and the associated rare earth and trace metal deposits [Riley 2003; Ernst & Bell 2010], with the main-ultramafic ore occurrences of Fe-Ti-V and Cr-Pt, PGE-Ni-Co ore specialization, Cu-Mo porphyry deposits and with a number of other ore types [Berzina & Borisenko 2008; de Boorder 2014]. The main reason of the close spatial relationship between the LIP provinces and the ore provinces is the idea of the emergence of provinces due to mantle plume activity. The initial activation of the LIP region is to form of a large uplift - swell caused by the pressure of the rising mantle plume on the lithosphere. Thus, the first portions of floor basalt, fissure volcanism, corresponded of basic tholeiitic basalts, are the earliest manifestation of magmatism. Plutonic magmatism, associated with this type of volcanism, forms mafic and ultramafic intrusive complexes with associated metallogenic specialization.

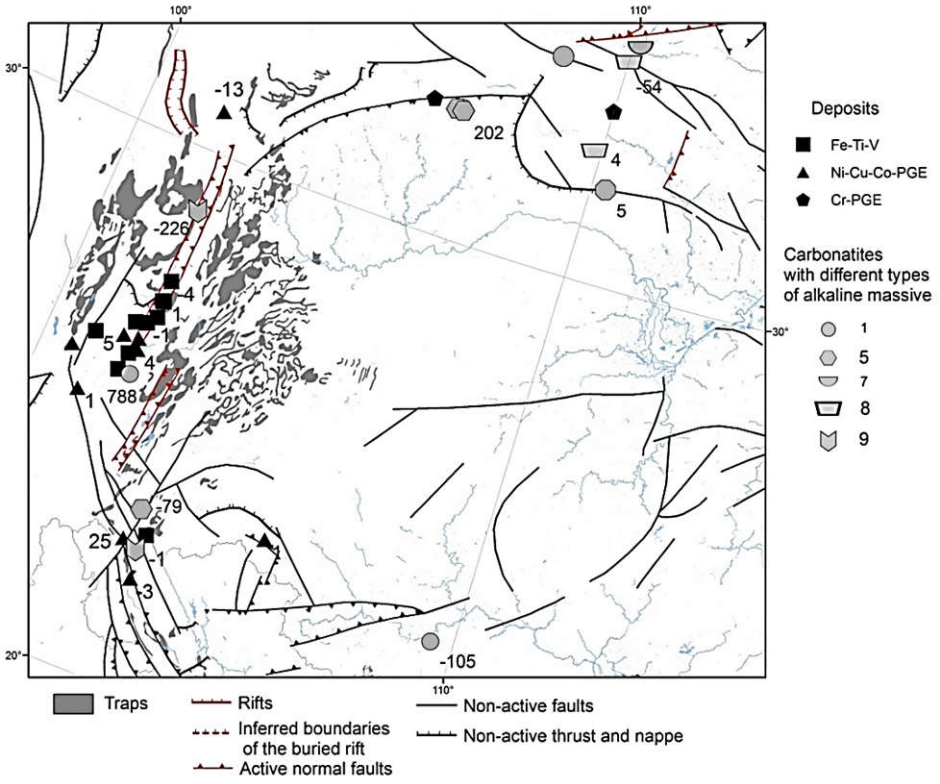

Fig. 1. Scheme location of large deposits in the ELIP province. The boundaries of basalts of ELIP coverings according to [Chung et al., 1998; Xu et al., 2007].

Later, within this global swell area, linear faults structures are formed: fault trough, rift structures, thrusts. There is no direct connection between these disruptive disturbances and the manifestations of magmatism. Within these linear depressions, there are shallow sedimentation basins (lake or shallow sea bays). Along the LIP boundaries the large alkaline provinces (Enisey, Udjinsky – Tomtor, Maimecha-Kotui) are formed, where carbonatite and rare metals ore deposits are found. This very simplified scheme for the development of LIP magmatism remains poorly detailed and contains many unresolved issues. There are many problems in LIP petrogenesis process. We have many questions: the relationship between the ages of alkaline and basalt volcanism, the causes of spatial asymmetry and spatial shift (on the South) of the LIP center and centers of mantle plumes, the spatial metallogenic zonation of alkaline and basic provinces, the genesis of rifting into the LIP provinces, moved and break-up of continental craton with these processes.

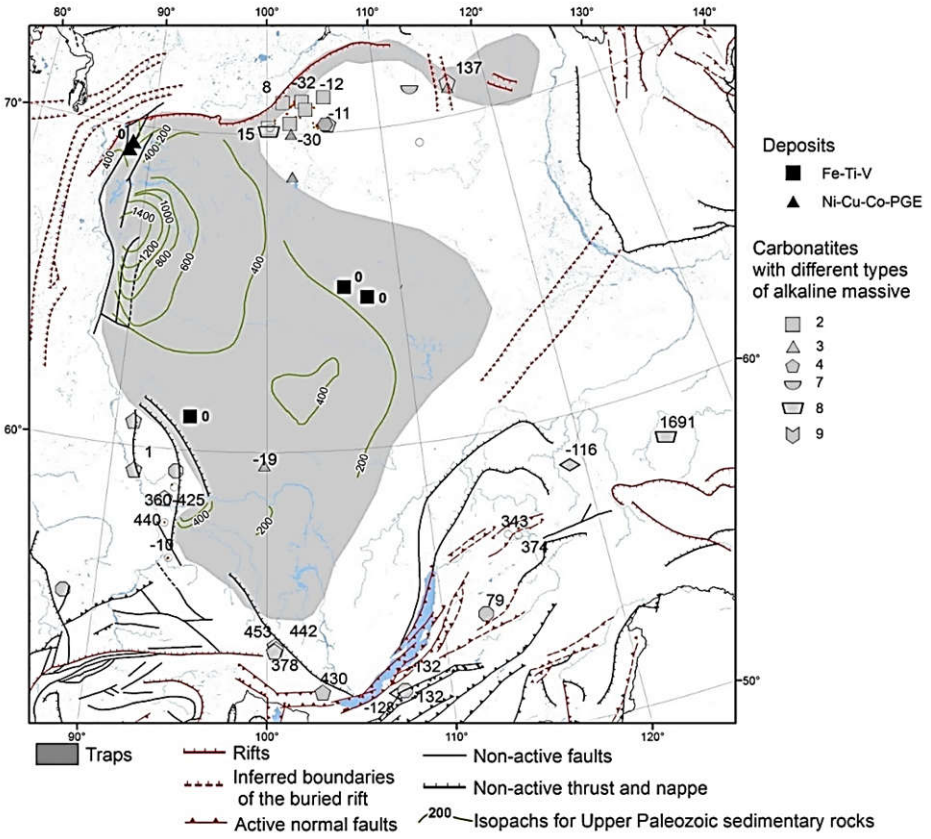

Fig. 2. Scheme location of large deposits in the Siberian LIP province. The boundaries of LIP according to [Czamanske et al., 1998, Fedorenko & Czamanske 1997; Fedorenko 2010] and the geological and mineralogical maps of Russia M1: 2500000 [Bogdanov et al., 2016; Afanasyev et al. 2016].

Thus, it is possible to distinguish such common structural elements as the boundaries and forms of the LIP region, the center of the uplift, the position of the rift zones, the position and size of the alkaline provinces, the position of the plume magmatism center and so on.

We prepared the GIS project, where we collected some published databases of deposits associated with basic and ultrabasic melts: sulphide Cu-Ni-PGE, low-sulfide layered platinum-bearing and chromite and titanomagnetite Fe-Ti-V [Schulz et al., 2012; Schulz et al., 2011; Schulz et al., 2014]. The data of the metallogeny of China were taken from survey work [Pirajno 2013; Wu et al., 1996; Yuwang et al., 2008].

Deposits associated with basaltic magmatism were divided into three groups: sulphide ore deposit (Cu-Ni-PGE), titano-magnetite layered pluton (Fe-Ti-V), and chromite layered low-sulfide intrusion(Cr-Pt). The figure also shows the number of large, ore-free stratified sills (Vilyuisky,

Kuzmovsky, Vavokansky) studied in [Egorova & Latypov 2013]. In addition, we used perspective occurrences of sulphide Cu-Ni-PGE ores where the resources of category P3 are estimated (http://p3.vsegei.ru/index.php).

Coordinates of deposits associated with plume magmatism - rare-earth-metal carbonatite massifs were taken from the Carbonatite World database [Woolley & Kjarsgaard 2009, Woolley & Kjarsgaard 2008] and databases [Frolov et al. 2005; Belov et al., 2008]. In the figures, icons indicate carbonatite deposits in accordance of the classification proposed by us [Asavin 2015]. In figures 1-2, next to the symbol of the deposit the difference between the age of massif and the age of the LIP are shown. We took 250 million years for Siberian LIP, and 260 million years for Emeishan LIP [Burgess & Bowring 2015].

Figure 2 also shows the isopachites of the Upper Paleozoic sedimentary rocks [Czamanske et al., 1998], which allows us to evaluate the internal structure of the trap field. Apparently, the great thickness of the sediments corresponded to the marginal troughs, and the position of the center of the uplift is fixed by the minimum of precipitation. It should be noted that according to Dobretsov [Dobretsov 1997] it was the center of the plume. In ELIP, the center was located on the western border.

The first regularities, we can see, is the spatial separation of the productive alkaline and mafic magmatism. The position of alkaline provinces and mafic intrusions with Ni-Cu-PGE sulphide mineralization of the same age-with LIP are located on different parts of the LIP. Ore mafic and ultramafic intrusions of Siberia are located along the western boundary of LIP, as well as Chinese deposits of the same type. Fe-Ti-V deposits are typical for the Chinese ELIP, and they are not found within the Siberian trap. Emeishan ore intrusions localize into rift inner area. Chromite deposits are located in the outer zone of LIP and their age is not defined. Alkaline provinces of the same age with LIP activity (the difference of ages from several million years to 20-30 million years) are located at a considerable distance from the mafic ore-genesis regions. For China, the massifs with carbonatites (206-265 million years) are located on the northeast margin. Other alkaline carbonatite magmatismis either too young or too old (Fig.2). In particular, carbonatite massifs located near sulfide deposits and near the center of ELIP are of age 34, 1048, 181 Ma. The second important observation is the combination of intrusions with different age within one province. Compared with LIP, the age difference reaches several hundred million years, and it can be younger and more ancient manifestations, regarding the activity of basaltic magmatism. This is the evidence that the source of this alkaline magmatism column'dt link with LIP but the same spatial locality is the evidence that is the same mantle plume source. We view this fact as evidence of the continuous plume activity in the region, which was not limited to the formation of the LIP province alone, and may be, a considerable (for several hundred km) displacement of the plume center from the beginning of its rise to the base of the lithosphere, to the finish of its activity. This drift can explain a different metallogenic typification of alkaline provinces (for example, Maimecha–Kotui and Yenisei Ridge). Such drift for the Siberian plume looks like a change in ages from the older ones on the Maimecha-Kotui province (range from -32 to 15) to more young (from 1 to -19) and for the Chadobetskii complex -19.

This is the paradox. How to explain that at a distance much larger (about 1400km) than the size of the plume area, activation of deep mantle sources and generation of alkaline magmatism occur simultaneously. That is, there was a certain chord (line) of mantle activity intersecting LIP, as an analogue of the track of an oceanic hot point along which an alkaline province is generated on opposite sides of the LIP. The Kotui province, specialized in the platinoids, consist mainly with ultrabasic and largest olivinite plutons. Yenisei province, consist mainly with nephelinites, with phosphorus and gold specialization [Grinev 2001; Romanova 2013; Romanova 2013].

Simultaneously c event. provinces, located at a considerable distance one from another (much larger than the size of the plume), have different metallogenic types. The simplest solution to this question is the suggestion, which made by [Dobretsov 1997] about two univocally activating plumes: the northern one in the Khatangsky region, responsible for the Maimecha-Kotui province and the southern one (approximately in the Chadobetsky complex). However, it seems to us that this is a questionable model, because this is contrary to modern models of the mantle plume dynamic. Existing estimates from geophysical data and from plate-tectonic modeling data do not give grounds for

assuming the existence of such neighboring mantle plumes, and even more so simultaneously acting, in relatively close regions of the earth's crust. The explanation of Ernst and other authors that single plume rising beneath a thick lithosphere can spread along the base of the lithosphere and rise to shallower levels along more than one edge of the craton--- producing multiple separate but coeval centres of plume magmatism. The key word of our hesitation here is "more then one edge". We need explain why these critical points of plume activity must be on the edge points of "plume chord line". For our opinion a more realistic model is the displacement of plume as a result of migration along "plume chord line" of a convection cell, caused by the appearance of LIP structures in the lithosphere. However, this idea must be proved on a more representative material.

References

Asavin A.M. Types of carbonatite and relative associated silicate rocks groups – by re-analysisis of the Database Woolley and Kjarsgaard // "Alkaline Magmatism of the Earth and Related Strategic Metal Deposits". Proceedings of XXXII International Conference. Apatity 7-14 August 2015, M.: GEOKHI 2015, P.13-17

Berzina A. P., and A. S. Borisenko Porphyry Cu-Mo mineralization and mantle plumes //Doklady Earth Sciences, 2008, V.423, N.1, P.1240-1244

Bryan, S. E., & Ferrari, L. Large igneous provinces and silicic large igneous provinces: Progress in our understanding over the last 25 years. //Geological Society of America Bulletin 2013, V.125, N.7-8, P.1053-1078.

Burgess, S. D., & Bowring, S. A. High-precision geochronology confirms voluminous magmatism before, during, and after Earth's most severe extinction. //*Science Advances*, 2015, V.*1*(7), e1500470, 14 pp.

Chung, S. L., Jahn, B. M., Genyao, W., Lo, C. H., & Bolin, C. The Emeishan Flood Basalt in SW China: A Mantle Plume Initiation Model and its Connection with Continental Breakup and Mass Extinction at the Permian-Triassic Boundary. //Mantle dynamics and plate interactions in East Asia 1998, P.47-58.

Czamanske, G.K., Gurevitch, A.B., Fedorenko, V., Simonov, O. Demise of the Siberian plume: Paleogeographic and paleotectonic reconstruction from the prevolcanic and volcanic record, North-Central Siberia //International Geology Review, 1998, V.40(2), P.95-115.

de Boorder, H. The Central European, Tarim and Siberian Large Igneous Provinces, Late Palaeozoic orogeny and coeval metallogeny. //Global Tectonics and Metallogeny 2014, V.10.1, P.1-22.

Egorova, V, and R Latypov. Mafic–ultramafic sills: New insights from M-and S-shaped mineral and whole-rock compositional profiles. //Journal of Petrology 2013, V.54.10, P.2155-2191.

Ernst R. E. & Bell K. Large igneous provinces (LIPs) and carbonatites //Miner Petrol 2010, V.98, N.1-4, P.55-76.

Ernst, R. E., & Jowitt, S. M. Large igneous provinces (LIPs) and metallogeny. //In book: "Tectonics, Metallogeny, and Discovery: the North American Cordillera and Similar Accretionary Settings". Edited by M. Colpron, T. Bissig, BG Rusk, and JFH Thompson. Soc. Of Economic Geologists Special Publ. 2013, V.17, Chapter 2, P.17-51.

Fedorenko V.A. & Czamanske G.K., Results of New Field & Geochemical Studies of the Volcanic & Intrusive Rocks of the Maymecha-Kotuy Area Siberian Flood-Basalt Province Russia //International Geology Review 1997, V.39 P.479-531.

Fedorenko V.A. Magmatism and Ni-Cu deposits of the Norilsk region (Review) //Personal communication 2010, 51 pp.

Pirajno F. The Geology and Tectonic Settings of China's Mineral Deposits //Springer 2013, 688 pp.

Schulz K. J., V. W. Chandler, S. W. Nicholson, N. Piatak, R. R. Seal, II, Laurel G. Woodruff, and M. L. Zientek Magmatic Sulfide-Rich Nickel-Copper Deposits Related to Picrite and (or) Tholeiitic Basalt Dike-Sill Complexes: A Preliminary Deposit Model //Open-File Report 2010–1179 U.S. Geological Survey, Reston, Virginia: 2010 http://pubs.usgs.gov/of/2010/1179/ 2010, Rep.2010, N.1179, 31 pp.

Zientek, M.L. Magmatic ore deposits in layered intrusions—Descriptive model for reef-type PGE and contact-type Cu-Ni-PGE deposits //USGS U.S. Geological Survey Open-File Report 2012, N.1010, 48 pp.

Schulz K. J., Laurel G. Woodruff, S. W. Nicholson, Robert R. Seal II, …and John L. Mars Occurrence Model for Magmatic Sulfide-Rich Nickel-Copper-(Platinum-Group Element) Deposits Related to Mafic and Ultramafic Dike-Sill Complexes. //USGS Scientific Investigations Open Report Geological Survey, Reston, Virginia 2010–5070–I http://dx.doi.org/10.3133/sir20105070I. 2014, Rep.2010, N.5070–I, 93 pp.

Woolley A. R., Kjarsgaard B. A. Paragenetic types of carbonatite as indicated by the diversity and relative abundances of associated silicate rocks: Evidence from a global database. //The Canadian Mineralogist 2008, V.46, N.4., P.741-752.

Woolley A. R., Kjarsgaard B. A. Book Review. //Journal of petrology. 2009, V.50, N. 1, P.195-196.

Wu, C. Z. Yuan and G. Bai, Rare earth deposits in China. //In Rare Earth Minerals: Chemistry, origin and deposits. Edited by Adrian P. Jones, Frances Wall and 1996, Chap.7, P. 280-310.

Xu, Y.-G., He, B., Huang, X., Luo, Z., Chung, S.-L., Xiao, L., Zhu, D., Shao, H., Fan, W.-M., Xu, J., Wang, Y.-J. Identification of mantle plumes in the Emeishan Large Igneous Province //Episodes, 2007, V.30 (1), P. 32-42.

Yuwang, W. A. N. G., Jingbin, W. A. N. G., Lijuan, W. A. N. G., & Lingli, L. O. N. G Metallogenic Series Related to Permian Mafic Complex in North Xinjiang: Post-collisional Stage or Mantle Plume Result?. //Acta Geologica Sinica (English Edition) 2008, V.82.4, P. 788-795.

Zhang M., O'Reilly S. Y., Wang Kuo-Lung, Hronsky J., Griffin W. L. Flood Basalts and Metallogeny: the Lithospheric Mantle Connection //Earth-Science Reviews 2008, V.86, Iss.1, P. 145-174.

Н.И. Афанасьева, В.Н. Белова, Б.И. Беневольский, Г.Н. Булатова, Л.И. Гурская, Е.С. Заскинд, Е.В. Зублюк, Е.В. Ершова, С.Н. Калабашкин, С.В. Кашин, В.А. Килипко, Д.С. Терехов, В.П. Феоктистов, В.А. Шамахов, В.В. Шатов. Прогнозно-минерагеническая карта Российской Федерации и ее континентального шельфа Масштаб 1:2500000 //МПР РФ, Федеральное Агентство по Недропользованию, ВСЕГЕИ, ред.: О.В. Петров, А.Ф. Морозов, В.В. Шатов, А.В. Молчанов, Е.М. Аксенов, П.П. Сенаторов, А.И. и др. 2016.

Белов С.В., Лапин А.В., Толстов А.В., Фролов А.А. Минерагения платформенного магматизма (траппы карбонатиты кимберлиты) // Изд. Со РАН Новосибирск 2008, 537 стр.

Ю.Б. Богданов, В.П. Кириков, Е.К. Ковригина, Б.А. Марковский, И.М. Мигович, Н.Н. Соболев, В.Л. Мараев. Геологическая Карта России и прилегающих акваторий Масштаб 1:2500000 //МПР РФ, Федеральное Агентство по Недропользованию, ВСЕГЕИ, ВНИИОКЕАНГЕОЛОГИЯ Ред. О.В. Петров, и др. 2016.

Гринев О.М. (2001). Провинции щелочных пород как районы комплексных золото-платиновых руд. //Материалы научной конференции, Петрология магматических и метаморфических комплексов посвященной 80-летию со дня рождения проф. Михаила Петровича Кортусова Томск, 28-30 ноября 2001 года Томский государственный университет 2001, Вып.2, С. 216-226.

Добрецов Н.Л. Пермо-триасовый магматизм и осадконакопление в Евразии как отражение суперплюма //Докл. РАН 1997, V.354 (2), P. 220-223.

Добрецов Н. Л., А. С. Борисенко, А. Э. Изох Термохимические глубинные мантийные плюмы – источник рудного богатства планеты //Наука из первых рук, Гипотезы и Факты 2011, V.6, N42, С. 36-43.

Романова И. В. (2013). Геохимия, минералогия и геохронология щелочных комплексов Енисейского Кряжа //Автореферат диссертации канд. г.м.н. Иркутск. Институте геологии и минералогии им. В.С. Соболева СО РАН и . 2013, 21 стр.

Фролов А.А,, Лапин А.В., Толстов А.В., Зинчук Н.Н., Белов С.В., Бурмистров А.А. Карбонатиты и Кимберлиты (взаимоотношения, минерагения, прогноз). НИА-Природа М. 2005, 540 стр.

A SEARCH CRITERION FOR ASSESSING THE POSITION OF ORE REEFS IN LOW-SULFIDE LAYERED BASIC-ULTRABASIC MASSIVE

Asavin A.M., Tyutyunnik O.A.
GEOHI RAS, Moscow, aalex06@lnbox.ru

The drilling operations in the geological exploration works and during the localization of ore layers in intrusive pluton complexes of low-sulfide platinum deposits, are the most costly. A large amount of holes is necessary to obtain a detailed picture of the internal structure of the intrusion, since usually the thickness of plutons is large up to be several kilometers, and the thickness of the ore horizon is only the first meters In this situation, it becomes necessary to develop effective search criteria for a previous theoretical forecast of the position of ore horizons into the massif.

On the basis of an our experimental work of the water-rock interaction (Asavin & Tyutyunnik 2018), we assumed that when an independent fluid (H2O) phase appears, into the layering complex necessarily there is infiltration columns are formed during cooling intrusion. Due to the acidity gradient within the rhythms, it becomes possible to transfer ore components and accumulate them as ore into local layer. Figure 1 shows the experimentally found dependence of the acidity of solutions on the parameter reflecting the composition of the rock, calculated by the CIPW normative recalculation.

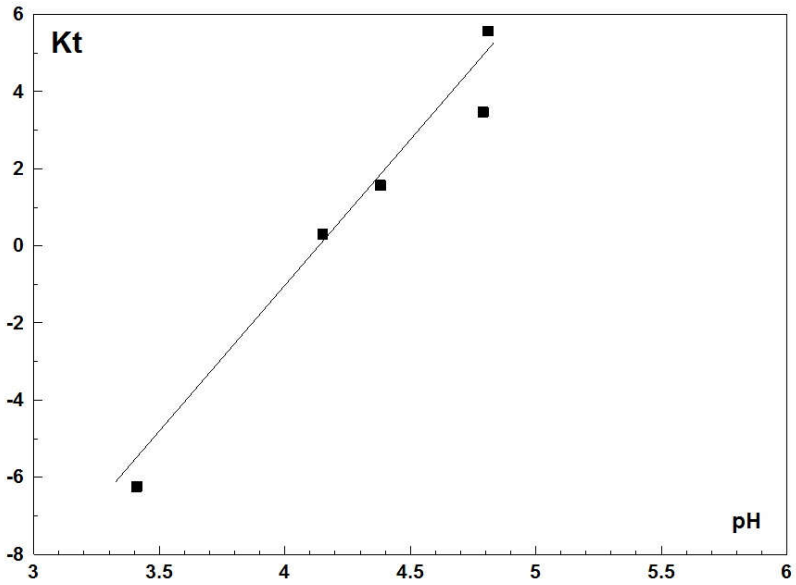

Fig. 1. Experimental line of the equilibrium solution pH in depend of the Kt calculate parameter as composition of the rock (Asavin & Tyutyunnik 2018).

The albitization reaction should be depend of both by the total value of the plagioclase content and by the ratio of the fraction of the albite minal to anorthite. The reaction of serpentinization and amphibolization will depend on the content of olivine and diopside in the rock. In addition, the calcite minal indicates the participation of carbon dioxide in the reaction. Proceeding from these considerations, we proposed to calculate the value of the interaction between water rocks (Kt) as:

Kt = An/(Ab –CC) - Di

Where An, Ab, Di, CC are the normative fractions of minerals anorthite, albite, diopside and calcite, calculated by CIPW procedure, respectively. The calculation was carried out according to a linear relationship (Fig. 1) established as a result of water-rock experiments (Asavin & Tyutyunnik, 2018).

The description of this process theoretically will make it possible to calculate the position into the intrusion section ore's layers, and made exploration mining work more chipper. In fact, these are areas with a most gradient sharp drop in pH value in fluid solutions. In more acidic solutions, the ore components are transported in dissolved form, and getting into the contrasting alkaline region there is a

unloading of the fluids and the deposition of ore minerals. With a constant pH gradient and a long process duration, a significant accumulation of ore matter and the formation of ore reefs will be possible.

It is interesting to test this hypothesis on the material of the already explored layered complex. Unfortunately, in the literature, there is no published detailed geochemical information including main components and ore elements concentration in the rock in depend of the section deep. We managed to find a single work, where simultaneously with the macrocomponents of the rocks, the content of rare elements was measured across the full layering section (Latypov & Chistyakova 2000) (the West Pansky Tundra deposit, Kola Peninsula). Using these data, we calculated the critical coefficient (Km), which determines the acidity of the solution that is in equilibrium with the rock.

Fig. 2 shows the correspondence between Kt parameter (which we calculate as pH solution) and the concentration of ore chalcophile components- Ni and Cu. The value of Kt is recalculated in the form more traditional conditional values of the acidity (pH) of the equilibrium solution with the rock. The calculation was carried out according to a linear relationship established as a result of water-rock experiments (Asavin & Tyutyunnik, 2018). The results in the figure can be assessed ambiguously. On the one hand, there is a certain correlation in the position of the maximums of the calculated pH and the concentration of Ni, Cu, and on the other hand the scatter of the points is quite large both with respect to the concentration of the ore elements and the calculated pH value.

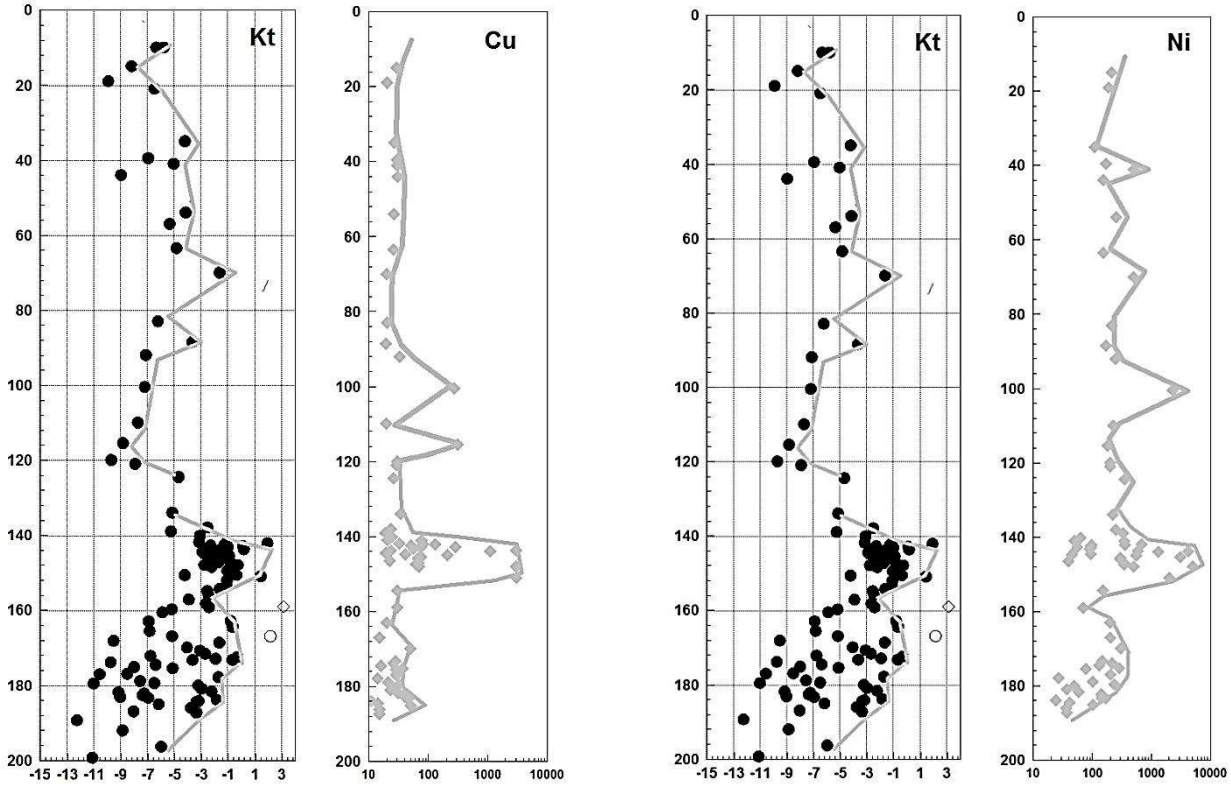

Figure 2. Distribution the Кт value (black points as calculate pH of the hypothetical equilibrium solution) into the section of the massif (m) and the concentration of Ni, Cu (gray dots in ppm).

What are the reasons for the scatter of the points on the low part on the Fig. 2? It is indicate a large fluctuation of the composition at a small distance in the lower part of the intrusion section. Probably the thickness of the rhythms in the stratified section decreases. Because of this, more detailed testing of such horizons is needed to find the correlation. Unfortunatly, according to the available data, such analysis cannot be performed. An increase in the detail of the research probing will allow us to answer the question of the effectiveness of the proposed method for determining the position of ore horizons. At the present time apparatus developed sufficiently comfortable local estimation macro

geochemical lithology - fluorescence spectrometry portable x-ray analyzers that can quickly evaluate the composition of the rocks (e.g., NITON XL2 950, NITON XL3t 950 [http://www.ccsservices.ru/]).

And, if earlier for these devices it was impossible to determine the light elements such as silicon, then now this problem is solved. That is, technically, it is easy enough to estimate the rock composition fluctuations composition and, consequently, use the proposed methodology for estimating the acidity of interstitial solutions. In practice, this means that it is possible to search the prospectively horizons with the highest Kt along the reference wells and, after that, to limit region were to conduct more detailed exploration and search for ore horizons. But at the present moment, we can only talk about the good prospects of developing this exploration method.

There are a number of theoretical difficulties in the application of the method into the real nature object. For example, amphibolization is likely to result in the drying of the environmental rocks, since water will be actively used to form an amphibole structure, but the same process will ensure the increase of ore components concentration in solution, since amphibole has low chalcophile elements distribution coefficients. In the case of solutions with a high content of CO2 will lead to processes of carbonization and therefore the formula for calculating Kt will not work. These are only obvious difficulties in using the proposed methodology, but nevertheless we are considering these approach quite optimistically, since no alternative forecasting method has not been published (Mitrofanov et al. 2006, 2012).

Thus, a calculation procedure for Kt (the coefficient of conditional acidity (pH) of the equilibrium solution with the rock) has been proposed. Estimating this value, it is possible to predict the position of ore layers – ore riff into the layered basic-ultrabasic complex.

References

Asavin A.M., & Tyutyunnik O. A. The water-rock interaction as the mechanism of the ore layers genesis in the basic magmatic complexes (by the experimental data) // Proceedings of the Russian Seminar on Experimental Mineralogy, Petrology and Geochemistry (ВЕСЭМПГ-2018)18-19 April 2018. Moscow. (in press)

Latypov R. M. & Chistyakova C. Yu. The mechanism of differentiation of the stratified intrusion of the Western Pansky Tundra // Kola Sci. Center RAS. 2000. 298 c.

Mitrofanov F.P., Zhirov D. V., T.B. Bayanova. Complex forecasting and search criteria of the main metallogenic specialization (low-sulfide Pt-Pd or sulfide Cu-Ni) of Early Proterozoic basite-hyperbasite stratified massifs of crystalline shields.// Kola Sci. Center RAS. 2012. V.1. P. 6-12.

Mitrofanov F.P., T.B. Bayanova. Pripatchkin V.A., Exploration indicators of new industrial deposits of rhodium-platinum-palladium, cobalt-copper-nickel and chrome ores on the Kola Peninsula // Otechestvennaiy Geology 2006. V. 200. P. 3-9.

ORE-CONTROLLING MAGMATIC COMPLEXES AS DERIVATES OF THE MANTIES PLUM

Baibatsha A.B., Omarova G.M., Shakirova G.S.

Kazakh National Research Technical University named after K.I. Satpayev, Almaty, baibatsha48@mail.ru

At present, the concept of the participation of mantle plumes and superplumes in the formation of geotectonics and geodynamics of certain regions of our planet characterized by large and unique mineral deposits is becoming increasingly recognized (David *et al*., 2007; Joachim *et al*., 2007; Pirajo, 2000; Baibatsha, 2016, 2017, 2018; Dobretsov *et al*., 2001).

In the modern geological structure of Kazakhstan, the inner and middle ring structures are rather fully preserved. The inner ring became elongated in the north-west direction, and its northwestern edge straightened, sometimes even concave. The middle ring from the south and south-east side due to the pressure of the above-mentioned corresponding lithospheric plates and the formation of the collision zone has become close to the inner ring, and the deformed north-eastern edge is traced along the Altai crushing zone. The outer ring also became flattened and crumpled into mountain-folded structures

from the south and south-east, from the north side it joins the Ural mountain-fold belt and the West Siberian plate, and from the northwest is cut by a shift-collision zone between Siberia (Figure 1).

Fig. 1. Scheme of ring structures of Kazakhstan on a tectonic basis.

We studied magmatic complexes within the Kyrgyz-Terskeisk and Karsakpai-Ulytau zones of the Second Ring and Shu-Ile zones and the Northern Balkhash area of the First Ring Geosuture. Thus, the analysis of the tectonic structure of the composition and interrelationship of magmatic formations of the Kyrgyz-Terskei mineragenic zone located within the North Tien Shan fold system reveals their homodromic sequence in a single tectonic-magmatic cycle of the Paleozoic. According to the newest geotectonic zoning, the Kyrgyz-Terskei mineralogical zone is confined to the Second Ring Geosuture structure, which was created by the Paleozoic superplume (Baibatsha, 2018).

Numerous deposits and ore occurrences predominantly of gold ore specialization are known in the Kyrgyz-Terskei metallogenic zone, including the Kokkiya gold deposit. The geological position of the deposit is determined by its confinement to the top of the granodiorite massif of the Upper Devonian intrusive complex. Stratified formations are represented by terrigenous and volcanogenic formations of the Aksai Formation and acidic crystallovitroclastic tuffs and conglomerates of the Taldysu Formation. The intrusive rocks of the Upper Devonian magmatic complex occupy about one-third of the area of the ore field and are exposed along the periphery of the site. Contacts of intrusive bodies, as a rule, are renewed with discontinuous tectonics (Mikolaichuk, 2003).

Intrusive rocks of the Paleozoic, confined to the deep faults of the Geosururec zone, form a significant part of the territory under consideration and form the following complexes: 1) Late Cambrian-Early Ordovician (Karaarcha); 2) medium-Ordovician (Almaly); 3) Late Ordovician-Silurian (Aktash); 4) Middle Devonian intrusive complex; 5) Late Devonian subvolcanic; 6) Late Devonian (Merke). A brief description of the isolated complexes is given by (Avdeev, 2001).

The Karaarcha intrusive complex (Є-O₁k). The complex's formations are found in the form of independent intrusive bodies among the enclosing rocks and in the form of remains in the plutons of the Aktash complex. In the first case, they form an independent massif in the basin of the river Karaarcha, in others - a group of remains on the right bank of the Shorlysu River and in the interfluve of the rivers Shorlysu-Tuyuktor. Host rocks, formations of sodium basalts are, along with the intrusive formations described, the constituent parts of a single ophiolite volcanoplutonic association, the

stratospheric-main plutonic and volcanic rocks of the mantle, covered with a cover of deep-sea sediments.

Gray fine-grained and medium-grained gabbro, dark gray and black fine-grained diabases, black coarse-grained and medium-grained pyroxenites and peridotites participate in the structure of the massif.

Formation is allochthonous, the initial material of which was formed at great depth. The characteristic formation is the beginning of the magmatic megarhythm (initial magmatism) of the Early Paleozoic stage of tectonomagmatic activation.

The Almaly intrusive complex (O_2al). The intrusive bodies of the complex are found both in the form of independent bodies among stratified formations, and in the form of large remains in polychronic plutons. In the first case, the bodies of the complex are noted in the valley of the Aspara River, east of the Kokdonen and Kunkir pass and east of the Makbel protrusion, in the second - in the form of "islands" among granitoids of the Ushbulak pluton. The complex is complex in composition. Its structure includes rocks of basic, medium and acidic composition: gabbro, diorites, quartz diorites, plagiogranites, dikes of basic and acidic composition. The complex is multiphase. In its composition the following are distinguished: the first intrusive phase - gray and dark gray coarse, medium-grained diorites and quartz diorites (δ_1O_2al); the second intrusive phase is gray coarse, medium-grained plagiogranites (γ_2O_2al).

Aktas intrusive complex (O_3-S_1at). The rocks of the complex participate in the structure of the two largest polychronic plutons of the described territory - Buzylgankol and Kankol, forming pluton plots in sizes from the first to 30-35 km^2. The rocks of the complex in the area of the Aktas pass, the Aulie mountains and the Aspara valley share active contact with the terrigenous rocks of the Early Middle Ordovician in the structure of the Buzylgankol pluton. Well-rounded pebble rock complex is noted in conglomerates of the Middle and Late Devonian. On numerous sections of the rock the complex is in contact with the younger granitoids of the Merke complex. The complex is multiphase, formed as a result of the introduction of a magmatic melt of different composition. It distinguishes: the first intrusive phase: gabbro, gabbro-diorites, diorites, quartz diorites - ν_1O_3-Sat, $\nu\delta_1O_3$-Sat, δ_1O_3-Sat; the second intrusive phase: granodiorites, granites - $\gamma\delta_2O_3$-Sat, γ_2O_3-Sat; dikes of the first and second stages.

The leading family of rocks participating in the structure of the second phase is the family of granodiorites. A secondary role in the structure of the main intrusive facies belongs to granites. In the diagram of D. Peacock, the character of the variational curves and the value of D. Peacock's index of 55.6 indicate that the formation belongs to the alkaline-calcareous series, and the petrochemical features of the composition of the constituent rocks indicate its transitional (to calcalkaline type) character. Among the rocks of the alkaline-calcareous group, the representatives of the middle group predominate (with the value σ = 1.8-3.0). The rocks of the weak group of the alkali-limy series and the transition group of the alkaline series are less common.

The Middle Devonian Intrusive Complex (D_2) has been identified in the process of carrying out work under the GDM-200 program. The northern part of the polychronous Ushbulak massif, located in the western part of the surveyed territory, is composed of the rocks of the complex. In addition, the individual bodies of the complex participate in the structure of other polychronous plutons (in the Aspara river basin) and form a series of intrusive bodies in the Karakystak river valley. The composition of the complex is complex: granodiorites, quartz diorites, diorites, syenites, quartz syenites, monzonites, monzodiorites and their subalkaline differences participate in its structure. The composition of the dike series is extremely diverse - from ultra-acid granites to dolerites and their subalkaline differences.

Late Devonian Merce's intrusive complex (D_3). The rocks of the complex play an important role in the geological structure of the described region, participating in the structure of two large polychronous granitoid massifs - Buzylgankol and Kankol.

With the introduction of the Aktas complex, the formation of the Caledonian orogeny, which along with the Makbel hard block in the Silurian, was a denudation area.

Conclusions

Different-age and different composition of intrusive complexes of the tectonic-magmatic zone considered are comagmatic formations. The basis for judging the comagmatic nature of intrusive formations of different composition is their location in a single space confined to the deep fault zone, and the time displacement from the Cambrian to the Devonian inclusive is homodromous from ultrabasites to acid rocks. The differentiation of intrusive rocks by composition and time is related to their physical properties and chemical composition. The source of the formation of intrusive complexes is the mantle plume introduced into the lithosphere at the beginning of the Caledonian tectonic magmatic activation of the continent Kazahia. The formation of a peculiar geotectonic of modern Kazakhstan and adjacent territories is associated with the active superplume that operated during the Paleozoic.

This work was supported by the scientific program 2018 BR05233713 «Comprehensive geological study of subsurface resources for the development of resource base and mining exploitation of new sources of ore raw materials in Kazakhstan».

References

David A. Yuen, Shigerenori Maruyama, Shun-Ichiro Karato, Brian F. Windley. Superplumes: Beyond Plate Tectonics. 2007. XIV. 569 p.

Joachim R.R., Ritter, Ulrich R. Christensen. Mantle Plums. 2007. VIII. 502 p.

Pirajno. F. Ore Deposits and Mantle Plumes. 2000. 576 p.

Avdeev A.V. Geodinamicheskaya karta Yuzhnogo Kazakhstana. Masshtab 1:500000. Almaty. 2001.

Baibatsha A.B. Plyum-tektonicheskaya priroda geologicheskikh struktur i geodinamiki territorii Kazakhstana // GeoBaykal, 2016. – Irkutsk, Russia.

Baibatsha A.B. The role of the Paleozoic superplume in the formation of the geological structures of Kazakhstan with large metal deposits// Magmatism of the Earth and related strategic metal deposits. Proceedings of XXXIV International Conference. Miass, 4-9 August 2017. GEOKHI RAS, 2017. p. 28-30.

Baibatsha A.B. Innovatsionnyye technologii prognoza poleznykh iskopayemykh. Almaty. 2018. 548 s.

Glubinnoye stroyeniye i mineral'nyye resursy Kazakhstana. T.1. Glubinnoye stroyeniye i geodinamika. Almaty. 2002. 224 s.

Dobretsov N.L., Kirdyashkin A.G. i dr. Global'naya geodinamika. Novosibirsk. SORAN. 2001. 409 s.

Mikolaichuk A.V., Sobel E. Strukturnaya evolyutsiya severnoy okrainy Tyan'-Shanskogo orogena // Izv. NAN KR. Bishkek, 2003.

NEW INSIGHTS INTO THE NEWLY DISCOVERED KIMBERLITE AND RELATED ROCKS IN THE CENTRAL EASTERN DESERT OF EGYPT

Barakat A.A.

The Egyptian Mineral Resource Authority (EMRA), 3 Salah Salem Road, Abbassyia, Cairo Egypt, alybarakat20000@gmail.com

The central portion of the Eastern Desert is geologically characterized by the presence of Hammamat basin which comprises 7500-m thick succession consisting of varies facies of basement and sedimentary rocks, Fowler and Osman (2013). This portion of the Eastern Desert comprises carbonates emplacements in several modes of occurrences. The source of carbonates in the Eastern Desert and Sinai is a matter of heated debate between researchers, (Stern and Gwinn, 1990 and references therein). The studied site occurs ~2-km south WadiZediun in the central part of the Eastern Desert of Egypt (Fig. 1), between latitudes 25 36 51- 25 37 56 N and longitudes 33 53 30- 33 54 00 E. Despite the several regional and detailed scale studies, which have been carried on the area of Wadi

Zeidun, there are no available studies dealing specifically within this site, except few lines within Francis et al. (1971), brief note on the occurrence of jasper deposit (Soliman and Barakat 2004) and the suggestion that the area may represent eroded astrobleme (Barakat, 2011). According to Francis et al., (op.cit.), the area surrounding the considered site is made up of metasediments, metavolcanics and serpentinites. The site attracted the scientific attention after recent quarrying processes exposed tough and compact siliceous carbonated rocks of reddish-buff color in the form of plugs intruding the country rocks. Recent studies (Barakat, et al., 2017) identified lamproite dyke, seven well-exposed pipes, as a result of quarrying activities, with a main kimberlitic dyke in the western side of the bottom of the crater. The pipes will label; beginning from south to north; 1-Hume (William Fraser Hume), 2-Afia (Mohamed SamehAfia), 3-El-Raghy (Sami El-Raghy), 4-Issawi (Bahy Issawi), 5-El Ramly (Mahmoud Fawzy El Ramly), 6-El-Gaby (El Sayed Samir Omar El Gaby) and 7-Soliman (Hassan A. Soliman) for their contribution to the geology and the economic geology of Egypt.

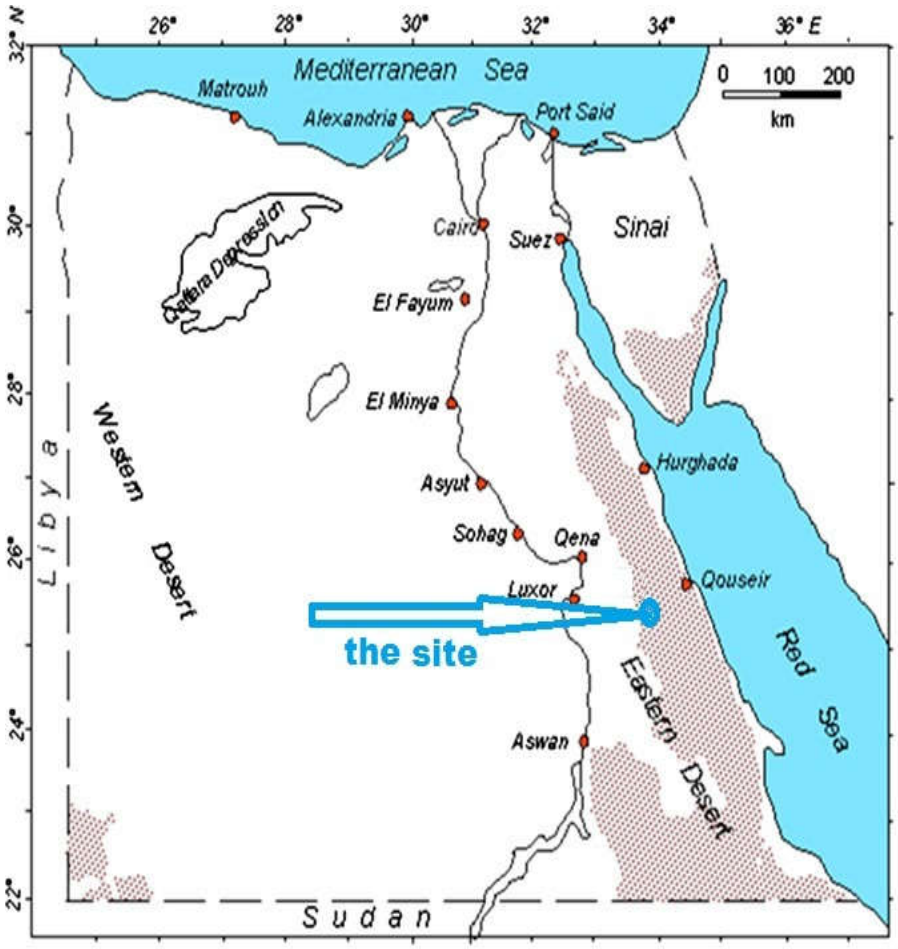

Fig. 1. location map of the site on the western flank of the Arabo-Nubian Shield.

Geological setting.

The considered site is of elliptical shape in the form of large tadpole with its enlarged part (head) in the southwestern side of the site, while its narrower part (tail) in the northwestern side of the site. The kimberlitic bodies occur in three forms; (i) lateral extension pipes alternate with (ii) vertical pipes and (iii) dyke(s). The best exposure of these objects occurs in southwestern side of the site. The vertical and lateral pipes form elliptical crater of nearly 30-m depth in the southwestern side of the site. The individual lateral extension pipes acquire the form of small tadpoles. Inside the site along its western side the kimberlitic rocks occur in the form of main dyke. Three main major faults strike the area around the site, the southern one (Fig. 2), crops out the suggested southern extension of the kimberlitic dyke along the Hammamt rocks.

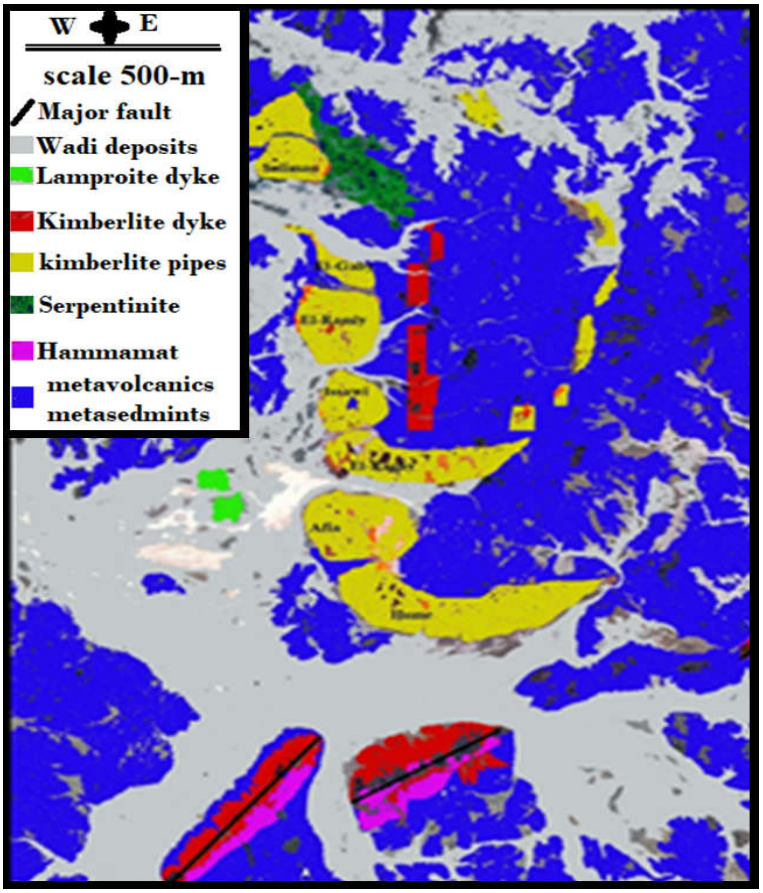

Fig. 2. Sketch geological map of the site.

The kimberlitic rocks and the associated alkaline mafic rocks are silicified, carbonated and serpentinized. This reflects different degree of alteration as well as different compositions of the same masses from parts to others along their surface exposures. The upper external parts of the pipes occur on the upper horizon of the country rocks of nearly 30-m high above the surrounding plain as viewed from the southwestern side of the site (Fig. 3) and they are characterized by buff-red color. The contact between the kimberlitic and the holding rocks is clear.

Fig. 3. The southwestern exposures of the pipes.

Fig. 4. Close up image of the greenish xenoliths.

Xenoliths of greenish rocks (including lamprphyres) are common feature in the kimberlitic rocks (Fig. 4). These xenoliths occur as small masses or as relatively large lenses and slabs some meters in length and several centimeters breadth. The contact between these xenoliths and the holding kimberlitic rock ranges from faint to sharp. In the heart of Afia pipe, red coloration spreading in the

greenish rock slabs, which gradually change to red color to be hardly distinguished from the holding rocks. Below the southeastern slopes of Afia pipe, there is ambiguous dark-brown rock acquire the appearance of iron ore. Close examination reveals that the rock consists of kaolintized minerals with appreciable amount of oxidized ilmenite and other unidentified mineral phases.

Minor phases.

The petrographic investigations aid with SEM study show that the rock contains, tiny grains of low oxygen fugacity phases (tistarite). In addition, some of the studied rocks contain irregular black color patches of carbon. Very tiny translucent to transparent grains of similar properties to microdiamond admixed with amorphous phases as well as tiny grains of graphite occur within these rocks. The present study reveals that microdiamonds may occur within some of the studied rocks in a relatively good concentration. Grain of microdiamond may occur within grains of Cr-rich spinel, (Fig. 5). The reasons are favors to identify this grain in particular as diamond; (i) the sharp edges of the grain, and (ii) its clear resistance decomposition compared with the surrounding spinel. The question is: what is the mineral except diamond can survive with perfect outlines, while the surrounding minerals were exceedingly decomposed?

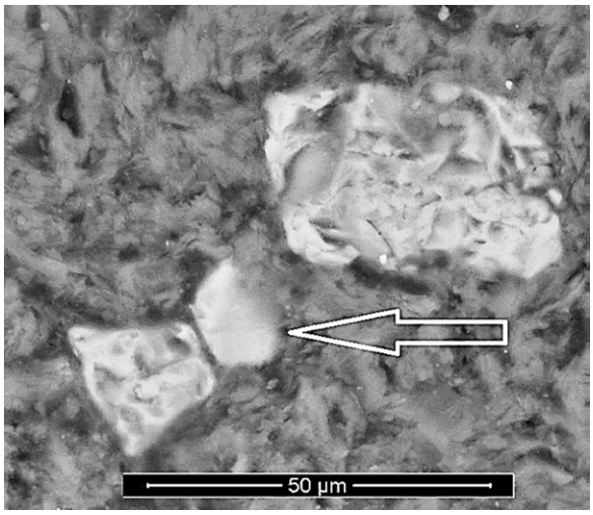

Fig. 5. SEM image of a possible grain of microdiamond.

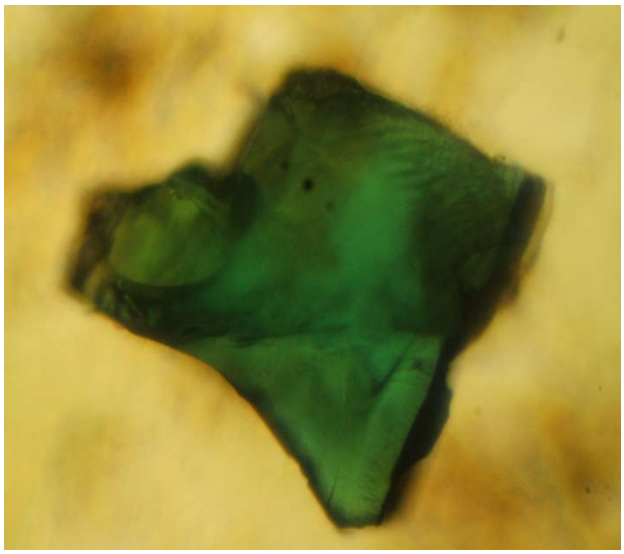

Fig. 6. Image of irregular bluish-green grain of moissanite (PPL) (the grain width ~ 0.14 mm).

In addition to this grain, several black grains have been traced by SEM imaging. EDX analysis proved that they are composed mainly of carbon in a carbonaceous silica patches. To avoid any doubt of contamination with grinding materials, fresh small chunk of the rock was extracted and studied by SEM, which showed regular grains composed essentially of carbon. The result may indicate occurrence of diamond. The same result has been traced in other rocks. In addition, the lamproite dyke contains a clear grain of irregular shape and bluish-green color (Fig. 6), which is very close in general characters to moissanite. This grain is the largest grain in the studied thin section (~0.14 mm diameter) associates other smaller grains of similar characters and others of orange-greenish color. The possibility that these grains is of grinding material is nearly excluded, as the grains are clearly embedded within the surrounding minerals as indicated by microscopic investigations and their occurrences as individual and aggregates of various sizes. Native and alloy metallic specks have been encountered in the studied rocks. These specks are mainly occurring within the carbon phases. Very few tiny grains of native Ni, Fe, Cu, Zn and Au have been detected in some of the studied samples.

Whole rock composition.

There is clear variation in both major (table 1), trace and REEs (table 2) in the studied rocks. Variation in kimberlite compositions is normally, since kimberlites are a hybrid rocks in general, e.g. Michel (1995). The results in general indicate that the studied rocks are of alkaline ultramafic affinity. i.e., kimberlites and lamproites and related rocks. Some of the studied rocks are enriched in Al_2O_3 and

depleted in MgO and K_2O than that of kimberlites, while the lamproiteare relatively enriched in Al_2O_3 and depleted in K_2O. The differences between the concentrations of these elements in the studied rocks and kimberlites seems normal in the light of the advanced weathering state of the studied rocks as indicating by different studies.

Table 1. Major oxides of some of the studied rocks.

	212	**213**	**213-A**	**214**	**215-R**	**215-RA**
SiO_2	54.75	57.07	56.66	41.32	45.34	43.718
TiO_2	1.4	0.86	1.02	0.34	0.32	0.341
Al_2O_3	14.8	13.8	13.57	5.92	8.2	8.009
Fe_2O_3	4.37	2.57	6.9	7.43	6.82	8.231
FeO	4.59	4.1	n.d.	1.26	2.7	n.d
MnO	0.11	0.13	0.16	0.16	0.16	0.168
MgO	6.02	10.8	12.39	8.66	12.3	20.131
CaO	3.81	1.16	1.26	17.3	10.3	11.61
Na_2O	4.46	0.4	<0.01	0.06	0.05	0.01
K_2O	0.333	1.26	1.5	0.048	0.053	0.32
P_2O_5	0.379	0.199	0.14	0.138	0.078	0.163
SO3	0.147	0.058	0.06	0.032	0.035	0.04
Cl	0.016	0.036	0.04	0.003	0.004	n.d
L.O.I.	4.84	6	6.04	16.66	12.86	7.032
Total	100.025	98.443	99.74	99.331	99.22	99.773

Table 2. REEs of some of the studied rocks.

	212	**213**	**214**	**215-R**	**G-889***
La	16.7	14.3	9.46	7.95	11.23
Ce	38.1	38.9	19.6	16.1	24.15
Pr	5.44	5.07	2.69	2.22	3.04
Nd	22.9	19.6	11.4	9.21	12.59
Sm	5.17	5.06	2.62	2.17	2.39
Eu	1.35	1.15	0.7	0.46	0.61
Gd	4.11	4.4	2.63	2.18	1.87
Tb	0.54	0.78	0.42	0.38	0.25
Dy	3.15	5.26	2.58	2.38	1.22
Ho	0.59	1.03	0.53	0.49	0.2
Er	1.48	2.87	1.4	1.44	0.5
Tm	0.24	0.49	0.21	0.23	0.06
Yb	1.23	3.28	1.3	1.34	0.44
Lu	0.16	0.41	0.19	0.19	0.06

* Data from Lapinet al., (2007).

Contamination by crustal rocks usually results in the addition of SiO_2, Al_2O_3 and Na_2O to kimberlites. In addition, this kimberlite contains appreciable percent of eclogite xenoliths, judging from the common occurrence of garnet and spinel. It seems likely that partial mantle metasomatic of these xenoliths, Windom and Boettcher (1980) originated the observed greenish-grey xenoliths in the kimberlitic, which match the composition and general characters of lamprophyric rocks. This may also elucidate the high aluminum contents within these kimberlitic rocks. The major oxides analysis (as it is) may match the composition of Akwatia kimberlitic (diamond field, Ghanna) rocks which some research consider them of being a hybrid rock with geochemical affinities to ultramafic lamprophyres such as minettes and alnoites (Asiedu, et al., 2007).

In the meantime, the studied kimberlitic samples are similar in REEs contents to some samples from the Russian Kimberlites (e.g. Nyurbinskaya, sample No. G-889, (Lapin, et al., 2007). The low concentration of REEs in particular the LREEs, in these rocks can being explained in many ways; (i) sampling e.g. some samples close to lamprophyric xenoliths, (ii) technical errors resulted from the used techniques and weathering. In addition, REEs, particularly LREEs, can be mobilized during alteration processes.

Conclusion

The study elucidates that the site acquires definite criteria candidate it of being one of the ideal sites of kimberlite and related rocks emplacement; such as, (i) it occurs on the western flanks of the Arabo-Nubian Shield, within or close to the suggested Paleoproterozoic–Archean age cratonic segments (Shlevin, et al., 2009), (ii) its occurrence in the heart of the assigned East Mediterranean–Nubian diamondiferous belt along the Levantine-Nubian volcanic fault system (Eppelbaum and Katz, 2012), (iii) associating low melting rocks, e.g. the nepheline mico-syanite of Jebel Hadarba, which formed along cratonic margins (Begg, et al., 2009), (iv) association of alkaline and mafic alkaline rocks, (v) the shape of each individual pipe as well as the shape of the whole pipes acquire the shape of tadpole like that of Argyle pipe, Australia, (vi) the crater form of the southwestern side of the site, (vii) detection of mineral suite characteristic of kimberlitic rocks, e.g.; picroilmenite, chromium spinel, carbon, tiny particles of native iron, Cu-Zn alloy and low oxygen fugacity phases (tistarite).

The author thanks Mr. Sami El-Raghy for his encouragements during all stages of the study. He also funded the charges of full chemical analysis of 32 rock samples in Australia. Thanks are also due to Mr. Youssef El-Raghy and Mr. Esmat El-Raghy for providing logistic support during the five field trips to the site.

References

Asiedu, D.K., Dampare, S.B., Sakyi, P.A. and Boamah, D. (2007) Major- and trace-element geochemistry of Kimberlitic rocks in the akwatia area of the Birim Diamondiferous field, southwest Ghana. *AJST, 8, No. 2,* 81-91.

Barakat, A.A. (2011) Ras Zeidun Eastern Desert of Egypt: A possible astrobleme. 2nd Arab Impact Cratering and Astrogeology Conference (AICAC II) Hassan II Casablanca University; Casablanca, Morocco: 2011 (Abstract).

Barakat, A.A., Soliman, Kh. A., Basal, A.K., Kandel, S.MR., and Abdesalam, K. (2017) A preliminary report on the occurrence of kimberlitic and related rocks in the central Eastern Desert of Egypt-abstract. The Ninth International Conference on the Geology of Africa, 7-9 November 2017 Assiut-Egypt, 47-48.

Begg, G.C., Griffin, W.L., Natapov, L.M., O'Reilly, S. Y., Grand, S., O'Neill, C. J., Hronsky, J.M.A, PoudjomDjomani, Y., Deen, T. and Bowden, P. (2009) The lithospheric architecture of Africa: Seismic tomography, mantle petrology and tectonic evolution. Geosphere 5, 23-50.

Eppelbaum, L.V. and Katz, Y.I. (2012) Mineral deposits in Israel: A contemporary view, *In*: (Eds. Ya"ari, A. and Zahavi, E.D.) Israel: Social, Economic and Political Developments, Nova Science Publishers, N.Y., USA, 1-41.

Fowler, T.J. and Osman, A.F. (2013) Sedimentation and inversion history of three molasse basins of the western Central Eastern Desert of Egypt: Implications for the tectonic significance of Hammamat basins. Gondwana Research, 23 1511–1534.

Francis, M.H., Qusa, M.E., Abd El Naby, A. and Phillips, P.W. (1971)The Geology of WadiZeidun Area. Unpublished Report, Egyptian Geological Survey and Mining Authority, Cairo, 34pp.

Hofmann, (1988) Chemical differentiation of the Earth: The relationship between mantle, continental crust, and oceanic crust. Earth and Planet. Sci. Lett., 90(3):297-314.

Lapin, A. V Tolstov, A. V. and Vasilenko, V. B. (2007) Petrogeochemical Characteristics of the Kimberlites from the Middle Markha Region with Application to the Problem of the Geochemical Heterogeneity of Kimberlites. Geochemistry International, 45 (12), 1197–1209.

Mitchell, R.H. (1995) Kimberlites, Orangeites and related rocks. Plenum Press, New York and London, 410 pp.

Shlevin, Y.B., Katzir, Y., Whitehouse, M.J. and Kleinhanns, I.C. (2009) Contribution of pre Pan-African crust to formation of the Arabian Nubian Shield: New secondary ionization mass spectrometry U-Pb and O studies of zircon. Geology, 2009, 37 (10), 899–902.

Soliman, Kh. A., and Barakat, A.A. (2004) A note on: New jasper deposit in the Eastern Desert. Ann. Geological Survey Egypt, 27, 599-604.

Stern, R.J. and Gwinn, C.J. (1990) Origin of late Precambrian intrusive carbonates, Eastern Desert of Egypt and Sudan: C, O and Sr isotopic evidence. Precambrian Res., 46: 259-272.

Windom, K.E and Boettcher, A.L. (1980) Mantle Metasomatism and the Kimberlite-Lamprophyre Association: Evidence from an Eclogite Nodule from Roberts Victor Mine, South Africa. Journal of Geology, 88 (6), 705-712.

SIGNIFICANCE OF BADDELEYITE FOR PLUME PROCESSES FROM PZ TO AR TIME IN THE N-E PART OF THE BALTIC SHIELD ARCTIC REGION

***Bayanova T.B.*[1], *Subbotin V.V.*[1], *Drogobuzhskaya S.V.*[2] , *Kamensky I. L.*[1], *Elizarov D.V.*[1]**

[1]*GI KSC RAS, Apatity, Russia tamara@geoksc.apatity.ru*

[2]*ICHREM KSC RAS Apatity, Russia Drogo_sv@chemy.kolasc.net.ru*

Baddeleyite of zirconium dioxide was discovered more than 100 year ago (Heaman, Cheminant, 1993) and widely using last 30 years in U-Pb geochronology together with zircon. Zircon can be originated as metamorphic, metacomatic and hydrothermal processes and are characterized by xenocryst nature to baddeleyite are almost have magmatic origin (Bayanova, 2006).

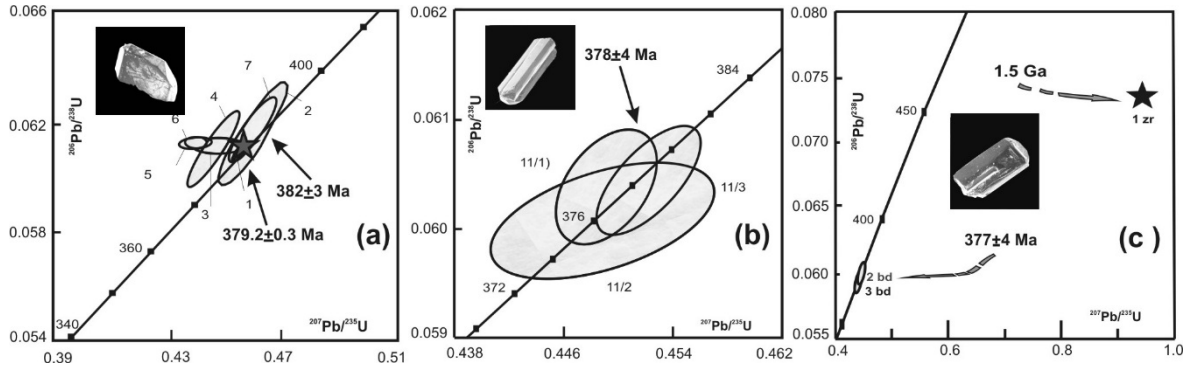

Fig. 1. Isotope U-Pb data on baddeleyite from foscorite ore Kovdor (a), baddeleyite from carbonatite Sebljavr (b) and zircon xenocryst (1) from pyroxenite and baddeleyite (2-3) from late carbonatiteVuorijarvi (c).

In Paleozoic time there are largest (Kovdor, Sebljavr, Vuoryarvi et set.) and super largest (Khibina and Lovozero) alkaline-subalkaline with carbonatites industrial deposits. Baddeleyite were separated and dated by U-Pb and LA-ICP-MS methods and at the first time distribution of REE and concentrations' of Ti and Zr have been studied due to knowing closure temperature of U-Pb systematic in the crystals (Fig. 1a, b, c). Multidisciplinary U-Pb, Sm-Nd and Rb-Sr ages data on the rocks, accessory and rocks-forming minerals from kimberlitic pipes, carbonatites and dike series reflect formation the biggest mantle reservoirs for primary magma of alkaline-ultraalkaline magmatism in the interval from 465-325 Ma (more than 140 Ma). Isotope (ε_{Nd} +4; I_{Sr} – 0.703-0.704; T_{Dm} – 980-700 Ma; enriched by LILE REE; $^3He/^4He$ up to $3.5x10^{-5}$) data on references rocks and Mgt and Ilm minerals these formation are suggested by primary mantle reservoirs DM и HIMU. Based on big bank isotope-geochemistry data on U-Pb and LA-ICP-MS baddeleyite dating from carbonatites and dykes complexes comes to conclusions about primary magmatic plume activity of Paleozoic magmatism which are connected with the breakup of Pangea supercontinent. New data on the distribution and concentration of REE , Ti and Zr in baddeleyite grains from Kovdor and Vyoriarvi massifs measured by LA-ICP-MS (ELAN 9000) methods are given much higher closure U-Pb temperatures than zircon equals –888^0 C and 984^0 C correspondingly.

In Paleoproterozoic time in frame in the Central Kola megablock are distinguished Kola Pt-metal province, which are the second and very important after Pt-metal Norilsk in Russia and includes Co-Cu-Ni (Monchegorsk ore region), Cr-Ti-Fe-V (Imandra lopolith), low sulfides Pt-Pd ores (with Au+Aq) of the Fedorovo-Pansky ore complex (Mitrofanov et al., 2013). Systematically U-Pb ages on

baddeleyite from gabbronorites, anorhtosites and dykes cutting complexes from these ores keys reflect time of the formation these large magmatic provinces or (LIP) from 2.53 Ga to 2.40 Ga (more than 130 Ma) (Fig. 2). Isotope-geochemistry data based on Nd-Sr-He systematic for the rocks and Ilm and Mgt minerals are suggested about mantle contributions of N-MORB, E-MORB and OIB sources for dykes' complexes. Primary mantle protolith for the rocks are characterized by (ε_{Nd} – 1-3; I_{Sr} – 0.702-0.704; T_{Dm}– 3.5-2.8 Ga; enriched by LILE REE elements; $^3He/^4He$ up to $1.5x10^{-6}$) and have an origin magmatic mantle reservoirs EM-1 also of plume genesis by Re-Os (Yang et al., 2016) investigations. Formation of the Cu-Ni-Cr-Ti-V-Fe and PGE deposits of the Kola Pt-metal province are connected with large plume magmatism and probably breakup of the oldest Kenorland Supercontinent (Lubnina, 2009).

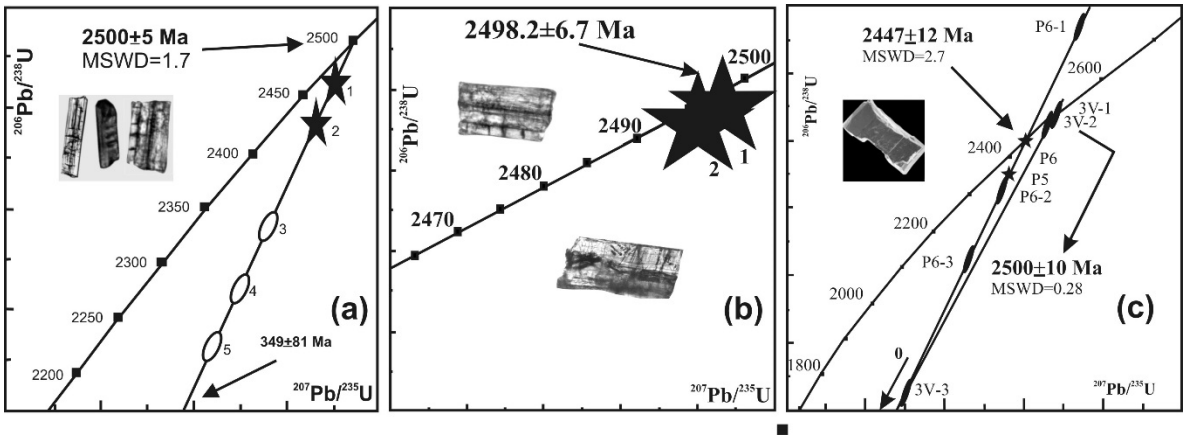

Fig. 2. a – Mt. Nyud, gabbronorite of "critical horizon" (Co-Cu-Ni ores);
b – Vurechuaivench Foothills, coarse-grained metagabbronorite (Pt-Pd reef) – Monchegorsk pluton;
c - U-Pb diagram for zircon from Mgt gabbro and baddeleyite from anorthosite of Fedorovo-Pansky massif.

The Paleoproterozoic Pechenga (Fig. 3) Cu-Ni deposits (1982±8) and carbonatites (Corfu et al., 2011) of Tiksheozero (Karelia region) apatite ores have a very coeval (1990±2) ages based on U-Pb data on single zircon-baddeleyite grains. A very coeval U-Pb ages have been measured using single crystals of zircon and baddeleyite (2055-2057 Ma) from the super large Pt-Ni and Cr Bushveld deposits (Mungall et al., 2016) of the South Africa. Isotope-geochemical data (ε_{Nd} + 2+4; I_{Sr} – 0.702-0.704; T_{Dm} – 2.5-2.3 Ga; enriched by LILE REE elements; $^3He/^4He$ up to $2x10^{-6}$) on references rocks reflect mantle plume sources for origin primary reservoirs and connected with the breakup of the Columbia supercontinent (Lubnina, 2009).

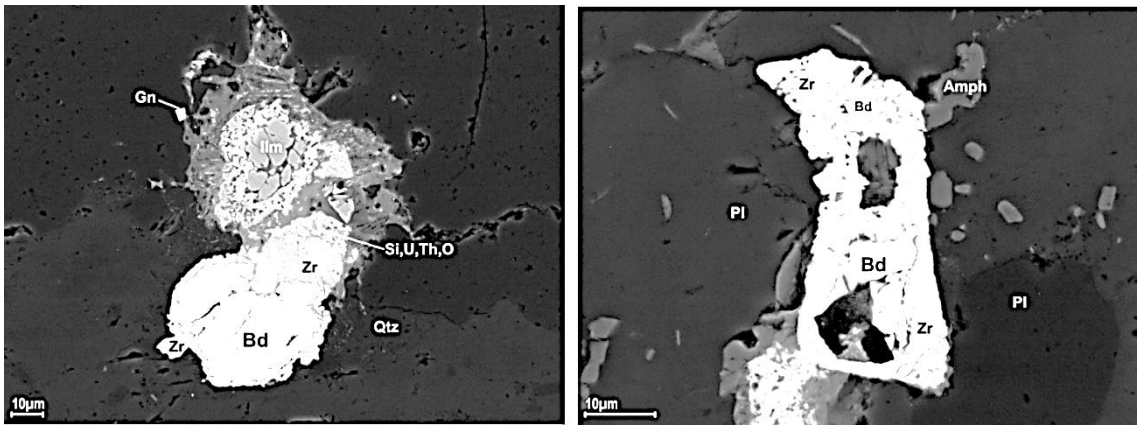

Fig. 3. Baddeleyite from Pt-Pd deposits of the Fedorovo-Pansky (2.5 Ga) layered intrusions.

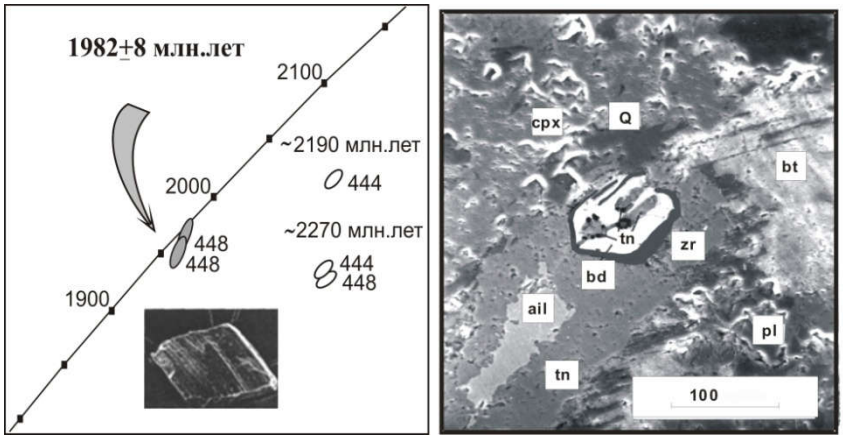

Fig. 4. Zircon and baddeleyite from gabbro Zhdanov Cu-Ni deposit of Pechenga; The microphotography of intergrowing baddeleyite (bd) and apoilmenite (ail) by reflected light. Ilmenite is replaced by titanite (tn). Zircon (zr) substitutes baddeleyit; (B) Chemical composition (wt %) of (1, 2) baddeleyite and (3, 4) zircon from anorthosites of the Imandra lopolith.

In frame in the N-E part of the Fennoscandinavian Shield baddeleyite at the first time was found in Central Kola megablokc in dykes' complexes, which are cutted largest Kirovogorsk deposits of the BIF Olenegorsk formation. New U-Pb age on zircon-baddeleyite minerals from the gabbronorites dykes yielded 2738±6 Ma (Fig. 5a). Isotope U-Pb ages on baddeleyite were measured for anorthosites of Tsaga massif with Ti-Cr-Mgt deposits in the Keivy terrane, during the studing monzogabbroes, anothtosites and gaddronorites from the intrusion with 2653±3 Ma, 2660±10 Ma and 2668±10 Ma respectively (Fig. 5b).

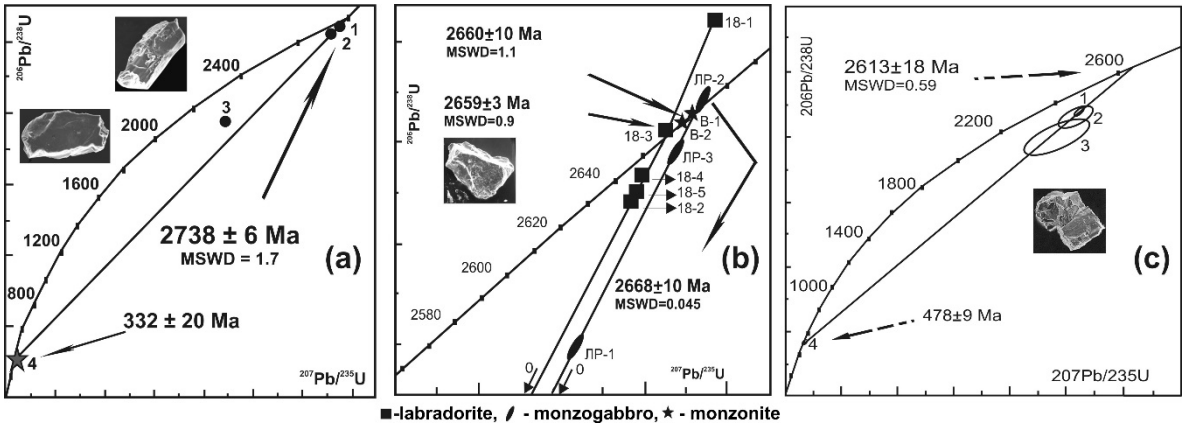

Fig. 5. a - U-Pb diagram for zircon (1-3) and baddeleyite (4) from basite dyke, Kirovogorsk (BIF);
b - U-Pb diagram for zircon and baddeleyite from different rocks, Tsaga; c - U-Pb diagram for baddeleyite (1) and zircon (2-4), Siilinjarvi (collection of A.Silvennoinen).

The very coeval U-Pb age on zircon-baddeleyite geochronometer was measured for Siilinijrvi carbonatites in Finland with (REE, Ap, Zr) deposit equals 2613±13 Ma (Fig. 5c). Systematically isotope-geochemistry investigations by different methods gave (ε_{Nd} – 0.4+2; I_{Sr} – 0.707-0.709; T_{Dm} – 3.2-3.0 Ga; enriched by LILE REE elements; $^3He/^4He$ up to $0.6x10^{-6}$) data for the rocks of the neoarchaean anorogenic intraplate magmatism with 2.74 Ga for sanukitoids according to (Mitrofanov et al., 2013). All data are considered about more than 100 Ma interval for the origin of multimetal deposits from 2.74 Ga to 2.61 Ga. Geochemical Nd-Sr-He data for the rocks and Mgt and Ilm minerals permit comes to conclusion about the primary magmatic enriched mantle plume reservoir EM-2, which connected with the origin and break up more older than Kenorland Supercontinent in the history of the Earth (Lubnina, 2009).

Baddeleyite were founded in the frame in Arctic region N-E part of the Fennoscandian Shield and studied by U-Pb и LA-ICP-MS methods during the time interval from 2.74 Ga up to 325 Ma, so baddeleyite origin more than 2.4 Ga.

Baddeleyite were investigated in the important active industrial deposits and references rocks of neoarchaean BIF formation, Paleoproterozoic, Cu-Ni and Pt-Pd layered intrusions and Paleozoic alkaline and ultraalkaline ore deposits and mostly are characterized by primary magmatic genesis. Baddeleyite is a very important mineral in U-Pb geochronology to study time origin and duration of magmatic activity and have significant value in progress of super continental reconstructions (Fig. 3, 6).

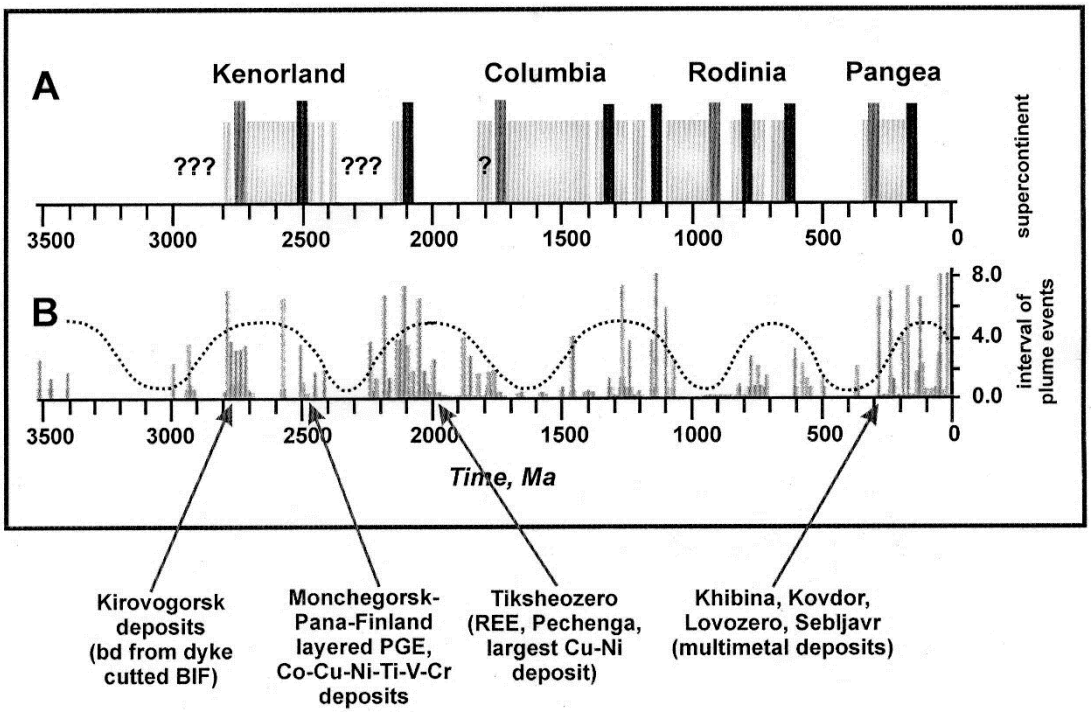

Fig. 6. Correlation of supercontinental cycles (A) with period 750-900 Ma for mantle-plume (B) activity.

All investigations are supported by RFBR 16-05-00305, and Program by Presidium RAS No. 48 and are devoted by memory of academician RAS Mitrofanov F.P. who was initiated baddeleyite studied in the Kola Pt bearing province of Arctic region.

References

Bayanova T.B. Baddeleyite: A Promising Geochronometer for Alkaline and Basic Magmatism // Petrology, 2006. Vol. 14. No. 2. P. 187-200.

Corfu F., Bayanova T. et. al. U-Pb ID-TIMS age of the Tiksheozero carbonatite: expression of 2.0 Ga alkaline magmatism in Karelia, Russia // Central European Journal of Geosciences, 2011. P. 302-308.

Heaman L.M., Le Cheminant A.N. Paragenesis and U-Pb systematic of baddeleyite (ZrO) // Chemical Geology, 1993. Vol. 110. P. 95–126.

Lubnina N.V. East-European craton from neoarhaean to paleozoic time based on paleomagnetic data // Manuscript of doctoral dissertation. Moscow: MSU, 2009. 40 p.

Mitrofanov F.P, Bayanova T.B, Korchagin A.Y. et al. East Scandinavian and Noril'sk Plume Mafic Large Igneous Provinces of Pd–Pt Ores: Geological and Metallogenic Comparison // Geology of Ore Deposits, 2013. Vol. 55. No. 5. P. 305–319.

Mungall J. et.al. U-Pb geochronology documents out-of-sequence emplacement of ultramafic layers in the Bushveld Igneous Complex of South Africa // Naturecommunications, 2016. /7:13385/DO 10.1038/ ncomms13383/ www.nature.com/ naturecommunications

Yang Sheng-Hong et. al. Mantle source of the 2.44-2.50 Ga mantle plume-related magmatism in the Fennoscandian Shield: evidence from Os, Nd and Sr isotope compositions of the Monchepluton and Kemi intrusions // Mineralium Deposita, 2016. Vol. 51. P. 1055-1073.

ON THE AGE AND GENETIC CHARACTERISTICS OF NIOBIUM-RARE METAL MINERALIZATION OF THE VUORIYARVI MASSIF (KOLA PENINSULA, RUSSIA)

***Belyatsky B.V.*[1], *Lepekhina E.V.*[1], *Antonov A.V.*[1], *Sorokhtina N.V.*[2], *Petrov O.D.*[1], *Sergeev S.A.*[1]**

[1]*A.P.Karpinsky All-Russian Geological Institute (VSEGEI), CIR, St.Petersburg, Sredniy ave., 74, Russia, bbelyatsky@mail.ru*

[2]*Vernadsky Institute of Geochemistry, RAS, Moscow, Russia*

The Vuoriyarvi massif (3.5×5.5 km, about 20 km^2) is located 20 km southwest of the Alakurti village on the north-eastern shore of Lake Vuoriyarvi (Murmansk region, Kola Peninsula). The Vuoriyarvi massif has a typical concentrically zoned structure. The earliest rocks are ultramafics composed mainly of pyroxenites, olivinites and peridotite dikes cross-cutting the host Archean granite-gneisses in the form of stock-like body (core zone about 12 km^2). Along the contact of ultramafics with host gneisses there is a ring-body of ijolites, active influence of which upon the granite-gneisses aroused formation of the eugerine-K-feldspar fenites (Brassinnes et al., 2005; Arzamastsev, Arzamastseva, 2013). Ultramafics under the influence of alkaline melts over a considerable area have been transformed into olivine-pyroxene, pyroxene, phlogopite-pyroxene and nepheline-pyroxene rocks. Rare-metal mineralization is common within two sites of the massif: essentially carbonatite (Neskevara), in which the stockwork of veins in pyroxenites with a small amount of apatite-magnetite carbonatite in endocontacts is localized. Within the tubular body of apatite-magnetite carbonatites in the same pyroxenites with a subordinate amount of carbonatites (Tukhtavara) rare-metal mineralization is also represented. Pyrochlore group minerals (Nb>Ta>Ti) are the main ore components composed Nb-rare-metal mineralization (Subbotin, Subbotina, 2000).

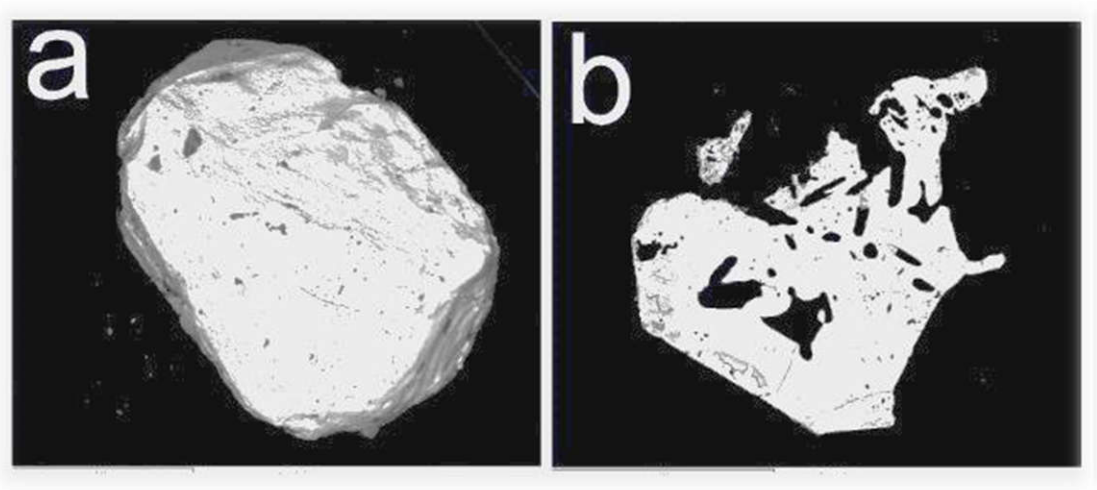

Fig. 1. Typical crystal morphology of pyrochlore variety from the Neskevara calcite carbonatite, Vuoriyarvi massif (a) and detail of grain with prominent oscillatory zoning and poikilitic structure (b).

Identification of genetic connection of Nb-mineralization with alkaline and/or carbonatite magmas and determination of their age limitation were the aim of the present study. Pyrochlore from calcite carbonatites, calcite-magnetite foscorites, and rare-earth dolomite carbonatites have been studied for chemical specification (EDS, CamScan2500) and local U-Th-Pb isotope composition by SHRIMP-II. Studied pyrochlore-group minerals are represented by subeuhedral octaedral grains up to 1 mm (Fig. 1), frequently with a prominent oscillatory zoning, located in the calcite matrix in association with apatite (Fig. 1b). At the expence of abundant microinclusions of calcite and apatite the

poikilitic structure is quite often marked. The variability in the composition of pyrochlore is mainly due to variations in the Ti, Th, and Ce content. These minerals are mainly classified as fluorcalciopyrochlore (Atencio et al., 2010) with characteristic high niobium contents – up to 70 wt.% Nb_2O_5 (Fig. 2a). According to Nb content pyrochlores of the Vuoriyarvi massif are the most enriched among those from the alkaline-ultrabasic massifs of the Caledonian complex of the Kola Peninsula (Subbotin, Subbotina, 2000). The analyzed crystals are predominantly characterized by the complete occupation of cation site "A" for the vast majority of the obtained compositions (Fig. 2c), taking into account the formula unit calculation based on the occupation of "B" site (Nb + Ta + Ti = 2 f.u.). The analytical points with a noticeable deficiency in site "A" are derived from those parts of grain affected by hydrothemal and secondary alteration, which cause an increase in such elements as Ta, Ba, REE, U, but not the characteristic Sr. A typical chemical feature of studied pyrochlores is the constant presence of thorium (up to 3.5±1 wt.%) and cerium - 1.5±1 wt.% Ce_2O_3. The increase in U content (up to 11 wt.% UO_2) in the altered parts of the crystals is accompanied by growth in the tantalum concentration (up to 9 wt.% Ta_2O_5). Th-enriched varieties are supposed to be connected with the earliest stages of foscorites and carbonatites [Subbotin, Subbotina, 2000]. Barium varieties of pyrochlore are found only as subordinate domains within the fluorocalciopyrochlores, the contents reach of 17 wt.% BaO. Ba-enrichment is accompanied by a decrease in the calcium and sodium contents, without any correlation with niobium (Fig. 2d).

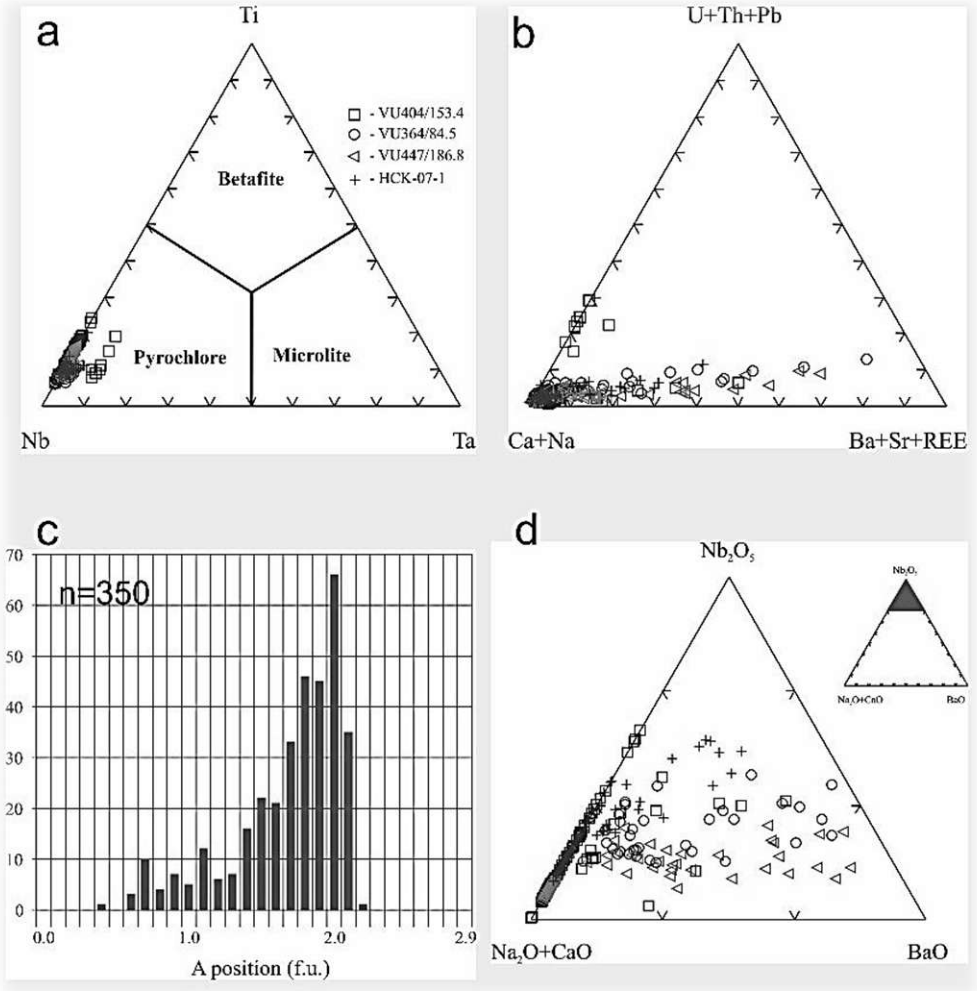

Fig. 2. Vuoriyarvi pyrochlore composition in main cation components (see text).

A total of 68 pyrochlore grains, differing in color, size, mineral inclusions, Th and U composition, from 4 samples have been studied and 103 U-Th-Pb SIMS SHRIMP-II analyzes have been performed with respect to the inhouse standard "pyrochlore-331" with an age of 231 ± 1.5 Ma

and U content of 1500 ppm according to the procedure described earlier (Lepekhina et al., 2016). The studied samples contain both dark-brown cloudy, opaque and reddish-brown transparent varieties of pyrochlore, as low-U ones - up to 2-10 ppm, as well as moderately and even high-U - up to 300-450 ppm, and in some cases up to 1000-1500 ppm. Moreover, all studied pyrochlore grains have permanently high-Th contents - up to 2-3×10^4 ppm, and significant variations in the Th/U ratio: from 5 to 14,600, while the radioogenic ^{206}Pb varies within 5-70 ppm, and the share of non-radiogenic lead is 10-80%.

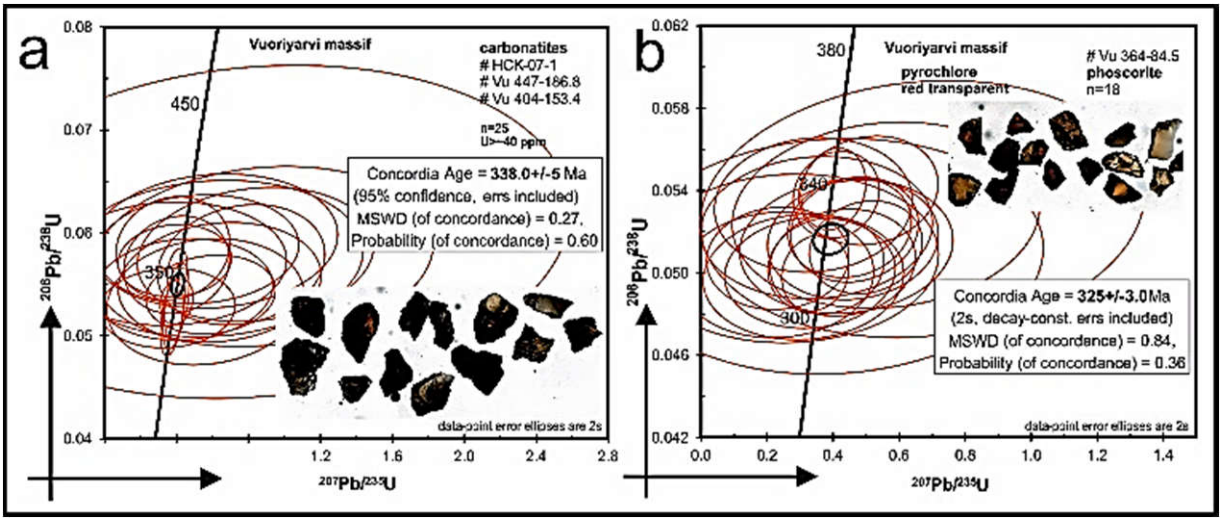

Fig. 3. U-Pb diagrams for Vuoriyarvi pyrochlore from carbonatites and phoscorites.

Variations of the calculated U/Pb ratios make it possible to estimate the age of pyrochlore for separate sample and for total set of 3 carbonatite samples of different composition: 332 ± 11 Ma, using the measured isotopic ratios uncorrected for the common lead composition (MSWD 6.9, 32 analyses). It should be noted that for this calculation analyses with uranium content above 40 ppm and 10 ppm of radiogenic ^{206}Pb were used. If we use the radiogenic lead to uranium ratios (Fig. 3a) with the correction of the nonradiogenic lead share from the measured isotope ^{204}Pb, the value of the concordant age: 338 ± 5 Ma coincides within the error with the previous estimate. At the same time, for the studied pyrochlore from the foscorite sample, the excess variability of U/Pb ratios is characteristic, which corresponds in the values of ^{206}Pb/^{238}U age to an interval of 310-420 Ma. The analysis of individual pyrochlore grains (opaque dark brown varieties) showed a distinctly older age: 410 ± 15 Ma, whereas the bulk of transparent red color grains have a concordant age of 325 ± 3 Ma (18 analyses, Fig.3b). Such a spread of data probably appears to be due to a distortion of the Th/U ratio in the mineral due to its high ability for cation-exchange processes, including secondary transformation, or/and to be the result of a multi-stage formation of rare-metal mineralization, which can accompany the intrusions of ijolites and carbonatite-phoscorites, and to form at the postmagmatic hydrothermal stage as well. The closeness of the obtained age estimates of pyrochlore from the carbonatite and foscorite samples: 332 and 325 Ma, respectively, and also the assumption of their common origin (Wu et al., 2013), makes it possible to calculate and construct a combined isochron for 67 analyses: in the coordinates of ^{207}Pb/^{206}Pb and ^{238}U/^{206}Pb measured ratios with satisfactory statistical parameters: 327 ± 9 Ma for MSWD equal to 14 (Fig. 4a). If we use a three-dimensional isochron calculation, the age estimate changes insignificantly: 326.7 ± 6.1 Ma, and the MSWD value decreases by a factor two down to 7.4 and the non-radiogenic component has ^{206}Pb/^{204}Pb and ^{207}Pb/^{204}Pb 18.84 and 15.68, respectively. The value of 319.4 ± 4.5 Ma obtained by the 3-D isochron calculation on 59 analyses (the most homogeneous analysis set, Fig. 4b) could be the best estimation of the Vuoriyarvi carbonatite-phoscorite pyrochlore age.

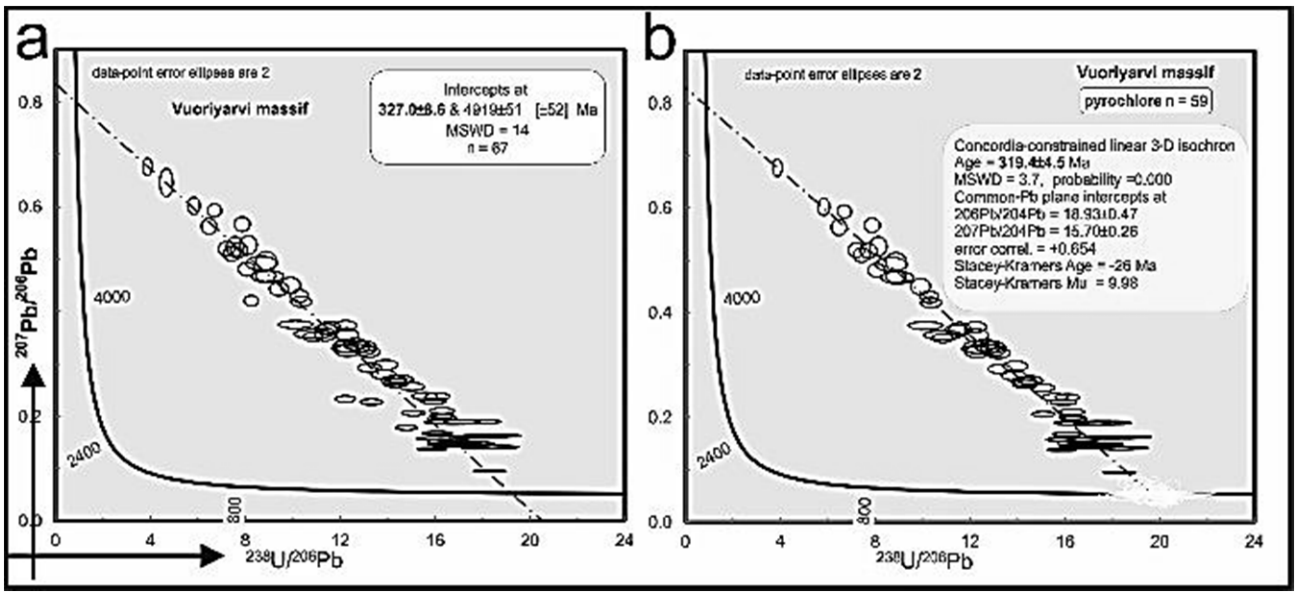

Fig. 4. Age estimation of Nb-rare metal mineralization of the Vuoriyarvi ultrabasic-alkaline massif.

Thus, Nb-rare-metal mineralization of Vuoriyarvi ultrabasic-alkaline massif formed 50 m.y. later crystallization of the main magmatic phases composing the massif - peridotite and ijolites, phoscorites and carbonatites, for which the specified age is in the range of 375-383 Ma according to the Rb-Sr, Sm-Nd and U-Pb isotopic data on rock-forming minerals and baddeleyite (Rukhlov et al., 2015). But the U-Pb analysis of perovskite from alkaline rocks indicates a little bit younger age of foidolite formation - 368-361 Ma (Arzamastsev, Wu, 2014). The process of pyrochlore mineralization formation was probably multistages: crystallization, dissolution and redeposition of ore-substances accompanying carbonatite-phoscorite stockwork formation and during subsequent hydrothermal-metasomatic reworking of these rocks. Nevertheless we can resume of this study: the time of the Vuoriyarvi Nb-rare metal mineralization on the massif, established by the pyrochlore U-Pb isotope system, corresponds to 320 Ma.

The study has been fulfilled as a part of CIR project: "Developments of new analytical methods and approaches for isotope dating of alkaline and basic-ultrabasic intrusive bodies applicated for geological mapping within 2014-2016" under financial support of the State Geological Survey.

References

Arzamastsev A.A., Arzamastseva L.V. Geochemical indicators of the evolution of the ultrabasic-alkaline series of Paleozoic massifs of the Fennoscandian Shield // Petrology. 2013. Vol. 21. Iss. 3 pp.249–279.

Arzamastsev A.A., Wu F.-Y. U-Pb geochronology and Sr-Nd isotopic systematics of minerals from the ultrabasic-alkaline massifs of the Kola Province// Petrology. 2014. Vol. 22. Iss. 5 pp.462–479.

Atencio D., Andrade M.B., Christi A.G. et al. The pyrochlore supergroup of minerals: nomenclature// The Canadian Mineralogist. 2010. Vol. 48 pp. 673–698.

Brassinnes S., Balaganskaya E., Demaiffe D. Magmatic evolution of the differentiated ultramafic, alkaline and carbonatite intrusion of Vuoriyarvi (Kola Peninsula, Russia). A LA-IC-MS study of apatite// Lithos. 2005. Vol. 85 pp.76–92.

Lepekhina E.N., Antonov A.V., Belyatsky B.V., et al. Some features of U-Pb SHRIMP dating of pyrochlore from alkaline-ultramafic polyphase Kovdor massif (North Karelia): isotope-geochemical characteristics of the evolution of pyrochlore-group mineral composition// Regional Geology and Metallogeny. 2016. Vol. 67 pp. 86–4 (in Russian).

Rukhlov A.S., Bell K., Amelin Yu.V. Carbonatites, isotopes and evolution of the subcontinental mantle: an overview// Symposium on strategic and critical materials Proceedings, November 13-14, 2015. British Columbia Geological Survey Paper 2015-3, 2015. pp. 39–64.

Subbotin V.V., Subbotina G.F. Pyrochlore-group minerals within phoscorites and carbonatites of the Kola Peninsula// Vestnik of MGTU. 2000. Vol. 3. Iss. 2. pp. 273–284 (in Russian).

Wu F.-Y., Arzamastsev, A.A., Mitchell, R.H. et al. Emplacement age and Sr-Nd isotopic compositions of the Africanda alkaline ultramafic complex, Kola Peninsula, Russia // Chemical Geology. 2013. Vol. 353 pp. 210–229.

AB INITIO SIMULATIONS OF THE ELECTRONIC PROPERTIES OF MULTICOMPONENT SILICATE MELTS - THE PYROLITE MODEL

Bobocioiu E.[1], Caracas R.[1,2]

[1]Ecole Normale Supérieure de Lyon, Laboratoire de Géologie de Lyon, Lyon, France

[2]CNRS

The structure of the Earth can be reduced to a silicate and oxide layer lying on top of a metallic iron-rich core. The average composition of the silicate layer was mainly determined from direct sampling, and partly inferred from the composition of the large class of meteorites and the sun photosphere (McDonough & Sun, 1995). As such, it is a multi-component system, whose study requires exploring complex phase diagrams. Things are even more complicated in the high-temperature regime, with many intersecting pressure-dependent liquidus lines. Direct experimental investigations of the physical properties of such silicate melts are made even more complicated by the inherent difficulties associated with the high temperatures and pressures. So far, the only reliable techniques that allow for the indirect measurement of electronic and magnetic properties of such a melt remain the X-ray Absorption Spectroscopies, usually as extended X-ray absorption fine structure (EXAFS) spectroscopy. This allowed the estimation of speciation (A. di Cicco, 2001; Cochain et al., 2015; M. Wilke, 2018) through inferring the local configuration environment for selected elements. As EXAFS is an electronic spectroscopy, the knowledge of the local electronic structure is fundamental in interpreting the experimental measurements.

Here we study the electronic structure of pyrolite melts employing ab initio calculations based on density functional theory (DFT).

First we perform molecular dynamics simulations of the melt. We work inside a temperature and pressure range that covers the conditions of the entire magma ocean. This ocean was formed in the early Earth from the condensation of the protolunar disk. The disk itself generated as a result of a giant impact (the Moon is the second body separated from this disk).

The melt simulations were realized in the NVT ensemble, using the VASP package (Kresse and Hafner, 1993). We used the Projector Augmented Wavefunctions flavor (Blöchl, 1994) of the DFT with the PBE96 functional for the exchange-correlation. Because of the presence of Fe, we considered spin-polarized systems.

Figure 1 shows the variation of the magnetic moment on each of the 4 Fe atoms present in the pyrolite melt. We analyze several pressure points along the 5000K isotherm. At low pressures all 4 Fe atoms are in a high-spin state almost the entire simulation. With increasing pressure, there is a statistical quantity of instances of lower Fe atoms. This population steadily increases with increasing pressure. At the highest pressure points the melt can be considered in a low spin state. However, at conditions typical of the magma ocean, one can safely assume the presence of the residual magnetic moment on the Fe atoms in the silicate melt.

Then we investigate the electronic band structure of the melt. For this we take snapshots from the simulations separated by 1 picosecond intervals and we perform an accurate calculation using the ABINIT package (Gonze et al., 2009). We compute the total electronic density of states for the two spin populations at several temperatures and pressures. Preliminary results are shown in figure 2, in the

form of the total the resulting density of states for one relevant snapshot taken at a density of 2.43 g/cm^3 and a temperature of 5000K, which is well beyond experimental reach.

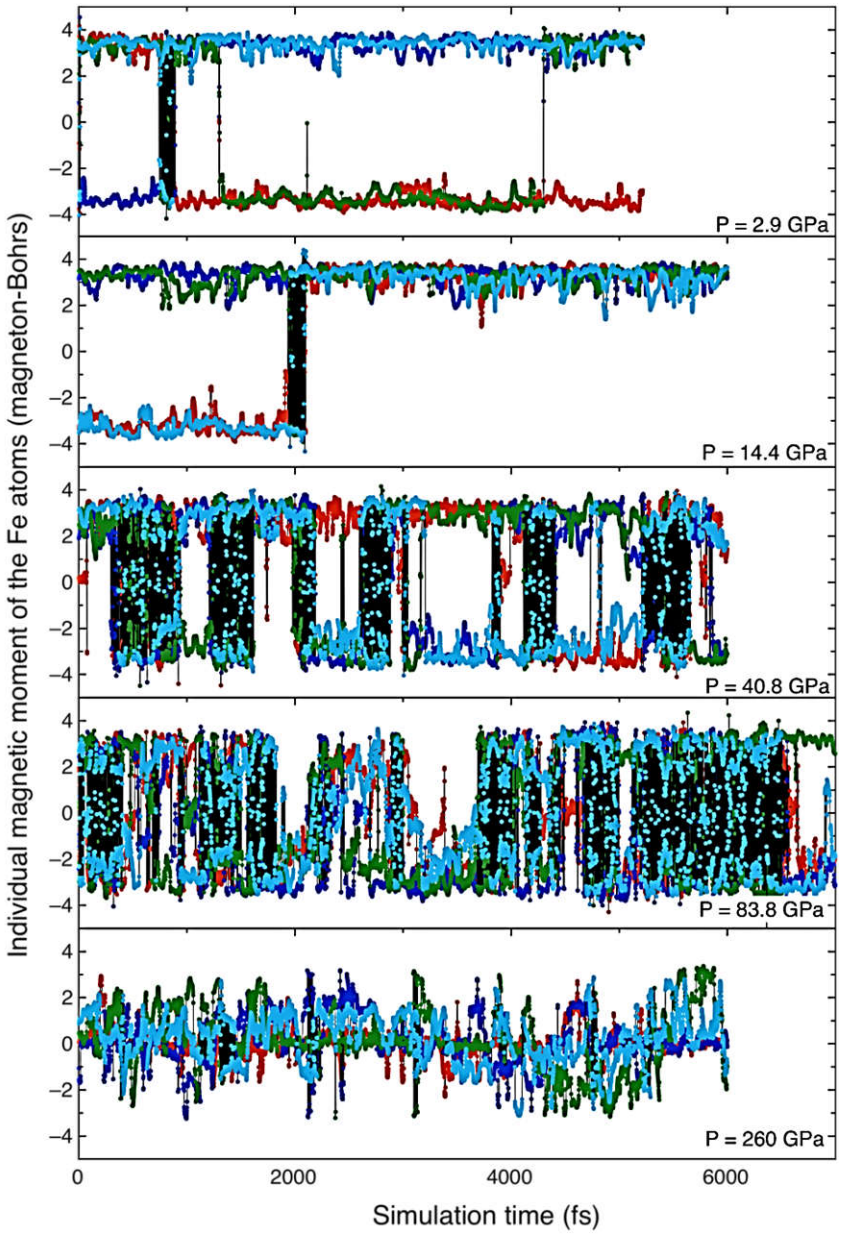

Fig. 1. Local magnetic moment on the Fe atoms at 5000K and several pressures. Each color represents one of the 4 Fe atoms present in our simulation box of the pyrolite melt.

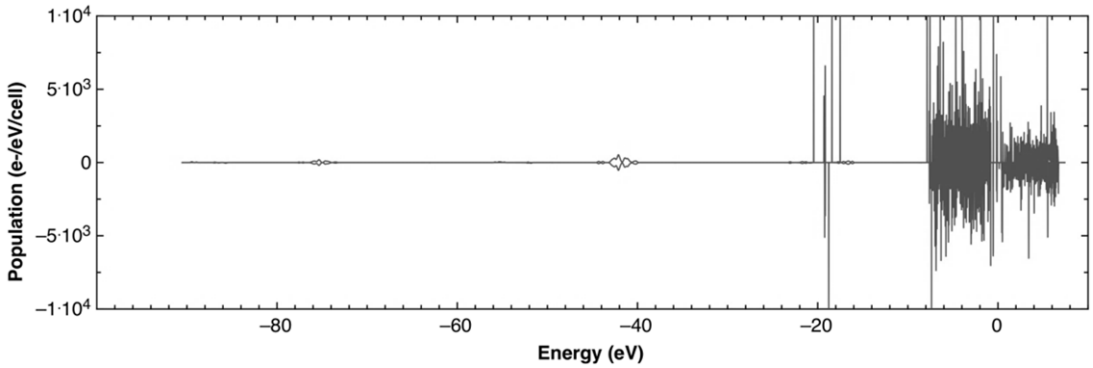

Fig, 2. Total electronic density of states in one snapshot at 2.431 g/cm^3 and 5000K.

On-going calculations aim at determining the projection on the s, p, and d Fe orbitals, and the effect of pressure on their occupancies.

References

Blöchl P. E. Projector augmented-wave method, Phys. Rev. B 50 17953 (1994).

di Cicco A. EXAFS for liquids, J. Phys: Condensed Matter 13, R23 (2001).

Cochain B., C. Sanloup, C. de Grouchy, C. Crepisson, H. Bureau, C. Leroy, I. Kantor, T. Irifune Bromine speciation in hydrous silicate melts at high pressure, Chem. Geol. 404, 18-26 (2015).

Gonze, X., Amadon, B., Anglade, P.-M., Beuken, J.-M., Bottin, F., Boulanger, P., Bruneval, F., Caliste, D., Caracas, R., Côté, M., and others. (2009) ABINIT: First-principles approach to material and nanosystem properties. Computer Physics Communications, 180, 2582–2615.

Kresse G. and Hafner J. Ab initio molecular dynamics for liquid metals. Phys. Rev. B 47, 558 (1993).

Wilke, M. X-ray absorption spectroscopy measurements, Chap. 6. pp. 155-178. in Magmas under pressure: advances in high-pressure experiments on structure and properties of melts, Eds: Y. Kono, C. Sanloup, Elsevier (2018).

MINOR ELEMENTS IN BRIDGMANITE: EXPERIMENTAL AND NATURAL DATA

***Bobrov A.V.*[1,2,3], *Matrosova E.A.*[2], *Bindi L.*[4,5], *Tamarova A.P.*[1], *Pushcharovsky D.Yu.*[1], *Irifune T.*[6]**

[1]*Geological Faculty, Moscow State University, Moscow, Russia*

[2]*Vernadsky Insitute of Geochemistry and Analytical Chemistry RAS, Moscow, Russia*

[3]*Institute of Experimental Mineralogy RAS, Chernogolovka, Russia*

[4]*Dipartimento di Scienze della Terra, Università di Firenze, Via La Pira 4, I-50121 Firenze, Italy,*

[5]*CNR, Istituto di Geoscienze e Georisorse, sezione di Firenze, Via La Pira 4, I-50121 Firenze, Italy,*

[6]*Geodynamic Research Center, Matsuyama University, Japan, dragon.of.rainbow@yandex.ru*

Bridgmanite is the major phase of the lower mantle ultrabasic association and the most abundant mineral in the Earth. It is observed as inclusions in natural UHP diamonds in association with magnesiowüstite, ringwoodite, $CaSiO_3$-perovskite, tetragonal almandine–pyrope phase (TAPP), high-pressure $(Mg,Fe)(Al,Cr)_2O_4$ polymorphs, native Ni, and sulfides. Bridgmanite is not stable in time and undergoes retrograde transformation into pyroxene with decreasing pressure. The newly formed phase inherits the chemical composition of bridgmanite and, importantly, the high aluminum content. Upper-mantle enstatite from inclusions in diamonds usually contains 0.3–0.9 wt % Al_2O_3 (but never > 1 wt %), whereas the concentration of Al_2O_3 in bridgmanite (former bridgmanite) is much higher: the maximal Al_2O_3 concentration registered in natural bridgmanite is 12.6 wt % (Kaminsky, 2012). The high Al content, as well as an association with ferropericlase (magnesiowüstite) are the typomorphic features of lower-mantle $(Mg,Fe)SiO_3$ bridgmanite. Andrault et al. (1998) suggested that Al^{3+} could enter bridgmanite via two competing mechanisms: (i) stoichiometric $Mg^{2+}_A + Si^{4+}_B = Al^{3+}_A + Al^{3+}_B$, where A and B are the eightfold and octahedral sites, respectively; (ii) nonstoichiometric $2Si^{4+}_B + O^{2-}_O = 2Al^{3+}_B + V_O$) with vacancies in the oxygen site.

Bridgmanites from inclusions in natural diamonds demonstrate quite wide ranges of Mg# (from 0.88 до 0.95) (Harte et al., 1999). These compositions are different from the experimental data showing the lower Mg# (0.80–0.88) (Fei et al., 1996; Lee et al., 2004; and others). Such differences may be mostly explained by instability of Fe-rich bridgmanite and its decomposition onto ferropericlase and SiO_2. Variations in Mg# may be controlled by the concentration of Al in $MgSiO_3$-perovskite as well, since there is the positive correlation between Al and Fe^{3+} in bridgmanite (McCammon, 1997). According to the results of experimental studies (Frost and Langenhorst, 2002),

increase in Al content in $MgSiO_3$-perovskite accompanied by increase in Fe^{3+} content, however, does not affect significantly the distribution of Fe^{2+} between bridgmanite and ferropericlase.

According to the pyrolite model (Ringwood, 1991), chromium, titanium, and sodium are characterized by the low bulk concentrations in the Earth's mantle (0.42 wt % Cr_2O_3, 0.2 wt % TiO_2, 0.57 wt % Na_2O). The influence of such elements on structural peculiarities of bridgmanite is poorly investigated (Andrault, 2007), although even their small concentrations may influence significantly on the physical properties of bridgmanite. At the same time, the minor-element composition is typomorphic for bridgmanite: incorporation of Cr indicates an ultrabasic mantle lithology, whereas Ti- and Na-rich bridgmanites may occur in the mantle as a result of oceanic crust subduction. Here we report the new experimental data on the minor-element composition of bridgmanite.

Bridgmanite with the ***highest chromium content*** of 10.35 wt % Cr_2O_3 was synthesized at 23 GPa and 1600°C (Bindi et al., 2014). The crystal structure and chemical composition of a crystal of $(Mg_{1-x}Cr_x)(Si_{1-x}Cr_x)O_3$ perovskite (with x = 0.07) are characterized by substitution for both Mg at the dodecahedral X site (with a mean bond distance of 2.187 Å) and Si at the octahedral Y site (mean: 1.814 Å) with Cr, according to the reaction $Mg^{2+} + Si^{4+} = 2Cr^{3+}$. Such substitutions cause a shortening of the <X-O> and a lengthening of the <Y-O> distances with respect to the values typically observed for pure $MgSiO_3$ perovskite. Although the compound was found to be orthorhombic, space group **Pbnm**, with lattice parameters **a** = 4.8213(5), **b** = 4.9368(6), **c** = 6.9132(8) Å, **V** = 164.55(3) $Å^3$ (Bindi et al. 2014), the differences from the perovskite structure are essential. The perovskite is characterized by tilting of the BO6 octahedra changes the coordination of an undersized A cation from 12 to 8. We observe the shortening of the <X-O> and a lengthening of the <Y-O> distances with respect to the values typically observed for pure $MgSiO_3$ perovskite (Horiuchi et al. 1987). In the Cr-bridgmanite the Mg and Si atoms specifically ordered into dodecahedral X site and octahedral Y site.

The ***highest sodium content*** of 1.53 wt % Na_2O was registered in bridgmanite synthesized at 24 GPa and 1700°C in the alkali carbonate–pyrolite system and associated with Na-rich (up to 4.4 wt % Na_2O) ringwoodite, ferropericlase, and quenched carbonate-silicate melt (Bindi et al., 2016). By analogy with Na-bearing majoritic garnet (Bobrov et al., 2008), we could expect that incorporation of Na in bridgmanite will increase with decreasing degree of partial melting, but our samples demonstrate the opposite regularity. The concentration of sodium increases with increasing temperature and degree of partial melting. There is the positive correlation between the concentrations of Na and Al in bridgmanie and negative, between Na and Fe^{3+}. This is explained by the different behavior of these elements during isomorphism. Al (especially in excess of Mg) predominantly entered the B-site and left the A-site for Na. The larger Fe^{3+} cation occupied an eight-fold site and prevented Na incorporation in bridgmanite. The cell volume of Na-bearing bridgmanite (166 Å) is much higher than that of pure $MgSiO_3$ bridgmanite (162.53Å, Dobson and Jacobsen, 2004). The results of our runs show that alkali carbonatitic melt metasomatism in the deep transition zone may lead to local Na-enrichment, and bridgmanite (as well as ringwoodite) may be an important host for Na in the deep transition zone. Subsequent convection or subduction of metasomatised mantle may lead to enrichment of alkaline elements in the upper and lower mantle.

Ti-rich bridgmanite with 25.20 wt % TiO2 was synthesized in the pyrope $Mg_3Al_2Si_3O_{12}$–geikielite $MgTiO_3$ system at 20 GPa 1600°C (Bindi et al., 2017). A new bridgmanite-like structure that can be described as a three-fold commensurate superstructure of the ideal $MgSiO_3$-perovskite structure was observed in a $[Mg_{5/6}Al_{1/6}][Si_{1/2}Ti_{1/3}Al_{1/6}]O_3$ crystal synthesized in the model system $Mg_3Al_2Si_3O_{12}$–$MgTiO_3$ at 20 GPa and 1600 °C. The compound was found to be orthorhombic, space group *Pnma*, with lattice parameters a = 14.767(3), b = 6.958(1), c = 4.812(1) Å, V = 494.4(2) $Å^3$, which represents a 3a × b × c superstructure of the typical *Pnma* perovskite structure. The structure was refined to R = 0.024 using 846 independent reflections. The superstructure mainly arises from the ordering of titanium in one of the octahedral positions. Crystal-chemical details of the different polyhedra in the superstructure are discussed in comparison to pure $MgSiO_3$. This is the first documented superstructure of a bridgmanite phase, and Ti-rich bridgmanite in the lower mantle arising from local Ti-enrichments may exhibit different physical properties and elemental partitioning

behavior from Ti-poor, peridotitic bridgmanite. In addition, large amounts of Ti can stabilize bridgmanite-like compounds at considerably lower pressure than lower mantle conditions.

This study was supported by the Russian Science Foundation, project no. 17-17-01169.

References

Andrault D. Properties of lower-mantle Al(Mg,Fe)SiO_3 perovskite// Advances in High-Pressure Mineralogy: Geological Society of America Special Paper (ed. by E. Ohtani). 2007. Vol. 421 pp. 15–36.

Andrault D., Neuville D.R., Flank A.M., Wang Y. Cation sites in Al-rich $MgSiO_3$-perovskites// Amer. Mineral. 1998. Vol. 83 pp. 1045–1053.

Bindi L., Sirotkina E.A., Bobrov A.V., Irifune T. Chromium solubility in perovskite at high pressure: the structure of $(Mg_{1-x}Cr_x)(Si_{1-x}Cr_x)O_3$ (with x = 0.07) synthesized at 23 GPa and 1600°C// Amer. Mineral. 2014. Vol. 99 pp. 866–869. DOI: 10.2138/am.2014.4784.

Bindi L., Tamarova A., Bobrov A.V., Sirotkina E.A., Tschauner O., Walter M.J., Irifune T. Incorporation of high amounts of Na in ringwoodite: possible implications for transport of alkali into lower mantle// Am. Miner. 2016. Vol. 101 pp. 483–486.

Bindi L., Sirotkina E.A., Bobrov A.V., Walter M.J., Pushcharovsky D.Yu., Irifune T. Bridgmanite-like crystal structure in the novel Ti-rich phase synthesized at transition zone condition// American Mineralogist. 2017. Vol. 102. No. 1 pp. 227–230. DOI: 10.2138/am-2017-5937.

Bobrov A.V., Litvin Yu.A., Bindi L., Dymshits A.M. Phase relations and formation of sodium-rich majorite garnet in the system $Mg_3Al_2Si_3O_{12}$–$Na_2MgSi_5O_{12}$ at 7.0 and 8.5 GPa// Contrib. Mineral. Petrol. Vol. 156. No. 2 pp. 243–257.

Dobson D.P., Jacobsen S.D. The flux growth of magnesium silicate perovskite single crystals// American Mineralogist. 2004. Vol. 89 pp. 807–811.

Fei Y., Wang Y., Finger L.W. Maximum solubility of FeO in (Mg,Fe)SiO_3 perovskite as a function of temperature at 26 GPa: Implication for FeO content in the lower mantle// J. Geophys. Res. 1996. Vol. 101 (B5) pp. 11525–11530.

Frost D.J., Langenhorst F. The effect of Al_2O_3 on Fe–Mg partitioning between magnesiowüstite and magnesium silicate perovskite// Earth and Planetary Science Letters. 2002. Vol. 199. No. 3–4 pp. 227–241.

Harte B., Harris J.W., Hutchison M.T., Watt G.R., Wilding M.C. Lower mantle mineral associations in diamonds from Sao Luiz, Brazil// Mantle Petrology: Field Observations and High Pressure Experimentation: A Tribute to Francis R. (Joe) Boyd: Geochemical Society Special Publication. 1999. No. 6 pp. 125–153.

Horiuchi H., Ito E., Weidner D. Perovskite-type $MgSiO_3$: single crystal X-ray diffraction study// Am. Mineral. 1987. Vol. 72 pp. 357–360.

Kaminsky F.V. Mineralogy of the lower mantle: A review of 'super-deep' mineral inclusions in diamond// Earth-Sci. Rev. 2012. Vol. 110 pp. 127–147.

Lee K.K.M., O'Neill B., Panero W.R., Shim S.H., Benedetti L.R., Jeanloz R. Equations of state of the high-pressure phases of a natural peridotite and implications for the Earth's lower mantle// Earth Planet. Sci. Lett. 2004. Vol. 223 pp. 381–393.

McCammon C.A. Perovskite as a possible sink for ferric iron in the lower mantle// Nature. 1997. Vol. 387 pp. 694–696, doi: 10.1038/42685.

Ringwood A. E. (1991). Phase transformations and their bearing on the constitution and dynamics of the mantle// Geochim. Cosmochim. Acta. Vol. 55. No. 8 pp. 2083–2110.

MONCHEGORSK PLUTON (KOLA PENINSULA): DECOUPLING OF SM-ND AND RE-OS DATA

***Bogina M.M.*[1], *Belyatsky B.V.*[2], *Krymsky R.Sh.*[2] , *Sharkov E.V.*[1], *Chistyakov A.V.*[1], *Zlobin V.L.*[3]**

[1]*IGEM RAS, Moscow, Russia, lekhta@mail.mail*

[2]*VSEGEI, St. Petersburg*

[3]*GIN RAS, Moscow, Russia, vzlobin@bk.ru*

The Archean-Paleoproterozoic boundary was marked by the formation of large igneous provinces (LIPs) made up of siliceous high-Mg series (SHMS) represented by dike swarms, PGE-Cu-Ni bearing mafic-ultramafic intrusions, and volcanics (Sharkov, Bogina, 2006). Several models were proposed to explain their origin: (1) high-degree melting of depleted mantle plume with subsequent crustal contamination of derived melts (Sharkov and Chistyakov, 2012; Puchtel et al., 1997, etc.); (2) melting of "enriched" metasomatized lithospheric mantle (Lauri et al., 2006); or (3) involvement of both the mechanisms (Amelin and Semenov, 1996). The lower-crustal sanukitoid-type rocks were proposed as a universal crustal contaminant for SHMS rocks (Bogina et al., 2018).

However, it is difficult to distinguish between crustal contaminant and enriched mantle source. Sm-Nd isotope study of SHMS rocks cannot provide unambiguous answer, because their narrow range of ε_{Nd} can be interpreted as both significant crustal contamination and melting of enriched mantle. The development of Re-Os technique opened new perspectives in estimating their sources, because difference in the Os content between mantle and crustal rocks is three orders of magnitude. Thus, even insignificant crustal input provides essential shift in the Re-Os isotope composition. Layered intrusions are suitable objects for this study, since their rocks, especially ultramafic varieties, have high Os contents as compared to the volcanic and dike rocks. We address this problem by studying Re-Os and Sm-Nd isotopic systems in the PGE-Cu-Ni Monchegorsk layered mafic-ultramafic intrusion ascribed to the early Paleoproterozoic LIP in the eastern Fennoscandian shield (Sharkov, Chistyakov, 2012).

The PGE-Cu-Ni-bearing Monchegorsk pluton (2504 $\pm$ 2 Ma; (Amelin et al., 1995)) is located in the central part of the Kola Peninsula. The massif from the bottom upward consists of the Marginal zone and Layered Series including: (1) Dunite zone of olivine-chromite cumulates, (2) Peridotite zone of rhythmic alternation of harzburgites (Ol+Opx±CrSp cumulates) and bronzitites (Opx±CrSp cumulates); (3) Bronzitite zone; (4) Norite zone (Opx+Pl±Cpx cumulates). Ore zones are restricted to the Bronzitite zone (Sopcha Ore Layer), Peridotite zone (massive ores of Mt. Nittis), Norite zone (Critical horizon of Mt. Nyud), and Sopcheozero chromite deposit in the Dunite lens, Mt. Sopcha (Sharkov, Chistyakov, 2012).

The Nd isotope composition was analyzed throughout the vertical section of the massif. Most of the rocks have near-chondritic ε_{Nd}: -0.3 in peridotite from the lower Layered series, -0.2 in the gabbros from the lower marginal zone, -0.8 and -0.6 in peridotites from the Sopcha ore layer, and -0.8 to -0.4 in the dunites and chromitites, respectively, from the Sopcheozero chromitite deposit. Slightly lower values were found in the harzburgite from the Critical Horizon (-1.9) and in the Bronzitite zone (-2.5 to -2.6), indicating restricted ε_{Nd} variations within 2 units in the whole range of ultramafic rocks.

The Re-Os isotope study was carried out for the same samples. The highest Os content (63 ppb) in combination with near-chondritic values of initial isotopic composition (0.1104) and γ_{Os} (0.5) was found in the chromitite from the Sopcheozero chromitite deposit. These values are closest to the initial composition of a mantle source and resemble plume-like mantle composition (Puchtel et al., 2004). Slightly lower initial $^{187}Os/^{188}Os$ of 0.08345 and negative γ_{Os}(-24) was determined in the dunite from the Sopcheozero deposit. In contrast, all other samples show much higher degree of crustal contamination with much more radiogenic initial Os isotope composition. In particular, peridotite from the lower Peridotite zone has $^{187}Os/^{188}Os$ of 0.17552 and γ_{Os} of +60. Even higher ratios of 0.18941 and 0.34976 and γ_{Os} of +72 and +218, respectively, were determined in the harzburgite and dunite of the Sopcha Ore layer, respectively. Extremely high, practically crustal Os signature (0.9707) was obtained for the bronzitite from the Critical Horizon. The crustal contribution in the studied rocks is also confirmed by the fact that all the data points define an "apparent isochron" in the $^{187}Os/^{188}Os$-$^{187}Re/^{188}Os$ diagram with a slope corresponding to an age around 2800 Ma and an initial ratio of 0.161

(Fig. 1). The well-expressed positive correlation between $^{187}Os/^{188}Os$ and $^{187}Re/^{188}Os$ can be explained by variable degrees of crustal contamination by ~ 2.8Ga-old crustal rock. This is consistent with the wide development of ~ 2.8-Ga granites in this area.

An extremely strong crustal contamination with a wide range of Os isotope composition is in conflict with a narrow range of slightly unradiogenic Nd isotopic composition. There are no Re-Os data on 2.8-Ga granitoids near the massif, while Archean gneisses from the Finnish Lapland have γ_{Os} at about +544 (Hanski et al., 2001). However, this composition requires much higher crustal contamination (> 50%) and even cannot provide some observed Re-Os signatures. Such high crustal contribution is hardly possible, because would result in significant increase in SiO_2 and LREE, which is not observed. In contrast, Nd data point to the lower crustal contribution. This indicates a decoupling of Re-Os and Sm-Nd isotopic systems, which is likely related to selective crustal contamination (Yang et al., 2012).

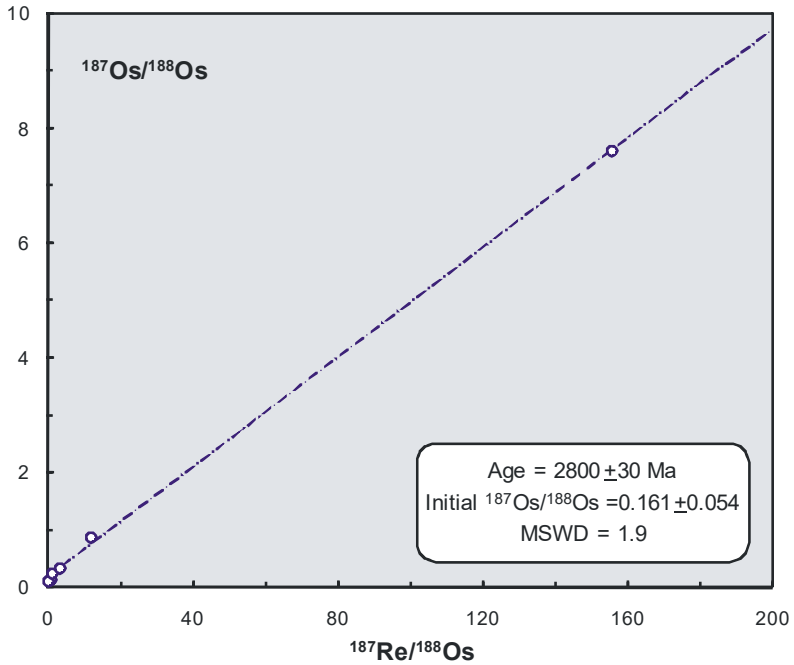

Fig. 1. $^{187}Re/^{188}Os$ *vs* $^{187}Os/^{188}Os$ for the rocks of the Monchegorsk pluton.

Different crustal material can be involved in contamination, even only volatiles (Lesher and Burnham, 2001), which are least stable during partial melting or devolatilization. Sulfides are less stable than silicates and can be easily molten and involved in melt. Assimilation of sulfides from crustal rocks would increase $^{187}Os/^{188}Os$ ratio, but will not affect the Nd isotope composition and REE contents. At the same time, relatively low-Os magmas are more strongly affected by crustal Os and have higher $^{187}Os/^{188}Os$ ratio. The crustal (sulfide) material can be derived from 2910-Ma granulites of the Kola Group consisting mainly of highly aluminous garnet-orthopyroxene-sillimanite, garnet-kyanite-biotite, garnet-sillimanite-cordierite crystalline schists (metapelites), quartzites, and banded iron formations. This process leads to sulfide saturation and formation of sulfide droplets and can explain the extremely radiogenic Os composition in the Ore Sopcha Layer and Critical Horizon of the Monchegorsk Pluton. Chondritic-like Os composition in the dunite and chromitite of the Sopcheozero deposit suggests that these rocks were derived from new portions of more primitive melt, which practically did not experience crustal contamination. The most primitive character of the Sopcheozero rocks is confirmed by the highest Pt/Pd up to 6, which subsequently decreases in the Peridotite zone (3.3), Bronzitite zone and Critical Horizon (0.38 and 0.42) and reaches minimum in the Sopcha Ore Layer (0.16).

Thus, decoupling of Sm-Nd and Re-Os isotopic systems found in the Monchegorsk pluton was caused by selective extraction of crustal sulfides from host metasediments.

This study was supported by the Russian Foundation for Basic Research (project no. 16-05-00708).

References

Amelin Yu.V., Heaman L.M., Semenov V.S. U-Pb geochronology of layered mafic intrusions in the eastern Baltic Shield: implications for the timing and duration of Paleoproterozoic continental rifting// Precambrian Res. 1995. Vol. 75. pp. 31–46.

Amelin Yu.V., Semenov V.S. Nd and Sr isotopic geochemistry of mafic layered intrusions in the Eastern Baltic Shield: implications for the evolution of Paleoproterozoic continental mafic magmas// Contrib. Mineral. Petrol. 1996. Vol. 124. pp.255–272.

Bogina M., Zlobin V., Svetov S., Sharkov E., Chistyakov A. Petrogenesis of siliceous high-Mg series: Evidence from Early Paleoproterozoic mafic volcanic rocks of the Vodlozero Domain, Fennoscandian Shield// Geosci. Front. 2018. Vol. 9, pp. 207-221.

Hanski, E., et al. The Os and Nd isotopic systematics of c.2.44 Ga Akanvaara and Koitelainen mafic layered intrusions in northern Finland // Precambrian Res. 2001. Vol. 109, pp. 73–102.

Lauri L.S., et al. Petrogenesis of silicic magmatism related to the ~2.44 Ga rifting of Archean crust in Koillismaa, eastern Finland// Lithos. 2006. Vol. 86, pp. 137–166.

Lesher C.M., Burnham O.M. Micromponent elemental and isotope mixing in Ni-Cu-(PGE) ores at Kambalda, Western Australia // Lithos. 2001. Vol. 39, pp. 421–446.

Puchtel I.S., Brandon A., Humayun M. Precise Pt-Re-Os isotope systematics of the mantle from 2.7-Ga komatiites// Earth Planet. Sci. Lett. 2004. Vol. 225, pp. 157–174.

Puchtel I.S., Haase, K.M., Hofmann, A.W., et al. Petrology and geochemistry of crustally contaminated komatiitic basalts from the Vetreny Belt, southeastern Baltic Shield: Evidence for an Early Proterozoic mantle plume beneath rifted Archean continental lithosphere // Geochim. Cosmochim. Acta. 1997. Vol. 61, pp. 1205–1222.

Sharkov E.V., Bogina M.M. Evolution of the Paleoproterozoic magmatism: geology, geochemistry, and isotopic constraints//Stratigr. Geol. Correl. 2006. Vol. 14. pp. 345-367.

Sharkov, E.V., and Chistyakov, A.V. The Early Paleoproterozoic Monchegorsk layered mafic-ultramafite massif in the Kola Peninsula: geology, petrology and ore potential// Petrology. 2012. Vol. 20, pp. 607–639.

Yang S.H., et al. Selective crustal contamination and decoupling of lithophile and chalcophile element isotopes in sulfide-bearing mafic intrusions: an example from the Jingbulake intrusion, Xinjiang, NW China//Chem. Geol. 2012. Vol. 302-303, pp. 106-118.

FERRIC/FERROUS RATIO IN SILICATE MELTS: NEW MODEL AND NEW MORBS FO2 ESTIMATIONS

Borisov A.A.

Institute of Geology of Ore Deposits, Petrography, Mineralogy, and Geochemistry Russian Academy of Sciences (IGEM RAS), aborisov@igem.ru

The ferric/ferrous ratio is a crucial parameter of natural silicate melts which controls crystallization of iron-containing phases and physical properties of silicate melts via the activities of FeO and F_2O_3 components. The ferric/ferrous ratio is also widely used for estimation of the redox conditions of magmas (e.g., Christie et al. 1986). The ferric/ferrous equilibrium in melts can be described by the reaction:

$$FeO + ¼\ O_2 = FeO_{1.5} \quad (1)$$

which leads to the following relation:

$$\log (X_{FeO1.5}/X_{FeO}) = ¼ \log fO_2 + \log K - \log (\gamma_{FeO1.5}/\gamma_{FeO}) \quad (2)$$

where X_i and γ_i are mole fraction and activity coefficients of iron oxides in silicate melts, respectively, fO_2 is the oxygen fugacity and K is the constant of the reaction (1). In practice the equation (2) can be replaced by an empirical equation in the form:

$$\log(X_{FeO1.5}/X_{FeO}) = k \cdot \log fO_2 + h/T + \Sigma d_i X_i + c \quad (3),$$

where T is the temperature in K, and k, h, d_i and c are constants and X_i are mole fractions of the main oxide components in silicate melts, such as SiO_2, Al_2O_3, MgO, CaO, Na_2O and K_2O (e.g., Sack et al. 1980; Kilinc et al. 1983).

Based on own (Borisov et al., 2013; 2015; 2017) and published experimental data a new Model is proposed to predict the ferric/ferrous ratio as a function of oxygen fugacity, temperature and melt composition. In contrast to previous equations, the compositional effect of melts on the Fe^{3+}/Fe^{2+} ratio is not only modelled by the sum of the molar fraction of the individual oxide components. Additional interactions terms have been incorporated ($d_{SiAl} \cdot X_{SiO2} \cdot X_{Al2O3}$ and $d_{SiMg} \cdot X_{SiO2} \cdot X_{MgO}$). The main advantage of the proposed model is its applicability for a wide compositional range. However, its application to felsic melts (> 68 wt% SiO_2) is not recommended.

Type (3) equations are widely used to estimate fO_2 values for MORB glasses, if ferric/ferrous in these samples are precisely determined. We used two last datasets (Berry et al., 2018; Zhang et al., 2018) and calculated fO_2, applying the equation of Kilinc et al. (1983), the equation of Kress and Carmichael (1991) and our new Model. The fO_2 calculation was performed assuming the temperature of 1200°C and fO_2 values relative quartz–fayalite–magnetite buffer (ΔQFM) were found.

It was demonstrated that MORB fO_2 estimations vary by up to one log unit depending on the analytical procedure to constrain ferric/ferrous in MORB glasses. For a given dataset, a variation of up to ca 0.5 log unit can be obtained, depending on the model that is applied to calculate fO_2. Assuming that the most recent data from Zhang et al. (2018) are correct and applying our new Model, we suggest that MORBs are equilibrated at fO_2 values corresponding to QFM+0.2±0.1.

References

Berry A.J., Stewart G.A., O'Neill H.St.C., Mallmann G., Mosselmans J.F.W. (2018) A re-assessment of the oxidation state of iron in MORB glasses. Earth and Planetary Science Letters 483, 114–123.

Borisov A., Behrens H., Holtz F. (2013) The effect of titanium and phosphorus on ferric/ferrous ratio in silicate melts: an experimental study. Contribution to Mineralogy and Petrology 166, 1577-1591.

Borisov A., Behrens H., Holtz F. (2015) Effects of melt composition on Fe^{3+}/Fe^{2+} in silicate melts: a step to model ferric/ferrous ratio in multicomponent systems. Contributions to Mineralogy and Petrology 169, Article 24.

Borisov A., Behrens H., Holtz F. (2017) Effects of strong network modifiers on Fe^{3+}/Fe^{2+} in silicate melts: An experimental study. Contributions to Mineralogy and Petrology 172, Article 34.

Christie D.M., Carmichael I.S.E. and Langmuir C.H. (1986) Oxidation state of mid-ocean ridge basalt glasses. Earth and Planetary Science Letters 79, 397-411.

Jayasuriya K.D., O'Neil H.St.C., Berry A., Campbell S.J. (2004) A Mössbauer study of the oxidation state of Fe in silicate melts. American Mineralogist 89, 1597-1609.

Kilinc A., Carmichael I.S.E., Rivers M.L., Sack R.O. (1983) The ferric-ferrous ratio of natural silicate liquids equilibrated in air. Contributions to Mineralogy and Petrology 83, 136-140.

Kress V.C., Carmichael I.S.E. (1991) The compressibility of silicate liquids containing Fe_2O_3 and the effect of composition, temperature, oxygen fugacity and pressure on their redox states. Contributions to Mineralogy and Petrology 108, 82-92.

Sack RO, Carmichael ISE, Rivers ML, Ghiorso MS (1980): Ferric-ferrous equilibria in natural silicate liquids at 1 bar. Contribution to Mineralogy and Petrology 75: 369-376

Zhang HL, Cottrell E, Solheid PA, Kelley KA and Hirschmann MM (2018) Determination of $Fe^{3+}/\Sigma Fe$ of XANES basaltic glass standards by Mössbauer spectroscopy and its application to the oxidation state of iron in MORB. Chemical Geology 479, 166–175.

POTENTIAL ENRICHMENTS OF INCOMPATIBLE ELEMENTS (BA-SR-LREE) AND LI IN A VOLCANIC SEQUENECES OF SEYITGAZI DISTRICT, ESKIŞEHIR, TURKEY

Budakoglu M., Kocaturk H., Unluer A.T., Kirikoglu M.S., Doner Z., Kumral M.
Istanbul Technical University, Faculty of Mines, Geological Engineering Department,
budak@itu.edu.tr

This study focus on the potential enrichments of incompatible elements (Ba-Sr-LREE) and Li in volcanic rocks located at Örencik-Aşağısöğüt-Yukarısöğüt-Yeşiltepe villages of Seyitgazi district of Eskişehir, Western Anatolia Turkey. For this purpose geological, mineralogical and petrographic examinations were performed on the different type of rocks and these examinations were also supported by ICP-MS analysis to determine LREE and HREE concentrations of these volcanic rocks. REE potentials were also identified on various diagrams. While ICP-MS analyses indicate that light rare earth elements have more potential compared to heavy rare earth elements, related various diagrams interpret REE potential of these lithological units. Pyroclastics and basaltic lava flows are two important geological units representing potential sources of REE enrichments. Pyroclastic occurrences are can be described as ignimbirites and tuffs intercalated with lacustrine carbonate rocks. Basaltic lava flows are represented with silica-undersaturated alkaline basaltic rocks. Determination of the mineralogical, petrographic, geochemical and geological properties for the separated pyroclastic formations and sedimentary rocks in the study area were also presented important data on the REE concentrations and their economic potential. Consequently, primitive studies conducted in the field were supported by examinations carried out in the laboratory and a sample work model was created for the detailed further efforts on this area.

Table 1. Major Oxide and Trace Element Ratios of Some Samples

	C-1	C-2	C-4	C-11	C-13		C-1	C-2	C-4	C-11	C-13
SiO2	69,65	68,44	50,42	50,28	49,97	**Gd**	5,636	5,299	4,311	9,346	12,869
Al2O3	13,63	13,42	16,3	18,93	16,82	**Tb**	0,826	0,713	0,601	1,052	1,432
Fe2O3	1,79	3,31	7,16	10,73	8,24	**Dy**	4,79	3,701	3,388	4,881	6,584
MgO	1,51	1,41	4,92	2,8	4,69	**Ho**	0,944	0,725	0,669	0,877	1,203
CaO	1,56	3,51	8,59	4,55	7,52	**Er**	2,84	2,192	1,997	2,512	3,463
Na2O	1,81	3,1	2,79	0,84	2,46	**Tm**	0,419	0,298	0,279	0,328	0,439
K2O	5,8	4,64	5,35	3,13	5,47	**Yb**	2,766	1,906	1,776	2,004	2,812
TiO2	0,11	0,62	1,24	1,86	1,55	**Lu**	0,416	0,29	0,256	0,301	0,406
P2O5	0,03	0,21	0,68	0,5	0,68	**Th**	23,886	24,093	20,722	14,883	21,803
MnO	0,09	0,06	0,14	0,15	0,13	**Li**	160,481	40,446	181,612	53,245	24,618
Cr2O3	0	0	0,04	0,06	0,04	**Be**	5,027	4,404	3,731	1,857	3,686
Cl	0,07	0,05	0,03	0	0	**Co**	15,194	14,679	14,526	25,235	38,101
SO3	0	0,03	0,02	0,01	0,05	**Ni**	30,694	8,386	26,271	19,757	26,19
LOI	3,81	0,93	1,89	5,68	1,93	**Cu**	8,686	4,187	7,965	23,402	14,7
Total	99,85	99,72	99,54	99,52	99,53	**As**	66,557	89,41	68,184	59,447	60,41
Sc	57,496	49,75	48,588	45,968	69,478	**Rb**	151,437	142,797	78,346	71,043	93,773
Y	26,977	21,133	18,666	24,656	32,531	**Sr**	305,248	319,855	311,898	775,464	1387,194
La	32,677	40,137	28,03	72,431	97,81	**Ag**	0,73	0,422	0,453	0,941	1,533
Ce	66,85	77,619	64,304	126,58	190,842	**Cs**	27,709	19,218	13,047	8,283	2,562
Pr	7,178	8,277	5,883	16,062	22,156	**Ba**	409,842	684,385	381,528	1255,086	1835,674
Nd	26,153	29,188	21,106	62,353	83,31	**Tl**	0,914	1,074	0,547	0,156	0,234
Sm	5,531	5,469	4,211	10,557	14,592	**Pb**	48,26	52,198	43,149	13,823	16,394
Eu	1,003	0,923	0,757	3,049	3,977	**U**	4,937	6,779	2,092	6,035	5,765

Geology and Geochemistry of Volcanic Rocks

The primary target for enrichment of incompatible element enrichments are pyroclastic occurrences and basaltic lava flows. Both volcanic rocks are products of accetionary tectonics, subduction processes and slab tearing (Prelevic at al 2015). The extensional tectonic regime in Eocene-

Pliocene period provides lacustrine basins and volcanic activities related with fault boundaries. The lavas are defined as trachytes and basalt units which are dark gray and black in color because of the abundant amount of anhydrous ferromagnesian minerals. Trachyte and basalts have holocyrstalline porphyritic texture. The clinopyroxene and amphibole fenocrystals and plagioclase microlites found in trachytic texture are the main identified properties of these rocks. On the other hand, the pyroclastic occurrences which can be described as unlithified tuffs, lithified ignimbrites and tuffites. Examination of the spider diagrams normalized to primitive mantle revealed that the rock specimens enriched in REE. The volcanic rocks in the region are thought to be a product of post-collisional, Eskişehir-Afyon-Isparta, late Cenozoic potassic-ultrapotassic volcanic province in southwestern Turkey. Partial melting and fractional crystallization of wehrlitic oceanic floor (Caran, 2016) and sub-continental lithospheric mantle led to the formation of Ba, Sr, LREE rich potassic-ultrapotassic magma (Dilek and Altunkaynak, 2010).

The potassic rocks in the region enriched by HFSE such as La (40-100 ppm), Ce (60-190 ppm), Nd (60-83 ppm) and Zr (390-440 ppm) some of the LILE, Ba 0.15% - 0.23% and Sr (0.09% and 0.15%). On the other hand, tuffs with high silica contents have lower Ba, Sr and REE concentration. These results indicate that the HFSE content is in positive correlation with K, Ba, Sr and negative correlation with silica content. Pyroclastic rocks with high silica content contain significantly less amounts of incompatible elements (both HFSE and LILE). There is a significant lithium enrichment in some of the pyroclastic samples (up to 180 ppm).

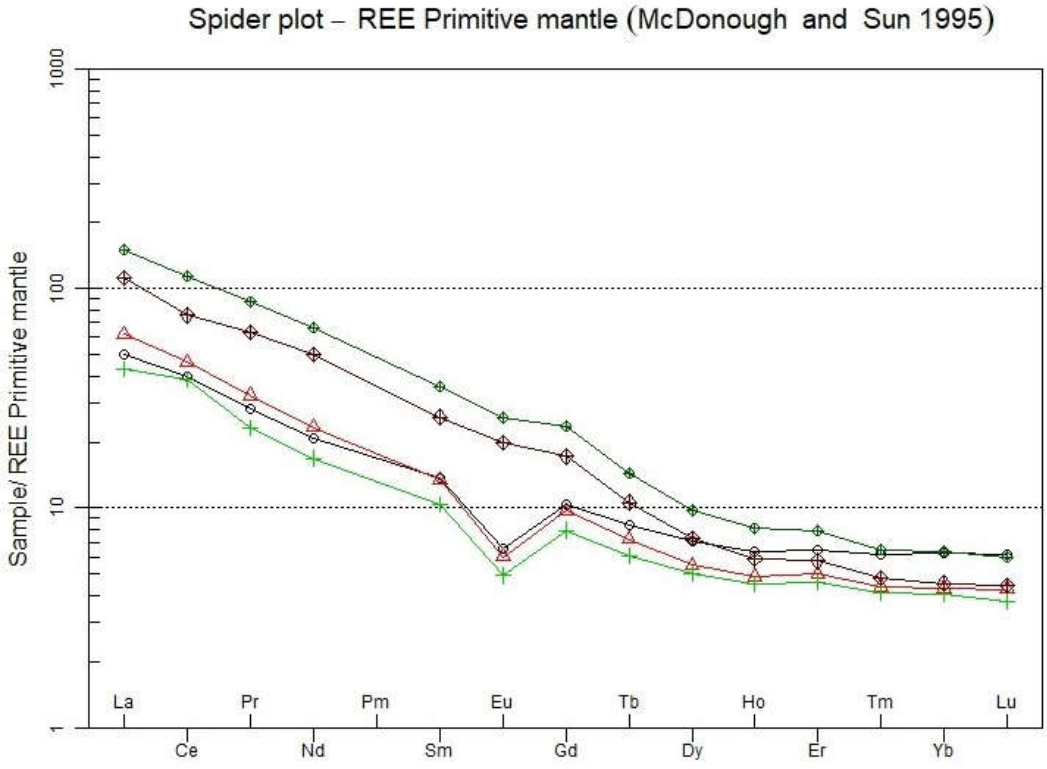

Figure 1. Samples Normalized to Primitive Mantle.

Financial support of this study is provided by The Scientific and Technological Research Council of Turkey (TÜBİTAK). Project Number is 114Y646 and Principal Investigator Prof. Dr. M. Sezai KIRIKOĞLU.

References

Caran, Ş. (2016). Mineralogy and petrology of leucite ankaratrites with affinities to kamafugites and carbonatites from the Kayıköy area, Isparta, SW Anatolia, Turkey: Implications for the influences

of carbonatite metasomatism into the parental mantle sources of silica-undersaturated potassic magmas. Lithos, 256, 13-25.

Dilek, Y., & Altunkaynak, Ş. (2010). Geochemistry of Neogene–Quaternary alkaline volcanism in western Anatolia, Turkey, and implications for the Aegean mantle. International Geology Review, 52(4-6), 631-655.

Dejan Prelević, Cüneyt Akal, Rolf L. Romer, Regina Mertz-Kraus, Cahit Helvacı; Magmatic Response to Slab Tearing: Constraints from the Afyon Alkaline Volcanic Complex, Western Turkey, Journal of Petrology, Volume 56, Issue 3, 1 March 2015, Pages 527–562.

McDonough, W. F., & Sun, S. S. (1995). The composition of the Earth. Chemical geology, 120(3-4), 223-253.

REE AND TRACE ELEMENT DISTRIBUTIONS OF FE-AL LATERITES ORIGINATED FROM YONCAYOLU METAMORPHICS, KAHRAMANMARAŞ (SE,TURKEY)

Budakoglu M., Kırıkoğlu S., Kocaturk H., Unluer A.T., Doner Z., Kumral M.

Istanbul Technical University, Faculty of Mines, Geological Engineering Department,

budak@itu.edu.tr

The Carboniferous-Permian Yoncayolu Metamorphic rocks are considered to be the lower units of the, Keban-Malatya Metamorphic group. These rocks can be described as gneisses, amphibolitschists, calchists, intercalated with metavolcanics, marbles and quartzites. The weathering products (bauxite nodules and Terra Rossa) of the Yoncayolu metamorphics are common in Northern parts of Kahramanmaraş area. Both Bauxite nodules and Terra Rossa enriched in iron (up to 80% Fe_2O_3) and aluminum (up to 52% Al_2O_3) due to the presence of goethite, hematite and diaspore minerals. Presence of high REE (100-500 ppm) indicates that the laterites are assembling the geochemical remarks of the metamorphic origin. On the other hand, Pb (up to 0,15 PbO %), Zn (up to 0,35 %) and As (up to 0,11 %) also enriched in both Terra Rossa and bauxite nodules, due to the hydrothermal activities circulating trough metamorphic units. These hydrothermal activities are thought to be originated from the volcanic and plutonic activities during the Cretaceous period.

Fig. 1. The Altered Metamorphic Rocks Near Acıelma Village & Bauxite Nodules.

1.1 Stratigraphy of the region

Yoncayolu Keban Methamorphics are the basement rocks in the area. These rocks are overlain by Upper Cretacous Goksun ophiolite and cut by some granitic intrusions (Yumun, Z.U & Kılıc, A.M 2002, Parlak, 2006). According to the field studies, the intrusive rocks such as acidic silts, monzonites and other granitoid rocks are folded together with Yoncayolu-Keban metamorphics. The folded

structure of the rock units causing misobservations of older units to overlaying younger rock units. The lower part of the Keban Yoncayolu metamorphics are dominated by gneisses and amphibolitschist, on the other hand middle levels are slightly less metamorphosed, micashists and calchists are main rock types. The metamorhic rocks are totally altered (Fig. 1) at the study area causing an in-stu enrichement of Iron, Aluminum and other elements. The Iron and Aluminium enriched bauxite nodules can be observed in various localities within the study field (Fig. 1.). The altered metamorphic rock units have an area of approximately 20 km^2.

In order to determine the REE a detailed XRD analysis was performed According to the XRD analysis, it is probable that the enrichment of REE is due to either hydrothermal or a supergene process. Some of the detected minerals in XRD studies suggest some Ce bearing (e.g. fluocerite) minerals can be found besides aluminum bearing diaspore and iron bearing hematite minerals the investigation area.

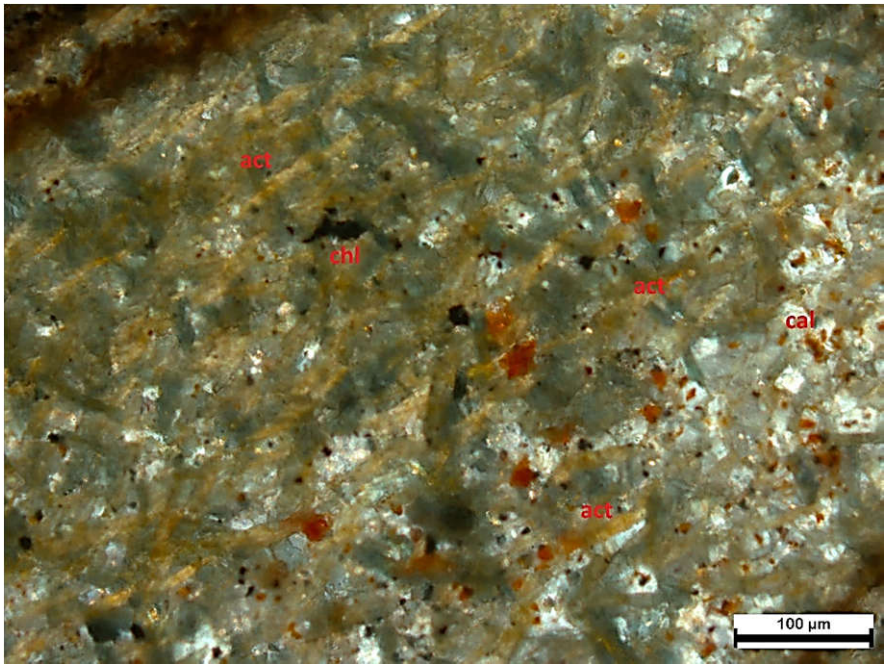

Fig. 2. Thin Section Image of a Metamorphic Sample (Xpl).

In order to determine the REE a detailed XRD analysis was performed According to the XRD analysis, it is probable that the enrichment of REE is due to either hydrothermal or a supergene process. Some of the detected minerals in XRD studies suggest some Ce bearing (e.g. fluocerite) minerals can be found besides aluminum bearing diaspore and iron bearing hematite minerals the investigation area.

Some samples are also enriched in Titanium. All of the samples have an evident depletion in mobile elements such as Na, Ca and Mg. This depletion of mobile elements and enrichment of immobile elements are were also correlated with the general behaviour of High field strength elements (HFSE) such as REE (Table 1). The enrichment of the immobile elements are in linear correlation with alteration strength.

Table 1. SiO_2, Al_2O_3 and Fe_2O_3 values and REE, Pb and Zn contents of the samples.

Elements	Values (ppm)		Elements	Values (%)	
REE	min	278.3	SiO_2	min	4.3
	avg	498.3		avg	32.3
	max	732		max	52.5
Pb	min	8.7	Al_2O_3	min	1.97
	avg	435		avg	20.2
	max	2576		max	51.5
	min	74.4		min	9.49

Zn	avg	554	Fe_2O_3	avg	34.4
	max	2800		max	80.1

Financial support of this study is provided by The Scientific and Technological Research Council of Turkey (TÜBİTAK) Project Number: 114Y646, Principal Investigator of this project is Prof. Dr. M. Sezai Kırıkoğlu.

References

Parlak, O. Petrology of Neotethyan ophiolites in Turkey: distinct magma generations and their tectonic significance. 2006.

Yümün, Z. Ü and Kılıç, A. M. 2002. Kamandağı ile Camdere Köyü Arasının Stratigrafisi (Göksun-K.Maraş),Cumhuriyet Üniversitesi Mühendislik Fakültesi Dergisi. 2002. Seri A Yerbilimleri Volume 2, pp. 193-202.

NEW DATA ON ISOTOPIC AND ELEMENTAL COMPOSITION OF NOBLE GASES AND MAJOR VOLATILE COMPONENTS IN ROCKS OF THE SEBLYAVR ALKALINE-ULTRABASIC MASSIF, KOLA PENINSULA

***Buikin A.I.*[1], *Verchovsky A.B.*[2], *Sorokhtina N.V.*[1]**

[1]*Vernadsky Institute of Geochemistry and Analytical Chemistry, Russian Academy of Sciences, Kosygina 19, Moscow, 119991 Russia, bouikine@mail.ru*

[2]*The Open University, Milton Keynes, United Kingdom*

The Seblyavr carbonatite alkali-ultramafic massif is located in the NW part of the Kola Peninsula. The massif was intruded during Paleozoic time and connected with plume magmatism; the relevant mantle-lithospheric geodynamic activities of Kola peninsula in Devon is confirmed by numerous geological and isotopic data (Arzamastsev et al., 2008; Ernst, Bell, 2010; Zhirov, 2015). According to geophysical data, the Seblyavr is the deepest massif among Devonian carbonatite intrusions (Arzamastsev et al., 2001). The massif comprises (from early to late types of rocks) of olivinites, pyroxenites, ijolites, different types of phoscorites and associated calcite carbonatites, dolomite and ankerite carbonatites. The earlier types of magmatic rocks are intensely altered by the later carbonatitic melts. Autometasomatic apatite-phlogopite-diopside and nepheline-diopside rocks were formed in the contact zones of the earlier magmatic rocks and carbonatites.

The RFA analyses (Table) of rocks demonstrate that the altered pyroxenites and ijolites are characterized by a high content of K_2O and CaO in comparison with the less altered samples (Balaganskaya et al., 2007). They also show relatively high loss on ignition, which should point to a high content of CO_2 and/or H_2O in the samples. The calcite carbonatites generally consist of a coarse-grained calcite up to 80 vol. % and termed soviet (Fig. 1) (Woolley, Kempe, 1989). The calcite and dolomite carbonatites are characterized by low K_2O contents.

Table. The content of some components in Seblyavr massif rocks, wt. %.

Sample	Rock	K_2O	CaO	Ignition
Sb1-97-23	pyroxenite	4.72	14.21	3.46
Sb1-97-47		2.58	27.28	13.79
Sbl-98-45		2.54	15.73	6.71
Data from literature	pyroxenite *	0.98-1.05	17.3-19.33	0.37-1.03
Sbl-98-25	ijolite	0.81	25.93	3.27
Sbl-98-74	calcite carbonatite	0.33	52.44	34.38
Sb1-97-11		0.11	38.83	54.11
Sbl-97-13		0.04	55.37	40.77
Data from literature	calcite carbonatite*	0.31-0.44	48.06-48.26	na
Sb1-96-22	dolomite carbonatite	1.54	27.66	27.01
Data from literature	dolomite carbonatite*	0.06	27.94	na

* - data from Balaganskaya et al. (2007); na - not analyzed.

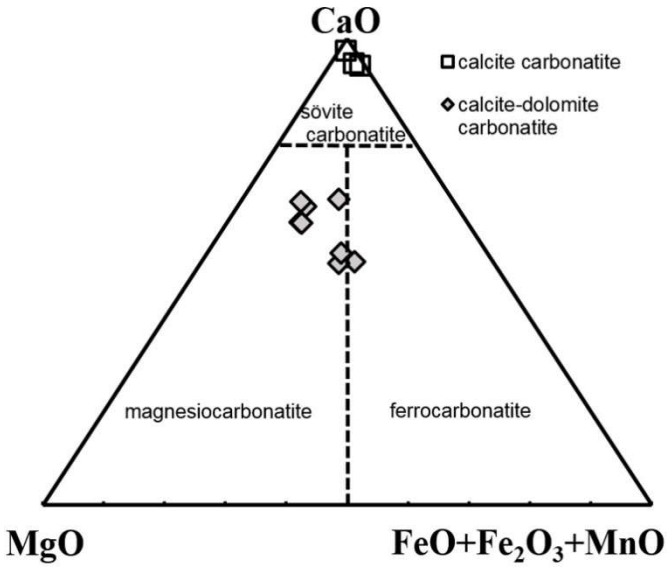

Fig. 1. Classification diagram of carbonatites in terms of CaO-MgO-(FeO + Fe203 + MnO) (wt. %) by (Woolley, Kempe, 1989). The data plotted are for calcite carbonatites (№ Sbl-97-11, Sbl-97-13, Sbl-98-74), dolomite and dolomite-ankerite carbonatites (№ Sbl-95-23, Sbl-95-25, Sbl-95-135, Sbl-95-141, Sbl-95-144, Sbl-95-232, Sbl-96-22, Sbl-96-24), including contact zone with phoscorites.

In order to better understand the sources and evolution of fluid phase during formation of the different stage rocks of the Seblyavr massif we have studied isotopic compositions and elemental ratios of Ar, N_2, He and CO_2 in mineral separates from pyroxenites (Sbl97-23, Sbl97-47, Sbl98-45, Sbl97-5), ijolites (Sbl98-25), early calcite carbonatites (Sbl97-11; Sbl97-13, Sbl98-74) and late dolomite carbonatite (Sbl96-22). The gases were extracted by stepwise crushing (Buikin et al., 2017a); their concentrations and isotope compositions were analyzed at high sensitivity Finnesse mass-spectrometric complex (The Open University, Milton Keynes, UK), the technique is described in Verchovsky et al. (2002).

The data show that ultrabasic and alkaline-ultrabasic rocks, representing the earlier stages of the massif formation, contain 1-2 orders of magnitude higher helium concentrations than the later carbonatites $((4...13)\times10^{-5}$ cm^3 STP/g and $(0.1...0.4)\times10^{-5}$ cm^3 STP/g, respectively). It could be explained in terms of preferential post magmatic He diffusion loss from calcites, which was previously observed in Guli massif carbonatites (Buikin et al., 2017b). Really, the noble gases diffusion constants in calcite are much higher than in silicates (Baxter 2010). This could be the reason why the pyroxenes contain 1-2 orders of magnitude more mantle helium than calcites. Contrary to helium, the CO_2 concentrations are 5-20 times higher in carbonatites in comparison to ultramafic rocks, which could point to increasing of CO_2 content at the transition from the ultrabasic to the carbonatite stage of formation of the massif. An exception is the feldspar from ijolite 98-25, in which the CO_2 content (1262 mcg/g) is much higher than in calcites from carbonatites. Nitrogen concentrations are generally higher in calcites (383 – 1175 ng/g) than in silica minerals (94 – 294 ng/g). Argon content varies from 0.4×10^{-5} to 2.0×10^{-5} cm^3 STP/g in all rocks/minerals independently on their origin.

Fig. 2 shows C/N and C/Ar ratios in crushing steps of mineral separates. One can observe broad ranges of the ratios – much wider for calcites than for pyroxenes. Another observation: calcite separates form trend which differs from that for pyroxenes. Moreover pyroxenes from ijolite and calcite carbonatite form a separate trend from that for pyroxenes from pyroxenites the former is between the latter and calcites' trend. It is interesting to note that experimental points for calcites form a fractionation trend similar to that observed for MORB glasses (see, for example, Cartigny et al., 2001; Buikin et al., 2018a). The steeper Px-trend most probably could be explained by the addition of an *in situ* radiogenic Ar from mica and/or amphibole impurities inside the Px-separates which are especially abundant in pyroxenes from pyroxenites (more explanations see in Buikin et al., 2018b).

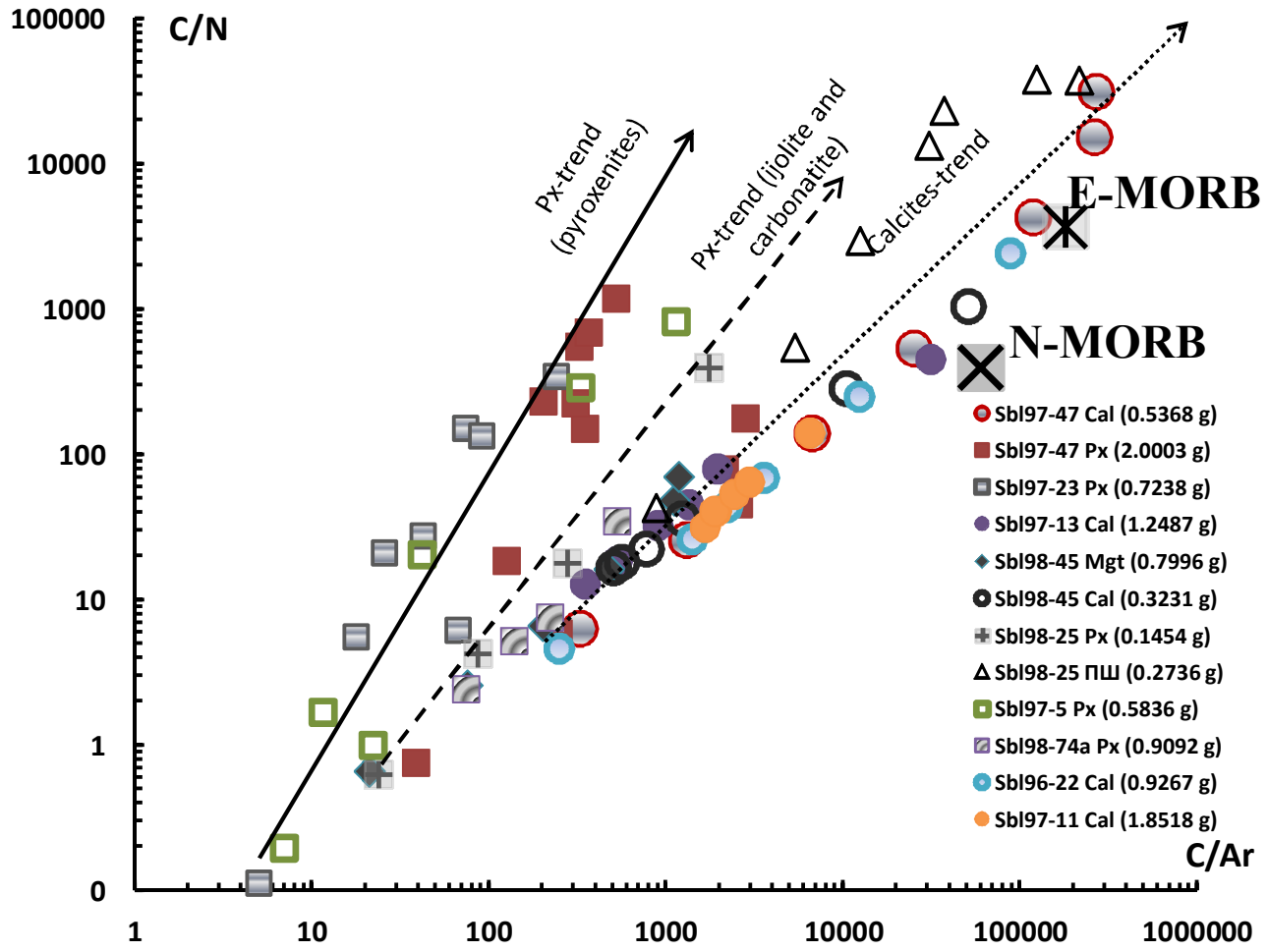

Fig. 2. Co-variations of C/N and C/Ar ratios in crushing steps of mineral separates selected from the rocks of different stages of Seblyavr massif formation.

Independently of the rock type and concentrations of nitrogen its isotopic composition in the samples differ from the MORB-source mantle, and varies in the range for $\delta^{15}N$ from -0.7 to +11 ‰, indicating the presence of subducted organogenic sedimentary nitrogen in the fluid source. The nitrogen-argon isotope systematic points to the presence of at least two generations of fluid inclusions in the samples: the first one carrying essentially mantle gases and the second one – representing a mixture of mantle and atmospheric gases in different proportions. The most likely agent to introduce atmospheric noble gases into the fluid source – the high temperature paleo-meteoric waters, which is supported by hydrogen isotopic composition in the fluid inclusions (Buikin et al., 2014).

The work was carried out within the framework of the state task under the project № 0137-2016-0012, analytical part was financially supported by RFBR grant №16-05-00974a.

References

Arzamastsev A.A., Glaznev V.N. Plume-lithosphere interaction in the presence of an ancient sublithospheric mantle keel: an example from the Kola alkaline province // Dokl. Earth Sci. 2008. Vol. 419. № 2. pp. 384-387.

Arzamastsev A.A., Bea F., Glaznev V.N., Arzamastseva L.V., Montero P. Kola alkaline province in the Paleozoic: estimation of the composition of primary mantle melts and magma generation conditions. Ross. Zh. Nauk o Zemle, 2001, vol. 3, №. 1, pp. 1–35.

Balaganskaya E.G., Downes H., Demaiffe D. REE and Sr-Nd isotope compositions of clinopyroxenites, phoscorites and carbonatites of the Seblyavr massif, Kola Peninsula, Russia // Min. Polonica. 2007. V.38. №1. P. 29-44.

Buikin A.I., Verchovsky A.B., Sorokhtina N.V., Kogarko L.N. (2014) Composition and Sources of Volatiles and Noble Gases in Fluid Inclusions in Pyroxenites and Carbonatites of the Seblyavr Massif, Kola Peninsula. Petrology, 22(5), 507–520.

Buikin A.I., Nevinny Yu. A., Kamaleeva A.I., Sevast'yanov V.S., and Kuznetsova O.V. (2017a) Equipment and Newly Developed Methodological Approaches for Isotopic–Geochemical Studying Fluid Phases in Rocks and Minerals. Geochem. Int. 55(1), 1–8.

Buikin A.I., Kogarko L. N., Hopp J., Trieloff M. (2017b) Light Noble Gas Data in Guli Massif Carbonatites Reveal the Subcontinental Lithospheric Mantle as Primary Fluid Source. Geochem. Int. 55(5), 457–464.

Buikin A.I., Verchovsky A.B., Migdisova N.A. (2018a) N-C-Ar-He isotope systematic of the chilled glasses form Bouvet triple junction. Geochem. Int. 56(13), xxx-xxx. In press.

Buikin A.I., Kamaleeva A.I., Sorokhtina N.V. (2018b) On the Separation Efficiency of Entrapped and in Situ Formed Noble Gas Components at Sample Crushing in Vacuum. Geochem. Int. 56(6), 601-607.

Cartigny P., Jendrzejewski N., Pineau F., Petit E., Javoy M. (2001) Volatile (C, N, Ar) variability in MORB and the respective roles of mantle source heterogeneity and degassing: the case of the Southwest Indian Ridge. Earth Planet. Sci. Lett. 194, 241-257.

Ernst R.E. & Bell K. Large igneous provinces (LIPs) and carbonatites // Mineral. Petrol. (2010) 98:55–76.

Verchovsky A.B., Sephton M.A., Wright I.P., Pillinger C.T. (2002) Separation of planetary noble gas carrier from bulk carbon in enstatite chondrites during stepped combustion. Earth Planet. Sci. Lett. 199, 243–255.

Zhirov D.V. Geodynamic Reconstruction of the Palaeozoic Kola Alkaline Large Igneous Province // Alkaline Magmatism of the Earth and related strategic metal deposits (2015) 148-150.

Woolley A.R., Kempe D.R.C. Carbonatites: nomenclature, average chemical compositions, and element distribution // In Carbonatites: Genesis and Evolution (K. Bell, ed.). Chapman & Hall, London, 1989. P.1-14.

GEOCHEMICAL FEATURES OF LATE PALEOZOIC DIKES WITHIN THE SPITSBERGEN ARCHIPELAGO AS A REFLECTION OF GEODYNAMIC CONDITIONS OF THEIR FORMATION

***Burnaeva M.Yu.*[1], *Sirotkin A.N.*[2]**

[1]*FGBU VNIIOkeangeologia, St.Petersburg, burnaevam@mail.ru*

[2]*AO PMGRE, Lomonosov, pechenga-67@yandex.ru*

There are different points of view on the nature of the Devonian Graben formation on the Western Spitsbergen Island. Researchers associate its occurrence with the formation of internal depressions filled with red-colored molassa at the final stages of the Caledonian collision orogeny, or attribute the graben to the epiorogenic rift zone, or they believe that the graben occurrence was due to the processes of intraplatform rifting (Sirotkin, 2010). It is known that tectonic processes are accompanied by characteristic magmatism and are reflected in chemical composition of magmatic bodies (Frolova, Burikova, 1997).

Currently, within the boundaries of the Devonian graben of the Western Spitsbergen Island, detected are over 30 late Paleozoic dikes of basic and ultrabasic composition, present both as separate bodies and in groups. All the dikes show submeridional and meridional strikes that correlate with the direction of graben structures. The dip of the bodies is subvertical and vertical, consistent with the subvertical dip of the axes in zones of the Billefjord (in the east) and the Braybogensky (in the west) deep faults the dikes are connected with. Thickness of the bodies is from 0.3 to 3.5 m at an average of 1.0 m, the revealed length is up to 5 km. Spatially, two groups of the dike rocks may be distinguished, belonging to the eastern and the western wings of the graben, respectively. Dikes of the eastern wing are more numerous and represent picrites, which break through terrigenous rocks of the lower-mid Devonian. In the west, two dikes of picrodolerites occur among the lower Devonian terrigenous deposits and one dike of ankaramites - in pre-Cambrian rocks framing the graben.

Macroscopically, the dikes are composed of fine-grained dense massive and amygdaloid carbonate rocks of dark gray to black color, of porphyric, less often aphiric structure. Most dikes of the eastern wing of the graben contain megacrysts usually represented by olivine, clinopyroxene or Mg-Fe mica; there are bodies with inclusions of deep xenoliths.

TAS diagram shows that compositions of the eastern dikes fall into the field of subalkaline picrites and basalts, and those of the western dikes - into the field of subalkaline basalts and trachybasalts. A feature of the dikes is the low content of silicic acid, which is compensated by high values of volatile components, that is probably due to the phenomena of desilication during contact interaction with the host rocks (Korzhinsky, 1993). The same process can explain the fact that the composition differs from the center to the edges in some eastern dykes. By alkalinity, the eastern dikes refer to potassium and potassium-sodium type, and the western - to sodium one. By the ratio of alumina, the rocks predominantly fall into the field of normal aluminous rocks.

The most important characteristic of rocks is their mineral composition. The main rock-forming minerals are clinopyroxenes, magnesian-ferruginous mica, olivine for the eastern dikes, and plagioclase (labrador), clinopyroxene and modified olivine for the western dikes. Pyroxene is present predominantly in its monoclinic variety. Orthopyroxene occurs as single cases in the composition of xenoliths included in the rock. In the eastern dikes, three varieties of clinopyroxenes occur: megacrysts (I) formed under deep conditions during the protomagmatic stage, phenocrysts (II) and microlites (III) manifested at different stages of rock crystallization. The total mineral content varies from 20 to 60%, of which I and II varieties account for less than 1%. For the phenocrysts and especially the microlites, high contents of aluminum and titanium are characteristic. In the western dikes, clinopyroxene is present both in phenocrysts (I) and in the bulk (II). Pyroxene (I) and (II) often contain sodium and chromium. Ca-Mg-ΣFe diagram shows that the studied compositions are located in the fields of diopside and augite, indicating two trends: calcium and ferruginous. The first is characteristic of pyroxenes III and the marginal zone of pyroxenes II of the eastern dikes. In the western dikes, the entire diversity of compositions corresponds to those of diopside-salite.

Olivine in the eastern dikes occurs in megacrysts and in the composition of xenoliths (I), phenocrysts (II) and in fine grains of the bulk (III); in the western dikes only rare olivine phenocrysts are present. Only olivine I from the western dikes is slightly modified; the remaining varieties of the mineral are completely replaced mainly by chlorite and/or carbonate. Olivine I contains 88-92% of forsterite minal and an admixture of nickel (up to 0.33 mass % NiO). Magnesian-ferruginous mica is common in the eastern dikes while is very rare in the western ones. Mica represents phlogopite and biotite from magnesian to ferruginous. The most magnesian is mica from the megacrysts and from central zones of the phenocrysts of the eastern bodies, and mica from the western dikes (1 grain analyzed). According to the content of titanium, the dike compositions predominantly fall into the fields of titanium-containing and titanium mica, which are characteristic of the potassium and potassium-sodium series of rocks.

Of accessory minerals in the rocks there are apatite, chrome spinels, garnet, ilmenite, tourmaline, moissanite; astrophyllite is rare, analcime is present in the tonsils of the eastern dikes. In the eastern dikes, deep xenoliths of dunites, lherzolites and verlites occur. The material and chemical compositions of the dikes are described in more detail in (Burnaeva, 2011).

The low thickness of the dikes and the high content of volatile components favor the fact that most dikes are almost completely metasomatically modified: chloritized, carbonatized. Isotope studies confirmed the crustal origin of the carbonate (Burnaeva, 2015).

Concerning chondrite (Fig. 1), the dikes show minima in Co, Ni, Cr contents that may be due to the processes of deep fractionation and low degrees of melting; as well as high contents of macro-ion lithophilic (K, Rb, Ba, Sr), high-charge (Sc, Nb, Ce, Hf, Th) and rare earth elements, that indicates the formation of rocks from an enriched magmatic source. The spider diagram shows that the eastern and western dikes have different content of LIL and TR elements, which in combination with different alkalinity may indicate different sources of magma formation. At the same time, the eastern dikes are deeper, formed from magma enriched with crustal component; in the area of their magma generation, probably there was a garnet - a concentrator of heavy rare-earth elements and Y.

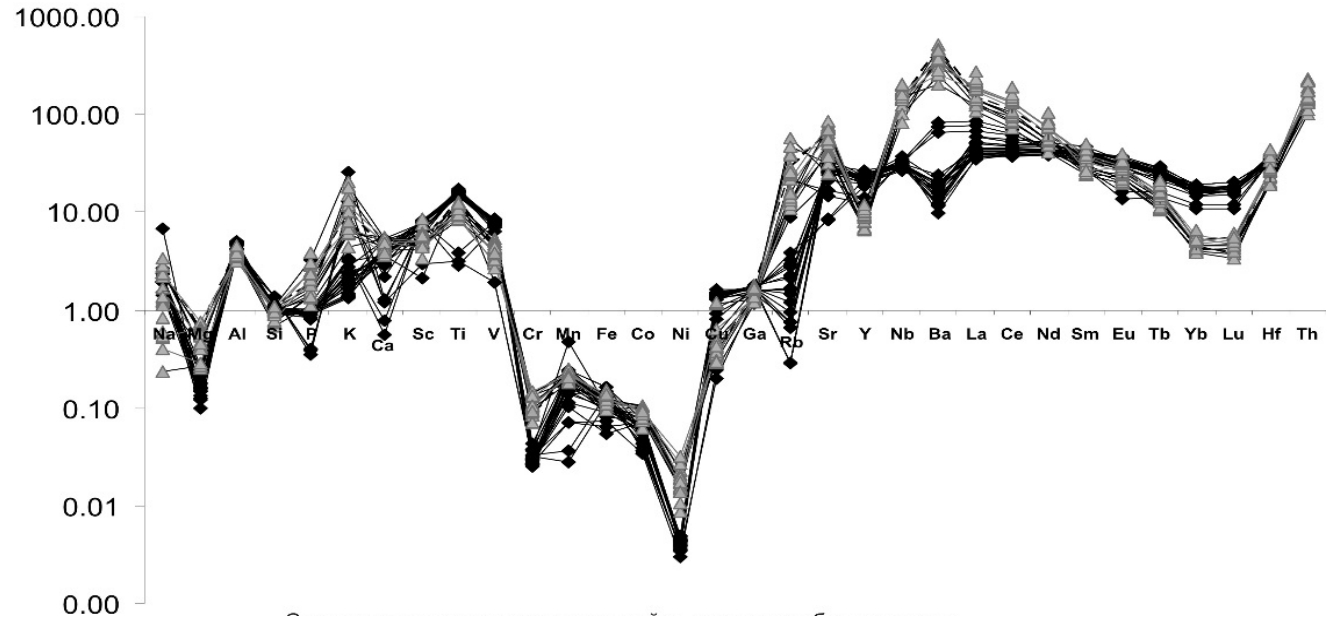

Fig. 1. Late Paleozoic dikes of Western Spitsbergen Isl. (normalized to chondrite) according to (Don L. Anderson, 1983). Composition of the dikes: eastern – gray triangles, western – black rhombuses.

Three eastern dikes are dated by Rb-Sr method (315.0, 326.8 and 334.8 Ma), one of the western dykes is dated in the outcrop where it dissects the lower Devonian terrigenous deposits and is overlain by carbonate deposits of the middle Carboniferous.

The ultrabasic and basaltic composition of the dikes may already testify in favor of stretching processes manifested within the graben during its formation. At the same time, the scarcity of volcanic manifestations indicates the passive development of the rift. The age of the dikes is consistent with the final stage of graben(rift)-formation (Sirotkin, 2010).

The ultrabasic composition, the high content of alkalis, including potassium (for the eastern dikes), the presence of megacrysts of magnesian olivine, clinopyroxene, phlogopite, the presence of deep ultramafic xenoliths in the eastern dikes testify in favor of considerable depths of magmogenesis and mantle enrichment by the crustal component. It should be noted that the above features are more evident in the eastern dikes. Within the graben there are no significant manifestations of acid rocks that are typical for rifts formed according to the epiogenic scenario (Frolova, Burikova, 1997). All of the above can serve as evidence in favor of the thesis of the graben formation under the processes of epiplatform rifting.

References

Burnaeva M.Yu. Towards the Issue about the Source of Carbonic Matter in Paleozoic Ultrabasic Dykes within Spitsbergen Archipelago //“Alkaline Magmatism of the Earth and related strategic metal deposits”. Proceedings XXXII international conference. Apatity, August 7-15, 2015. M:GEOKHI RAS, 2015, pp 28-30.

Don L. Anderson Chemical composition of the mantle // J. of Geoph. Res. 1983. Vol. 88, Issue S01. Pp. B41-B52.

Burnaeva M.Yu. Mineralogical and petrochemical features of Paleozoic picrites of the Spitsbergen archipelago. // Regional geology and metallogeny. 2011. No 48. Pp. 37-49. (in rus)

Korzhinsky D.S. Selected proceedings. Fundamentals of metasomatism and metamagmatism. M. Nauka. 1993. 239 pages. (in rus)

Sirotkin A.N. The Spitsbergen Archipelago: geodynamics of the early-mid Paleozoic development stage of the Barents Sea Plate basement // Tectonics and geodynamics of folded belts and Phanerozoic platforms. Proceedings of XLIII Tectonic Meeting. Vol. 2, M., GEOS, 2010, pp. 254-261. (in rus)

Frolova T.I., Burikova I.A. Magmatic formations of the recent geotectonic environments. - Moscow: PH MGU, 1997. 317 pages. (in rus).

P-T AND FLUID CONDITIONS OF INTERACTION BETWEEN MAFIC XENOLITHES AND PLAGIOGRANITES IN THE RIVER LOTTA AREA OF THE LAPLAND GRANULITE BELT

Butvina V.G., Safonov O.G.

Korzhinskii Institute of Experimental Mineralogy (IEM) RAS, Chernogolovka, butvina@iem.ac.ru

Garnet and orthopyroxene plagiogranites within the Lapland Granulite Belt (LGB) are confined to the northeastern part of the complex, building large areas in the Lotta river and Lovnaozero lake regions and extending westward to northern Norway (Mitrofanov et al., 1974; Kozlov and Kozlova, 1998). They are usually associated with peraluminous granulites (khondalites), showing intrusive contacts with these country rocks. Based on chemical and mineral composition of plagiogranites, which are typical for the S-type granites, the plagiogranites are usually considered as products of anataxis of khondalites at the peak of D3/M3 metamorphism during ~1.91 Ga at temperatures 800-850°C within a wide pressure interval 6.8-9.5 kbar (Mitrofanov et al., 1974; Kozlov, Kozlova, 1998; Mints et al., 2007, 2015; Kaulina et al., 2014). Magmatic origin of the plagiogranites is confirmed by a presence of xenoliths of various lithologies, which are products of earlier metamorphic stages at 1.97-1.96 Ga (e.g. Kaulina et al., 2014). Among the xenolith rocks, mafic rocks are abundant, but are not investigated in detail. Therefore, the object of this study are mafic (amphibolized two pyroxene-plagioclase-quartz rocks) xenoliths in plagiogranites of the river Lotta Area of the Central Zone of the LGB. These xenoliths reflect interaction of mafic rocks with fluids issued by granitic magmas during their crystallization.

Mafic xenoliths are equally grained granoblastic rocks consisting of low-aluminous clinopyroxene (10-15 %, X_{Mg} = 0.56 - 0.58, 2 - 2.5 wt. % Al_2O_3), orthopyroxene (25 - 30 %, X_{Mg} = 0.43 - 0.44, 1-1.3 wt. % Al_2O_3), plagioclase (30-40 %; An_{47-54}), and quartz (5-10 %). Clinopyroxene cores contains thin lamellae of orthopyroxene. Accessory magnetite, ilmenite and pyrrhotite form both separate grains and complex grains. In addition, the rocks contain fluor-apatite and zircon. Ti-bearing (up to 2 wt. % TiO_2) pargasite-edenite amphibole forms elongated grains, rims and coarse-grained symplectites with quartz at the contacts of pyroxenes, magnetite, ilmenite and pyrrhotite with plagioclase. It is mostly developed after orthopyroxene, which is preserved, in this case, as resorbed relics. In contacts with clinopyroxene with plagioclase, amphibole is either absent or forms just thin rims. Thus, the process of amphibolization can be represented by the following schematic reaction Opx + Ilm + Mt + Pl + H_2O = Amph ± Qtz, where clinopyroxene participates just indirectly. Amphibole formation is locally accompanied by the biotite, as well as the formation of magnetite ± pyrite along cracks in orthopyroxene suggesting addition of alkali-bearing oxidizing fluids.

Using the TWQ 2.32 software (Berman, 2007), a pressure of 6.0-6.4 kbar was estimated for equilibrium clinopyroxene + orthopyroxene + plagioclase + quartz in non-amphibolized domains of xenoliths (***Table 1***). The temperatures corresponding to this association are 800-860 °C and are within the crystallization temperature range of plagiogranites (Kaulina et al., 2014), as well as peak temperatures of the tectono-thermal stage M2 in the Lapland granulite belt (Mints et al., 2007). The amphibole-plagioclase equilibrium (Blundy, Holland, 1990) recorded the temperatures of the process of amphibolization of xenoliths 740-780 °C at a pressure of 5.0-5.5 kbar (***Table 2***). Based on certain thermodynamic conditions for the formation of the main xenoliths in the Lotta region of LGB, we can confidently confirm the assumption that the formation of plagiogranite magmas probably occurred at depths of the order of 25-30 km. As they uplifted, they captured a variety of xenoliths (Kozlov, Kozlova, 1998). The results of new thermobarometric studies, data on fluid inclusions and isotope data for carbon in these rocks confirmed these conclusions (Safonov et al., 2017).

Conclusions. Using the TWQ 2.32 software package (Berman, 2007), a pressure of 6.0-6.4 kbar was estimated for clinopyroxene + orthopyroxene + plagioclase + quartz equilibrium in non-amphibolized sections of xenoliths.

Table 1. P-T conditions for the equilibrium clinopyroxene + orthopyroxene + plagioclase + quartz in non-amphibolized domains of xenoliths estimated using the TWQ 2.32 software (Berman, 2007).

Pl,№№	Opx,№№	Cpx,№№	T,C	P, kb
40*	16	9	804	6,2
41	18	9	804	6,4
43	20	17	862	6,0
43	21	17	839	6,0
38	29	6	802	6,2
39	29	6	800	6,2

Table 2. Thermodynamic conditions of granulite amphibolization process determined by means of amphibole-plagioclase equilibrium (Blundy, Holland, 1990).

Amph,№№	24c	25r	27c	28r	35r	42c	43r
SiO2	42,49	42,16	42,99	42,38	43,44	43,26	42,86
TiO2	1,71	1,32	1,88	1,71	0,80	1,34	1,57
Al_2O_3	11,65	11,67	11,94	11,97	11,82	11,14	11,52
FeO	20,59	20,34	20,37	20,98	19,67	19,90	20,81
MgO	8,39	8,50	8,26	8,34	9,31	8,91	8,40
MnO	0,38	0,28	0,35	0,13	0,33	0,31	0,29
CaO	12,24	12,19	11,09	12,23	12,14	12,46	12,11
Na_2O	1,47	1,35	1,44	1,14	1,16	1,56	1,21
K_2O	1,25	1,32	1,29	0,95	0,99	1,24	1,10
F	0,00	0,00	0,00	0,00	0,00	0,00	0,00
Cl	0,00	0,00	0,00	0,00	0,00	0,00	0,00
Sum	100,17	99,13	99,61	99,83	99,66	100,12	99,87
Pl							
xAb	0,53	0,53	0,53	0,53	0,53	0,53	0,53
xAn	0,47	0,47	0,47	0,47	0,47	0,47	0,47
T,°C	**766**	**756**	**780**	**763**	**746**	**740**	**760**
P, kbar	**5,0**	**5,3**	**4,9**	**5,3**	**5,5**	**5,2**	**5,0**

Temperatures corresponding to the association, make 800-860°C and are within the crystallization temperature range plagiogranites (Kaulina et al., 2014), as well as peak temperatures of the tectono-metamorphic stage D2/M2 in the Lapland granulite belt (Mints et al., 2007). Amphibole-plagioclase equilibrium (Blundy, Holland, 1990) recorded the temperatures of the process of amphibolization of xenoliths 740-780 °C at a pressure of 5.0-5.5 kbar. Variations in the composition of the amphibole are in the direction of lowering the temperature. It was probably connected with the interaction of a substantially aqueous fluid from the cooling plagiogranite magma with xenoliths as they were captured and uplifted. Indeed, the xenoliths are intersected by veins of plagiogranite composition. The abundance of water-salt (12-20 % NaCl eq.) inclusions and a subordinate amount of carbonic inclusions in minerals of plagiogranites (Safonov et al., 2017) confirm this assumption.

This work was supported by the Russian Foundation for Basic Research (grant 16-05-00266).

References

Berman R.G. WinTWQ (version 2.3): A software package for performing internally-consistent thermobarometric calculations // Geological Survey of Canada Open File 5462, 2007.

Blundy J.D., Holland T.J.B. Calcic amphibole equilibria and a new amphibole-plagioclase geothermometer // Contribution to Mineralogy and Petrology, 1990. Vol. 104, pp. 208-224.

Kaulina T.V., Nerovich L.I., Bayanova T.B., Yapaskurt V.O. Sequence of geological processes in the Central and North-Eastern part of the Lapland granulite belt: isotope-geochemical data on zircon and the results of geological-petrological studies // Geochemistry, 2014. Vol. 7, pp. 625-645.

Kozlov N.E., Kozlova N.E. On the Genesis of Pomegranate Plagiogranitoids of the Lapland Granulite Belt // Bulletin of the Murmansk State Technical University, 1998. Vol. 1, pp. 43-52.

Mints M.V., Kaulina T.V., Konilov A.N., Krotov A.V., Stupak V.M. The thermal and geodynamic evolution of the Lapland granulite belt: Implications for thermal structure of the lower crust during granulite-facies metamorphism // Gondwana Research, 2007. Vol. 12, pp. 252-267.

Mitrofanov F.P., Kravtsova E.I., Manuilova M.M. Early Precambrian granitoid formations. 1974. Moscow, Science, 292 p.

Safonov O.G., Reutsky V.N., Golunova M.A., Butvina V.G., Yapaskurt V.O., Varlamov D.A., Shcherbakov V.D., Van Rinnen D.D. Isotopic characteristics of carbon as an indicator of the source of high-temperature granitoids in granulite complexes // "Geodynamics of the Early Precambrian: Similarity and Differences with the Phanerozoic", Proceedings of the Conference, Petrozavodsk, May 29-31, 2017, pp. 216-218.

IN SITU EXPERIMENTAL STUDY OF BASALT – COH SYSTEM AT THE UPPER MANTLE CONDITIONS

Chertkova N.V.*, *Ohfuji H.*, *Irifune T.

Ehime University, Geodynamics Research Center, Matsuyama, Japan, chertkova.nadezda.sj@ehime-u.ac.jp

Experimental investigation of the complex systems involving silicate and C-O-H components at simultaneous high temperatures and high pressures is a challenging task, since volatile components can easily change aggregate state and escape upon quenching and opening of the sample chamber. Recent technological advances provide an opportunity to observe and analyze such systems *in situ*, directly at the pressure and temperature conditions of interest (e.g., Chertkova and Yamashita, 2015; Thompson et al., 2016; Masotta and Keppler, 2017; Mysen, 2018).

In the present work, we applied a lever-type diamond anvil cell with an external heater to study interaction between basaltic (MORB) and C-O-H components at the conditions of cold subduction zones. The starting material was first compressed in the diamond anvil cell, which was placed under the microscope, connected to a highly confocal Photon Design Raman system, and then heated to temperatures exceeding 900°C. Visual observations of the sample and Raman measurements were performed *in situ* during heating (Fig. 1).

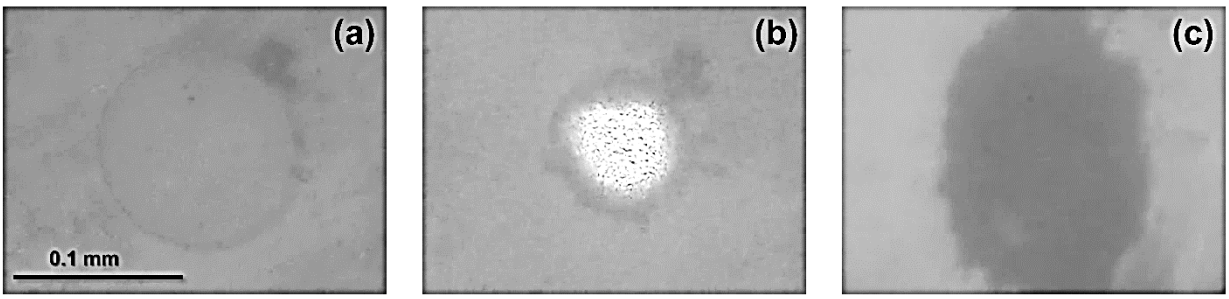

Fig. 1. Microphotographs of the sample (80 wt.% basalt + 20 wt.% $C_2H_2O_4$), taken during experiment in the diamond anvil cell: (a) compressed mixture at 25 °C and 0.8 GPa; (b) decomposition of oxalic acid, 395 °C and 4.0 GPa; (c) coexistence of opaque polymeric phase and silicate phases at 900 °C and 4.7 GPa.

In the chosen basalt – $C_2H_2O_4$ system, an appearance of polymeric phase with the dominant *G* bond-stretching mode and *D* breathing mode in the Raman spectra, common for carbon materials (Ferrari and Robertson, 2000), was detected at temperatures above 600 °C and pressures above 4 GPa along with the silicate minerals (Fig. 1c). This observation indicates that $C_2H_2O_4$ compound is not suitable as a fluid source at the mentioned experimental conditions. In the future work, water-rich compounds with lower carbon content will be used for experiments, modeling fluid and rock interaction in the geological settings of subduction zones.

References

Chertkova N., Yamashita S. In situ spectroscopic study of water speciation in the depolymerized $Na_2Si_2O_5$ melt// Chem. Geol. 2015. Vol. 409 pp.149–156.

Thompson E.C., Campbell A.J., Liu Z. In-situ infrared spectroscopic studies of hydroxyl in amphiboles at high pressure // Am. Min. 2016. Vol. 101. Iss. 3. Pp.706–12.

Masotta M., Keppler H. A new hydrothermal moissanite cell apparatus for optical in-situ observations at high pressure and high temperature, with applications to bubble nucleation in silicate melts// Am. Min. 2017. Vol. 102 Iss. 10 pp.2022–2031.

Mysen B. Mass transfer in the Earth's interior: fluid-melt interaction in aluminosilicate–C–O–H–N systems at high pressure and temperature under oxidizing conditions// PEPS. 2018. Vol. 5. Iss. 1. Pp. 6.

Ferrari A.C., Robertson J. Interpretation of Raman spectra of disordered and amorphous carbon// Phys. Rev. 2000. Vol. 61 Iss. 20 pp.14095–14107.

PETROLOGICAL AND VOLATILE EVOLUTION OF THE NORRA KÄRR LANTHANOID (REE) DEPOSIT

***Dobrzański A.*[1], *Walcott R.*[2], *Kirstein L.*[1], *Schröder C.*[3], *Butler I.*[1], *Ngwenya B.*[1]**

[1]*School of Geosciences, The Grant Institute, Kings Buildings, Edinburgh, UK, EH9 3FE, a.j.dobrzanski@ed.ac.uk*

[2]*Department of Natural Sciences, National Museums Scotland, Edinburgh, UK, EH1 1JF*

[3]*Biological and Environmental Sciences, University of Stirling, Stirling FK9 4LA, UK*

Lanthanoids or 'Rare Earths' are critical to a range of advanced technologies; however, the formation processes that result in concentrated economic deposits of lanthanoids remain enigmatic. This research has focused on the evolution of the Norra Kärr syenite which has measured ore grades up to 0.61% TREO (of which 52.6% are HREO) and an indicated resource of 31.1 Mt at 0.4% TREO cut-off grade (Saxon et al. 2015) making it mainland Europe's largest lanthanoid resource. Core samples and analytical data kindly supplied by Tasman Metals Ltd. has provided an unrivalled opportunity to further investigate the evolution of this complex and to build on the previous studies of Sjöqvist et al. (2013) and Atanasova et al. (2017). Using a combination of detailed petrographic, geochemical, and structural data this study has shown that the Norra Kärr complex represents two separate intrusive phases, each with its own petrological and volatile fractionation sequence which in turn influences the evolution of the lanthanoid concentrations within specific minerals.

Mössbauer analysis was used to determine the Fe^{2+}/Fe^{3+} ratios of minerals within bulk-rock powders from different lithologies within Norra Kärr. This analysis revealed that the two intrusive phases have distinct redox properties. The first intrusive phase comprises of the ore bearing magma which was oxidised and rich in Fe^{3+}. The second intrusive phase was non-ore bearing and more reduced than the first phase with minerals from included enclaves being the richest in Fe^{2+}.

The differences between the two intrusive phases has been further highlighted by petrographic work and electronprobe (EPMA) analysis. This has shown that the overall crystallisation sequence of each lithology (aegirines followed by zirconosilicate phases and finally feldspars) also contains separate trends in volatile and lanthanoid evolution. These trends can be picked out using data from amphiboles, biotites and zirconosilicates. Previous modelling work by Andersen et al. (2013) has shown that the order in which these phases form in an alkaline magma is controlled by the relative activity of a given volatile (F^-, Cl^-, OH^-) in the magma. Future work will involve modelling the relationship between the volatile and lanthanoid trends and synthesising the available data into a holistic ore-deposit model for exploration purposes.

References

Andersen, T., Erambert, M., Larsen, A. O., & Selbekk, R. S. (2013). Petrology of nepheline syenite pegmatites in the Oslo Rift, Norway: Zr and Ti mineral assemblages in miaskitic and agpaitic pegmatites in the Larvik Plutonic Complex. Mineralogia, 44(3-4), 61-98.

Atanasova, P., Marks, M. A. W., Heinig, T., Krause, J., Gutzmer, J., & Markl, G. (2017). Distinguishing Magmatic and Metamorphic Processes in Peralkaline Rocks of the Norra Kärr Complex (Southern Sweden) Using Textural and Compositional Variations of Clinopyroxene and Eudialyte-group Minerals. Journal of Petrology, 58(2), 361-384.

Saxon, M., Leijd, M., Forrester, K., and Berg, J., (2015) British Columbia Geological Survey Paper 2015-3, pp. 97-107

Sjöqvist, A. S., Cornell, D. H., Andersen, T., Erambert, M., Ek, M., & Leijd, M. (2013). Three compositional varieties of rare-earth element ore: eudialyte-group minerals from the Norra Kärr Alkaline Complex, Southern Sweden. Minerals, 3(1), 94-120.

COMPOSITION AND GENESIS OF SILICATE-CARBONATE ROCKS OF CHAROITE COMPLEX

Dokuchits E.Yu.[1], Vladykin N.V.[2]

[1]Institute of Geochemistry SB RAS, Irkutsk, Russia, esfor@rambler.ru

[2]Institute of Geochemistry SB RAS, Irkutsk, Russia, vlad@igc.irk.ru

Charoite complex in the Murun geological massif is located in the Chara River area, in border of Irkutsk region and Yakutia. It was formed by evolution from alkaline ultrabasic to alkaline granite melts by differentiation and layering of a potassic alkaline magma.

In this work silicate-carbonate rocks of charoite complex are described. Charoite complex is formed by microclinites, microcline-pyroxene rocks, microcline-pyroxene-quartz-calcite rocks, charoite rocks and carbonatites. These rocks originated in a silicate and silicate-carbonate layering process of residual magmaof the Murun massif. Double correlation plots of petrogenic elements of these rocks are plotted and described.

Composition and genesis

The Murun alkaline complex is the largest complex of potassic agpaitic rocks, which is located in north-west part of Aldan shield (the border of Irkutsk region and Yakutia). This complex is one of Mesozoic alkaline complexes of Aldan alkaline province and it doesn't have any analogues in the world. In the Murun massif the entire range of differentiates was found, from K-ultrabasic-alkalic rocks through basic and medium ones to alkali granites and unique calc-silicate rocks (benstonite Ba-Sr carbonatites and charoite rocks). The area of the Murun massif is 150 km^2; its age is about 135 mln years [Dokuchits, 2016].

According to scheme of four stages of magmatism of the Murun massif, silicate-carbonate rocks originated in a silicate and silicate-carbonate layering process of residual magma.

Four stages of magmatism of the Murun massif [Vladykin, 2009]:

1. Early (cumulative) stage: olivine-spinel rocks and zones of olivine-pyroxene-phlogopite-monticellite rocks with melilite. A layered complex of ultrapotassic ultrabasic rocks: Bt-pyroxenites (Ap + Bt + Py), Ol-lamproites (Ol + Bt + Py + Plc + Fsp), K-ijolites (Gr + Bt + Py + Ks), leucite fergusites (Plc + Bt + Py), and shonkinites (Fsp + Bt + Py).

2. Main stage: a layered complex of Plc, Fsp-Ks, Bt-Py-Fsp syenites, quartz syenites, alkali granite dikes and stocks.

3. Volcanic stage: a layered flow of Plc-melaphonolites, leucitites, Plc-lamproites, with patches of their tuff lavas and tuff breccias. Dike complex: Plc-tinguaites, richterite-sanidine lamproites, trachyte porphyries, syenite porphyries, and eudialyte lujavrites.

4. Late stage: a banded layered complex of potassic calc-silicate rocks: potassic microsparites, Qu-Kc-Fsp-Py rocks with schlieren and veins of carbonatites (benstonite, calcite, and quartz-calcite)

and charoite rocks. The most recent formations in the massif are hydrothermal veins and zones with ore components: U, Th, Au, Ag, Cu, Pb, Zn, Mo, Ti, and Nb.

Charoite complex has area about 10 km^2; it's formed by microclinites, microcline-pyroxene rocks, microcline-pyroxene-quartz-calcite rocks, charoite rocks and carbonatites. Microclinites are leucocratic fine-grained rocks. As well as microcline, these rocks may contain spherolite aggregates of tinaksite and pyroxene (not more than 1-3%). All these rocks are close together in time of origin; the earliest rock of them is microclinite.

There are three types of carbonatites in charoite complex. *Benstonite carbonatites* are the earliest carbonatite type. These carbonatites form geobody 40 m width and more than 1 km length, which cuts earlier microcline-pyroxene rocks. Benstonite carbonatites are composed by benstonite, pyroxene, microcline, tinaksite and sulphides. *Calcite carbonatites* form small dykes in different parts of charoite complex. They are composed by calcite, pyroxene and microcline. Accessory minerals of these type of carbonatites are tinaksite, titanite, charoite, thorite, dalyite and sulphides. *Quartz-calcite carbonatites* form geobody 3 m width and 20 m length. They are composed by quartz-calcite graphic concretions, in which pypoxene and various sulphides can be found. All varieties of carbonatites are cut by small dykes of charoite rocks [Vladykin, 2016, Vladykin, Tsaruk, 2003].

Double correlation plots of petrogenic elements (fig. 1) show common trends of composition changes from microclinites to pyroxene-concentrated rocks, which is indicative of their magmatic origin.

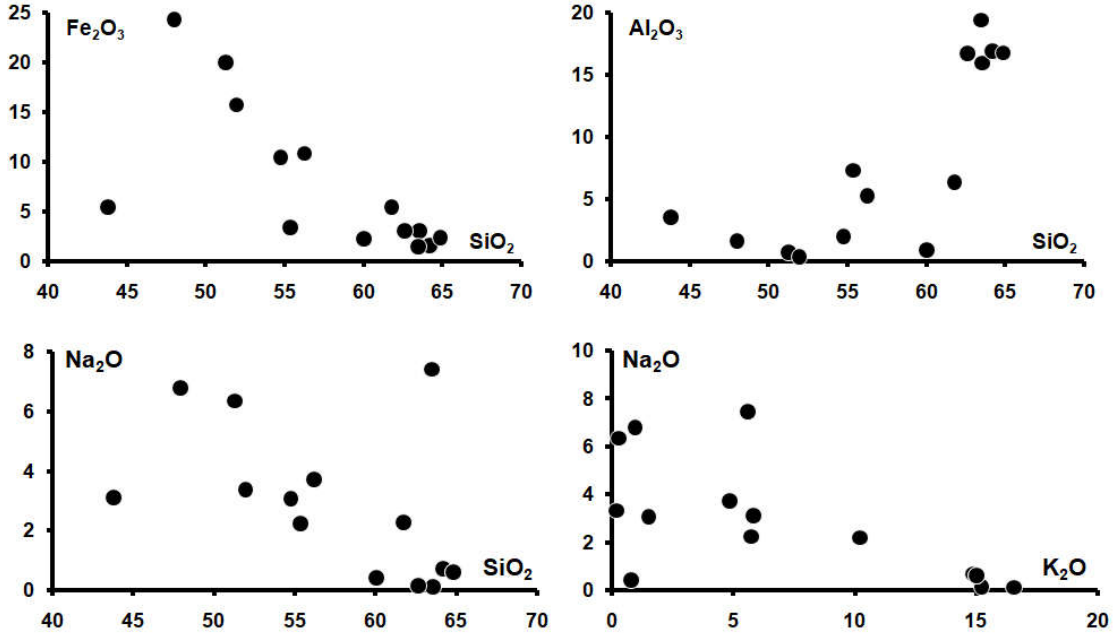

Fig. 1. Double correlation plots of rock-forming elements of microclinites and microcline-pyroxene rocks of charoite complex [Dokuchits, 2018].

Silicate-carbonate rocks are of practical importance because of their hardness (Mohs' hardness is 6-6,5) and good decorative features. On geological and petrographic features showing these rocks have magmatic origin.

The work was supported by the Russian Foundation for Basic Research (grants 18-05-00073 and 17-55-45028).

References

Dokuchits E.Yu. Mineralogical and geochemical features of rocks of charoite complex of Murun massif//Dissertation. Institute of geochemistry SB RAS, Russia, 2016. [in russian].

Dokuchits E.Y., Vladykin N.V. Compositional variations of charoite and its paragenous minerals from charoite rocks // Proceedings of Siberian Department of the Section of Earth Sciences, Russian Academy of Natural Sciences. Geology, Prospecting and Exploration of Ore Deposits. 2016. No. 2 (55). Pp. 51–60. DOI 10.21285/0301-108X-2016-55-2-51-60. [in russian].

Dokuchits E.Yu. Silicate rocks of charoite complex of Murun massif // Natural science issues / № 2, 2018 [in russian].

Vladykin N.V. Potassium alkaline lamproite-carbonatite complexes: petrology, genesis, and ore reserves / Russian Geology and Geophysics 50 (2009) 1119–1128.

Vladykin N.V. Genesis and crystallization of ultramafic-alkaline carbonatite magmas of Siberia: ore potential, mantle sources and relationship with plume activity / Russian Geology and Geophysics 57. 2016. pp 698–712.

Vladykin N.V. Unique Murun massif of ultrabasic agpaitic rocks and carbonatites, their magmatism and genesis // collection of IMGRE "Genetic types of ore deposits", No. 7, 2005, p. 20. [in russian].

Vladykin N.V., Tsaruk I.I. Geology, chemism and genesis of Ba-Sr («benstonite») carbonatites of Murun massif // Geology and geophysics, vol. 44, № 4, 2003, pp. 325-339. [in russian].

ALBITITES FROM DMYTRIVKA (THE OKTRIABSKI MASSIF, UKRAINE) - EVIDENCE OF FLUID-ROCK INTERACTION TRIGGERED BY FENITIZATION PROCESSES

Dumańska-Słowik M.[1], Powolny T.[1], Heflik W.[1], Sikorska M.[2], Natkaniec-Nowak L.[1], Giro L.[2]

[1]Department of Mineralogy, Petrography and Geochemistry, Faculty of Geology, Geophysics and Environmental Protection, AGH - University of Science and Technology, 30 Mickiewicz Av., Krakow 30-059, Poland; e-mail: dumanska@agh.edu.pl

[2]Polish Geological Institute - National Research Institute, 4 Rakowiecka St., 00-975 Warsaw, Poland

Albitites represent very uncommon rocks of a quite simple mineralogy, which are almost entirely composed of albite with subordinate amounts of quartz, K-feldspar, mica, apatite, zircon, and titanite (e.g. Castorina et al., 2006; Mohammad et al., 2007). The possible origin proposed for these rocks include: (1) metasomatism of granitic rocks by hydrothermal fluids (Cathelineau, 1988), (2) direct precipitation from solution (Jahnson and Harlow, 1999), and (3) crystallization from sodium enriched magma (Schwartz, 1992). Hence, they are found in both magmatic and hydrothermal geological settings. Albitites from Dmytrivka form vein- like structure within pyroxene fenites. They occur in a near vicinity of granitoids, pyroxenites, and mariupolites (albite-aegirine nepheline syenite) belonging to the Oktiabrski Massif. According to Krivdik (2017), albitites were formed as a result of metasomatic alteration of host fenites. Albitite of Dmytrivka are mostly composed of albite forming either larger non-turbid euhedral plates, or fine-grained (up to 0.3 mm), non-turbid crystals which are characterized by anhedral shape and straight grain boundaries exhibiting interfacial angles of 120° (triple-point junctions). All forms of albite show characteristic red CL colours activated by Fe^{3+} (White et al., 1986; Götze 2000). Locally, poorly-laminated texture, characterized by subparallel arrangement of tabular albite crystals, is observed. Sodium plagioclase is accompanied by relatively larger (up to 1.0 mm) cross-hatched microcline, acicular pyroxene (aegirine), and zircon. The latter forms large, bipyramidal-like crystals with sizes of 0.1-1.0 mm irregularly scattered within the rocks. The vast majority of K-feldspars exhibit pink, brown-red, or brown CL colours attributed to Fe^{3+} impurities occupying Al^{3+} tetrahedral sites in feldspar (White et al., 1986; Götze, 2000). Only a few of them luminescence in grey-blue and blue which is caused by emission centres of Al-O^--Ti (Kayama et al., 2010) and Al-O^--Al (Götze, 2000). Zircon crystals are strongly fractured and show irregular domains with yellow and dark navy-blue cathodoluminescence colours. The dominant yellow CL is attributed to extrinsic defects such as Dy^{3+} and Tb^{3+} (Götze, 2000;Gorobets and Rogojine, 2002; Blanc et al., 2000;Gaft et al., 2005), whereas dark blue CL is mainly caused by intrinsic defects in the zircon structure (Gorobets and Rogojine, 2002;Gaft et al., 2005). The relatively large size and distinctive shape of zircon crystals may imply their hydrothermal origin. On the other hand, strong fracturing

indicate that they might be also overprinted by strong deuteric alteration (Yang et al., 2013). Chlorite, ilmenite-pyrophanite minerals occur as accessory phases of albitites.

CL observations of albitites show that all feldspars were strongly affected by fluid-rock interaction triggered by migration of fenitizing solutions enriched in Fe^{3+} (Marshall, 1988; Finch and Klein, 1999). Moreover, the local presence of granoblastic texture, reflected by the presence of polygonal albite crystals, indicate subsolidus textural maturation of these rocks (Suikkanen and Rämö, 2017) which is consistent with CL observations. Nevertheless, the metasomatic origin of these rocks suggested by Krivdik (2017) still demand further investigations. The reason is that no traces of typical replacement of K-feldspar by albite were observed during CL and microscopic observations, although pervasive fluid overprint seems to be undisputed.

This study was supported by Grant No. 11.11.140.158 (AGH University of Science and Technology, Krakow).

References

Blanc P., Baumer A., Cesbron F., Ohnenstetter D., Panczer G., Remond G. Systematic Cathodoluminescence Spectral Analysis of Synthetic Doped Minerals. In: Cathodoluminescence in Geosciences (Eds. Pagel M., Barbin V., Blanc P., Ohnenstetter D.). 2000. pp.127-160.

Castorina, F., Masi, U., Padalino, G., and Palomba, M. Constraints from geochemistry and Sr-Nd isotopes for the origin of albitite deposits from Central Sardinia (Italy) // Miner Depos.2006. Vol. 41 pp. 323–338.

Cathelineau, M. Accessory mineral alteration in peraluminous granites at the hydrothermal stage: A review // RendSoc Ital Mineral Petrol. 1988. Vol 43. Pp. 499–508.

Finch A.A., Klein J. The causes and petrological significance of cathodoluminescence emission from alkali feldspars // Contrib Mineral Petrol.1999. Vol.135 pp. 234-243.

GaftM.,.Reisfeld R.,PanczerG. Luminescence Spectroscopy of Minerals and Materials. Berlin, Heidelberg, New York: Springer-Verlag. 2005. 356 p.

Gorobets, B.S., Rogojine, A.A. Luminescent spectra of minerals. Moscow.2002. 300 p.

Götze J. Cathodoluminescence microscopy and spectroscopy in applied mineralogy. Freiberg: Forschungshefte. 2000. 128p.

Johnson, C.A., and Harlow, G.E. Guatemala jadeitites and albitites were formed by deuterium-rich serpentinizing fluids deep within a subduction zone // Geology.1999.Vol. 27. Pp. 629–632.

Kayama M., Nakano S., Nishido H. Characteristics of emission centers in alkali feldspar:A new approach by using cathodoluminescence spectral deconvolution // Am. Mineral. 2010. Vol. 95. Pp. 1783-1795.

KrivdikS. Apofeniticalbitites of Ukrainian Shield.//Heokhimiya ta rudoutvorennya.2017.Vol. 38 pp. 58-69 [in Ukrainian].

Marshall D.J. Cathodoluminescence of geological materials. Boston. 1988. 146 p.

Mohammad Y., Maekawa H., Lawa F.A.Mineralogy and origin of Mlakawaalbitite from Kurdistan region, northeastern Iraq // Geosphere.2007. Vol.3 No. 6 pp. 624-645.

Schwartz M.O. Geochemical criteria for distinguishing magmatic and metasomatic albite-enrichment in granitoids: examples from Ta-Li granite Yivhun (China) and the Sn-W deposit Tikus (Indonesia) // Miner Depos.1992.Vol. 27 pp. 101–108.

Suikkanen E., Rämö O.T. Metasomatic alkali-feldspar syenites (episyenites) of the Proterozoic Suomenniemi rapakivi granite complex, southeastern Finland // Lithos. 2017. Vol. 294 pp. 1-19.

White W.B., Matsumara M., Linnehan D.G., Furukawa T., Chandrasekhar B.K. Absorption and luminescence of Fe^{3+} in single crystal orthoclase // Am Mineral. 1986. Vol. 71, 1415-1419.

Yang W.B., Niu H.C., Shan Q., Sun W.D., Zhang H., Li N.B., Jiang Y.H., Yu X.Y. Geochemistry of magmatic and hydrothermal zircon from the highly evolved Baerzhe alkaline granite: implications for Zr–REE–Nb mineralization // Miner Depos. 2014. Vol. 49 No. 4. Pp. 451-470.

MINERALS – CONCENTRATORS OF ARSENIC IN NONSULFIDE ENDOGENEOUS PB-ZN-SB ORES IN PELAGONIAN MASSIF, MACEDONIA

***Ermolaeva V.N.*[1,2], *Varlamov D.A.*[1,3], *Chukanov N.V.*[3], *Jančev S.*[4]**

[1]*Institute of Experimental Mineralogy RAS, Chernogolovka, Russia, cvera@mail.ru*

[2]*Vernadsky Institute of Geochemistry and Analytical Chemistry RAS, Moscow, Russia*

[3]*Institute of Problems of Chemical Physics RAS, Chernogolovka, Russia*

[4]*Faculty of Technology and Metallurgy, Saints Cyril and Methodius University, Skopje, Macedonia*

Nonsulfide endogeneous mineral associations with high contents of chalcophile elements are relatively rare. Along with the orogenic zone related to the so called "Mixed Series" of the Pelagonian massif, the well-known examples of such objects are Franklin and Sterling Hill Fe-Zn deposits in New Jersey, USA (Tarr, 1929; Palache, 1929a,b; Wilkerson, 1962), as well as Långban, Nordmark (including Jakobsberg) and Pajsberg (including Harstigen) Fe-Mn deposits in the Bergslagen ore province, Värmland, Sweden (Palache, 1929b; Holtstam, Langhof, 1999), some types of ores of Kombat deposite in Namibia (Innes, Chaplin, 1986; Dunn, 1991).

Metasomatic rocks forming exo-contact aureoles around the Early Paleozoic meta-rhyolite formation and apo-rhyolite schists with dolomite marbles near the village of Nezhilovo (Pelagonian massif, Macedonia – see Barić, 1960) are characterized by high concentrations of chalcophile elements (S, As, Sb, Zn, Pb, Cu). Unlike most polymetallic endogeneous ores, in this object sulphides are practically absent, and chalcophile elements are concentrated in oxysalts – predominantly oxides, silicates, phosphates and arsenates (Chukanov et al., 2015, 2016, 2018; Ermolaeva et al., 2016; Ermolaeva et al., in press; Jančev et al., 2016; Varlamov et al., 2017). We believe, that the absence of sulfides and sulfosalts in these ores is a result of a high barium activity and, as a result, sulfur immobilization in the barite form. The most probable sources of barium in metasomatites of Nezhilovo are post-magmatic fluid related to rhyolites, as well as hydrothermally alterated K feldspar of rhyolites. Another factor which has affected mineral composition of nonsulfide ores of the Pelagonian massif is a relatively high oxygen activity: practically in all minerals of the ores elements of variable valence have the highest oxidation number degree: Fe(III), Mn(III), Mn(IV), Sb(V), As(V).

In this work we studied minerals – concentrators of arsenic in ore-bearing metasomatites of the Pelagonian massif. Electron microprobe analyses were carried out using a Tescan VEGA-II XMU electronic microscope (EDS mode, 20 kV, 400 pA). Data reduction was carried out by means of a modified INCA Energy 450 software package.

As-bearing minerals are present in two types of mineral associations. The **oxide association** contains two main zones. The earlier zone is composed by fine-grained aggregates of Zn-spinels (mainly, gahnite and franklinite, with accessory hetaerolite and zincochromite) and contains minor amounts of Zn-bearing talc, barite and zircon. Another zone (hydrothermally alterated one) contains both Zn-spinels and zincovelesite-6*N*6*S*. The latter forms epitaxial growths on gahnite (Chukanov et al., 2017). The rare and accessory components of this zone are barite, quartz, dolomite, Zn-containing talc, Mn-dominant analogue of plumboferrite, hydroxycalcioroméite and almeidaite. Ferricoronadite forms late veins up to 8 mm thick (Chukanov et al., 2016). As-rich fluorapatite (Fig. 1) forms zonal xenomorphic grains. This mineral is the only concentrator of As in the oxide association and is present there in all zones.

The **oxysalt associations** are mainly composed of silicates, carbonates, barite and tilasite which are present in different proportions and form fine- to medium-grained aggregates. Among arsenates, only tilasite belongs to the main rock-forming minerals. In some rock types its relative content may be more than 50%. Various other arsenates are present as accessory components. Among them, the most important concentrators of arsenic in most studied mineral assemblages are members of the apatite supergroup, namely As-rich fluorapatite and mimetite. Fluorapatite was found in all types of nonsulphide endogenous Pb-Zn-Sb ores. It forms xenomorphic grains and often has complex zoning. Other mempers of the apatite supergroup (As-containing hydroxylapatite, hedyphane) are rare. The content of As in fluorapatite and hydroxilapatite varies in a wide rainge (Table 1), but continuous

isomorphism between these minerals and mimetite is not observed. In particular, boundaries between hydroxilapatite and mimetite in their intergrowths are sharp (Fig. 2).

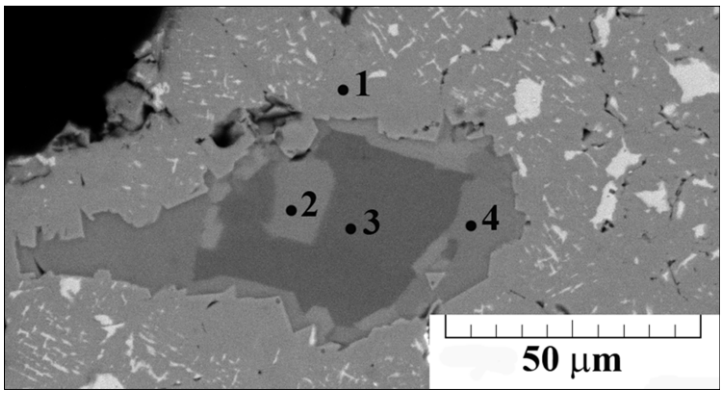

Figure 1. Zoned fluorapatite grain with As-rich (2, 4) and As-poor (3) zones in gahnite (1), in association with franklinite and baryte. Sample FeCor-1. Polished section. BSE image.

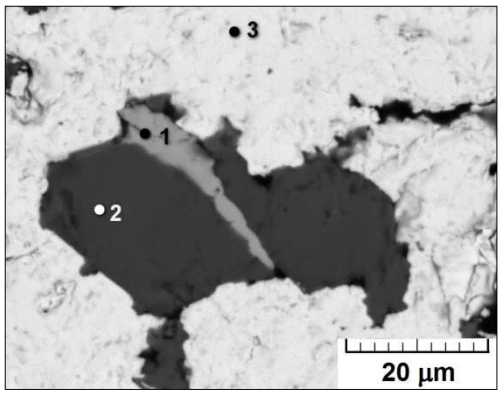

Figure 2. Monazite-(Ce) inclusion (1) in As-containing hydroxilapatite (2) forming core of a mimetite crystal (3). Sample Sh-1. Polished section. BSE image.

Table 1. Variations of arsenic content in As-bearing minerals from nonsulfide Pb-Zn-Sb ores of the Pelagonian massif.

Minerals	As_2O_5, wt.%	As, apfu
Tilasite $CaMg(AsO_4)F$	42.86–52.79	0.95–1.00
Fluorapatite $Ca_5(PO_4)_3F$	0.22–21.45	0.05–1.16
Mimetite $Pb_5(AsO_4)_3Cl$	18.63–24.35	2.67–3.00
Hedyphane $Pb_3Ca_2(AsO_4)_3Cl$	33.95–36.25	2.86–2.93
Adelite $CaMg(AsO_4)(OH)$	38.52–44.44	1.00
Mottramite* $PbCu(VO_4)(OH)$	14.70	0.41
Gasparite-(Ce) $Ce(AsO_4)$	26.81–33.24	0.74–0.77
Gasparite-(La) $La(AsO_4)$	31.12–37.11	0.81–0.88
Monazite-(Ce) $Ce(PO_4)$	5.19–19.84	0.10–0.45
Chernovite-(Y) (Y,*REE*)$[AsO_4]$	38.19–41.38	0.79–0.91
Foggite $CaAl(PO_4)(OH)_2 \cdot H_2O$	16.89–21.14	0.43–0.50

*Single analysis.

Mimetite was detected mainly in associations mainly composed by silicates and barite. Hedyphane is mainly related to tilasite and silicate zones, in which it forms small individuals up to several tens of microns. In tilasite-carbonate-silicate associations, minerals of adelite-descloizite group (adelite and mottramite) form small inclusions in tilasite. Minerals of the monazite group are presented by P-containing arsenates gasparite-(Ce) and gasparite-(La), as well as As-containing phosphate monazite-(Ce). Gasparite-(Ce) and gasparite-(La) are present as accessory components in metasomatites containing predominantly barite and tilasite, with subordinate carbonates and silicates and accessory members of the högbomite supergroup and other oxide phases. Gasparite-(Ce) is crystallized in the interstitial space between barite and zincohögbomite grains (Fig. 3). Individuals of gasparite-(Ce) reach up to 200 microns in length. Gasparite-(La) forms small (up to 5 microns) grains in carbonate-silicate veinlets crosseding granular tilasite aggregate. In amazonite-containing pegmatoid rock monazite-(Ce) and chernovite-(Y) forms equant xenomorphic inclusions up to 50 microns in quartz-microcline aggregate, as well as irregular grains in As-bearing fluorapatite, located as cores of large mimetite crystals (Fig. 4).

Chernovite forms skeletal crystals up to 600 microns (Fig. 5). Individes of monazite-(Ce) are characterized by complex zonatity, mainly due to variations of the As:P ratio (Table 1). As-rich variety of foggite is noted as a rare accessory component of the tilasite-silicate rock, where this mineral forms small inclusions in As-bearing fluorapatite (Fig. 6). The atomic ratio As:P in this mineral reaches 1:1.

Except for above-mentioned AsO_4-containing minerals, in non-sulphide Pb-Zn-Sb ores of Nezhilovo minor amounts of As were detected in accessory Sb oxides belonging to the pyrochlore supergroup and ilmenite group. In Sb-dominant minerals of the pyrochlore supergroup (roméite-group members), As content reaches 0.16 apfu (Varlamov et al., 2017).

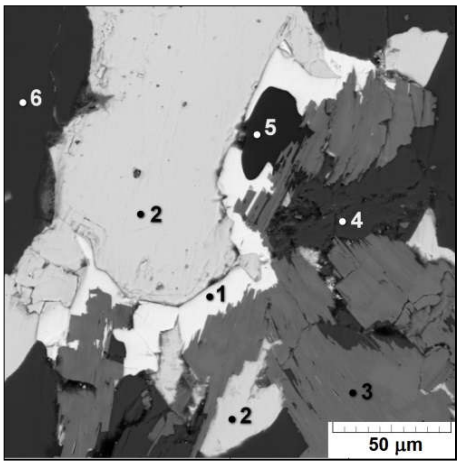

Figure 3. Gasparite-(Ce) (1) in association with barite (2), zincohögbomite (3), Zn-containing talc (4), quartz (5), dolomite (6). Sample R-11-7-1. Polished section. BSE image.

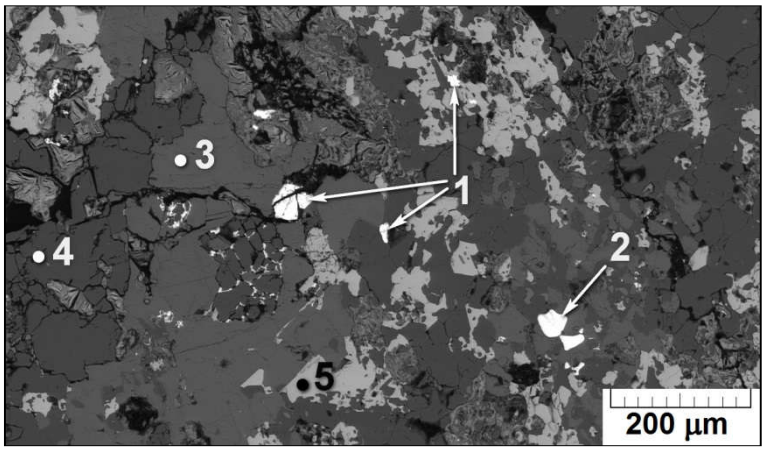

Figure 4. Monazite-(Ce) (1) and chernovite-(Y) (2) grains in a polymineral aggregate composed of K-feldspar (3), quartz (4), and hematite (5). Sample Sh-1. Polished section. BSE image.

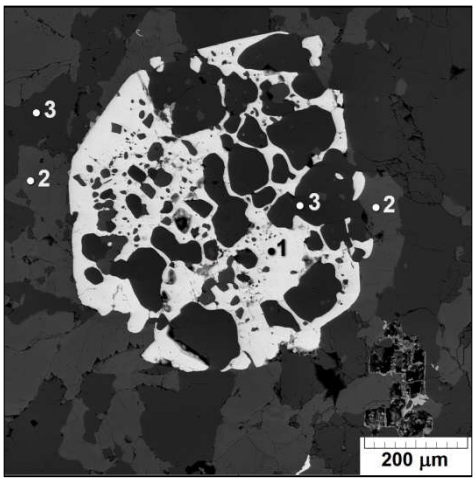

Figure 5. Skeletal crystal of chernovite-(Y) (1) in association with amazonite (2) and quartz (3). Sample Sh-1. Polished section. BSE image.

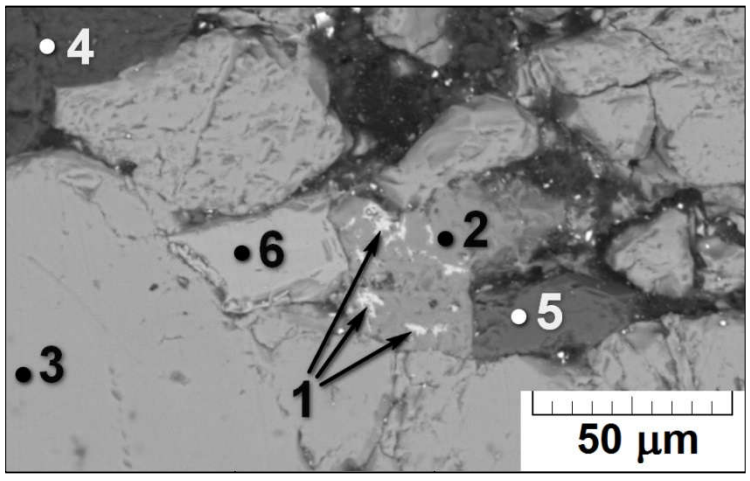

Figure 6. Foggite inclusions (1) in As-containing fluorapatite (2), in association with tilasite (3), Zn-containing talc (4), magnesioribekite (5) and braunite (6). Sample 13. Polished section. BSE image.

Comparison of chemical compositions of associated As-containing minerals in Nezhilovo metasomatites show several regularities. As-bearing fluorapatite is a regular accessory component of ore-bearing metasomatites of the Pelagonian massif, whereas the arsenates (gasparite-(Ce), gasparite-(La), adelite), vanadate (mottramite) and phosphate (foggite) are located only in high-tilasite zones. Zonality of As-bearing fluorapatite indicates that in the course of metasomatites formation there were at least two maxima of As activity. In oxysalt associations, As-mineralization is much more diverse and includes different arsenates (tilasite, hedyphane, mimetite, adelite, gasparite-(La), gasparite-(Ce), chernovite-(Y)) and As-containing phosphates (fluorapatite, hydroxilapatite, monazite-(Ce), foggite)

and vanadate (mottramite). Unlike adelite, tilasite shows strong affinity towards fluorine: F contents in tilasite in all cases are more than 0.8 apfu, and in adelite in all cases they are below 0.2 apfu. Possibly, strong hydrogen bonds in minerals of the adelite-descloizite group lead to stabilization of this structure type. Other feature of adelite-descloizite group minerals, which distinguishes them from tilasite, is a high affinity to chalcophile elements: arsenic member of this group (adelite) selectively accumulates Zn (up to 0.4 apfu), and vanadium member (mottramite) concentrates Cu (up to 0.54 apfu) and Pb (up to 0.65 apfu). In addition, mottramite is riched in Ca (0.2 apfu), Mg (0.3 apfu) and As (0.4 apfu). Thus, adelite and mottramite are presented by varieties, transitional to austinite $CaZn(AsO_4)(OH)$ and adelite, respectively. Associated phosphates and arsenates of *REE* are another example of selective concentration of chemical components: chernovote-(Y) accumulates *HREE*, whereas monazite-(Ce) contains mainly *LREE*. Pb,As-containing foggite forms partial pseudomorphs after fluorapatite. Foggite formation may be related to a late hydrothermal stage, during which supply of Al, Pb, As и H_2O took place (Chukanov et al., 2016, 2017).

The study was supported by the Russian foundation for basic research, grant No 17-05-00179_a.

References

Barić L. Piemontit, gahnit und rutil aus dem Fundort der Blei und Zinkerze bei dem Dorfe Nezilovo in Mazedonien // Glasnik Prirodnjackogo Muzeja. Beograd., Ser. A. 1960. Vol. 13. P. 200–204 (in German).

Chukanov N.V., Jančev S., Pekov I.V. The association of oxygen-bearing minerals of chalcophile elements in the orogenetic zone related to the “Mixed Series” complex near Nežilovo, Republic of Macedonia // Macedonian J. of Chem. and Chem. Eng. 2015. Vol. 34(1). P. 115–124.

Chukanov N.V., Aksenov S.M., Jančev S., Pekov I.V., Göttlicher J., Polekhovsky Yu.S., Rusakov V.S., Nelyubina Yu.V., Van K.V. A new mineral species ferricoronadite, $Pb[Mn^{4+}_6(Fe^{3+},Mn^{3+})_2]O_{16}$: mineralogical characterization, crystal chemistry and physical properties // Phys. Chem. Miner. 2016. Vol. 43. No. 7. P. 503–514.

Chukanov N.V., Krzhizhanovskaya M.G., Jančev S., Pekov I.V., Varlamov D.A., Göttlicher J., Rusakov V.S., Polekhovsky Y.S., Ermolaeva V.N. Zincovelesite-6N6S, IMA 2017-034. CNMNC Newsletter No. 38, August 2017. P. 1037; Mineral. Magaz. 2017. Vol. 81. P. 1033–1038.

Chukanov N.V., Zubkova N.V., Schäfer C., Varlamov D.A., Ermolaeva V.N., Polekhovsky Yu.S., Jančev S., Pekov I.V., Pushcharovsky D.Yu. Ferriakasakaite-(La): new data, new findings and crystal-chemical relationships with other epidote-supergroup minerals // Eur. J. Miner. 2018 (accepted for publication).

Dunn P.J. Rare minerals of the Kombat Mine // Mineral. Rec. 1991. Vol. 22(6). P. 421–425.

Ermolaeva V.N., Chukanov N.V., Jančev S., Van K. Endogenic oxide parageneses with chalcophile elements in the orogenetic zone related to the “Mixed Series”of the Pelagonian massif, Republic of Macedonia // New Data on Minerals. 2016. Vol. 51. P. 12–19.

Ermolaeva V.N., Varlamov D.A., Jančev S., Chukanov N.V. Spinel-group and högbomite-supergroup minerals from a nonsulfide endogenous Pb-Zn-Sb-As association in the Pelagonian massif, Macedonia // Zap. Ross. Mineral. O-va. 2018 (in press) (in Russian).

Holtstam D., Langhof J. (Eds.) Långban: The mines, their minerals, geology and explorers. Stockholm: Raster Förlag, 1999. 217 pp.

Innes J., Chaplin R.C. Ore bodies of the Kombat mine, South West Africa/Namibia. In: C.R. Anheusser and S. Maske (eds.), Mineral deposits of southern Africa, Geological Society of South Africa, 1986. P. 1789–1805.

Jančev S., Chukanov N.V., Ermolaeva V.N. Association of oxide minerals - concentrators of chalcophile elements (Pb, Zn, Sb) from the “Mixed series” near Nežilovo village, Macedonia // Materials of the Third Congress of Geologists of Republic of Macedonia. Struga, 30 September – 02 October, 2016. Vol. 2. P. 401–404.

Palache Ch. Paragenetic classification of the minerals of Franklin, New Jersey // Am. Mineral. 1929a. Vol. 14(1). P. 1–18.

Palache Ch. A comparison of the ore deposits of Longban, Sweden, with those of Franklin, New Jersey // Am. Mineral. 1929b. Vol. 14(2). P. 43–47.

Tarr W.A. The origin of the zinc deposits at Franklin and Sterling Hill, New Jersey // Am. Mineral. 1929. Vol. 14. P. 207–221.

Varlamov D.A., Ermolaeva V.N., Jančev S., Chukanov N.V. Pyrochlore-supergroup minerals from a nonsulfide endogeneous association of Pb-Zn-Sb-As minerals in the Pelagonian massif, Macedonia // Zap. Ross. Mineral. O-va. 2017. Part 146. №. 4. P. 65–78 (in Russian).

Wilkerson A.S. The minerals of Franklin and Sterling Hill, New Jersey. – Bulletin 65. New Jersey Geological Survey. Trenton, New Jersey: Department of Conservation and Economic Development. 1962. 80 pp.

NEW CAMECA SXFIVETACTIS AND SOME OF THE LATEST APPLICATIONS

***Fedik I.V.*[1], *Moret M.P.*[2]*, *Robbes A.-S.*[2], *Henderson C.*[2]**

[1]*CAMECA Nu Instruments Russia, Moscow, Russia, igor.fedik@ametek.com*
[2]*CAMECA SAS, Gennevilliers, Paris, France *mona.moret@ametek.com*

Thanks to its precision, its reproducibility and its stability, Electron Microprobe is a well suited technique for accurately analyzing nearly all chemical elements at concentration levels down to few 10's ppm with a spatial resolution of about 1 µm, which is relevant to microstructures in a wide variety of materials and mineral specimens.

Fig 1. New CAMECA EPMA SXFive TACTIS

CAMECA leader in scientific instruments has been manufacturing Electron Microprobe (EPMA) since 1958 and will present its latest CAMECA EPMA model, SXFive TACTIS released in December 2018. One of the main add-on is the new Tactile interface to allow non-frequent or beginner users to easily use the instrument while still allowing experienced users to perform advanced tasks. Further integration of the EDS as well as an additional low energy BSE will be described.

Examples of the latest applications, usage of the CAMECA EPMA will be presented in Earth science.

IN-SITU ISOTOPIC ANALYSIS METHODS IN GEOCHEMISTRY

***Fedik I.V.*[1], *Peres P.* [2], *Horréard F.* [2], *Zhao Y.*[3]**

[1] *CAMECA Nu Instruments Russia, Moscow, Russia, igor.fedik@ametek.com*

[2]*CAMECA SAS, Gennevilliers, Paris, France*

[3]*CAMECA Nu Instruments, Wrexham, United Kingdom*

Geological samples generally are highly heterogeneous, with complex phase and chemical composition. Analyzing objects of micron and nanometer scale for example dust particles, impurities, thin layers in intergrain space in minerals becomes increasingly important in modern geochemistry. Therefore recently the methods of local analysis become more widely spread and developed.

At the same time, requirements to detection limits of analytical methods increase.

However due to physical limitations a combination of high spatial resolution (or lateral resolution if only the sample's surface is investigated) and high detection limit (sensitivity) is a general challenge in development of analytical instruments. Therefore selection of an analytical technique comes down to a compromise between lateral resolution and detection limit. This is particularly important for isotopic analysis.

The current discussion is to raise a problem of selection of appropriate in-situ isotopic analysis technique for various applications in geochemistry.

Secondary Ion Mass Spectrometry (SIMS) is a technique of ever-growing use in geochemistry.

SIMS is the most sensitive method of the in-situ elemental and isotopic analysis. In this method sample surface is bombarded with a focused beam of primary ions which leads to local ionization of the sample and to sputtering of the secondary ions which are analyzed with a mass-spectrometer. Generally in geochemistry O^-, O_2^+, Cs^+ are used as primary ions (Werner, et al., 2003).

SIMS method provides an unique combination of high sensitivity for all elements from hydrogen to uranium and further (with detection limits for the majority of elements down to ppb levels), high spatial resolution (down to 50 nm) and extremely wide dynamic range (more than 5 orders). It is the only method which allows to examine surface and volume distribution of elements in both organic, and inorganic solid bodies. Like every mass-spectrometry method SIMS is destructive, however this feature allows to perform in-depth analysis and 3D-mapping.

CAMECA had developed a range of SIMS instruments which are particularly useful in geological applications:

The IMS 1300-HR^3 (Fig 1.) which is the high sensitivity/ high precision SIMS required for precise trace elements (U/Pb dating, REE, …) or ultra-fast stable isotope measurements in FC multicollection mode. Typical analytical performance:

- down to or below 1E-4 range (0.1 permil) reproducibility for stable isotope measurements in automated, FC multicollection mode (Schuhmacher, et al., 2004) ,
- high throughput - high precision U/Pb geochronology on zircons from smaller spots (5-15µm) in automated, EM monocollection mode.

Fig.1. IMS 1300-HR^3 new generation large geometry SIMS instrument.

The NanoSIMS 50L which is the SIMS instrument allowing to reach spatial resolution down to 50 nm without loss of sensitivity for light elements thanks to unique design of coaxial ion optics.

Studying of some geological and cosmochemical samples require ultimately high spatial resolution. For example this instrument has been used for studying distribution of H, D, ^{12}C, ^{13}S-, ^{18}O, ^{28}Si, ^{29}Si, ^{30}Si isotopes and ^{26}CN, $^{12}C^{14}N$-, $^{12}C^{15}N$ compounds in chondrites and presolar grains (Remusat, et.al, 2008, Bose, et al, 2014, Piani, et al, 2015).

Other distinctive features of NanoSIMS 50L are:

- Multicollector allowing the parallel detection of seven masses. Each multicollection trolley can receive one EM and one FC. Mass dispersion for parallel detection Mmax/Mmin is 21 and the minimum mass interval is Mmax/58.

- High reproducibility of isotopic measurements thanks to the development of software routines for automated secondary ion beam alignment in the optics and addition of field compensating coils before the entrance slits.

- All moveable slits and apertures of the optics as well as the hexapole and the Z-axis of the sample stage have are automated.

Operating the NanoSIMS 50L in multiple FC mode allows to envision earth science applications requiring permil isotopic ratio reproducibility at sub-µm scale.

Despite of its uncompromised sensitivity, lateral and depth resolution SIMS technique is prone to serious matrix effects. This requires using reference samples which resemble the sample to be analyzed as much as possible in order to achieve highest precision in isotopic measurements. These reference samples are not always readily available, therefore alternative methods might be preferred.

Since its invention in the 1990s, the multicollector ICP-MS (MC-ICP-MS) technique is generally known as a bulk analysis method of dissolved samples. Solution MC-ICP-MS can provide good accuracy, precision better than 0.2‰ (2SD) (Craddock, et.al, 2008, Clough, et al, 2006, Pribil, et al, 2015), and sample demand is lower than GS-MS. Recent studies have shown that solution MC- ICP-MS can be used to measure very low sulfur samples (e.g., glacier, snow, and rainwater samples), having a sulfur demand as low as 2 mg (Paris, et.al, 2013, Das, et al, 2012). Though bulk analytical techniques have very high precision, it is difficult to distinguish sulfur isotopes of zonation within a single grain or multi-genesis minerals in micro-areas.

For mass spectrometry analysis, isotopic interferences from molecular ions (e.g., ^{16}O-^{16}O+, ^{32}S-^{1}H+ and ^{17}O-^{16}O-^{1}H+) and doubly charged ions (e.g., $^{64}Zn^{2}$+) have a negative effect on sulfur isotope analysis (Craddock, et.al, 2008, Pribil, et al, 2015, Bendall, et al, 2006). This problem is commonly resolved using sufficient mass resolution to enable the detection of S isotopes on the interference-free plateau. However, the sulfur plateau is too narrow compared with the mixed peak, and values might be significantly affected by instrument stability. This can be solved by using a high-resolution large geometry MC-ICP-MS Nu 1700. Nu 1700 is able to completely separate any interference peaks in ^{32}S using medium resolution mode (resolution power = 10 000) and in ^{33}S using a higher resolution mode (resolution power = 18 000) (Fig.1).

References

Bose M., Zega T.J., Williams P. (2014) Earth and Planetary Science Letters. Vol. 399, P. 128–138.

Piani L., Robert F., Remusat L. (2015) Earth and Planetary Science Letters. Vol. 415, P. 154–164.

Remusat L., Guan Y., Eiler J.M.(2008) 39th Lunar and Planetary Science Conference. Texas (USA),. P. 2477.

Schuhmacher M., Fernandes F., De Chambost E.. (2004) Applied Surface Science 231–232.

Werner H.W. (2003) Surf. Interface Anal.. Vol. 35, P. 859–879.

Craddock P. R., Rouxel O. J., Ball L. A., Bach W., Chem. Geol., 2008, 253, 102-113, DOI: 10.1016/j.chemgeo.2008.04.017.

Clough R., Evans P., Catterick T., Evans E. H., Anal. Chem., 2006, 78, 6126-6132.

Pribil M. J., Ridley W. I. Emsbo, P., Chem. Geol., 2015, 412, 99-106.

Paris G., Sessions A. L., Subhas A. V., Adkins J. F., Chem. Geol., 2013, 345, 50-61.

Das A., Chung C.-H., You C.-F., Shen M.-L., J. Anal. At. Spectrom., 2012, 27, 2088.

Bendall C., Lahaye Y., Fiebig J., Weyer S., Brey G. P., Appl. Geochem., 2006, 21, 782-787,

COMPOSITIONAL VARIATIONS AND ALTERATION OF GADOLINITE-GROUP MINERALS FROM THE HEFTETJERN GRANITIC PEGMATITE, SOUTHERN NORWAY

***Ermolaeva V.N.*[1,2], *Varlamov D.A.*[1,3], *Chukanov N.V.*[3]**

[1]*Institute of Experimental Mineralogy RAS, Chernogolovka, Russia, cvera@mail.ru*

[2]*Vernadsky Institute of Geochemistry and Analytical Chemistry RAS, Moscow, Russia*

[3]*Institute of Problems of Chemical Physics RAS, Chernogolovka, Russia*

The Heftetjern granitic pegmatite situated in Telemark, Southern Norway consists dominantly of albite, microcline, quartz, dark and light micas, with minor oligoclase. The main accessory minerals are beryl, spessartine, gadolinite-(Y), cassiterite, scandian ixiolite, zircon, monazite-(Ce), Sc-bearing pyrochlore-group minerals, milarite and phenakite. Recently a new member of the gadolinite group, the OH-dominant analogue of gadolinite-(Y) with the idealized formula $(Y,Ca)_2(Fe,\square)Be_2Si_2O_8(OH,O)_2$ ("hydroxylgadolinite-(Y)") has been discovered in this association (Chukanov *et al*., 2017).

Crystals of gadolinite-group minerals studied in this work occur in close association with albite (Figs. 1-5).

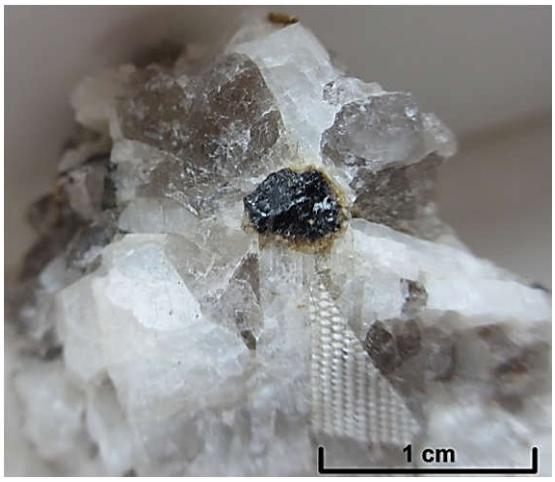

Figure 1. Grain of gadolinite-(Y) partly substituted by hingganite-(Y) in albite-quartz aggregate. Sample 1.

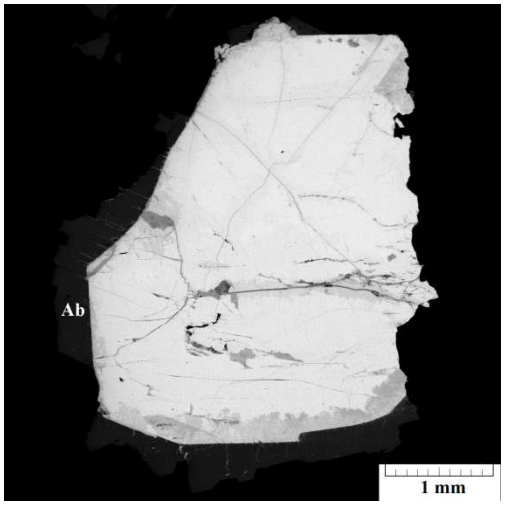

Figure 2. Gadolinite-(Y), partly substituted by Fe-deficient gadolinite-(Y) and hingganite-(Y). Around the gadolinite-(Y) crystal is observed albite rim. Sample 1. BSE image.

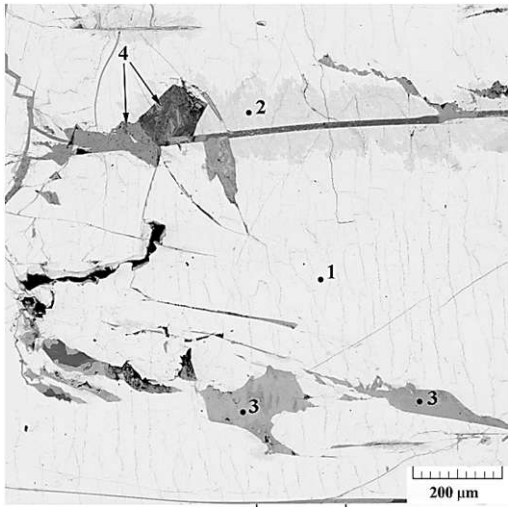

Figure 3. Fragment of Figure 2. Gadolinite-(Y) (1), partly substituted by Fe-deficient gadolinite-(Y) (2), hingganite-(Y) (3) and nonidentified secondary hydrous Y-bearing silicates (4). BSE image.

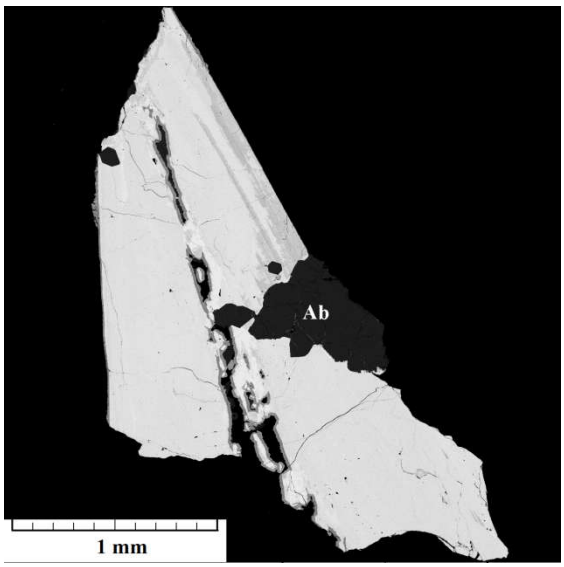

Figure 4. Grain of an individual with zones of gadolinite-group minerals in association with albite. Sample 2. BSE image.

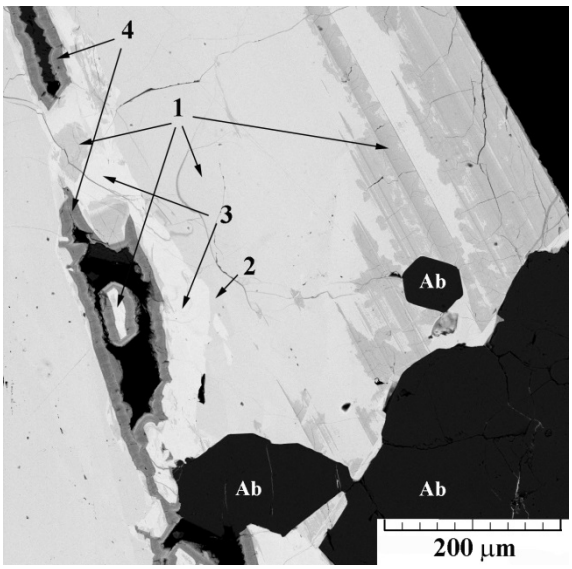

Figure 5. Fragment of Figure 4. "Hydroxylgadolinite-(Y)" (1) with relics of gadolinite-(Y) (2) and hingganite-(Y) (3), with rims of nonidentified secondary hydrous Y-bearing silicates (4) in association with albite. BSE image.

Two samples have been investigated. One of them (Sample 1) belongs to an earlier association and forms a grain with pleochroic halo (Fig. 1). It is rather uniform in composition which corresponds to typical gadolinite-(Y), with the exception of a thin peripheral zone and a thin zone along a crack which are composed of Fe-deficient gadolinite-(Y) and hingganite-(Y). Irregular shape of the borders between gadolinite-(Y) and hingganite-(Y) (Fig. 2) indicates that the zonality does not have a growth origin, but is due to partial substitution of gadolinite-(Y) with secondary phases. The typical empirical formulae of these minerals in Sample 1 are: $(Y_{1.47}Dy_{0.11}Nd_{0.07}Er_{0.06}Ce_{0.06}Yb_{0.06}Ho_{0.05}Tm_{0.04}Sm_{0.03}Gd_{0.03}Pr_{0.02}Eu_{0.02}Tb_{0.01}Ca_{0.01}Lu_{0.01})_{\Sigma 2.05}Fe_{0.84}Be_2Si_{2.00}O_8[O_{1.83}(OH)_{0.17}]_{\Sigma 2}$ (gadolinite-(Y)) and $(Y_{1.03}Ca_{0.70}Dy_{0.08}Gd_{0.05}Er_{0.05}Sm_{0.03}Yb_{0.03}Tb_{0.03}Nd_{0.02}Ho_{0.02}La_{0.01}Tm_{0.01})_{\Sigma 2.07}Fe_{0.40}Be_2Si_{2.00}O_8[(OH)_{1.72}O_{0.28}]_{\Sigma 2}$ (hingganite-(Y)). The OH contents were calculated taking into account charge balance requirement.

Another one (Sample 2) presumably belongs to a later association and shows distinct signs of profound late alterations. Its inner zone principally consists of *REE*,Ca-deficient "hydroxylgadolinite-(Y)" with the typical composition $(Y_{0.94}Ce_{0.14}Nd_{0.13}Dy_{0.10}Yb_{0.09}La_{0.05}Sm_{0.04}Er_{0.04}Ca_{0.03}Pr_{0.03}Ho_{0.03}Lu_{0.03}Gd_{0.02}Tb_{0.02}Eu_{0.01}Th_{0.01})_{\Sigma 1.71}(Fe_{0.63}Al_{0.13})_{\Sigma 0.76}Be_2(Si_{1.96}P_{0.04})_{\Sigma 2.00}O_8[(OH)_{1.12}O_{0.82}]_{\Sigma 2}$, and contains subordinate areas of gadolinite-(Y) and hingganite-(Y). The typical empirical formulae of these minerals in Sample 2 are: $(Y_{1.27}Ce_{0.13}Yb_{0.08}Ca_{0.07}Nd_{0.05}Er_{0.05}Dy_{0.05}La_{0.03}Sm_{0.03}Ho_{0.03}Tb_{0.02}Pr_{0.02}Gd_{0.01}Eu_{0.01}Tm_{0.01}Lu_{0.01})_{\Sigma 1.87}(Fe_{0.43}Al_{0.21})_{\Sigma 0.64}Be_2(Si_{1.96}P_{0.04})_{\Sigma 2.00}O_8[O_{1.07}(OH)_{0.93}]_{\Sigma 2}$ (Al-bearing gadolinite-(Y)) and $(Y_{1.13}Ce_{0.17}Nd_{0.15}Dy_{0.09}Sm_{0.06}Ca_{0.06}Pr_{0.05}Gd_{0.05}Yb_{0.05}Er_{0.03}La_{0.02}Ho_{0.02}Tb_{0.02})_{\Sigma 1.84}Fe_{0.43}Be_2Si_2O_8[(OH)_{1.5}O_{0.5}]_{\Sigma 2}$ (hingganite-(Y)). Light zones of the crystal in Sample 2 contain slightly more *REE* (1.82-1.92 apfu) then darker zones (1.68-1.82 apfu). Hypothetically, crystallization of "hydroxylgadolinite-(Y)" and gadolinite-(Y) in Sample 2 occurred during the albitization stage, at a high activity of Al which resulted in the presence of unusually high amounts of aluminium in these minerals.

The latest generation of Y-bearing silicates is presented by interstitial grains and crusts of nonidentified hydrous phases on the walls of cavities with low sums of electron microprobe analyses (points 4 in Fig. 3 and Fig. 5). In particular, the stoichiometry of the mineral forming late crusts (the point 4 in Fig. 5) is close to that of hingganite, but unlike hingganite this phase is characterized by a very high content of Ca and lowered sums of electron microprobe analyses (table 1). As a result of

high Ca contents, charge-balanced empirical formulae of this phase calculated on 2 Si atoms contain more than 2 OH groups. Due to insufficient amount of available substance, reliable identification of this mineral was impossible.

Table 1. Chemical composition of of nonidentified secondary hydrous Y-bearing silicates.

	Sample 1	**Sample 2**
CaO	3.37	13.41
FeO	1.96	2.57
Y_2O_3	25.07	24.45
La_2O_3	0.19	0.64
Ce_2O_3	0.13	1.98
Pr_2O_3	н.п.о.	0.50
Nd_2O_3	0.63	0.87
Gd_2O_3	0.40	н.п.о.
Dy_2O_3	2.62	1.28
Ho_2O_3	0.92	н.п.о.
Er_2O_3	1.26	1.15
Tm_2O_3	0.38	0.93
Yb_2O_3	1.39	1.16
SiO_2	30.46	31.87
P_2O_5	н.п.о.	0.34
Total	68.78	81.15
Ca	0.24	0.89
Fe	0.11	0.13
Y	0.88	0.81
La	0	0.01
Ce	0	0.05
Pr	0	0.01
Nd	0.01	0.02
Gd	0.01	0
Dy	0.06	0.03
Ho	0.02	0
Er	0.03	0.02
Tm	0.01	0.02
Yb	0.03	0.02
Si	2.00	1.98
P	0	0.02
Basis of calculation	Si=2	(Si+P)=2

As a conclusion, four stages of evolution of Y-bearing minerals can be distinguished: a) crystallization of gadolinite-(Y), b) formation of intermediate gadolinite-(Y) – hingganite-(Y) members and “hydroxylgadolinite-(Y)”, c) substitution of the earlier phases by Ca,*REE*-deficient hingganite-(Y) and d) crystallization of late hydrous Y-bearing silicates in interstitial space and cavities. The assumption on a late-stage origin of “hydroxylgadolinite-(Y)” is in a good agreement with its non-metamict state, which is confirmed by its perfect crystal structure (Chukanov *et al*., 2017) and perfect cleavage (Fig. 5).

We are thankful to R. Kristiansen for the samples kindly provided for the investigations.

The study was supported by the Russian Scientific Foundation, grant No 14-17-00048.

TITANIUM-RICH POTASSIUM AMPHIBOLE OF THE AGPAITIC SYENITE (KOLA PENINSULA, RUSSIA)

Filina M.I., Kogarko L.N., Kononkova N.N.
Vernadsky Institute, Moscow, Russia, makimm@mail.ru

Sodium and sodium-calcium amphiboles are typical for alkaline, especially agpaitic rocks, pegmatites and metasomatites associated with alkaline intrusions (Deer et al., 1997; Hawthorne, 1976). Potassium is a typical component of many alkaline amphiboles, but the K_2O content usually does not exceed 1-2% wt %. In 2004 was approved, a new mineral form - potassium arfvedsonite KNa2Fe2 + 4Fe3 + Si8O22 (OH)2, it found in alkaline pegmatites from three alkaline complexes: the Ilimaussaq, Lovozero and Khibiny (Pekov et al., 2004).

Titanium-rich potassium amphibole from the agpaitic syenites of the Niva intrusion and the dyke "Mohnatye Roga" have been investigated. It is situated in the northwestern part of the Belomorian mobile belt (Kola Peninsula, Russia). The syenites from these objects are almost identical in chemical and mineral composition (Akimenko et al., 2014; Arzamastsev et al., 2000). The main minerals of agpaitic syenites are potassium feldspar (25-30 vol.%), natrolite (10-15 vol.%), aegirine-augite (10-15 vol.%), aenigmatite (10-15 vol.%), titanium-rich potassium amphibole (5-10 vol.%), a characteristic feature of the rock, is the presence among rock-forming minerals in an amount up to 20 vol. % minerals of the lamprophyllite group (LGM): lamprophyllite, fluorlamprophyllite, baryitolamprophyllite, and fluorobarytol lamprophyllite. Compared with the nepheline syenites of the Khibiny and Lovozero massifs, the studied rocks contain less silica, while the iron and titanium content is much higher, which is reflected in the chemical composition of rock-forming minerals (Akimenko et al., 2014; Arzamastsev et al., 2000).

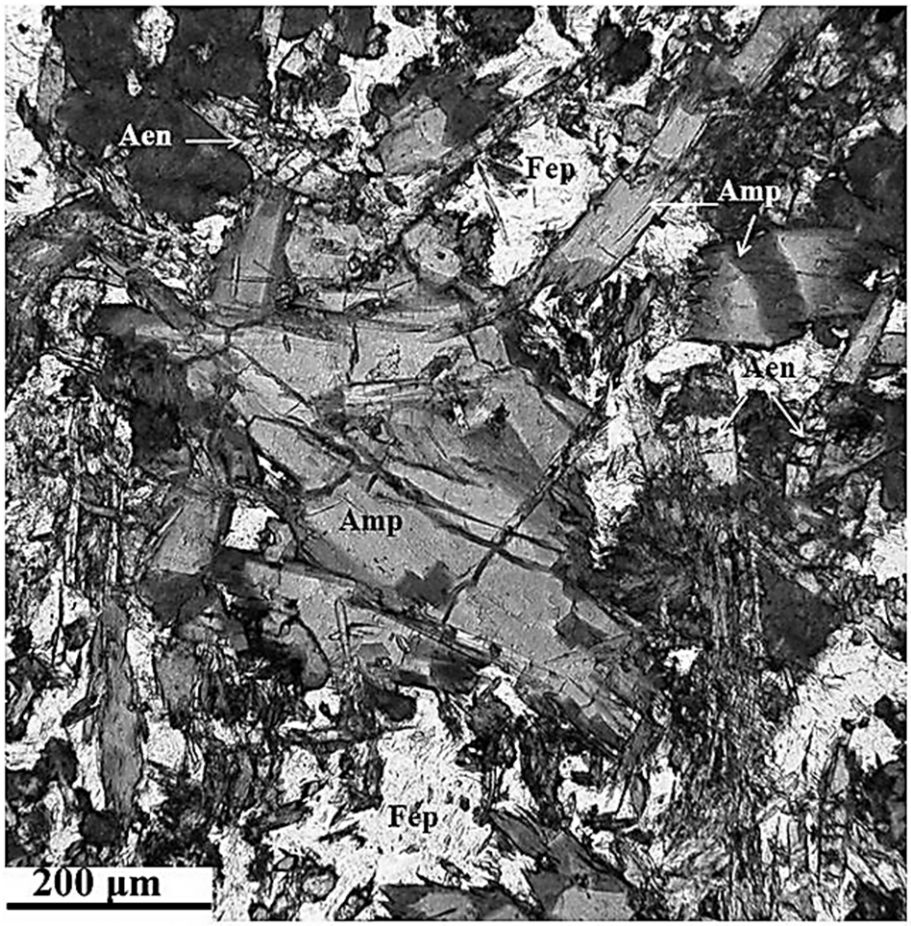

Fig. 1. Accumulation of crystals of potassium amphibole (Amp) in association with aegirine-augite (Aen) in a matrix of feldspar and natrolite (Fep), agpaitic syenite of the Niva intrusion.

Table. 1. Representative analyses (wt.%) of zonal amphibole crystals from the dyke and Niva intrusions.

	1C *	2 R	3 C **	4 R	5 C	6 R	7 C	8 R	9 C
SiO_2	52.62	50.08	49.86	48.65	50.91	49.57	51.03	50.61	50.81
TiO_2	3.16	2.74	3.02	2.11	4.36	2.83	4.38	2.02	4.71
Al_2O_3	0.76	0.83	0.75	0.88	1.57	0.18	1.42	0.59	1.83
MnO	0.52	0.33	0.53	0.27	0.46	0.72	0.55	0.60	0.53
FeO	14.16	25.90	14.19	24.20	13.92	29.32	14.86	25.54	14.15
MgO	12.53	5.69	12.40	6.49	11.64	1.13	11.43	4.58	11.73
CaO	3.11	0.79	3.05	0.75	2.86	0.06	2.97	0.22	3.35
Na_2O	6.43	7.06	6.36	7.15	6.72	7.21	6.63	6.88	6.44
K_2O	3.76	4.55	3.60	4.19	3.25	4.81	3.16	4.77	3.11
ZrO_2	0.79	0.00	0.85	0.06	0.48	«-»	0.12	«-»	0.12
BaO	0.11	0.05	0.07	0.05	0.29	0.22	0.13	0.13	«-»
SrO	0.49	0.03	0.57	0.17	0.33	0.05	0.28	0.07	0.60
Cr2O3					0.03	0.01	0.02	«-»	0.06
Nb_2O_5	0.02	0.01	0.05	0.10					
UO_2	0.64	0.73	0.73	0.88					
F	3.34	0.83	3.54	1.44	3.04	0.02	3.13	0.21	2.97
Total	102.51	99.62	99.76	97.39	99.86	96.13	100.11	96.22	100.41
O=F	1.41	0.35	1.49	0.61	1.28	0.01	1.32	0.09	1.25
Total	101.10	99.27	98.27	96.78	98.58	96.12	98.79	96.13	99.16
Formula coefficients									
Na	0.38	0.24	0.43	0.33	0.45	0.30	0.15	0.45	0.45
K	0.71	0.89	0.70	0.84	0.62	1.00	0.96	0.63	0.59
Ca	0.49	0.13	0.50	0.13	0.46	0.01	0.04	0.39	0.54
Σ_A	1.09	1.14	1.13	1.17	1.07	1.30	1.12	1.08	1.05
Ca	0.49	0.13	0.50	0.13	0.46	0.01	0.04	0.39	0.54
Sr	0.04	0.00	0.05	0.02	0.03	0.01	0.01	0.04	0.05
Na	1.46	1.87	1.45	1.86	1.51	1.99	1.96	1.57	1.41
Σ_B	2.00	2.00	2.00	2.00	2.00	2.00	2.00	2.00	2.00
Ti	0.28	0.18	0.10	0.08	0.43	0.35	0.24	0.47	0.44
Zr	0.06	—	0.06	0.01	0.04	—	—	0.01	0.01
Al	—	—	—	—	—	0.04	0.11	—	—
Fe^{3+}	—	0.79	0.40	1.02	—	—	0.48	—	—
Mn^{2+}	0.07	0.04	0.07	0.04	0.06	0.10	0.08	0.08	0.07
Fe^{2+}	1.75	2.54	1.41	2.17	1.75	4.01	2.89	2.08	1.77
Mg	2.77	1.31	2.82	1.52	2.61	0.28	1.08	2.27	2.61
Σoct.	4.92	4.87	4.87	4.83	4.89	4.77	4.89	4.90	4.90
Si	7.79	7.71	7.62	7.66	7.66	8.10	8.00	7.69	7.59
Al	0.13	0.15	0.14	0.16	0.28	—	—	0.26	0.32
Ti	0.08	0.14	0.25	0.17	0.06	—	—	0.05	0.09
Σtetr.	8.00	8.00	8.00	8.00	8.00	8.10	8.00	7.99	8.00
OH	0.44	1.60	0.29	1.28	0.55	1.99	1.90	0.73	0.60
F	1.56	0.40	1.71	0.72	1.45	0.01	0.11	1.27	1.40
Σ_w	2.00	2.00	2.00	2.00	2.00	2.00	2.00	2.00	2.00

Note. 1-4 – amphiboles from the dyke (samples № 11-UK-8, 11-UK-32). 5-9 – amphiboles from the Niva intrusion (samples № N-8-1, N-8-3). Zones of crystals: C – core, R-rim. Formula coefficients calculated on the basis of 24 (OH, F, Cl, O). The values of the OH content were obtained on the basis of the electroneutrality condition. «-»–below the detection limit. In the amount included: *ThO_2-0.07; ** ThO_2 - 0.07, Ta_2O_5 – 012.

Amphiboles in the rock form elongated coarse grains, 1-1.5 mm in size, brown colored, with a faint bluish tint, the cross sections often have a hexagonal shape. The mineral is noticeably pleochroic in greenish-brown and bluish-green tones with a reverse absorption pattern. Amphibole is most often associated with aegirine-augite, the fine needle-like grains of which are located both on the edges and inside the crystals (Fig. 1), also amphibole can be located along the rim of aenigmatite grains, and it can be assumed that aenigmatite in comparison with amphibole earlier.

According to the modern classification of the amphibole group (Hawthorne et al., 2012), the studied amphibole belong to the sodium-calcium and sodium groups, the K_2O content is 3.11-4.81% wt.%, which allows K to dominate over Na in position A. A characteristic feature of the amphibole is the high content of titanium - 4.71 wt. %, as well as fluorine - up to 3.54 wt. % (Table 1). Crystals are zonal: the cores correspond to titanium-rich potassium cathophorite, potassium cathophorite or titanium-rich potassium enkermanite, the rims of titanium-rich potassium arfvedsonite or potassium arfvedsonite. From core to rim increase contents of sodium, potassium, and iron, and decrease in the content of magnesium and calcium. The central parts of the crystals enriched of titanium and fluorine, the fluorine content correlating with the titanium: the content of titanium decreases, the fluorine content also decreases (Table 1), which indicates a high activity of fluorine in the early stages of crystallization of the melt. In earlier experimental studies of the stability fields of amphiboles, depending on the oxygen fugacity and temperature, it was shown that the trend of a change in the amphibole composition from Ca through Na-Ca to Na amphiboles reflects a decrease in temperature and oxygen fugacity at or below the QFM buffer (Mitchell, 1990).

Also, the evolution of amphibole compositions corresponds to the general trend in the evolution of pyroxene compositions in the studied agpaitic syenite (Filina et al., 2017). Zonality of pyroxenes is expressed in an increase in the contents of sodium, iron and titanium from the core to the periphery, and a decrease in the contents of magnesium and calcium. Pyroxenes also contain significant amounts of titanium to 6.05 wt. % TiO2 in the marginal parts of the crystals, which allows us to refer it to the titanic aegirine-augite.

The evolution of the composition of rock-forming minerals from alkaline complexes can be used to study the evolution of igneous systems from early stages to late stages, which are controlled by such factors as magmatic melt composition, oxygen fugacity, alkali, temperature of mineral equilibria, etc.

The work was carried out at the expense of the funds allocated for the execution of the state assignment.

References

Akimenko M.I., Kogarko L.N., Sorokhtina N.V., Kononkova N.N., Mamontov V.P. A New Occurrence of Alkaline Magmatism on the Kola Peninsula: An Agpaitic Dyke in the Kandalaksha Region // Doklady Earth Sciences. 2014. Vol. 458. pp. 193-197.

Arzamastsev A.A., Belyatskiy B.V., Arzamastseva L.V. Agpaitic magmatism in the northeastern Baltic Shield: a study of the Niva intrusion, Kola Peninsula, Russia // Lithos. 2000. № 51. pp. 27-46.

Deer W.A., Howie R.A., Zussman J. Rock-Forming Minerals // London, Geol. Soc. Volume 2B Double-Chain Silicates. 1997. 764 pp.

Filina M.I., Kogarko L.N., Kononkova N.N. Evolution of pyroxene from peralkaline magmatic systems: Dyke complex of agpaitic syenite and Niva Intrusion (Kola Peninsula) // Geochem Int. 2017. № 7 pp. 1-7.

Hawthorne, F.C. The crystal chemistry of the amphiboles: V. The structure and chemistry of arfvedsonite // Canadian Mineralogist. 1976. № 14 pp. 346-356.

Hawthorne F.C., Oberti R., Harlow G.E., Maresch W.V., Martin R.F., Schumacher J.C., Welch M.D. IMA Report Nomenclature of the amphibole supergroup // American Mineralogist. 2012.V. 97. pp. 2031–2048.

Mitchell R.H. A review of the compositional variation of amphiboles in alkaline plutonic complexes // Lithos. 1990. 135-156.

Pekov, I.V., Chukanov, N.V., Lebedeva, Yu.S., Pushcharovsky, D.Yu., Ferraris,G., Gula, A., Zadov, A.E., Novakova, A.A., Petersen, O.V. Potassicarfvedsonite, KNa2Fe2+4Fe3+Si8O22(OH)2, a K-dominant sodic amphibole of the arfvedsonite series from agpaitic pegmatites – Mineral data and type of disorder in the A site // Neues Jahrbuch für Mineralogie - Monatshefte. 2004. № 12. pp. 555–574.

LINKAGE OF MIASKITES FROM VISHNEVOGORSKY ALKALINE MASSIVE AND KYSHTYMITES (CORUNDUM ANORTHOSITES) OF THE SOUTHERN URALS, RUSSIA: EVIDENCE FROM MINERALOGY AND GEOCHEMISTRY

***Filina M.I.*[1], *Sorokina E.S.*[1], *Rassomakhin M.A.*[2], *Kogarko L.N.*[1], *Kononkova N.N.*[1]**

[1]*Vernadsky Institute of Geochemistry and Analytical Chemistry RAS (GEOKHI RAS), Kosygin st., 19, Moscow. E-mail: makimm@mail.ru*

[2]*Ilmen State Reserve, Chelyabinsk region, Miass*

Kyshtymite is a high-alumina variety of anorthosites. In 1823, K.F. Fuchs first described kyshtymite on the gold mine close to Borzovka River, South Urals of Russia (Koptev-Dvornikov et al., 1931; Kolesnik, 1976; Kolesnik et al., 1974).

Studied material was collected on the corundum deposit "5 versta" located northeast of the Borzovsky corundum deposit and on the boundary of the eastern flank of the Vishnevogorsky alkaline massif (Koptev-Dvornikov et al., 1931; Nedosekova et al., 2009). Bodies of meta-ultramafites with the lenses of kyshtymites were detected within the quartzites of the meta-terrigenous Saitovsky series. Studied kyshtimite vein is a lenticular body, found in an open pit of 3 m in depth. Meta-ultramafite host rocks mostly composed of enstatite. There is a reaction rim (10-25 cm) consisting of chrysotile-asbestos on the contact between host rocks and kyshtimites. According to the classification diagram of igneous rocks (Cox et al., 1979), studied kyshtimites belong to the alkaline rocks - iolite, alkaline gabbros and syenite-diorites (the average content of Al_2O_3 is 36.38 wt.%, SiO_2- 45.53 wt.%, CaO- 3.55 wt.%, Na_2O-3.55 wt.%, K_2O-0.91 wt.%). The rock-forming minerals of kyshtimite are corundum (up to 50% vol.), plagioclase - An_{61-93} (30-50 vol.%), muscovite (up to 10 vol.%), clinochlore, clinozoisite, accessory zircon and xenotime.

The formation of high-alumina associations within the Ilmenogorsky-Vishnevogorsky polymetamorphic complex likely links with the intrusions of the miaskites at 440-420 Ma and further development of the geological structure. This miaskite magma provided re-mobilization and redistribution of aluminum, as well as titanium, HFSE and LILE-elements under the lower crustal-conditions and partial melting of ultramafic host rocks producing kyshtymites at the stage of tectonic deformations (280-320 Ma).

The work was supported by a grant from the President of the Russian Federation (Project No. MK-4459.2018.5).

References

Koptev-Dvornikov VS, Kuznetsov EA, Borzovskoe corundum deposit: Petrological study., Moscow. Tekhizdat, 1931, 320 p.

Kolesnik Yu.N. High-temperature metasomatism in ultramafic massifs, 1976, 240 p.

Kolesnik Yu.N. Korolyuk V.N. Lavrent'ev Yu.G., Spinels and ore minerals of the Borzovsk deposit of corundum plagioclasites., ZVMO. 1974, Ch. 103, Iss. 3, c. 373-378.

Nedosekova IL, Vladykin NV, Pribakin SV, Bayanova T.B. the structure of the Ilmeno-Vishnevogorsk Mayskite-Carbonatite Complex: origin, ore-bearing. Sources of matter (Ural, Russia). Geology of Ore Deposits, 2009, Vol. 51, No. 2, p. 157-181.

Cox, K.G., Bell, J.D, Pankhurst, R.J. The Interpretation of Igneous Rocks, 1979, London, U.K.

SHRIMP U-PB ZIRCON AND OPAL GEOCHRONOLOGY, ISOTOPE GEOCHEMISTRY, AND GENESIS OF THE SUPER LARGE BE DEPOSIT AT SPOR MOUNTAIN, UTAH, USA

Foley N.K.*, *Ayuso R.A.

U.S. Geological Survey, Reston, Virginia, 20192 USA, nfoley@usgs.gov

Ongoing studies of the Spor Mountain beryllium (Be) deposit are focused on (1) characterizing the role of igneous rocks in the genesis of the ore zones, (2) determining the timing and duration of magmatic-hydrothermal events, and (3) establishing processes related to beryllium transport and

accumulation. The Spor Mountain Formation (SMF) hosts the deposit, which is the largest known volcanic rock-related Be deposit in the world (Foley et al., 2017). Discovery of the Be deposit at Spor Mountain in the 1960s displaced beryl as the main commercial source of beryllium in the global supply chain. Technological advances in mineral processing enabled bertrandite ($Be_4Si_2O_7(OH)_2$) ore of variable grade and composition from Spor Mountain to compete with beryl ore derived from pegmatite (Lederer et al., 2018; Foley et al., 2018). The deposit currently accounts for approximately 85% of the global beryllium mine production.

The Be deposit is in the Basin and Range province of North America, which is characterized by Oligocene and Eocene calderas, extensive alkalic rhyolitic lava and ash flow tuffs, widespread uranium and fluorite occurrences, and Precambrian to Paleozoic sedimentary rocks. The SMF consists of a hydrothermally-altered, fluorite-bearing, lithic-rich (clasts of carbonate, quartzite, and older volcanic rocks) pyroclastic tuff (informal name: Be tuff member) that is overlain by altered, porphyritic, and topaz-rich rhyolite (alkali rhyolite member) (Fig. 1). The tuff encloses elongate mineralized layers containing numerous nodules that consist of calcite, chalcedony, opal, fluorite, and bertrandite ($Be_4Si_2O_7(OH)_2$, the main ore mineral (Fig. 2).

Fig. 1. Photograph of the Spor Mountain Formation, Utah, showing gray rhyolite overlying bertrandite-mineralized pink tuff (Fluro Pit); vertical scale of opposite wall is approximately 50 m.

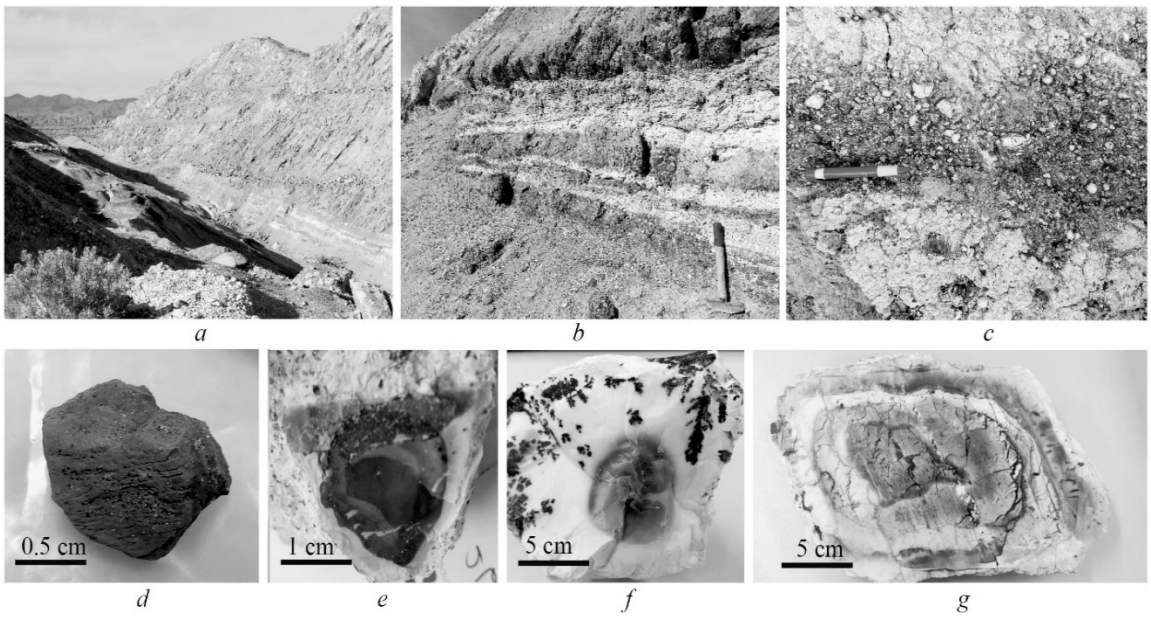

Fig. 2. a) Photograph of the Spor Mountain Formation, Utah, showing gray rhyolite overlying bertrandite-mineralized pink tuff at the Fluro Pit; vertical scale of opposite wall is approximately 50 m. b) View of the Be tuff member. c) Nodule-bearing layer in the Be tuff member. d-g) Various types of nodular ore.

Sensitive High-Resolution Ion Microprobe (SHRIMP) U-Pb zircon age determinations of the two members of the SMF (Ayuso et al., 2018) show that the weighted mean $^{238}U/^{206}Pb$ crystallization age of the Be tuff is between ca. 25.6 Ma and 25.1 Ma (Fig. 3a). The overlying capping rhyolite yields weighted mean $^{238}U/^{206}Pb$ crystallization ages between ca 26.2 Ma and 25.1 Ma (Fig. 3b). Thus, the ages of both the fluorite- and bertrandite-rich Be tuff and the overlying topaz-rich rhyolite are coeval. Ore zones in the Be tuff consist of bertrandite-rich elongate irregular bands and layers (Fig. 2b,c) with mineralized nodules (Fig. 2d-g). The nodules formed over time by hydrothermal replacement of Paleozoic carbonate rock fragments, which were rafted up from underlying sedimentary rock sequences during the catastrophic explosive eruptions that formed the Spor Mountain volcanic rocks. The layered nodules mainly consist of bertrandite, fluorite, opal, and lesser amounts of Mn-oxides and carbonate. Submicroscopic grains of bertrandite are mixed with abundant fine-grained fluorite, opal, and, rarely, calcite in the nodules; bertrandite-rich layers alternate with opal, opal+calcite, and opal+Mn-oxide+fluorite layers. Thin, outermost fluorite and bertrandite reaction rinds have up to ~100,000 ppm Be; layers of fluorite+bertrandite+opal contain >10,000 ppm Be.

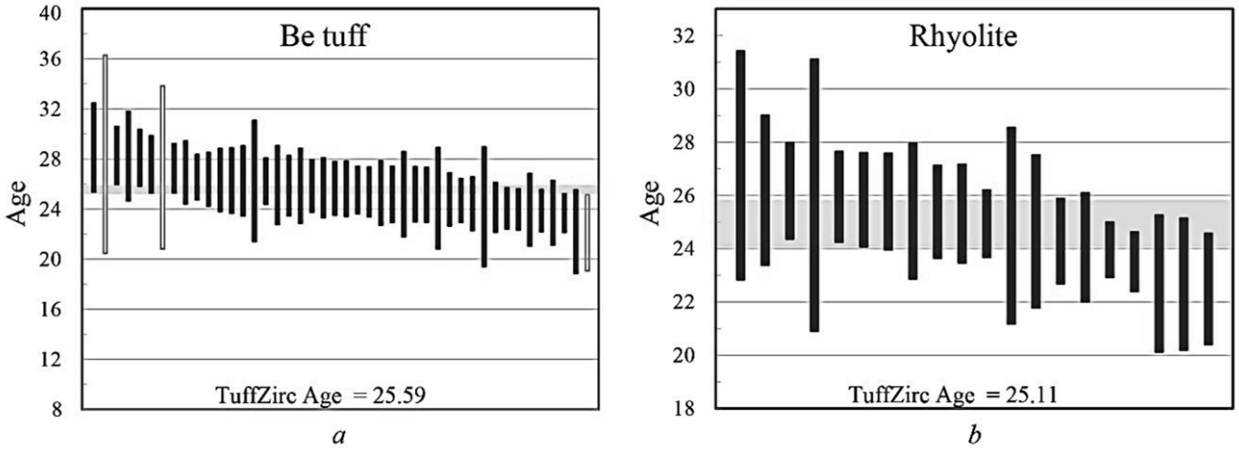

Fig. 3. Weighted mean $^{238}U/^{206}Pb$ crystallization ages (TuffZirc): a) Sample 16-110 is from the Be tuff (n = 41 spot analyses) at ca. 25.6 Ma. b) Sample 16-106 is from the capping rhyolite (n = 20 spot analyses) at ca. 25.1 Ma. Box heights are 2 σ.

New SHRIMP U-Pb age and geochemistry data monitor the evolution of these nodules and the timing of enrichment stages of Be and other metals (e.g., REE, Li, U, Th). Be concentrations of carbonate-free opal layers analyzed by SHRIMP methods range from 10 to 5,500 ppm. U-Pb analyses of opal indicate a range of $^{206}Pb/^{238}U$ ages ca. 25-26 Ma (nodule cores) to ca. 2 Ma (outermost layers) (technique adapted from Neymark et al., 1980). Together with fluctuations in Be contents, the protracted development of opal nodule layers documented by the U-Pb SHRIMP data (Ayuso et al., 2018; and this study) agrees with bulk thermal ionization mass spectrometry data (Ludwig et al., 1980) and supports the notion that the influx of Be into the deposit was part of a long-lived, multi-stage opal-depositing magmatic-hydrothermal system. Precipitation of Be-rich opal at ca. 25 Ma records the initiation of a magmatic-to-hydrothermal stage of mineralization that is generally coeval with crystallization of the host tuff (Ayuso et al., 2018). Younger opals likely record remobilization effects related to circulation of cooling hydrothermal fluids (some from external recharge).

The Be tuff is highly evolved (Zr/Ti ~0.1-0.3) and alkalic (Nb/Y ~0.6-2; rhyolite to trachyte). The tuff is also relatively depleted in Ba, Sr, Ti, P, Nb, etc., enriched in Cs, U, and Pb (Fig. 4a), and generally has flat rare earth element (REE) patterns with pronounced negative Eu anomalies (Fig. 5a). The capping rhyolite shares all the chemical features found in the Be tuff (Fig. 4a and 5a). Opal layers from nodules also generally mimic the compositional variations of the Be tuff (Fig. 4b).

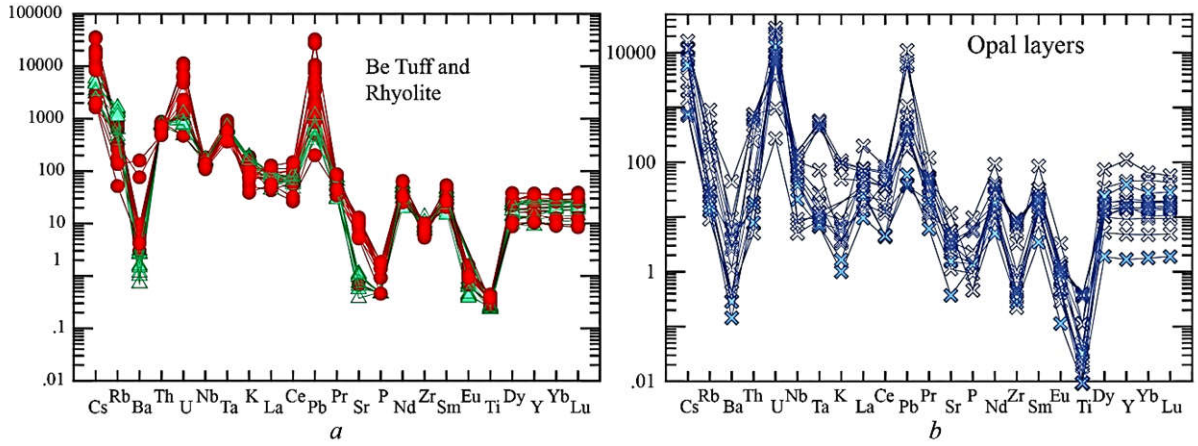

Fig. 4. Mantle-normalized abundances: a) Be tuff member and capping rhyolite of the Spor Mtn. Formation. b) Opal layers in nodules.

Trace element and REE contents of zircons from the two members of the SMF have overlapping values (U/Yb >0.1; REE patterns with positive Ce anomalies and pronounced negative Eu anomalies). Be concentrations in zircon from the Be tuff (1 to 300 ppm) and capping rhyolite (<100 ppm) also overlap. Bulk rock Be concentrations of the Be tuff (~10-4000 ppm) are significantly higher than the capping rhyolite (<50 ppm). These features are consistent with bulk rock and opal values for $^{206}Pb/^{204}Pb$ ~19.00-19.64, $^{207}Pb/^{204}Pb$ ~15.62-15.79, $^{208}Pb/^{204}Pb$ ~ 39.20-39.85 (Ludwig et al., 1980; and this study), $^{143}Nd/^{144}Nd$ values of ~0.51202-0.51226, and $^{87}Sr/^{86}Sr$ ~0.7120 that indicate magmatic sources originating from the lithosphere.

New geochemical modeling shows that critical features of the deposit were established early in its evolution when hydrothermal fluids enriched in aqueous fluoride complexes of Be, derived from Be-rich glass in the tuff, reacted with Paleozoic limestone clasts to form high-grade fluorite + bertrandite rims at contacts between tuff and limestone clasts. Be remobilization and reworking of ore continued intermittently over 10s of millions of years, as suggested by the opal data, primarily under pH-buffered, isothermal to cooling conditions (250º-100ºC).

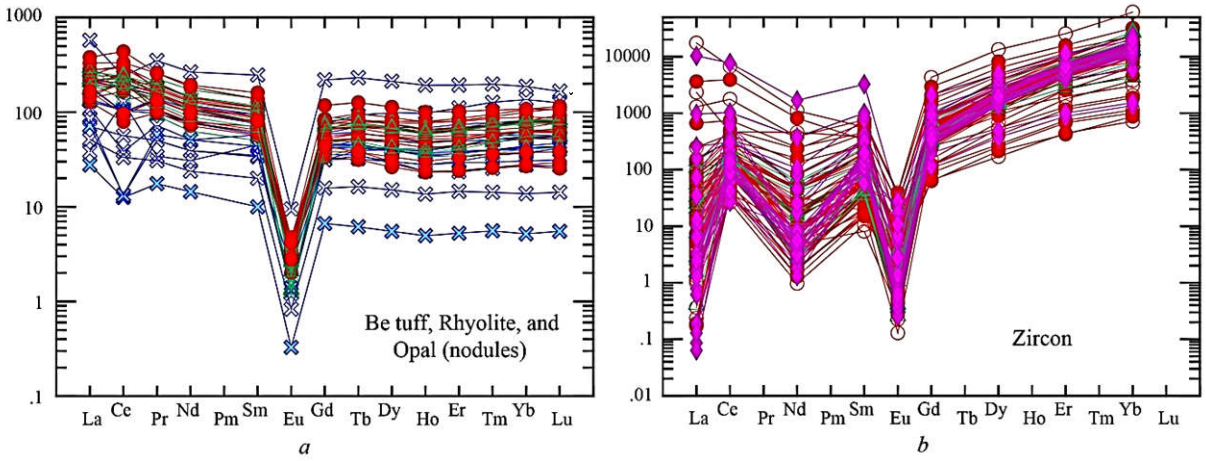

Fig. 5. Chondrite-normalized abundances: a) Bulk compositions of the Be tuff, rhyolite, and opal nodules in the Be tuff member. The Be tuff (circles) and rhyolite (triangles) overlap; the opal nodules (crosses) resemble the compositions of the Be tuff and have similar REE patterns but are significantly more diverse. b) Zircon compositions of the Be tuff member (circles) and capping rhyolite (triangles and rhombs). The two members of the SMF overlap.

The Be deposit likely formed as a result of protracted magmatic-hydrothermal processes (see Foley et al., 2018) initiated by eruption of rift-related alkalic and lithophile element-rich magmas at ca.

25-26 Ma. The magmas originated from the continental lithosphere. The widespread occurrence of geochemically similar volcanic rocks in the Basin and Range province of the western United States highlights the likelihood of additional resources of economically important volcanic-hosted Be deposits.

References

Ayuso, R.A., Foley, N.K., Vazquez, J.A., Lederer, G.W, Jaskula, B.W. (2018) SHRIMP U-Pb Geochronology of zircon and opal and geochemistry of the world-class volcanic-related beryllium deposit at Spor Mountain, Utah, USA [abs]: Resources for Future Generations, Vancouver, Canada.

Foley, N.K., Jaskula, B.W., Piatak, N.M., Schulte, R. (2017) Chapter E: Beryllium, Schulz, K.J., Bradley, D.C., DeYoung, J.H., Jr., and Seal, R.R., II (eds) Critical mineral resources of the United States—Economic and environmental geology and prospects for future supply. U.S. Geological Survey Prof. Paper 1802. 44 p.

Foley, N.K., Ayuso, R.A., Vazquez, J.A, Lederer, G.W., Jaskula, B.W. (2018) Genesis of the super large Spor Mountain, Utah, USA beryllium deposit: Timing and duration of dynamic magmatic-hydrothermal processes [abs]: Resources for Future Generation, Vancouver, BC, Canada.

Lederer, G.W., Foley, N.K., Jaskula, B.W., Ayuso, R.A. (2018) Global Beryllium Supply Chain and Materials Flow Analysis [abs]: Resources for Future Generation, Vancouver, BC, Canada.

Lindsey, D.A. (1977) Epithermal beryllium deposits in water-laid tuff, Utah. Econ. Geol. 72:219–232.

Ludwig, K.R., Lindsey, D.A., Zielinski, R.A., Simmons, K.R. (1980) U-Pb ages of uraniferous opals and implications for the history of beryllium, fluorine, and uranium mineralization at Spor Mountain, Utah. Earth Planet. Sci. Letters. 46:221–232.

Neymark, L.A., Paces, J.B. (1980) Ion-probe U-Pb dating of authigenic and detrital opal from Neogene-Quaternary alluvium.// Earth Planet. Sci. Letters. 1980. v. 361 p. 98–109. 2013.

TI-NB MINERALIIZATION IN LATE CARBONATITES OF THE PETYAYAN-VARA (VUORIYARVI)

***Fomina E.N.*[1], *Kozlov E.N.*[1], *Sidorov M.Yu.*[1], *Shilovskikh V.V.*[2]**

[1]*Geoological Institute of Kola Science Centre RAS, Apatity, fomina_e.n@mail.ru*

[2]*"Geomodel" Resource Centre of St. Petersburg State University, St. Petersburg*

The deposits of critical elements (HFSE and REE) in carbonatite complexes are mainly associated with the latest carbonatite differentiates. The leading role in the formation of the latter is played by carbo(hydro)thermal-metasomatic processes, which are often multi-stage. Therefore, deciphering the petrogenesis of late carbonatites is a complex and fascinating task. The use of genetic mineralogy methods for titanium and niobium oxides, which are widespread in late carbonatites, is effective for petrogenetic interpretation.

Here we consider the poorly studied carbonatites of the Petyayan-vara area located in the eastern part of the Vuoriyarvi alkaline-ultrabasic carbonatite complex composed of (in the formation order) olivinites, pyroxenites, foidolites and nepheline syenites. The latest formations are stockworks of various carbonatites, occupying several isolated fields. Most of them are calciocarbonatites with ore specialization for apatite, magnetite and pyrochlore.

In most carbonatite fields, late varieties are rare. On the Petyayan-vara area, carbonatites stand out by a diversity of mineral parageneses and widely spread late mineralization. They are unusual for both the Vuoriyarvi massif and the Kola Alkaline Province in general. There are magnesiocarbonatites within the Petyayan-vara field, but unaltered dolomite carbonatites are uncommon. The rocks underwent at least 3 stages of metasomatic processing: (1) alkaline aluminosilicate metasomatism simultaneously with apatitization, (2) Ba-REE-Sr metasomatism and (3) hydrothermal action of a fluid supersaturated with Si and REE.

In the Petyayan-vara carbonatites, the bulk of titanium and niobium oxides was formed during alkaline-aluminosilicate metasomatism, which was the earliest of the superimposed processes.

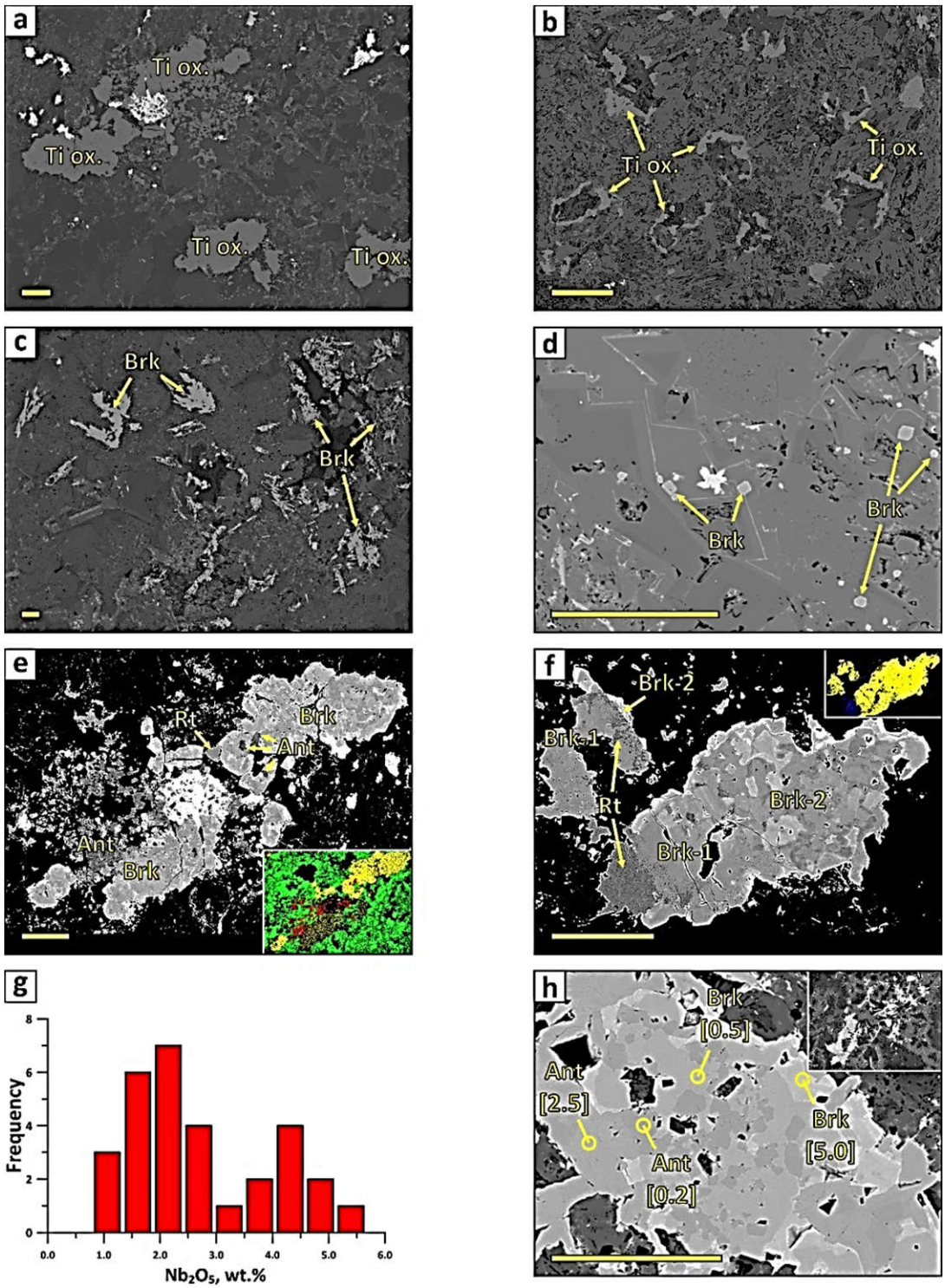

Fig. 1. Morphotypes of titanium oxides (Ti ox.) from Ti-carbonatites: (a) amoeboid segregations; (b) xenomorphic rims around carbonate grains; (c) segregations of elongated brookite (Brk) crystals; (d) idiomorphic individuals of brookite. BSE images. Anatomy of amoeboid TiO_2: (e) and (f), contrasting BSE images. On the inserts - phase distribution maps within the same sections, obtained by the EBSD: yellow - brookite (Brk), red - anatase (Ant), blue - rutile (Rt). Histogram of the Nb2O5 contents in titanium oxides - (g). An example of the Nb_2O_5 distribution in the "penetrating" rim developing both in anatase and brookite in the segregation of titanium oxides from TiO_2-dolomite-calcite veins - (h). The square brackets show the Nb_2O_5 content (wt. %). The morphology of these segregations is shown on the insert. Scale rulers are 100 μm.

Consequently, these minerals "witnessed" the entire path of the formation of late carbonatites. In addition, titanium oxides in carbonatites that underwent this process are rock-forming minerals. Geochemically this is expressed in the enrichment of rocks by Ti. Ti-rocks are enriched with other components specific for carbonatites: Si, Al, K. Furthermore, only samples enriched in titanium are sometimes have significant amount of apatite, although in most of these rocks the phosphorus content is not great. In comparison with other carbonatites of the Petyayan-vara, titaniferous carbonatites have high amounts of Fe concentrated in the ankerite minal of dolomite and in oxides-hydroxides of Fe. Compared with the most common in the Petyayan-vara Ba-Sr-REE-carbonatites, titanium-rich varieties are characterized by low contents of Ba, Sr, REE, like unaltered dolomite carbonatites do. To date, the authors do not have an unambiguous answer, whether the latter were a protolith for the titanic species or they were formed autometasomatically over the carbonatites of an additional intrusion phase. However, the high importance of fluid processing in the formation history of Ti-carbonatites is doubtless. Near the titanic varieties, thin TiO2-dolomite-calcite veinlets are observed in the "ordinary" dolomite carbonatites. They were formed in cracking zones and indicate fluid mobility of titanium. Rarely, the same cracks are filled with a pyrochlore minerals.

Optical diagnostics of titanium oxides in the studied rocks proved to be unclear. Obviously, anatase, brookite and rutile do not differ in chemical composition as well. In view of this, for their determination, we used methods based on the structural characteristics of the phases: Raman spectroscopy (RS) and electron backscatter diffraction (EBSD). The first was used for express identification, the second allowed to visualize the ratios of TiO_2 polymorphs. Researches were conducted in the "Geomodel" Resource Centre of SPbSU.

Ti oxides are represented by three polymorphic modifications: anatase, rutile and brookite. The most common is brookite. Titanium carbonatites contain four morphotypes of this mineral. These are (I) amoeboid segregations, (II) xenomorphic rims around the carbonate grains, (III) segregation of elongated crystals and (IV) small idiomorphic individuals (Figs. 1a-d). Types I-III are present mostly in the matrix of the rock, while IV are observed exclusively near selvage of secant calcite veins along with the late association of dolomite. In a single structural position with brookite IV, single idiomorphic grains of pyrochlore have been found. Most of them are zonal: (a) the F-free Th-variety forms submicron nucleuses, (b) the bulk is occupied by Ca-F-pyrochlore replaced at the edges and cracks by (c) F-free Pb-pyrochlore.

In a detailed examination of the amoeboid segregations anatomy, three polymorphic modifications of TiO_2 were detected in their structure (Fig. 1e, f). The anatase grains are fragments, the largest of which are included into the brookite segregations, while the smaller ones form clusters outside of these (Fig. 1e). Brookite accounts for more than 80% of the formations. It was grown in at least two stages. Brookite of early generation Brk-1 is chemically homogeneous and is prone to be replaced by radial-ray paramorphoses of spongy rutile containing Ca, Si and P admixtures (Fig. 1f). The late generation of brookite (Brk-2) overgrown both Brk-1 and rutile that substituted the latter. In addition, Brk-2 is very heterogeneous in Nb content, therefore it has a mosaic appearance on BSE-images.

In the investigated grains of titanium oxides, the Nb_2O_5 content varies from 0.8 to 5.2% by weight. Thus, due to its maximum prevalence, brookite is the main concentrator of niobium in Ti-rich rocks. The distribution of niobium oxide in the sampling was bimodal with pronounced maxima of 2.2 and 4.3 wt.% (Fig. 1g). There is also a Nb enrichment tendency towards the late generation of brookite. The key to understanding the mechanism of niobium accumulation is its distribution in glomeroblastic clusters of titanium oxides from TiO_2-dolomite-calcite veins common in dolomite carbonatites surrounding Ti-rocks. Anatase and brookite are present in equal parts in them, and rutile is absent (Fig. 1h). Anatase forms the spindle-shaped crystals of excellent cut, while brookite either includes it, or coexists with it in the form of idiomorphic isometric grains. We note that the appearance of TiO_2 glomeroblasts is similar to that of Brookite III (cf. Fig. 1c and the inset in Fig. 1h). This allows us to assume the paramorphic genesis of the latter. Probably, anatase in Ti-carbonatites was initially spread more widely, but the superimposed fluid processes ruined it. Of interest is the presence of rims that penetrated both anatase and brookite edges in the glomeras under discussion. In these rims, the Nb

content increases by an order of magnitude (Fig. 1)! We believe this is a direct indication of the responsibility of the residual fluid phase for the Nb enrichment of rocks. This is confirmed by the presence of chain pyrochlore mineralization without titanium oxides in dolomite carbonatites. This pyrochlore is identical to that previously described in titanic carbonatites, even by its zonality.

We came to the following conclusions: (1) the coexistence of three polymorphs of TiO2 and their paramorphic transitions indicate abrupt changes in physicochemical conditions during mineral formation; (2) a residual Ti-Nb fluid took part in the formation of Ti-carbonatites and complementary rocks; (3) when the fluid influenced, the separation of Ti and Nb occurred.

The work was carried out in the GI KSC of the Russian Academy of Sciences within the framework of state order No. 0231-2015-0009.

INCORPORATION OF NITROGEN INTO LOWER-MANTLE MINERALS FROM HIGH P-T EXPERIMENTS UNDER CONTROLLED FE-FEO BUFFER

***Fukuyama K.*[1], *Kagi H.*[1], *Inoue T.*[2,3], *Shinmei T.*[3], *Kakizawa S.*[3], *Takahata N.*[4], *Sano Y.*[4]**

[1]*Geochemical Research Center, Graduate School of Science, The University of Tokyo*

[2]*Department of Earth and Planetary Systems Science, Hiroshima University*

[3]*Geodynamics Research Center, Ehime University*

[4]*Atmosphere and Ocean Research Institute, The University of Tokyo*

(ko.fukuyama@eqchem.s.u-tokyo.ac.jp)

Nitrogen occupies about 80% of the Earth 's atmosphere and is an essential element of life. Moreover, it is suggested that nitrogen had an impact on the climate in the early Earth (e.g. Goldblatt et al., 2009; Wordsworth and Pierrehumbert, 2013). Therefore, nitrogen is an important volatile element in the early Earth evolution process and origin of the life. However, we still cannot fully understand the behavior of nitrogen in the deep Earth. For example, nitrogen is depleted compared to other volatile elements in deep mantle (Marty et al., 2012). The "missing" nitrogen is an important subject in Earth Science.

In this study, we compared nitrogen incorporation into lower-mantle minerals (bridgmanite, periclase and stishovite) synthesized using multi-anvil apparatus installed at Geodynamics Research Center, Ehime University under the conditions of 27 GPa and 1600℃-1700℃. In these experiments, we used Fe-FeO buffer in order to reproduce the redox state of the lower mantle. Two types of starting materials having dry bridgmanite composition and wet bridgmanite composition: a powder mixture of SiO_2 (quartz) and MgO and a powder mixture of SiO_2, MgO, Al_2O_3 and $Mg(OH)_2$ were used for starting materials. We used $^{15}NH_4{}^{15}NO_3$ as nitrogen source and the nitrogen source was installed into sample capsules. Nitrogen in recovered samples was analyzed using NanoSIMS installed at Atmosphere and Ocean Research Institute.

A series of experimental results revealed that stishovite and periclase can incorporate more nitrogen than bridgmanite. This suggests that periclase, a major mineral in the lower mantle, may be a nitrogen reservoir. Moreover, stishovite which is formed by the transition of the SiO_2-rich oceanic crustal sedimentary rocks transported to the lower mantle via subducting slabs can incorporate more nitrogen than bridgmanite (about 5-55 ppm nitrogen concentration reported by Yoshioka et al. (2018)). In addition, metallic iron containing almost no Pt remained in the Fe-FeO buffer after experiments, which suggested that redox state of the lower mantle was achieved in our experiments.

Our study suggests that nitrogen would continue to be supplied to the lower mantle via subducting slabs since approximate 4 billion years ago when the plate tectonics initiated, forming a “hidden” nitrogen reservoir in the lower mantle. Furthermore, this “hidden” nitrogen reservoir may play a role in decreasing high-concentration nitrogen which enhanced greenhouse effect in the early atmosphere (Goldblatt et al., 2009) to the present nitrogen concentration level.

References

Goldblatt, C., Claire, M. W., Lenton, T. M., Matthews, A. J., Watson, A. J., & Zahnle, K. J. Nitrogen-enhanced greenhouse warming on early Earth// Nature Geoscience. 2009. Vol. 2 Iss. 12 pp.891-896.

Marty, B. The origins and concentrations of water, carbon, nitrogen and noble gases on Earth. Earth and Planetary Science Letters. 2012. Vol. 313 pp.56-66.

Wordsworth, R., & Pierrehumbert, R. Hydrogen-nitrogen greenhouse warming in Earth's early atmosphere// science. 2013. Vol. 339 Iss. 6115 pp.64-67.

Yoshioka, T., Wiedenbeck, M., Shcheka, S., & Keppler, H. Nitrogen solubility in the deep mantle and the origin of Earth's primordial nitrogen budget// Earth and Planetary Science Letters. 2018. Vol. 488 pp.134-143.

ALKALI-ULTRABASIC ROCKS IN THE NORTHEAST OF TAYMYR (RUSSIA)

Goloburdina M.N.

A. P. Karpinsky Russian Geological Research Institute Saint Petersburg, Russia,
marina_goloburdina@vsegei.ru

An intruding thin body of alkali-ultrabasic rocks has been revealed in the Northeast Taimyr during regional mapping of an ultrabasic massif in the middle reaches of the Stanovaya River. In a context of the region ore potential, it is important to scrutinize compositional features of the ultrabasic and alkali-ultrabasic rocks and to determine their formational belonging.

The ultrabasic rocks form elongated bodies up to first tens of meters as thick, extending for several of kilometers (Vernikovsky, 1996). The rocks are confined to the NNE fault zone with the length of 30 km. Their host rocks are metamorphosed under amphibolite, epidote-amphibolite and greenschist facies conditions and are of the Proterozoic age.

In the studied massif the ultramafic rocks are completely serpentinized. The relict structural and mineralogical characteristics and chemical composition (SiO_2 25-36, Al_2O_3 0.3-5.9, MgO 31.3-41.7, $K_2O + Na_2O$ <0.1, TiO_2 <0.01, MnO 0.08-0.9%, average (N=21) Ni = 2000 ppm, average (N=21) ΣREE = 0.27 ppm, average (N=21) La/Yb = 0.88) suggest that the rocks correspond to apo-dunite and apo-harzburgite serpentinite of dunite-harzburgite formation. Chrome-spinelide, occurring in the ultrabasic rocks, has a Cr – Al trend (Fig.1). At the massif fringes and in fractured zones their compositions change to ferrous-chromite and chromium-magnetite with Cr – Fe^{+3} trend. Their zonal character of alumo-chromite substitution indicates their metamorphic-metasomatic nature.

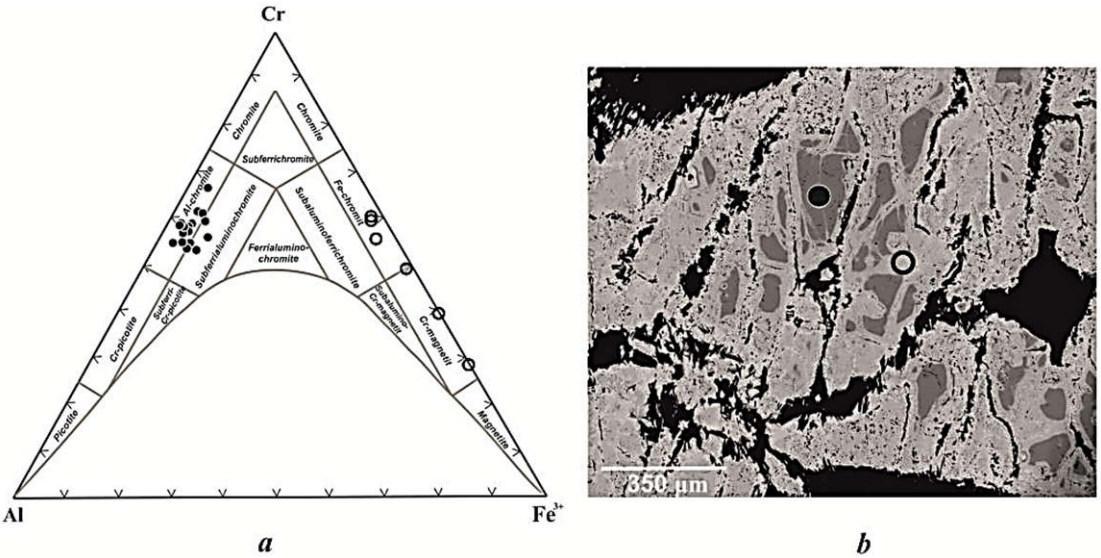

a *b*

Fig. 1. *a* - compositional features of chrome-spinelides from the rocks of dunite-harzburgite formation in the Pavlov classification diagram (1949). *b* - compositions of the chrome-spinel grains.

An ultrabasic rock dating is problematic. The ultrabasic rocks are accompanied by chromite (Cr_2O_3 up to 32.3%) and sulphide-nickel mineralization.

The alkali-ultrabasic rocks form a horizontally sheet body, probably a sill (c. 0.3 m thick) cutting the described ultrabasic rocks (Fig. 2). Contacts are abrupt, intrusive. The exocontact comprises an up to 1 cm thick band of lightened serpentinite. The rocks contain lenticular boudins of serpentinite.

The alkali-ultramafic rock is an apatite-pyroxene phlogopitite of gray color with a greenish-brownish hue, fine-grained and massive. Microscopically, the rocks have a hypidiomorphic-grained and poikilitic textures. It is composed of phlogopite (60%), clinopyroxene (20%), apatite (15%), titanite (<1%). The rock is unevenly carbonated (up to 10% vol.). Its endocontact zone contains an increased up to 40% amount of clinopyroxene and the rock texture gradually passes to a finer-grained prismatic granular due to a prismatic appearance of minerals forming radial aggregates. EDX analysis (analysts A. V. Antonov and E. L. Gruzova) of the rock revealed some accessory minerals: allanite, baddeleyite, zircon, thorianite and Mn-ilmenite (MnO 8.9-10.0%). According to the content and distribution pattern of REE, the studied rock is comparable to a foscorite of the Maimecha-Kotui Province (Fig. 2). The apatite-pyroxene phlogopitite compositionally correspond to rocks associated with ore bodies of an alkaline-ultramafic formation comprising foscorite and carbonatite. Similar rocks are known in zoned ultrabasic - alkali complexes of the Kola Peninsula and Maimecha-Kotui Provinces.

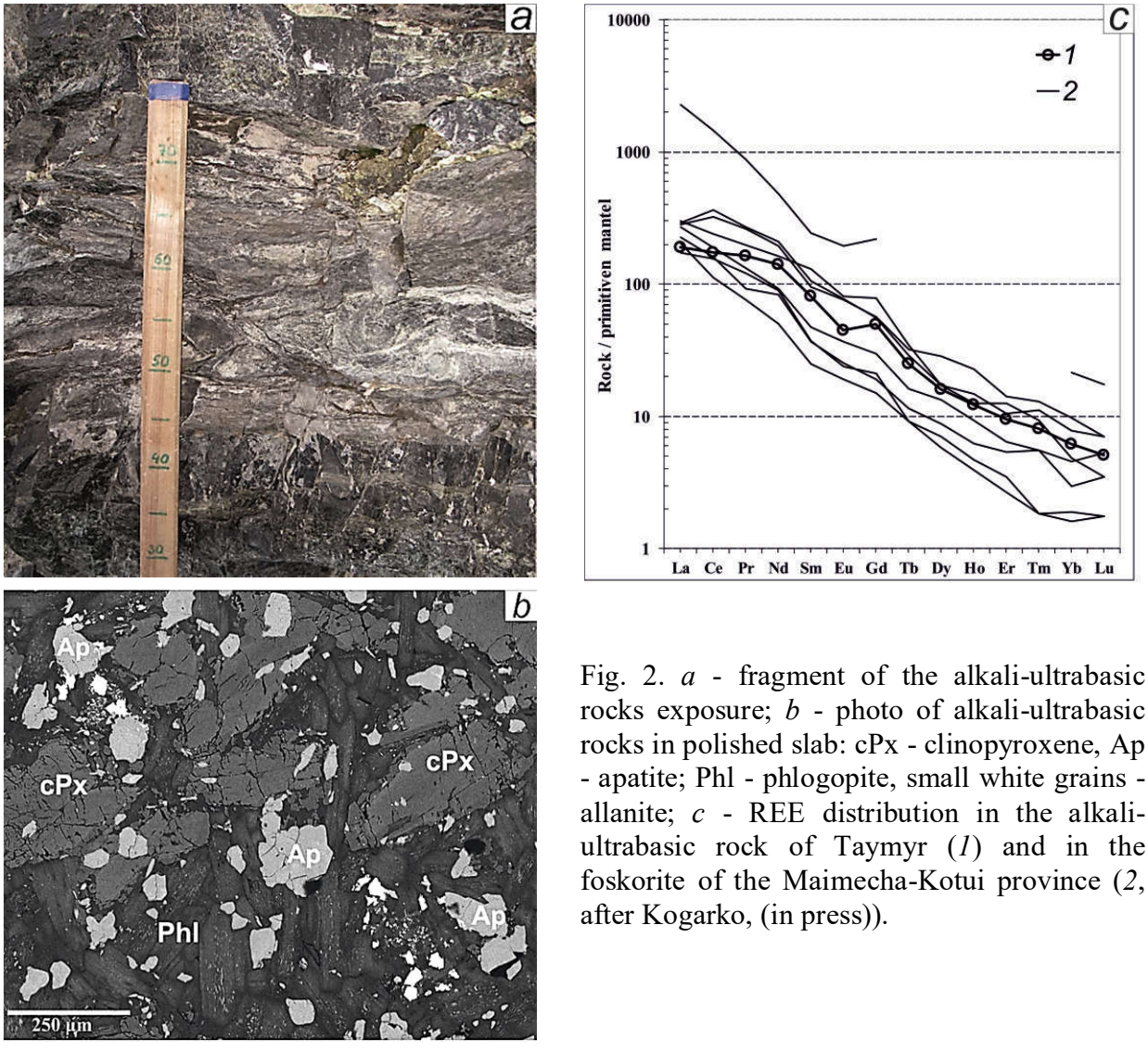

Fig. 2. *a* - fragment of the alkali-ultrabasic rocks exposure; *b* - photo of alkali-ultrabasic rocks in polished slab: cPx - clinopyroxene, Ap - apatite; Phl - phlogopite, small white grains - allanite; *c* - REE distribution in the alkali-ultrabasic rock of Taymyr (*1*) and in the foskorite of the Maimecha-Kotui province (*2*, after Kogarko, (in press)).

The combination of ultrabasic rocks of the dunite-harzburgite formation with apatite-pyroxene-phlogopite rocks of the alkali-ultramafic formation looks very unusual, taking into account differences of their nature. However, an increasing number of publications on the finding of carbonatite in atypical tectonic settings (Jones et al., 2013) allows to consider those settings as potentially valuable for trace element and rare-earth ores.

In the Taimyr Peninsula, a carbonatite are known as gold-bearing, copper-polymetallic-sulphide-bearing and having a fluorite-barite mineralization (Proskurnin et al., 2010). The conducted study has demonstrated that alkali magmatism took place in the NE Taimyr. It is potentially ore-bearing and associates with trace-element and REE mineralization. The described rock association is promising for further identification of ore-bearing carbonatite bodies.

References

Jones A.P., Genge M., Carmody L. Carbonate Melts and Carbonatites**.** // Reviews in Mineralogy and Geochemistry. 2013. Vol. 75, pp. 289-322.

Kogarko L. N. (in press) Potential of strategic metals in alkali rocks of Polar Siberia (rare earth and radioactive metals).

Proskurnin V .F., Petrov O. V., Gavrish A. V., Paderin P.G., Mozaleva I.N., Petrushkov B.S., Bagaeva A.A. Early Mesozoic belt of carbonatites of the Taimyr Peninsula. // Lithosphere. 2010. No. 3, pp. 95-102.

Vernikovsky V.A. Geodinamic evolution of Taimyr folded area. Novosibirsk: Published by Siberian Branch RAS, SPC UIGGM, 1996. 202 p.

FLOOD BASALT AND ORE-BEARING INTRUSIONS OF THE NORILSK REGION: SOURCES AND CONDITIONS FOR THE FORMATION OF ORE-BEARING MAGMA

Gorbachev N.S.

IEM RAS, Chernogolovka, gor@iem.ac.ru

Deposits of sulfide ores of the Norilsk region are among the largest deposits of nickel and platinum metals. They are confined to stratified intrusions, the formation of which is associated with the permo-triassic flood basalt magmatism of the Siberian platform. Although a large number of publications (Dodin et.al., 2000; Gorbachev 2005, 2006, 2010, 2012; Krivtsovet.al., 2001; Lightfoot et.al., 1990, 1994, 2005; Naldrett et.al., 1992, 1998; Sobolev et.al., 2009), the main problem is the sources and conditions for the formation of super-concentrations of sulfides and metals in them in small (up to 10 km^3) intrusions are still debatable. In this connection, the features of tectono-magmatic activation of the Noril'sk region, stratigraphy and geochemistry of the effusive strata, intrusions of the Norilsk type and its ores are considered. Based on geological, geochemical and experimental data, a genetic model for the formation of ore-bearing magma is proposed, scales and further perspectives of the region in relation to sulfide mineralization, and their search characteristics are estimated.

Geology and magmatism. The Permian–Triassic flood basalt magmatism of the Noril'sk district developed in part of the Siberian Platform with Archean–Paleoproterozoic basement broken into blocks and overlapped by a sedimentary cover up to 13 km thick and a volcanic sequence reaching 3.7 km in thickness. The geophysical data show that remnants of the subducted ancient oceanic crust exist in the mantle and fragments of transitional magma chambers and conduits are retained at different levels of the Earth's crust. The cyclic tectonomagmatic evolution of the territory was characterized by alternation of extension with intense volcanic activity and compression accompanied by waning of volcanic eruptions. The early rifting, transitional stage, and late dispersed spreading are distinguished. The associations of volcanic (lavas and tuffs) and intrusive rocks were formed during each stage. The volcanic sequence is subdivided into 11 suites. Two of primary magmas differ in geochemistry of lavas and intrusions: (1) OIB type high-Ti magma (iv, sv, gd formations of the first stage from bottom to top) and (2) low-Ti magma (hk, tk, nd formations of the second stage and mr–mk formations of the third stage). The nd formation depleted in ore elements and the ore-bearing cumulus composed of

silicate and sulfide melts in combination with early silicate minerals and chromite are products of the fractionation of the primary low-Ti magma.

The intrusions of the Talnakh and Noril'sk ore fields are distinguished by two level structure with the Upper Noril'sk ore-bearing intrusions above and the Lower Noril'sk barren intrusions below. As follows from geochemical parameters, intrusions of the Lower Noril'sk type are comagmatic to the evolved lavas of the nd_3 subformation, whereas intrusions of the Upper Noril'sk type are comagmatic to the lavas of the mr–mk formations. Geochemical similarity with volcanic rocks provides evidence for the composition of the initial magma and the time of intrusion emplacement. The ore bearing intrusions of the Upper Noril'sk type were formed at the onset of the third stage, when the primitive low-Ti magma similar to the lavas of mr–mk formations in composition was emplaced. When intruding, this melt captured and transported ore-bearing cumulus (drops of sulfide melt, early olivine and chromite grains) into the magma chamber. Separate portions of sulfide liquid were involved into movement as a self-dependent intrusive subphase during formation of the Talnakh and Kharaelakh intrusions.

Sulfur solubility. An extremal effect of pressure on sulfur concentration in fluid-bearing and sulfide-saturated mafic magmas has been established in experiments at P = 1–4 GPa. In this interval of pressure, the S concentration in sulfide-saturated magmas increases in the following sequence: dry magma ≤ (H_2O+CO_2)-bearing magma < H_2O-bearing magma. In the regions of low (< 0.3 GPa) and high (> 2.5 GPa) pressures, the S contents (0.1–0.2 wt.%) are commensurable. The experimentally established extremal nature of the effect of pressure on the sulfur concentration in fluid-containing mafic magmas under conditions of sulfide saturation with a maximum (up to 0.9 wt.% S) in the range P = 1.0-2.0 GPa and very low solubility (≤ 0.1 wt.% S) at P ≤ 0.1 GPa and at P ≥ 2.5 GPa can play an important role in the formation of ore-bearing magmas and the transport of sulfides from deep magmatic foci to the upper horizons of the earth's crust.

Isotopic composition of sulfur. The sulfur enrichment of the sulfides of the deposits with a heavy isotope at a constant ratio of mantle and crustal sulfur to them can be explained by the admixture of the sulfur crust in the mantle source containing protoliths of the subducted oceanic crust, during melting of which sulfide-silicate and silicate magmas, and also the fluids were initially enriched with 34S.

Experimental simulation of the formation of ore-bearing magmas from mantle chamber containing protoliths of the subducted oceanic crust could serve as a source of volatile and primary trap magma. Our experimental modeling of magma formation from such a source showed that in the interval P=1.5-4.0 GPa, the formation of melts of the picrite-basalt composition occurs already at T=1250-1350ºC and is accompanied by pyroxenization of the mantle peridotite resulting from the reaction with the melt. These features determined the large volume of generated melts, their enrichment with olivine-compatible elements.

Sulfide ores. Fractional crystallization and emanation differentiation of sulfide magma and related mineralogical and geochemical zoning are exemplified in massive sulfide ores of the Oktyabr'sky deposit, Noril'sk district. The mineralogical zoning is expressed in the change of mineral types of ore from pyrrhotite (Po) to chalcopyrite (Cp) (from the flanks to the center of the ore lode). In terms of geochemistry, the Cu content, Cu/(Cu + Ni) ratio, and contents of noble metals incompatible with Mss (Pt, Pd, and Au) increase in this direction, while the S and Fe contents decrease. The distribution of elements compatible with Mss (Ir, Os, Rh, and Ru) is more complex. Their contents decrease from Po to high-Cu Cp ore, although there is a second maximum for Cb-type ore. The distribution of ore elements in the vertical and horizontal sections of massive ores at the deposit is different. The upper outer contact zone and frontal parts of massive ore lodes are enriched in all ore elements and a light sulfur isotope. The succession of enrichment is correlated with the relative affinity for sulfur and remains independent of the affinity of these elements for Mss (Pd–Rh, Os–Au). The possible role of liquid immiscibility of sulfide magma in the development of the mineralogical and geochemical zoning of massive ore is discussed.

Conclusion. The calculation results show that the amount of sulfides in the known deposits does not exceed 2% of geological resources of the sulfides separated from the flood basalts. Therefore, the

chance of discovery of new deposits remains rather high. Proceeding from the conditions of ore-bearing magma formation and geological setting of the known deposits, criteria for recognition of potentially ore-bearing areas are proposed and such areas are outlined.

I thanks Naldrett A., Lightfoot P., Fedorenko V. long-term cooperation in the study of the Noril'sk ore district; V.E. Kunilov and A.I. Stekhin for their assistance in conducting fieldwork, visiting mines and sampling. The work was supported by the RFBR grant 17-05-00930a.

References

Dodin D. A., N. M. Chernyshov, and B. A. Yatskevich. PGM Deposits of Russia (Nauka, St. Petersburg, 2000) [in Russian].

Gorbachev N. S., Kostyuk A. V., Nekrasov A. N. Influence of water on sulfur solubility in mafic melts at high pressures // Doklady Earth Sciences. 2005. Vol. 401, no. 3. P. 421–423.

Gorbachev N.S. Mineralogical and geochemical zoning and genesis of massive sulfide ores at the Oktyabr'sky deposit // Geology of Ore Deposits, 2006, Vol. 48, No. 6, pp. 473–488.

Gorbachev N.S. Experimental study of interaction between fluid-bearing basaltic melts and peridotite: a mantle-crustal source of trap magmas in the Norilsk Area // Petrology, 2010, Vol. 18, No. 4, pp. 416–431.

Gorbachev N.S. Sources and formation conditions of sulfide-silicate magmas in the Noril'sk district // Geology of Ore Deposits, 2012, Vol. 54, No. 3, pp. 155–178.

Krivtsov A. I., V. I. Kochnev-Pervukhov, O. M. Konkina, et al. Cu-Ni-MPG Deposits of the Noril'sk Type (TsNIGRI, Moscow, 2001) [in Russian].

Lightfoot P.C., Naldrett A.J., Gorbachev N.S. et al. Geochemistry of the Siberia trap of the Noril'sk area USSR with implications for the relative contributions of crust and mantle to flood basalt magmatism. // Contrib Mineral Petrol. 1990. V.104. p.631-644.

Lightfoot P.C, Naldrett A.J., Gorbachev N.S., et al. Chemostratigraphy of Siberia trap lava, Noril'sk district, Russia: Implications for the source of flood basalt magma and their associated Ni-Cu mineralization, //Can. Mineral. Sudbery - Noril'sk Symposium Volume, OGS Special Publication N.5. 1994. p.1-52.

Lightfoot P. C. and R. R. Keays, "Siderophile and Chalcophile Metal Variation in Flood Basalts from the Siberian Trap, Norilsk Region: Implications for the Origin of the Ni_Cu_PGE Sulfide Ores," Econ. Geol. 2005. 100, p.439-462.

Naldrett A.J., Lightfoot P.C, Fedorenko V.A., Gorbachev N.S. et al. Geology and geochemistry of intrusions and flood basalt of the Noril'sk Region, USSR with implication for the origin of the Ni-Cu ores. //Econ. Geol. v.87, N4, 1992. p. 975-1004.

Naldrett A.J., Lightfoot P., Gorbachev N.S. e.a. A model for formation of the Ni-Cu-PGE deposits of the Norils'k region. 1998. International Platinum. S.-Peterburg. Atheus. P. 92-106.

Sobolev A.V., Krivolutskaya N.A., and Kuz'min D.V. Petrology of the Parental Melts and Mantle Sources of Siberian Trap Magmatism // Petrology 17 (3), 2009. P.276-310.

SUWAŁKI VS. SEJNY JOTUNITES – AN ATTEMPT OF COMPARISON (NE POLAND)

Grabarczyk A.

Institute of Geochemistry, Mineralogy and Petrology, Faculty of Geology, Warsaw University, anna.grabarczyk@student.uw.*edu.pl*

The crystalline basement of Polish part of East European Craton (EEC) is covered by a thick layer of Phanerozoic sediments ranging from 600 m in NE part of Poland up to 6,500 m along the Trans European Suture Zone (TESZ) and it is explored only by geophysics and drillings (Wiszniewska at al., 2002). The Mezoproterozoic Mazury Complex (Fig. 1) is composed mostly of rapakivi type granites, which have been interpreted as A-type, and several more mafic intrusions of anorogenic character and bimodal composition. Three massive-type anorthosite-norite massifs were recognized: Suwałki, Kętrzyn and the smallest one – Sejny (Wiszniewska and Bagiński, 2003), which together

with granitoids create, common in Proterozoic, AMCG (anorthosite-mangerite-charnockite-granite "rapakivi") suite (Bagiński et al., 2007). Because of appearance of oxides Fe-Ti-V ore deposites only two anorthosite massifs were investigated on a greater extent. Massifs show in a cross-section a diapiric character, where the centre is built of anorthosite and norite with ferrolites and diorites appear in the external part. Jotunitic rocks, were also described, but their composition is slightly different in each massif (Wiszniewska et al., 2002). Recent Re-Os dating indicates 1559 ± 37 Ma of oxide minerals and anorthosites (Wiszniewska et al., 2002).

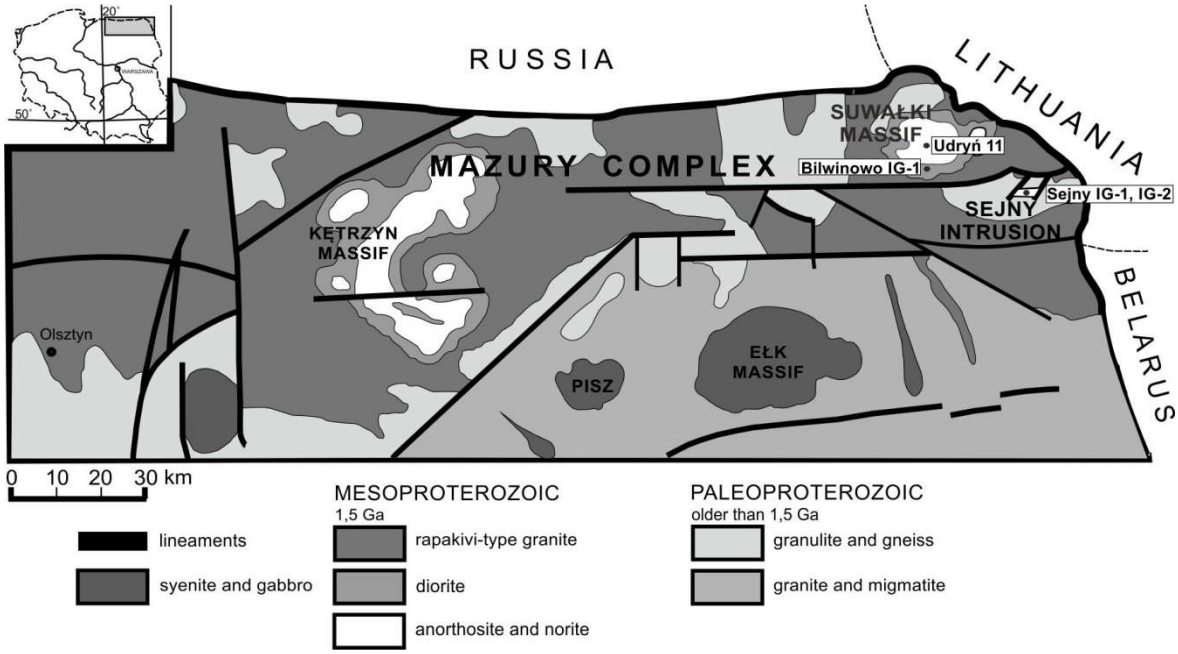

Fig. 1. Geological map of Mazury Complex (after Wiszniewska et al., 2002, modified).

The jotunitic rocks from Bilwinowo IG-1, Sejny IG-1 and Sejny IG-2 (Fig. 1) were initially analyzed under the polarizing microscope. The selected samples of jotunites from three boreholes: Bilwinowo IG-1, Sejny IG-2 and Udryń 11 were studied for major and trace elements. Major elements were analysed using ISP-ES and trace elements were analyzed by ISP-MS method in ACME Laboratory in Vancouver, Canada. Analyses of main rock-forming minerals were carried out on thin sections from a Bilwinowo IG-1 borehole with a Cameca SX–100 electron-probe microanalyzer at the Electron Microprobe Laboratory of the Inter-Institute Analytical Complex for Minerals and Synthetic Substances at the Institute of Geochemistry, Mineralogy and Petrology, Warsaw University. An acceleration voltage of 20 kV and a beam current of 15 nA were used.

Jotunites are fined-grained rocks with high Fe-Ti-P contents. They contain antyperthitic plagioclase of andesine composition, high Ca and low Ca pyroxenes. The rocks are characterized by presence of hypersthene, so they are the synonymous of hypersthene monzodiorite or monzonorite and belong to charnockitic group of rocks (Duchesne, 1999). They are also rich in apatite elongated crystals and small rounded Fe–Ti oxides. Accessory biotite enriched in Ti (up to 4,8% of TiO_2) also appeares. Characteristic texture of chilled type of these rocks and dyke forms crosscutting anorthosites and norites, indicate the fast cooling of magma. Jotunites are now widely considered as parental magma of anorthosite which was experimentally proved by Longhi et al. (1999).

Analyzed samples of Polish jotunites come from two anorthosite massifs: S1-877 from the Sejny Intrusion and B1-1953, B1-1980 and U11-1518 from the Suwałki Massif. They were compared to two other samples, which were studied earlier: 97-4, the Suwałki Massif and 97-18, the Sejny Intrusion (Wiszniewska, 2002). Jotunites show slight diversity in geochemistry between massifs. A sample 97-18 contains unzoned plagioclase (labradorite with An_{63}), low Ca pyroxenes (#mg = 59) and high Ca pyroxenes (#mg = 74). Other samples from the Suwałki Massif are made up of much more albitic plagioclase with An_{50}, low Ca pyroxenes (#mg = 57) and high Ca pyroxenes (#mg = 70). Samples

from the SAM indicate significant enrichment in Fe (up to 20,71% Fe_2O_{3t}), Ti (up to 4,18% TiO_2) and P (up to 1,26% P_2O_5). Contents of these elements in the Sejny Massif are lower, but still higher than in related rocks, norites and anorthosites. The REE distribution indicates low $[La/Yb]_N$ = 6,16-9,97 for Sejny samples, to medium for Suwałki samples $[La/Yb]_N$ = 10,91-14,18, level of fractionation. Jotunites from Sejny do not show clear Eu anomaly while Suwałki jotunitic rocks exhibit small negative one (Fig. 2), which is related to high amount of apatite crystals. The same distinction between jotunites from the Suwałki and Sejny Massifs is well visible on multielement diagrams (Fig. 3), where Sejny jotunites are depleted in Th and Nb, while Suwałki jotunites have higher amounts of Th, Nb, P, Ti and REE. On variation diagrams jotunitic samples from Polish anorthosite massifs are located close to jotunites from other anorthosite massifs like Rogaland, Norway or Korosten, Ukraine and display *the liquid line of descent* (Auwera at el., 1998).

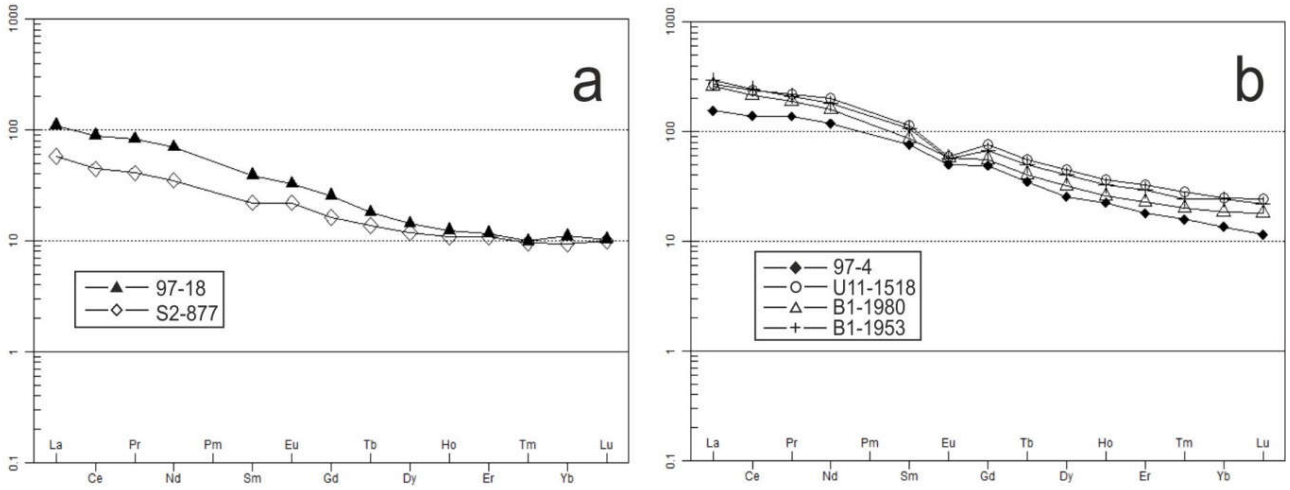

Fig. 2. Chondrite-normalized REE distributions in jotunites in a) the Sejny Intrusion, b) the Suwałki Massif (Boynton, 1984).

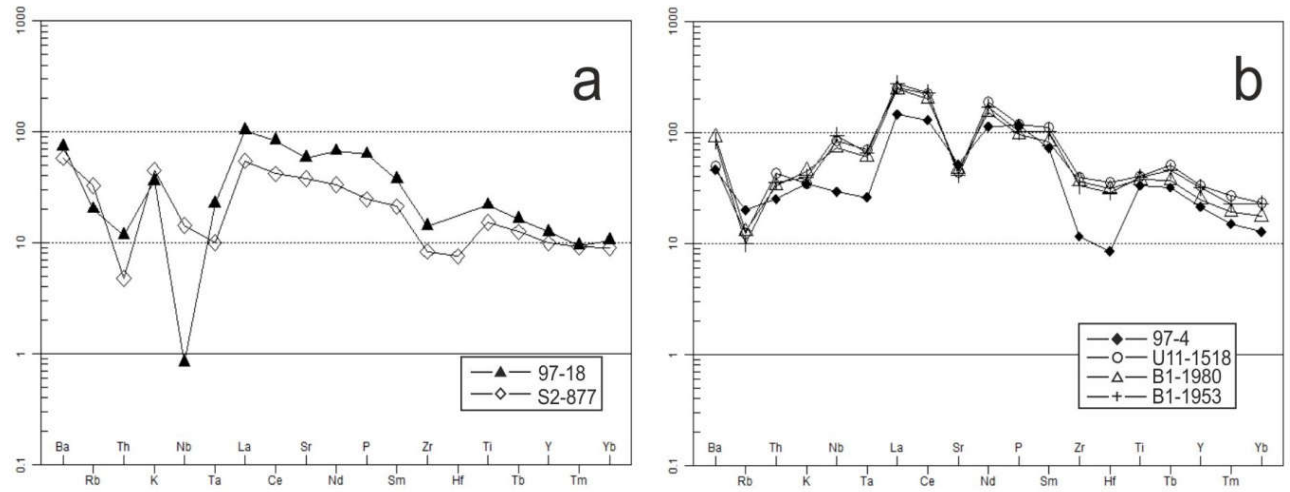

Fig. 3. Multielement diagrams of the jotunitic rocks in a) the Sejny Intrusion, b) the Suwałki Massif (Thompson, 1982).

A chemical composition of jotunitic rocks from anorthosite massifs within the Mazury Complex can be divided into two groups. These two types of jotunites do not exist together within one anorthosite massif. Sejny jotunites seem to be primitive ones due to the presence of more Ca plagioclase and lower content of incompatible elements including REE. These results are very similar to jotunites from other massive-type anorthosite occurrences like Rogaland Province, Norway. Jotunitic rocks from the Suwałki Massif indicate more evolved features of rocks with higher amount of Fe, Ti, P and higher content of REE. The variability of jotunites do not reveal within single massifs

which is confirmed by the same chemical composition of jotunitic rocks from the central (the Udryń borehole) and the external (the Bilwinowo borehole) part of the Suwałki Massif. This diversification can point to a different evolution of two massifs and extra processes which result in higher fractionation of jotunites from the SAM.

References

Auwera J.V., Longhi J., Duchesne J.C. A liquid line of descent of the jotunite (hypersthene monzodiorite) suite// Journal of Petrology. 1998. 39(3). pp. 439-468.

Bagiński B., Duchesne J.C., Martin H., Wiszniewska J. Isotopic and geochemical constraints on the evolution of the Mazury granitoids, NE Poland// Granitoids in Poland. 2007. pp. 11-30.

Duchesne J.C., Liégeois J.P., Auwera J.V., Longhi J. The crustal tongue melting model and the origin of massive anorthosites// Terra Nova. 1999. 11(2-3). pp. 100-105.

Longhi J., Auwera J.V., Fram M.S., Duchesne J.C. Some phase equilibrium constraints on the origin of Proterozoic (massif) anorthosites and related rocks// Journal of Petrology. 1999. 40(2). pp. 339-362.

Wiszniewska J., Claesson S., Stein H., Auwera J.V., Duchesne J.C. The north-eastern Polish anorthosite massifs: petrological, geochemical and isotopic evidence for a crustal derivation// Terra Nova. 2002. 14(6). pp. 451-460.

Wiszniewska J., Bagiński B. Petrogenesis of Proterozoic Anorogenic Granitoids from the Mazury Complex (NE Poland) // "The Ishihara Symposium: Granites and Associated Metallogenesis". July 2003. pp. 145-147.

LIPOVKA COLORED TOURMALINES FROM VERNADSKY STATE GEOLOGICAL MUSEUM

Gvozdenko T.A.[1], Gerasimova E.I.[1], Sinopalnikov N.I.[1], Kononkova N.N.[2]

[1]Vernadsky State Geological Museum of Russian Academy of Sciences, t.gvozdenko@sgm.ru

[2]Vernadsky Institute of Geochemistry and Analytical Chemistry RAS

Tourmaline is one of the most attractive and diverse gemstones. Its varieties include: rubellite, indicolit, verdelit, achroite, paraiba, schorl, dravite, etc. The majority of them are widely used in jewelry industry. Gem-quality tourmaline deposits are widespread all around the globe (Russia, Brazil, Mozambique, Madagascar, Pakistan, United States and so on). As far as Russian deposits are concerned, one of the most famous and valuable historical deposits is Lipovka.

Lipovka pegmatite deposits were discovered at the beginning of the XX century (app. 1900) (Pekov and Memetova (2008)). It used to be source with the greatest quantity of gem-quality colored tourmaline in the history of Russia. However, some of the modern researches are still sure about the potential of the location to the later discoveries.

Lipovka is 75 kilometers nortwest of Ekaterinburg, in a "wedge" of Lower Paleozoic metamorphic rock in contact with the Murzinka granite pluton from the north side, the Adui pluton from the south and Sokolovsky pluton from the east. Tourmaline-bearing pegmatite occurs in serpentinite, gneiss and crystalline schist, although gem-quality colored tourmaline occurs in just serpentinite (Kievlenko, 2003).

Lipovka pegmatites have been classified differently. As for the colored tourmaline-bearing pegmatites, the rare-metal – gem-bearing pegmatites type suggested by Pekov and Memetova (2008) might be the most appropriate name.

We examined colored tourmalines from Lipovka granitic pegmatites (totally 27 samples, all from the funds of Vernadsky State Geological Museum of RAS). The studied samples are mainly represented by pink, green and polychrome varieties, including so-called "water-melon type" (concentric-zoned crystals with usually pink core and green rim). Some of the samples are shown in Figures 1,2.

Fig. 1. Rubellite crystal, 3.2 cm., Lipovka, Middle Urals, Sample №19929, SGM RAS. Photo: Gvozdenko T.A.

Fig. 2. Tourmaline crystals in pegmatite, Lipovka, Middle Urals, Sample №33627, SGM RAS. Photo: Gvozdenko T.A.

Previously, the chemistry of tourmalines from Lipovka was studied by Serdyuchenko et.al (1984), Pekov and Memetova (2005, 2008), Zaharov et.al (2010). The chemical measurements of our samples were carried out by electron microprobe analysis on the Camebax SX 100 in GEOCHI RAS (Moscow), focused electron beam of 15 kV and 30 nA, 5 μm (Table 1).

Table 1. Chemical composition (wt.%) of tourmalines from Lipovka, Middle Urals.

Component	1	2	3	4	5	6	7	8	9	10
SiO_2	37.23	37.39	37.33	37.4	38.13	37.45	37.85	38.61	37.28	37.56
Al_2O_3	38.09	40.17	41.48	42.98	43.65	41.47	39.65	40.63	39.96	38.92
CaO	0.65	0.39	0.38	0.21	0.03	0.22	0.06	0.26	1.31	1.27
Na_2O	2.12	1.88	1.63	1.81	1.57	2.1	1.53	2.11	1.64	1.91
MgO	0.02	0.11	0.04	0.02	0.01	0.22	1.17	0.15	0.15	0.11
MnO	2.64	0.75	0.26	0.08	0.08	0.36	0.95	1.3	0.45	1.89
FeO	1.31	0.65	0.28	bdl	bdl	1.29	3.9	1.24	1.25	0.94
TiO_2	0.2	0.05	0.03	bdl	0.02	0.05	0.01	0.05	0.06	0.2
LiO_2	1.82	1.76	1.57	1.28	1.46	1.34	0.98	1.97	1.71	1.86
Total	84.08	83.15	83	83.78	84.95	84.5	86.1	86.32	83.81	84.66
Formula coefficients (calculated per six silicon atoms)										
Si	6	6	6	6	6	6	6	6	6	6
Al	7.24	7.6	7.86	8.13	8.1	7.83	7.41	7.44	7.58	7.33
Ca	0.11	0.07	0.07	0.04	0.01	-	0.01	0.04	0.23	0.22
Na	0.66	0.58	0.51	0.56	0.48	0.65	0.47	0.64	0.51	0.59
Mg	-	0.03	0.01	-	-	0.05	0.28	0.03	0.04	0.03
Mn	0.36	0.1	0.04	0.01	0.01	0.05	0.13	0.17	0.06	0.26
Fe	0.18	0.09	0.04	-	-	0.17	0.52	0.16	0.17	0.13
Ti	0.02	0.01	-	-	-	0.01	-	0.01	0.01	0.02
Li	1.22	1.18	1.05	0.86	0.89	0.9	0.66	1.2	1.15	1.25

Notes: 1-4 – concentric-zoned crystal of elbaite: 1-green rim, 2-greenish yellow zone, 3-pink core, 4- yellowish pink zone inside the pink core; 5-rubellit crystal; 6-green crystal of elbaite; 7-8 – polychromic crystal of elbaite: 7-black zone, 8-green zone; 9-11 – concentric-zoned crystal of elbaite: 9-green rim, 10-pink core.

bdl – below detection limit.

Li content have been calculated (to 6 atoms Si).

Tourmalines have a very complex chemical composition which gives rise to a wide range of colors. Moreover, even similar colored crystals could greatly vary in content of elements: points 1-4 in comparison with points 9-10 to name a few. Both are concentric-zoned elbaite crystals, but the content of elements in the same colored zone differ: the green rim in point 1 is Mn-enriched (2.64 wt.%), whereas the green rim in point 9 contains much less Mn (0.45 wt.%). The content of Mn and Fe in the pink core in point 3 and point 10 considerably vary as well. If compare pink tourmalines from Lipovka pegmatites with, for example, pink tourmalines from another famous Russian pegmatite deposit – Malkhan district, the latter Ca-enriched (up to 2.1 wt.%) and contain quite high amount of Li (up to

2 wt.%) and Mn (up to 1.3 wt.%), which depends on mineral formation environments (Zagorsky and Peretyazhko, 1999).

It is common knowledge that tourmalines, especially polychrome varieties, are a matter of significant scientific research, which could lead to the deep understanding of chemical evolution and mineral formation processes.

Nowadays Lipovka pegmatite deposits make part of the Natural and Mineralogical Reserve "Rezevskoi". The majority of open-pit mines are flooded. Nevertheless, one of the authors (Tatiana Gvozdenko) visited Lipovka earlier this year (May 2018) and collected some samples, which are currently under examination. In addition, the research could be continued with the samples from museums' funds and private collectors.

References

Kievlenko E.Y. (2003) Geology of Gems. Ocean Pictures Ltd., Littleton, USA, 432 p.

Pekov I.V., Memetova L.R. (2005) Chemistry and zoning of tourmaline from the granitic pegmatites of the Lipovka, Middle Urals, Russia. Vth International Symposium "Mineralogical Museums" Saint Petersburg, pp.151-153.

Pekov I.V., Memetova L.R. (2008) Minerals of the Lipovka Granitic Pegmatites, Central Urals, Russia. Mineralogical Almanac, pp. 7-44.

Serdyuchenko et.al (1984) Tourmaline from pegmatites and granites of Lipovka, the Urals, Zapiski VMO, pp. 478-485.

Zagorsky V.E. and Peretyazhko I.S. (1999) Granitic pegmatites, v.3 Miarolitic pegmatites, Novosibirsk, Nauka, 499 p.

Zaharov A.V. et al (2010) Geochemistry of polychromic tourmaline from the Lipovka granitic pegmatites (Middle Urals), Ural Mineralogical School, pp. 69-72.

THE ROLE OF FRACTIONATION AND CONTAMINATION PROCESSES IN THE FORMATION OF COEXISTING QUARTZ AND NEPHELINE SYENITES AT ABU KHRUQ RING COMPLEX, SOUTHEASTERN DESERT, EGYPT

Hegazy H.A.

Assiut University, Egypt, hhegazy4451@yahoo.com

Abu Khruq is one of the youngest Egyptian ring complexes, i.e. 89± 2 Ma and is related to the structural lineament trending N30°W parallel to the Red Sea. It crops out over a roughly circular area of approximately 50 km^2 and intruded into the late – Proterozoic gneisses and schists at about 85 km from the Red Sea and 130 km NW of Aswan.

Field investigation revealed that the Abu Khruq ring complex (ARC) present as slightly elliptical epizonal polyphases of alkaline rocks, rising up to 874 m.a.s.l. It composes of early volcanics (mainly trachyte, phonolite and rhyolite as well as their pyroclastic equivalents) successively intruded by uralitized alkaline essixitic gabbro and both silica over and more common undersaturated nepheline syenites.

The field relationships as well as the petrographic and chemical characteristics of the ARC reflect the cogenetic nature of the entire suite. The chemical data support a model in which a mantel derived alkaline mafic magma was emplaced at a lower crustal block and then extensively fractionated to give an evolved syenitic liquid. The incompatible trace elements (e.g. Nb, Zr, Ce) show enrichment trends with silica increasing, consistent with fractional crystallization. Moreover the low Cr- content in gabbros is consistent with the derivation from an evolved mafic magma.

The large range of major and trace element concentrations and identification of cumulates in some of the studied rocks indicate extensive fractional crystallization in the petrogenesis of coeval silica-saturated and silica-undersaturated alkaline rocks. However isotopic results indicate that quartz syenite bear the signature of substantial amount of crustal contamination. This provides important insight into the processes that occur in subvolcanic complexes in continental settings.

QUANTITATIVE ANALYSIS OF DETECTED MAGNETIC MINERAL USING MAGNETIC SURVEY METHOD

Ikusika A.[1], Poppola O.I.[2]
Department of Physics
[1]Adeyemi College of Education, Ondo, akintayodavies@gmail.com.
[2]University of Ibadan, Ibadan.

Local inhabitants especially the blacksmiths made use of mined minerals in the making of hoes, cutlasses and some other metallic materials through the bloomery-hearth process without identifying the usefulness of tantalite, a magnetic mineral in Iseyin, Southwest, Nigeria. Based on this, the study was aimed at carrying out ground magnetic survey of the study area so as to investigate the presence of tatantalite, and the sub-surface geology on the basis of anomalies in Earth's magnetic field resulting from magnetic properties of the underlying rock using the portable proton precession magnetometer. A total of ten geophysical traverses were established in the study area. The acquired magnetic field data were corrected for drift. The trend analysis was adopted to remove regional gradient from the observed data and the resulting results were presented as profiles. Quantitative interpretation only was adopted to obtain the depth to basement using Peter half slope method. From the geological setting of the area and the information obtained from the magnetic survey, a conclusion can be made that the study area is underlain by a rock unit of accumulated minerals. It is therefore suspected that the overburden is relatively thin within the study area and the metallic minerals are in disseminated quantity and at a shallow depth.

INTERPRETATION OF THE SULFIDE ASSEMBLAGES IN GARNET SHEARED PERIDOTITES FROM THE UDACHNAYA-EAST KIMBERLITE PIPE

Ilyina O.V., Sharygin I.S., Agashev A.M., Golovin A.V., Pokhilenko L.N.
IGM SB RAS olgailyina88@igm.nsc.ru

The sheared peridotites from the Udachnaya-East kimberlite pipe represent a root part (180-230 km) of the lithospheric mantle of the Siberian craton (Pokhilenko et al., 1999; Agashev et al., 2013). They display two types of grains by size, large (1-12 mm) porphyroclasts of olivine, orthopyroxene, clinopyroxene and garnet resided in fine-grained (usually less than 0.1-0.2 mm) neoblasts matrix of olivine with minor orthopyroxene and clinopyroxene. The sheared peridotites from the Udachnaya-East kimberlite pipe are unusually fresh with rare or without any secondary alterations. All studied the sheared peridotites from the Udachnaya-East kimberlite pipe have diverse types of sulfide occurrence.

Here, we focus on careful examination of sulfide mineralogy of one sample UV-268/02. Following distinct types of sulfide occurrence were defined based on texture, size, mineralogy, and location within the xenolith:

1a) Large rounded sulfide inclusions (globules) up to 70 μm in silicates. These inclusions composed of pentlandite, pyrrhotite and chalcopyrite. These globules are surrounded by radial disk-shaped cracks, which presumably do not communicate with the grain boundaries of host silicates (Fig. 1a, b, c).

1b) Large sulfide globules up to 70 that contain djerfisherite, K- and Cl-bearing sulfide, in addition to pentlandite, pyrrhotite and chalcopyrite. These inclusions are also surrounded by radial cracks. Inclusions of this type are intersected by another type of cracks, which communicate with the grain boundaries of host silicates and often cut entire grain (Fig. 1d). It was suggested that these cracks are pathways for K-Cl-bearing melt/fluid (Sharygin et al., 2012).

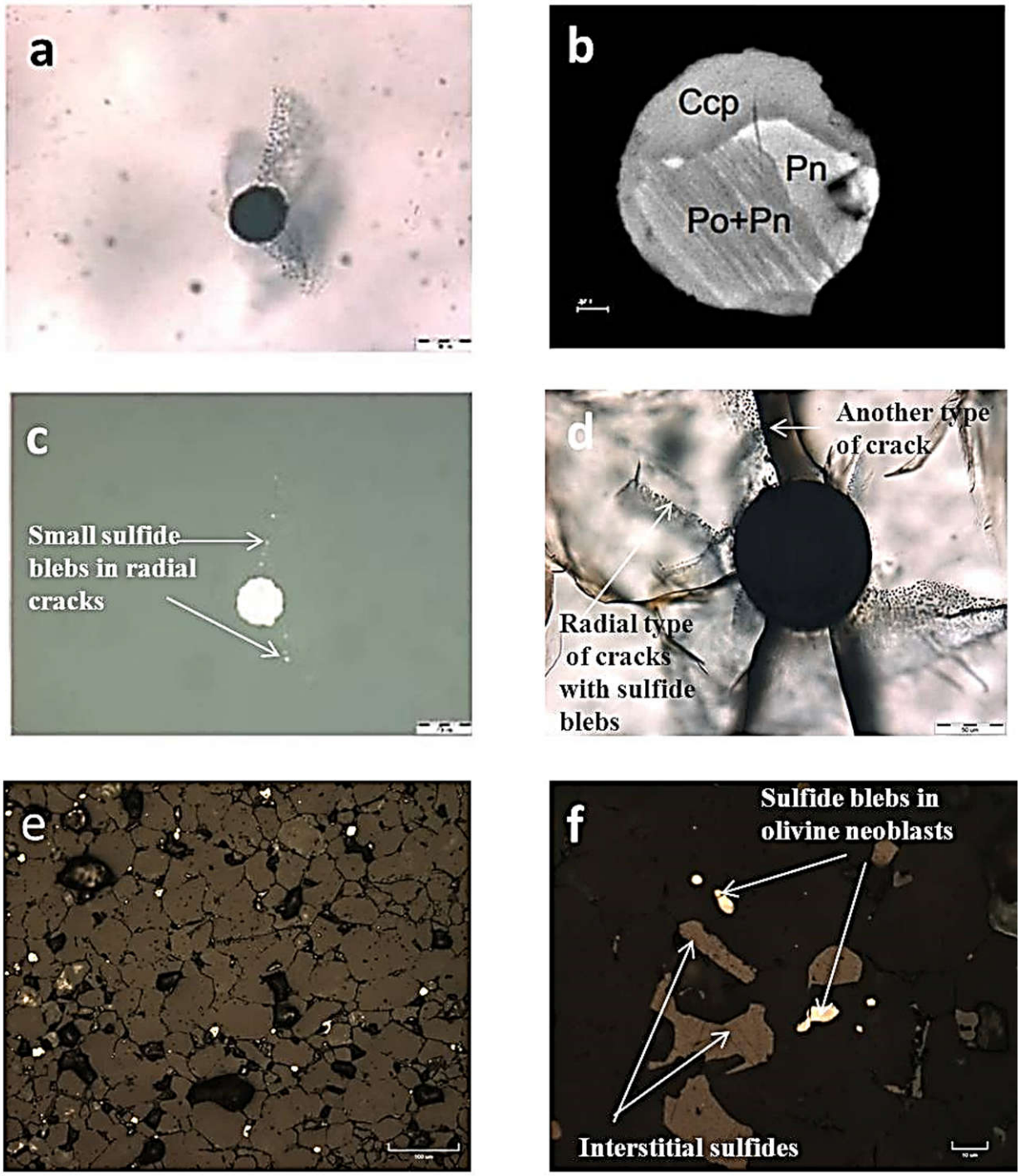

Fig. 1. Sulfide occurrences in sheared peridotite UV-268/02 from Udachnaya-East kimberlite pipe: (a, b, c) - sulfide globules (type 1a) in garnet porphyroclast surrounded by radial disk-shaped cracks, Po = pyrrhotite, Pn = pentlandite, Ccp = chalcopyrite, scale bar = 20, 2 and 20 μm, respectively; (c) - a small sulfide blebs within the radial cracks around large sulfide globule in garnet porhyroclast (type 2); (d) - sulfide inclusion in garnet porphyroclast with djerfisherite (type 1b), scale bar = 50 μm; (e) - discrete djerfisherite grains dispersed between olivine neoblasts (type 3), scale bar = 100 μm; (f) - small sulfide inclusions in olivine neoblasts (type 5) with interstitial sulfide grains (type 4). (a, d) - plane polarized transmitted light, (b) - back-scattered electron image, (c, e, f) plane polarized reflected light.

2) Trails of small sulfide blebs (1-2 μm) in porphyroclasts scattered along radial cracks surrounding large sulfide globules (Fig. 1c). These blebs consist of pentlandite, pyrrhotite and chalcopyrite.

3) Discrete small (<25 μm) euhedral to subhedral djerfisherite grains scattered randomly in matrix of olivine neoblasts (Fig. 1e).

4) Large segregations of djerfisherite (up to 80 μm) with irregular shape in interstitial spaces (Fig. 1e). Sometimes these djerfisherite segregations contain pentlandite and pyrrhotite in the central part.

5) Rounded small sulfide blebs up to 15 μm in size in olivine neoblasts (Fig. 1f). These blebs are composed of pentlandite, chalcopyrite and pyrrhotite.

We proposed the following interpretation of such a variety of sulfide types in the sample UV-268/03. Apparently the porphyroclastic texture of sheared peridotites resulted from recrystallization of coarse-grained peridotites under a very high-stress and high strain-rate deformation and this process occurred shortly before kimberlite eruption (Harte, 1977; Mercier, 1979). Thus, we suggest that large rounded sulfide inclusions (type 1a) in porphyroclasts represent the pristine sulfide material. During recrystallisation of initial coarse olivine grains this sulfide material was both trapped by newly formed olivine neoblast (type 5) and stored interstitially between these neoblasts (type 4). This process suggests that sulfide material was molten, i.e. it was sulfide melt. The small droplets (type 2) in radial cracks were formed during xenoliths transport to the surface by kimberlite magma. We interpreted radial cracks as a result of release of external pressure caused by expansion of the sulfide melt within the globules under decompression. Sulfide melt from large inclusions infiltrated along cracks. Sulfide melt in large inclusions and in small droplets in porphyroclasts and sulfide inclusion in olivine neoblast was crystallized in pentlandite, pyrrhotite and chalcopyrite upon cooling (type 1a, 2, 5). The absence of djerfisherite in intact large globules in porphyroclasts and small sulfide inclusions in neoblasts suggests that it is not related to pristine sulfide material and was formed after recrystallisation and olivine porphyroclasts cracking. We suggest that kimberlite or protokimberlite melt infiltrated into xenoliths along grain boundaries and cracks within porphyroblasts and react with primary sulfide to form djerfisherite (type 1b, type 4). Djerfisherite that form discrete small grains directly crystallized from (proto)kimberlite melt.

References

Agashev A.M. et al., Metasomatism in lithospheric mantle roots: constraints from whole-rock and mineral chemical composition of deformed peridotite xenoliths from kimberlite pipe Udachnaya // Lithos. 2013. Vol. 160. pp. 201-215.

Harte B. Rock nomenclature with particular relation to deformation and recrystallisation textures in olivine-bearing xenoliths // The Journal of Geology. 1977. Vol. 85. №. 3. pp. 279-288.

Mercier J.C.C. Peridotite xenoliths and the dynamics of kimberlite intrusion // The Mantle Sample: Inclusion in Kimberlites and Other Volcanics. 1979. pp. 197-212.

Pokhilenko et al., Peculiarities of distribution of pyroxenite paragenesis garnets in Yakutian kimberlites and some aspects of the evolution of the Siberian craton lithospheric mantle // Proceedings of the 7th International Kimberlite Conference. Cape Town: Red Roof Design, 1999. Vol. 2. pp.689-698.

Sharygin I.S. et al., Djerfisherite in xenoliths of sheared peridotite in the Udachnaya-East pipe (Yakutia): origin and relationship with kimberlitic magmatism // Russian Geology and Geophysics. 2012. Vol. 53. №. 3. pp. 247-261.

PETROLOGY AND GEOCHEMISTRY OF THE LATE CENOZOIC COLLISION VOLCANISM IN THE LESSER CAUCASUS

***Imamverdiyev N.A.*[1], *Romanko A.E.*[2], *Veliyev A.A.*[3], *Gasanguliyeva M.Ya.*[4]**

[1]*Baku State University, Azerbaijan, Academic Zahid Khalilov str. 23, Baku city, AZ 1148, Republic of Azerbaijan, inazim17@yahoo.com*

[2]*Geological Institute, Academy of Sciences, Moscow, Russian Federation*

[3]*Azerbaijan International Mining Company, Hanifa Aleskerov str. 16, Nasimi, Baku, AZ 1022, Azerbaijan)*

[4]*Institute of Geology and Geophysics, Azerbaijan National Academy of Sciences, H. Javid Av. 119, Baku, AZ 1143, Azerbaijan*

Late Cenozoic igneous rocks are widespread within the Caucasus and are one of the major components of the continental crust in the Alpine–Himalayan intracontinental orogenic belt. Their formation was synchronous with the regional continental collision. According to modern concepts, the Caucasus folded structures resulted from the convergence of the Afro-Arabian and Eurasian Plates. N.V.Koronovsky and L.I.Demina (1999) believe that the Late Cenozoic volcanism was manifested at the Caucasus segment of the Alpine–Himalayan orogenic belt during the submeridional compression of the latter. The compression was caused by the rapid northward transition of the Arabian Plate as a result of the opening of the Red Sea in the Middle Miocene (about 15–10 Ma). The Late Cenozoic volcanism was manifested in the central part of the Lesser Caucasus in two stages: Late Miocene–Early Pliocene and Late Pliocene–Quaternary. Differentiated andesite–dacite–rhyolite association formed at the first stage, and bimodal rhyolite and weakly differentiated trachybasalt–trachyandesite associations, at the second stage (Imamverdiev, 2000). Andesite–dacite–rhyolite association. The association rocks form a continuous series from andesites to rhyolites by SiO_2 contents ($SiO_2 \geq 60$ wt.%). The rocks of the andesite–dacite–rhyolite association show regular variations in the contents of trace and rare-earth elements. All this indicates that the rocks formed mainly through crystallization differentiation caused by the fractionation of clinopyroxene, magnetite, and olivine. Rhyolite association. In contrast to the rocks of the previous association, these rocks are characterized by an ultrafelsic composition, high alkalinity, nearly equal Na_2O/K_2O ratios, and low contents of CaO, MgO, and FeO. In contrast to the rocks of the andesite–dacite–rhyolite association, the similar rocks of the rhyolite association are depleted in femic components, iron group elements, and HFSE and are enriched in ore and lithophile (Pb, Th, U). Trachybasalt–trachyandesite association. These moderately alkaline rocks form a continuous series from basalts to andesites according to SiO_2 contents. The rocks of the trachybasalt–trachyandesite association show nearly the same lithophile-element pattern as the rocks of the andesite–dacite–rhyolite association, but it is better pronounced. These rocks have high contents of LILE (Rb, Ba, La, and Sr) and high La/Yb and La/Sm ratios. The geochemical data indicate that the diversity of the rocks is due to their fractional crystallization. In contents of lithophile elements the rocks of the Lesser Caucasus trachybasalt–trachyandesite association are close to oceanic-island and rift zone rocks formed from enriched mantle sources. The primitive-mantle-normalized (Sun and McDonough, 1989) magmatophile-element diagrams show that the mafic and intermediate rocks of the andesite–dacite–rhyolite and trachybasalt–trachyandesite associations are enriched in LILE, LREE, and HFSE, have high LILE/HFSE (e.g., Ba/Nb) ratios, and are depleted in Ti, Y, and HREE as compared with the primitive mantle. The intermediate calc-alkalic rocks of the former association are depleted in Ti relative to the moderately alkaline rocks of the latter association. The REE patterns of the mafic and intermediate rocks are similar and show a weak negative Eu anomaly. The rhyolites of the andesite–dacite–rhyolite association demonstrate similar REE patterns and are slightly depleted in REE. Compared with the intermediate and mafic rocks, they show a higher La/Sm ratio and a small negative Eu anomaly and are depleted in HREE. The mafic and intermediate (??) rocks of the rhyolite association show a stronger negative Eu anomaly (Imamverdiev, 2003). The rocks show steep chondrite-normalized patterns and are enriched in LREE (Imamverdiev, 2003). As shown above, the Late Miocene–Quaternary volcanic rocks in the Azerbaijan area (part) have similar geochemical features (dependence of the contents of major and trace elements on the MgO content).

This suggests that their primary magmas were generated from similar sources in similar conditions. These Late Cenozoic volcanics have low contents of Cr and Ni (up to 450 and 110 ppm, respectively, in the least differentiated basaltic lavas) as compared with the primary magmas. The contents of Cr (up to 710 ppm), Ni (up to 350 ppm), and MgO (8–13 wt.%) in the gabbroid inclusions are higher than those in the host basaltoids. The inclusions are probably close in major- and trace-element composition to the primary magmas. Nevertheless, the contents of MgO, Cr, and Ni in these inclusions are lower than those in the parental melts. We assume that these are cumulates and schlieric rocks. The upper-mantle primary magmas are characterized by high Mg# values (>0.7%), high contents of Ni (>400–500 ppm) and Cr (>1000 ppm), and SiO2 < 50 wt.% (Condie, 2001; Taylor and McLennan, 1985; Thirwall et al., 1994; Wilson, 1989). Thus, the primary magmas that generated the rocks of both associations were probably weakly differentiated. As shown above, the rocks of the early association formed from high-alumina basaltic magma, whereas the parental melt that produced the rocks of the late association was close in composition to weakly differentiated moderately alkaline olivine basalts containing equilibrium olivine Fo84 at KD = 0.33 (Imamverdiev, 2000). Note that the Neogene–Quaternary volcanic associations are characterized by nearly the same REE and trace-element patterns. The normalized spidergrams of the mafic and intermediate rocks show negative Nb, Ta, Hf, and Zr anomalies. The salic rocks are strongly enriched in Rb, Ba, Th, and La and are depleted in Ti, Yb, and Y relative to the primitive mantle. The enrichment of rocks in incompatible elements suggests that the parental melt was generated from the metasomatized lithospheric mantle enriched in K and incompatible elements. Negative Nb–Ta anomalies are considered to be intrinsic to suprasubductional magmatism. In subduction zones, K, Rb, Th, and La localized above the mantle wedge pass into a melt, whereas Nb and Ta stay in solid peridotite restites and thus cause depletion of suprasubductional magmas in these elements (Condie, 2001). In contrast to IAB, the studied samples are enriched in LILE. Similar geochemical features were earlier revealed in other postcollisional areas (Pearce et al., 1990). The geochemical data, in particular, the high Th/Nb, Ba/Nb, and K/Ti ratios and low Nb/Y and Ti/Y ratios, and the regional geological data show that the mantle sources beneath the Lesser Caucasus were metasomatized by more ancient subduction processes and contain HFSE-depleted high-K water fluids. Gabbroid nodules and the least differentiated Miocene–Quaternary basaltoids have similar compositions indicating their formation from the enriched lithospheric mantle. Thus, volcanism in the central part of the Lesser Caucasus was developed in two stages: Late Miocene–Early Pliocene (high-K calc-alkalic volcanism) and Late Pliocene–Quaternary (moderately alkaline volcanism). All volcanic rocks are characterized by similar primitive-mantle-normalized trace-element and REE patterns, negative Nb and Ta anomalies, enrichment in Rb, Ba, Th, and La and depletion in Ti, Yb, and Y. This indicates the presence of the subduction-metasomatized lithospheric mantle in the magma source. Magma evolution was controlled by the partial melting of the subcontinental mantle lithosphere and assimilation-fractional crystallization developed in the postcollisional magmatic belts of the Lesser Caucasus (Imamverdiyev et al., 2015). The increase in the rock alkalinity in the period from Late Miocene to Quaternary, the high La/Yb ratios, and the LILE enrichment of the rocks are due to the influence of a suprasubductional source. These features indicate the presence of the suprasubductional metasomatized mantle material beneath the recent Turkish–Iranian plateau, including the Lesser Caucasus (Dilek et al., 2010). The partial melting of the rising asthenosphere in the Arabian–Eurasian collision zone favored the enrichment of magmas with alkaline components of younger volcanic rocks and probably resulted in the regional lithospheric delamination.

References

Condie, K.C., 2001. Mantle Plumes and Their Record in Earth History. Cambridge University Press, Cambridge, 306 p.

Dilek, Y., Imamverdiyev, N., Altunkaynak, Ş., 2010. Geochemistry and tectonics of Cenozoic volcanism in the Lesser Caucasus (Azerbaijan) and the peri-Arabian region: collision-induced mantle dynamics and its magmatic fingerprint. Int. Geol. Rev. 52 (4-6), 536–578.

Imamverdiev, N.A., 2000. Geochemistry of Late Cenozoic Volcanic Complexes in the Lesser Caucasus [in Russian]. Nafta Press, Baku,192 p. [in Russian].

Imamverdiev, N.A., 2003. Rare earth element geochemistry of Late Cenozoic volcanic series in the Lesser Caucasus. Geochem. Int. 41 (4), 379–394.

Imamverdiyev, N.A., Gasangulieva, M.Ya., Veliev, A.A., 2015. Petrogeochemical model for the Late Pliocene–Quaternary collision volcanism in the Lesser Caucasus. Vestnik Bakinskogo Universiteta. Ser. Estestvennykh Nauk, No. 1, 66–80. [in Russian].

Koronovsky, N.V., Demina, L.I., 1999. Collision stage in the evolution of the Caucasian sector of the Alpine Orogenic Belt: geodynamics and magmatism. Geotektonika, No. 2, 17–35. [in Russian].

Pearce, J.A., Bender, J.F., De Long, Kidd, W.S.F., Low, P.J., Güner, Y., Saroğlu, F., Yilmaz, Y., Moorbath, S., Mitchell, J.G., 1990. Genesis of collision volcanism in Eastern Anatolia, Turkey. J. Volcanol. Geotherm. Res. 44, 189–229.

Sun, S.S., McDonough, W.F., 1989. Chemical and isotopic systematics of oceanic basalts: Implications for mantle composition and processes, in: Saunders, A.D., Norry, M.J. (Eds.), Magmatism in the Ocean Basins. Geol. Soc. London Spec. Publ. 42, 313–345.

Taylor, S.R., McLennan, S.H., 1985. The Continental Crust: Its Composition and Evolution. Blackwell, Oxford, 312 p.

Thieblemont, D., Tegyey, M., 1994. Une discrimination géochimique des roches différenciéestémoin de la diversité d'origine et de la situation tectonique des magmas. Comptes Rendus del'Académie des Sciences, Paris, Vol. 319, No. II, pp. 87–94.

Thirwall, M.F., Smith, T.E., Graham, A.M., Theodorou, N., Holling, P., Davidson, J.P., Arculus, R.D., 1994. High field strength element anomalies in arc lavas: Source or process? J. Petrol. 35, 819–838.

Wilson, M., 1989. Igneous Petrogenesis: A Global Tectonic Approach. Unwin Hyman, Boston, MA: Unwin Hyman. 1989, ISBN: 0045520259, 496 p.

EXISTENCE OF WATER IN THE LOWER MANTLE

Inoue T.[1,2], Kakizawa S.[1], Kuribayashi T.[3], Noda M.[1], Sakamoto N.[4], Yurimoto H.[4,5,6], Sano-Furukawa A.[7], Hattori T.[7]

[1]Geodynamics Research Center, Ehime University, Matsuyama 790-8577, Ehime, Japan.

[2]Department of Earth and Planetary Systems Science & Hiroshima Institute of Plate Convergence Region Research (HiPeR), Hiroshima University, Higashi-Hiroshima 739-8526, Hiroshima, Japan, toinoue@hiroshima-u.ac.jp

[3]Department of Earth Science, Graduate School of Science, Tohoku University, Sendai 980-8578, Japan

[4]Isotope Imaging Laboratory, Hokkaido University, Sapporo, Hokkaido 001-0021, Japan

[5]Natural History Sciences, Hokkaido University, Sapporo, Hokkaido 060-0810, Japan

[6]Institute of Space and Astronautical Science, JAXA, Sagamihara, Kanagawa 252-5120, Japan

[7]J-PARC Center, Japan Atomic Energy Agency, Tokai, Naka, Ibaraki 319-1195, Japan

High pressure experimental studies show that wadsleyite and ringwoodite, which are the most abundant minerals in the mantle transition zone, can contain water up to ~3 wt% [e.g. Inoue et al., 1995, 1998, Kohlstedt et al., 1996]. Actually in a natural diamond inclusion, hydrous ringwoodite was found which includes ~1.5 wt% H_2O (Pearson et al., 2014). These results show that the mantle transition zone is a strong water reservoir in the Earth's interior. On the other hand, the water storage capacity in the lower mantle is a matter of debate.

We have been conducting the study for the stability and water solubility of hydrous and nominally anhydrous minerals, and we reported H incorporation in bridgmanite with Al. The possible H substitution mechanism can be proposed by means of chemical compositional relationship between Mg, Si, Al and H. In addition, we clarified the possible H position in the bridgmanite by means of the powder neutron diffraction analysis in J-PARC, together with the single crystal X-ray structural analysis in PF. This shows that the significant amount of H (water) can be stored in the Earth's lower mantle.

Still more, we also investigated the nature of Al-bearing anhydrous bridgmanite for the comparison. We will introduce about our recent progress of our Al-bearing hydrous and anhydrous bridgmanite studies.

CHEMICAL COMPOSITIONS OF THE MANTLE TRANSITION REGION AND THE UPPERMOST LOWER MANTLE INFERRED FROM HIGH-PRESSURE MINERAL PHYSICS

Irifune T., Gréaux S.

Geodynamics Research Center, Ehime University, Matsuyama 790-8577, Japan, irifune@dpc.ehime-u.ac.jp

Recent studies on the inclusions in natural diamond revealed the presence of almost all major high-pressure phases predicted to occur in the deep mantle based on high-pressure experimental studies, including the cubic form of $CaSiO_3$ perovskite (CaPv). We have recently measured sound velocities of CaPv under the entire pressure and temperature conditions of the mantle transition region by a combination of in situ X-ray observations and ultrasonic interferometry measurements in multi-anvil apparatus. Elastic properties of both tetragonal and cubic forms of CaPv have been obtained, yielding the shear modulus of cubic CaPv substantially lower than the theoretically predicted values. The present results, combined with the corresponding elastic properties of other high-pressure forms of major minerals in the mantle and subducting slabs, suggest the existence of a harzburgite-rich region near the bottom of the mantle transition region. In contrast, basaltic compositions have significantly lower shear velocities relative to the surrounding pyrolitic mantle, and may explain the low velocity region atop of the lower mantle and the seismic scatters in the upper parts of the lower mantle.

SYNTHESIS OF THE PHASES IN THE SYSTEM CA–AL–O AT 15 GPA AND 1600°C

***Iskrina A.V.*[1], *Spivak A.V.*[2], *Bobrov A.V.*[1,2,3], *Dubrovinsky L.S.*[4], *Eremin N.N.*[1], *Marchenko E.I.*[1]**

[1]*M.V. Lomonosov Moscow State University, Department of Geology, Moscow*

[2]*Institute of Experimental Mineralogy RAS, Chernogolovka*

[3]*V.I. Vernadsky Institute of Geochemistry and Analytical Chemistry RAS, Moscow,*

grigoryeva_av888@mail.ru

Aluminates may be the hosts of aluminum under the conditions of the transition zone and lower mantle of the Earth (Ringwood, 1976; Irifune and Tsuchiya, 2007). There are Ca-aluminates, among which several compounds are registered in the Ca–Al–O system. To date, several intermediate compounds are known in the CaO-Al2O3 system ($CaAl_2O_4$; $CaA_{l4}O_7$; $CaAl_{12}O_{19}$; $Ca_3Al_2O_6$; $Ca_2Al_2O_5$; $Ca_{12}Al_{14}O_{33}$) (Ito et al, 1980, Lazic et al, 2006, Janakova, Salavcova, Renaudin et al, 2007, Jerebtsov and Mikhailov, 2001, Filonenko and Lavrov, 1949, Ivanova et al, 2002, Ma,. Kampf et al, 2011, Mikouchi, Zolensky et al, 2009). They are stable over a wide range of pressures and temperatures.

Experiment on synthesis of the phases on the CaO-Al2O3 join was carried out using a high pressure - high temperature 1200-t multi-anvil Sumitomo press at Bayerisches Geoinstitute (BGI). The phases of $CaA_{l2}O_4$ and $Ca_2Al_6O_{11}$ were synthesized at 15 GPa and 1600°C. The latter phases was obtained for the first time. Compounds of these phases were studied by different methods including optical microscopy, SEM and microprobe analysis. The method of single-crystal X-ray diffraction allowed us to refine the structures (Fig. 1, 2) and to determine the crystal chemical formulae of the phases. Both studied phases are synthesized at 15 GPa so they stable in the transition zone. Thus they can be considered as potential aluminum concentrators in the transition zone and lower mantle of Earth. The new data requires refinement of the P-T diagram for the Ca-Al-O system.

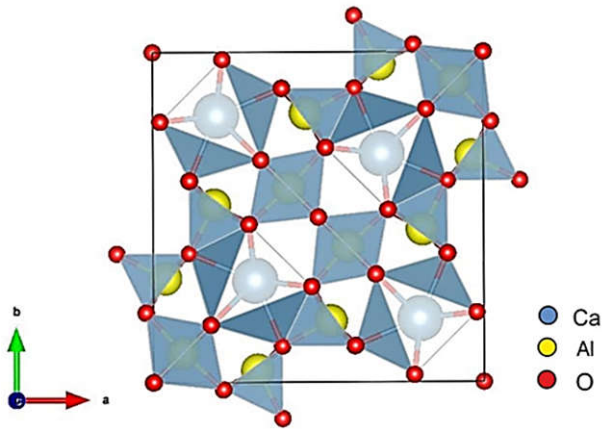

Fig. 1. Crystal structure of $Ca_2Al_6O_{11}$.

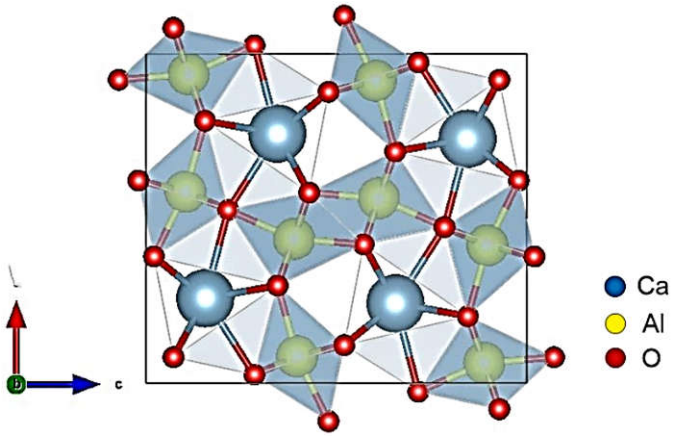

Fig. 2. Crystal structure of $CaAl_2O_4$.

This work was supported by the Russian Science Foundation, project no. 17-17-01169.

References

Filonenko, N.E., Lavrov, I.V. Critical evaluation and optimization of the thermodynamic properties of the CaO-Al2O3, Dokl. Akad.Nauk S.S.S.R.,1949, Vol.66., P. 673 – 676.

Irifune T., Tsuchiya T. Mineralogy of the Earth – Phase Transitions and Mineralogy of the Lower Mantle, Ehime University, Matsuyama, Japan, 2007.

Ivanova M.A., Petaev M.I., MacPherson G.J., Nazarov M.A., Taylor L.A., Wood J.A. The first known natural occurrence of calcium monoaluminate, in a calcium-aluminum-rich inclusion from the CH chondrite Northwest Africa 470, Meteoritic and Planetary Science 37, 2002, P. 1337-1344.

Ito S., Suzuki K., Inagaki M., Naka S. High pressure modifications of CaAl2O4 and CaGa2O4, Mat. Res. Bull.,Vol. 15, 1980, P. 925-932.

Janakova S., Salavcova L., Renaudin G., Filinchuk Y., Boyer D., Boutinaud P. Preparation and structural investigations of sol–gel derived Eu3+-doped CaAl2O4, Journal of Physics and Chemistry of Solids 68, 2007, P. 1147–115.

Jerebtsov D.A., Mikhailov G.G. Phase diagram of CaO±Al2O3 system, Ceramics International 27, 2001, P. 25-28.

Lazic B., Kahlenberg V., Konzett J., Kaindl R. On the polymorphism of CaAl2O4 — structural investigations of two high pressure modifications, Solid State Sciences 8, 2006, P. 589–597.

Ma C., Kampf A.R., Connolly Jr. H.C., Beckett J.R., Rossman G.R., Smith S.A.S., Schrader D.L. Krotite, CaAl2O4, a new refractory mineral from the NWA 1934 meteorite, American Mineralogist, Vol. 96, 2011, P. 709–715.

Mikouchi T., Zolensky M.,Ivanova M., Tachikawa O., Komatsu M., Le L., Gounelle M. Dmitryivanovite: A new high-pressure calcium aluminum oxide from the Northwest Africa 470 CH3 chondrite characterized using electron backscatter diffraction analysis, American Mineralogist,Vol. 94, 2009, P. 746–750.

Ringwood A.E. Earth's mantle, Composition and Petrology of the Earth's Mantle, McGraw-Hill, Dusseldorf, 1976 , 618 pp.

STABILITY OF SKIAGITE-MAJORITE GARNETS AND FE SPINELS AT HIGH-PRESSURES AND TEMPERATURES

Ismailova L.S.[1], Bobrov A.V.[2], Dubrovinsky L.S.[3]

[1]Skolkovo Institute of Science and Technology, Skolkovo Innovation Center, 3, Moscow 143026, Russia

[2]Department of Petrology, Geological Faculty, Moscow State University, Leninskie Gory, 119991 Moscow, Russia

[3]Bayerisches Geoinstitut, University of Bayreuth, Universitätsstrasse 30, D-95440 Bayreuth, Germany

Iron-bearing minerals mantle oxides and silicates are of petrologic and geochemical interest because of their ability to incorporate in their structure both divalent and trivalent cations (Fe^{2+} and Fe^{3+}). Ferric iron ratios (Fe^{3+}/Fe_{tot}) in garnet and spinel from xenoliths have been used to derive oxygen fugacity profiles from upper-mantle assemblages (Koch, Woodland, & Angel, 2004; Luth et al., 1990). The only samples currently available from greater pressures are mineral inclusions in diamonds. The presence of mixed valence iron oxides as inclusions could provide an approximate indication of the oxygen fugacity prevealing in diamond-precipitating fluids in the mantle. For example, almost-pure Fe_3O_4 magnetite inclusions (Kaminsky & Wirth, 2011; Stachel, 2001) have been found in diamonds and evidence of $(Mg,Fe)Fe_2O_4$ exsolution from ferropericlase (McCammon et al., 1998) has also been observed. Knowledge of the thermodynamic properties of iron oxides at high pressure is an important prerequisite for understanding the fluids in which such oxides form.

The stability and phase relations of skiagite garnet was studied by (Woodland & O'Neill, 1995). They performed high-pressure experiments in the join andradite-skiagite as function of pressure at 1100 C. The maxim solubility of of skiagite in andradite increases from 12 mol.% at 1.7 GPa to 48 and 64 mol.% at 6 and 7 GPa, respectively. The solubility of skiagite in almandine is lower than in andradite. Recently, ferric iron-rich majoritic garnet was found as inclusions in a host garnet within an eclogite xenolith originating in the deep mantle (Xu et al., 2017). Based on Mossbauer spectroscopy, majoritic inclusions shows the very high ferric iron content (Fe^{3+}/Fe_{tot}=0.81±0.01).

The FeO-Fe_2O_3-SiO_2 model system can, in the very first approximation, characterize iron-rich phases of various parts of the Earth's mantle, outline the formation and decomposition reactions of the skiagite and skiagite-Fe-majorite garnets, as well as other iron-bearing minerals with increasing pressure and temperature conditions. Additionally, high-pressure and high-temperature experiments can possibly show the influence of incorporation of ferrous and ferric iron on the properties of typical mantle minerals.

As a starting composition was used mixture of oxides FeO-Fe_2O_3-SiO_2 corresponding to skiagite $Fe_3Fe_2Si_3O_{12}$. High-pressure high-temperature experiments at 7 GPa were performed using anvil with hole press at Vernadsky Institute, Moscow, Russia and experiments at 7.5-12.5 GPa using Kawai-type multi anvil press at Bavarian Geoinstitute, Bayreuth, Germany. Temperatures varied from 1000 °C to 1600 °C.

Recovered samples from high pressure synthesis were studied by means of electron microprobe analysis. Metallic Fe and Si were used as standards for Fe and Si. X-ray diffraction measurements were performed on selected single crystals with various compositions.

The main phases obtained in experiments were skiagite-majorite garnets $Fe_3Fe_2Si_3O_{12}$-$Fe_4Si_4O_{12}$, Fe_2SiO_4-Fe_3O_4 spinel structured solid solutions, clinoferrosilite $Fe_2Si_2O_6$, coesite SiO_2 и stishovite SiO_2. Spinel solid solution forms a continuous series with almost pure magnetite Fe_3O_4 and Fe_2SiO_4 with spinel-type structure, as well as intermediate compositions.

At moderated pressures, 7 GPa and 1000° C in the system FeO-Fe_2O_3-SiO_2 coexist magnetite, pyroxene and coesite. With increasing temperature, this phase assemblage persists up to 1300°C, when magnetite-ringwoodite solid solution starts to form.

Further increase in pressure and temperature skiagite-majorite solid solution (Ski-Maj) replaces pyroxene-magnetite-coesite (Px+Mgt+Coe), according to the following reaction:

$2Fe^{2+}SiO_3$ (*Px*) + SiO_2 (*Coe*) + $Fe^{2+}Fe^{3+}{}_2O_4$ (*Mgt*) = $Fe^{2+}{}_3Fe^{3+}{}_2Si_3O_{12}$ (*Ski*)

Since SiO_2 is constantly present as an independent phase (coesite, which is replaced by stishovite with increasing pressure), excess of it leads to forming of Fe-majorite component ($Fe_4Si_4O_{12}$) in garnet. The presence of Fe-majorite end-member is compensated by the appearance of a magnetite-ringwoodite (spinel) solid solution in association with the garnet according to the reaction:

$Fe^{2+}{}_3Fe^{3+}{}_2Si_3O_{12}$ (Ski) = $2SiO_2$ (*Coe*) + $Fe^{2+}Fe^{3+}{}_2O_4 \cdot Fe^{2+}{}_2SiO_4$ (*Mag-Rwd*)

The texture of the experimental sample is formed by relatively large spinel crystals and small uniform skiagite-majorite crystals (rarely bigger than 20 um). Pyroxene crystals can reach up to 60 um.

With increasing pressure, at 8.5 GPa the assemblage of skiagite-majorite, magnetite-ringwoodite and coesite is present. (Fig. 1). However, in comparison with lower pressure synthesis, spinel crystals are much larger.

The run products recovered from a series of experiments performed at 9.5 GPa reveals different assemblages depending on temperature. At 9.5 GPa and 1100-1300 °C, skiagite-majorite garnet is stable assemblage, coexisting with the spinel solid solution (Fig. 1). With increasing temperature, the size of skiagite-majorite garnet crystals gradually decreases, and the size of spinel crystals increases. Further temperature increasing leads to partial melting with a portion of liquid and large crystals of pure Fe2SiO4 (with no presence of solid solution with magnetite).

The phase relation study of pure skiagite starting composition performed at 10 GPa and 1100 °C performed by Woodland and O'Neill (1993). At this pressure-temperature conditions, a multiphase assemblage appears - skiagite garnet coexist with spinel and stishovite (red circle on the diagram). Authors assumed pure skiagite and pure spinel, probably due to technical limitations.

At 10.5 GPa and 1200 °C, skiagite-majorite solid solution coexist with spinel solid soluton, magnetite and stishovite. Further increasing of temperature, at 1300 °C skiagite-majorite garnet coexist with spinel solid solution, stishovite and Fe_2SiO_4 instead of magnetite.

At 11.5 GPa and 1200 skiagite-majorite garnet becomes unstable and the phase assemblage is represented with spinel solid solution crystals and stishovite.

At maximum reached pressure 12.5 GPa and 1200 °C the sample consists of skiagite garnet, magnetite, magnetite-ringwoodite spinel. At 1300 °C these phase assemblage is replaced by magnetite-ringwoodite spinel and stishovite, as it happens at 11.5 GPa and 1300 °C.

Thus, the stability of skiagite-majorite garnet is limited to 11.5 GPa at 1200 °C and 12.5 1300 °C the solid line on the diagram (Fig. 1). Above it skiagite-majorite is replaced with Fe_3O_4-Fe_2SiO4 spinel and stishovite, and further (above 12.5 GPa and 1200 °C) with magnetite, Fe_2SiO_4 and stishovite by the reaction:

$Fe^{2+}{}_3Fe^{3+}{}_2Si_3O_{12}$ (Ski) = $2SiO_2$ (*Sti*) + $Fe^{2+}Fe^{3+}{}_2O_4$ (*Mag*)+ $Fe^{2+}{}_2SiO_4$ (*Rwd*) (1)

This reaction has a clear tendency to shift to the left with temperature.

Melts were observed in the run products from experiments at 1400 C, 1500, 1600 in this study. Big crystals of ringwoodite coexists with melts. Experimental results are summarized in Figure 1.

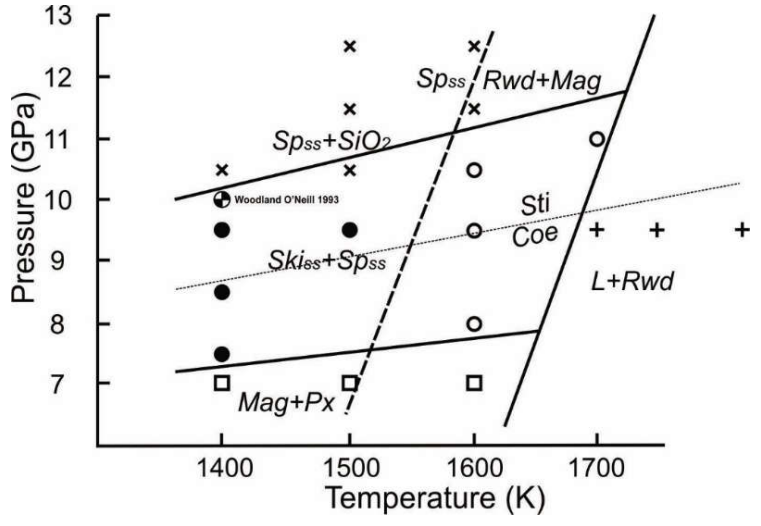

Fig. 1. Phase relation of $Fe_3Fe_2Si_3O_{12}$ at high pressures and temperatures.

Our experimental results show that there is an excess of Si (over 3 p.f.u.) on the octahedral site in garnet in all experimental assemblage. This suggest that Fe majorite component $Fe_4Si_4O_{12}$ can enter skiagite garnet structure. The maxim solubility of iron majorite in skiagite garnet reaches 76 % at 9.5 GPa and 1100 C. There is a strong disagreement with experimental data on knorringite [Sirotkin at al.,2015] and other majorite garnets [Gasparik, 2000; Stachel at al.,2015], where the amount of majorite component (Si on the octahedral site) increases with pressure. We assume, this can be connected with formation of spinel solid solution (magnetite-Fe_2SiO_4) where the solubility of Fe_2SiO_4 (Si and Fe^{2+}) increases with pressure. The amount of magnetite-spinel polymorphs present in the experimental runs is correlated to the amount of skiagite-majorite garnet.

The ferric iron concentration in iron-bearing spinel and oxides from the upper mantle may reflect prevailing redox conditions, and used for geothermeters and geobarameters. It may also provide information on redox reactions involving recycled carbonate and fertile mantle silicate or fluids.

References

Kaminsky, F. V., & Wirth, R. (2011). Iron carbide inclusions in lower-mantle diamond from juina, brazil. Canadian Mineralogist, 49(2), 555–572.

Koch, M., Woodland, A. B., & Angel, R. J. (2004). Stability of spinelloid phases in the system Mg 2 SiO 4 – Fe 2 SiO 4 – Fe 3 O 4 at 1100 ◦ C and up to 10 . 5 GPa, 144, 171–183.

Luth, R. W., Virgo, D., Boyd, F. R., Wood, B. J., (1990). Ferric iron in mantle-derived garnets. Implications for thermobarometry and for the oxidation state of the mantle, 104, 56–72.

Stachel, T. (2001). Diamonds from the asthenosphere and the transition zone. European Journal of Mineralogy, 13(May 2000), 883–892.

Woodland, A. B., & O'Neill, H. S. C. (1995). Phase relation between Ca3Fe2Si3O12-Fe3Fe2Si3O12 garnet and CaFe2Si2O6-Fe2Si2O6 solutions. Contributions to Mineralogy and Petrology, 121, 87–98.

Xu, C., Kynický, J., Tao, R., Liu, X., Zhang, L., Pohanka, M., … Fei, Y. (2017). Recovery of an oxidized majorite inclusion from Earth's deep asthenosphere. Science Advances, 3(4).

MINERALOGY OF OGOL BASALTIC LAVAS (CRATER HIGHLANDS, TANZANIA)

***Ivashchenkova O.V.*[1], *Arzamastsev A.A.*[2,3], *Zaitsev A.N.*[1,4]**

[1]*Department of Mineralogy, St. Petersburg State University*

[2]*Department of Petrology, St. Petersburg State University*

[3]*The Institute of Precambrian Geology and Geochronology RAS, St. Petersburg*

[4]*Imaging and Analysis Centre, Natural History Museum, London, UK, lelia1991@yandex.ru*

The Gregory Rift extends approximately 900-1000 km, between Turkana Lake in Kenya to the lakes of Manyara and Balangida in northern Tanzania. Geological activity within the Gregory Rift began approx. 35-30 Ma within the northern part, and continues currently within the southern part (carbonatite-nephelinite-phonolitic Oldoinyo Lengai active volcano). The geological time frames of volcanism development in the area of the modern Gregory Rift is examined in various publications and many geological, geochemical and mineralogical studies of various volcanic rocks have been described (e.g. Dawson, 2008).

The Crater Highlands area is located within the northern part of the Gregory Rift. This area is formed by large volcanoes and separate lava flows, the formation of which had taken place between 4.5 and 0.8 Ma (Mollel and Swisher, 2012). The volcanoes are distinguished into two types by the chemical composition of eruptive rocks. The first type - volcanoes of mainly basaltic and trachytic composition (Ngorongoro, Lemagrut and Oldeani), and the second type – volcanoes with predominately nephelinitic rocks (Sadiman and possibly Embakai). Separate lava fields that are spatially not connected with large volcanoes are located in the South-Western part of the upland. These lavas are known as Ogol lavas, which are the subject of our research.

Previous studies (Hay, 1987) postulate that the Ogol lava flows erupted from small separate channels (craters) or cones. These channels and cones stretch in a west to easterly direction for approx. 25 km, and are 0.5 to 1.5 km in diameter and from 50 to 150 m in height.

There is only one scientific publication, dedicated to the research of Ogol lava mineralogy and geochemistry – a PhD thesis by Mollel (2007). In this thesis only four rock samples have been studied (bulk chemical composition of rocks and chemical composition of major minerals). According to Mollel (2007) the Ogol lavas are basaltoid porphyritic rock with olivine, augite, biotite, alkali feldspar phenocrysts, as well as with plagioclase and nepheline microphenocrysts. By chemical composition the Ogol lavas are high-magnesian rocks (Mg# = 56-59) with high chromium content (514-863 ppm). In comparison to other volcanic rocks, known in the Crater Highlands, these are the most primitive (poorly differentiated) volcanic rocks.

The studies are performed on rock material, available in Saint Petersburg State University and Institute of Precambrian geology and geochronology collections. At the author's disposal there is a collection, consisting of 13 specimens, picked out from seven outcrops. At the moment we have studied seven specimens of Ogol lava, obtaining the following results:

1) The major (forsterite, plagioclase, diopside, magnetite), minor (apatite, amphibole, calcite) and accessory (pyrrhotine, chromite, baryte) minerals were determined in the rocks. Na and K silicates that are not diagnosed properly yet are also present in the groundmass.

2) Two mineral assemblages were observed in basalts: primary (magmatic) (forsterite, plagioclase, diopside, magnetite, apatite, amphibole, chromite) and secondary (hydrothermal) (baryte, calcite, as well as an undiagnosed Mg hydrous silicate that forms after forsterite).

3) Among the studied specimens at the very least two basalt varieties can be distinguished: a) olivine-pyroxene basalts and b) plagioclase basalts.

The new data acquired from the Ogol lavas basalt mineralogy will help to improve the understanding of the volcanism history of the Crater Highlands, and together with the future geochemical (including radigenic isotopes) data permits answering the question of whether the genetic relationship between the Ogol lavas and large volcanoes exist.

This research is supported by the Russian Foundation for Basic Research (grant 18-05-00835), St. Petersburg State University (Geomodel Resource Centre) and Alexander von Humboldt-Stiftung.

References

Dawson J.B. The Gregory Rift Valley and Neogene-Recent volcanoes of northern Tanzania Geological Society Memoirs. Vol. 33. 2008. 102 p.

Hay R.L. Geology of the Laetoli area. In Laetoli: a Pliocene Site in Northern Tanzania. Oxford: Oxford University Press. 1987. pp. 23-47.

Mollel G.F. Petrochemistry and Geochronology of Ngorongoro Volcanic Highland Complex (NVHC) and its relationship to Laetoli and Olduvai Gorge, Tanzania. PhD thesis, Rutgers University, 2007. 254 p.

Mollel G.F., Swisher III C.C. The Ngorongoro Volcanic Highland its relationships to volcanic deposits at Olduvai Gorge and East Africa Rift volcanism // Journal of Human Evolution. 2012. Vol. 63. pp. 274-283.

PETROCHEMICAL FEATURES OF REE MINERALIZATION RELATED INTRUSIVE ROCKS, MONGOLIA

***Jargalan S.*[1], Oyunbaatar U.[1], Garamjav D.[2], Enkhjargal B.[1], Odbayar O.[3]**

[1]School of Geology and Mining Engineering, Mongolian University of Science and Technology

[2]Oyu Tolgoi LLC, Mongolia Science and Technology, Ulaanbaatar, Mongolia

[3]Institute of Paleontology and Geology, Mongolian Academy of Sciences, Mongolia

A number of geological processes can lead to concentration of rare earth elements in specific types of rock or sediment and to enrichment of REE. Igneous REE deposits are mainly associated with

carbonatites and peralkaline silicate rocks, including some subeconomic mineralization in pegmatites associated with metaluminous granites (Chakhmouradian and Zaitsev 2012). As a result, understanding the distribution and origin of REE deposits and identifying and quantifying REE resources have become strategic priorities of Mongolia. Unlike other metals like gold, copper etc, the REEs were not discovered and relatively little studied in Mongolia. Understanding the petrology and petrogenesis REE mineralization related rocks is essential for unraveling the complexities of REE deposits intimately associated with these rock types.

The objective of this study is to make clear petrochemical features of intrusive rocks which have spatial and genetic relation with REE mineralization in Mongolia and furthermore to overview regional scale characteristics.

Types REE Mineralization of Mongolia

The majority of REE deposits occur in intracontinental, anorogenic, extensional settings. Economic concentrations of REE-bearing minerals occur in some alkaline rocks, skarns and carbonate-replacement deposits associated with alkaline intrusions, veins and dikes cutting alkaline igneous complexes and surrounding rocks, soils and other weathering products of alkaline rocks. REE mineralization is poorly studied in Mongolia, but result of various types of geological study including geological mapping and scientific research results and exploration reports indicate that we have 4 deposits, 80 occurrences and more than 280 anomalous areas of REE mineralization. We studied ore mineralogy, petrography and geochemistry of more 80 locations of REE mineralization and regarding top result we can distinguish five main genetic types REE mineralization. These are

- Alkaline granitoid related REE
- Nepheline-syenite related REE
- Carbonatite related
- Ion adsorption type REE mineralization
- Placer deposits

REE mineralization related with alkaline granitoid is mainly distributed in wide range in whole country and they are characterized to be as alkaline metsomatite bodies in two main age period. Devonian and carboniferous REE bearing alkaline granitoids are mainly distributed at the western and north western part, and Permian and younger REE bearing alkaline granitoids are distributed at the central and eastern part of Mongolia. Carbonatite related REE deposits found in only south Mongolia and they are Jurassic and Cretaceous in age. REE mineralization related with nepheline-syenite is distributed in northern Mongolia. Ion adsorption type mineralization is not yet found but some sedimentary and roll front type uranium deposits are enriched by REE. There are a few occurrences of monazite bearing placer in the north east part of Mongolia.

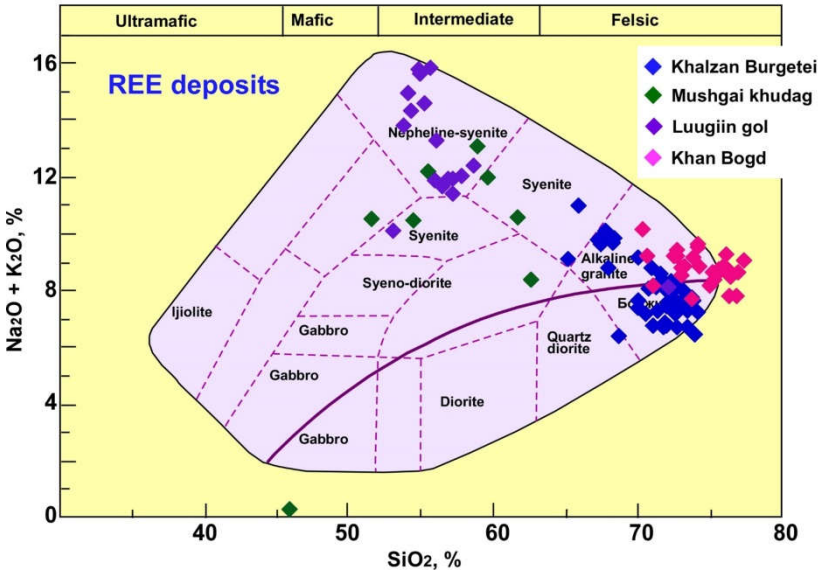

Fig 1. Figure 1. TAS диаграм granitoids of REE deposits.

Petrochemical features of REE related intrusive rocks

We studied more than 80 localities of REE mineralization and analyzed more than 250 samples for major, trace and REE content by ICP-MS method at "ActLab" laboratory. Result of these analyzes summarized using various discrimination diagrams in order to distinguish magma type REE characteristics as well as tectonic setting of REE mineralization in Mongolia. First, we checked TAS diagram (Fig 1) to make clear rock types. Khalzan Burgetei deposit and Khan Bogd occurrence are alkaline related REE mineralization and granitoid rocks show alkaline granite in composition, but in case carbonatite related deposits as Luugin gol and Mushgai khudag REE related intrusive rocks show completely different and they are mainly syenite and nepheline-syenite in composition.In order to make clear REE characteristics in relation with magma differentiation we checked correlation between silica content and REE on Figure 2. Granitoid rocks of Mushgai khudag deposit show clear negative correlation, but Khalzan Burgetei deposit shows positive correlation. In case of Luugiin gol and Khan Bogd they are scattered but show weak correlation.

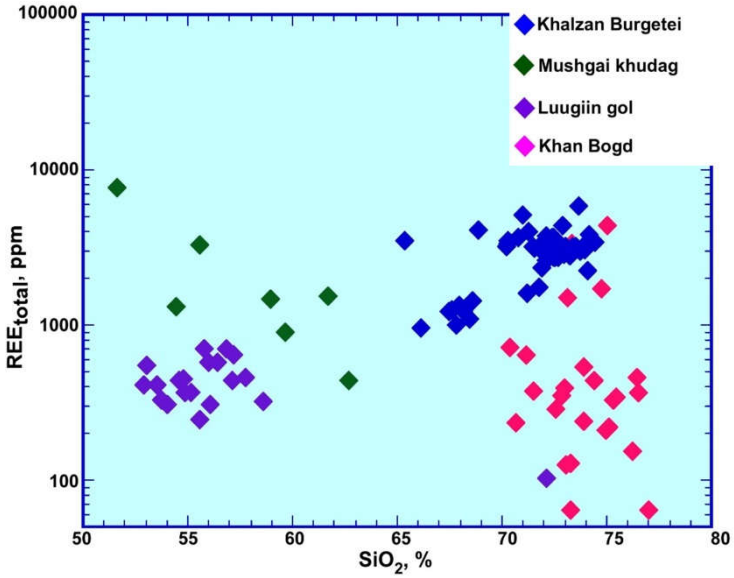

Fig. 2. Caption uses Times Roman 9 and centered.

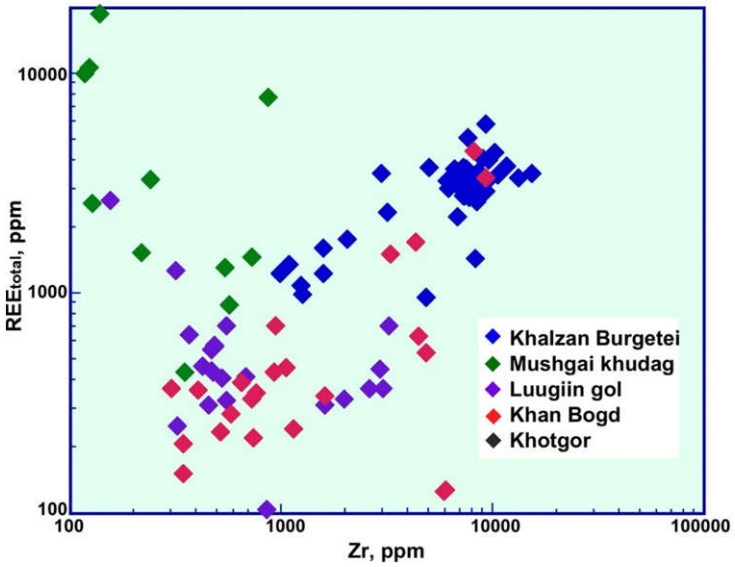

Fig. 3. Correlation between zirconium and REE composition of REE deposits.

Alkaline granitoid related REE mineralization usually associates with zirconium silicate minerals. Therefore, we cchecked how REE and Zr content correlates each (Figure 3) other. Zircon content of azan Burgetei and Khan Bogd is high ranging from 200ppm to 11000ppm and show very

good positive correlation with REE (Figure 3) content.In case of carbonatite related REE deposits Mushgai khudag, Khotgor and Luugiin gol zirconium content is lower (100-99 ppm) and now correlation is identified.

Ittrium content varies from 80 ppm to 1100 ppm and shows very good positive correlation in all (Figure 4) deposits.

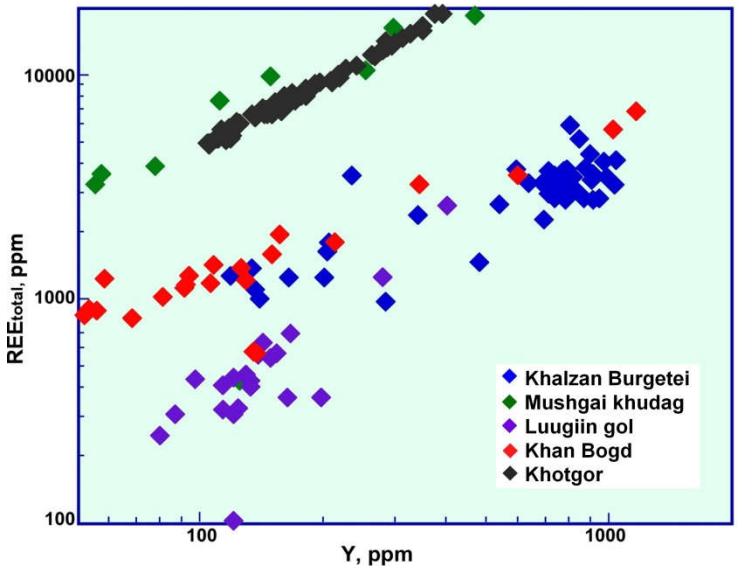

Fig. 4. Correlation between ittrium and REE composition.

Chondrite normalized REE pattern show completely different characteristics for deposits. Khalzan Burgetei deposit, which is related with alkaline granitoid has very clear europium (Figure 5) anomaly, indicating plagioclase fractionation. REE pattern of Mushgai khudag, which is carbonatite related deposit, it shows highly enrichment of light REE without any europium (Figure 5) anomaly.

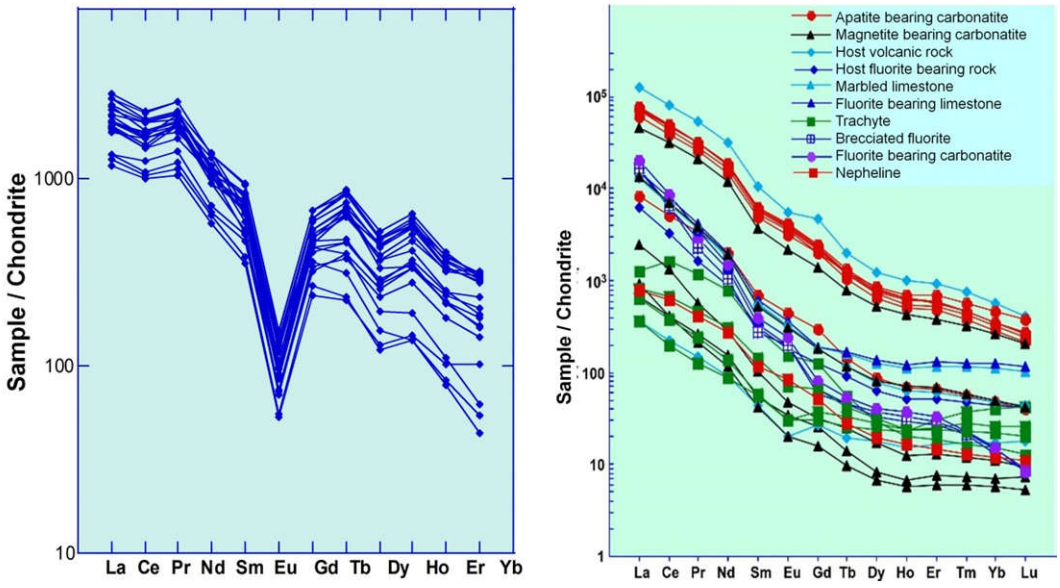

Figure 5. REE pattern of main deposits: A) Khalzan Burgetei alkaline related deposit; B) Mushgai khudag carbonatite related deposit.

Source of magma is very important for formation of REE mineralization, therefore, we tried to make clear magma source of REE related intrusives of main deposits using gallium and aluminum ratio versus zirconium. Figure 6 clearly shows REE mineralization related intrusive rocks are mainly A type or anorogenic granites.

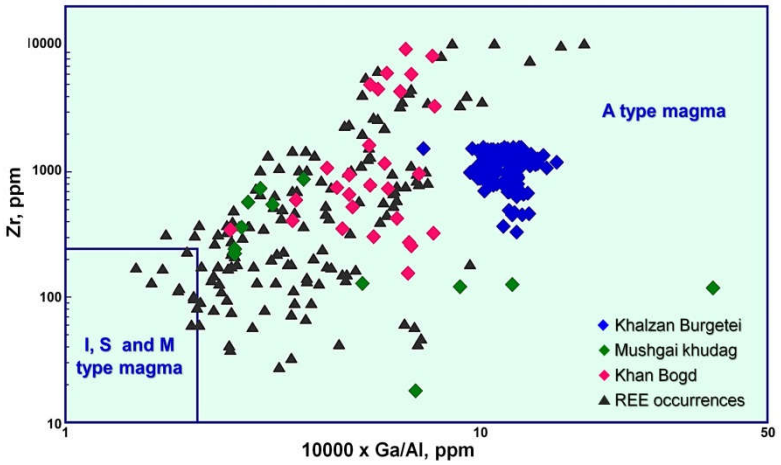

Figure 6. Discrimination of magma source (Whalen, 1987).

Tectonic environment of REE deposits of Mongolia is checked on Pearce's tectonic (Figure 7) discrimination diagram and result shows that rocks are formed on several types of tectonic environment.

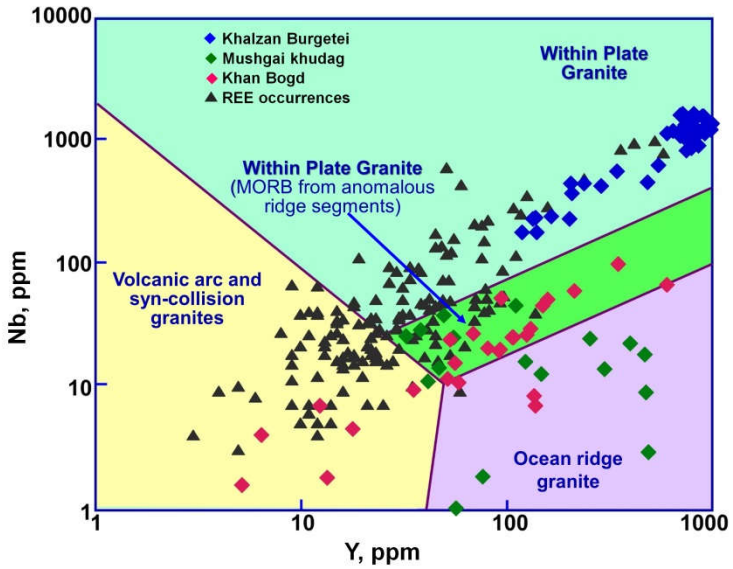

Figure 7. Tectonic discrimination diagram (Pearce, 1974).

Khalzan Burgetei deposit is formed on within plate tectonic setting but Mushgai kudag deposit, Khan Bogd and other occurrences show scattered and continuous trend from volcanic arc to within plate setting

Summary

We studied more than 80 locations of REE mineralized occurrences and deposits and analyzed more than 200 hundred samples of intrusive rocks which have spatial and genetic relation with REE mineralization. Result of geochemical study of intrusive rocks of REE occurrences and deposits can be summarized as following:

- Intrusive rocks show compositional difference regarding to their genetic types: carbonatite related REE occurrences show more alkaline and mainly syenite and nepheline syenite, but alkaline related REE occurrences show alkaline granites.
- REE content of intrusive rocks show various tendency with content of silica. REE composition of Mushgai khudag deposit decreases with increasing silica content but other deposits and occurrences increases.

- REE content of all deposits and occurrences has very good positive correlation with ittrium.
- All rocks are A-type granites indicating anorogenic source.
- REE deposits and occurrences show mainly within plate tectonic setting but partly volcanic arc, oceanic ridge granite tectonic environment.

CHARACTERIZATION OF TURKALI PLUTON & YUNTDAG VOLCANICS RELATED ORE GENESIS (MANISA-TURKEY)

Kabiru M., Kocaturk H., Yıldırım D., Kumral M., Unluer A.T., Budakoglu M.
Istanbul Technical University, Faculty of Mines, kocaturkhu@itu.edu.tr

The Investigation area is structurally characterised by Permo-Triassic rock unit known as the Karakaya Complex in northwestern Anatolia which intends divided into two sub-units; Nilüfer unit is the basement with structurally deformed rock; metabasite, phyllite and marble, then overlaid by upper Karakaya complex. Hodul unit that consists of volcaniclastics and volcanic rocks with exotic block of Permian limestones. Field fall within upper Karakaya complex and Miocene Yuntdağ volcanic rocks consisting of andesite and dacite and Tertiary sediments from Soma formation with plutonic rocks such as granite and granodiorite. The aim of this study is to understand differences between polymetallic Cu-Zn-Pb-Au and Ag mineralization and Porphyry Cu-Mo-Ag-Au (Zn-Pb) breccias and veins at Turkali by deciphering geochemistry, fluid inclusion and ore paragenesiss. Polymetallic epithermal veins are structurally controlled by Cenozoic-aged detachment faulting related to exhumation and core complex development of Kazdag massif during Oligo-Miocene and strike-slip faults which started during Early Miocene by the formation process of North Anatolian Fault Zone (NAFZ). The fluid characteristics are favorable for the precipitation of both precious and base metal Au-Ag-Cu-Pb-Zn-Sb and are mostly found in low temperature hydrothermal environment. During the Miocene, lead, zinc silver and gold deposits are usually treated as same because they are mostly associated with hydrothermal base metal mineral deposits. Zinc and lead are the 24th and 36th common elements with crustal abundant of 70 ppm and 15ppm and enrichment factor of 600 and 400 respectively. The potential source of a mineralization fluid is of high interest to study the origin and pathway of a deposit. This deposit is hosted by subvolcanic rocks with andesitic character. Yigit (2012), highlighted the mineral deposits of the area are shaped by Cenozoic calc-alkaline magmatism ranging from 52 to18 Ma, which is related to collisional and post-collisional tectonic regimes. These deposits include epithermal Au-Ag (low, intermediate and high) sulphidation, porphyry. The Oligocene formed deposits are of economic significance and include epithermal and porphyry deposits.

Ore Paragenesis and Fluid Inclusison Investigations

Ore paragenesis confirmed the intermediate epithermal vein-type by the precipitation of coarse-grained to massive aggregates of sphalerite, galena, pyrite, chalcopyrite and other sulphide minerals like tennantite, tetrahedrite, realgar and orpiment in open space fractures. The texture shows colloform banding of sulphide minerals which probably indicate a change in fluid characteristics from high (H) to intermediate (I) sulphidation mineralization and occur as hydrothermal veins replacement or open space fillings. Also, the main gangue minerals are quartz, carbonates and barite with supergene enrichment of malachite, azurite, covellite, cerussite, smithsonite and anglesite. Also, barite probably characterised deposition of fluid under decreasing temperature and oxidising environment. Gold and silver were observed only in the geochemical data and not as ore minerals. Porphyry Cu-Mo is probably derived from an I-type Türkali granodiorite stock which is from a post-collisional setting and is the source of presumably Cu-Mo deposit. The presence of hydrothermal breccia and vein zones probably. Double polished-sections of quartz, calcite, barite and sphalerite samples were used for petrography and Heating/Freezing stage connected to microscope with a camera to capture the fluid inclusion images.

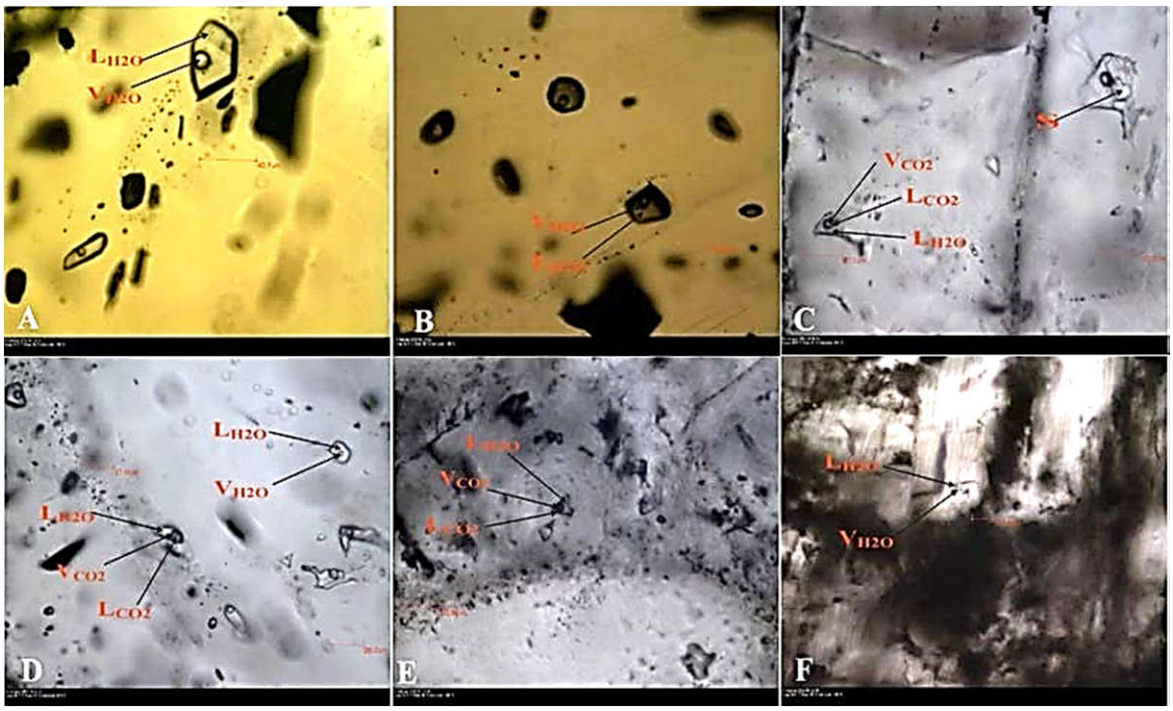

Fig. 1. Photomicrographs of fluid inclusions; (a) Liquid phase (LH2O) and Vapour phase (VH2O) in sphalerite (MLG4-1), (b) (LH2O) and (VH2O) in sphalerite (MLG2-4), (c) Liquid phases LH2O and LCO2, Solid (S) and vapour (VCO2) in Calcite (ML10), (d) Liquid phases LH2O and LCO2, and vapour (VCO2) in Calcite (KB6B), (e) Liquid phases LH2O and LCO2, and vapour (VCO2) in quartz (KB6C) and (f) Liquid phase (LH2O) and Vapour phase (VH2O) in Barite (KB3).

The samples dominantly of massive aggregates of pyrite (Py), galena (Gn), sphalerite (Sl) and chalcopyrite (Ccp) within brecciated veins of quartz (Qtz), carbonates and barites (Brt). Hypogene ore minerals; realgar (Rg), orpiment (Opt), tennantite (Tn), tetrahedrite (Tt), molybdenite (Mo), boulangerite (Bno) and hematite (He), as well as supergene enrichment of covellite (Cv), malachite (Ma), azurite (Az), carbonate; cerussite (Cer) and smithsonite (Sm) and sulphate; anglesite (Ang) were recognised. Photomicrographs of the examined samples show the ore minerals present in the study area with various textures and crystal forms of both the hydrothermal veins and supergene environment. The existence of both low-temperature minerals such as realgar, orpiment, barite, and high-temperature minerals like molybdenite, pyrite, chalcopyrite, sphalerite and galena indicate intermediate epithermal hydrothermal system.

Conclusion

As a result, based on the above features obtained from field observations, ore microscopy, fluid inclusion studies, geochemistry, and literature reviews, the genesis of the ore fluid is likely to occur in the hydrothermal and polymetallic intermediate epithermal vein type mineralization. Polymetallic epithermal vein mineralizations are structurally controlled by feature characterized by detachment faults Oligo-Miocene NE- direction related to north Anatolian Fault Zone (NAFZ). NE-SW, E-W and NW-SE fault directions which started during Early Miocene and continue during Quaternary and serves as a fluid migration pathway and causes surrounding volcanic rocks mostly andesite to become permeable which acted as the reservoir for the sulphide minerals (Bingol et al 1975; Orgun et al. 2005). The presences of breccia vein zone probably overprint intrusion-related Au-Ag-Zn-Pb stock and subhorizontal breccia for porphyry Au mineralization.

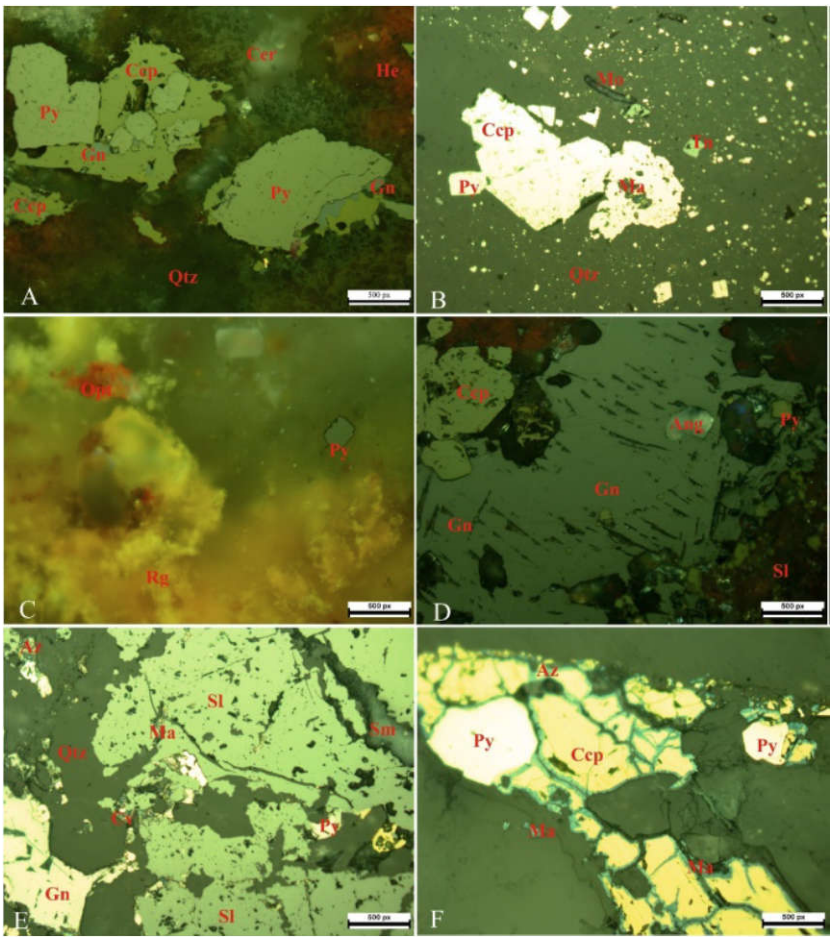

Figure 2. Photomicrographs of Türkali ore minerals: A (KB3); replacement of pyrite (Py) by chalcopyrite (Ccp) and chalcopyrite by galena (Gn), B (KB6B); Molybdenite (Mo), tennantite (Tn), Pyrite and chalcopyrite in quartz, C (KB6B); Arsenic minerals realgar (Rg) and orpiment (Opt), D (KB6C) Galena with triangular pits formed by deformation, E (KB9); Massive sphalerite (Sl) with smithsonite (Sm) and quartz (Qtz) veins and F (KB11) Supergene zone with malachite (Ma) and azurite (Az).

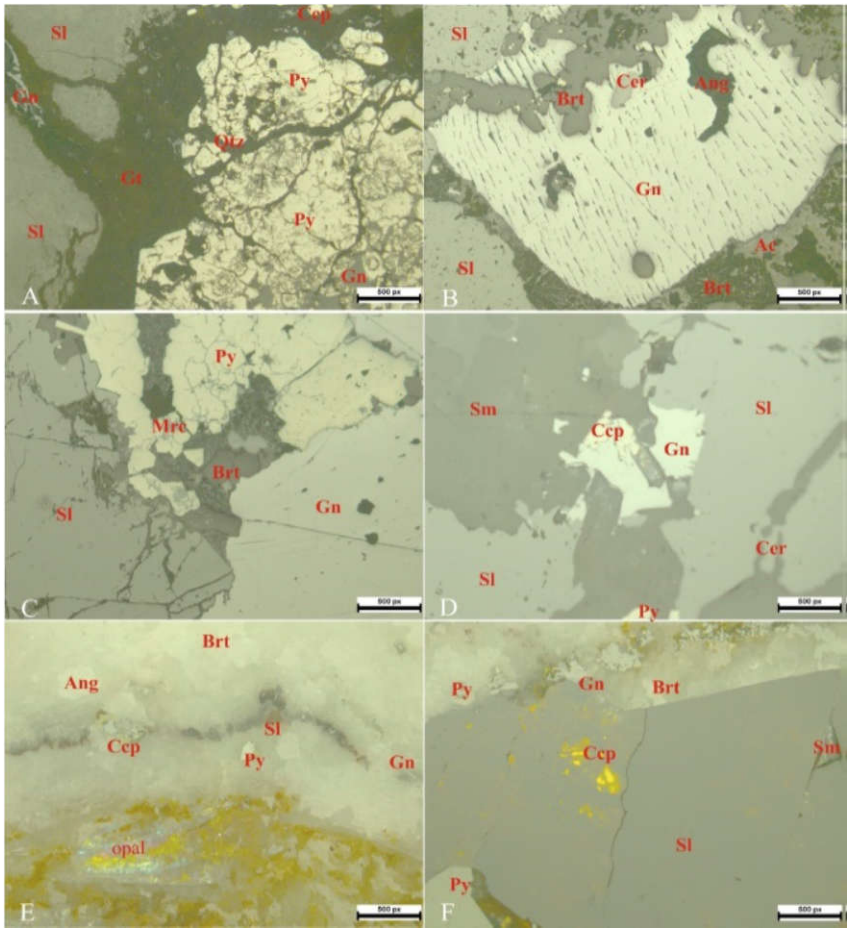

Figure 3. Photomicrographs of Yayladali ore minerals: A (MK2); botryoidal pyrite (Py) indicating early formed pyrite, B (MK6A) Massive galena (Gn) with triangular pits and barite (Brt), Cerussite (Cer) and anglesite (Ang), C (MK with smithsonite (Sm) matrix, E (MKG2) Colloform structure with pyrite, chalcopyrite, sphalerite, galena and opal, F (MKG4); Exsolution of Chalcopyrite (disease) in sphalerite.12); Massive Pyrite replaced by marcasite (Mrc), D (MK16); replacement of sphalerite (Sl) by galena.

References

Bingol, E., Akyurek, B. and Korkmazer, B. Geology of the Biga peninsula and some characteristics of the Karakaya block series. Proceedings of the 50th Anniversary of the Turkish Republic Earth Science Congress, Mineral Research and Exploration Institute of Turkey Publications. 1975. pp 70-75.

Orgun, Y., Gultekin, A.H., Onal, A. Geology, mineralogy and fluid inclusion data from the Arapucan Pb–Zn–Cu–Ag deposit, Canakkale, Turkey. J. Asian Earth Sci. 2005. Vol. 25. pp 629–642.

Yigit O. A Prospective sector in the tethyan metallogenic belt: Geology and geochronology of mineral deposits in the Biga Peninsula, NW Turkey. Ore Geology Reviews. 2012. Vol 46. pp 118-148.

PRESSURE-INDUCED REACTIONS ON ORGANIC COMPOUNDS: PREBIOTIC MOLECULAR EVOLUTION IN ICY BODIES

***Kagi H.*[1], *Fujimoto C.*[1], *Takahshi S.*[1], *Shinocaki A.*[2], *Mimura K.*[3]**

[1]*Graduate School of Science, The University of Tokyo, kagi@eqchem.s.u-tokyo.ac.jp*

[2]*Graduate School of Science, Hokkaido University*

[3]*Graduate School of Environmental Studies, Nagoya University*

Organic compounds are crucial for the evolution and origin of life. Since organic compounds behave as a soft material with compression, intermolecular interactions of organic molecules drastically increase at high pressure. For this reason, high pressure can induce substantial structural changes and chemical reactions on organic compounds even at ambient temperature. We have reported polymerization and dehydration condensation of organic compounds (ex. pyridine, benzene, trimethyl silanol, naphthalene, etc.) under high pressure and ambient temperature conditions (Shinozaki et al., 2013; Shinozaki et al., 2014; Shinozaki et al., 2016; Yasuzuka et al., 2011). It is noteworthy that the products from pressure-induced reaction are significantly different from those from shock-induced reactions mainly because of the contrast of temperatures between the two experiments.

Pressure-induced dehydration condensation resulting in peptide formatin occurs on amino acids. We have reported peptide formation from an aqueous solution of L-alanine at pressures greater than 5 GPa and room temperature (Fujimoto et al., 2015). The maximum length of peptides has reached up to 11-mer. It is curious that the peptide formation was found from aqueous solution of amino acids, because the peptide formation is a dehydration reaction and the intermolecular interactions between amino-acid molecules weakens in aqueous solution. We have proposed a pressure-induced freeze concentration associated with crystallization of ice VII (a high-pressure polymorph of ice) is a key process, which explain the peptide formation occurring in the aqueous solution of amino acid at high pressure. Our experimental results suggest that the interior of icy bodies may be responsible for prebiotic peptide formation.

In the presentation, I would like to introduce our recent results on pressure-induced ester formation reactions, optical isomer formation, etc.

References

Fujimoto C., Shinozaki A., Mimura K., Nishida T., Gotou H., Komatsu K. and Kagi H. (2015) Pressure-induced oligomerization of alanine at 25 ℃. Chemical Communications, 51, 13358-13361.

Shinozaki A., Noguchi N. and Kagi H. (2013) In-situ spectroscopic observations of pressure-induced condensation of trimethylsilanol and behavior of dehydrated molecular water. Chemical Physics Letters, 574, 66-70.

Shinozaki A., Mimura K., Kagi H., Komatsu K., Noguchi N. and Gotou H. (2014) Pressure-induced polymerization of benzene at room temperature as a precursory reaction of amorphization. Journal of Chemical Physics, 141, 084306.

Shinozaki A., Mimura K., Nishida T., Inoue T., Nakano S. and Kagi H. (2016) Stability and partial oligomerization of naphthalene under high pressure at room temperature. Chemical Physics Letters, 662, 263-267.

Shinozaki A., Komatsu K., Kagi H., Fujimoto C., Machida S., Sano-Furukawa A., Hattori T. (2018) Behavior of intermolecular interactions in α-glycine under high pressure. Journal of Chemical Physics, 148, 044507.

Takahashi S., Kagi H., Fujimoto C., Shinozaki A., Gotou H., Nishida T. and Mimura K. (2017) Pressure-induced freeze concentration of alanine aqueous solution as a novel field of chemical reaction. Chemistry Letters, 46, 334-337.

Yasuzuka T., Komatsu K. and Kagi H. (2011) A revisit to high pressure transitions of pyridine: a new phase transition at 5 GPa and formation of a crystalline phase over 20 GPa. Chemistry Letters 40, 733-735. doi:10.1246/cl.2011.733

THE ALYARMAUT UPLIFT: FEATURES OF ORE MINERALIZATION (BASED ON REE PATTERNS)

Kalko I.A.*, Nikolaeva I.Yu., Nikolaev Yu.N., Prokofiev V.Yu., Krivitckaya N.N., Lubkova T.N., Bychkov D.A.

Geology Department of Lomonosov Moscow State University, ildarkalko@yandex.ru

New prospects were revealed in the process of geochemical works in the territory of Chukotka (Far East of Russia). Their characteristics are similar to objects of industrial value. The Alyarmaut uplift is located 100 kilometers north of the Bilibino (Chukotka Autonomous District). Geochemical works were carried out on the territory with testing of bottom sediments, soils, background rocks and ore samples.

The area concerns to Anyui-Chukotka Fold Belt allocated sediments carboniferous - triassic shown shale, siltstone, marbled limestone, quartzites, triassic gabbroides Anyui complex. At the outer frame portion positioned acidic intrusive formation tymkiveemsky and suharninsky suits diorite-granite complexes whose age formation is 116 - 108 million years (Katkov, 2007). In the area are known industrial gold placers, non-industrial placer deposits of tin, prospects of gold, tin, antimony. The mineral resources of the region are associated with intrusive rocks of Cretaceous age.

According to the results of geochemical works, area contrasting secondary halos of silver, gold, lead, copper were installed. The ore formations contain the contents of silver, gold, arsenic, lead, selenium, antimony and zinc. The gold content up to 13 ppm, silver up to 1700 ppm, tenth percent - percentages of antimony, copper, lead, zinc, arsenic have been established by testing ore samples. Of the most interesting samples, thin sections were made to study the fluid inclusions. The composition of the complex phases was determined using microprobe studies. In the samples of background rocks and ore formations, the contents of rare-earth and incompatible elements were determined in order to determinate the source of mineralization.

Copper, lead and zinc sulfides mineral associations predominate, in some cases it intersects with early arsenopyrite-pyrite association. Among minerals four associations identified: pyrite-arsenopyrite and gold (1), the association of simple sulfide (galena, sphalerite, chalcopyrite, pyrrhotite) (2), precious metal associations on (gold, silver, naumannite, acanthite, petzite) (3) association of lead-antimony sulfosalts (stibnite, zinkenite, plagionite) (4). In accordance with primary sulphides are developed supergene minerals represented scorodite, malachite, azurite, siderite, bornite, covellite, oxyplumboroméite. In the ore samples of gold extraction have a sample of 794 ‰, and in placers from 876 to 913 ‰.

On the temperature of homogenization (Prokofiev, 2018) two classes of fluid inclusions are distinguished: mesothermal and epithermal; salinity is varied from high (33-43% eq. NaCl) to salinity characteristic of epithermal deposits (0.2-9.6% eq. NaCl). According to the calculated pressures, there are two types of fluid inclusions in quartz: the first high-pressure, the second low-pressure. The difference in pressure shows a rising from a depth of about 7 km to a depth of about 1 km (Prokofiev, 2018).

The granitoids of the Alyarmaut Uplift are classified in the paper (Luchitskaya, 2010) have geochemical features of collisional and subduction types.

The article (Tikhomirov, 2017) assumes the existence of an early Cretaceous volcanogenic belt, the relics of which are also noted on the Alyarmaut Uplift.

Geochemical characteristics of the ore formations of the Alyarmaut Uplift reveal similarities with the host rocks (fig. 1, 2).

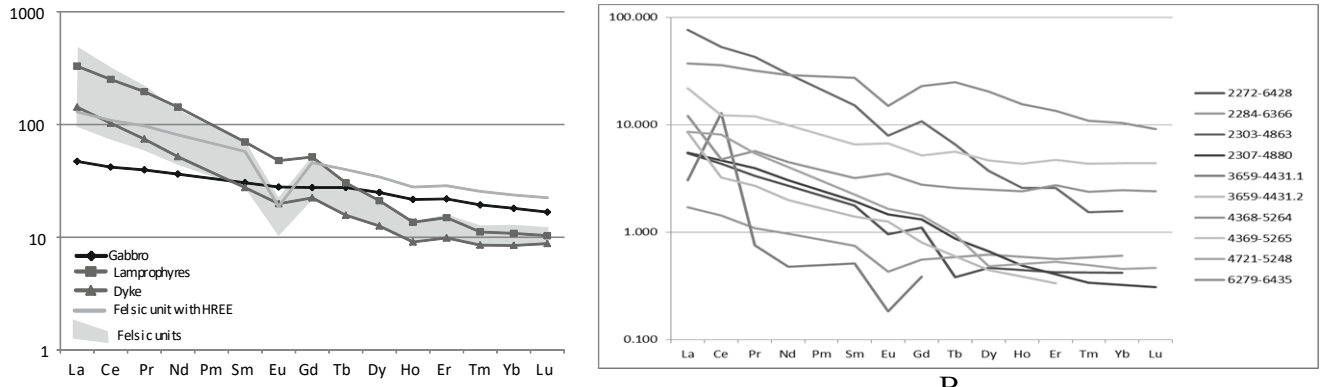

Fig. 1. The patterns of rare-earth elements in Alyarmaut uplift's a) rocks; b)ores (normalized to CI-chondrites concentration (Anders, 1989)).

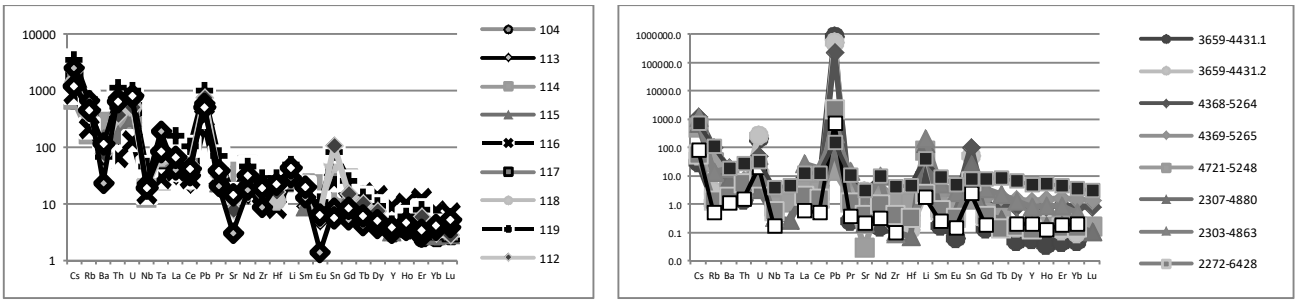

Fig. 2. Mantle-normalized (Sun, 1989) diagram a)rocks; b) ores.

The patterns of distribution of rare and incompatible elements in rocks and ores with Alarmaut are close to each other. In ore samples, intensive enrichment occurs Pb, Li. All other elements in relation to rocks are weakly or strongly extricated or diluted. There is a slight europium maximum in two ore samples.

References

Anders E., Grevesse N. Abundances of the elements: Meteoritic and solar. //Geochim. Cosmochim. Acta. 1989. Vol. 53 pp. 197-214.

Katkov S. M., Strickland A., Miller E. L., Toro J. Age of Granite Batholiths in the Anyui–Chukotka Foldbelt.// Doklady Earth Sciences. 2007. Vol. 414 No. 4 pp. 515–518

Luchitskaya M.V., Sokolov S.D., Katkov S.M., Bondarenko G.E. Composition and geodynamic setting of granitoid magmatism in The Alyarmaut Uplift, Western Chukchi Peninsula. // Geochemistry International. 2010. Vol. 48 No 9 pp. 891-916.

Prokofiev V. Yu., Kalko I. A., Volkov A. V., Nikolaev Yu. N., Krivitskaya N. N., Sidorov A. A. Features of Ore Mineralization of Alyarmaut Rise (Western Chukotka). // Doklady Earth Sciences. 2018. Vol. 479 Part 1 pp. 310–315.

Sun, S.-S., McDonough, W.F. Chemical and isotopic systematics of oceanic basalts: implications for mantle composition and processes. // Magmatism in Ocean Basins. Geol. Soc. Spec. Publ. 1989. pp. 313–345.

Tikhomirov P. L., Prokof'ev V. Yu., Kal'ko I. A., Apletalin A. V., Nikolaev Yu. N., Kobayashi K., Nakamura E. Post-collisional magmatism of Western Chukotka and Early Cretaceous Tectonic Rearrangement in Northeastern Asia. // Geotectonics. 2017. Vol. 51 No. 2 pp. 131–151.

WATER IN THE EARTH'S LOWER MANTLE

Kaminsky F.V.

KM Diamond Exploration Ltd., West Vancouver, British Columbia, Canada, felixvkaminsky@aol.com

The presence of water in the mantle affects various physical properties of the deep Earth, such as electrical conductivity, elastic properties, phase boundaries, melting, etc. At the early stages of the Earth's history water played an important role during the solidification of the magma ocean and in core segregation. Moreover, water played a significant role during the formation of the Earth and Moon from a supraplanetary gas-dust body (Galimov, 2011). The effect of water on phase transformations in the mantle transition zone and the core-mantle boundary may lead to a significant revision of temperature distribution inside the Earth and its spatial and temporal energy balance (Litasov and Ohtani, 2007).

However, the presence of water below the transition zone (deeper than 660 km), in natural lower mantle minerals is poorly constrained to date, although there is direct evidence on this subject. Diamonds from the lower mantle contain the structural impurity of hydrogen several times more than is found in lithospheric diamonds. Recently, in a diamond from Namaqualand were found crystalline inclusions of ice-VII, formed at depths of between 610-800 km (Tschauner et al., 2018). Furthermore, the development of experimental, high-pressure techniques over the last two decades has facilitated the study of synthetic lower-mantle mineral phases.

All major, rock-forming lower-mantle minerals (bridgmanite, CaSi-perovskite, ferropericlase and stishovite) are 'nominally anhydrous minerals' (NAMs), in which hydrogen comprises less than 1 wt.% and whose chemical formula would be normally written without hydrogen. In NAMs, hydrogen occupies various defects of the crystal lattice and is bonded to structural oxygen, forming hydroxyl groups. The most reliable estimates of water concentrations in lower-mantle minerals vary widely: 1400-1800 ppm in bridgmanite, 10-80 ppm in ferropericlase, and 20-150 ppm in stishovite (Table 1).

Table 1. Estimates of concentrations and mass of water in the lower mantle and the core.

Reference	H_2O in the lower mantle			H_2O in the core		Total H_2O mass in the Earth, 10^{24} grams
	Concentration, ppm	Mass, 10^{23} grams	Rate to the mass of ocean	Concentration, ppm	Mass, 10^{23} grams	
Litasov et al. 2003	1500	34.2	~2.5			
Keppler and Bolfan-Casanova 2006	~10	0.29	0.02			
Mottl et al. 2007	20-500	0.59-14.7 (av. 1.4)	0.04-1			22.1
Bodnar et al. 2013	100	3.00	~0.2			3.04
Nestola and Smith 2016	2000	61.0	~7	80-500	1.5-10 (av. 4.73)	12.1
Peslier et al. 2017	100-2000 (av. 1340)	3.0-61 (av. 40.6)	~2.9	20-7300 (av. 1000)	2.4-960 (av. 17.4)	24.7
This work	1500	45.5	~3.3			25.2

The average concentration of water in the lower mantle is ~1500 ppm. Despite such minor concentrations in lower-mantle minerals, water forms a great reservoir within the lower mantle, probably amounting ~45.45 × 10^{23} grams H_2O, i.e., ~3.3 times the mass of the Earth's oceans. Some amount of water is transported into the lower mantle by subducting lithospheric slabs; this amount is balanced by the water flux from the lower mantle to the transition zone. Within areas of partial melting in the lower and upper parts of the lower mantle, as well as in some local areas, stress and thermal increase initiate release of water from lower-mantle minerals into melt. The enrichment of partial melts with H_2O depends on the *P-T* conditions, oxygen fugacity values, and percentage of melting. It causes major geodynamic processes that are initiated within the deep Earth. The major source of the water reservoir in the lower mantle is primordial water stored early in the Earth's evolution.

References

Bodnar R.J., Azbej T., Becker S.P., et al. Whole Earth geohydrologic cycle, from the clouds to the core: the distribution of water in the dynamic Earth system. Geol. Soc. Amer. Spec. Pap. 2013 .Vol. 500 pp. 431–461.

Galimov E.M. Formation of the Moon and the Earth from a common supraplanetary gas–dust cloud. Geochem. Internat. 2011. Vol. 49 Iss. 6 pp. 537–554.

Keppler, H., Bolfan-Casanova, N. (2006) Thermodynamics of water solubility and partitioning. Rev. Mineral. Geochem. 2006. Vol. 62 Iss. 1 pp. 193–230.

Litasov K.D., Ohtani E. Effect of water on the phase relations in Earth's mantle and deep water cycle. In: Ohtani, E. (Ed.), Advances in High-Pressure Mineralogy. Geol. Soc.Amer. Spec. Pap. 2007. Vol. 421 pp. 115–156.

Litasov K., Ohtani E., Langenhorst F., et al. Water solubility in Mg-perovskites and water storage capacity in the lower mantle. Earth . Planet. Sci. Lett. 2003. Vol. 211 pp. 189-203.

Mottl M.J., Glazer B.T., Kaiser R.I., et al. (2007) Water and astrobiology: Chemie der Erde/Geochemistry 2007. Vol. 67 Iss. 4 pp. 253–282.

Nestola, F., Smyth, J.R. Diamonds and water in the deep Earth: a new scenario. Internat. Geol. Rev. 2016. Vol. 58 Iss. 3 pp. 263-276.

Peslier, A.H., Schönbächler, M., Busemann, H., et al. Water in the Earth's interior: Distribution and origin. Space Sci. Rev. 2017. Vol. 212 Iss. 1-2 pp. 743-810.

Tschauner O., Huang S., Greenberg E., et al. (2018) Ice-VII inclusions in diamonds: Evidence for aqueous fluid in Earth's deep mantle. Science 2018. Vol. 359 Iss. 6380 pp. 1136-1139.

DECOMPOSITION OF MAGNESITE IN THE PRESENCE OF REDUCED C-H-O FLUID UNDER UPPER MANTLE CONDITIONS

Kawamura H.*, *Ohfuji H.

Ehime Univ., kawamura@sci.ehime-u.ac.jp, ohfuji@sci.ehime-u.ac.jp

Magnesite, $MgCO_3$ is the representative carbonate mineral which is subducted to the deep mantle along with the oceanic crust and has been reported to be stable at pressure and temperature conditions corresponding to the bottom of the lower mantle (Isshiki et al., 2004; Solopova et al., 2015). However, we recently found that its stability was significantly influenced by the presence of a methane-rich C-H-O fluid in our preliminary experiments using laser-heated diamond anvil cell. In the present study, we performed a series of multi-anvil experiments to study the detail of the decomposition mechanism of magnesite and its significance in the deep carbon cycle. Experiments were conducted at 10 and 17 GPa and at 600-1400°C with a heating duration of 1 hours. Powdered natural magnesite and stearic acid (as a fluid source) (Yamaoka et al., 2002) were used as the starting material and were enclosed in a Pt capsule that was placed inside a Mo outer capsule (used as an oxygen fugacity (fO_2) buffer). Recovered samples were carefully sectioned (polished) by Ar^+ ion milling (using JEOL, Cross Section Polisher) and then examined by micro-focus XRD, SEM-EDS and TEM-EDS. FIB was used to prepare foil sections for TEM analysis.

At 17 GPa, the decomposition of magnesite was observed at 800°C and higher temperature, where a methane-rich C-H-O fluid was produced from stearic acid. The decomposition products in the sample recovered from 800°C were periclase, MgO and graphite/diamond mixture, while those from higher temperatures were brucite, $Mg(OH)_2$ and diamond (+graphite). The formation of brucite is likely due to the subsequent hydrolysis of the initially produced periclase crystals. The sample from 600°C showed no signs of decomposition, which is likely because the temperature was too low to produce C-H-O fluid from stearic acid. We also observed the formation of periclase and graphite/diamond from magnesite at 10 GPa and 800°C. TEM observation of the magnesite grains that were partly replaced with periclase showed a distinct coaxial relation between their lattices, Mas [-110] // Per [110], which suggests the solid-solid transformation from magnesite to periclase as a result of the decarbonation reaction. This means that the decomposition of magnesite occurred spontaneously

under the low fO_2 condition where methane was the dominant component of the coexisting fluid rather than by the chemical reaction with the methane molecules. In the Earth's mantle, the composition of C-H-O fluid depends largely on the surrounding fO_2 and at depths below 300 km methane is thought to be the most dominant component (Frost and McCammon, 2008). Our result suggests that carbonates transported by the subducting slab decompose under reducing environment at the lower upper mantle, and diamond takes over the role as the major carbon source which further subducts to the deeper mantle. Furthermore, the formation of periclase at shallower conditions (10 and 17 GPa) suggests that periclase inclusions solely-present in diamond can not always be used as indicator of lower-mantle origin.

References

Frost, D.J. and McCammon, C.A. (2008) The Redox State of Earth's Mantle. Annu. Rev. Earth Planet. Sci., 36, 389-420.

Isshiki, M., Irifune, T., Hirose, K., Ono, S., Ohishi, Y., Watanuki, T., Mishibori, E., Takata, M. & Sakata, M. (2004) Stability of magnesite and its high-pressure form in the lowermost mantle. Nature, 427, 60-63.

Solopova, N. A., Dubrovinsky, L., Spivak, A. V., Litvin, Yu. A., Dubrovinskaia, N. (2015) Melting and decomposition of $MgCO_3$ at pressures up to 84 GPa. Phys. Chem. Minerals., 42, 73-81.

Yamaoka, S., Shaji Kumarb, M. D., Kanda, H., Akaishi, M. (2002) Formation of diamond from $CaCO_3$ in a reduced C–O–H fluid at HP–HT. Diamond and Related Minerals 11, 1496-1504.

PHASE RELATIONS OF THE MODEL SEDIMENT-PERIDOTITE SYSTEM UNDER THE CONDITIONS OF THE EARTH'S MANTLE

***Kharitonova A.A.*[1,2], *Bobrov A.V.*[1,2,3], *Sirotkina E.A.*[2], *Irifune T.*[4]**

[1]*Department of Petrology, Geological Faculty, Moscow State University,* garmr9@gmail.com

[2]*Vernadsky Institute of Geochemistry and Analytical Chemistry RAS, Moscow, Russia*

[3]*Institute of Experimental Mineralogy RAS, Chernogolovka, Russia*

[4]*Geodynamic Research Center, Matsuyama University, Japan*

The processes of crust-mantle interaction have significant influence on the composition of phase assemblages in the deep Earth. It is known that subduction at mantle temperatures and pressures upon interaction of mantle peridotite and subducted crustal material (GLOSS) may result in the formation of melts enriched in Na, K, Al, Ti, REEs, and other elements, which may be parental for many deep-seated rocks. In addition, participation of the crustal material may affect significantly on the major solid-state reactions under the conditions of the Earth's mantle. Study of phase transformations upon partial melting of the crust-mantle material under the conditions of the uppermost lower mantle is an important and actual problem.

The main objective of our research is experimental study of the interaction between the model sediment GLOSS (Global Ocean Subducting Sediment) (Plank and Langmuir, 1998) and peridotite (with the composition of garnet lherzolite and weight proportions of $Ol_{60}Opx_{18}Cpx_{16}Grt_{12}$). Experimental data of such kind are rather limited (Bulatov et al., 2014; Woodland et al., 2018). In addition, our experiments were focused on the study of partitioning of such elements as Al, Cr, Ca, Ti, and others between the GLOSS and peridotite zones of the samples.

The experiments were performed at pressures of 7, 18 and 24 GPa and temperatures of 900–1600°C using a 1000-, 2000-, 3000-t Kawai-type multi-anvil high-pressure apparatus at the Geodynamics Research Center, Ehime University (Matsuyama, Japan) and at pressure 7 GPa in wide range of temperatures on a toroidal anvil-with-hole apparatus at the Vernadsky Institute of Geochemistry and Analytical Chemistry, Russian Academy of Sciences. To model crust-mantle interaction, the starting materials were loaded into Re ampoules in a 1:1 weight proportion with peridotite in the hot zone of an ampoule.

The samples after runs demonstrate clear zoning with the peridotite, GLOSS, and intermediate zones. At 7 GPa, the peridotite zone is composed of olivine, garnet and pyroxene. With decreasing

temperature, garnets become depleted in Mg and enriched in Ca. The concentration of Cr_2O_3 reaches 4 wt % and has no clear correlation with temperature. Pyroxenes in this zone are low-Ca (up to 0.6 wt % CaO). The GLOSS zone contains garnet and omphacitic pyroxene. The concentration of jadeite in pyroxene increases with temperature and reaches a maximum of 48 mol %. The compositions of associated minerals in two zones of the samples change simultaneously. With increasing temperature, garnets from both zones show increase in Mg content and Fe/Ca ratio. Pyroxenes from the peridotite zone demonstrate increase in Mg/Fe ratio with temperature, whereas pyroxenes from the GLOSS zone become enriched in Al with slight decrease in Mg/Ca ratio.

The samples produced in the GLOSS–peridotite system at 18 GPa are also characterized by the clear zoned structure. The phase associations include garnet, akimotoite, wadsleyite, stishovite, and high-Al phases. With increasing pressure, Al-bearing $MgSiO_3$ akimotoite transforms to bridgmanite.

The samples produced in the GLOSS–peridotite system at 24 GPa are also characterized by the clear zoned structure with a strong predomination of bridgmanite in both zones. Bridgmanite shows wide compositional variations with typomorphic features in each zone. Bridgmanite from the GLOSS zone is characterized by the higher concentrations of Al_2O_3 (up to 8 wt %) and presence of titanium (~0.7 wt % TiO_2). Bridgmanite from the peridotite zone is Cr-rich (~ 1 wt % Cr_2O_3), whereas the concentration of Al_2O_3 does not exceed 5 wt %. In both zones, bridgmanite associates with ferropericlase and $CaSiO_3$-perovskite. The samples usually contain an intermediate zone with the monomineral Al-rich bridgmanite composition.

Bridgmanite contains variable concentrations of Помимо железистого компонента Fe_2O_3, Al_2O_3 and their incorporation proceeds via two concurring mechanisms: coupled substitution, with almost constant Mg/Si ratios, and and nonstoichiometric (vacancy), with increasing Mg/Si ratio with substitution of Si with Al in the octahedral site (Andrault, 2007). The stoichiometric scheme predominates in bridgmanites produced in our runs (Fig. 1).

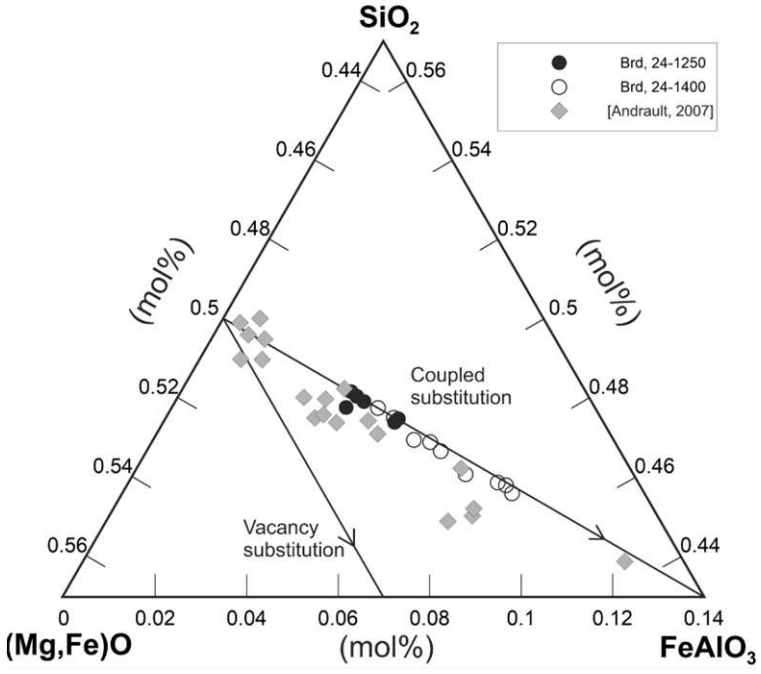

Fig. 1. Ternary diagram, showing the chemical compositions of bridgmanite.

In addition to the formation of high-Al bridgmanites, the high concentrations of Al in the intermediate zone of the samples results in the formation of several high-Al phases. The first phase most likely corresponds to NAL (new aluminous) (Akaogi, 2007) with a general formula $Mg_2CaAl_6O_{12}$ ($2MgAl_2O_4 \cdot CaAl_2O_4$). This phase in our runs in the GLOSS-peridotite system is characterized by the high concentrations of Al_2O_3 (up to 53 wt %), TiO_2 (up to 8,25 wt.%), and FeO(total) (~11 wt %). The formula of this phase is $Mg_2Fe_{0.5}Ca_{0.5}Na_{0.2}Al_{4.5}Si_{0.5}Ti_{0.45}O_{12}$. The

concentrations of Al_2O_3 in the second phase reach 55 wt % and it may be formed in the reaction like $(Mg_{0.9}Al_{0.1})(Al_{0.1}Si_{0.9})O_3 = MgSiO_3 + Al_2O_3$ (Ak = Brd + Al_2O_3).

In addition, the intermediate zone is characterized by the formation of two high-Al hydrous phases. The first phase (*AL*) (up to 56 wt % Al_2O_3) is the solid solution between $MgSiO_2(OH)_2$ (phase H) and AlOOH (phase δ), with the formula $((Mg_{0.09},Fe_{0.07})Si_{0.15}Al_{0.69})OOOH$. The second phase (*HAL*) (up to 18 wt % Al_2O_3) corresponding to the formula $Mg_2AlSi_3O_9(OH)$ was most likely formed via the reaction: *2Grt + Wad + 5Sti +2H₂O → 4HAL.*

The ternary diagram (Fig. 2) shows the compositions of $MgSiO_3$ and Al-bearing phases synthesized in our runs at pressures of 18 and 24 GPa. The general compositional trend of Al-bearing $MgSiO_3$ continues to the high-Al area, where the field of high-Al phases is observed.

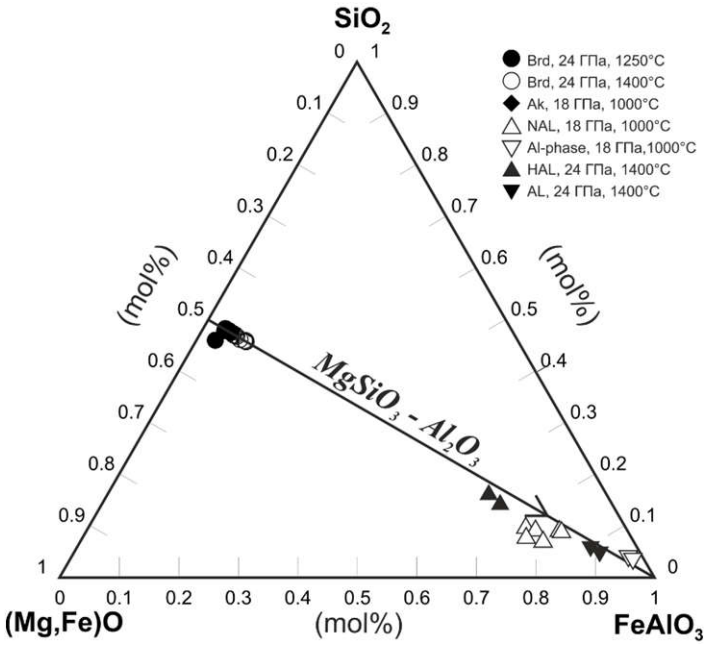

Fig. 2. Ternary diagram illustrating the compositions of bridgmanite, akimotoite, and Al-rich phases.

Thus, experimental study of interaction in the GLOSS-peridotite system in a wide P-T range allowed us to investigate phase relations, interphase element partitioning, and patterns of isomorphism in high-pressure minerals including hydrous phases. Most of the samples contain the intermediate (reaction) zones between the zones of GLOSS and peridotite modeling the crust-mantle interaction at different pressures corresponding to the upper mantle (7 GPa), transition zone (18 GPa) and uppermost lower mantle (24 GPa). Experiments of such kind at 18 and 24 GPa were carried out for the first time. We simulated the reactions between peridotite and GLOSS resulting in the formation of hydrous phases in the transition zone and lower mantle. The phase associations obtained in our runs show probability of the formation of hydrous Al-rich phases (up to 8 wt % H_2O) upon crust-mantle interaction; some of this phases may supply water to the Earth's transition zone and lower mantle.

This study was supported by the Russian Science Foundation (project no. 17-17-01169). The study of Cr, Ni, Ti interface partition at 7 GPa was supported by the Russian Foundation for Basic Research (project no. 17-55-50062) and by the Foundation of the President of the Russian Federation (Grant No MK-1277.2017.5).

References

Andrault D. Properties of lower-mantle Al-(Mg,Fe)SiO_3 perovskite // Advances in High- Pressure Mineralogy (ed. By E. Ohtani). 2007. Special paper 421, p. 15-36.

Akaogi M. Phase transitions of minerals in the transition zone and upper part of the lower mantle // Advances in High-Pressure Mineralogy (ed. By E. Ohtani). 2007. Special paper 421, p. 1-13.

Bulatov V.K., Brey G.P., Girnis A.V., Gerdes A., Hofer H.E. Carbonated sediment- peridotite

interaction and melting at 7.5-12 GPa // Lithos. 2014. V200-201. P. 368-385.

Plank T., Langmuir C.H. The chemical composition of subducting sediment and its consequenses for the crust and mantle // Chemical Geology. 1998. V. 145, p. 325-394.

Woodland A.B., Bulatov V.K., Brey G.P., Girnis A.V., Hofer H.E., Gerdes A. Subduction factory in an ampoule: Experiments on sediment-peridotite interaction under temperature gradient conditions // Geochimica et Cosmochimica Acta. 2018. V. 223. P. 319-349.

IMPURITIES REMOVAL FROM FINE QUARTZ USING FROTH FLOTATION PROCESS

***Kheloufi A.*[1], Bobocioiu E.[2], Medjahed S.A.[1], Hamou M.O.[3], Kefaifi A.[1]**

[1]*Research Center of Semiconductors Technology for Energetic (C.R.T.S.E), Dep. Raw material and crystal growth, kheloufi@yahoo.co.uk*

[2]*Ecole Normale Supérieure (ENS), Geology Dep.*

[3]*Ecole Nationale Polytechnique d'Alger*

We study of microstructural properties of Algerian quartz from Timimoun deposits and their enrichment for silicon production. The Timimoun deposit is located about 600 Km south of Algiers, and it is characterized by a quartz rich petrofacies. The quartz represents the gangue of a gold-bearing mineralization in association with pyrite and chalcopyrite (M. Thomas, 2011).

About 60 kilograms of quartz have been investigated by X-ray fluorescence (XRF) and optical microscopy in the laboratory of CRTSE – Algeria. A total of 40 representative samples were taken all along the deposit, of which 20 samples were taken from the northern part (sample 1) and 20 others from the southern part of the area (sample 2).

The microscopic investigations of samples revealed primary metamorphic origin of the quartz. The crystals were strongly affected by brittle and ductile deformation. The brittle deformation caused numerous fractures and cracks at the outcrup scale as well as at the intracrystalline scale. Local quartz recrystallizations are also present.

The size of the quartz grains is very heterogeneous ranging from 10-20 μm to few centimeters (fig.1a). The quartz is relatively poor in solid inclusions. We remark the presence of muscovite ($KAl_2Si_3AlO_{10}(OH,F)_2$) with sizes up to 200 μm. Small quantities of opaque minerals such as Fe oxides are present.

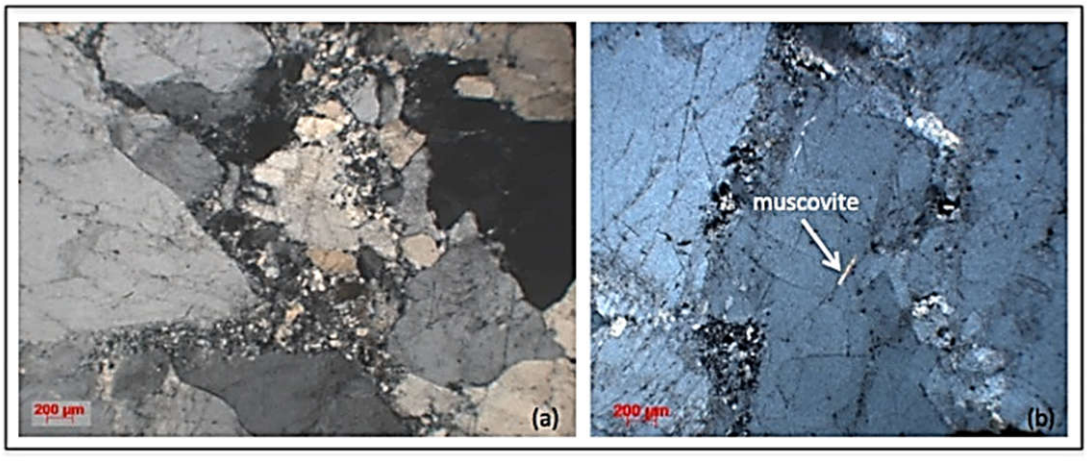

Fig. 1. Quartz from Timimoun deposits. a – Quartz granules with very varied sizes; b – Muscovite crystal in quartz. Images in polarized light.

The X-ray fluorescence highlights quartz with considerable purity (93 – 94 % SiO_2) (Table 1). However, this percentage is not enough to use the quartz in electrometallurgy applications. Based on these results, samples need to be subject to enrichment processes, to increase the required purity for solar-grade silicon production $SiO_2 > 98$ % (fig. 2).

Table 1. X-ray fluorescence analysis of silica.

Compound	Al_2O_3 ppm	SiO_2 %	SO_3 ppm	Cl ppm	CaO ppm	Fe_2O_3 ppm	CdO ppm	SnO_2 ppm
Sample 1	5947.2	93.637	1665.8	713.1	282.5	650.9	11.7	62.4
Sample 2	3800	94.99	750.2	583.4	270	410,50	48.2	23.7

We use the froth flotation process in acid and neutral environment to investigate the impact and the optimal amount of depressant reagent (HF) on the process and also the role of pH in the pulp, which influence on the purity and the recovery of SiO_2.

The flow-sheet of the flotation is represented in Fig. 2.

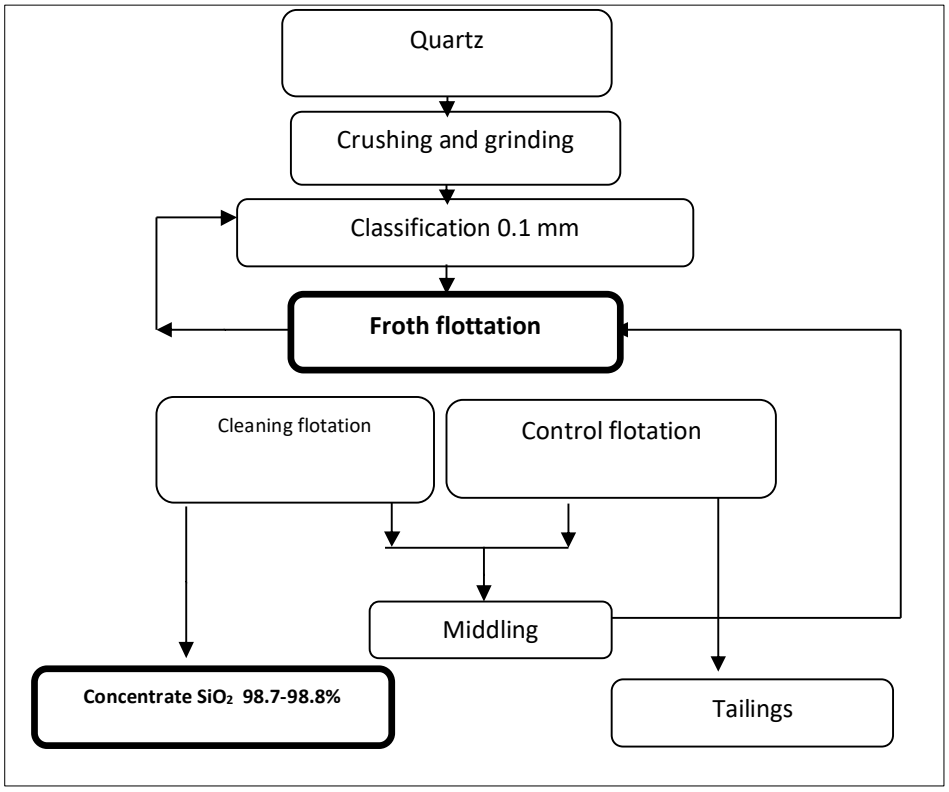

Figure 2. Flow-sheet of flotation of Timimoun quartz deposit.

The results of flotation experiments in acid solution showed a quartz concentrate containing 98.8% SiO_2, 0.01% Fe_2O_3 and 0.04% Al_2O_3 with 86:75% recovery. However, the flotation in neutral environment leads to a concentrate containing 97.61% SiO_2, 0.02% Fe_2O_3 and 0.05% Al_2O_3 with 62.21% recovery.

The effect of the pH of the pulp and the HF as depressant reagent on the content and recovery of SiO_2 was presented in Figure 2 and 3. We observe that in acidic environment the optimal values of SiO_2 concentration and recovery were obtained for the pH value less than 3 with the amount of HF around 500 g/t. This is due to the role of HF in the selective flotation of minerals that have close flotation properties. Minerals that relate to the same class (eg. The oxides) float with the same collector. The use of depressant makes it possible to increase the selectivity of the action of the collector to the minerals belonging to the same class.

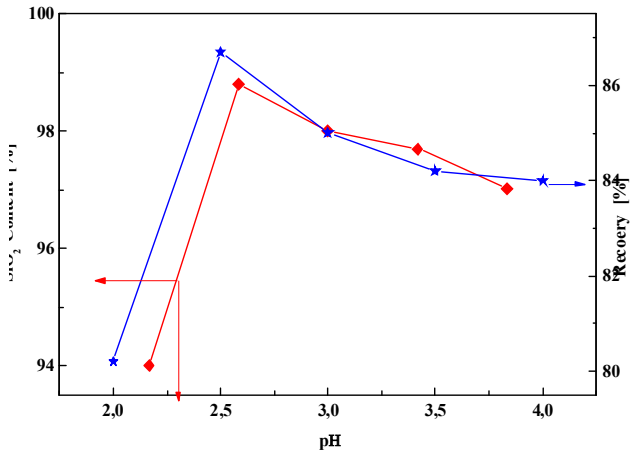

Figure 3. The effect of pH on the SiO_2 the SiO_2 content and recovery

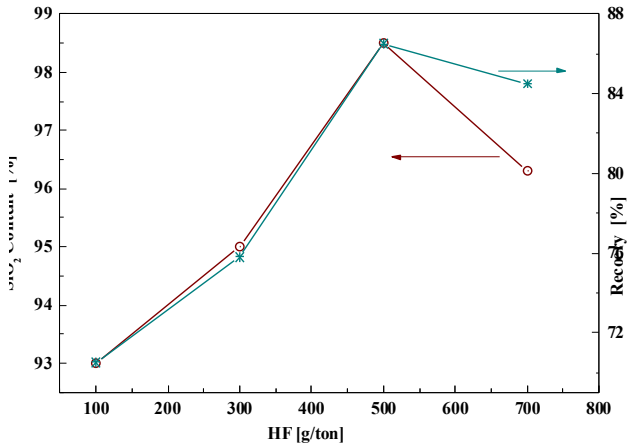

Figure 4. The effect of the depressant amount on amount on the SiO_2 content and recovery

Consequently, the best flotation conditions were obtained for first group experiments, with a pH of 2.25 (for H_2SO_4, NaOH, HF: 500 g/t, Aero 840: 500 g/t, DF 250: 50 g/t).

We can conclude that the optical and spectroscopic characterizations of the quartz from Timimoun deposits show the presence of numerous fractures and cracks. The muscovite and Fe oxides are the only mineral inclusions observed at the microscopic scale.

XRF analyses highlight an initial SiO_2 content of 93-94%. The removal of impurities such Al_2O_3 and SO_3 and Fe_2O_3 was carried out using a froth flotation method. In this context, we determined the influence of depressant reagent HF and pH pulp on the purity and recovery of SiO_2. The results of flotation experiments in acid solution showed a quartz concentrate containing 98.8% SiO_2, 0.01% Fe_2O_3 and 0.04% Al_2O_3 with 86:75% recovery. The flotation leads to a concentrate containing 97.61% SiO_2, 0.02% Fe_2O_3 and 0.05% Al_2O_3 with 62.21% recovery. The quartz product obtained in acidic medium meets the suitable properties and can be used for silicon production.

References

Kheloufi A., Bobocioiu E., Kerkar F., Kefaifi A., Anas S., Medjahed S.A., Belkacem Y., Keffous A. Optical and spectroscopic characterizations of Algerian silica raw material to predict high quality solar-grade silicon // Optic. Mat. 2017. Vol.65 pp. 142-149.

Braga F., Moreira S.P., Zamperi P.R., Bacchin J.M.G. Mei P.R. New processes for the production of solar-grade polycrystalline silicon // J. Sol. energy Mater.2008. Sol. cells Vol.92 Iss. 4 pp. 418-424.

Farmer, A.D., Collings, A.F., Jameson, G.J. The Application of Power Ultrasound to The Surface Cleaning of Silica and Heavy Mineral Sands //Ultras. Sonochem. 2000. Vol.7 pp. 243-247.

Ay, N., Arica, E., Refining Istanbul's Silica Sand //The American Ceramic Society Bulletin August.2000., pp.89-91.

Désindes. L. Silice ultra-pure pour l'électrométallurgie. Dissertation : gîtologie et caractéristiques physiques et chimiques du minerai quartz. Dissertation. Université Henri pointcaré Nancy 1, Nancy, France.2004. 433 p.

Thomas M. Sedimentology and Basin Context of the Numidian Flysh Formation; Sicily and Tunisia. Dissertation. University of Manchester. United Kingdom. 2011 254 p.

Deniz F., Halime A., Temel A., Bozkurt V.. Removal of Impurities from Tailing (Quartz) Obtained from Bitlis Kyanite Ore by Flotation Method.International.// Journal of Applied Science and Technology. 2011. Vol. 1 Iss.1 pp.74-81.

ISOTOPIC FEATURES AND FLUID CHARECTERIZATION OF ORE FORMING PROCESS GURGENYAYLA AND BOGAZOVA PLUTONS (KÜTAHYA/BURSA/BILECIK-TURKEY)

***Kocaturk H.*[1], *Sendir H.*[2], *Kumral M.*[1], *Unluer A.T.*[1], *Budakoglu M.*[1]**

[1]*Istanbul Technical University, Faculty of Mines, kocaturkhu@itu.edu.tr*

[2]*Eskisehir Osmangazi University, Geological Engineering Department, hsendir@ogu.edu.tr*

Investigation field is located between Kutahya-Bursa-Bilecik provincial borders. The key factor for the ore formation is the effect of hydrothermal activities which is originated from Guregenyayla(Domanic) and Bogazova Granodiorites. These granodiorites show similar geochemical and petrographic characteristics and it is logical to whether they are produced from the same magma chamber. All the ore genesis processes are related to these intrusions and their relevant products. Intrusions are identified as granodiorites with the distinct petrographic subgroups such as granodiorite porphyry, diorite porphyry, granite, diorite. Intrusions are cutting through different lithological units such as limestone, marble, schist and sedimentary units. Main goal of the study is to understand the geological setting and determine the characteristics of the ore carrying fluid. Ore deposition which is formed over Sarıcayıryayla region can be identified as vein type Cu-Mo mineralization with the disseminated gold enrichments. In this region identified ore minerals are chalcopyrite, pyrite, sphalerite and rutile. Another deposit which is formed over Arapdede region. Dominant ore minerals for Arapdede region is galena and chalcopyrite. Iclaliye mineralization has similar character with Hayriye mineralization and it is mainly formed as skarn type deposit which observed on the border of granodiorite, marble and schists. Additionally, Copper enrichment is much more at these regions and it is possible to see some high copper included minerals such as bornite in this field. Specimens are striking to be highly enriched of both LREE (light rare earth elements) and HREE (heavy rare earth elements) in the normalization pattern according to the chondrite. LREE and HREE enrichment in the SDT and ICL specimens are similar and relative enrichment is less than in the SY specimens. In all cases, the enrichment seen in the LREE elements indicates that the magma is rich in trace elements, or in parts of different proportions, resulting in eruptions. The negative Eu anomalies observed in HYR, ICL and SDT specimens and lesser examples of SY can be interpreted as the source of feldspar minerals during fractionation or partial melting of plagioclase minerals.

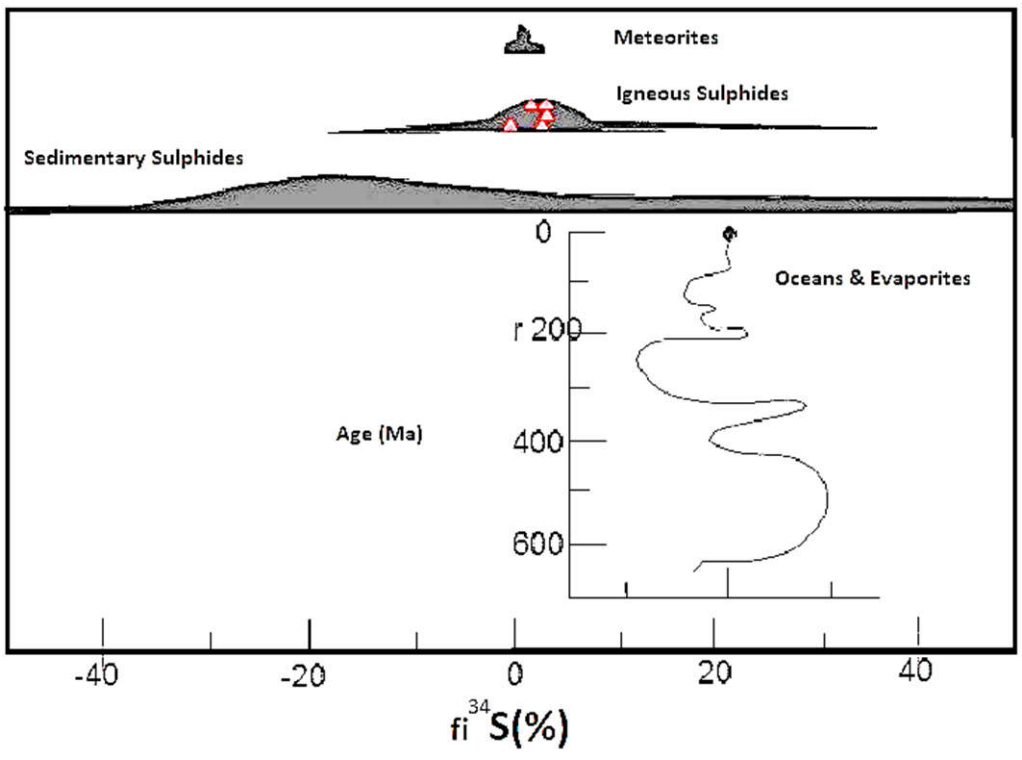

Fig. 1. Environmental analysis of sulfur samples according to Ohmoto and Rye (1979).

Isotope Geochemistry

Sulfur isotope values measured from pyrite, chalcopyrite, sphalerite minerals from Hayriye and Saadet mineralizations. As a result of the measurements, it was determined that the sulfur isotope values were changed between % 2.95 and 3.5 ‰. According to Ohmoto and Rye (1979), these results in the area of magmatic sulphides (Fig. 1) and according to the Hoefs (1987) they are located in the granitic rocks (Fig. 2).

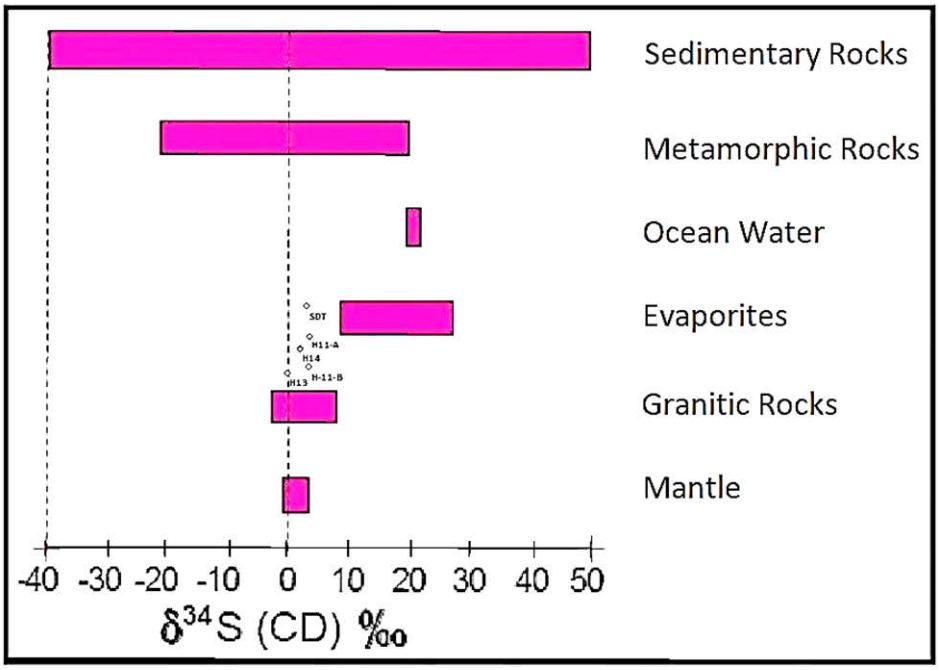

Fig. 2. The Locations of the Sulfur Samples in The Hoefs (1987) Diagram.

Lead isotope measurements were carried out on Galena specimen which is selected from Arapdede and Hayriye mineralizations. The Pb^{208} / Pb^{204} values ranged from 38.2 to 40.1, the Pb^{207}/ Pb^{204} values ranged from 15.5 to 16.01 and the Pb^{206} / Pb^{204} values ranged from 18.66 to 19.19 (Fig.3). Lead isotope values of mineralization around Hayriye and Arapdede are far away from the lower crust, but fall into the upper crust-areas suggesting that the lead forming the mineralization comes from the Upper Crust.

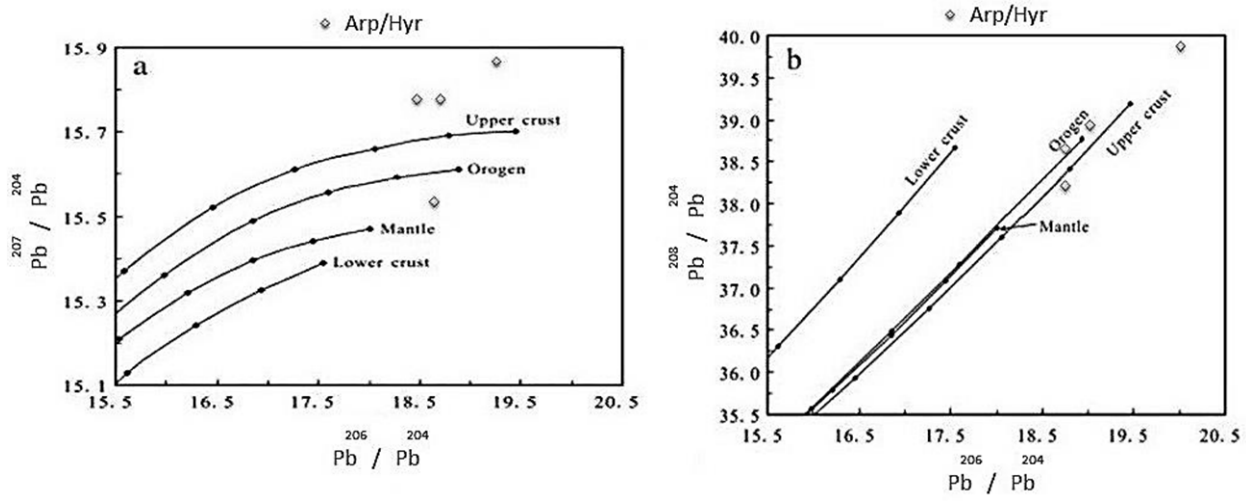

Fig. 3. a) Pb^{207}/Pb^{204} versus $Pb^{206}/Pb204$ b) Pb^{208}/Pb^{204} versus Pb^{206}/Pb^{204}. Figure Giving the Origin Areas for Pb Isotope Data According to Doe&Zartman (1981).

Fluid Inclusion Investigations

According to 32 measured values taken from Hayriye region, the homogenization temperature of inclusions is between 210-350^{0}C. Condensation is observed especially at temperatures between 220-290^{0}C. The salinity of the two-phase (liquid+gas) inclusions varies between 1.6% and 3.4% NaCl equivalents (Fig.4). Accordingly, the system is considered to have medium/high temperature and low/medium salinity values in the NaCl-H2O systems. According to the 23 measurements made in the sample taken from Sarıcayıryayla mineralization, the homogenization temperature of the inclusions varies between 290-390^{0}C. Condensation is observed especially at temperatures between 290 and 350^{0}C. The salinity of the two-phase (liquid+gas) inclusions varies between 5.4% and 13.9% NaCl equivalents. Fluid inclusion studies were carried out in translucent and semi-transparent quartz minerals in the Arapdede region (Fig.4). According to the 15 measured values, the homogenization temperature of the inclusions is between 220-330^{0}C. When the histogram is evaluated above, it is seen that the homogenization temperatures are concentrated especially at temperatures between 260-330^{0}C. Results obtained from multi-phase (liquid + gas + solid 1 + solid 2) inclusions, the salinity of the melt forming the inclusions ranged from 3.20% to 3.90% NaCl equivalent.

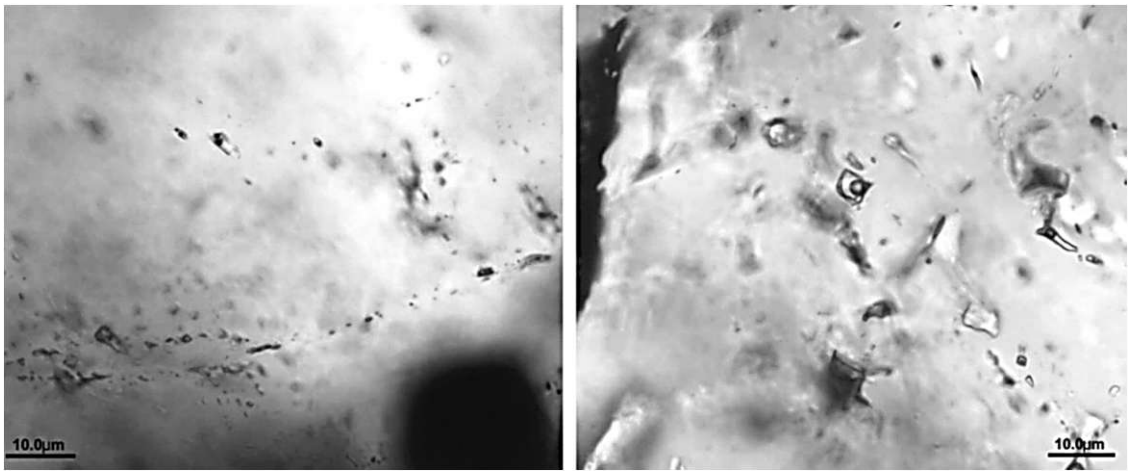

Fig. 4. Primary Inclusions Observed in Quartz Crystals (Left Side Arapdede-Right Side Hayriye).

Conclusion

Sarıcayıryayla Region: granite, granite porphyry, granite, granite porphyry and granodiorite zones were determined from the surface to the deep in drillings. The main components of the granites are quartz and orthoclase. Mineralogical compositions of granitic porphyries consist of quartz, orthoclase, plagioclase. As a result of petrography and, mineralogical studies, it was concluded that this region represent the the potassic zone.

Hayriye Region: It is determined as the result of the field survey the marble, granodiorite, calc-schist, quartz-schist rocks accompanying mineralization. Pyrite, chalcopyrite, galena, sphalerite, bornite minerals were determined in Hayriye village mineralization.

Saadet Region: As a result of field investigations, it was determined that the rocks accompanying mineralization are mostly quartz and epidote.

Arapdede Region: wall rock rich in actinolith-tremolite minerals, especially in the contact with granitic body. Galena, sphalerite, pyrite and chalcopyrite minerals were identified in the Arapdede mineralization.

All the features obtained from field observations, geochemistry and fluid inclusion studies, the genesis of the ore fluid is likely to occur in the hydrothermal and polymetallic intermediate epithermal vein type mineralization. It is also possible to say that hydrothermal activity is syngenetic with orogeny.

References

Hoefs J. Stable Isotope Geochemistry. Springer Verlag, Berlin.1987. p 241.

Ohmoto H., and Rye R.O. Isotopes of Sulphur and Carbon, Geochemistry of Hydrothermal Ore Deposits, New York, Wiley-İntersci., (1979). Pp 509-567.

Zartman R. E. e Doe, B.R. Plumbotectonics - The Model. Tectonophysics. 1981. 75: 135-162.

FRACTIONATION OF COHERENT ELEMENTS (ZR AND HF) DURING THE PROFOUND DIFFERENTIATION OF PERALKALINE MAGMATIC SYSTEMS: A CASE STUDY OF THE LOVOZERO COMPLEX

Kogarko L.N.

GEOKHI RAS, Kogarko@geokhi.ru

Coherent elements of such pairs as Zr–Hf, Nb–Ta, and of REEs group usually behave analogously in magmatic and some other natural processes. The fractionation of elements in these pairs provides insight into extremal physicochemical conditions under which these elements can be fracionated from each other, and hence, data on the fractionation of such analogously behaving elements are of paramount importance for evaluating such parameters of natural processes as oxygen fugacity, crystallization of mineral phases characterized by different distribution coefficients of coherent elements because of differences in the structures of these minerals, pressure, temperature, etc.

Zirconium and hafnium are industrially valuable metals, whose closely similar crystal chemical characteristics (such as ionic radii and charges) make them elements analogues.

All magmatic deposits of Zr and Hf are genetically related to alkaline magmatism. Being typical lithophile elements, zirconium and hafnium are accumulated late in the course of the magmatic process when alkaline rocks are produced. Among all varieties of alkaline rocks, the association of agpaitic nepheline syenites is characterized by the most significant enrichment of these elements: as much as a few percent in eudialyte lujavrite and eudialytite and as much as a few fractions of a percent for Hf in these rocks.

According to literature data, the Zr distribution coefficients between equilibrium melts and crystals of major rockforming minerals are relatively low but are still much higher for mafic minerals, such as micas, amphiboles, and pyroxenes, than for leucocratic minerals, such as feldspars and feldspathoids. The extent to which Zr can substitute other cations in rockforming minerals depends on their crystallization timing (crystallization temperature) and on the alkalinity of the mineral_forming medium (its Na_2O and K_2O concentrations). Hafnium concentrations in magmatic systems are more than one order of magnitude lower.

The chondritic Zr/Hf ratio is 37 (McDonough and Sun, 1995). In alkaline magmas, substitutions like Zr^{4+}+ Hf^{4+} ± Na^{+} + Fe^{3+} or 3M = 2 $2Na^{+}$ +Zr^{4++}+Hf^{4+} (where M = Ca^{2+}, Fe^{2+}, and/or Mg^{2+}) can likely occur. Alkaline pyroxenes and amphiboles in agpaitic nepheline syenites can contain more than 2 wt % ZrO_2 (its normal concentrations in alkaline calcalkaline rocks are no higher than a few tenths of a percent; Kogarko et al., 1988). The usual Hf concentrations are a few tenths of a percent.

Our research was centered on studying the distribution of Zr and Hf in nepheline syenites and their minerals in the Lovozero Massif in order to estimate the fractionation of these elements in the process of alkaline magma evolution.

Zirconium and hafnium were analyzed by ICP MS on a Finnigan Element, using the internationally certified BEN and IFG standards. Zirconium and hafnium concentrations in minerals were analyzed on a CAMECA 100 microprobe and by laser ablation in situ.

We studied the distribution of Zr and Hf in all types of rocks and ores of the Lovozero Massif and in the major rockforming, ore, and accessory minerals. We have analyzed 41 rock samples and seven mineral varieties.

The differentiation of the alkaline magma of the Lovozero intrusion (starting with phase I toward younger complexes) was associated with its enrichment in Zr (and, to a lesser extent, Hf), which reflects the earlier fractionation of leucocratic minerals (nepheline and potassic feldspar) than mafic minerals (pyroxene and amphibole) and eudialyte, the main concentrators of these elements. The

enrichment in the Zr + Hf pair in the latest products of the evolution of the Lovozero intrusion was mentioned in (Gerasimovskii et al., 1966), but we were the first to discover this trend for Hf individually. The highest Zr and Hf concentra tions were detected in the eudialyte ores: up to 6–8% for Zr and up to a few tenths of a percent for Hf.

To understand the behavior of elements in the process of magmatic differentiation, one should know the distribution coefficients of these elements in mineral–melt pairs. We have determined the Zr distribution coefficient for alkaline pyroxene of the Lovozero intrusion (Kogarko, 2015).

HAFNIUM DISTRIBUTION COEFFICIENT FOR PYROXENE IN PERALKALINE MAGMATIC SYSTEMS

As was mentioned above, the Lovozero agpaitic massif, a vast alkaline intrusion in the Kola Peninsula, contains hypabyssal nepheline syenites, which are thought to be the dike suite of the eudialyte lujavrite complex. The Hf distribution coefficients between equilibrium aegirine and alkaline melt were assumed to be equal to the ratio of the Hf concentration in the aegirine phenocrysts (which are not zoned) to the Hf concentration in the groundmass. The aegirine phenocryst and groundmass material were hand_picked, the groundmass was then homogenized via grinding and pulverizing for a long time, and 50mg portions of the material were loaded into Pt ampoules (which were then welded) and fused at a temperature of 1250°C and then quenched. The glass thus obtained was tested for homogeneity.

The procedures used to determine the Hf distribution coefficient of pyroxene were described in several publications (Marks et al., 2004; Lemerchand, 1987; Green et al., 2000), but none of these publications reports Hf distribution coefficients for aegirine in equilibrium with agpaitic nepheline syenite, such as in the Lovozero Massif. The data in (Marks et al., 2004; Lemarchand, 1987) for the compositionally closely similar Ilimaussaq Massif pertain to equilibrium of low Fe pyroxene with Ilimaussaq augite syenite, whose composition is very significantly different from that of the alkaline melts of the Lovozero porphyritic lujavrite.

Our Zr and Hf distribution coefficients obtained for aegirine in the porphyritic lujavrite are 0.40 for Zr and 0.58 for Hf (Kogarko, 2015). Comparison of these values with data on the Zr and Hf distribution in basalts shows that in alkaline magmatic systems, these elements are somewhat more significantly enriched in pyroxene. The Zr and Hf distribution coefficients of aegirine from the Lovozero Massif are remarkably higher that these values of pyroxene in basalt (**Green et al., 2000**).

Nevertheless, it is worth mentioning that in all publications devoted to Zr and Hf distribution in pyroxenes, the Hf distribution coefficient is always lower than that of Zr. Our data also demonstrate that pyroxenes in the Lovozero intrusion are richer in Hf than Zr. With regard for the high Zr and Hf distribution coefficients of aegirine and the leading role of pyroxenes in the process of crystallization differentiation of the Lovozero intrusion (whose rocks contain 35–45% pyroxenes), it is reasonable to believe that approximately 25% Zr and Hf of the whole magmatic system should be contained in pyroxenes. This implies that pyroxenes should have played an important part in Zr and Hf distribution during the evolution of peralkaline magmas.

ZIRCONIUM AND HAFNIUM FRACTIONATION DURING THE EVOLUTION OF THE PERALKALINE MAGMATIC SYSTEM OF THE LOVOZERO INTRUSION

In spite of their similar chemical properties, Zr and Hf can be separated in certain natural processes. The chondritic Zr/Hf ratio is 37 (McDonough and Sun, 1995). In tholeiitic MORB, whose origin is related to the partial melting of upper mantle material, Zr and Hf are not fractionated and the Zr/Hf ratio is close to 37.

In basalts generated in relation to plumes, basalts of ocean islands (OIB), the Zr/Hf ratio varies within very broad limits reportedly not only because of crystallization differentiation and/or fractional melting of the mantle source but also because of mantle metasomatism (Pfander et al., 2007; David and Schiano, 2000). It was proved that phoscorites, the oldest components of carbonatite complexes, posses elevated Zr/Hf ratios as high as 60 (Chakhmouradian, 2006). Carbonatite melts are active agent of mantle metasomatism, and Zr and Hf are fractionated in the metasomatized source material in the course of this processes, and its Zr/Hf ratio increases.

In this context, it is pertinent to mention that primary magmas (melilite nephelinites) in polar Siberia and the Kola Peninsula posses elevated Zr/Hf ratios up to 80. The evolution of the Lovozero magmatic system was accompanied by the fractionation of Zr and Hf.

The Zr/Hf ratio of the phase I rocks is 38, and that ratio reaches 44 in the differentiated complex, 51 in the Eudialyte Complex, and 53 in the porphyritic lamprophyllite–murmanite lujavrite. Our ICP MS data on Zr and Hf distribution in minerals of the Lovozero Massif (Table 2) show that the alkaline pyroxene has the lowest Zr/Hf ratio of 28 among those of the minerals with elevated Zr and Hf concentrations. The Zr/Hf ratio of the amphibole and eudialyte is slightly higher: 33 and 40, respectively. This ratio of the titanite, whose Zr concentration is a few tenths of a percent, is relatively low: 29. The Zr/Hf ratio of the accessory loparite and lamprophyllite, which contain very little Zr and Hf, is very low: 29 and 27. An unexpectedly very high Zr/Hf ratio up to 77 was detected in minerals of the mosandrite group. Minerals of this group are fairly rare in rocks of the Lovozero Massif and likely did not play any appreciably role in Zr and Hf fractionation.

The major Zr and Hf concentrators in rocks of the Lovozero Massif are eudialyte and alkaline pyroxene.

The fractionation of pyroxene, which has a higher Hf distribution coefficient compared to zircon and, hence, is characterized by a lower Zr/Hf ratio, should inevitably lead an increase in this ratio of the later differentiation products. This is reflected in an increase in the Zr/Hf ratio from intrusive rocks of phase I to the differentiated and eudialyte complexes of the Lovozero Massif. Zirconium and hafnium fractionation in the course of crystallization differentiation of the Lovozero perlakaline magmatic system was evaluated by the equation of equilibrium and fractional crystallization (Shaw, 1953; Ryabchikov, 1965). The results of these calculations show that the fractionation of approximately 95% magmatic sediment containing 40% alkaline pyroxene from parental magma whose composition corresponds to that of the first intrusive phase should result in a ZrO2 concentration close to 1.5% in the final differentiation product, which is consistent with the data in (Gerasimovskii et al., 1966), and a Zr/Hf ratio of 48, which is slightly lower than the value we determined in the lujav rite (51). The difference can likely be explained by the fractionation of amphibole, which also (similar to alkaline pyroxene) has a relatively low Zr/Hf ratio of 33.

We have previously demonstrated that the evolution of peralkaline magmatic system of Lovozero Complex was controlled by crystallization differentiation coupled with magmatic layering at stationary convection (Kogarko, 1976; Kogarko and Khapaev, 1987; Kogarko et al., 2006). Hence, the main process responsible for Zr and Hf fractionation was fractional crystallization differentiation with the crystallization of pyroxene (and amphibole), which has a higher Hf distribution coefficient than that of Zr. The accumulation of Hf during the evolution of alkaline magma was also controlled by the earlier crystallization of leucocratic minerals, which posses lower distribution coefficients of both Zr and Hf.

References

Chakhmouradian A.R. High-field-strength elements in carbonatitic rocks: Geochemistry, crystal chemistry and significance for constraining the sources of carbonatites// Chem. Geol. 2006. Vol. 235 pp. 138–160.

David K., Schiano P., Alle`gre C.J. Assessment of the Zr/Hf fractionation in oceanic basalts and continental materials during petrogenetic processes. Earth Planet, Sci. Lett. 2000. Vol. 178 Iss. 3–4 pp. 285–301.

Gerasimovskii V.I., Volkov V.P., Kogarko L.N., Polyakov A.I., Saprykina T.V., and Balashov Yu.A., Geochemistry of the Lovozero Alkaline Massif (Nauka, Moscow, 1966) [in Russian].

Green T.H., Blundy J.D., Adam J., and Yaxley G.M. SIMS determination of trace element partition coefficients between garnet, clinopyroxene and hydrous basaltic liquids at 2–7.5 GPa and 1080–1200°C// Lithos. 2000. Vol. 53 pp. 165–187.

Kogarko L.N. and Khapaev V.V. The modelling of formation of apatite deposits of the Khibina Massif (Kola Peninsula)// in Origins of Igneous Layering, Ed. by I. Parsons (D. Reidel, Dordrecht. 1987. pp. 589–611.

Kogarko L.N. Fractionation of zirconium in pyroxenes of alkaline magmas// Geochem. Int. 2015. Vol. 53 Iss. 1 pp. 1–8.

Kogarko L.N., Lazukina L.N., and Krigman L.D., Conditions of Zirconium Accumulation in Magmatic Processes (Nauka, Moscow, 1988) [in Russian].

Kogarko L.N., Williams C.T., and. Woolley A.R, “Compositional evolution and cryptic variation in pyroxenes of the peralkaline Lovozero intrusion, Kola Peninsula, Russia// Mineral. Mag. 2006. Vol. 70 Iss. 4 pp. 347–359.
Lemarchand F., Villemant B., and Calas G. Trace element distribution coefficients in alkaline series// Geochim. Cosmochim. Acta. 1987. Vol. 51 pp. 1071–1081.
Marks M., Halama R., Wenzel T., and Markl G. Trace element variations in clinopyroxene and amphibole from alkaline to peralkaline syenites and granites: implications for mineral–melt traceelement partitioning// Chem. Geol. 2004. Vol. 211 pp. 185–215.
McDonough W. F. and Sun S.-S. The composition of the Earth// Chem. Geol. 1995. Vol. 120 pp. 223–253.
Pfänder J.A., Münker C., Stracke A., and Mezger K. Nb/Ta and Zr/Hf in ocean island basalts—implications for crust–mantle differentiation and the fate of niobium// Earth Planet. Sci. Lett. 2007. Vol. 254 pp. 158–172.
Ryabchikov I.D. Thermodynamic Analysis of the Behavior of Minor Elements during Crystallization of Silicate Melts (Nauka, Moscow, 1965) [in Russian].
Shaw D.M., “The camouflage principal and trace element distribution in magmatic minerals// J. Geol. 1953. Vol. 61 Iss. 2 pp. 142–151.

GEOCHEMICAL FEATURES OF CAPE VERDE ARCHIPELAGO PRIMARY MELTS

Kogarko L.N., Migdisova N.A.
Vernadsky Institute of Geochemistry and Analytical Chemistry of Russian Academy of Sciences, 19, Kosygin str., Moscow, Russia, 119991. nat-mig@yandex.ru.

New data obtained on the content of rare and lithophilic elements in the primary magmas of the Cape Verde Islands significantly expand the already existing database. Especial importance to our study gives the fact that it was carried by modern research methods on contemporary equipment that allows measurements on a qualitatively and quantitatively new level.

Distribution of rare earth elements (Fig. 1) in primary magmas of Cape Verde Islands is typical for alkaline rocks with a predominance of light rare earth elements (LREE) over heavy rare earth elements (HREE).

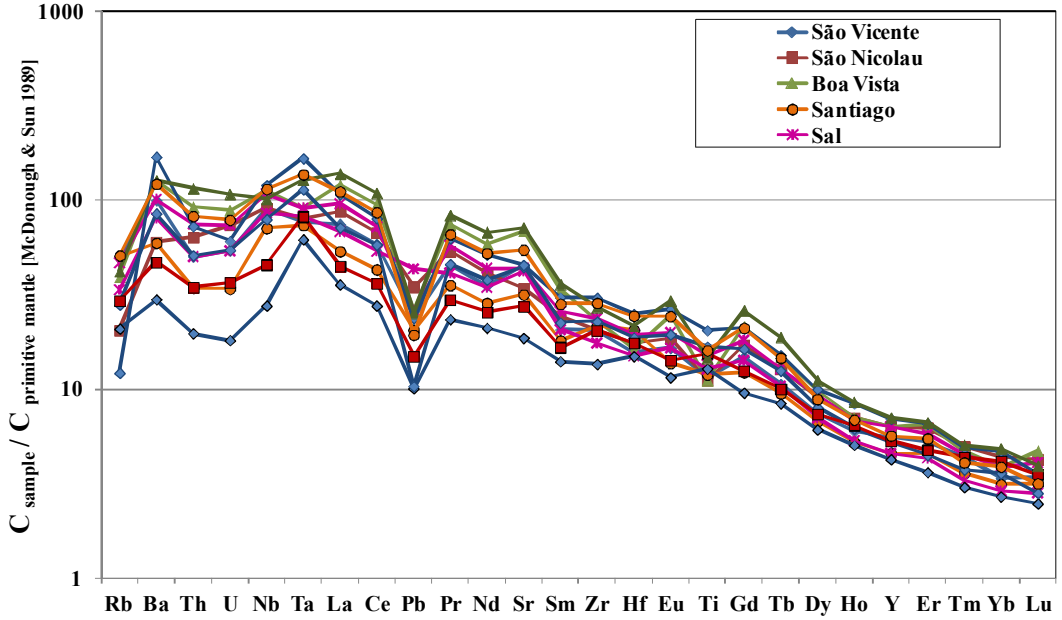

Figure 1. Distribution of rare elements in the rocks of individual Cape Verde islands: Sao Vicente, Sao Nicolau, Boa Vista, Santiago and Sal

The overwhelming number of primitive melts of the Cape Verde Archipelago is characterized by the maximum on Ti, Nb, Ta, Ba, La, U and the minima of K, Th, Zr, Sr, Yb. We note a general decrease in the concentrations of incompatible elements from left to right of the spectra. The fractionation type of rare elements normalized to the composition of the primitive mantle by (Sun and McDonough, 1989) demonstrates the similarity of primary magmas erupted on individual Cape Verde Islands of different ages. Despite of this prominent affinity in the distribution spectrums of rare elements of high magnesium melts on different Cape Verde Islands, certain differences in their characteristics are revealed as well. The diversity in incoherent elements spectra of distinct islands indicates the non- homogenous nature of their sources. The most recent eruptions were on the islands of Santiago and San Vicente. We can remark that the degree of rare elements increment in such young melts decrease. The last observation correlates with the previous studies supposing the depletion of alkaline-gabbroid magmas by rare elements, whereas to alkaline basalts is typical the significant enrichment in incompatible rare elements (Mazarovich et al., 1990).

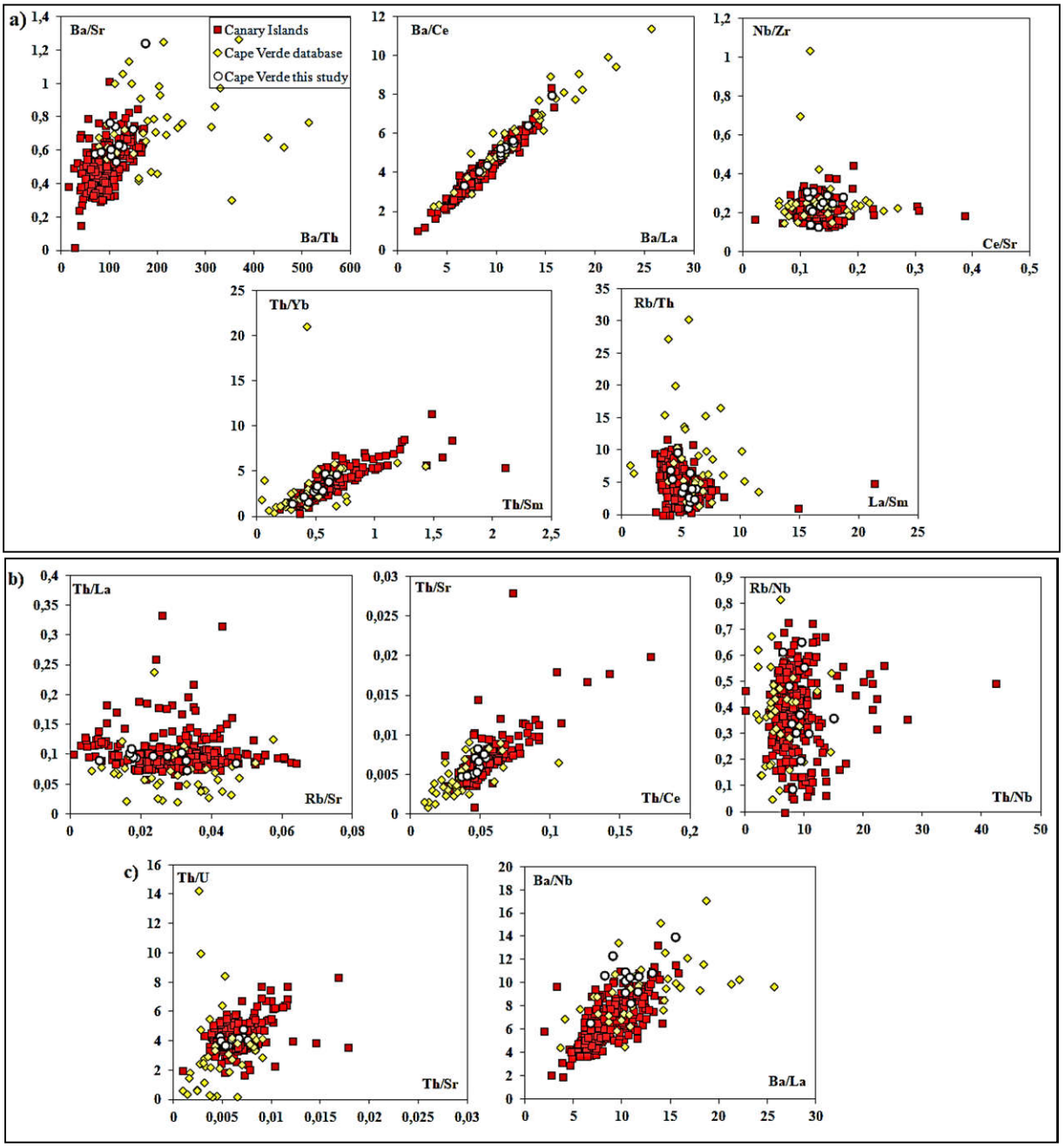

Fig. 2. Variations of incoherent elements in primary magmas of Cape Verde Islands in comparison with characteristics of Canary Archipelago primary magmas.

The first group is the most numerous, such feature indicates the enrichment of the mantle substrate of the Cape Verde Islands with incompatible elements. The Ba/Th ratio in the primary magmas of Cape Verde Islands (except undifferentiated magmas of the Sal island) is markedly higher than those for the chondrites and the Canary Archipelago. The ratio varies in a wide range – from 60 in the primary melts of the island of Sal to 250 in the Santiago magmas. The Ba/La and Ba/Ce ratios are generally close to those in the Canary Archipelago, although there is also an area of elevated values of these parameters. The Ba/Sr characteristic ratio does not fluctuate much. Compared to the chondrite value the ratios of Th/Sm and Th/Yb are very high. Although they are much lower in Cape Verde Island rocks in comparison with the primary magmas of the Canary Archipelago reflecting the Cape Verde flatter spectrum of HREE (Fig. 3). The Nb/Zr ratio is quite constant in all high-magnesium magmas of the Cape Verde Islands and it is similar to one in the primary magmas of the Canary Islands. The ratio of Rb/Th in the primary magmas of the Cape Verde Islands is very high in comparison with Canary Islands. The ratio of Ce/Sr ranges from 0.008 to 0.28 likewise this parameter does in the rocks of the Canary Islands.

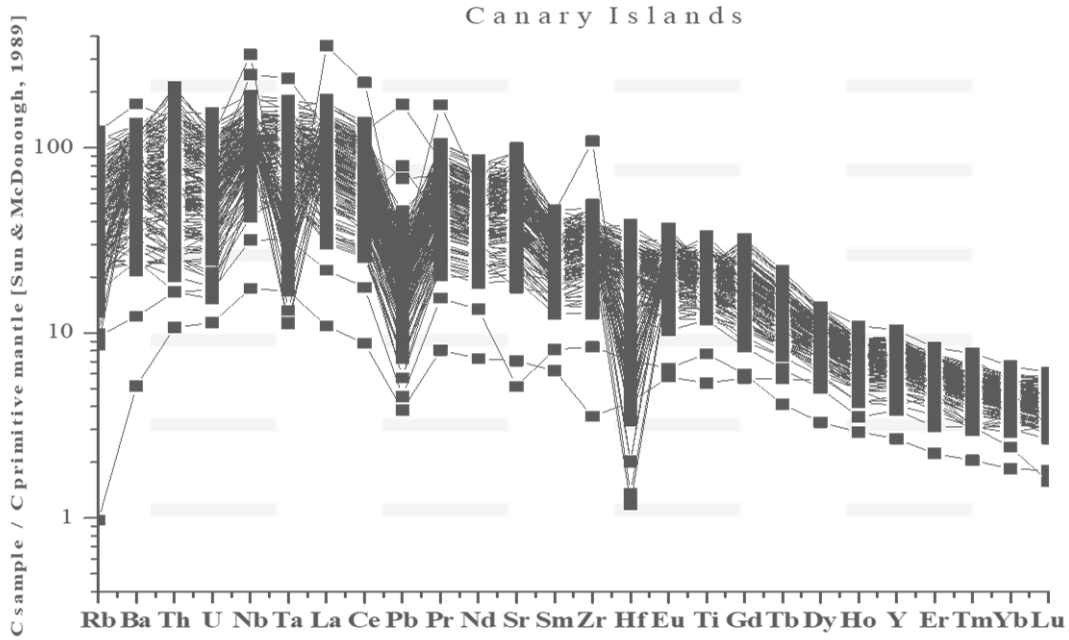

Fig. 3. The distribution of rare incompatible elements in Canary Archipelago rocks (petdb).

The ratio of Th/Ce, Th/La in the primary magmas of the Cape Verde Islands is almost two times lower than established for chondrite and significantly lower than that of the primary magmas of the Canary Islands, due to the strong LREE enrichment of OIB alkaline magmas. Th and La have direct correlations in the primary magmas of most of the distinct Cape Verde islands. The ratio of Rb / Sr is almost an order of magnitude lower in comparison with chondrites, somewhat lower than the Canary rocks. The Rb/Nb ratio varies from 0.1 to 0.9, and is similar to those for primary magmas of the Canary Islands. The Th/Nb ratio varies from 3 to 15 and is close to the Canary Islands. The fluctuations of this value in the rocks of the Cape Verde possible reflect the heterogeneity of the mantle source. The Ba/La and Ba/Nb ratios vary in a wide range: 3-4 times in the rocks of a Cape Verde and 5-6 times in the Canary Islands rocks. The Th/Sr ratio is similar in the rocks of two archipelagos and varies between 0 and 0.01. The Th/U ratio varies in both archipelagos within the same interval – from 2 to 8, but the group of compositions with higher values of this parameter in the Canary archipelago is higher.

The geochemical study of the alkaline magmatism of the Cape Verde Archipelago revealed a significant enrichment of LREE, Ti, Ba, Nb. Such geochemical characteristics are typical for the alkaline rocks of continental rifts.

This work was supported by Program of Presidium RAS №0137-2015-0087.

References

Мазарович А.О., Фрих-Хар Д.И., Когарко Л.Н., Копорулин В.И., Рихтер А.В., Ахметьев М.А., Золотарев Б.П. Тектоника и магматизм островов Зеленого Мыса. (Тр. ГИН; Вып. 451). - М.: Наука, 1990. - 246с. - ISBN 5-02-002090-7.

Sun S.-S., McDonough W.F. Chemical and isotopic systematics of oceanic basalts: implications for mantle composition and processes. // Magmatism in the ocean basins. Eds.Suanders A.D., Norry M.J., Geol.Soc.Spec.Publ., 42, pp.313-345, 1989.

Thompson RN. Magmatism of the British Tertiary Volcanic Province. Scott J Geol, 18, p.50–107, 1982.

GEODYNAMIC CONDITIONS, MAGMATISM AND COMPOSITION OF ORES OF GOLD DEPOSITS IN UZBEKISTAN (WESTERN TIEN SHAN)

Koneev R.I.[1], Seltmann R.[2], Khalmatov R.A.[3]

[1]National University of Uzbekistan, Tashkent. ri.koneev@gmail.com

[2]CERCAMS, Natural History Museum, London, r.seltmann@nhm.ac.uk.

[3]Educational and Experimental Center for High Technologies, Tashkent. r.khalmatov@yahoo.com

According to up-to-date conceptions (A.S.Yakubchuk, R.Seltmann, R.Goldfarb, etc.), industrial gold mineralization in Uzbekistan is located within the South Tien Shan orogenic belt and the Beltau-Kuramin volcanic-plutonic arc, which were formed as a result of the subduction of the crust of the Turkestan paleocene under the Kazakhstan continent , its collision with the Karakum Continent and subsequent post-collisional processes. The deposits are grouped into three ore regions: Kyzylkum, Nurata and Kuramin, which were formed as a result of intersection of the belts with hidden, transformational, deep faults (Fig.).

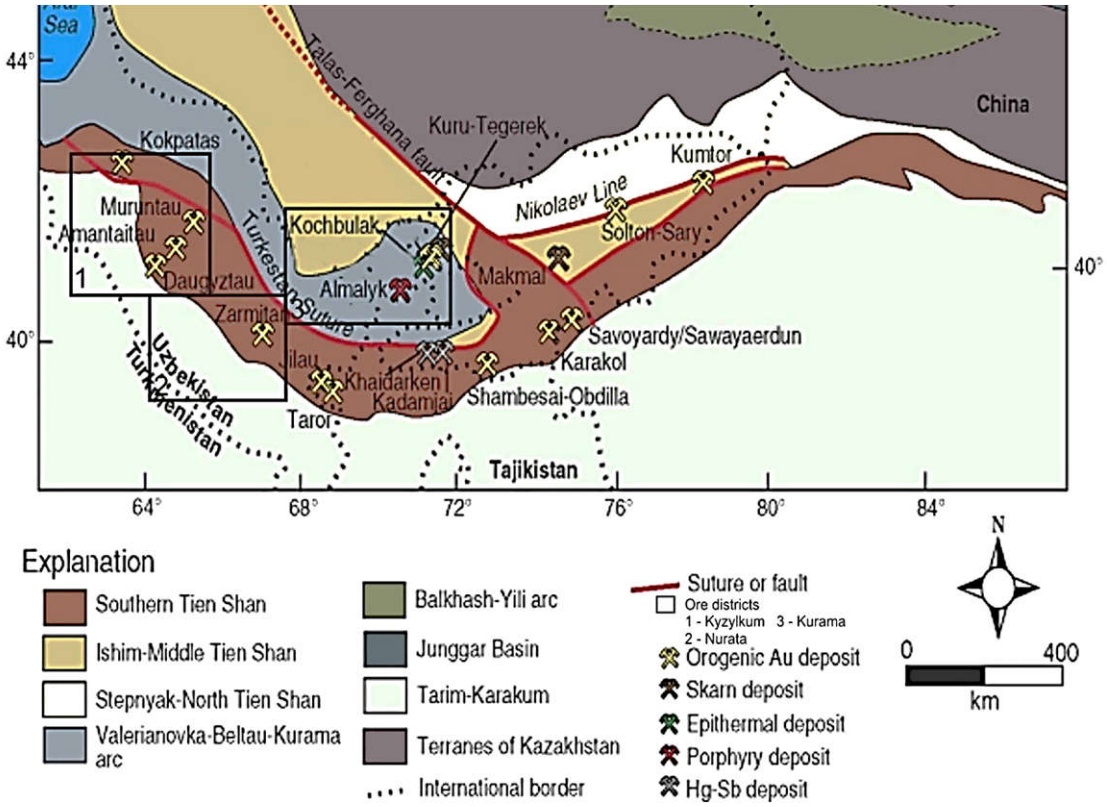

Fig. 1 The position of gold deposits in geodynamic structures of the Tien Shan (Goldfarb et all., 2013).

As a result, orogenic deposits of gold were formed in the South Tien Shan belt, and in the Beltau-Kurama Au-Cu (Mo) porphyry and epithermal deposits.

The different nature of the geodynamic and ore-forming processes occurring in the two belts is confirmed by the results of determining the absolute age of the U-Pb by the zircon method of 40 intrusive massifs in Uzbekistan (Dolgopolova et all, 2016). It was revealed that magmatism of two tectonic stages is manifested in the territory of Uzbekistan: Hercynian and Caledonian. Hercynian ages are divided into two intervals: 270-290 million years and 300-320 million years. The first interval corresponds to the post-collisional magmatism of the South Tien Shan orogenic belt, the second refers to the subduction period and developed in the Beltau-Kuramin volcanic-plutonic arc. The study of the most common, early sulfides (arsenopyrite, pyrite, molybdenite) Re-Os method showed that the age of gold mineralization corresponds to the age of Hercynian granitoid magmatism, but for supersubduction deposits of the volcanic-plutonic arc - Kochbulak, Kyzylalmasay, Kalmakyr, it refers to the upper-Carboniferous period (296-316 million years), for the orogenic deposits Muruntau, Myutenbay, Zarmitan – to the Lower Permian period (286-288 million years).

Table.1 The main types of gold mineralization in the fields of Uzbekistan.

Type, impurity elements	**Mineral association**	**Gold compounds**	**Micro- nanoensemble**	**Example of deposits**
Au-Hg As, Sb, Se, Tl	Mercurial: cinnabar, realgar,	Amalgam Au, Au_2Ag, AuAg	Kongsbergite, schwatzite, tiemannite, crookesite	Karasu Jasaul Akchisay
Au-Sb Pb, Cu, Ag, Se, Hg	Antimony-sulfoantimony: antimony, pyrite, tetrahedrite	Aurostibite ($AuSb_2$) Au_4Ag, Au_3Ag	Jamesonite, bournonite, boulangerite, miargyrite, andorite	Amantaytau Daugyztau Guzhumsay Zarmitan
Au-Ag-Se Sb, Cu, Te, Hg	Sulfosal-selenide: pyrite, galena, freibergite, akantite	Petrovskaite (AuAgS) Fishesserit ($AgAuSe_2$), AuAg	Pyrargyrite, polybasite, stephanite, naumannite, aguilarite, cervellite	Kosmanachi Visokovol'tnoe Adzhibugut Kyzylalmasay Chadak
Au-Ag-Te Sb, Cu, Pb, Bi, Se, Hg	Silver-telluride: pyrite, galena, chalcopyrite, tetrahedrite	Calaverite ($AuTe_2$) Petzite (Au_3AgTe_2), Au_8Ag, Au_2Ag	Hessite, altaite, tellurantimony, coloradoite, tetradymite, junoite, chatkalite	Amantaytau Visokovol'tnoe Kochbulak Kayragach Samarchuk
Au-As Co, Ni	Pyrite-arsenopyrite: As-pyrite, arsenopyrite	FeAuAsS, $FeAuS_2$	Cobaltite, gersdorffite, loellingite, pentlandite, violarite	Muruntau Zarmitan Kyzylalmasay Kochbulak
Au-Bi-Te Se, Sb, Zn	Bismuth-telluride: Arsenopyrite, pyrite, bismuthinite, sphalerite	Maldonite (Au_2Bi), Au_8Ag, Au_4Ag, Au_3Ag	Pilsenite, hedleyite, tsumoite, joseite, kobellite, gustavite, Te-canfieldite	Muruntau, Myutenbay, Zarmitan, Urtalik
Au-W Mo, REE	Rare-metal: scheelite, molybdenite	Dispersed	Wolframite, tungtenite	Muruntau Zarmitan

The deposits of the Kyzylkum and Nurata regions belong to the hypo- mesothermal, Kurama to meso-epithermal. They are located in rocks of different composition - black shales, sedimentary-volcanogenic rocks, granosyenites, andesidzacite volcanics, granites, carbonate rocks. All rocks are changed as a result of metasomatic processes to create a favorable environment for the deposition of gold mineralization, leveling the diverse composition of the enclosing rocks.

Ore formation is in principle a standard physicochemical process that leads to the formation of regular, zonal series of mineral-geochemical types in all gold deposits, regardless of the composition of the host rocks (from the bottom up): /Au-W/Au-Te-Bi/Au-As/Au-Te-Ag/Au-Ag-Se/Au-Sb/Au-Hg/

(Koneev et al., 2010). Each type is characterized by its own formation conditions, mineral associations, gold compounds and regular micro-nanoassembles (table).

In the orogenic deposits of the Kyzylkum and Nurata districts, all types of ores are shown, in the epithermal Kuramin region only Au-As, Au-Ag-Te and Au-Ag-Se. Depending on the conditions for the formation of deposits and their erosion cut in ore can be combined and determine the industrial resource of a different number of types. For example, in Muruntau - Au-W, Au-As, Au-Te-Bi; Charmatine Au-W, Au-As, Au-Te-Bi, Au-Sb; Kyzylalmasay - Au-As, Au-Ag-Se; Kochbulak - Au-As, Au-Ag-Te.

We note the constant presence of Au-As, pyrite-arsenopyrite type on all deposits, which determines the main volume of quartz-sulfide ore bodies and the main resource of early, scattered, invisible gold.

The convergence in time with granitoid magmatism, the confinement to the nodes of the intersection of deep structures, the constancy of the standard series of mineral-geochemical types irrespective of the host rocks, the contrast composition of each type, the regular, zonal nature of their deposits allows to suggest the genetic relationship of gold mineralization with granitoid magmatism and transform faults. The source of gold and associated ore elements, apparently, were mantle plumes. The average content of elements in stone chondrites, taken as the standard of the upper mantle, is ten times higher than their clark in the earth's crust (g/t): Au 0.17 (0.0043), Te 0.5 (0.001), Se - 10 (0.05), Hg-3 (0.083), Ni-1% (58 g/t).

The research was carried out with the support of the grant of the Ministry of Innovative Development of the Republic of Uzbekistan OT-F8-01.

References

Dolgopolova A., Seltmann R., Konopelko D. & Koneev R., Divaev F. Geodynamic evolution of the western Tien Shan, Uzbekistan: Insights from U-Pb SHRIMP geochronology and Sr-Nd-Pb-Hf isotope mapping of granitoids // Gondwana Research, 2016. P. 1-34. http://dx.doi.org/10.1016/j.gr.2016.10.022

Goldfarb R., Taylor R, Gregory S. Collins et. al. Phanerozoic continental growth and gold metallogeny of Asia // Gondwana Research, 2013. P. 1-55. http://dx.doi.org/10.1016/j.gr.2013.03.002

Koneev R., Khalmatov R. and Mun Yu. Nanomineralogy and nanogeochemistry of ores from gold deposits of Uzbekistan // Geology of ore deposits, Vol. 52, No 8, 2010, pp.755-766.

NEW DATA ABOUT BRECCIA WITH QUARTZ - POTASSIUM FELDSPAR - PORPHYRY CEMENT ASSOCIATED WITH RAPAKIVI-GRANITE, SALMI BATOLITH, SOUTH KARELIA

***Konyshev A.A.*[1,2], *Rusak A.A.*[1], *Alferyeva Ya.O.*[3], *Kovalchuk E.V.*[4]**

[1]*GEOKHI RAS*

[2]*IEM RAS*

[3]*MSU*

[4]*IGEM RAS*

This work contains new data about sub-effusive magmatic breccias with quartz-potassium feldspar-porphyry cement of rhyolite-trachyriolite composition. These breccias are associated with biotite-hornblende granites (rapakivi), probably, form the feeding channel of an effusive center confined to the Salmi Batholith.

At the end of the Paleoproterozoic – the beginning of the Mesoproterozoic (1.8-1.5 Ga), wide effused intraplate felsic magmatism of increased alkalinity took place on Earth. These events occurred on the site of stabilized Early Paleoproterozoic orogens. Large non-metamorphosed intrusions of anorthosite-rapakivigranite complexes (ARGC) are associated with the belts of this magmatism. Biotite-hornblende granites (rapakivi) is the earliest felsic rocks included in the ARGK. These rocks

are rich in K, Fe, F, and oxygen fugacity during their formation was below the FMQ buffer. These granites have the largest area of distribution among the acid rocks of the ARGK. Effusive formations associated with rapakivi granite are known, but rare, often strongly altered, some of them are described in (Belyaev, 2013; Ehrlich et.al, 2013; Vorma, 1975; Kisvarsanyi, 1972).

The Salmi Batholith is a member of the ARGK, located in South Karelia on the eastern shore of the Ladoga lake at the junction of the Svekofen crust and the Karelian craton. In the southwestern extremity of the Lupikko gneiss-granite dome (AR_2-PR_1) some researchers noted quartz-porphyrites and magmatic breccia outcrops (Trustedt, 1907; Sviridenko, 1968; Belyaev, 1985), but according to the descriptions the rocks are brown, rich in K and heavily altered.

As a result of the field work carried out by the authors in 2017 in the area of the flooded "central pegmatite quarry" southward of the breakstone quarry "Mosavtodor") the outcrop of altered magmatic breccia was observed, which were identical to those previously described. In the dumps along the sides of the quarry breccia of the host rocks with gray quartz-potassium feldspar-porphyry cement were found.

Xenoliths in the breccia are represented by the coarse fragments of the rocks hosting the Salmi batholith: gneiss-granite domes, amphibolites and mica schists of the Ladoga series; as well as earlier amphibole-biotite granites with a typical texture of rapakivi (plagioclase ovoid around the gigantic granular crystals of potassium feldspar).

The breccia cement was separated from the xenoliths by a diamond circular saw, examined for petrochemical and trace element composition by the methods of XRF (IGEM RAS), ICP-MS and ICP-AES (IPTM RAS) (see Table 1, and Fig. 1) and also by the methods of optical microscopy and X-ray spectral microanalysis (IEM RAS).

Table 1. Petrochemical and trace element composition, sample 220617-1_2 (ground mass of breccia)

Component	Wt%	Element	ppm	Element	ppm	Element	ppm	Weight Ratio	
SiO_2	74,95	Li	19,5	Mo	5	Tb	2,9	Zr/Hf	33
TiO_2	0,197	Be	7,1	Pd	-	Dy	17,1	Nb/Ta	14
Al_2O_3	12,19	Sc	5	Ag	-	Ho	3,5	K/Rb	185
Fe_2O_3*	2,74	V	7,3	Cd	0,93	Er	9,5	La/Nb	2,8
MnO	0,028	Cr	9,7	In	-	Tm	1,4	La/Ta	39
MgO	0,3	Co	2,8	Sn	6	Yb	9,8	K/Ba	124
CaO	1,01	Ni	16	Sb	3,3	Lu	1,4	Y/Ho	28
Na_2O	2,6	Cu	38	Te	-	Hf	11,7	Sr/Eu	127
K_2O	5,13	Zn	194	Cs	3	Ta	3,5		
P_2O_5	0,022	Ga	26,1	Ba	343	W	2,5		
S_{tot}*	0,072	As	<0,1	La	136	Pt	-		
F	-	Se	-	Ce	277	Au	-		
Сумма	99,24	Rb	230	Pr	31,7	Tl	1,4		
ППП	0,72	Sr	77,8	Nd	111	Pb	55		
K/N*	1,3	Y	96,4	Sm	21,1	Bi	0,22		
A/CNK*	1,05	Zr	385	Eu	0,61	Th	21,5		
NK/A*	0,81	Nb	48,2	Gd	18,2	U	6,8		

The total content of iron and sulfur is given in the form Fe_2O_3 и S_{tot}; K/N, A/CNK, NK/A – molal ratios, K_2O/Na_2O, $Al_2O_3/(CaO+Na_2O+K_2O)$, $(Na_2O+K_2O)/Al_2O_3$.

The REE spectrum from breccia cement shows similarity with the spectrum of a typical representative of biotite hornblende granite-rapakivi (sample Ch-37/1). A more profound Eu minimum, a slight LREE depletion and HREE enrichment are observed. The gray cement of Breccia has cryptocrystalline ground, phenocryst secretions up to 5 mm. in the diameter: smoky quartz (di-pyramidal shape without the prism facets) and sanidine (Kfs 0,87, Ab 0,13) with the iridescence in the greyish-bluish tones. The phenocrysts of quartz and K-feldspar have "caverns" from the surface to deep into the grain, filled with a ground fine-crystalline mass. This can be evidence of either rapid dissolution of phenocrysts in the melt or rapid growth or dissolution with subsequent growth. Elongated inclusions of fine crystalline mass, completely overgrown with a host mineral, can speak in

favor of the last two assumptions. Also there is the large number of melt inclusions from the first microns in width up to 200 in these minerals. Inclusions in quartz are, as a rule, isometric and represented by negative forms of crystals (β-quartz). All inclusions are completely crystallized, no gas bubbles are found, but Mn-Fe-containing calcite and a fine grained impregnated fluorite are observed.

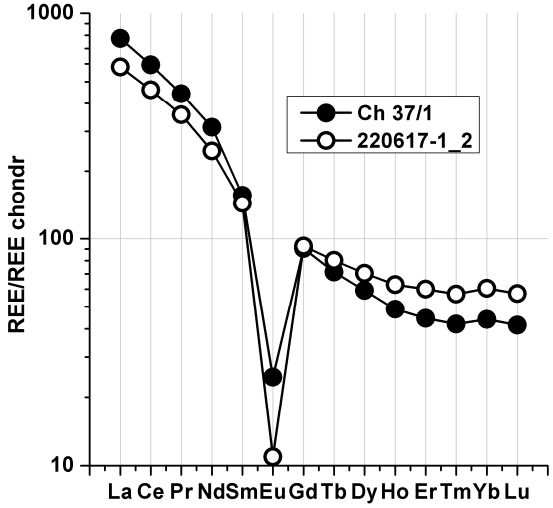

Fig. 1. REE spectra normalized to chondrites (Andres and Grevese, 1989) from rocks of the Salmi batholith.

Composition of the ground mass of breccia: potassium feldspar $Or_{0.978}$ $Ab_{0.022}$, albite $Ab_{0.92}$ $An_{0.08}$, apatite (3.5 wt% F), amphibole (0.34 wt% Cl), monazite, zircon, ilmenite (up to 0, 65 wt% Nb), rutile, fluorite, calcite (0.4-0.8 wt% Mn and 0.7 wt% Fe), REE fluorocarbonates, and a variety of S-mineralization: pyrite, sphalerite, chalcopyrite, galena.

Fine grained impregnated fluorite (1-2 microns), fieldspars, apatite identical to apatite of the ground mass, amphibole, REE fluorocarbonate, calcite (2.3 wt% Mn and 0.88 wt% Fe), galena, rutile, zircon are observed in the melt inclusions on the surface of a polished sample.

The melt inclusions are opened when heated at atmospheric pressure above the phase transition temperature in quartz inclusions. The study of inclusion homogenization at excess external pressure in a high-pressure vessel with internal heating "gas bomb" is being conducted now. At a temperature of 950 ° C and below homogenization does not occur.

Estimation of temperature formation of quartz and zircon.

Zircon, quartz phenocrysts and quartz in the ground mass were analyzed for Ti-content using the JEOL JXA-8200 electron probe microanalyzer (IGEM RAS). This allowed us to estimate the formation temperatures of minerals, according to (Watson et al., 2006; Wark & Watson, 2006).

Conditions of analyzing: accelerating voltage 20 kV, 300 nA, beam diameter 1 micron. The corrections were calculated using the ZAF correction method. For Ti (Kα, PETH): in zircon - the exposure time was 100 seconds at the peak and 50 seconds on the background; for quartz - 200 sec at the peak and 100 sec on the background. The detection limit was 0.003% by weight Ti (3σ).

Since ilmenite is widely distributed in the rock and rutile is also noted - in calculations it was assumed that $\alpha Ti = 1$.

Two types of zircons are distinguished: the first type has internal parts formed at lower temperatures than external: 720-870°C; the second type grew under isothermal conditions in the temperature ranges: 824-950°C.

Phenocrystals of quartz showed mixed values of formation temperatures from the center to the edges: colder in the inner part, equivalent center-periphery values, and lower boundary values. The average values of all zones are about 760°C with a spread of values from 726°C to 787°C. In the quartz of ground mass calculated temperatures are on average lower than in phenocrysts: 735°C with a spread of values from 620 to 792°C. But it should be taken into account that ground mass contains fine-grained Ti- mineralization, which can lead to the distortion of the result.

The error of determining the temperature according to the calculations does not exceed 10°C. Due to the small number of determinations of Ti content in quartz (20) and zircon (15) and a large spread of values, these data must be considered preliminary.

A calculated range of temperatures, in general, is higher than in the rhyoliths of the island of Hogland (Suursaari), associated with Wiborg batholith (Ehrlich et.al, 2013).

Discussion

The described breccias are localized in the frame of the Luppikko gneiss-granite dome and lie subparallel to its outer boundaries. Probably, the gneiss-granite dome was a rather monolithic microblock, significant part of the melt and fluids appeared at its junction with meta-sedimentary rocks. The layers of metacarbonates with skarns with ore mineralization are located on outer boundaries of the gneiss-granites domes at modern erosion surface. One of the problems of this region is the relationship between ore mineralization and the source of matter.

According to the data (Belyaev, 1985), xenoliths of skarns were found in quartz porphyrites. Sn-content in skarns xenoliths is up to 500-630 ppm, in xenoliths of amphibolites - up to 42 ppm Sn, but the amount of Sn in breccia ground mass remained low 3.5 -4 ppm. In the rocks considered by us the Sn content is slightly higher (6 ppm), but the difference is not significant. Breccia ground mass does not contain high concentrations of Cu, Zn, Pb, but their content is somewhat higher with comparison with the samples of another granitic rocks in our collection from this area. But in connection with low oxygen activity and presence of sulfur these elements are not a dissipate, form their own sulfide phases and can be easily mobilized as a result of postmagmatic activity.

Conclusion

According to the presented data - before the intrusion of quartz-potasium feldspar-porphyrites the melt was heated, probably due to the entry of more heated felsic magma from a deeper source.

The breccias associated with granite-rapakivi considered in this work can be a source of ore matter at postmagmatic stage of deposit forming. In this area the relationship between ore objects and the source of matter is not completely clear.

Such breccias and effusive formations associated with the ARGK haven't been studied thoroughly due to their relative rareness. The further study of this object can shed light on the physicochemical conditions of precambrian ARGK formation and associated ore mineralisation and deposites.

This work is supported by RFBR grant 18-05-01101.

References

Belyaev A.M. Petrology of volcanic rocks of rapakivi formation (Gogland island) // Regional geology and metallogeny, No 55, 2013. (in Russian)

Belyaev A.M. Distribution Regularities of ore elements in pegmatites, pegmatoid granites and gneiss-granite of the Northern Ladoga area. In the book. "Regularities of the concentration of ore elements in granitoid formations of the Karelo-Kola region", Apatity, 1985, p. 89-96. (in Russian)

Sviridenko L.P. Petrology of Salmi granite-rapakivi massive (Karelia) Petrozavodsk: Karelia pub., 1968, p. 116. (in Russian)

Andres E., Grevese N. Abundances of the elements: meteoritic and solar // Geochimica et Cosmochimica acta 1989 vol 53 pp. 197-214

Ehrlich K., Ver E., Kirs J., Soesoo A. Using a titanium-in-quartz geothermometer for crystallization temperature estimation of the Palaeoproterozoic Suursaari quartz porphyry // Estonian Journal of Earth Sciences, 2012, 61, 4, 195.204

Kisvarsanyi E.B. Petrochemistry of Precambrian igneous province, St. Francois Mountains, Missouri // Report of Investigations. N 51. Rolla, Missouri, USA, 1972. – 97 p.

Trüstedt, O., 1907. Die Erzlagerstätten von Pitkäranta amLadoga-See. Bulletin de la Commission Geologique de Finlande no 19. Frenckellska Tryckeri-Aktiebolaget, Helsingfors.

Vorma A. On two roof pendants in the Wiborg rapakivi massif, Southeastern Finland // Geological Survey of Finland Bull. 272, Geologinen tutkimuslaitos Espoo, 1975. – P. 2–46.

Wark, D.A. & Watson, E.B. 2006. TitaniQ: a titanium-inquartzgeothermometer. Contributions to Mineralogy and Petrology, 152, 743.754.

Watson E.B., Wark D.A., Thomas J.B. Crystallization thermometers for zircon and rutile // Contrib Mineral Petrol (2006) 151: 413–433.

RARE METAL DEPOSITS (W, MO, BE) OF CENTRAL KAZAKHSTAN AND THEIR CONNECTION WITH INTRUSIVE ROCK

Kopobayeva A.N.
Karaganda State Technical University (Karaganda, Kazakhstan), aiman_25.87@mail.ru

Kazakhstan's subsoil contains over half of the world's tungsten reserves, with the country ranked fourth globally and first among the countries of Asia in molybdenum reserves. Tungsten has the greatest industrial importance for the country from among other rare metals. The base reserves are centered in 6 large and unique deposits: Upper Kayrakty, Boguty, Karaoba, North Katpar, Koktenkol, Bayan, Aksoran, and a part of commercial ore is contained in deposits Nurataldy, Solnechnoye, Akmaya (Bekzhanov et al., 2006; Bekzhanov et al., 2006; Gubaidulin, 2008; Uzhkenov et al., 2011). With growing world consumption of tungsten, we witness growing interest to different genetic types of tungsten deposits, and first of all, to stockwork deposits. A specific feature of stockwork deposits in Kazakhstan is large scale of mineralization and, accordingly, significant reserves. Among the deposits, there are giant deposits with reserves exceeding hundreds of thousands tons (Gubaidulin, 2008, Lehmann et al., 1994). Over 87% of commercial tungsten reserves account for stockwork ores in such deposits as Upper Kayrakty, Koktenkol, Karaoba, North Katpar (Uzhkenov et al., 2011).

A characteristic feature of most rare metal deposits of Central Kazakhstan is their genetic and spatial connection with intrusives of the Akchatau complex (Shcherba 1960, Kudryashov 1964, Shatov et al., 2000).

A genetic feature of the deposits is connection with leucocratic granite intrusives. The most productive ones are the deposits formed in superintrusive zones of granite intrusions; the deeper the intrusion, the greater the vertical range of mineralization, from 200-300 m (Southern Zhaur) to 2000 m (Upper Kayrakty), and the greater the practical significance of the objects (Uzhkenov et al., 2011). These deposits, according to G.N. Shcherba (1960), are associated with apical or superintrusive zones of the Permian granite massifs of the Akchatau complex.

Until early seventies, all intrusives of ultra-acid granitoids fell into the Akchatau complex: sub-granite (East Kounrad, Zhamankarabas, etc.), leucogranite (Akchatau, Airtau, etc.), alaskite leucogranites (Bektauata, Karkaraly, etc.), alaskite and alkaline alaskites (Maytas, Mamyr, etc.). Serykh and others (1974) came to two conclusions. First, the previously distinguished Kaldyrminsky complex combines, on the one hand, granitoids, which in fact should fall within Topar complex (granodiorites, adamellites, granites), and on the other hand the Kaldyrminsky complex (leucocratic granites), which in no way differs from Akchatau complex, including in ore-bearing property, and logically should be combined with the latter. By tradition deeply rooted in the minds of geologists for decades, the terms "Akchatau" and "ore-bearing" have become synonymous. Without violating this tradition, we keep the name "Akchatau" for the new complex. Second, intrusives of alaskites and alaskite leucogranites (Karkaraly, Kent, Mamyr, etc.), which earlier in the northern part of the Tokrau region fell within Aktauau complex, correspond to the most acid, mostly ore-free, intrusives in the south of the zone. All of them characteristically exhibit specific tectonic position, age, composition, formation conditions, ore content, and other features, and should be classified as an independent Kyzylaray complex (Serykh et al., 1974).

In the last proposed version (Serykh, 2009) the "Akchatau" complex unites plutons of almost exclusively leucogranite composition (only 1 phase of single massifs Zhamankarabas, Zhamankoitas, Kyzylkaragan, Shaltas is composed of subnormal granites). In its distribution, intrusives of the complex are closely connected in the tectonomagnetic activation zones with the intrusives of Topar complex, mixing with them in single polychronous plutons, making up the Topar-Akchatau potassium-type granitoid series (Serykh, 2009). Just like the Topar intrusives, the "Akchatau" intrusives are most widely spread in Uspenskaya, Akbastau-Akzhal and East Zhamansarysu tectonomagnetic activation zones. Uspenskaya zone comprises the intrusives of Koktenkol, Kaldyrma, Karakoitas, Nurataldy, Berikty, Katpar, Zhamantas, Kotyrkyzyltau, Karatemir, Murzatay, Belkoytas and others; Akbastau-Akzhalzone comprises Kyzyltau, Airtau, Zhamankarabas; East Zhamansarysu zone includes Akchatau,

Batystau, Uzunbulak, Keregetas, Saran, etc. Ortau massif is located at the junction of Uspenskaya and Akbastau-Akzhal zones.

Geological studies in Central Kazakhstan, Northern Balkhash region in particular, found that industrial tungsten mineralization and associated molybdenum, bismuth and rare earth mineralization are genetically related to a specific type of intrusives: Late Carbonaceous – Early Permian leucocratic and alaskite granites (Ivanov, Serykh 1969). Central Kazakhstan exhibits many intrusives of this type. Within almost all ore fields we witness a complex combination of successive intrusives threading the Caledonian and Hercynian structural complexes of sedimentary and volcanic rocks. Rare metal deposit themselves spatially lean toward Late Carbonaceous – Early Permian "Akchatau" complex, laying in super-intrusive, near-intrusive zones and within the massifs themselves (Kudryashov, 1964). The most important pneumatolytic-hydrothermal rare metal-tin-molybdenum-tungsten mineralization is associated with the plutons of the leucogranite formation in Central Kazakhstan. Central Kazakhstan shows widely spread plutonogenic hydrothermal-greisen rare metal deposits of W, Mo, Be, Sn, Bi, Ta, Nb (over 60 deposits). Genetically they are associated with the plutons of leucogranite and alaskite formations. However, the ore-bearing properties of leucogranite and alaskite plutons are sharply different: among leucogranite plutons, every second pluton is ore-bearing (and ore occurrences are in connection with each pluton), whereas among the alaskite ones, only every 25th pluton is ore-bearing, and the deposits in these cases are not larger than the middle ones (Serykh, 2009).

The table shows the classification of rare metal deposits in Central Kazakhstan up to the level of ore formations confined to "Akchatau" complex.

Table 1. Endogenous formations of the W, Mo, Be deposits of Central Kazakhstan (classification by Ivanov, 1975)

Magmatic complexes	Metallogenic formations	Ore formations	Forms of ore bodies	Typical deposits
Akchatau complex by V.I. Serykh (Aktachau and Kaldyrminsky, unified)	Orogenic paragenosynclinal bismuth-beryllium-molybdenum-tungsten-rare-earth	Skarn-carbonate-greisen chalcopyrite-bismuthin-wittichenite-molybdenite-scheelite	Quartz-vein stockwork zones	North Katpar, Koktenkol, Promezhutochny
		Hydrothermalite K-feldspar-sericite-pyrite-molybdenite-scheelite	Quartz-vein stockwork zones	Batystau, Upper Kayrakty, South Zhaur, Koktenkol
		Hydrothermalitic quartz-beryl-molybdenite-wolframite	Quartz-vein greisen zones	East Kounrad, Akshatau, Molybdenum area of Karaoby
		Hydrothermalitic quartz-muscovite-beryl-molybdenite-bismuthin-wolframite	Quartz-vein greisen zones	Bainazar, Nurataldy, Northern Konyrat

Central Kazakhstan boasts concentrations of over 60 rare metal and rare-earth deposits, including stockwork deposits unique in their reserves: Upper Kayrakty, Koktenkol, and North Katpar. Therefore, further study of their genetic connections, structural association, morphology, and forecasting criteria is a highly relevant task in the light of the onset of development of individual rare metal deposits (Syrymbet). This article outlines the main problems of the forthcoming studies.

References

Bekzhanov G.R., Ivanov L.B., Rare Metals of Kazakhstan. Molybdenum. // Geology and Conservation of Mineral Resources. 2006. No. 2. pp. 17-24.

Bekzhanov G.R., Ivanov L.B., Rare Metals of Kazakhstan. Tungsten. // Geology and Conservation of Mineral Resources. 2006. No. 3. pp. 37-43.

Gubaidulin F.G., Laumulin T.M., Kuzovenko A.I., Tungsten Deposits of Kazakhstan (Condition and Prospects) // Izvestiya NAS RK. Geological series. 2008. No. 4. pp. 17-53.

Ivanov L.B., Towards the Classification of Hydrothermalite Rare Metal Deposits in Kazakhstan. In: Non-Ferrous and Noble Metals of Kazakhstan. Alma-Ata. "Nauka" KazSSR. 1975.

Laumulin T.M., Gubaidulin F.G., Sheptura V.N. et al., Deposits of Rare Metals and Rare Earths in Kazakhstan: Handbook. Almaty. 1998.136 p.

Lehmann B., Seltmann R., Rare metal granites and associated mineralization of Central Kazakhstan // Erzmetall 48. 1995. No.3. pp. 128-132.

Serykh V.I., Ivanov O.V., Some Petrographic and Mineralogical-Geochemical Indications for the Search for Tungsten Deposits in Central Kazakhstan // Theses of Proceedings at II All-Union Council on Mineralogy, Geochemistry and Genesis of Tungsten Deposits. USSR. Leningrad, Leningrad State University. 1968. pp. 15-17.

Serykh V.I., Rybaltovsky Ye.V., Features of the Material Composition, Radiogeochronology, Age Ratio and Patterns of the Location of intrusives of Ultra-Acid Granitoids of the Northern Balkhash Region // Theses of Proceedings at II Kaz. Petrograph. Council. Alma-Ata. Science of the Kazakh SSR. 1974.

Serykh V.I., Paleozoic Granitoid Complexes and the Balkhash Series, Proceedings of Academy of Sciences of Kazakh USSR, Geological Series. 1977. No.3. pp. 8-17.

Serykh V.I., Geology, Petrology and Metallogeny of the Ultra-Acid Granitoids of Central Kazakhstan. Karaganda. 2009. 318 p.

Uzhkenov B.S., Bekzhanov G.R., Ivanov L.V., Rare Metals and Rare Earths of Kazakhstan. Almaty. 2011. 277p.

Shatov V.V., Plyushchev E.V., Belova V.N., Russkikh S.S., R. Seltmann // Alternation Controls on Localization of Scheelite Stockwork Mineralization in the Verkhnee Qairaqty Deposit Area, Central Kazakhstan. Geodinamics and Metallogeny:Theory and Implications for Applied Geology. Moscow. 2000. Pp. 373-387.

Shcherba G.N., Formation of Rare Metal Deposits of Central Kazakhstan. Alma-Ata: Nauka. 1960. 381 p.

TRACE-ELEMENT DISTRIBUTION AT DIFFERENT STAGES OF CRYSTALLIZATION DIFFERENTIATION

Kopylova A.G.

Diamond and Precious Metal Geology Institute, SB RAS, Yakutsk, Russia, kopylova@diamond.ysn.ru

Within the eastern Siberian platform, basic magmatism repeatedly manifested itself under different geodynamic conditions over a long period of time. In the Precambrian and Middle Paleozoic it was related to rifting processes and in the Late Paleozoic-Early Mesozoic to the initiation and development of trap syneclises. Differences in the geodynamic setting of magma generation are well displayed in compositional variations of the rocks. Magmatites of the trap syneclises are characterized by moderate alkalies contents, a slight REE fractionation trend, and the presence of a Ta-Nb minimum. The composition of parent magmas varies significantly in the process of fractional-crystallization differentiation that takes place at various stages of the magmatic system evolution. The intra-chamber crystallization differentiation of reasonably thick intrusions of the trap syneclises gives rise to a wide range of rocks from basic magnesian to acidic alkaline ones. The process involves active distribution of trace elements. The analysis of the trace-element distribution in differentiated intrusions allows understanding the particularities of their behavior in the course of the magmatic system evolution in general. The Lower Tomba intrusion is a typical example of a layered trap massif with a differentiation trend from troctolite gabbro-dolerites to schlieren and lenses of gabbro-pegmatite, granophyre and ferro-gabbro. The degree of differentiation is rather high - Mg# varies from 48 to 33 reaching 12-17 in the acidic varieties. The content of trace elements which enter into the composition of the early phases tends to decrease in the course of successive evolution of the rocks. Cr and Ni are among the first to escape from the magmatic melt. At the middle stages of evolution, a tendency toward accumulation of V, Sc, Zn, and Cu is evident. But the amount of siderophile elements in the schlieren of high-siliceous alkaline gabbro-pegmatites and granophyres is minimum. When Zn and Co exhibit their chalcophile properties to form their own minerals they are most heavily concentrated in schlieren. Minimum

values of all incompatible elements, except for Sr, are established in the troctolite dolerites and maximum ones in the acidic differentiates. Most of Sr in the magmatic rocks is concentrated in early plagioclase of basic composition. Spider diagrams for the final products of differentiation exhibit Sr and Eu minima. This may result from the reduced Ca content and, in the case of Eu, may also be connected with the oxidizing conditions and the lagging of Eu^{2+} behind other more strongly oxidized REE. The evolution of melts of normal alkalinity in intra-chamber conditions proceeds with the growing ΣREE content from 49.1 in troctolite dolerites to 193.4 in the acidic differentiates and the $(La/Yb)_n$ ratio varying within a narrow range (2.37-2.72) in that same direction. Lenses of ferro-gabbro are composed of moderate-basicity plagioclase (An_{50-45}), ferro-augite (Fs_{39-45}) and a high proportion of ore minerals. They differ from normal dolerites in having higher contents of iron (17, 20% FeO), titanium (2, 13 % TiO_2) and HFSE (Ti, Zr, Hf, Nb and V) whose geochemical history in the basites is related to oxide ore minerals and, partly, to clinopyroxene. The Sr minimum is less pronounced in them than in the gabbro-pegmatite schlieren, and the Eu minimum is virtually absent. Multi-element diagrams for all differentiates of the Lower Tomba intrusive clearly show a Ta-Nb minimum, which is typical for traps magmatism of the Siberian platform.

The derivatives of the Precambrian and Devonian rift-related magmatism are characterized by elevated contents of Ti, P, K and all incompatible elements, a high degree of REE differentiation, and the absence of the NB/Nb* minimum. The Nyurba dike provides a good example of both intra- and pre-chamber differentiation of a basic melt. Microdolerites of the marginal zones of the dike are replaced by quartz gabbro-dolerites, and its central part is composed of monzonite porphyries of the second intrusive stage of the melt. A low value of Mg#=36, reduced Ni, Co and Cr contents, and large amounts of alkalies in the rocks of the marginal zones testify to a high degree of pre-chamber differentiation of the melt which was further differentiated in intra-chamber conditions with the formation of rocks still more enriched in SiO_2, K_2O and incompatible elements and depleted in compatible ones. But the process of intra-chamber differentiation alone cannot explain a sharp increase in SiO_2 and K amounts in the direction from quartz gabbro-dolerites to monzonite porphyries. This may be related to a long-term evolution of the alkaline basaltic melt as a result of its retardation in an intermediate chamber (15-20 km deep from the paleosurface, at P=5-8 kbar). This process is known as the monzonitoid-type differentiation of a basaltic melt (Koroleva, 1991). The repeated pulsatory opening of the magma feeder brought about discontinuity of the then partly crystalline Nyurba dike. The monzonitoid melt intruded, as a second phase, into the central part of the dike to form sharp contacts with the quartz gabbro-dolerites. The monzonite porphyries are porous rocks with abundant amygdules. They are made up of andesine, K-feldspar, apatite, ilmenite, amphibole-chlorous aggregate, hornblende, sphene and zircon. Typical for them are maximum values of K (up to 5.6%), Rb, Ba, Th and U as well as ΣREE =618.8 and $(La/Yb)_n$ =10.6. A distinctive geochemical feature of the alkali basites is a high content of the zircon-group elements – Zr, Y, Yb, Ta and Nb. These elements tend to accumulate in ilmenite, but the highest values are found in accessory apatite, zircon and sphene. The latter minerals are most abundant in the quartz gabbro-dolerites and monzonite porphyres which therefore contain maximum concentrations of these elements. At the same time, as compared to other differentiates of the dike, these rocks are distinguished by a lower Sr content and the maximum negative Eu anomaly (Eu/Eu^*=0.65), which is no doubt due to the absence of the early magmatic phases of plagioclase from them. The initially low concentrations of siderophile elements (Na, Co, Cr) in the alkali basites of the dike further decrease in the course of the intra-chamber differentiation reaching a minimum value in the quartz gabbro-dolerites and monzonite porphyres.

Among the Precambrian bodies of the Anabar massif there are also found composite differentiated dikes with evidence of the monzonitoid-type differentiation. They differ from the Devonian riftogenic intrusions by lower Ti, K and P contents and by prevalence of Na over other alkalies in the monzonite porphyries. But the character of distribution of most trace elements in them is, in general, the same as in the Middle-Paleozoic basites. The exception is the presence of the Na-Nb minimum (Nb/Nb^*=0.26 and 0.44) and a higher $(La/Yb)_n$ ratio: 11.82 in the monzonites versus 5.02-4.32 in normal dolerites.

Under depth conditions, the melt appears to have undergone the anorthosite-type differentiation (Oleinikov and Tomshin, 1976). This is evidenced by the presence of anorthosite gabbro-dolerite clusters in the cross-sections of intrusive bodies. Such bodies occur both among the traps and the Middle-Paleozoic dikes, and they include minerals incompatible with the conditions of intra-chamber differentiation of a tholeiitic melt at a hypabyssal level. These are anorthite-bytownite, chrysolite, chrome-spinellid, moissanite, garnet, disthene and native elements. The bodies were formed at the closure of magma-feeding zones in the setting of a deep-seated intermediate chamber. The melt started to evolve at a depth of 35-40 km from the paleosurface, at a pressure of no less than 10 kbar and a temperature of 1450-1300^{0}C as derived from the homogenization temperature of melt inclusions in bytownite. That gravitation-crystallization stage of the melt evolution led to a decrease in the total amount of Fe and Mg due to gravity settling of the earlier iron-magnesium and oxide-ore phases and to increased amounts of alumina and calcium, which provided preconditions for crystallization of the early plagioclase. Geochemically this is expressed in the lower concentrations of Ni, Co, Cr and Zn and maximum Sr values in the rocks enriched in the early magmatic plagioclase. At high pressures, the anorthosite rocks also become relatively rich in Ba which enters the early plagioclase to replace Ca. These trends in the behavior of these elements are characteristic both of the traps and the Middle-Paleozoic riftogenic magmatites. However, the Middle Paleozoic anorthosites retain, in general, the main features characteristic of this age group of rocks, i.e., higher K, Ti and P contents. The anorthosite-dolerites of Middle Paleozoic age contain, along with basic plagioclase, its more acidic varieties characteristic of the intra-chamber evolutionary stage, as well as accessory minerals such as apatite, biotite and hornblende that concentrate many of incompatible elements. That is why the Middle Paleozoic anorthosite-dolerites, as compared to the traps, are characterized by higher concentrations of all incompatible elements.

In summary it can be said that distribution of trace elements in the rocks of differentiated intrusions during the shallow-depth intra-chamber crystallization differentiation of the melt is close to processes occuring in the course of pre-chamber differentiation at great depths, and thus can serve as a model for the pre-chamber evolution of tholeiitic-basaltic magmas in general. A wide variety of chemical compositions of basaltic magmas may be due not only to deep partial melting of a mantle source but to further fractionation of the melt in intermediate magma chambers too.

References

Koroleva O.V. Compositional features and genesis of basic and intermediate magmatic rock associations in the Siberian and Hindustan platforms. Traps of Siberia and Deccan: similarities and differences. Novosibirsk: Nauka, 1991, pp. 39-63 (in Russian).

Oleinikov, B.V. and Tomshin, M.D., 1976. Deep-level differentiation of magma of platformal basites // DAN SSSR, V. 231, no. 1, pp. 177-180.

Sun, S., McDonough, W.F. Chemical and isotopic systematics of oceanic basalts: implications for mantle composition and processes.// Geol. Soc. Amer. Spec. Publ. 1989. V. 42. P. 313-345.

EXPERIMENTAL DATA ON NI PARTITIONING BETWEEN OLIVINE AND HIGHLY ALKALINE SILICATE MELTS

Koshlyakova A.N.[1], Sobolev A.V.[1,2], Krasheninnikov S.P.[1], Batanova V.G.[1,2], Borisov A.A.[1,3]

[1]Vernadsky Institute of Geochemistry and Analytical Chemistry, RAS, Moscow, Russia

an.koshlyakova@gmail.com

[2]Institut des Sciences de la Terre (ISTerre) Université Grenoble Alpes, Grenoble, France

[3]Institute of Geology of Ore Deposits, Petrography, Mineralogy and Geochemistry RAS, Moscow, Russia

Olivine-melt equilibrium is often used in petrological models to determine the conditions of formation and evolution of mantle melts. Nickel contents in magnesian magmatic olivine are widely used to indicate mantle source lithology (Sobolev et al., 2005). At present, there is a large amount of

experimental data on Ni partitioning between olivine and melt. However, the authors usually use low-alkali compositions or note the loss of alkalis during the experiments (Leeman and Lindstrom, 1978; Hart and Devis, 1978; Takahashi, 1978; Kinzler et al., 1990; Ehlers et al., 1992; Mysen, 2007; Wang and Gaetani, 2008).

We present the results of 60 high-temperature (1250-1450°C) experiments at atmospheric pressure and oxygen fugacity at the NNO buffer level. The starting compositions were mixtures of Hawaiian picrites and lamproites of Gaussberg with the addition of MgO. We used the crucible-supported loop technique (Borisov et al. 2006), by which the samples on Pt loops are placed into a quartz crucible, above the alkali-rich mixture (Fig. 1).

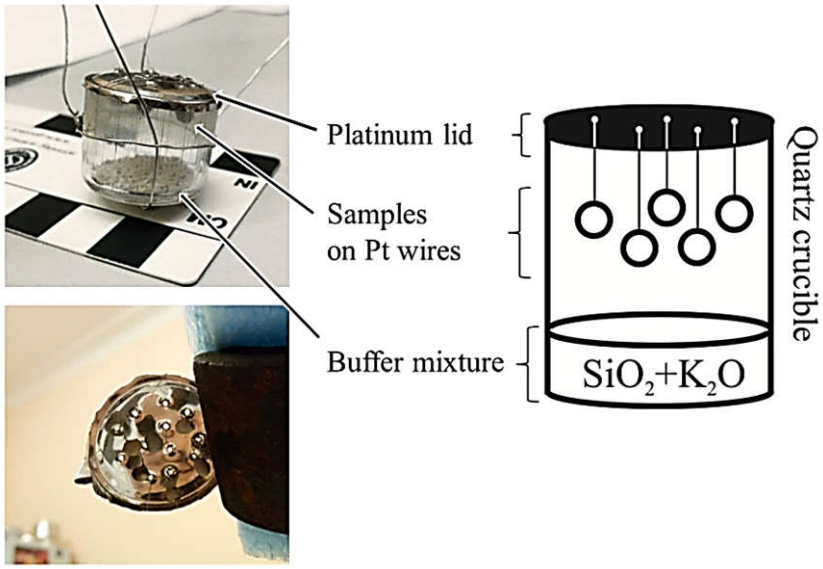

Fig. 1. Photos and scheme of crucible-supported loop technique

The composition of mixture corresponds to liquidus temperature for each experiment. The buffers used are mixtures of SiO_2+K_2O+CaO, SiO_2+K_2O, SiO_2+K_2O+Na_2O, SiO_2+Na_2O. Testing of this technique showed that the composition of each mixture after a 6 and a 20 hour experiment remained the same. Thus, the usage of this technique enables high and constant potassium and/or sodium concentration to be maintained in melt during experiments.

Quenched runs were analyzed by electron microprobe analysis at ISTerre, Grenoble, France (Batanova et al., 2018). The products of the experiments are olivines and glass (Fig. 2).

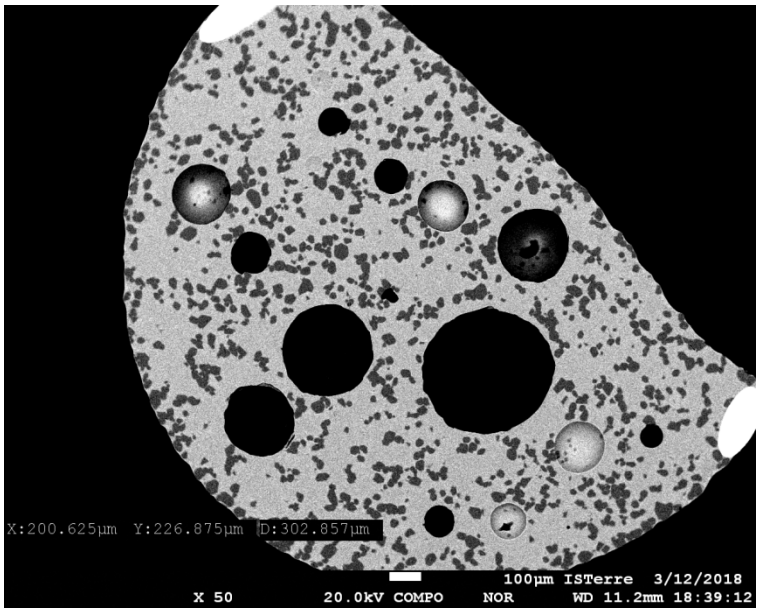

Fig. 2 BSE image of K-Na experiment products: olivines (dark phase) and glass.

The range of alkalis content in glass is given in the Table. 1.

Table. 1 Alkalis content in glass of samples using different buffers.

	K_2O-SiO_2-CaO	K_2O-SiO_2	K_2O-Na_2O-SiO_2	Na_2O-SiO_2
K_2O in glass (wt. %)	2-7	6-12	3-7	1-3
Na_2O in glass (wt. %)	<1	<1	4-5	6-8

We model the Ni-Mg partitioning between olivine and melt by using the following exchange reaction:

$MgSi_{0.5}O_2^{ol} + Ni^{liq} \leftrightarrow NiSi_{0.5}O_2^{ol} + Mg^{liq}$

The equilibrium constant of this exchange reaction and, at the same time, the Ni-Mg distribution coefficient is:

$$Kd = \frac{X(NiSi0.5O2)ol}{X(NiO)liq} \frac{X(MgO)liq}{X(MgSi0.5O2)ol}$$

For our data we derived an equation, which predicts Kd from temperature and melt composition:

$LnKd = -2.132(\pm0.200) + 2685(\pm271)/T + 1.890(\pm0.260)*X_{SiO2} - 1.618(\pm0.388)*X_{Na2O} - 6.865(\pm0.488)*X_{K2O}$.

One standard error of each coefficient is given in the brackets. The effects of Na_2O and K_2O on Ni-Mg partitioning turn out to be significant. Both K and Na reduce an exchange equilibrium constant whereas Si raises it. The effect of K is four times higher than that of Na.

Then, after calculating the partitioning coefficient D(Ni) from Kd, we compared it to the observed D(Ni) from analysis. Almost all experiments are predicted well within two standard errors (Fig. 3).

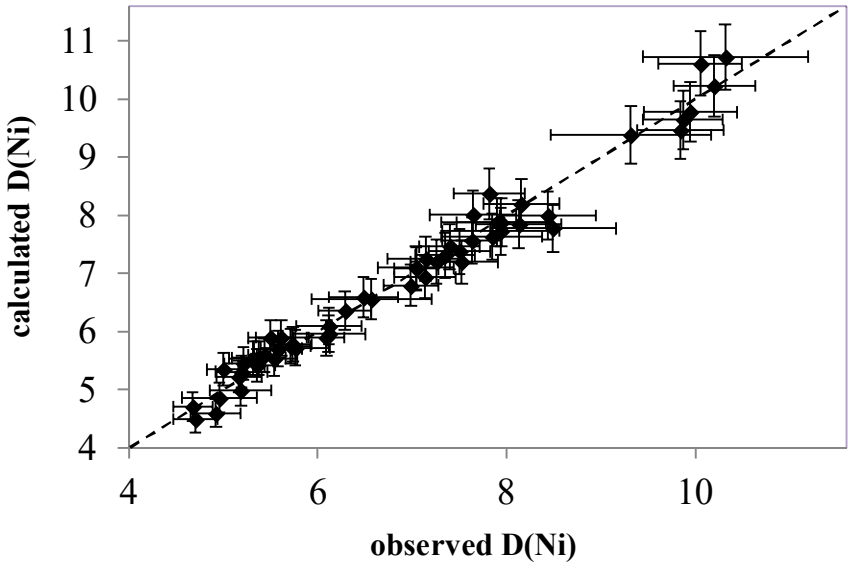

Fig. 3. Calculated vs observed D(Ni) for the experiments.

The experiments at temperatures lower than 1400 were supported by Russian Basic Research Foundation, grant 17-05-00856a, while experiments at higher temperatures were supported by the Russian Science Foundation, grant 14-17-00491.

References

Batanova V. G., Sobolev A. V., Magnin V. Trace element analysis by EPMA in geosciences: detection limit, precision and accuracy// IOP Conference Series: Materials Science and Engineering. – IOP Publishing. 2018. Vol. 304 №1 p. 012001.

Borisov A., Lahaye Y., Palme H. The effect of sodium on the solubilities of metals in silicate melts// American Mineralogist. 2006. Vol. 91 №. 5-6 pp. 762-771.

Ehlers K. et al. The effect of oxygen fugacity on the partitioning of nickel and cobalt between olivine, silicate melt, and metal// Geochim. Cosmochim. Acta. 1992. Vol. 56 №10 pp. 3733-3743.

Hart S.R., Davis K.E. Nickel partitioning between olivine and silicate melt// Earth. Planet. Sci. Lett. 1978. Vol. 40 №2 pp. 203-219.

Kinzler R.J., Grove T.L., Recca S.I. An experimental study on the effect of temperature and melt composition on the partitioning of nickel between olivine and silicate melt// Geochim. Cosmochim. Acta. 1990. Vol. 54 №5 pp. 1255-1265.

Leeman W.P., Lindstrom D.J: Partitioning of Ni2+ between basaltic and synthetic melts and olivines—an experimental study// Geochim. Cosmochim. Acta. 1978. Vol. 42 №6 pp. 801-816.

Mysen B.O. (2007): Olivine/melt transition metal partitioning, melt composition, and melt structure—influence of Al3+ for Si4+ substitution in the tetrahedral network of silicate melts// Geochim. Cosmochim. Acta. 2007. Vol. 71 №22 pp. 5500-5513.

Sobolev A.V. et al. An olivine-free mantle source of Hawaiian shield basalts// Nature. 2005. Vol. 434 №7033 p. 590.

Takahashi E. Partitioning of Ni2+, Co2+, Fe2+, Mn2+ and Mg2+ between olivine and silicate melts: compositional dependence of partition coefficient// Geochim. Cosmochim. Acta. 1978. Vol. 42 №12 pp. 1829-1844.

Wang Z., Gaetani G.A. Partitioning of Ni between olivine and siliceous eclogite partial melt: experimental constraints on the mantle source of Hawaiian basalts// Contrib. Mineral. Petrol. 2008. Vol. 156 №5 pp. 661-678.

CRYSTAL CHEMISTRY OF ARSENATE AND VANADATE GARNETS FROM FUMAROLE EXHALATIONS OF THE TOLBACHIK VOLCANO, KAMCHATKA, RUSSIA

Koshlyakova N.N.[1], Pekov I.V.[1,2], Zubkova N.V.[1], Agakhanov A.A.[3], Turchkova A.G.[1], Sidorov E.G.[4], Pushcharovsky D.Yu.[1]

[1]Moscow State University, Moscow, Russia, nkoshlyakova@gmail.com

[2]Vernadsky Institute of Geochemistry and Analytical Chemistry, RAS, Moscow, Russia

[3]Fersman Mineralogical Museum of RAS, Moscow, Russia

[4]Institute of Volcanology and Seismology, Petropavlovsk-Kamchatsky, Russia

Arsenate and vanadate garnets of the berzeliite–schäferite series were found by us in exhalations of the Arsenatnaya fumarole, the Second scoria cone of the Northern Breakthrough of the Great Tolbachik Fissure Eruption, Tolbachik volcano, Kamchatka peninsula. They turned out among the major minerals in the deepest and hottest levels of the fumarole. These garnets were formed at temperatures above 450ºC (the most probable temperature interval is 500–750ºC), under atmospheric pressure and high oxygen fugacity. The minerals were deposited directly from fumarolic gas, as volcanic sublimates, or formed in the result of gas-rock interactions in fumarole cameras where basalt could be a source of low-volatile Mg and Ca. In general, anhydrous arsenates are very abundant and diverse in the exhalations of Arsenatnaya, more than 50 arsenates including alkaline ones were described here (Pekov et al., 2018). Vanadate phases are less common and most of the vanadium is concentrated in the As-bearing vanadate garnet schäferite.

The chemical composition of the garnets was determined by electron microprobe analysis and crystal structures of three garnet samples with different As:V ratio were studied by single-crystal X-ray diffraction (XRD).

Most garnet supergroup minerals are cubic, space group *Ia*-3*d*. There are four crystallographically non-equivalent atomic positions in the structure: three cation sites, namely dodecahedrally coordinated *X*, octahedrally coordinated *Y*, and tetrahedrally coordinated *Z* and an anion site *O* typically occupied by O^{2-}. The crystal structure consists of alternating isolated ZO_4 tetrahedra and YO_6 octahedra, which share corners to form a three-dimensional framework. Extra-framework sites contain the *X* cations. The current IMA-accepted form of general garnets formula is $\{X_3\}[Y_2]\ (Z_3)O_{12}$ (Grew et al., 2013).

The berzeliite–schäferite series garnets occur in exhalations of the Arsenatnaya fumarole as aggregates of transparent crystals of different shapes. They have yellow to orange color and strong vitreous luster. Sometimes the crystals are well formed and can reach 0.5 mm in size, but the most common form is 50-100 thick crusts intergrown with anhydrite (Fig. 1) or overgrowing its crystals. The garnets are associated with diopside, feldspars, andradite, haüyne, hematite, magnesioferrite, minerals of the svabite–fluorapatite solid-solution series, tilasite, Na-Ca-K sulfates, barite, powellite, minerals of the rhabdoborite-(V)–rhabdoborite-(W) series (IMA 2017-108 and 2017-109), *etc*.

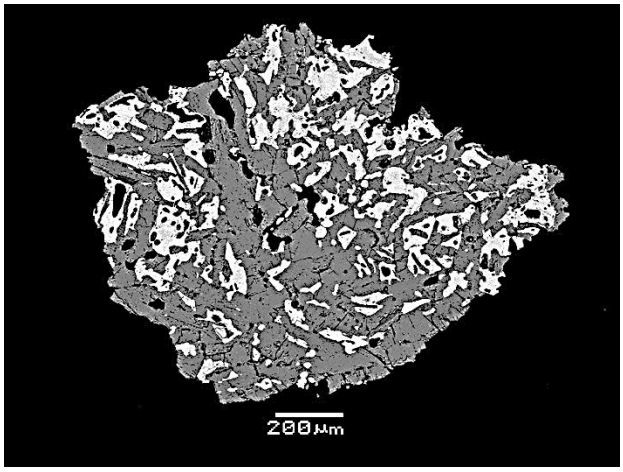

Fig. 1. BSE image of berzeliite (lighter phase) intimately intergrown with anhydrite (darker phase).

The greatest chemical variation in studied garnets occurs in the *Z* site: they form an almost complete solid-solution series between berzeliite and schäferite, $\{Ca_2Na\}[Mg_2](As_3)O_{12}$ - $\{Ca_2Na\}[Mg_2](V_3)O_{12}$. We found samples close to the arsenate end-member (3.02 wt.% V_2O_5 = 0.09 *apfu* V) while arsenic is never less than 10.83 wt.% As_2O_5 = 0.48 *apfu* As: Fig. 2, left. The corresponding maximum arsenic and vanadium concentrations are: 58.7 wt.% As_2O_5 = 2.90 *apfu* As and 41.2 wt.% V_2O_5 = 2.46 *apfu* V. Besides V^{5+} and As^{5+} the *Z* sites contain up to 0.2 *apfu* P^{5+} = 2.4 wt.% P_2O_5 and up to 0.3 *apfu* Si^{4+} = 3.7 wt.% SiO_2.

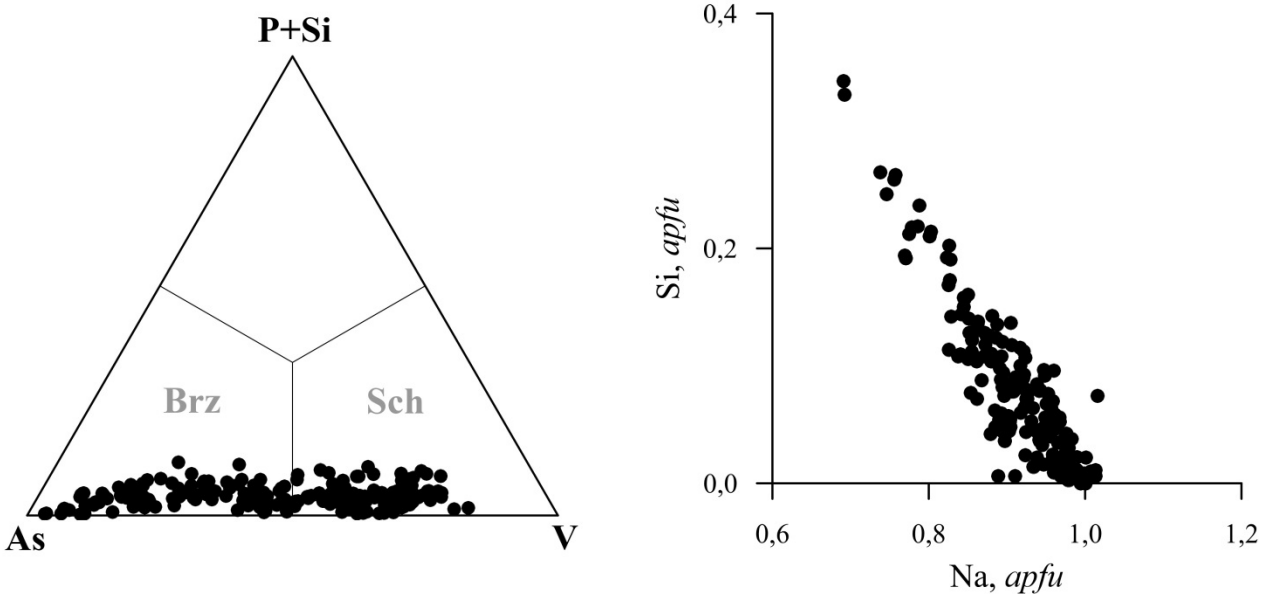

Fig. 2. Isomorphism in the *Z* (left figure) and *X* (right figure) sites contents in berzeliite-schäferite series garnets from the Arsenatnaya fumarole.

No significant substitutions except As^{5+} <=> V^{5+} were found in these minerals and composition of non-tetrahedral sites varies only slightly and in general is close to $^{X}(Ca_2Na)^{Y}Mg_2$. In the octahedral *Y* site the content of each of admixtures, Al, Ti, Mn, Fe, Cu, and Zn is lower than 0.05 *apfu* and the

total concentration of all above-mentioned cations is lower than 0.1 *apfu*. The dodecahedrally coordinated *X* position is occupied only by Na and Ca in the ratio controlled by charge-balance requirement (1:2 in the ideal case). Substitution of Z^{5+} for Si^{4+} leads to decrease of the total positive charge and is balanced by the increase of Ca^{2+} concentration according to the scheme $^{X}Ca^{2+} + {}^{Z}Si^{4+} = {}^{X}Na^{+} + Z^{5+}$ (Fig. 2, right). The highest Si^{4+} concentration of 0.3 *apfu* (3.8 wt.% SiO_2) corresponds to the lowest Na concentration of 0.7 *apfu* (3.9 wt.% Na_2O) and the highest Ca concentration of 2.3 *apfu* (23.7 wt.% CaO). Values of the measured Na and Ca total content is close to 3.0 *apfu.*

Crystal structures of three samples with different As:V ratios were studied and the garnet structure was confirmed. All three crystals are cubic, *Ia*-3*d*, *Z* = 8. The formulae based on both XRD and microprobe data, unit-cell parameter *a* and final *R* values are listed in Table. No significant variations in polyhedral sizes were found.

Table. Crystal chemical formula, unit-cell parameter *a* and final *R* values for three studied crystals of berzeliite–schäferite series garnets from the Arsenatnaya fumarole.

№	Formula	*a* (Å)	*R*
(1)	$\{Ca_{2.15}Na_{0.85}\}_{\Sigma3}[Mg_{2.0}](V_{1.95}As_{0.90}Si_{0.15})_{\Sigma3}O_{12}$	12.39737(7)	0.0210
(2)	$\{Ca_{2.00}Na_{1.00}\}_{\Sigma3}[Mg_{2.0}](As_{1.90}V_{0.90}P_{0.20})_{\Sigma3}O_{12}$	12.35366(10)	0.0181
(3)	$\{Ca_{2.05}Na_{0.95}\}_{\Sigma3}[Mg_{2.0}](As_{2.35}V_{0.60}Si_{0.05})_{\Sigma3}O_{12}$	12.36093(10)	0.0251

A berzeliite polymorph with the alluaudite structure was found by us in exhalations of the same Arsenatnaya fumarole and named paraberzeliite (IMA No. 2018-001). It is interesting that in paraberzeliite the tetrahedral sites are occupied by As without any significant admixtures, while the compositions of octahedrally coordinated and large cation sites vary in wide ranges. The main scheme of cationic substitutions in paraberzeliite is $^{A}Na^{+} + {}^{M}Fe^{3+} = {}^{A}Ca^{2+} + M^{2+}$, where *M* means octahedrally coordinated sites, occupied by Mg > Ca, Mn, Fe^{3+}, and *A* means large cation sites, occupied by Na, Ca, and vacancies.

The berzeliite–schäferite solid-solution series have not been reported yet either for natural or synthetic compounds, although the structure and properties of synthetic vanadate and arsenate garnets have been the subject of detailed studies (*e.g.*, Bayer, 1965; Ito, 1968; Schwarz and Schmidt, 1972; Mill and Ronniger, 1973; Nagashima and Ambruster, 2012; Iishi and Ikuta, 2006).

This study was supported by the Russian Foundation for Basic Research, grant 17-05-00179.

References

Bayer G. Vanadates $A_3B_2V_3O_{12}$ with garnet structure// J. Am. Ceram. Soc. 1965. Vol. 48 Iss.11 p.600.

Grew E.S. et al., Nomenclature of the garnet supergroup// Am. Mineral. 2013. Vol. 98 Iss. 4 pp.785-811.

Iishi K., Ikuta Y. Isomorphous substitutions in vanadate garnets// Neues Jahrb. Mineral., Abh. 2006. Vol. 182 pp.157-163.

Ito J. Synthesis of the berzeliite ($Ca_2NaMg_2As_3O_{12}$) - manganese berzeliite ($Ca_2NaMn_2As_3O_{12}$) series (arsenate garnet)// Am. Mineral. 1968. Vol. 53 pp.316-319.

Nagashima M., Armbruster T. Palenzonaite, berzeliite, and manganberzeliite: (As^{5+}, V^{5+}, Si^{4+})O_4 tetrahedra in garnet structures// Mineral. Mag. 2012. Vol. 76 Iss. 5 pp.1081-1097.

Pekov I.V. et al., Fumarolic arsenates – a special type of arsenic mineralization// Eur. J. Mineral. 2018.

Schwarz H., Schmidt L. Neue Verbindungen mit Granatstruktur. IV. Arsenate des Typs $\{Na_3\}[M_2^{III}](As_3)O_{12}$// Zeitschrift fur Annorganische und Allgemeine Chemie. 1972. Vol. 387 pp.31-42.

Mill B., Ronniger G. Vanadates with garnet structure// Physics and Chemistry of Ferrites. 1973. pp.98-115 (in Russian).

MELTING OF ECLOGITE WITH CARBONATES AND CHLORIDES ALKALY: FORMATION OF CARBONATE AND SILICATE MELTS (FOR EXPERIMENTAL DATA)

Kostyuk A.V.*, Gorbachev N.S., Soultanov D.M., Nekrasov A.N.
IEM RAS, Chernogolovka nastya@iem.ac.ru, gor@iem.ac.ru

Eclogites as peridotites are widespread among the xenoliths of mantle rocks. Nodules of mantle eclogites show signs of mantle metasomatism (Pyle, Hggerty, 1998; Ukhanov et.al., 1988). The formation of alkaline and carbonatite magmas is associated with the melting of the metasomatically amended carbonatized upper mantle. As a rule, carbonatites occur in association with alkaline rocks of the Na series, much less often - with enriched potassium rocks (Na/K < 1). The main components of metasomatic fluids along with H_2O and CO_2 are the salts (carbonates, chlorides) of Na and K. They are represented in fluid-melt inclusions in the minerals of the upper mantle xenoliths of peridotites and eclogites, as well as in tectonically embedded carbonate-bearing peridotite and eclogite massifs (Weiss et.al., 2009; Bogatikov et.al., 2010). Formation of carbonate and silicate melts during melting of eclogite with Na_2CO_3, K_2CO_3 and NaCl, KCl was studied in two systems: eclogite-$CaCO_3$-Na_2CO_3-K_2CO_3-H_2O and eclogite-$CaCO_3$-NaCl-KCl-H_2O+CO_2 at P=4 GPa, T=1100-1300°C.

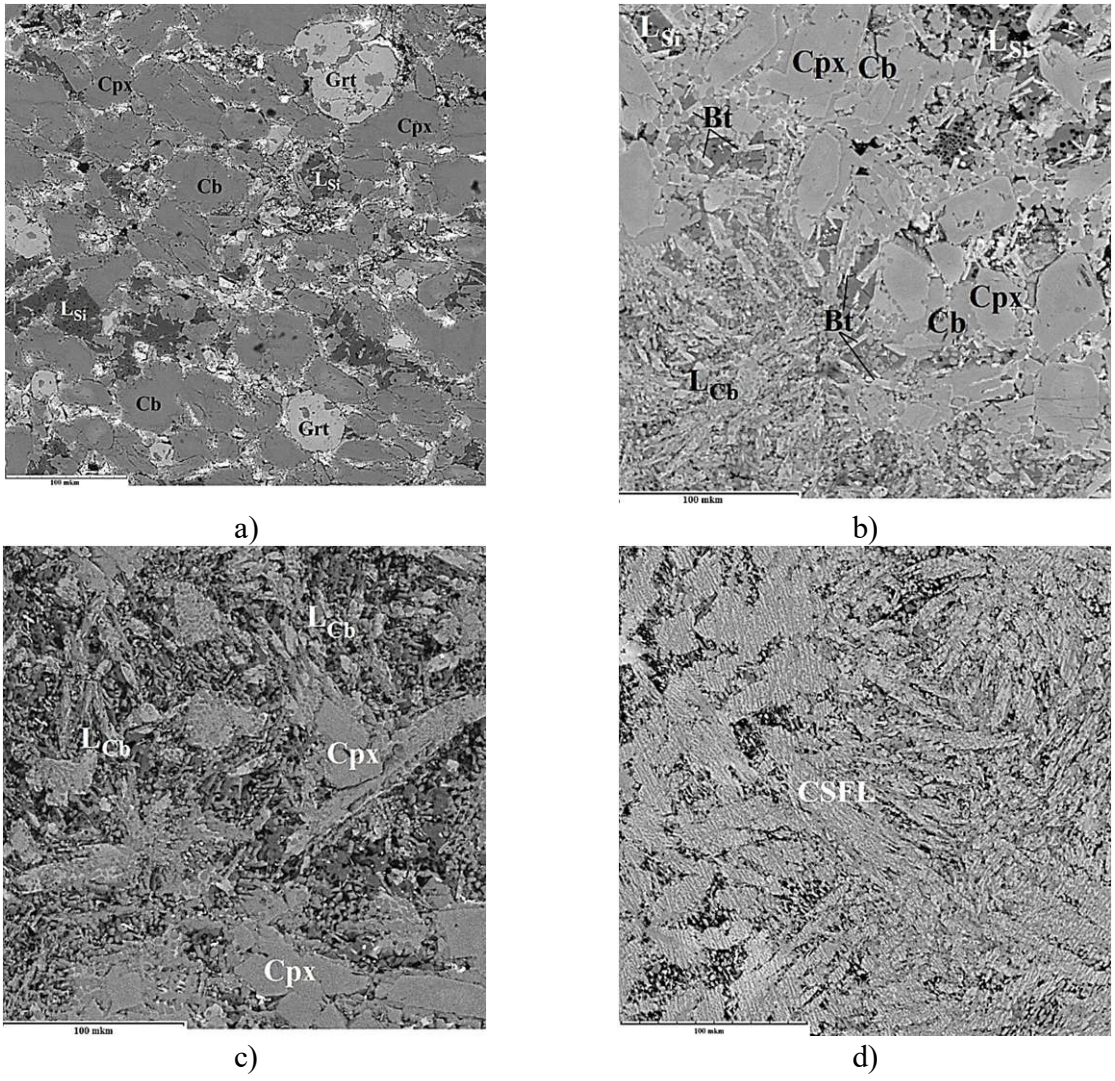

Fig. 1. Microphotographs of experimental samples in secondary electrons, which characterize the texture and phase composition in the eclogite-Na_2CO_3-K_2CO_3-H_2O system at: a) T=1100°C, b) T=1200°C, c) T=1250°C, d) T=1300°C, P=4 GPa.

Experiments were carried out in IEM RAS on an anvil-with-hole apparatus in Pt, Au, and Au-Pd ampoules using a multi-ampoule technique (Gorbachev, 1989). Starting materials: eclogite – tholeiitic basalt, $CaCO_3$ – calcitic carbonate of Kovdor, reagents of Na_2CO_3, K_2CO_3, NaCl and KCl. The source of H_2O is distilled water, H_2O+CO_2 – oxalic acid dihydrate $H_2C_2O_4 \cdot 2H_2O$. The temperature was measured by a Pt30Rh/Pt6Rh thermocouple, the pressure at high temperatures was calibrated along the quartz-coesite equilibrium curve. The accuracy of determining the temperature and pressure in the experiments is estimated at ±5°C and ±1 kbar (Litvin, 1991). The duration of experiments was from 8 to 24 hours. Polished samples were studied and analyzed on a microprobe.

Eclogite-$CaCO_3$-Na_2CO_3-K_2CO_3-H_2O system. In experiments on the melting of eclogite with calcium and alkali carbonates, the following sequence of changes in the phase composition was observed with increasing temperature and degree of melting: L_{Sil} + R – L_{Sil} + L_{Cb} + R – CSFL, where L_{Sil} – silicate melt, R – restite, liquid phases coexisting with melts, L_{Cb} – carbonate melt, CSFL – carbonate-silicate fluid melt.

At T=1100°C, the alkaline silicate melt coexisting with Cpx, Grt, and Cb is formed first in the melting of eclogite (Fig. 1a). With temperature increase up to 1200-1250°C, immiscible L_{Sil} and L_{Cb}, coexisting with Cpx and Grt, are formed (Fig. 1b, c). In the interval T=1250-1300°C there is a "critical" point T_K of the equilibrium L_{Sil} and L_{Cb}, above which there is complete mixing between them (Fig. 1d). An "supercritical" silicate-carbonate fluid-melt (CSFL) is formed. Hence it follows that the T_K of the equilibrium L_{Sil} + L_{Cb} is equal to 1275±20°C.

Eclogite-CaCO3-NaCl-KCl-H_2O+CO_2 system. The texture and phase relationships of quenching samples depend on temperature (Table 1, Fig. 2a). At T=1200°C, P=4 GPa, quenching samples of a massive texture are consist of Cpx, Grt, Cb (Fig. 1a). Cpx predominates among the silicate phases. Grt occurs on contact with Cpx, and also forms micro inclusions in it. Calcite carbonate contains MgO (up to 4 wt.%), FeO (up to 1 wt.%), SiO_2, Al_2O_3 - not more than 1 wt.%. The volatile content is about 48 wt.%.

At T=1250°C, a silicate-carbonate melt appears as a heterophase fine-dispersed mixture of the carbonate and silicate phases coexisting with Cpx + Grt. Silicate glass was not found. Cpx contains inclusions of Grt (Fig. 2b). The composition of undersolidus Cpx and Grt is similar to subsolidus (Table 1).

Table 1. Representative chemical composition (wt.%) of coexisting phases in the eclogite-NaCl-KCl+H_2O+CO_2 system at T=1200-1300°C, P=4 GPa.

	SiO_2	TiO_2	Al_2O_3	FeO	MnO	MgO	CaO	Na_2O	K_2O	Cr_2O_3	P_2O_5	Total
	T = 1200°C											
Cpx	49.92	0.07	11.37	1.73	-	12.81	22.56	1.40	0.02	0.14	-	100.02
Grt	39.19	0.49	22.31	6.76	0.18	9.45	21.01	0.20	0.00	0.16	-	99.75
Cb	0.00	0.00	0.27	0.92	0.21	3.35	46.96	0.00	0.08	0.00	-	51.79
	T = 1250°C											
Cpx	47.38	0.31	13.05	1.04	0.02	11.77	23.91	0.89	0.00	0.31	-	98.68
Grt	39.91	0.25	21.87	3.38	0.00	8.14	25.32	0.21	0.04	0.29	0.03	99.44
Ap	1.40	0.02	0.22	0.25	0.14	1.92	50.79	1.59	0.32	0.05	30.39	87.09
L_{Cb}	9.30	0.30	2.99	0.47	0.05	4.68	39.63	0.48	0.81	0.00	2.63	61.35
	T = 1300°C											
CSFL	14.88	0.65	5.23	1.78	0.26	6.59	42.02	0.60	1.27	0.00	2.95	76.22

At T=1300°C, only the heterophase mixture of the carbonate and silicate phases (CSFL) is present in quenching samples (Fig. 2c). The absence of liquidus minerals and silicate glass indicates the under-liquidus experimental conditions and complete mixing of silicate and carbonate melts.

Thus, unlike eclogite systems with carbonates of Ca, Na and K ± fluid, at partial melting of which silicate and carbonate melts are formed, in the system of eclogite-$CaCO_3$-chlorides of alkalis with fluid (with the same ratio of eclogite with fluid-containing phases) in the interval T=1200-1300°C only carbonate melt is formed. The composition of the melts in both systems depends on the temperature.

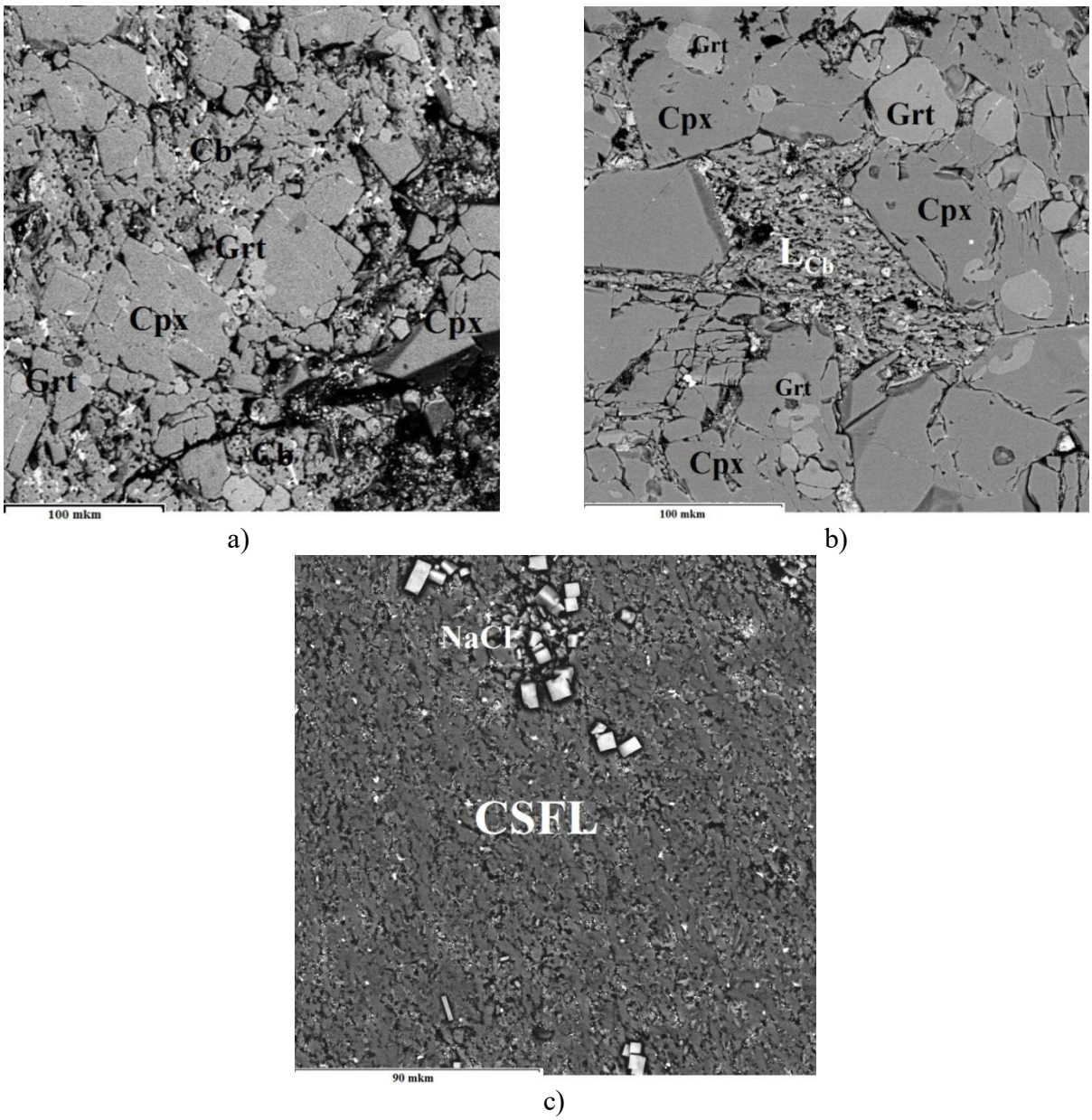

Fig. 2. Microphotographs of experimental samples in secondary electrons, which characterize the texture and phase composition in the eclogite-NaCl-KCl-H_2O+CO_2 system at: a) T=1200°C, b) T=1250°C, c) T=1300°C , P=4 GPa.

The existence of an alkaline fluid-chloride-carbonate melt at high pressures and low temperatures in eclogite systems can play an important role in mantle metasomatism. Particularly interesting in this respect are the subduction zones with the characteristic water-alkaline-chloride type of fluids (Bogatikov et.al., 2010), in which low-temperature chlorine-containing carbonate melts can exist even for the PT conditions of cold subduction in the subsolidus of silicate rocks of the submerged slab.

The work was supported by the RFBR grant 17-05-00930a.

References

Pyle, J.M., Haggerty, S.E. Eclogites and the metasomatism of eclogites from the Jagersfontein Kimberlite: Punctuated transport and implications for alkali magmatism // Geochimica et Cosmochimica Acta, 1998, V.62, p.1207-1231.

Weiss Y., Kessel R., et.al. A new model for the evolution of diamond-forming fluids: evidence from microinclusion-bearing diamonds from Kankan, Guinea // Lithos, 2009, v. 112S, p . 660—674.

Богатиков О.А., Коваленко В.И., Шарков Е.В. Магматиз, тектоника, геодинамика Земли. 2010. М. Изд. Наука. С.605.

Горбачев Н.С. Флюидно-магматическое взаимодействие в сульфидно-силикатных системах. 1989. М. Изд. Наука.

Литвин Ю.А. Физико-химические исследования плавления глубинного вещества Земли. 1991. М. Изд. Наука.

Уханов А.В., Рябчиков И.Д., Харькив А.Д. Литосферная мантия Якутской кимберлитовой провинции. 1988. М. Изд. Наука. С.286.

EXPERIMENTAL STUDY OF AMFIBOLIZATION IN GABBRO FROM TIKSHEOZERSKY MASSIF (NORTH KARELIA)

Kovalskaya T.N., Varlamov D.A., Shapovalov Yu.B., Kalinin G.M., Kotelnikov A.R.

Institute of experimental mineralogy, Chernogolovka, Osipyana str., 4, Moscow dictrict, Russia, Tatiana76@iem.ac.ru

The Tikshozero massif belongs to the formation of ultrabasic alkaline massifs with carbonatites, but it is located south of the main cluster of carbonatite massifs in the Karelian-Kola province, in the circumpolar part of North Karelia, to the south of the city of Kandalaksha (Metallogeny ..., 2001). A detailed study of rock-forming minerals and their parageneses in all types of rocks of the Tiksheozero Massif (North Karelia) revealed that they are all subject to intense postmagmatic changes. The development of chlorite and serpentinite is characteristic of ultrabasic rocks (olivinites, clinopyroxenites). In a number of cases, these minerals almost completely replicate grains of olivine and clinopyroxene (Kovalskaya et al., 2017). In gabbroids, a secondary amphibole develops. It forms rims around the cores of clinopyroxene, often with resorption (Fig. 1). Sometimes amphibole completely replaces clinopyroxene. By composition, the newly formed amphibole responds to pargasite, a typical mineral of postmagmatic associations (Perchuk, Ryabchikov, 1976).

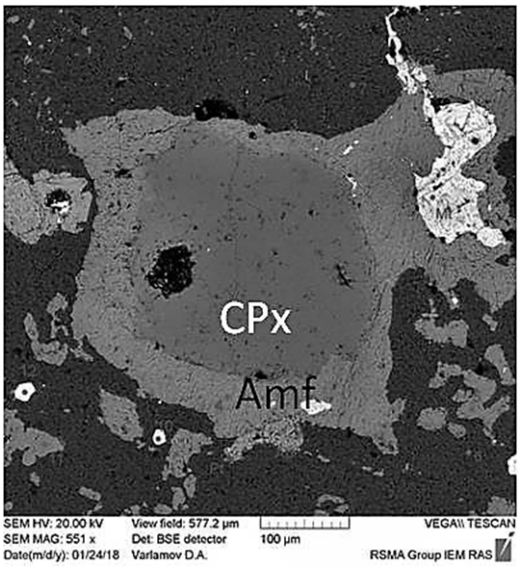

Fig. 1. Clinopyroxene with an amphibole rim. Gabbro. Tiksheozero massif.

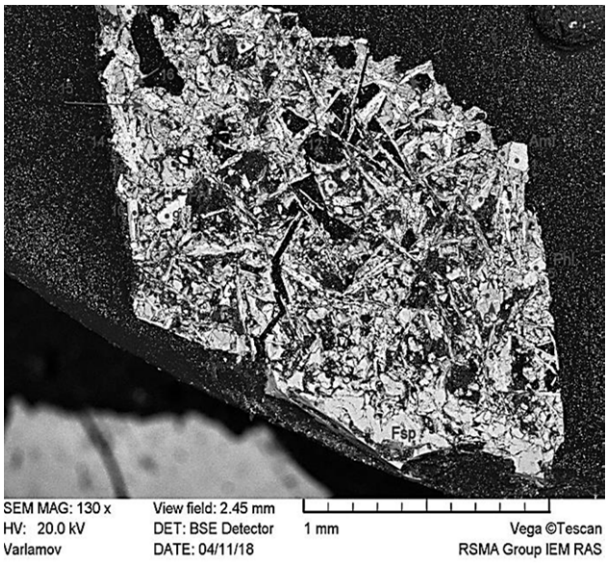

Fig. 2. Products of experiments on amphibolization of gabbro.

In order to recreate the conditions for the formation of postmagmatic changes in the gabbro, experiments were conducted to simulate gabbro amphibolization, since amphibole fringes around clinopyroxenes were found in gabbro samples from the Tiksheozero massif (Fig. 1). As initial components in the experiments, we took: a ground gabbro from the array of Lukkulaisvaara (Table 1), KF solutions of 1M and 2 M in a ratio of 1:10 to the weight of the sample. The duration of the

experiments was 10 days. First, the reaction mixture was heated to 1100 oC and P = 3 kbar, kept at these parameters for 1 hour, then wasobaric cooling to 850 oC, P = 3kbar followed by holding for 10 days at these parameters. For the experiment we used platinum ampoules with a diameter of 5 mm. The experiments were carried out on a high pressure gas installation. The products of the experiments were a small-crystalline mass (Fig. 2) of a greenish-gray color. Investigation using a microprobe CamScan MV2300 showed that amphiboles formed in the experiments from the grinded gabbro massif of Luqqulaisvaara were formed, similar in composition to the amphiboles of the Tiksheozero massif of the pargasite group (Fig. 3).

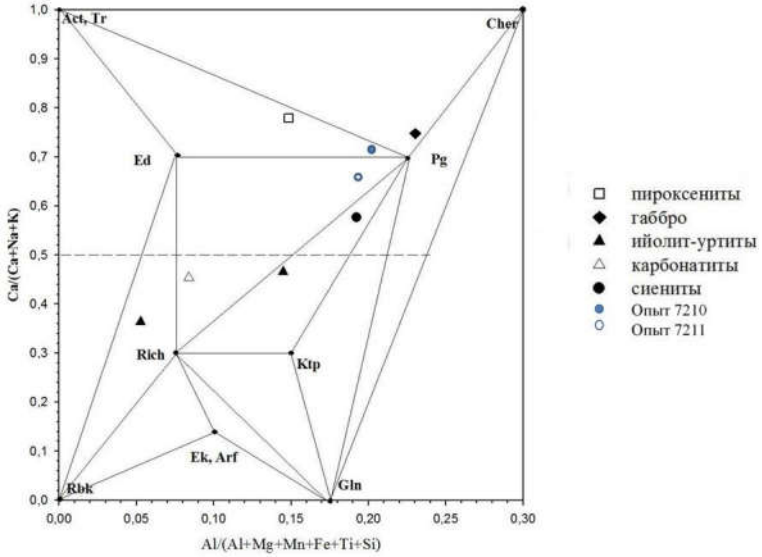

Fig. 3. Amphiboles of the Tikshozero Massif.

On the basis of the obtained data, it is possible to assume two variants of coexistence of pyroxenes and amphiboles in rocks of the Tmksheozero massif:

1. Natural amphiboles encountered in rocks along with pyroxenes are not paragenetic with them. 2. Natural amphiboles encountered in rocks together with pyroxenes have been altered (with increasing Ca content) during the evolution of the massif, possibly during carbonatization and development of the K-containing fluid. In favor of the second assumption is the presence in all these rocks along with pyroxene and amphibole and essentially calcium carbonate, as well as the presence of potassium minerals and the results of experimental studies.

References

Kovalskaya T.N., Kotelnikov A.R., Varlamov D.A. ROCK-FORMING MINERALS OF TIKSHEOZERSKY MASSIF (NORTH KARELIA, RUSSIA) //Magmatism of the Earth and related strategic metal deposits" Proceedings of XXXIV International Conference, 4-9 August 2017, Miass, Russia, GEOKHI RAS, c. 115-117.

Kukharenko AA, Orlova MP, Bagdasarov E.A. Alkaline gabbroids of Karelia. (In Rusian) Leningrad: Leningrad State University, 1969, 184 p.

Metallogeny of magmatic complexes of intraplate geodynamic environments (in Russian), Moscow, GEOS, 2001, 640 p.

Perchuk L.L., Ryabchikov I.D. Phase matching in mineral systems(In Russian). M .: Nedra, 1976. 287 p.

TECTONIC AND MAGMATIC FACTORS OF THE PT-CU-NI DEPOSITS FORMATION INSIDE THE SIBERIAN TRAP PROVINCE

***Krivolutskaya N.A.*[1], *Latyshev A.V.*[2,3], *Belyatsky B.V.*[4], *Bayanova T.B.*[5], *Gongalsky B.I.*[6], *Svirskaya N.M.*[1], *Asavin A.M.*[1], *Dolgal A.S.*[7], *Bychkova Ya.V.*[2]**

[1]*GEOKHI RAS, nakriv@mail.ru, nsvirsk@mail.ru, aalex06@ inbox.ru*

[2]*MSU, anton.latyshev@gmail.com, yanab66@yandex.ru*

[3]*IPE RAS*

[4]*VSEGEI, bbelyatsky@mail.ru*

[5]*Geological Institute, KSC RAS, Tamara@geoksc.apatity.ru*

[6]*IGEM RAS, brgon@mail.ru*

[7]*Perm University, dolgal@mi-perm.ru*

The Noril'sk deposits take outstanding place among magmatic deposits due to their enormous Ni and PGE reserves. They are different from other PGE-Cu-Ni deposits around the world because they are spatially associated with the world's largest continental Siberian trap province (251 Ma, Kamo et al., 2003) and related to thin (100-150 m) basic-ultrabasic intrusive bodies in contrast with large Proterozoic plutons (Naldrett, 2004). The high economic value and unusual geological structure of the Noril'sk deposits arise a question on their origin which is discussed during several decades.

The modern widespread model of deposits origin suggests the ore formation inside an open magmatic system (Rad'ko, 1991; Naldrett, 2004; Li et al., 2009;) where Noril'sk intrusions are horizontal parts of magma conduits s to the surface. It is based on the geochemical similarities of basalts and ore-bearing intrusions and suggests the essential contamination of sedimentary rocks by magmas. This model does not take into account the position of intrusions inside the Siberian platform and does not explain the selective mineralization of some intrusions in comparing with thousands intrusive bodies located around the province. The last problem was regarded in many Russian publications (Godlevsky, 1959; Malitch et al., 1987; Dyuzhikov et al., 1992) where ore origin was examined within a close magmatic system. According to this model the localization of ore-bearing magmas was controlled by deep faults which served the channels for mantle magmas to the upper crust (Likhachev, 2006). These faults are concentrated in the north-western part of the platform, inside the paleorift zone (Malitch et al., 1987).

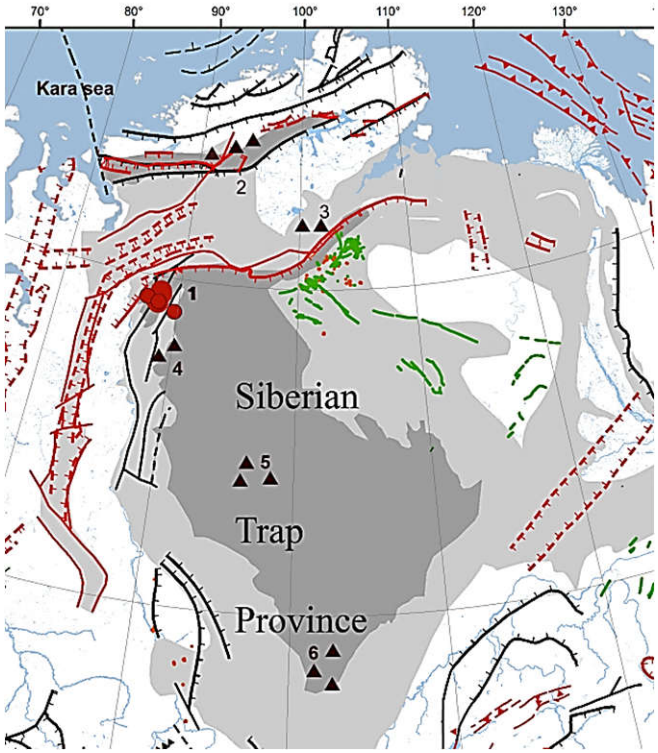

Fig. 1. Position of the studied intrusions inside the Siberian trap province.
Areas: 1-Noril'sk, 2-Taimyr, 3-Maymecha-Kotuy, 4- r. Kulyumder valley, 5 – r. Lower Tunguska valley, 6 – Angara-Tasseva depression. Colors: dark grey – magmatic rocks of the trap formation, light grey – sedimentary rocks. Lines: red – rift zones, black – main fault zones, green-dikes. Red circles are Cu-Ni deposits.

The last concept needs in some corrections because new data have been recently obtained. Firstly, it was demonstrated that the ore-bearing intrusions are characterized by crust geochemical features (Nesterenko & Al'mukhamedov, 1973; Geology and…, 1994), secondly, many faults of the Noril'sk area are not mantle-penetrating. Thus, parental magmas for the Noril'sk ore-bearing intrusions could not directly derive from the mantle.

To understand better the origin of the Noril'sk deposits it is important to analyze magmatic and tectonic features of this area in comparing with the other regions of the Siberian trap province. For this purpose we studied intrusive and effusive rocks (paleomagnetic and geochemical data) inside the six areas of the province: 1-Noril'sk, 2-Taimyr, 3- Maymecha-Kotuy, 4- r. Kulyumber valley, 5 – r. Lower Tunguska valley, 6 – Angara-Tasseva depression (Fig. 1) located in different tectonic structures.

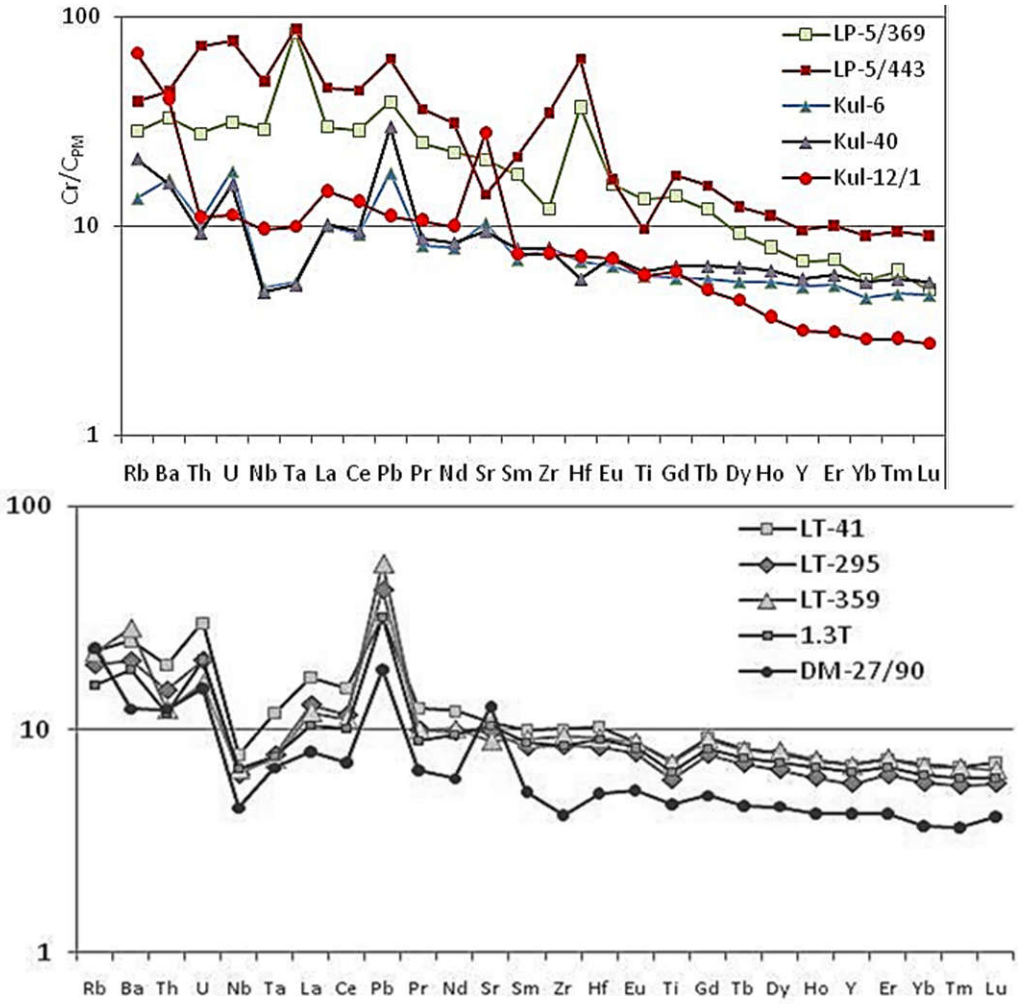

Fig. 2. Spider-diagrams for intrusive rocks from the key areas of the Siberian trap province: (a) Taimyr and r. Kulyumber valley, (b) r. Lower Tunguska valley. Samples: (a) LP-5/369, LP-5/443 – central Taimyr; Kul-6, Kul-40, Kul-12/1 – r. Kulyumber; (b) LT-41, LT-295, LT-359 –r.Lower Tunguska; 1.3 T – Angara-Tasseva sincline; DM-27/90 – Noril'sk area (Noril'sk 1 intrusion).

Particular attention was paid to intrusive rocks from these areas, in which contents of the major, rare elements and radiogenic isotopes were determined. 23 intrusions outside the Noril'sk area have been studied. It has been established that the maximum diversity of compositions is typical of the intrusions of the northern part of the province, namely, the Noril'sk, Maymecha-Kotuy and Taymyr regions (Fig. 2a), while the intrusions of the southern part (Angara-Taseeva syncline and valley of the Lower Tunguska river, mainly referred to as the Katangsky complex) are characterized by consistency of geochemical parameters (Fig.2b). Despite they are coeval to the intrusions of the Norilsk complex as suggested from paleomagnetic data (Latyshev et al., 2018) and have similar distribution of rare

elements (Fig.2b, sample DM-27/90 is gabbro-dolerite from the Noril'sk 1 ore-bearing intrusion, LT samples are intrusions from river Lower Tunguska valley) they differ significantly in geochemistry due to elevated titanium concentrations (1.2 - 1.6 TiO_2 wt.%) and ε_{Nd} (+ 1.0 - + 3.8) and low MgO contents (6 wt.%) in comparison with the average values for the intrusions of the Noril'sk complex (0.9 wt% TiO_2, ≥10 wt.% MgO and ε_{Nd} ±1).

The Angara-Taseeva sincline is characterized by the presence of large intrusive bodies (sills). Sometimes, they stretch for hundreds of kilometers and reach thicknesses of up to 400 m. Nevertheless, they are not or weakly differentiated and are composed of ordinary gabbro that is similar in composition to the intrusions of the Katangsky complex. But all of these sills have reverse polarity in contrast with Noril'sk intrusions and, probably, they emplaced just after the termination of the main stage of the volcanic activity in the Siberian platform. The Kulyumber area is located on the border of the Noril'sk region and Tunguska syneclise, so the both types of intrusions typical of these areas were found here (Fig. 2a).

Analysis of intrusions location indicates that ore-bearing massifs are situated only within the paleorift zones. Based on the medium-scale gravimetric and magnetic survey data (1: 200000 scale), the submeridional Noril'sk-Igarka paleorift system, which has high values of the gravitational field and a width of approximately 100-200 km, borders the ancient craton (Dolgal et al., 2006; Dolgal, 2012) and was identified on the northwestern margin of the Siberian platform. This paleorift zone with Kulyumber and Dyupkum branches, as the Yenisei-Khatanga trough, are characterized by the maximum diversity of igneous rocks with elevated MgO. They represent long-lived zones developed on substrate enriched in sulfur. Cu-Ni ores relate to products of crystallization both mantle and crustal parental magmas and were formed as a result of successive geological processes.

References

Dyuzhikov O. A.. Distler V. V.. Strunin B. M. et al. Geology and metallogeny of sulfide deposits Noril'sk region USSR. 1992. Econ Geol. Monogr 1. Ontario. Spec. Volume. 241 p.

Geology and ore deposits of the Noril`sk region. Guidebook of the VII International Platinum Symposium. 1994. Moscow: Moskovsky contact Press.

Godlevsky M.N. Traps and ore-bearing intrusions of the Noril'sk district. 1959.Moscow: Gosgeoltekhizdat. 61p.(in Russian).

Kamo S.L.. Czamanske G.K.. Amelin Y. et al. Rapid eruption of Siberian flood-volcanic rocks and evidence for coincidence with the Permian-Triassic boundary and mass extinction at 251 Ma.// Earth Planet. Sci. Lett. 2003. Vol.214. pp.75–91.

Latyshev A.V., Veselovskiy R.V., Ivanov A.V. Paleomagnetism of the Permian-Triassic intrusions from the Tunguska syncline and the Angara-Taseeva depression Siberian Traps Large Igneous Province: evidence of contrasting styles of magmatism. Tectonophysics. 2018. 723. pp.41-55.

Li C.S.. Ripley E.M.. Naldrett A.J. A new genetic model for the giant Ni–Cu-PGE sulfide deposits associated with the Siberian flood basalts. //Economic Geology. 2009. V.104. pp. 291–301.

Likhachev A.P. Platinum–Copper–Nickel and Platinum Deposits. Moscow: Eslan.2006.496 p.(in Russian).

Malitch N.S.. Mironyuk E.P.. Tuganova E.V. et al. Geological structure of the USSR and regularities of distribution of mineral deposits// "The Siberian Platform". 1987. V.4. Leningrad: Nedra. pp. (in Russian).

Naldrett A.J. Magmatic sulphide deposits. Geology. geochemistry and exploration. 2004. Berlin. Heidelberg. New York: Springer. 727 p.

Nesterenko G.V., Al'mukhamedov A.I. Geochemistry of differentiated traps. 1973. Moscow: Nauka. 187 p. (in Russian).

Rad'ko V.A. Model of the dynamic differentiation of intrusive traps from the Northwestern Siberian Platform: Geology and Geophysics. 1991. N 11. pp. 19–27. (in Russian).

SOURCES OF MATTER FOR RARE METAL PEGMATITES OF THE GREENSTONE BELT KOLMOZERO-VORONYA (KOLA REGION): ISOTOPE-GEOCHRONOLOGICAL STUDY OF TOURMALINE-MUSCOVITE GRANITES

***Kudryashov N.M.*[1], *Udoratina O.V.*[2], *Coble M.A.*[3], *Steshenko E.N.*[1]**

[1]*Geological Institute of Kola SC RAS, Apatity, Russia, nik@geoksc.apatity.ru*

[2]*Institute of Geology of Komi SC UB RAS, Syktyvkar, udoratina@geo.komisc.ru*

3Stanford University, USA, coblem@stanford.edu

An important task of study of rare metal pegmatites is the establishment of their genetic relations with granites, if any, and the determination of the time of occurrence of the ore mineralization. To address these questions, we connected zircon U-Pb geochronology aimed at determining the time of formation of both the granites ancestral for the pegmatites and the pegmatites themselves.

The Kolmozero-Voronya greenstone belt is confined to the central part of the suture zone separating the Murmansk domain from the Central Kola and Keivsky domains. The belt is represented by Late Archaean sedimentary-volcanogenic rocks (2.9-2.5 Ga). Within its limits the deposits of rare metal pegmatites (Li, Cs with associated Nb, Ta, Be) are concentrated. The pegmatite fields are located among amphibolites and gabbroic intrusions in the north-western and south-eastern parts of the belt. The age of the pegmatites within the belt, according to the available U-Pb datings for monazite and Rb-Sr isochronous method for bulk samples, was estimated at 2.7-2.6 Ga . Until now there is no generally accepted view on the genetic affiliation of the pegmatites. Various authors suggest association of the pegmatites with all types of granitoids within the region: plagiogranites, tonalites, amphibole-biotite granodiorites, microcline granites, alkaline granites, and also muscovite-tourmaline granites. The connection of the rare metal pegmatites with the processes of granitization has been also suggested to be associated with the formation of microcline granites (palingenic metasomatic granites).

Prior to this study, isotope dating has been obtained for a number of rock complexes, which may be possible candidates for the role of source granites for the rare metal pegmatites. These rocks belong to the differentiated sanukitoid Porosozersky massif represented by a series of gabbrodiorite - quartz monzodiorite - granodiorite - microcline-plagioclase granite. U-Pb (ID TIMS) age of the zircon from the rocks of the series is within the range of 2.73-2.68 Ga (Kudryashov et al., 2013). The age of the plagiogranites and tonalites from the Murmansk block, framing the rocks of the Kolmozero-Voronya greenstone belt, is defined as Late Archaean 2.8-2.7 Ga. The massifs of alkaline granites, located within the Keyvsky block, have the age of 2.65-2.67 Ga (Zozulya et al., 2005). Zircon in the pegmatites is overwhelming represented by broken crystals fragments due to fluid processes, and cannot be reliably used as a geochronometer to determine the crystallization age of the pegmatites. The use of non-traditional minerals-geochronometers with specially developed methods of separation of uranium and lead, allow estimating the time of formation and/or alteration of the pegmatites. The isotope-geochronological studies of tourmaline (shorl) from muscovite-tourmaline are Pb-Pb isochronous age of 2520±70 Ma. From the sample of the pegmatites taken from the Vasin-Mylk pits, tantalite and microlite were isolated for U-Pb isotope-geochronological study. The grains of tantalite and microlite are characterized by intraphase heterogeneity reflecting postcrystallization processes of changes of the mineral, probably metamictization. For the tantalite, a discordant age 2503±36 Ma was obtained, and for the microlite, a discordant age was 2454±8 Ma (Kudryashov et al., 2015). The obtained values ages of the tantalite and microlite possibly fix the time of crystallization of these minerals during the formation of rare metal pegmatites at the Archaean-Proterozoic boundary.

To determine the U-Pb crystallization age of zircon from the tourmaline-muscovite granites, a local isotope-geochronological study of the zircon grains was performed at the Stanford University and U.S. Geological Survey SHRIMP-RG microprobe. The isolated zircon from the tourmaline-muscovite granite sample (KV-76) is represented by slightly modified brownish crystals of zircon type with the size 100-150 μm. The internal structure is characterized by the intraphase heterogeneity expressed both as the alternation of dark and light zones in the marginal parts of grains, and as diffused dark spots in the center of the grains. The contours of the zones are blurred, rectilinear and, apparently, reflect the

growth of the crystals from the melt. The Pb-U isotope results of the analyzed zircon grains are shown in Fig. 1.

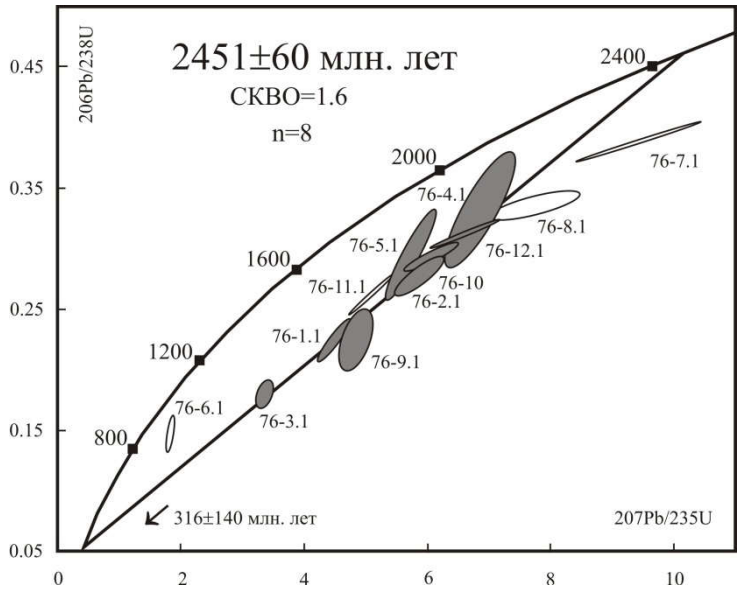

Fig. 1. Diagram with concordia for the tourmaline-muscovite granites. Gray ellipses - analytical data included in the calculation of the discordia; transparent ellipses - not included in the calculation.

The discordant age, calculated for 8 analyzed points of zircon, was 2451±61 Ma, MSWD=1.6. As can be seen in Fig. 1, the analytical points are strongly discordant, which indicates the original U-Pb system is not in equilibrium. The zircon is highly enriched in uranium - 2500-3000 ppm and has low U/Th=0.01-0.04, which possibly indicates the metasomatic processes. Thus, the upper intersection of the discordia with an intercept age of ~2.45 Ga likely reflects the crystallization time of zircon during the formation of the tourmaline-muscovite granites, and the high discordance is associated with a subsequent change in the zircon.

Zircon from the sample (KV-45) was extracted from the central part of the intrusion of tourmaline-muscovite granites of lake area Litsa (Gordienko, 1970). Grains are represented by slightly modified brown crystals of zircon type with the size of 100-200 μm. The internal structure is characterized by intra-phase heterogeneity. The central parts of the grains are light and translucent, rims dark and opaque. In the center of the individual grains is observed thin zoning. The Pb-U isotope results of the analyzed zircon grains are shown in Fig. 2. The discordant age, calculated for 8 analyzed points of zircon, was 2726±9 Ma, MSWD=2.5. The isotope age of the analytical data for the three points (45-4.1, 45-6.1 and 45-3.1) with respect to 207Pb/206Pb was in the range of 2.9-2.8 Ga and was not taken into account for the discord. The analytical points are sufficiently discordant and indicate a violation of the U-Pb system, due to the removal of lead. Zircon is enriched with U - 950-2500 ppm and has a low ratio of U/Th = 0.03-0.08. For three ancient zircon values, this ratio is higher than U/Th = 0.14-0.45. Thus, the upper intersection of the discord with a concordia with an age of 2726±9 Ma, probably reflects the crystallization time of zircon during the formation of tourmaline-muscovite granites. Older values of the age of zircon, apparently, can indicate both the presence of an ancient component preserved in zircon, and the xenogenic of zircon.

Zircon from the sample (KV-45) was extracted from the central part of the intrusion of tourmaline-muscovite granites of lake area Litsa (Gordienko, 1970). Grains are represented by slightly modified brown crystals of zircon type with the size of 100-200 μm. The internal structure is characterized by intra-phase heterogeneity. The central parts of the grains are light and translucent, rims dark and opaque. In the center of the individual grains is observed thin zoning. The Pb-U isotope results of the analyzed zircon grains are shown in Fig. 2. The discordant age, calculated for 8 analyzed points of zircon, was 2726±9 Ma, MSWD=2.5. The isotope age of the analytical data for the three points (45-4.1, 45-6.1 and 45-3.1) with respect to 207Pb/206Pb was in the range of 2.9-2.8 Ga and was

not taken into account for the discord. The analytical points are sufficiently discordant and indicate a violation of the U-Pb system, due to the removal of lead. Zircon is enriched with U - 950-2500 ppm and has a low ratio of U/Th = 0.03-0.08. For three ancient zircon values, this ratio is higher than U/Th = 0.14-0.45. Thus, the upper intersection of the discord with a concordia with an age of 2726±9 Ma, probably reflects the crystallization time of zircon during the formation of tourmaline-muscovite granites. Older values of the age of zircon, apparently, can indicate both the presence of an ancient component preserved in zircon, and the xenogenic of zircon.

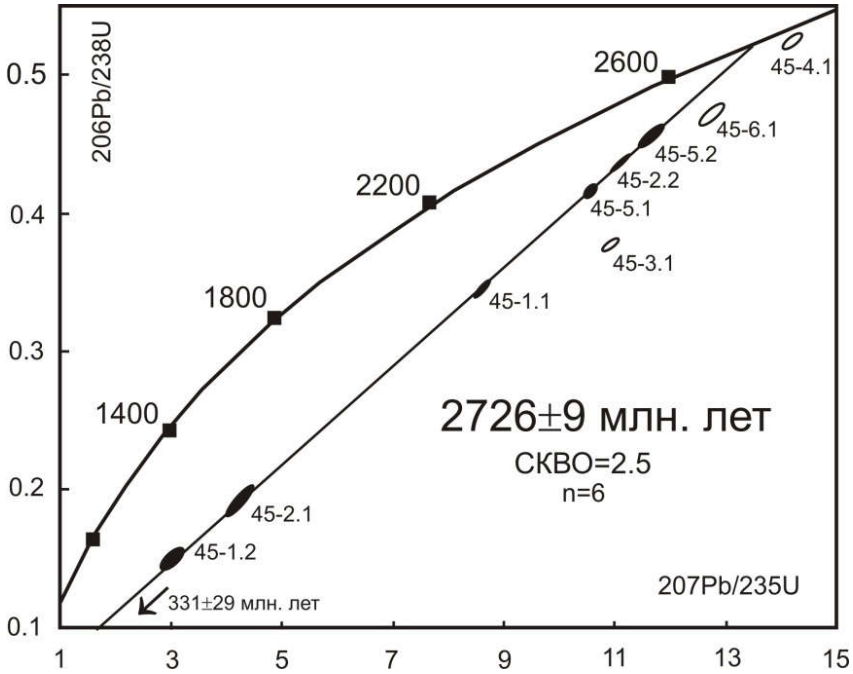

Fig. 2. Diagram with concordia for the tourmaline-muscovite granites. Gray ellipses - analytical data included in the calculation of the discordia; transparent ellipses - not included in the calculation.

The obtained zircon ages from two tourmaline-muscovite intrusions located in the northwestern and southeastern parts of the greenstone belt of Kolmozero-Voronya reflect the different stages in the formation of these granites. Thus, rare-metal pegmatites of the sodium-lithium type of the Kolmozero deposit were replaced in time by the development of lithium-cesium type pegmatites.

The studies were carried out with the financial support of the Russian Foundation for Basic Researches, grant No. 16-05-00367. The state project No. 0231-2015-0005.

References

Gordienko V.V. Mineralogy, geochemistry and genesis of spodumene pegmatites. Leningrad: Nedra, 1970. 240 p. (in Russian).

Kudryashov N.M., Lyalina L.M., Apanasevich E.A. Age of Rare-Metal Pegmatites from the Vasin_Myl'k Deposit (Kola Region): Evidence from U–Pb Geochronology of Microlite // Doklady Earth Sciences. 2015. V. 461. Part 2. P. 321–325.

Kudryashov N.M., Petrovsky M.N., Mokrushin A.V. and Elizarov D.V. Neoarchean Sanukitoid Magmatism in the Kola Region: Geological, Petrochemical, Geochronological, and Isotopic–Geochemical Data // Petrology. 2013. V. 21. № 4. P. 351–374.

Zozulya D. R., Bayanova T.B., Eby G.N. Ceology and Age of the Late Archean Keivy Alkaline Province, Northeastern Baltic Shield // Journal of Geology. 2005. V. 113. P. 601-608.

KARELIA'S ALKALINE AND MODERATELY ALKALINE MASSIFS AS SOURCES OF RARE-EARTH ELEMENTS

Kuleshevich L.V., Dmitrieva A.V.
IG KaRC RAS, Petrozavodsk, kuleshev@krc.karelia.ru; dmitrievaa-v@yandex.ru

Most known promising ore bodies in Karelia's alkaline and moderately alkaline rocks are complex, containing Ti, P, REE, Ba, Sr, Zr, Nb and other rare metals. Rare-earth (REE) and rare element (RE) concentrations in the rocks were estimated by ICP-MS analysis, concentrator minerals were studied on a VEGA II LSH, Tescan electron microscope with an EDS INCA Energy 350 attachment at IG KarRC EAS, Petrozavodsk. The highest REE concentrations were estimated in the following major types of alkaline and moderately alkaline ores (Kuleshevich & Dmitrieva, 2015; Mineral.., 2005): 1 – moderately alkaline granites, pegmatites and associated metasomatic rocks (feldspar, skarns, greysens) of AR and PR age; 2 – Neoarchean differentiated moderately alkaline gabbro-pyroxenite-syenite massifs of the Syargozero complex (0.13-0.14 %); 3 – ultramafic alkaline pegmatoid rocks of the Yeletozero and carbonatites of the Tiksheozero massifs (ΣREE 0.36 %); 4 – ultramafic alkaline rocks and titanite-apatite ores of the Elisenvaara complex (0.22-1.7 %); 5 – Riphean rapakivi granites and associated metasomatic rocks; 6 – lamproites of the Kostomuksha structure.

REE and their mineral associations in Karelia's alkaline and moderately alkaline complexes and associated metasomatic rocks.

West Karelia's Archean *granites, pegmatites and K-feldspar metasomatic rocks* contain elevated ΣREE concentrations of 0.13-0.41 %.

Neoarchean moderately alkaline massifs of gabbrio-pyroxenite-monzonite (Panozero, Elmus) and gabbro-pyroxenite-syenite (Syargozero, Sharavalampi and West Khizhjarvi) composition contain elevated REE (particularly LREE) concentrations. Maximum rare-earth concentrations are typical of an early gabbro-pyroxenite phase and alkaline metsomatic rocks after them that accompany the formation of a late monzonite-syenite phase. As silicic acid concentration in the rocks increases, REE concentration decreases. Total REE concentration in pyroxenites and gabbro of the Syargozero and Sharavalampi complexes, which have combined to form the Syargozero complex, varies from 584 to 1458 ppm, that of the West Khizhjarvi complex from 447 to 588 ppm, that of the Panozero complex from 172 to 494 ppm and that of the Elmus complex from 399 to 1342 ppm. ΣREE concentration in later-phase monzodiorites, monzonites and syenites is 200-600 ppm. Apatite, titanite, epidote, allanite and later REE-F-carbonat are concentrator minerals of rare earths. Moderately alkaline complexes also typically contain high Ba (2200-4300 pmm) and Sr (1700-4000 ppm) concentrations. They are part of K-feldspar, barite and celestine.

The Tiksheozero-Yeletozero alkaline-ultramafic rock complex in North Karelia combines the Yeletozero and Tiksheozero massifs. The 2.086 Ga Yeletozero massif is differentiated from ultrabasic rocks to nepheline syenites, while the Tiksheozeo massif also comprises carbonatites. Associated with alkaline-ultramafic rocks are various types of useful minerals such as titanomagnetite and apatite ores, carbonatites and feldspar, phlogopite as well as RE and REE mineralization. All differentiates of the complex, particularly pegmatites, are enriched in LREE. Ore gabbro-pyroxenites contain 0.26 % SrO and up to 2.7 % BaO. ΣREE in titanomagnetite ore does not exceed 38-140 ppm; at the contact with alkaline pegmatites ΣREE increases to 970 ppm. Apatite-bearing ore contains 0.15-0.56 % Nb_2O_5, 0.01-0.015 % Ta_2O_5, 0.13-1 % ZrO_2, 0.0046-0.03 % Hf and 0.1-036 % ΣREE (Yeletozero-1 occurrence).

The Karbonatitovoye deposit in the Tiksheozero massif is confined to the boundary of two blocks. Carbonatites form a steeply dipping body elongated in a N-S direction (Shchiptsov et al., 2012). Carbonatites contain 70-90 % calcite, 5-20 % apatite, 5-10 % dolomite, 5-7 % oxides (magnetite, ilmenite, Cr-Fe-oxides), 1-3 % phlogopite, ~1-4 % pyroxenes and amphiboles and rare accessories. Evolving at the exocontact and around xenoliths are zonal metasomatic rocks. Forming after phase-I pyroxenites are amphibole-carbonate metasomatic rocks; forming after alkaline rocks are biotite-phologopite and high-Ca metasomatic rocks enriched in rare accessories (baddeleyite, zircon,

pyrochlore and REE-minerals). Average P_2O_5 concentration in apatite ore is 2.94-4.18 % (до 16.2 %). Associated with them are the highest Sr and REE concentrations. Sr is part of Sr-apatite, Sr-carbonates (ancylite and carbocernaite) and Sr-barite. Sr concentration (1317-4163 ppm) is correlated with apatite concentration. REE (Σ 970-1250 ppm) in apatite ore is concentrated by phosphates and carbonates such as apatite, monazite, rabdophanite, bastnesite, synchisite, ancylite, carbocernaite (Kuleshevich et al., 2015). Zr is regularly distributed, its major phases are baddeleyite and zircon. Zr concentration in amphibole-phologopite carbonatites is up to 337-1000 ppm and Hf concentration is up to 12.6 ppm. Nb concentration varies from 8 to 930 ppm and Ta concentration from 1 to 35.5 (Nb/Ta =30÷9). Y concentration is 15-48, Th concentration is 3-30 and U concentration is 0.3-1.7 ppm. Higher U concentrations (up to 255 ppm) are associated with the presence of U-betafite and hatchettolite. Pyrochlore and betafite contain up to 0.8-5.92 % Ce. Carbonate-feldspar metasomatic rocks contain Zr-perovskite, strontiobarite and strontianite.

The Elisenvaara complex (~1.775 Ga), located in the NW Lake Ladoga area, consists of the Kaivomäki and Raivomäki massifs. It has been studied in detail by R.A. Khazov (1993). The alkaline complexes are differentiated from ultramafic to mafic and intermediate rocks. The highest REE concentrations are associated with ladogalites (local rock names), toensbergites and Ba-Sr-P-Ti ores in them. The typomorphic minerals of these rocks are clinopyroxene, amphibole, K-feldspar with microperthite (up to 20-80 % in various differentiates), titanite, apatite and accessory REE and RE-minerals. P_2O_5 concentration is 0.43-10.5 % (average 2.5-5 %), SrO concentration is 0.45-2.2 %, BaO concentration is 0.23-2.0 % and F concentration is 0.12-1.5 %. Ba and Sr are part of K-feldspar. Rocks of the complex contain (in ppm): ΣREE 1307-10380, Y 50-170, Nb 10-128, Ta 0.4-9, Ga 166-346, Th 10-77, Zr 120-940, Hf 2-14.7 (Kuleshevich et al., 2014). ΣREE is 1.36 % in apatite concentrates and 1.7 % in titanite concentrates. R.A. Khazov estimated REE resources at 15 Mt (average ΣREE concentration is 0.25 %). REE-concentrator minerals are represented by phosphates (monazite and TR-apatite), silicates (titanite, allanite and TR-epidote) and carbonate. REE-enriched zonal titanite predominates in mafic rock varieties. Zircon and baddeleyite prevail in differentiates with perthitic Ba-Sr-feldspar. Formed at the low-temperature stage of rock alteration are late and rare minerals such as lantanite, bastnesite and Ca-Sr-Ce-carbonates.

Early Riphean (~1.54 Ga) *Salmi and Ulyalega moderately alkaline rapakivi granite massifs* are located in South Karelia and in the NE Lake Ladoga area (Larin, 2011). They contain elevated REE and Y concentrations. Phase-1 and 2 granites carry ΣREE (180-1050 ppm), Nb (16-103), Ta (1.3-38), Zr (190-632), Hf (up to 6-16.4), Sr (21-100), Ba (60-1400), Rb (123-437) and Y (60-325 ppm) (Y concentrations in phase-2 rocks are as high as 0.1 %), (Kuleshevich & Dimitrieva, 2017). Confined to the massifs are small occurrences (ΣREE – 0.12-0.63 %) such Myuzilambi, Kamen-navolok, Sodder, Kairoilampi. Phase-2 granites in the Salmi massif aureole are accompanied by greysens resting on skarns. Greysens of the Lyupikko occurrence, in the aureole of phase-2 Li-F-granites contain 0.1 % Y and up to 0.1 % Yb. The granites contain monazite, xenotime, bastnesite, parisite, zircon, uraninite, Y-Zr-bearing thorite, Y-Th-Zr-silicate-phosphates and fluorite. Bastnesite accompanies later low-temperature alterations of the granites and grows onto Y-bearing monazite (Y 0.1 %) (Kuleshevich & Dmitrieva, 2017). Phase-2 granites and greysenized skarns of ore occurrences typically display elevated Be, Sn, Mo, W, Bi, Th, U, REE and Y concentrations. Uraninite is often overgrown with Y-thorite rim. Li-F-granites and pegmatites contain aeshynite, fergusonite, monazite, pyrochlore, zircon, allanite, tantalite-columbite, xenotime and bastnesite. REE carbonates and TR-bearing coffinite are occasionally encountered in the weathering crust of the Salmi massif and at the Karku U-deposit in overlying Riphean rocks.

Lamproites (1.23 Ga) of the Kostomuksha structure form several clusters (Taloveis, Kostomuksha and Korpanga) that comprise 50 dykes. RE concentrations in the lamproites (in ppm) is: ΣREE 1275-1300, Nb 223, Ta 10, Zr 933, Y 25, Sr 2950 and Ba 2346. As the dykes are thin and short, they are not promising.

The mineralogical and geochemical study of rocks and ore samples from moderately alkaline complexes with elevated REE concentrations, conducted by the Institute of Geology, KarRC, RAS,

under a research programme, is expected to contribute to the discovery of occurrences promising for REE and their forecast evaluation in Karelia's Precambrian rock sequences.

References

Dmitrieva A.V. Metallogenic specialization of Neoarchean moderately alkaline magmatism in Central Karelia // Abstract. 2017. 20 p.

Kuleshevich L.V. Rare-earth mineralization of the Tiksheozero-Yeletozero alkaline complex, North Karelia // Geology and useful minerals of Karelia. Petrozavodsk. 2016. No. 18. P. 71-87.

Kuleshevich L.V. & Dmitrieva A.V. Mineral associations and ore types of REE in Karelia // «Mineralogy as meant by this word». Proceedings of the 12th Congress of the Russian Mineralogical Association, 12-16 October. 2015. S-Pb. P. 116-118.

Kuleshevich L.V. & Dimitrieva A.V. Rare-earth mineralization in alkaline and moderately alkaline intrusive complexes of the northern Lake Ladoga area, Karelia // «Deep structure and geodynamics of the Lake Ladoga area (Priladozhye)». Proceedings of the All-Russian Conference. Petrozavodsk. 2017. P. 110-114.

Kuleshevich L.V., Dmitrieva A.V., Khazov R.A. Ba-Sr-P-Ti-TR-feldspar raw material of the Elisenvaara alkaline complex, Karelia: geochemistry and mineralogy of rare-earth elements // Uchenye zapiski PetrGU. Series: Natural and technical sciences. 2014. No. 4. P. 67-70.

Larin A.M. Rapakivi granites and associated rocks. S.-Pb: «Nauka». 2011. 402 p.

Mineral resources of the Republic of Karelia / Mikhailov V.P. & Aminov V.N., Eds. Petrozavodsk: «Karelia». 2005. Book 1. 278 p.

Shchiptsov V.V., Bubnova T.P., Garanzha A.V., Skamnitskaya L.S., Shchiptsova N.I. Geologo-technological and economic evaluation of carbonatite resources in the Tiksheozero massif (ultramafic-alkaline rock and carbonatite formation) // Geology and useful minerals of Karelia. 2007. No 10. P. 159-170.

MINERAL COMPOSITION OF THE ALKALINE TRACHYANDESITES OF THE LATE DEVONIAN OF BELARUS (PARAMETRIC WELL PRYBOR)

Kuzmenkova O.F.[1], Laptsevich A.G.[1], Nosova A.A.[2], Yutkina E.V.[2], Pospelov A.V.[3]

[1]State Enterprise "Research and Production Center for Geology", Minsk, Belarus, kuzmenkovaof@mail.ru, laptsevich@geology.org.by

[2]Institute of Geology of Ore Deposits, Petrography, Mineralogy and Geochemistry, Russian Academy of Sciences, Moscow, Russia, nosova@igem.ru, eyutkina@gmail.com

[3]Belarusian State Technological University, Minsk, Belarus

Parametric well Prybor was drilled in 2017 at the west of the Gomel Structural Lintel. This structure joins the Pripyat Trough, the Voronezh Crystal Massif, the Zhlobin and Bragin-Loevsky Saddles at the west of the East European Platform. In the section of the well the platform cover deposits with a capacity of 965.0 m lie on the porphyry granites PR_1 and belong to the *Quaternary, Paleogene, Cretaceous, Jurassic, Triassic* and *Devonian Systems*. The *Late Devonian* alkaline volcanic formation in the borehole section is represented by: an effusive-pyroclastic stratum of the intermediate composition of the *Vasilievo Suite* D_3v, that is interbedded with terrigenous-carbonate rocks of the *Upper Frasnian Substage* D_3f_3 in the depth interval 352,7 – 723,0 m; and alkaline syenites, syenite-porphyries and nephelinites of the *Pripyat Complex* $\varepsilon,\omega\xi D_3pr$, that break through the sedimentary *Devonian* rocks in the depth interval 727,5 – 926,0 m.

The following rocks are found in the volcanogenic stratum D_3v: the alkaline orthoclase and anorthoclase trachyandesites and the lapillium xenotufs of mixed (nephelinite-trachyandesite) composition with carbonate cement of pore-basal type (Tabl.). The outflow of lavas occurred in the conditions of the sea basin (Махнач, Корзун, 1977, Веретенников и др., 2000), so rocks are characterized by carbonatization (dolomite, calcite). The most carbonatization is manifested in the orthoclase trachyandesites, that form coverlets with a thickness of 3,0 – 39,0 m; and the least

carbonatization – in anorthoclase trachyandesites composing the powerful (64,0 m) cover (or dome) in the range of 590,0 – 654,0 m. The mineral composition of anorthoclase trachyandesites was studied on a scanning electron microscope JEOL JSM-5610 LV with JED-2201 in Belarusian State Technological University (Minsk).

The aegirine-augite–hornblende anorthoclase trachyandesites are the massive rocks of dark brownish-gray color, that contain 25 – 30 vol% of porphyry phenocrysts. The rocks contain xenoliths up to 6 – 8 cm in size: biotite gneisses of the *Kulazhin Series* AR_1kl, dolomites D_2, syenites $\varepsilon\xi D_3pr$ and fine-grained hornblendites (?).

Table. 1 Chemical composition of the alkaline trachyandesites, mass%.

depth, m	rock	SiO_2	TiO_2	Al_2O_3	Fe_2O_3	MnO	MgO	CaO	Na_2O	K_2O	P_2O_5	LOI
555,0	Ort t	54,51	0,89	20,05	5,01	0,16	2,51	4,89	3,38	8,31	0,29	8,47
557,0	Ort t	54,14	0,84	20,55	6,17	0,14	2,53	3,94	3,31	8,06	0,31	6,92
558,5	Ort t	55,35	0,87	20,48	6,08	0,15	2,31	3,66	4,20	6,57	0,33	5,85
561,4	Ort t	54,47	0,92	20,05	6,81	0,11	2,49	3,42	3,04	8,37	0,33	4,95
563,8	Ort t	56,04	0,81	21,05	5,10	0,14	2,03	3,53	4,07	6,94	0,29	6,01
575,0	Ort t	55,20	0,95	20,51	4,11	0,16	1,79	5,24	4,33	7,38	0,33	6,53
679,2	Ort t	55,63	0,83	21,33	3,02	0,10	2,15	4,36	3,21	9,09	0,29	6,65
597,8	Ant t	53,65	1,41	18,02	7,45	0,17	3,13	5,05	5,45	5,16	0,51	8,14
599,3	Ant t	54,88	1,27	18,95	6,75	0,19	1,60	4,25	7,47	4,08	0,58	2,71
600,5	Ant t	53,74	1,47	18,44	8,14	0,13	2,33	4,38	4,51	6,34	0,53	4,40
602,0	Ant t	54,96	1,12	18,95	6,95	0,17	1,89	4,08	7,11	4,23	0,56	2,36
636,1	Ant t	55,13	1,18	19,24	6,75	0,15	1,54	4,20	7,54	3,73	0,54	1,91
651,7	Ant t	55,53	1,11	19,42	6,26	0,16	1,38	3,80	7,54	4,32	0,49	2,10

Analyzes performed by XRF, Axios PANalytical, Belarusian State Technological University (Minsk) and recalculated by 100%. Ort t - orthoclase trachyandesite, Ant t - anorthoclase trachyandesite.

The phenocrysts are represented by feldspar leaves of the size from 2 x 1 mm to 10 x 3 mm (15 vol% oligoclase-andesine An_{10-38} with clearly manifested direct zonality, and in an insignificant amount – anorthoclase Anrt); elongated-prismatic grains of titanium basaltic hornblende Ti-Hbl with black color (10 vol%) in size from 1 x 2 mm to 15 x 40 mm; prismatic grains of sodium augite Na-Av and aegirine-augite Aeg-Av (10 vol%) with an average size of 0,5 x 0,1 mm; envelope-shaped micro phenocrysts of sphene Sph up to 0,8 x 0,3 (1 – 2 vol%) and titanomagnetite Ti-Mt of subisometric form 0,1 – 0,5 mm in size (1 – 2 vol%).

The rock bulk mass of the trachyte structure consists of felt of feldspars microlites (50 vol%) with a size of 0,07 x 0,01 mm. Anrt (35 vol%) prevails among them, albite Ab (An_{1-3}) (about 10 vol%) and orthoclase Ort (3 – 5 vol%) are found in a smaller amount. Ab and Ort mutually germinate with the formation of a spotted perthite structure as a result of the decomposition of the solid solution. Microlites of Aeg-Av and Na-Av (15 vol%) with a size of 0,03 x 0,02 mm are weighed into the felt and Ti-Mt grains (4 vol%) less than 0,05 mm in size are uniformly scattered. In the accessory quantity there are elongated-prismatic apatite Ap grains. The presence of Ti-Mt and Ap grains in the marginal parts of Ti-Hbl and Cpx grains in the form of poikillite inclusions is haracteristical.

The direct zonation is characteristic for the Ti-Hbl grains – from the center to the edge part the content of titanium and iron increases (TiO_2 from 2,53 mass% to 5,26 mass%; FeOt from 10,9 mass% to 24,46 mass%) and the content of magnesium decreases (MgO from 13,14 mass% to 5,94 mass%), that is emphasized by an increase in the intensity of the brown color. Less common is reverse zonation, when saturated with iron and titanium nucleus are replaced by an intermediate light-colored zone, and then – with a brown ferrous fringe. Ti-Hbl contains up to 3,83 mass% SrO, up to 1,25 mass% BaO, up to 2,35 mass% Y_2O_3, up to 1,69 mass% Yb_2O_3.

Aeg-Av contain 1,57 – 5,77 mass% Na_2O and 4,60 – 12,28 mass% Al_2O_3, while Na-Av contains 0,15 – 1,25 mass% Na_2O and 2,80 – 4,77 mass% Al_2O_3. The normal zoning is manifested in the grains of both varieties of augite with increasing in the green color intensity from the nucleus to the periphery. The content of sodium and magnesium decreases (MgO from 13,14 mass% to 5,94 mass%) and the content of iron increases (FeOt from 9,64 mass% to 27,13 mass%) in the marginal parts of

grains Aeg-Av. The sodium content in the marginal parts of the Na-Av grains increases and the magnesium content decreases (MgO from 8,3 mass% to 6,64 mass%) (Fig.).

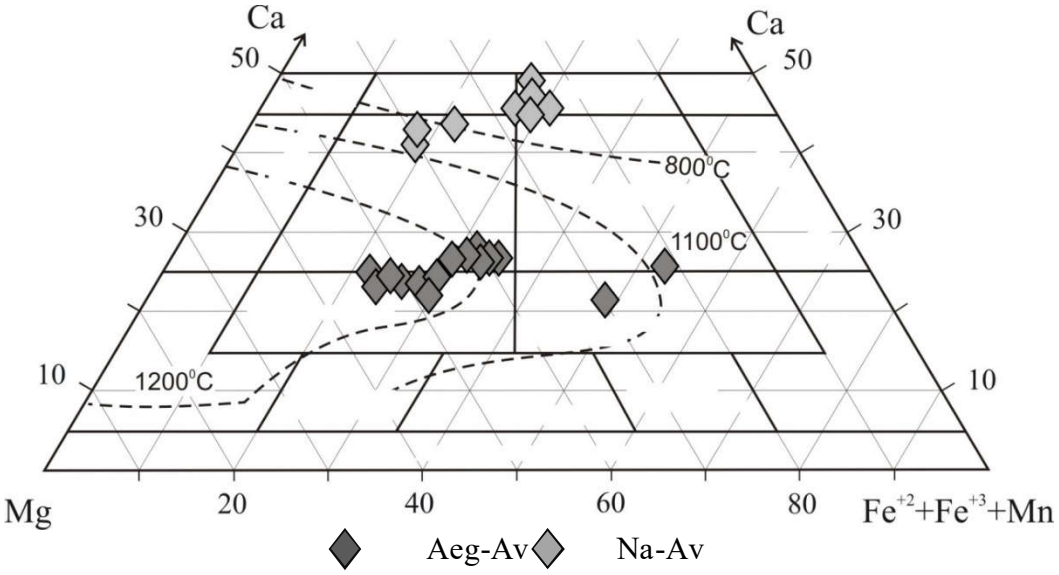

Fig. 1 Chemical composition of the pyroxenes in the coordinates Ca – Mg – (Fe^{+2} + Fe^{+3} + Mn), at%.

Sph is closely associated with Aeg-Av. It has significant contents: strontium (SrO = 2,75 – 3,08 mass%), niobium (Nb_2O_5 to 1,0 mass%) and REE (Y_2O_3 = 1,89 – 3,05 mass%). Ti-Mt contain impurities of vanadium (V_2O_5 = 0,3 – 1,19 mass%) and chromium (Cr_2O_3 = 0,15 – 1,6 mass%, up to 4,96 mass% in chromium Ti-Mt), the largest grains contain more titanium and vanadium.

In addition to synconsolidate carbonatization, hydrothermal mineralization is developed in the form of differently oriented veins and nests, that made with the pinkish-white carbonates (calcite and dolomite), the dark-violet fluorite, the pyrite powder, the fluorapatite and, to a lesser extent – analcime, quartz and hydromica.

The presence of andesine, non-alkaline amphibole – titanic basaltic hornblende, high pyroxene content (25 vol%) with SiO_2 = 53,65 – 55,53 mass% give the basis for attributing the studied rocks to trachyandesites. However, the presence of alkaline pyroxene (Aeg-Av) and a large amount of sodium feldspars (Ab and Anrt) are reflected in the increased alkalinity of the rocks (Na_2O + K_2O = 10,61 – 11,85 mass%), that has potassium-sodium type (Na_2O/K_2O = 0,71 – 2,02). The rocks are also highly potassium (K_2O = 3,73 – 6,34 mass%). The intermediat rocks of alkaline suboder with such chemical composition according to (Petrographic, 2012) refer to tephrifonolites, that contain nepheline and leucite, but it is not observed in the studied rocks.

Thus, the studied rocks by its chemical and mineral composition occupy the boundary position between the trachyandesites of the mid-alkaline suborder and tephriphonolites of the alkaline suborder and are in fact trachyandesites of the alkaline suborder.

The study was supported by the Belarusian Foundation for Basic Research (project no. X18P-109) and the Russian Belarusian Foundation for Basic Research (project no. 18-55-00006).

References

Веретенников Н.В., Корзун В.П., Махнач А.С., Лапцевич А.Г. Верхнедевонские вулканогенные образования Гомельской структурной перемычки // Докл. НАН Беларуси. 2000. Т. 44, № 5. С. 107 – 109.

Махнач А.С., Корзун В.П. Верхнедевонская щелочная вулканогенная формация Припятской впадины. Минск: Наука и техника, 1977. 161 с.

Petrographic code of Russia: magmatic, metamorphic, metasomatic, impact formations, edited by O. A. Bogatikov ... [et. al.]; translated from Russian A. V. Bobrov. – VSEGEI Press. 2012. 196 p.

COMPOSITION OF MINERALS FROM INCLUSIONS WITHIN GARNETS MEGACRYSTS FROM THE GRIB KIMBERLITE PIPE, AS EVIDENCE OF KIMBERLITE MELT EVOLUTION

***Lebedeva N.M.*[1], *Nosova A.A.*[1], *Kargin A.V.*[1], *Sazonova L.V.*[1,2], *Peresetskaya E.V.*[2], *Selutina N.V.*[2]**

[1]*Institute of Geology of Ore Deposits, Petrography, Mineralogy and Geochemistry,*

[2]*Lomonosov Moscow State University*

Large garnet crystals from kimberlite often contain polymineralic inclusions that are considered to be trapped at an early stage of the kimberlite melt modified by the host mineral during the kimberlite ascent. Therefore, one of the ways to trace down the evolution of the kimberlite melt is to study monomineralic and polymineralic inclusions in the garnets. We investigate petrographic and geochemical composition of these inclusions and host garnets from the Grib kimberlite, Arkhangelsk province.

Host garnets are split by a large amount of winding veins that can reach about ten microns in width. These veins often include isometric bulges. We can also see individual inclusions. The inclusions were found in different composite garnets: low-Cr megacrysts, middle-Cr megacrysts, high-Cr megacrysts, peridotite, eclogite A and C. Most of them have a predominant pyrope component (68-78 %) and eclogite C contains about 29 % of the pyrope component (Levedeva et al., 2018 in press).

Garnets show depletion in LREE patterns. An increase is observed in the LREE concentration from low-Cr to high-Cr megacrysts. The garnet megacrysts were in equilibrium with the enriched kimberlite melt. The absence of signs of a sinusoidal REE distribution for average and high-Cr megacrysts indicates that the garnets were in equilibrium with the LREE-enriched kimberlite melt. Low-Cr megacrysts show flat patterns of distribution near Gd. This may be due to parent peridotite. High Ti, Zr, Y contents in all megacrysts suggest that they were formed as a result of high-temperature melt-associated mantle metasomatism (Kargin et al., 2016a). The eclogite garnets show depletion in the REE distribution, which confirms that they were not in equilibrium with the kimberlite melt.

Polymineralic inclusions differ in position in the host crystal, the morphology of the inclusions and their mineral composition (Lebedeva et al., 2018 in press). The chemical variations of the minerals from the inclusions are described below.

Clinopyroxene composition from a polymineralic inclusion and a monocrystall overlap: Mg# from 0.91 to 0.89, Cr_2O_3 0.87-1.54, Al_2O_3 1.84-2.64 and TiO_2 0.30-0.53. The composition of clinopyroxene inclusions is between clinopyroxene megacrysts and clinopyroxene from garnet peridotite (Kargin et al., 2016a) and clinopyroxene from shared peridotite (Kargin et al., 2016b) (fig. 1). A single-cpx thermobarometer (Nimis, 2000) was used to obtain P–T estimates of equilibration for Cr-diopside megacrysts. The calculation showed temperatures 1082-1188°C and pressures around 5 GPa assuming that clinopyroxene was in equilibrium with garnet. The estimate temperatures are close to those of clinopyroxene megacrysts (Kargin et al., 2017).

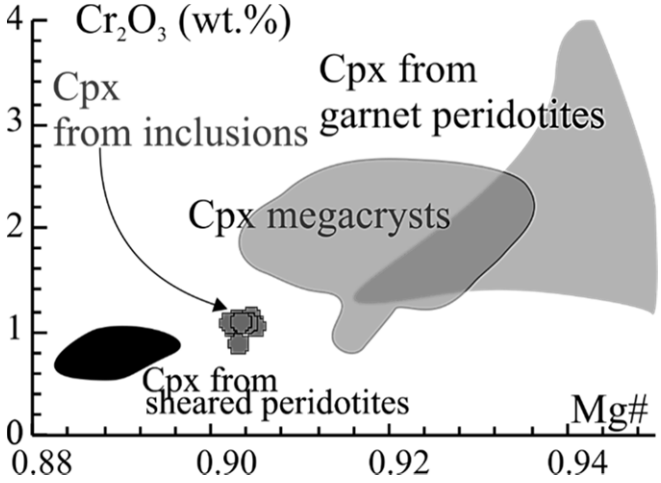

Fig. 1. Clinopyroxene (Cpx) from different associations (all from the Grib kimberlite pipe): sheared peridotites P: 7 GPa; T: 1200 °C (Kargin et al., 2016b), garnet peridotites P: 4.3-4.4 GPa (Kargin et al., 2016a); T: 730-841 °C and clinopyroxene megacrysts P: 3.6-4.7 GPa; T: 765-992 °C (Kargin et al., 2017) and clinopyroxene from poly and monomineralic inclusion within garnet.

Cr-Spinel composition with carbonate inclusions. It is the same as the kimberlite trend according to (Mitchell 1995) and they are concentrated: Cr_2O_3 32.57-37.19, Al_2O_3 3.97-5.74 and TiO_2 7.19-11.49 and Fe_2O_3 12.90 - 17.21. In addition, zonal Cr-spinels occur and they contain Cr_2O_3 12.37-37.88, Al_2O_3 9.86-52.85, TiO_2 0.39-5.22 and Fe_2O_3: 2.70-12.94.

Phlogopite is the most popular mineral, which occurs in most of the described inclusions. Phlogopite composition depends on garnet composition, grain size and its location in the inclusion. The central part of phlogopite grains from low, middle and high-Cr garnet megacrysts have a wide TiO_2 concentration range from 1.01 to 4.25 according to the garnet TiO_2 concentration and a relatively narrow Cr_2O_3 concentration range from 1.2 to 2.66 (fig. 2). The central part of phlogopite grains in an inclusion from eclogite garnets contained TiO_2 from 1.62 to 2.29 and Cr_2O_3 from 0.28 to 0.42. Towards the edge of the grain the content of Cr_2O_3 in phlogopite from megacrysts decreases. The content of Cr_2O_3 in phlogopites from eclogitic garnets increases, on the contrary. The TiO_2 content remains practically unchanged from the center to the rim. Phlogopite rims from low, medium, high-Cr megacrysts and eclogite garnets have a TiO_2 concentration from 1.25 to 3.25, Cr_2O_3 from 0.15 to 1.43.

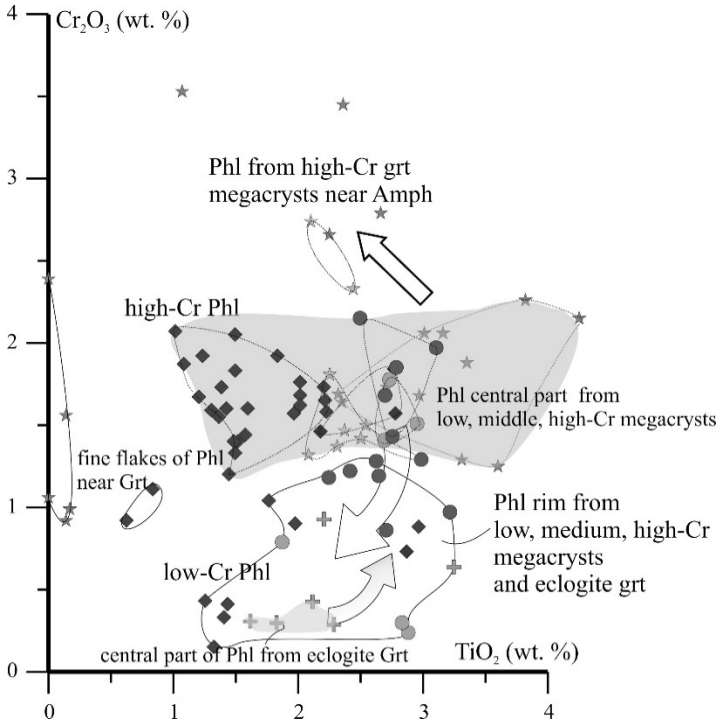

Fig. 2. Different type of phlogopite (Phl) from garnets megacrysts and eclogite garnet.

Thin flakes of phlogopite located on the rims of the inclusions have a low TiO_2 concentration near the detection limit. This type of phlogopite is in equilibrium with the host garnet.

Amphibole was formed after phlogopite, clinopyroxene and Cr-spinels. The amphiboles corresponded to the Ca-subgroup and the content of oxides varied: Na_2O from 0.14 to 3,6; Al_2O_3 from 12.49 to 20.47; Cr_2O_3 to 5.78; TiO_2 from 0.47 to 8.91. Cr_2O_3 content in the amphiboles touching the garnet are higher than in ones in the center of the inclusion.

We can suggest that the kimberlite melt evolution includes the following stages:

1) Garnet megacrysts were formed by mantle metasomatism during the first stage. Clinopyroxene, perovskite and ilmenite were probably formed then and later the garnets were captured by the host melt. The capture depth could correspond to P = 5 GPa and T around 1082-1188 °C (for Cpx, Nimis 2000).

2) Host high-Ti kimberlite melt carried megacrysts and peridotite fragments. The garnets cracked and the veinlets were formed. High-Cr phlogopite and zoned spinel were formed in these veinlets and inclusions. The garnets were probably partially melted due to the kimberlite melt.

3) Later changes occur due to the low-Cr, low-Ti and high-Ba, high-Sr post-kimberlite fluid. The phlogopite rims from garnet megacrysts and eclogite were probably composed at this stage.

Amphibole was formed in some of the inclusions. The amphibole in the inclusions may indicate the depths of their formation corresponding to P < 3 GPa, which is line with our estimates of their formation. Barite-celestine grew together into certain inclusions.

This study was supported by the Russian Foundation for Basic Research, project nos. 16-05-00298 and by the Russian President Grant for State Support of Yong Russian Scientists project nos. MK-575.2017.5.

References

Achterbergh V., Griffin W.L., Ryan C.G., et al. Melt inclusions from the deep Slave lithosphere : implications for the origin and evolution of mantle-derived carbonatite and kimberlite // 2004. T. 76.

Bussweiler Y., Stone R.S., Pearson D.G., et al. The evolution of calcite-bearing kimberlites by melt-rock reaction: evidence from polymineralic inclusions within clinopyroxene and garnet megacrysts from Lac de Gras kimberlites, Canada // Contrib. to Mineral. Petrol. 2016. T. 171.

Kargin A.V., Sazonova L.V., Nosova A.A., Lebedeva N.M., Tretyachenko V.V., Abersteiner A. Cr-rich clinopyroxene megacrysts from the Grib kimberlite, Arkhangelsk province, Russia: relation to clinopyroxene–phlogopite xenoliths and evidence for mantle metasomatism by kimberlite melts // Lithos. 2017. V. 292–293. P. 34-48.

Kargin A.V., Sazonova L.V., Nosova A.A., et al. Composition of garnet and clinopyroxene in peridotite xenoliths from the Grib kimberlite pipe, Arkhangelsk diamond province, Russia: Evidence for mantle metasomatism associated with kimberlite melts // Lithos. 2016a. T. 262.

Kargin A.V., Sazonova L.V., Nosova A.A., et al. Sheared peridotite xenolith from the V. Grib kimberlite pipe, Arkhangelsk Diamond Province, Russia: Texture, composition, and origin // Geosci. Front. 2016b.

Lebedeva N.M., Nosova A.A., Kargin A.V., Sazonova L.V., Tikhomirova Y.S., Peresetskaya E.V. The kimberlite melt composition evolution: evidence from polymineralic inclusions within garnet from the V. Grib kimberlite. Russian conference for young scientists. Irkutsk. 29 May-2 June.

Nimis P. Single clinopyroxene thermobarometry for garnet peridotites . Part I . Calibration and testing of a Cr-in-Cpx barometer and an enstatite-in-Cpx thermometer // 2000. C. 541–554.

GEOCHEMICAL AND ISOTOPIC HETEROGENEITY OF OPHIOLITES ORIGINATED IN BACK-ARC SETTINGS: AN EXAMPLE FROM THE ULTRAMAFIC-MAFIC COMPLEX OF THE MATACHINGAI RIVER, EAST CHUKOTKA, RUSSIA

***Ledneva G.V.*[1], *Bazylev B.A.*[2], *Moiseev A.V.*[1], *Sokolov S.D.*[1], *Ishiwatari A.*[3], *Kuzmin D.V.*[4,5], *Belyatsky B.V.*[6]**

[1]*Geological Institute, RAS, 7, Pyzhevski per., Moscow 119017, Russia, ledneva@ilran.ru*

[2]*V.I. Vernadsky Institute of Geochemistry and Analytical Chemistry, 19, Kosygina Str., Moscow, 119991, Russia, bazylev@geokhi.ru*

[3]*Nuclear Regulation Authority, Roppongi, Minato-ku, Tokyo 106-8450, Japan stepstone@tulip.ocn.ne.jp*

[4]*V.S. Sobolev Institute of Geology and Mineralogy, Siberian Branch Russian Academy of Sciences, 3, Akademika Koptyuga prospect, Novosibirsk, 630090, Russia, kuzmin@igm.nsc.ru*

[5]*Novosibirsk State University, 2, Pirogova str., Novosibirsk, 630090, Russia*

[6]*A.P. Karpinsky Russian Geological Research Institute, 74, Sredny prospect, 199106, St. Petersburg, Russia, bbelyatsky@mail.ru*

As known lavas erupted in different segments of back-arc spreading ridges commonly exhibit geochemical and isotopic heterogeneity (Fretzdorff et al., 2002; Pearce et al., 2005 and etc.). A main reason for such heterogeneity is a variable degree of a partial melting of originally different mantle peridotites variably enriched in subduction components as well as different conditions and mechanisms of a partial melting. Assuming similar processes in the past, geochemical and isotopic heterogeneity

can be expected to be expressed in ophiolite complexes originated in a back-arc setting, where it can be studied in both volcanic and plutonic (both mantle and crustal) rocks. Here we present one of such examples.

The ultramafic-mafic complex exposed to the north of the Kresta Bay in the basin of the Matachingai River is one of ophiolites in East Chukotka (Akinin, 1990; Kosygin et al., 1974), which are interpreted as tectonically displaced fragments of proto-Arctic Ocean lithosphere (Sokolov et al., 2009; 2014). The complex investigated is represented by several tectonic blocks restricted by nearly vertical faults of the northwestern strike, which are confined to the regional share zone of the same orientation. The blocks are locally overlain by Albian-Campanian deposits of the Okhotsk-Chukotka volcanic block and conglomerates of the lower Cretaceous molasses at the angular discontinuity (Kosygin et al., 1974). The blocks are made of a) spinel harzburgites containing rare podiform dunites and veins of pyroxenites, olivine gabbros and leucocratic gabbros, b) ±turmaline-hornblende-bearing gabbros, diorites and plagiogranites and their metamorphosed equivalents, c) volcanic-chert deposits; d) sandstones and gravels with beds of spilites, and e) chert-carbonate deposits of the upper Jurassic - lower Cretaceous. Plutonic rocks and lavas are not dated by geochronological methods; shellstones interbedded with clay limestones contain bivalves of the Valanginian. The molasses overlying tectonic blocks bear pebbles of hyperbasites, basalts and cherts (Kosygin et al., 1974).

The inner structure of blocks is poorly preserved. Spinel harzburgites with primary textures and mineral relicts compose central parts of the blocks; they are variably serpentinized and locally cut by veins of pyroxenites, olivine gabbros and leucocratic gabbros. Ultramafic rocks composing the outermost zones of the blocks are commonly replaced by talc-magnesite and quartz-magnesite rocks containing relicts of primary spinels. Gabbroic rocks occur as eluvium and colluvium deposits, their relationships with diorites and plagiogranites were not observed. The volcanic-chert deposits contain flows of pillow clinopyroxene-plagioclase porphyritic basalts.

The studies of plutonic and volcanic rocks of the complexes led us to the following conclusions:

1. Spinel harzburgites are residual mantle peridotites; pyroxenite and olivine gabbro of veins are cumulates; ±turmaline-hornblende-bearing gabbro and basalts are mixtures of quenched melts and minor amounts of cumulative minerals. These rocks constituting different tectonic blocks exhibit mineral compositions, parameters of formation, bulk geochemistry and lead, strontium and neodymium isotope compositions indicative of their formation in a setting of back-arc basin.

2. Lead, strontium and neodymium isotope compositions of plutonic rocks and basalts suggest generation of their parent melts via a partial melting of sources different in isotope composition: a) DMM (Depleted MORB mantle) reworked by subduction fluids for ±turmaline-hornblende gabbros, and b) DMM-EM I (Enriched Mantle I) reworked by subduction fluids for olivine gabbro of the vein and basalts. The latter differ from each other in εNd(t) as well. Melts trapped by mantle peridotites and dunites are geochemically enriched by the most strongly incompatible lithophile and light rare earth elements, and Cr-spinel of dunites shows Cr-number typical of that of boninites. Bulk compositions of basalts probably correspond to integral melts while melts trapped by spinel harzburgites and dunites are partial ones.

3. Assuming volcanic and plutonic rocks investigated to be nearly coeval, tectonic blocks composed of rocks different in modal composition and genesis probably represent relicts of an oceanic lithosphere of different parts of a back-arc basin but not fragments of an originally united and lately disintegrated lithospheric section.

This study was supported by RFFI (grant No 15-05-04543) and RSF (grant No 16-17-10251), whose funds were spent for geochemical and isotope investigations, respectively.

References

Akinin V.V., Miller E.L. Evolution of calc-alkaline magmas of the Okhotsk-Chukotka volcanic belt // Petrology. 2011. Vol. 19 Iss. 3 pp. 237–277.

Fretzdorff S., Livermore R.A., Devey C.W., Leat P.T., Stoffers P. Petrogenesis of the back-arc East Scotia Ridge, South Atlantic Ocean // J. Petrol. 2002 Vol. 43 No 8 pp. 1435–1467.

Kosygin Yu.A., Voevodin V.N., Zhitkov I.G., Solov'ev V.A. The east Chukchi volcanic zone and tectonic nature of volcanogenic belts // Dokl. Akad. Nauk SSSR 1974 Vol. 216 Iss. 4 pp. 885–888.

Pearce J.A., Stern R.J., Bloomer S.H., Fryer P. Geochemical mapping of the Mariana arc-basin system: Implications for the nature and distribution of subduction components // Geochemistry. Geophysics. Geosystems. 2005 Vol. 7 No 6 Q07006.

Sokolov S.D., Bondarenko G.Ye., Khudoley A.K., Morozov O.L., Luchitskaya M.V., Tuchkova M.I., Layer P.W. Tectonic reconstruction of Uda-Murgal arc and the Late Jurassic and Early Cretaceous convergent margin of Northeast Asia–Northwest Pacific. Stephan Mueller Spec. Publ. Ser. 2009 Vol. 4. pp. 273–288.

Sokolov S.D., Ledneva G.V., Tuchkova M.I., Luchitskaya M.V., Ganelin A.V., Verzhbitsky V.E. Chukchi Arctic continental margins: tectonic evolution, link to the opening of the Amerasia Basin // ICAM VI: Proceedings of the International conference on Arctic margins. St. Petersburg: VSEGEI, 2014. p. 97–113.

U-PB PYROCHLORE SHRIMP-II AGE OF THE RARE-METAL DEPOSIT OF THE TATARKA MASSIF (YENISEY RIDGE, SIBERIA)

Lepekhina E.N., Antonov A.V., Belyatsky B.V., Sergeev S.A.

A.P.Karpinsky All-Russian Geological Institute (VSEGEI), CIR, St.Petersburg, Sredniy ave., 74, Russia, avlan.online@gmail.com

The Tatarskoe niobium ore-deposit (Tatarka) is confined to the granite massif of the same name (the Yenisey Ridge, Siberia), located 85 km to the northwest of the Motygino village, in the upper reaches of the Tatarka River (58°52'36"N, 93°58'8"E). The deposit belongs to the formation of the fault-related alkaline metasomatites and carbonatites, and is controlled by the Panimbinsko-Murozhninsky fault zone, which is a branch of the Tatarskoe deep fault. Mineralization is localized in the western exocontact of the Tatar-Ayakhtin granite complex with shales and calcite marbles of the Early Proterozoic Pencheng Formation and amphibolites of the Indiglinsky complex. According to geological and structural features and spatial location several ore zones are distinguished at the deposit. Down to the depth of 150-250 m different crusts of chemical weathering are developed, to which the main part of ore bodies is confined. Morphologically, bodies are represented by lenticular and ribbon-like deposits of phosphate-niobium ores steeply dipping to the west. A total of 13 primary ore bodies and about 80 bodies located within the weathering crust are identified at the deposit. Primary ores are concordant to and sub-concordant with the host rocks and form layered and lenticular bodies, the extent of which stretches from 70 to 2450 m along the strike, and from 20 to 570 m along dip, and a thickness of 5 to 33 m. The extent of ore bodies located in the weathering crusts is up to 36-2045 m along strike and up to 90 m along the dip, with thikness at about of 3 to 109 m. The ore bodies within the weathering crust are characterized by pinch and swell, flexure curvature, and wedging out along the strike. In primary ores Nb2O5 content varies from 0.07 to 0.57%, in oxidized ores it ranges from 0.1 to 5%. The rare earths (TR2O3), tantalum (Ta2O5), strontium (SrO), rubidium, yttrium, hafnium, germanium and scandium are also present in the ores. The main ore minerals are: pyrochlore, columbite, frankolite, apatite, fluorapatite, ilmenorutil, vermiculite, iron and manganese hydroxides.

Pyrochlore is a typical accessory mineral of primary magmatic association. Light-yellow pyrochlore is most common in carbonatites and contact-reaction rocks, but red-brown variety is also found. Both varieties occur in octahedral crystals. The pyrochlore selected for the geochronological study refers to the primary magmatic association and is represented by large crystals of Ca-Na-pyrochlore (or fluornatropyrochlore, Atencio et al., 2010). Grains retain primary crystallographic forms, intergrowth imprints (Fig. 1a-b) and induction shading. Late fluorstrontiopyrochlore variety typical for the weathering crust of the Tatarka massif (Popova et al., 2017) was not detected in our samples. The internal grain structure is characterized by a homogeneity (absence of any appreciable zoning) and often a large number of apatite inclusions (up to poikilitic structure, Fig. 1c). The grains

selected for U-Pb dating are characterized by fairly chemical conformity (at the given sensitivity level of EDS method) (Fig. 1d).

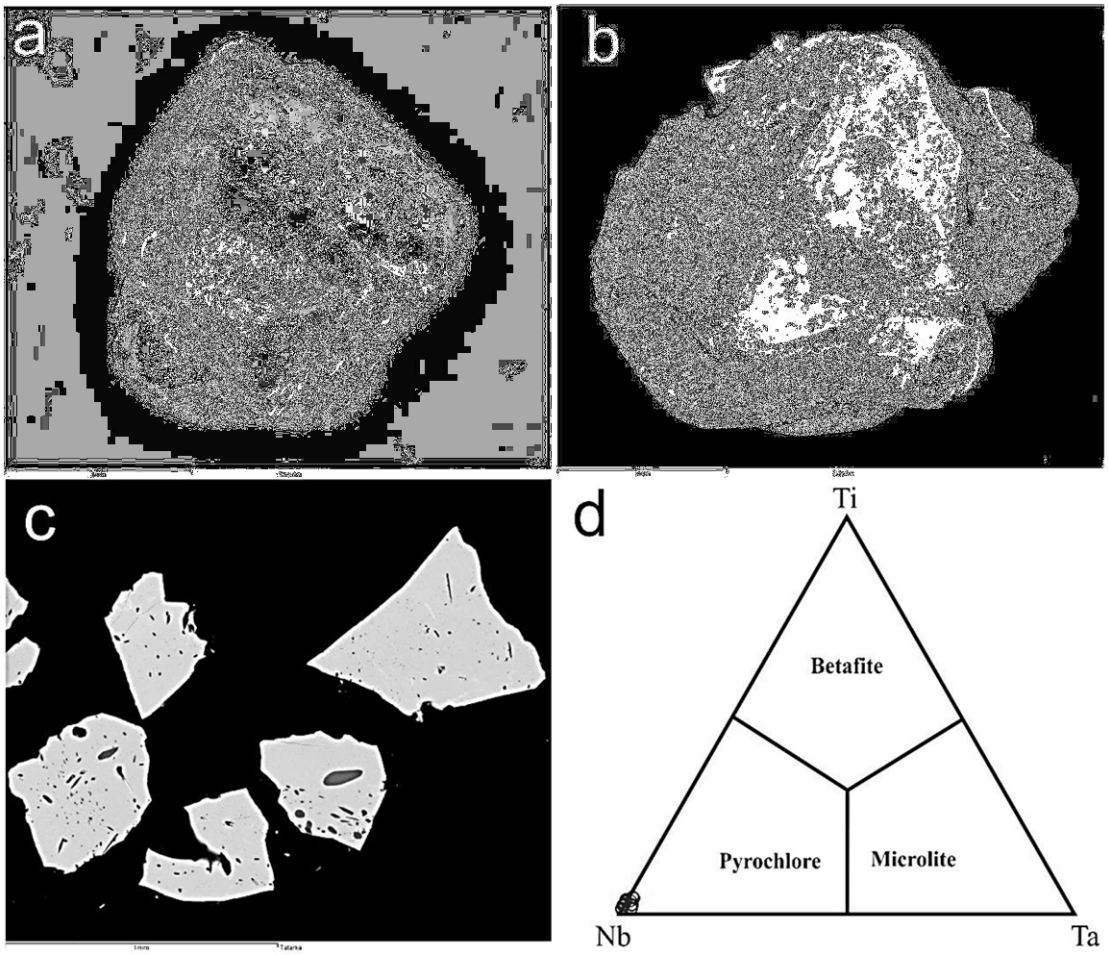

Fig. 1. Typical examples of the external shape of the pyrochlore crystals (a-b) and the internal structure and chemical composition (in a.p.f.u.) of the pyrochlore grains from the Tatarka Nb ore-deposit (carbonatites).

To estimate the time of rare-metal mineralization, single pyrochlore grains have been studied. The grains are represented by large fragments of light slightly-colored, but opaque due to abundant of mineral and fluid inclusions, larger crystals (Fig. 2e), composition of which varied insignificantly both within individual grain and between grains (Fig. 1d). U-Th-Pb isotope composition measurements have been performed on the SIMS SHRIMP-II (St. Petersburg) relative to the inhouse laboratory standard "pyrochlore-331" with an age of 231 ± 1.5 Ma and U content of 1500 ppm (Lepekhina et al., 2016). 31 analyses of isotope composition in 14 grains were carried out during one measurement session (Fig. 2). The uranium content in the studied grains varies more than 20 times: from 15 to 366 ppm, while the thorium content is fairly constant: 300-730 ppm, which leads to significant variations in the Th/U ratio: from 0.8 to 34. Meanwhile, the radiogenic lead content (^{206}Pb) is less than 45 ppm and is accompanied by the presence of a significant amount of common lead ($^{206}Pb_{com}$ share from 27 to 84%), which leads to an enhanced error in the calculated U/Pb ratios and ages. In the U-Pb diagram of the measured ratios of $^{207}Pb/^{206}Pb$ vs $^{238}U/^{206}Pb$ all analyses (31) form a single mixing linear trend with MSWD equal to 4.8 and radiogenic component of which has an age of 634 ± 20 Ma (Fig. 2a). For the most homogeneous 29 analyses this calculation leads to an age of 625 ± 13 Ma at MSWD corresponding to the value of 1.9 (Fig. 2b). If only analyses with uranium content of more than 40 ppm (n = 19) are used to estimate the age, we can calculate the concordant age of 640 ± 11 Ma at MSWD of less than 0.01 and probability of concordance of 0.94 (Fig. 2c). Whereas the weighted average

$^{206}Pb/^{238}U$ age estimation using correction of lead isotopic composition for nonradiogenic component according the measured ^{204}Pb isotope is 638 ± 10 Ma at MSWD 0.89 (Fig. 2d).

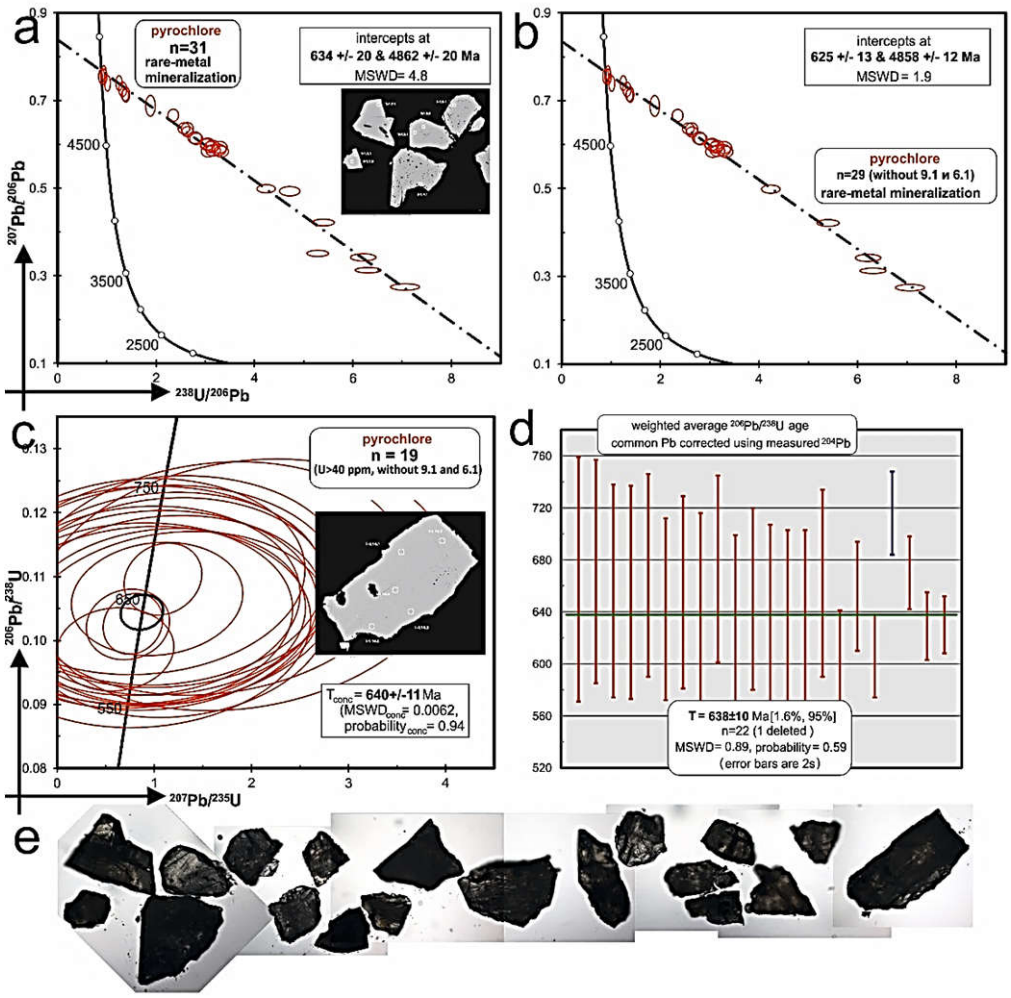

Fig. 2. Dating of the rare-metal mineralization from the Tatarka ore-deposit: a-d – estimation of the pyrochlore age according to U-Pb isotopic SHRIMP-II data on the single grain analysis, e – optic view of the dated pyrochlore grains.

Thus, for the age of rare-metal mineralization formation at the Tatarka deposit represented by pyrochlore mineralization in the weathering crust, a value of 640 ± 11 Ma can be assumed. It should be noted that the existing understanding of the sequence of geological events in this region does not contradict the obtained result, so the intrusion of granitoids of the Tatarka massif occurred 642 ± 16 m.y. ago, and the last tectono-thermal event, manifested in the formation of metasomatic zones, was no later than 630 m.y. ago (Vernikovskaya et al., 2013). The formation of carbonatite bodies (dykes and lenses), associated with rare-metal mineralization, apparently accompanied the formation of granitoid intrusions.

The study was done as a part of CIR project: "Developments of new analytical methods and approaches for isotope dating of alkaline and basic-ultrabasic intrusive bodies applicated for geological mapping within 2014-2016" under financial support by the State Geological Survey.

References

Atencio D., Andrade M.B., Christi A.G. et al. The pyrochlore supergroup of minerals nomenclature// The Canadian Mineralogist. 2010. Vol. 48 pp. 673–698.

Lepekhina E.N., Antonov A.V., Belyatsky B.V., et al. Some features of U-Pb SHRIMP dating of pyrochlore from alkaline-ultramafic polyphase Kovdor massif (North Karelia): isotope-geochemical

characteristics of the evolution of pyrochlore-group mineral composition// Regional Geology and Metallogeny. 2016. №67 pp. 86–94 (in Russian).

Popova V.I., Kozlov P.S., Lapin A.V., et al. New data on pyrochlore from the Tatarka deposit (Yenisei Ridge, Russia)// Mineralogy. 2017. №1 pp. 23–37 (in Russian).

Vernikovskaya A.E., Datsenko V.M., Vernikovsky V.A., et al. Magmatism evolution and carbonatite-granite association in the Neoproterozoic active margin of the Siberian Craton: thermochronological reconstructions// Doklady Earth Sciences. 2013. Vol. 448(2) pp. 161–167.

EXPERIMENTAL STUDY OF THE FLOGOPITE-FORMING REACTIONS IN THE SYSTEM PYROPE-GROSSULAR-ENSTATITE IN PRESENCE OF THE H2O-KCL FLUID AT 5 GPA

Limanov E.V., Butvina V.G., Safonov O.G.

Korzhinskii Institute of Experimental Mineralogy (IEM) RAS, Chernogolovka, butvina@iem.ac.ru

A typical mineral indicator of the modal mantle metasomatism is phlogopite. Appearance of this mineral in the mantle rocks as a result of their interaction with potassium-bearing aqueous fluids is explained by the reaction (Aoki, 1975; van Achterbergh et al., 2001; Safonov, Butvina, 2013, 2016):

$$5MgSiO_3 + CaMg_2Al_2Si_3O_{12} + [K_2O + 2H_2O] = K_2Mg_6Al_2Si_6O_{20}(OH)_4 + CaMgSi_2O_6 \quad (1)$$

or 5En + Grt + [K_2O + 2H_2O] = Phl + Di, which is a combination of two end-member reactions

$$1/2Prp + 3/2En + [1/2K_2O + H_2O] = Phl \quad (2)$$

$$1/2Grs + 9/2En + [1/2K_2O + H_2O] = Phl + 3/2Di \quad (3)$$

In the above reactions, the alkaline component is K_2O for clarity. However, in real fluids potassium exists in the forms of chlorides, carbonates, etc.

In this paper preliminary results of the study at a pressure of 5 GPa and temperatures of 900-1250 °C of reactions (2) and (3) are presented in the presence of a H_2O-KCl fluid with initial X_{KCl} = KCl/(KCl + H_2O) from 0.05 to 0.4. To reproduce the reaction (2) as a starting material, a mixture of pyrope gel, brucite and quartz was used, in which the H_2O content was ~ 8 wt. %. KCl was added to this mixture based on the required X_{KCl} in the starting fluid. To reproduce reaction (3), a gel of the grossular composition was added to the mixture. The mutual relations of phases and their compositions in the products of the experiments indicate a consistent realization of the reactions:

$$En + 1/3Prp + [2/3KCl + 1/3H_2O] = 1/3Phl + 1/3Cl\text{-}Phl \quad (4)$$

$$En + 1/5MgTs + [2/5KCl + 1/5H_2O] = 1/5Phl + 1/5Cl\text{-}Phl, \quad (5)$$

where MgTs is the Mg-Tschermack molecule ($MgAl_2SiO_6$), and Cl-Phl – is the $KMg_3AlSi_3O_{10}Cl_2$ end-member in the phlogopite solid solution. These reactions cause a regular disappearance of the garnet, a decrease in Al content in orthopyroxene, and an increase in Cl concentration in the newly formed phlogopite with an increase in the KCl content in the starting fluid. In the Ca-containing system, an increase in the concentration of KCl leads to destabilization of the pyrope-grossular garnet with the formation of clinopyroxene and phlogopite according to the reaction (3). Such relationships are well known in upper mantle xenoliths in kimberlites and alkaline basalts [exam. 4].

Thus, the ratios of Al concentrations in orthopyroxene and Cl in phlogopite according to reaction (5) are good indices of KCl activity in the fluid. These effects can be used in the future to quantify this activity, and hence the concentration of KCl in water-salt fluids in the processes of modal mantle metasomatism.

The study was supported by the Russian Foundation for Basic Research (project 16-05-00266).

References

Aoki K. (1975): Origin of phlogopite and potassic richterite bearing peridotite xenoliths from South Africa // Contrib. Mineral. Petrol. V. 53. P. 145-156.

Safonov O.G., Butvina V.G. (2013). Interaction of the model peridotite with the H2O-KCl fluid: an experiment at a pressure of 1.9 GPa and its application to the processes of upper mantle metasomatism. Petrology, Vol. 21, No. 6, pp. 654-672.

Safonov O.G., Butvina V.G. (2016) Reactions are indicators of K and Na activity in the upper mantle: natural and experimental data, thermodynamic modeling. Geochemistry, №10, pp.893 - 908.

van Achterbergh E., Griffin W. L., Stiefenhofer J. (2001): Metasomatism in mantle xenoliths from the Letlhakane kimberlites: estimation of element fluxes // Contrib. Mineral. Petrol. V. 141. P. 397-414.

CARBON-BEARING MAGMAS IN THE EARTH'S DEEP INTERIOR

Litasov K.D.*, *Shatskiy A.F.

Sobolev Institute of Geology and Mineralogy SB RAS, Novosibirsk, Russia

klitasov@igm.nsc.ru

Geodynamic models considering fast mantle upwelling without volatile-bearing components are inapplicable due to high melting temperatures of mantle silicates. Here, we discuss the possible nature and composition of melts in the deep upper and lower mantle, which can enhance material transport under superplumes and hot spots originating from the transition zone or from the core–mantle boundary of the Earth (Litasov and Shatskiy, 2018). We emphasize fundamental differences between melting in the petrologically important systems containing H_2O, CO_2, and with a reduced C–O–H fluid (Fig.1). Significant melting of subducted carbonates is expected at transition zone depths, especially if the slab stagnates above the 660 km discontinuity. Mantle melting in the presence of volatiles depends strongly on the redox state. An increase or decrease of the fO_2 causes redox melting or freezing in defined parts of the mantle. The role of sluggish kinetics of solid-solid and even melting reactions involving carbonates in the deep mantle is also of great important. Slow reaction rates allow subducted carbonates to penetrate as deep as the core–mantle boundary.

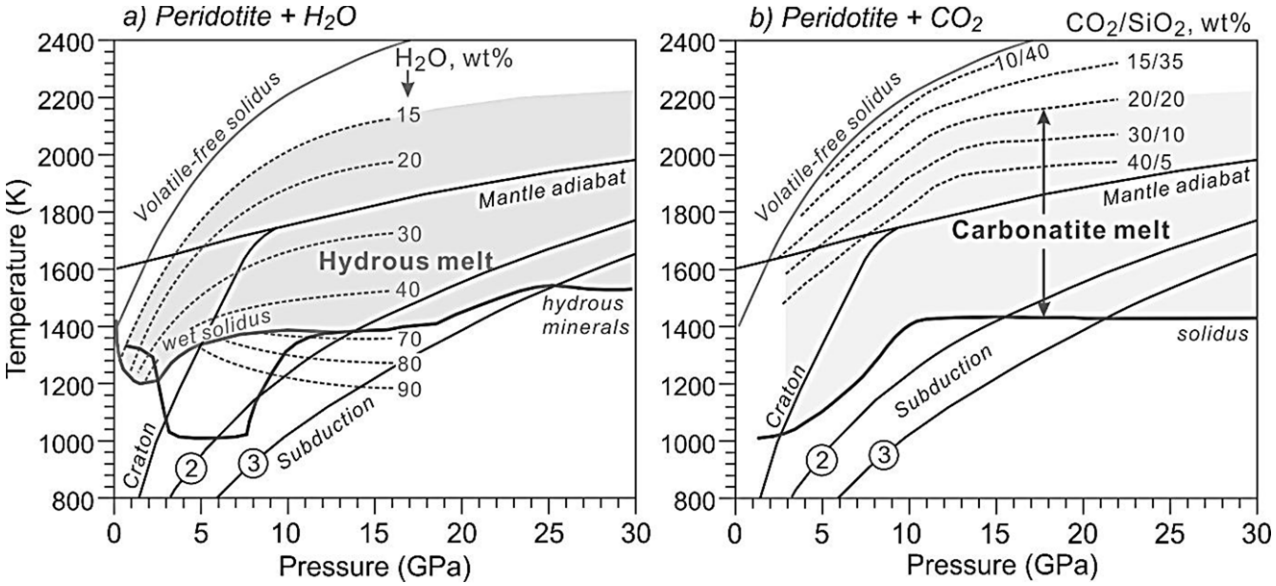

Figure 1. Solidi and melt compositions in the peridotite–H_2O (a) and peridotite–CO_2 (b) systems (Litasov and Shatskiy, 2018).

An important requirement for diapiric motion is stress-induced melting and dissolution–precipitation of fusible components at the front and rear of the plume, respectively. Carbonated or carbonatite melt is the best candidate for the fusible component of the plumes, especially for the upper mantle and transition zone (Fig.2). Hydrocarbon-bearing hydrous melt serves as the liquid component in mantle plumes arising from the core–mantle boundary. The conclusions are based on the recent data on melting in mantle systems with CO_2 and reduced C–O–H fluid, the stability of diamond and carbide phases, and the role of redox conditions in carbon and hydrogen cycles.

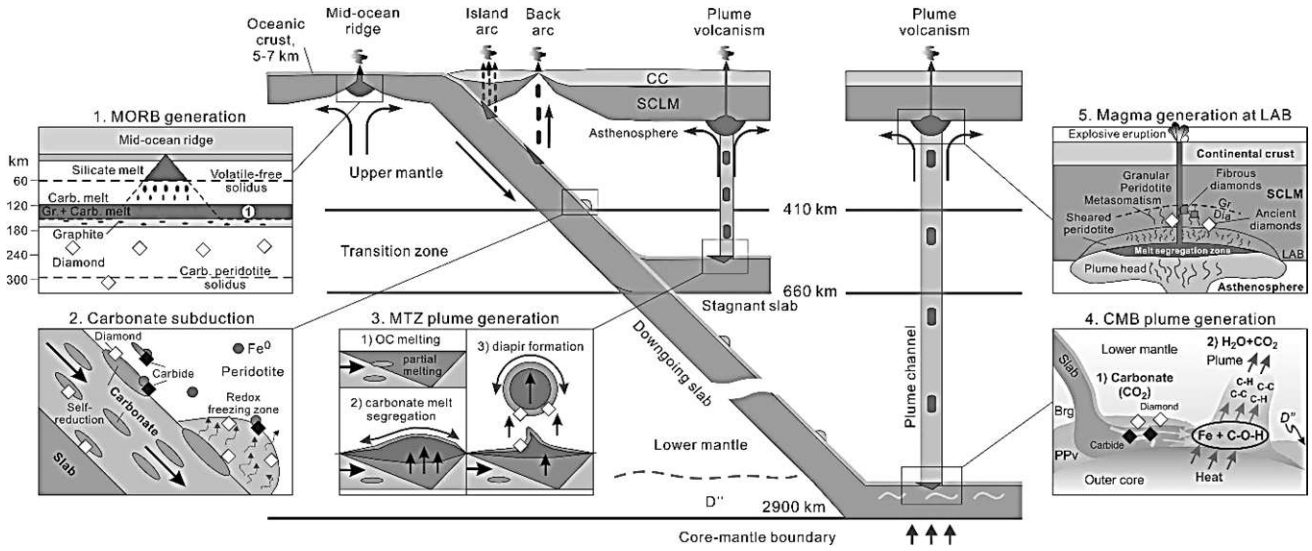

Figure 2. Schematic model for subduction of carbonates down to the transition zone (stagnant slab) and core–mantle boundary combined with the major redox processes associated with burial and remobilization of carbon-bearing compounds (Litasov and Shatskiy, 2018). Abbreviations: OC – oceanic crust, CC – continental crust, SCLM – subcontinental lithospheric mantle, Gr – graphite, Dia – diamond, Brg – bridgmanite, Ppv – postperovskite $(Mg,Fe)SiO_3$.

We emphasize five important processes related to carbonate or carbon-bearing compounds activity in the post-Archean deep mantle (Fig.2). 1. MORB generation induced by deep melting of carbonates, circle (1) shows field of the redox reaction $2Fe_2O_3 + C = 4FeO + CO_2$. 2. Carbonate subduction inside crustal layer (sediments+basalts) of the slab showing partial reduction at the slab–mantle interface, formation of the local redox freezing zones and self-reduction by Fe-disproportionation in slab silicates. 3. Mantle transition zone (MTZ) plume generation showing carbonatite melt diapir formed by melting of carbonates in the stagnant slab. 4. Carbonate reduction at the core–mantle boundary (CMB) and generation of the CMB plume. 5. Carbonatite or hydrocarbon-bearing hydrous melts approach the lithosphere–asthenosphere boundary (LAB), where they can solidify to form the source for later magmatism or, in case of high enough capacity, immediately cause lithosphere erosion, deformation and metasomatism with formation of carbonatite, kimberlite or other alkaline magmas.

The work was supported by Russian Science Foundation (No 14-17-00609P).

References

Litasov, K.D., Shatskiy, A.. Carbon-bearing magmas in the Earth's deep interior // "Magmas under pressure: Advances in High-Pressure Experiments on Structure and Properties of Melts", Kono, Y., Sanloup, C, eds., 2018, Elsevier, p. 43–82.

FRACTIONAL ULTRABASIC-BASIC EVOLUTION OF THE UPPER MANTLE MAGMAS: ROLE OF OLIVINE AND ORTHOPYROXENE PERITECTIC REACTIONS BY EXPERIMENTAL EVIDENCE

Litvin Yu.A., Kuzyra A.V.

D.S. Korjinsky Institute of Experimental Mineralogy litvin@iem.ac.ru, shu25@rambler.ru

The potentials of eclogites formation from garnet peridotites at fractional ultrabasic-basic magma evolution have been considered at the dawn of the age of high pressure physico-chemical experiments (O'Hara and Yoder, 1967). At the time, however, the problem could not be solved for the lack of insight into the physico-chemical mechanisms of olivine and orthopyroxene disappearance in the peridotite-to-eclogite transitions (Yoder, 1976). Experimental study of melting relations at 4 GPa of

the ultrabasic peridotite-pyroxenite multicomponent system olivine Ol-orthopyroxene Opx – clinopyroxene Cpx -garnet Grt has revealed invariant peritectic reaction of orthopyroxene and komatiitic melt with formation of clinopyroxene. The peritectics provides the consecutive change from univariant cotectics of Ol+Opx+Cpx+Grt+L (melt) to that of Ol+Cpx+Grt+L with temperature depression (Litvin, 1991). It makes possible to construct the equilibrium diagram-complex of liquidus structure for the ultrabasic-basic system olivine–(clinopyroxene/omphacite)–corundum–coesite (Fig. 1) (Litvin, 2017). The diagram consists of two ultrabasic and three basic elementary simplexes. The ultrabasic part is presented by peridotite-pyroxenitic symplex with peritectics P_1 and Ol-eclogitic simplex with eutectic E_1. The basic part consists of eclogitic simplexes - corund-kyanitic (eutectic E_2), kyanite-coesitic (eutectic $E_{3)}$, coesite-orthopyroxenitic (peritectics P_2).

The diagram-complex demonstrates significant restrictions for the evolution of ultrabasic-basic magma at the temperature maxima (‘’thermal barriers”) in piercing points between the adjacent simplexes for the univariant curve Opx+Grt+(Cpx/Omph)+L (#2 +15) between peritectics P_1 and P_2 as well as for the univariant curve Crn+Grt+(Cpx/Omph)+L (#6+7) between eutectics E_1 and E_2. The thermal barriers are impassable for ultrabasic-basic magmatic evolution under both the regimes of equilibrium and fractional crystallization. Thus, the peritectic reaction with loss of orthopyroxene may promote the evolution of the upper-mantle primary magma exclusively within the ultrabasic peridotite-pyroxenite- Ol-eclogite compositions with the use of the common univariant curve Ol+(Cpx/Omph)+Grt+L. Experimentally based data on the ultrabasic-basic evolution of the upper-mantle magmatism are applicable to the magma ocean activity in the early Earth and fractionation of Archean komatiitic magma.

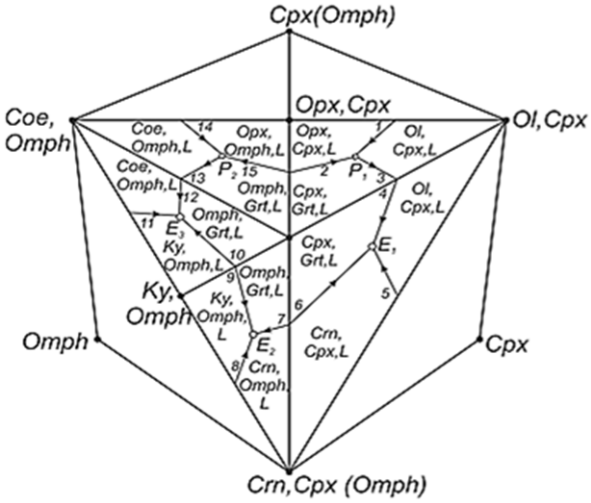

Fig. 1. Diagram-complex of ultrabasic-basic liquidus structure for upper mantle Ol-Opx-Crn-Coe system in projection onto isothermal section Ol,Cpx - Crn,Cpx(Omph) - Coe,Omph. P_1 – peritectics Ol+Opx+Grt+Cpx+L and E_1 – eutectic Ol+Crn+Grt+Cpx+L; for basic compositions: P_2 – peritectics Coe+Opx+Grt+Omph+L and eutectics E_2 – Crn+Ky+Grt+Omph+L and E_3 – Ky+Coe+Grt+Omph+L. Numbers by curves– ultrabasic: 1 – Ol+Opx+Cpx+L, 2 – Opx+Grt+Cpx+L, 3 and 4 – Ol+Grt+Cpx+L, 5 – Ol+Cpx+Crn+L , 6 – Crn+Grt+Cpx+L; basic: 7 – Crn+Grt+Omph+L, 8 – Crn+Ky+Omph+L, 9 и 10 – Ky+Grt+Omph+L, 11 – Ky+Coe+Omph+L, 12 and 13 – Coe+Grt+Omph+L, 14 – Coe+Opx+Omph+L, 15 – Opx+Grt+Omph+L. Symbol Omph for omphacite. Arrow by univariant curve for direction of temperature lowering

However this scenario does not hold under natural conditions as judged from the absence of Ol-eclogites among the upper-mantle ultrabasic xenoliths in kimberlites. At the same time the upper-mantle rocks are reported as the ultrabasic garnet peridotites and basic eclogites in kimberlites (Sobolev, 1977; Dawson, 1980). Primary diamond-hosted inclusions are also of peridotitic and eclogitic paragenesises. Probability of ultrabasic-basic magma evolution is marked by petrochemical trends with uninterrupted change of clinopyroxenes and garnet compositions between Ol-normative peridotites and SiO_2-normative eclogites (Fig. 2).

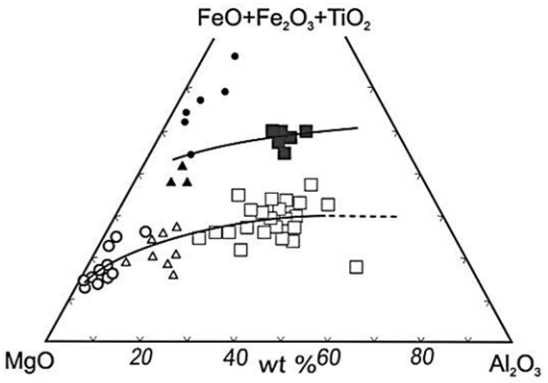

Fig. 2. Petrochemical diagram for ultrabasic and basic upper mantle rocks (plotted from data of Marakushev, 1984). Notations: Mg-Al rocks (white signs): circles –garnet dunites and peridotites; triangles - garnet pyroxenites; squares – bimineral eclogites and Ky-eclogites. Fe-Ti-rocks (black signs): circles – phlogopite-ilmenite peridotites; triangles – phlogopite-ilmenite pyroxenites; squares – rutile eclogites.

Encauraging perspective for a rigorous understanding the physico-chemical mechanism of ultrabasic-basic evolution of the upper mantle magma has appeared with experimental discovery of the reaction of forsterite and jadeite components with formation of pyropic garnet in the system forsterite-jadeite at pressures higher 4.5 GPa (Gasparik and Litvin, 1997). This is of particular interest in the experimental study of melting relations on the ultrabasic-basic olivine-diopside-jadeite system which composition is in closer approximation to the native upper mantle matter (after the loss of orthopyroxene). Contents of Na_2O in clinopyroxenes of peridotites and pyroxenites averages between 1.5 – 4.5 wt.% and are noticeably growing in omphacites of eclogites (2.5 – 6.5 wt.%) and grospydites (4.5 – 9.9 wt.%) that indicates the commensurable increase of concentration of the jadeitic component in the ultrabasic-basic magmatic system (Sobolev, 1977; Dawson, 1980). The contents of Na_20 in omphacitic primary inclusions in diamonds are even higher (6.4 – 10.7 wt.%). The growing of Na_2O and jadeitic components in peridotitic Cpx and eclogitic Omph reflects increase in their concentrations for the ultrabasic-basic melts during their evolution. This could be compatible with the regime of fractional crystallizations of the magmatic melts.

Melting relations of the olivine-diopside-jadeite system are studied at 6 GPa for the polythermal sections Ol – Omph ($Jd_{62}Di_{38}$) (Fig. 3) and Ol – Cpx($Di_{90}Jd_{10}$). As a result the peritectic reaction of olivine and jadeite-bearing melt with formation of garnet and the univariant assembly omphacite+garnet+basic liquid phase has been established.

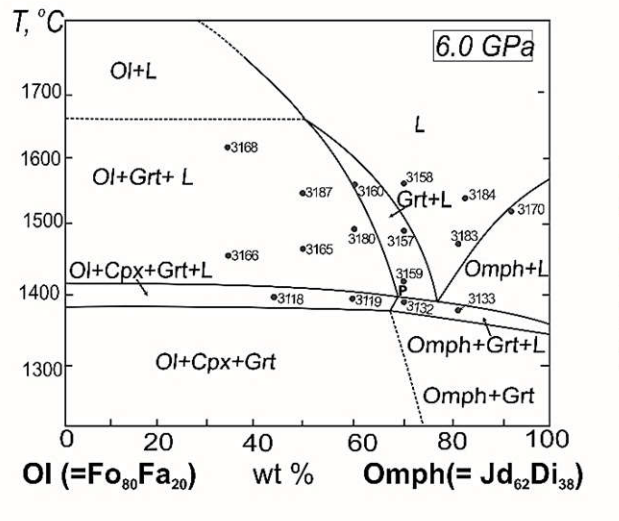

Fig. 3. Diagram of melting relations for polythermal section Ol-Omph of the ultrabasic-basic Ol-Di-Jd system. Black points for experimental compositions with sample numbers. Symbols: L = liquid phase, Fo – forsterite, Fa – fayalite, Di – diopside, Jd – jadeite.

The polythermal sections Ol – Omph and Ol – Cpx are propagated, respectively, through the three Ol +L, Grt + L, (Cpx ↔ Omph) +L and the two Ol+l, (Cpx ↔ Omph) +L liquidus associations. This clearly demonstrates the principal peritectic liquidus structure of the ternary Ol–Di–Jd system (Fig. 4). Experimental melting relations on the olivine-diopside-jadeite system at 6 GPa reveals peritectic reaction of olivine and jadeite-bearing melt with formation of the eclogitic garnet and omphacite assembly. Finally, the experimentally-based generalized diagram-simplex for melting

relations of the olivine-diopside-jadeite-garnet system (Fig. 5) has given insight into the physico-chemical mechanism of ultrabasic-to-basic transfer for the upper mantle magmas. The final stage of the ultrabasic magmatic evolutions is regulated by the cotectic curve Ol+(Cpx↔Omph)+Grt+L with growing concentration of Ld component in fractionated melts between eutectic E and peritectic P.

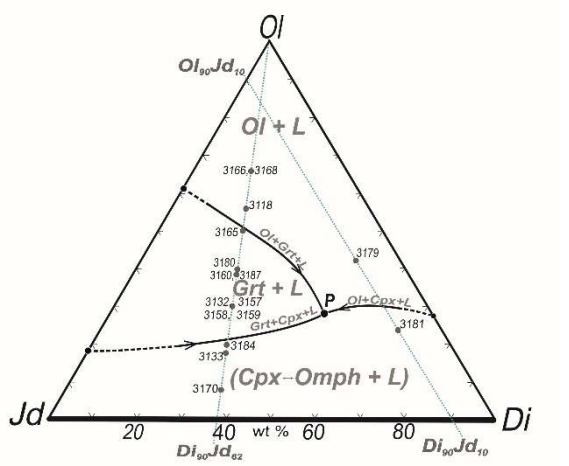

Fig. 4. Liquidus surface of ultrabasic-basic system Ol-Di-Jd. Positions of the polythermal sections Ol - $Jd_{62}Di_{38}$ and $Ol_{90}Jd_{10}$ – $Di_{90}Jd_{10}$ are marked by dotted lines. Positions of the experimental poits of the polythermal sections are presented by their projections onto the liquidus surface.

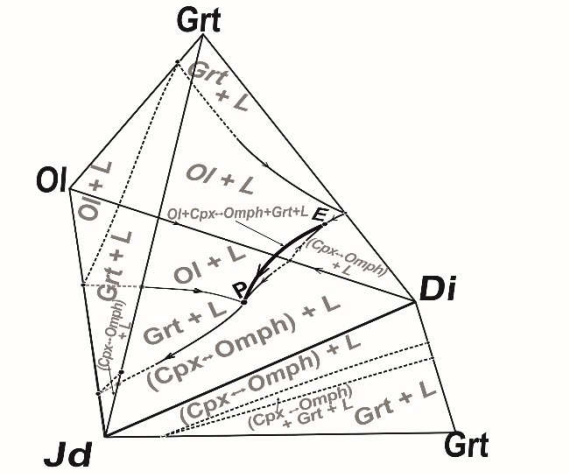

Fig. 5. Liquidus structure of quadruple ultrabasic-basic Ol-Di-Jd-Grt system (the ternary boundary Di-Jd-Grt join is developed toward observer for convenience). Cotectic curve Ol+(Cpx↔Omph)+Grt+L (marked with bold line) is disposed inside the tetrahedral volume between eutectic E and peritectucs P.

Peritectic reactions of orthopyroxene and olivine with melts are efficient in governing the regular fractional evolution of the ultrabasic and basic magmas and correlates well with petrochemical trends for the garnet-bearing peridotite and eclogite rocks. Thus, the role of olivine and orthopyroxene peritectic reactions with formation of garnet and clinopyroxene is crucial as a physico-chemical "bridge" for the fractional magmatic evolution of the material of the upper-mantle garnet-peridotitic facies between the ultrabasic peridotite-pyroxenitic and basic eclogitic compositions.

Support by the Program of the RAS №I.P.08.

References

Dawson J.B. (1980). Kimberlites and Their Xenoliths. Berlin:Springer-Verlag, 252 p.

Gasparik T., Litvin Yu.A., 1997. Stability of Na2Mg2Si2O7 and melting relations on the forsterite-jadeite join at pressures up to 22 GPa. Eur. J. Mineral. 9, 311-326.

Litvin Yu.A. (1991). Physico-Chemical Study of Melting Relations of the Deep-Seated Earth's Substance. Nauka, Moscow, 312 p. (in Russian).

Litvin Yu.A. (2017). Genesis of Diamonds and Associated Phases. Springer. 137 p.

Marakushev, A.A., (1984). Nodules of peridotites in kimberlites as indicators of the deep-seated structure of the lithosphere. In: Lectures of Soviet Geologists at the XXYII Session of the International Geological Congress. Petrology. Nauka, Moscow, p. 153-160 (in Russian).

O'Hara M.J., Yoder H.S. (1967). Formation and fractionation of basic magmas at high pressures. Scott. J. Geol. 3, 67-117.

Sobolev N.V. (1977). Deep-seated Inclusions in Kimberlites and the Problem of the Composition of the Upper Mantle. Washington, D.C.: Amer. Geophys. Union. 1977. 279 p.

Yoder H.S. (1976). Generation of Basaltic Magma. Nat,Acad. Sci., Washington.

FRACTIONAL ULTRABASIC-BASIC EVOLUTION OF THE LOWER MANTLE MAGMAS: ROLE OF BRIDGMANITE PERITECTIC REACTION BY EXPERIMENTAL EVIDENCE

Litvin Yu.A., Spivak A.V.

D.S. Korjinsky Institute of Experimental Mineralogy, litvin@iem.ac.ru, spivak@iem.ac.ru

The lower mantle rocks have not been found among the deep-seated xenoliths in kimberlites. However ferropericlase FPer=(Mg,Fe)O, ferrobridgmanite FBrd=(Mg,Fe)SiO_3, Ca-perovskite CaPrv=$CaSiO_3$, magnesiowustite MWus=(Fe,Mg)O and stishovite Sti=SiO_2 can be thought of as the lower mantle minerals of determining importance by indirect evidence from diamond-hosted inclusions (Kaminsky, 2018) and experimental subsolidus transformations of the Ringwood's "pyrholite" at lower-mantle PT-conditions (Akaogi, 2007). The lower-mantle diamond-hosted minerals have crystallized together with diamonds from silicate-oxide-carbonate-carbon melts-solutions (Litvin, 2017), whereas the lower-mantle rocks are bound to be products of crystallization of silicate-oxide magma. Nevertheless, it must not be ruled out genetic links between the lower mantle minerals and diamond-hosted inclusions. Most likely the mantle minerals could be dissolved in diamond-parental carbonatite melts at early stages of their formation, then in the closing stages the dissolved components were crystallized into similar minerals being trapped by the growing diamonds.

The lower mantle ultrabasic assemblages with ferropericlase and ferrobridgmanite-as well as basic ones with magnesiowustite and stishovite belong to the system MgO – FeO – SiO_2 – $CaSiO_3$. It must be taken into account that FPer and MWus are the phases of the continuous solid solutions on the join MgO-FeO. Experimental at 26 ГПа melting relations over the polythermal section $(MgO)_{49}(FeO)_{21}(CaSiO_3)_{30}$ – $(SiO_2)_{49}(FeO)_{21}(CaSiO_3)_{30}$ of the MgO – FeO – SiO_2 – $CaSiO_3$ system demonstrate the peritectic interaction of ferrobridgmanite and melt resulting in formation of stishovite and magnesiowustite (Figs. 1 and 2). In the case a key reaction may be presented as L + FBrd = Sti + MWus with disappearance of FBrd andis determined as the effect of stishovite paradox (Litvin, 2014). The experimental phase diagram (Fig. 1) demonstrates that L + FPer and L + Sti are the liquidus assemblies. Solidus assemblies L + FBrd + MWus + Sti + CaPrv and L + MWus + Sti + CaPrv reveal a disappearance of ferrobridgmanite by the action of the peritectic reaction (P). Stable subsolidus assemblies are presented by the FPer + FBrd + CaPrv, Fbrd + MWus + Sti + CaPrv and MWus + Sti + CaPrv.

Experimental results are in good agreement with liquidus structure of the system MgO – FeO - SiO_2 –$CaSiO_3$ (Fig. 2) characterizing melting relations of native material of the lower mantle.

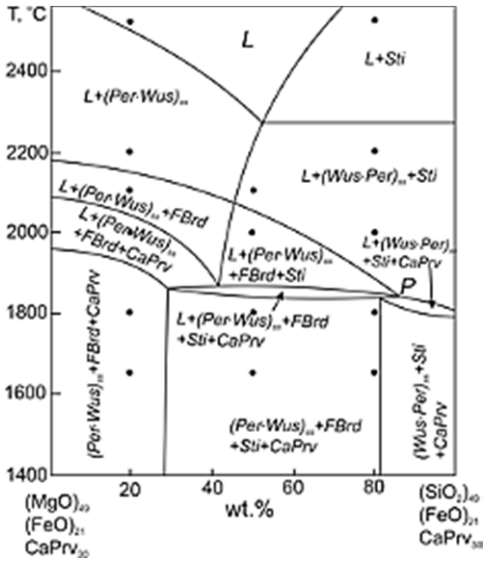

Fig. 1. Melting relations on the polythermal section $(MgO)_{49}(FeO)_{21}(CaSiO_3)_{30}$-$(SiO_2)_{49}(FeO)_{21}(CaSiO_3)_{30}$ at 26 GPa. Black points for experimental conditions. Symbols: L - melt; Per - periclase; Wus - wustite; FPer - ferropericlase; MWus - magnesiowustite; FBrd - ferrobridgmanite; CaPrv - Ca-perovskite; Sti – stishovite; invariant peritectic point L+FBrd+[(Per·Wus)ss↔(Wus·Per)ss]+Sti+CaPrv with the key reaction L+FBrd=Sti+(Wus·Per)ss of "stishovite paradox".

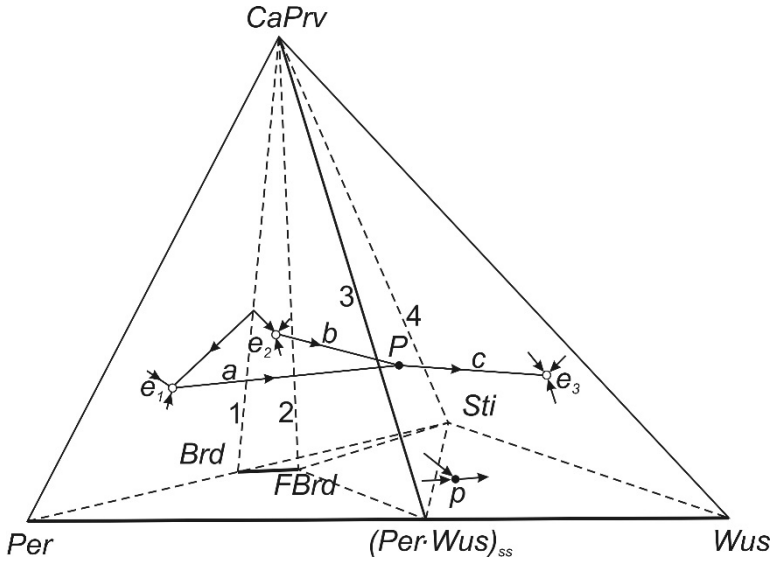

Fig. 2. Liquidus structure at 26 GPa of the lower mantle system Per-Wus-Sti-CaPrv. Symbols: Per – periclase, Brd – bridgmanite, FBrd – ferrobridgmanite, CaPrv – Ca-perovskite, Sti – stishovite. Wus – wustite, (Per·Wus) – periclase – wustite solid solutions. Subsolidus volumes of triangulation are marked as 1 – 4, eutectic and peritectic points – as e_1 (L+Per+Brd+CaPrv), e_2 (L+Brd+Sti+CaPrv), e_3 (L+Sti+Wus+CaPrv), p P – invariant peritectic point L+(FPer↔MWus)+FBrd+Sti +CaPrv of 4-component system with the key reaction L+FBrd=Sti+(Wus·Per)ss of «stishovite paradox»; univariant cotectic curves: (a) ultrabasic L+FPer+FBrd+CaPrv; (b) basic L+Sti+FBrd+CaPrv; (c) basicL+Sti+MWus+CaPrv.Brd=Sti+MWus).

Eutectic e_1 of the boundary system Per – Brd - CaPrv controls melting of low ferroferous lower mantle rocks and generation of primary ultrabasic magma. With temperature depression, the magma composition should change along the univariant cotectics L + FPer + FBrd + CaPrv («a») indirection to the peritectic point L + FBrd + MWus + Sti + CaPrv («P») where FBrd is disappeared due to the reaction of "stishovite paradox". The further temperature depression leads to formation of univariant cotectics L + MWus + Sti + CaPrv («c») terminating in the eutectic e3 of the boundary join Wus – Sti – CaPrv. It should be realized that the peritectic reaction of the "stishovite paradox" is of fundamental importance as the physico-chemical mechanism which provides the mere possibility of the ultrabasic-basic evolution of the lower-mantle magmatism. As this take place, the regime of fractional

crystallization is able to provide continual changes in formation from ultrabasic to basic minerals at lower mantle conditions.

Components of the lower mantle diamond-forming melts-solvents of carbon belong to the system MgO-FeO-$CaSiO_3$-Carb*$_{50}$ (where Carb* symbolizes the carbonate component $(MgCO_3)_{25}(FeCO_3)_{25}(CaCO_3)_{25}(Na_2CO_3)_{25}$). Expimental study at 26 GPa of melting relations on the polythermal section $(MgO)_{20}(FeO)_{15}(CaSiO_3)_{15}$Carb*$_{50}$ - $(SiO_2)_{20}(FeO)_{15}(CaSiO_3)_{15}$Carb*$_{50}$ (Fig. 3) reveals the peritectic interaction of ferropericlase and Mg-Fe-Ca-Na-carbonate-bearing melts with formation of the basic assembly of stishovite, magnesiowustite and carbonates. In this case the peritectic assembly is presented as L + FBrd + (MWus/FPer)ss + CaPrv + Sti + Carb* with the key reaction of carbonate-bearing melt and ferrobridgmanite - L + FBrd = Sti + (MWus/FPer)ss + Carb* and disappearance of FBrd ("effect of stishovite paradox"). As the liquidus phase FPes and Sti so the subsolidus paragenesises FPer + FBrd + CaPrv + Carb* and FBrd + (MWus/FPer)ss + Sti + CaPrv + Carb*demonstrate ultrabasic-basic composition change.

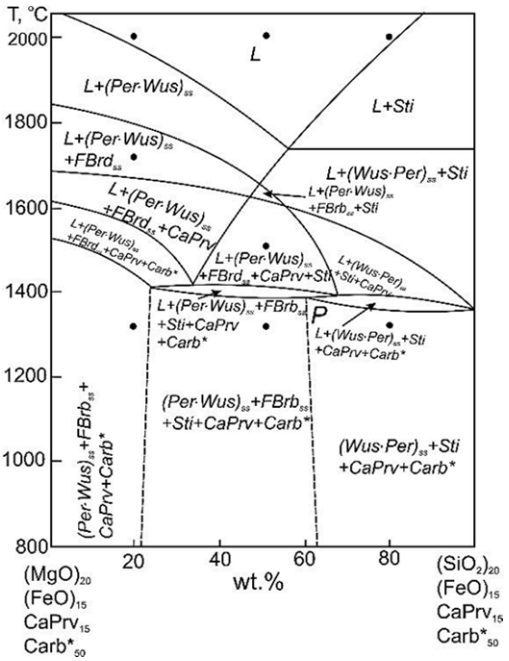

Fig. 3. Melting relations on polytheram section $(MgO)_{20}(FeO)_{15}CaPrv_{15}Carb^*_{50}$-$(SiO_2)_{20}(FeO)_{15}CaPrv_{15}Carb^*_{50}$ at 26 GPa.
Symbols: see for the Fig. 1, and Carb* - simplified notation for multicomponent carbonate composition $(MgCO_3)_{25}(FeCO_3)_{25}(CaCO_3)_{25}(Na_2CO_3)_{25}$.

Symptomatic that liquidus structure at 26 GPa of the diamond-forming system Per-Wus-Sti-CaPrv-Carb* is topologically similar to that of the native lower mantle system Per-Wus-Sti-CaPrv (Fig. 1). In both the cases the ultrabasic-basic magmatic evolution is governing with the peritectic disappearance of ferrobridgmanite due to the effect of "stishovite paradox" and the process has been made in the regime of fractional crystallization.

Experimental physico-chemical data can be used for construction of the fractional diagram of syngenesis for lower-mantle diamonds and associated mineral phases (Fig. 4). The diagram is constructed at plane of the polythermal section *FPer, FBrd, CaPrv, Carb**[→*MWus,Sti,CaPrv,Carb**] – diamond. The distinguishing characteristic of the syngenesis diagram lies in the fact that its general composition is not fixed but changeable at the crystallization processes. The fractional syngenesis diagram includes the PTN_c – curve of diamond solubility in completely miscible silicate-carbonate melts (N_c –solubility symbol).

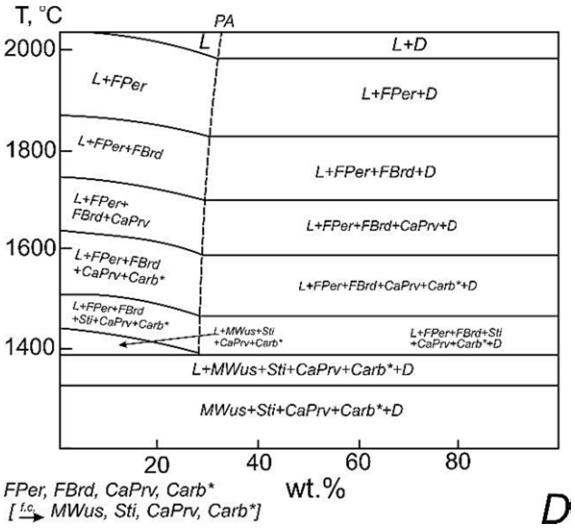

Fig. 4. Syngenesis fractional diagram for the diamong-forming ultrabasic-basic system FPer-FBrd-CaPrv-Carb*-D with the closing formation of the basic assembly MWus+Sti+CaPrv+Carb*+D. Symbols: see Figs 1 and 3, D – diamond.
Special labelling: FPer-FBrd-CaPrv-Carb* - starting ultrabasic phase composition;
MWus, Sti, CaPrv, Carb* - closing basic phase composition; f.c.→ regime of fractional crystallization; PA- curve of diamond solubility in silicate-carbonate melts.

The diamond solubility curve restricts the field of saturated silicate-carbonate melts-solutions in respect to diamond. The oversaturation to diamond, necessary for its nucleation and growth, is kept automatically by temperature lowering. The associated ultrabasic and basic mineral phases are formed together with diamond. The syngenesis diagram demonstrates that changeable compositions of the diamond-parental melts-solutions have to transfer through the phase fields of the paragenetic mineral phases. This creates conditions for their trapping by growing diamonds.

Support: Program of the RAS № I.P.08.

References

Kaminsky F.V. The Earth's Lower Mantle. Composition and Structure. Springer. 2018. 331 p.

Akaogi M. Advances in High-Pressure Mineralogy (Ohtani E., ed.). Geol. Soc. Amer. Spec. Pap. 2007. №421 pp. 1-13.

Litvin Yu.A. Genesis of Diamonds and Associated Phases. Springer. 2017. 137 p.

Litvin Yu.A. The stishovite paradox in genesis of ultradeep diamonds. Doklady Earth Sciences.2014. Vol. 455 No. 1 pp. 274-278.

BEHAVIOR OF LITHOPHILE ELEMENTS IN THOLEIITIC BASALT OF THE AZORES PLUME IMPACT REGION BASED ON THE RESULTS OF HOLE 332B (36ºN)

***Lobanova A.Y.*[1,2], *Sushchevskaya N.M.*[1], *Migdisova N.A.*[1], *Zshilkina A.V.*[1], *Sherbakov V.D.*[2]**

[1]*Vernadsky Institute of Geochemistry, RAS, Moscow, Russia*

[2]*Lomonosov Moscow State University,* ambercloudberries@gmail.com

Rift province of the North Atlantic - north of the Azor-Gibraltar member (Fig. 1) between 33-70º N reveals a unique for the mid-oceanic ridges manifestation of tholeiitic magmatism supposedly associated with a generation of primary melts at greater depths. This conclusion correlates with the configuration of seafloor and gravity signatures that reflect more heated mantle under this province (Dmitriev, et al., 1985; Klein and Langmuir, 1987; Dosso *et al*., 1999).

The specifics of the Azores plume are represented in the increasing degree of the enrichment of the tholeiitic magma with the decreasing of its age, the most enriched tholeiites are developed in the modern spreading zone (Leg 37 cruise synthesis, 1977). According to the geological and geophysical data, to the south of the Azores on the V-shaped fragment of the ridge an abnormally thick crust reaching ~10-15 km in comparison with the normal oceanic crust is established. This feature indicates the considerable influence of the hot substance of the Azores plume on the formation of the magmatism in this zone (Shilling, 1985, Gente et al, 2003, Montelli et al., 2006). Basalts from the Hole 332b Leg 37 DSDP were analyzed to establish the specificity of the evolution of the Azores plume and its probable impact on the magmatism of the Mid-Atlantic Ridge (MAR). The depth of the hole is

more than 580 meters, tholeiitic magmas were formed at this segment of MAR about 3.5 million years ago. The main part of the hole consists mostly of extrusive horizons of massive pillow-lavas of mafic composition interplayed by sediments and zones of breccias with fragments of basalts.

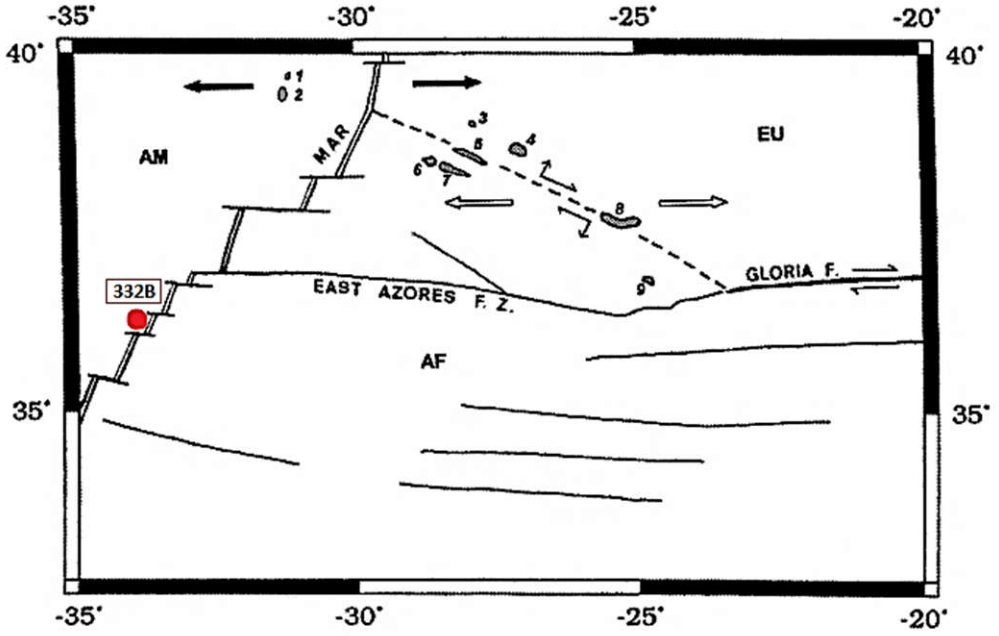

Fig. 1. Tectonic setting of the site 332b near Azores archipelago (Madeira and Ribeiro, 1990).

The first crystallizing phase was olivine, often found in the form of phenocrysts. Next crystallizing phase was plagioclase, in some cases in equilibrium with olivine, as evidenced by the presence of phenocrysts of plagioclase in olivine. Clinopyroxene is the last major crystallizing phase, marked mainly in the bulk in skeletal clusters with plagioclase. The low porosity of the samples may indicate a low content of volatiles in the melts and a relatively slow rise of magmas to the point of outflow.

The olivine and spinel compositions were analyzed in order to determine the main parameters of the crystallization process. Olivines are from idiomorphic to suidiomorphic grains (average size 0.1-0.5 mm). Some grains have a direct implicit zoning (the central part is more magnesian), several grains, however, have an inverse zonation, and probably are xenoliths captured by the ascending magma. Composition of olivines are mainly Fo_{84-91}. The contents of Ni, Mn and Ca for high Mg# olivines are 2400-2500 ppm, 1000 ppm, 2400 ppm, respectively, which is typical for depleted MORB.

Grains of chrome spinel in the rock are presented in small quantities, only as inclusions in grains of olivine and have a limited range of compositions - $Mg/(Mg + Fe^{2+})$ от 0.58 до 0.70 и $Cr/(Cr + Al)$ от 0.40 до 0.54. The temperatures of magma crystallization were calculated using the geothermometer based on the dependence of the distribution of Al_2O_3 between the olivine and chromospinelides by Zhihuan Wan et al. (2008). The calibration data reproduces the temperatures with an accuracy of about ± 22°C. 15 olivine graines were measured by an electron microscope with wave spectrometers that contained spinel inclusions with already known content. The calculated temperatures for the olivines Fo_{90} are 1200-1270°C. In general, this coincides with the liquidus temperatures supposed by Dmitriev et al. (1995).

Geochemical features of lavas were estimated by specially original methodic developed in the GEOKHI RAN for mass spectrometer with inductively coupled plasma (ICP-MS) (Сущевская и др., 2018).

Mafic rocks were decomposed in an open system with concentrated acids, while samples of felsic composition were analyzed in laboratory. Each analyzed sample was doped with stable In in case to control the complete dissolution of samples and possible losses during decomposition. The contents of trace elements in obtained solutions were determined by inductively coupled plasma mass

spectrometry (ICP-MS X Series 2) with the working parameters of the analysis: the output power of the generator is 1400 W, the flow rate of the plasma-forming gas (Ar) is 13 l/min, the auxiliary is 0.95 l/min, the Ar flow through the sprayer is 0.87 l/min, the sample consumption is 0.8 ml/min. With these settings, the CeO+/Ce+ oxide ion level is not higher than 2%, the relative fraction of doubly charged ions (Ba ++/Ba+) is not higher than 3%.

Relative standard deviation for all analyzed elements was no more than 0.2 for element contents below the five-fold detection limit and below 0.1 for contents above the five-fold detection limit. The correctness of the analyses was verified by the measurement of standard samples of basalts (BHVO-2 and BCR-2) and empty probes in every batch.

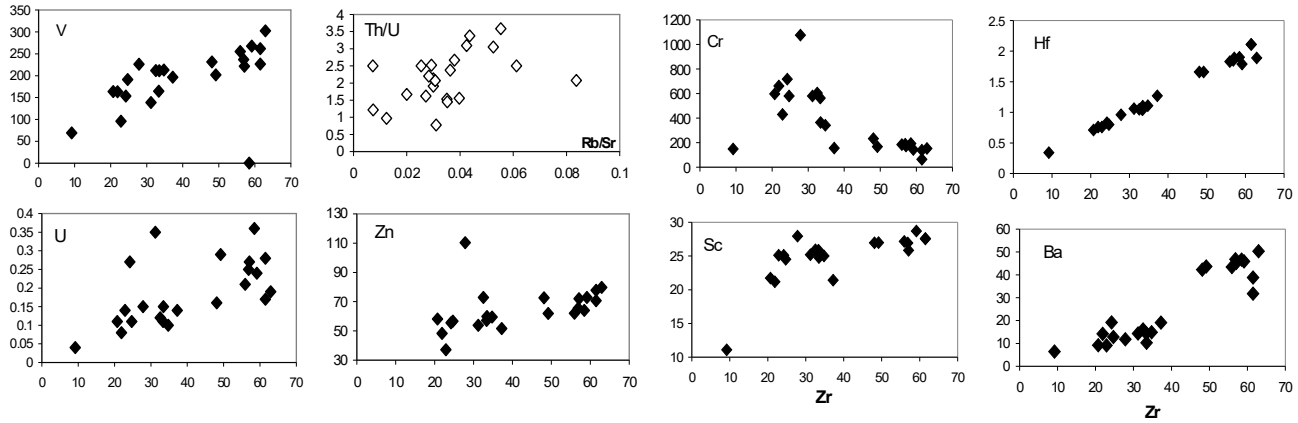

Fig. 2. Dependence of elements concentrations from Zr concentration

The measured spectra were processed using iPlasmaProQuad (GEOHI RAS) programs, which imports all measured data into the MS Access database and subsequent processing of the database (a system of approximately 60 requests including calculations). Processing includes the construction of calibration dependencies, calculation of isotope concentrations, introduction of amendments to the internal standard, compliance control, and an assessment of the uncertainty of the results (data consolidation, validation of standard samples and other functions).

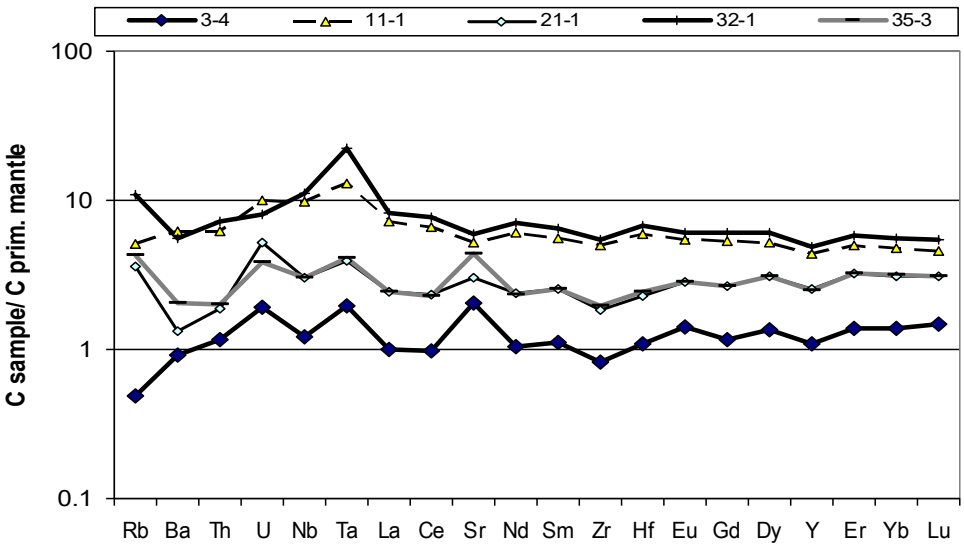

Fig. 3. Trace element patterns normalized to primitive mantle (McDonough & Sun,1995) for bulk-rocks.

The data obtained for 20 samples is shown in the series of figures Zr-element (Fig. 2) and on spidergrams of normalized values for lithophile elements (Fig. 3). The behavior of the incompatible

elements is shown on the graphs Zr – element. During the fractionation the concentrations of all incompatible elements regularly increase (U, Ba, Hf are given), the Cr content decreases. Increased V, Sc contents indicate the absence of Cpx in the paragenesys. The ratios of the more incompatible to the more compatible elements (Th/U, Rb/Sr) during fractionation increase, supposing the fractionation in a relatively closed system, with no continuous mixing of melts with different ratios of lithophile elements. On Fig. 3 the normalized values for the samples studied of different degrees of fractionation are shown. Samples 3-4 are plagioclase porphyry basalts from the uppermost horizon. They demonstrate the least enriched character: the ratio (La/Sm)n is lesser than 1. The other samples are more magnesian and are similar in composition to the primary magnesian melts (average series of representative samples in the figure) reveal poorly enriched spectra (Fig. 3). The Sr maxima for a number of samples is probably associated with the presence of the plagioclase in the melts. The weakly fractioned samples and the depleted sample 3-4 have a small negative Nb anomaly reflecting the characteristics of the melting source. For more enriched samples elevated Rb contents are noted.

Petro-geochemical study of basalts of hole 332b DSDP-37 Leg located near the MAR in the Azores Plateau area supports the tezis that about 3.5 million years ago rift magmatism in this region was presented by a poorly enriched type of MORB. For magmas of similar magnesia, two types of magmas have been identified: depleted and enriched. The established crystallization temperatures of about 1270°C for $Fo_{90.5}$ are typical for tholeiitic magmas. The origin of magmas is associated with the melting of the peridotite mantle (Dmitriev et al., 1985). At the same time the melting source had a poor enrichment with lithophilic elements probably reflecting the addition to the depleted asthenosphere the substance from enriched sources such as the enriched metasomatic mantle of the Azores Plateau formed at earlier stages of the MAR opening (40-35° N).

References

The Shipboard Scientific Party, Deep Sea Drilling Project Initial Reports, 1977, V. 37, SITE 332.

Dmitriev L. V., A. V. Sobolev, N. M. Suschevskaya, and S. A. Zapunny: Abyssal glasses, petrologic mapping of the oceanic floor and “geochemical Leg” 82. 1985.In: Bougault, H; Cande, SC; et al. (eds.), Initial Reports of the Deep Sea Drilling Project, Washington (U.S. Govt. Printing Office), 82, pp. 509-518.

Dosso, L., H. Bougault, C. Langmuir, C. Bollinger, O. Bonnier, and J. Etoubleau. The age and distribution of mantle heterogeneity along the Mid-Atlantic Ridge (31–41°N) // Earth Planet. Sci. Lett. 1999, 170, pp. 269–286.

Gente P., Dyment J., Maia M., Goslin J. Interaction between the Mid-Atlantic Ridge and the Azores hot spot during the last 85 Myr: Emplacement and rifting of the hot spotderived plateaus. // Geochemistry Geophysics Geosystems, 2003, V.4. №10. pp. 1–23.

Klein E.M., Langmuir C.H. Global correlations of ocean ridge basalt chemistry with axial depth and crustal thickness // J. Geophys. Res. 1987. Vol. 92. № B4. P. 8089–8115.

Madeira, J. & Ribeiro, A. Geodynamic models for Azores triple junction: A contribution for tectonics// Tectonophysics 1990. V.184, pp. 405 – 415.

McDonough W.F., S.-S.Sun The composition of the Earth Chemical Geology. 1995. Volume 120, Issues 3–4, 1, pp. 223-253.

Schilling J.-G./ Azores mantle blob: Rare-Earth evidence // *Earth Planetary Sci. Lett.* 1975 V. 25. pp. 103-115

Zhihuan Wan, Laurence a. Coogan, and Dante Canil Experimental calibration of aluminum partitioning between olivine and spinel as a geothermometer // American Mineralogist, 2008. V. 93, pp.1142–1147.

Сущевская Н.М., Б.В. Беляцкий, Д.А. Ткачева, Г.Л. Лейченков, Д. В. Кузьмин, А. В. Жилкина. Раннемеловой щелочной магматизм восточной Антарктиды (специфика, условия формирования, взаимосвязь с плюмом Кергелен) //Геохимия 2018, №11.

COMPOSITIONAL AND OSMIUM-ISOTOPE EVIDENCE FOR DISTINCT SOURCES OF PLATINUM-GROUP MINERALS FROM THE KONDYOR CLINOPYROXENITE-DUNITE MASSIF (ALDAN PROVINCE, RUSSIA)

Malitch K.N.[1], Badanina I.Yu.[1], Belousova E.A.[2], Khiller V.V.[1]

[1]Zavaritsky Institute of Geology and Geochemistry, Ural Branch of the Russian Academy of Sciences, Vonsovsky str. 15, Ekaterinburg 620016, Russia (dunite@yandex.ru)

[2]Department of Earth and Planetary Sciences, Macquarie University, Sydney, NSW 2109, Australia (elena.belousova@mq.edu.au)

The Kondyor massif is one of several zoned clinopyroxenite-dunite complexes within the Aldan Province, southeastern part of the Siberian Craton (Gurovitch et al., 1994; Malitch, 1999). About 100 metric tons of platinum have been mined from associated placer deposits in the past. The ultramafic rocks of the Kondyor massif have been subdivided into three lithologies (Burg et al., 2009): a main dunite core, an apatite-phlogopite-magnetite-rich clinopyroxenite that cuts dunite in the southwestern part of the massif, and a pyroxenite rim. The significant variability of ages, collected using different geochronological methods, has been reported for platinum-bearing rocks (86-2477 Ma) and platinum-group element mineralization (112-340 Ma), inviting contrasting interpretations of their origin (Efimov et al., 2012; El'yanov, Andreev, 1991; Gurovitch et al., 1994; Malitch, Thalhammer, 2002; Malitch et al., 2012; Nekrasov et al., 1994; Pushkarev et al., 2002; Shukolyukov et al., 2012, among others).

In order to gain further insights into genesis of platinum-group minerals (PGMs) we have carried out a combined compositional and osmium-isotope study of PGMs from: (i) chromitite within a dunite core, (ii) apatite-phlogopite-magnetite-rich clinopyroxenite and (iii) placer deposits. We integrate an application of a specific separation technique to concentrate PGMs from their host rocks, electron microprobe analyses to study composition of PGMs and Re-Os LA-MC-ICP-MS analyses of Os-rich alloy and laurite to date melt extraction and constrain the source region at the time of its formation.

To constrain textural relationships of PGMs with the associated gangue minerals, samples of chromitite and clinopyroxenite were first investigated in polished sections. Bedrock samples (1.0 kg each) were then disintegrated and milled, followed by sieving and removal of the fine fractions <56 and 56–100 microns. The heavy minerals (including PGMs) within these two fractions were concentrated by a hydroseparation technique (Knauf, 1996; Malitch et al., 2001) at NATI Research JSC, St. Petersburg, Russia. This technique reduces the amount of pure material from the disintegrated and sieved chromitite/clinopyroxenite fraction down to 1-4 milligrams. Each heavy-mineral concentrate was mounted in epoxy blocks and polished for further detailed microanalytical studies. Microprobe analyses of PGMs were carried out with an ARL-SEMQ microprobe with four wavelength-dispersive spectrometers (WDS) and equipped with a LINK energy dispersive analyser (Montanuniversität Leoben, Austria) and a CAMECA SX-100 equipped with five WDS spectrometers and a Bruker energy dispersive spectrometer system (Institute of Geology and Geochemistry, UB RAS, Ekaterinburg). Quantitative WDS analyses were performed at 25 kV accelerating voltage and 20 nA sample current, with a beam diameter of about 1 mm. The following X-ray lines and standards have been used: RuLα, RhLα, PdLβ, OsMα, IrLα, PtLα, NiKα (all native element standards); FeKα, CuKα, SKα (all chalcopyrite); AsLα (sperrylite). Corrections were performed for the interferences involving Ru-Rh, Ru-Pd and Ir-Cu. Details of the analytical procedures are described by Malitch et al. (2001) and Badanina et al. (2013). In-situ Os-isotope analyses of Os-bearing PGMs were carried out at Geochemical Analysis Unit at the CCFS/GEMOC laboratories (Macquarie University, Sydney, Australia) using analytical methods described in detail by Pearson et al. (2002) and Malitch et al. (2017).

Investigation of PGM grains from the chromitite and placer deposits revealed similar PGM assemblage dominated by Pt–Fe alloys with subordinate amounts of osmium (Os), laurite (RuS_2), erlichmanite (OsS_2), hollingworthite (RhAsS), irarsite (IrAsS), platarsite (PtAsS), sperrylite ($PtAs_2$) and tulameenite (Pt_2CuFe). PGM assemblage from stockwork clinopyroxenites contain predominant

cooperite and sperrylite, with subordinate Pt–Fe alloys, together with osmium, tulameenite, sobolevskite, braggite, keithconnite, irarsite, malanite, mertieite II, and a number of unnamed Pd-rich phases. Pt-Fe alloys from studied rocks show systematic compositional differences. Pt-Fe alloys from chromitite carry high contents of Ir (up to 4.87 mas %), whereas Pt-Fe alloys from apatite-phlogopite-magnetite-rich clinopyroxenite host rocks are enriched in Pd (up to 8.88 mas %). Therefore, high contents of Ir or Pd in Pt-Fe nuggets from placers are considered a diagnostic feature of their bedrock sources (e.g., chromitite vs apatite-phlogopite-magnetite-rich clinopyroxenite).

The Os-isotope data for four Os-rich alloy grains from chromitite show a restricted range of unradiogenic $^{187}Os/^{188}Os$ values between 0.1249 and 0.1254, with a mean of 0.1251±0.0001 (2 sigma, n=4), and $^{187}Re/^{188}Os$ <0.00003. This is consistent with the Os-isotope study of Os-rich alloys from chromitite and placer deposits (Malitch, Thalhammer, 2002), which gave a narrow range of $^{187}Os/^{188}Os$ values (between 0.1248 and 0.1252), indicative of a subchondritic mantle source of platinum-group elements (PGE). In contrast to Os-rich alloys with subchondritic $^{187}Os/^{188}Os$ values, Os-bearing PGMs from clinopyroxenite and placer deposits revealed much more pronounced range of radiogenic $^{187}Os/^{188}Os$ values (from 0.1295 to 0.1308, n=9), indicative of a suprachondritic source of PGE. This feature can be interpreted as evidence of a 'radiogenic' crustal component or an indication of an enriched mantle source. Consequently, suprachondritic $^{187}Os/^{188}Os$ values (>0.12863, Chen et al., 1998), which have been detected in detrital Os-bearing PGMs, clearly indicate their derivation from apatite-phlogopite-magnetite-rich clinopyroxenite host rocks of the Kondyor massif.

This study was supported by Russian Foundation for Basic Research (grant № 16-05-00967-a).

References

Badanina I.Yu., Malitch K.N., Murzin V.V. et al., Mineralogical and geochemical characteristics of PGE mineralization of the Verkh-Neivinsk dunite-harzburgite massif (Middle Urals, Russia) // Trudy IGG UrO RAN. 2013. Vol. 160. P. 188-192 (in Russian).

Burg J. P., Bodinier J.-L., Gerya N. et al., Translithospheric mantle diapirism: Geological evidence and numerical modeling of the Kondyor zoned ultramafic complex (Russian Far-East) // Journal of Petrology. 2009. Vol. 50. P. 289-321.

Chen J.H., Papanastassiou D.A., Wasserburg G.J. Re-Os systematics in chondrites and thefractionation of theplatinum-group elements in theearly solar system // Geochimica et Cosmochimica Acta. 1998. Vol. 62. P. 3379-3392.

Efimov A.A., Ronkin Yu.L., Malich K.N., Lepikhina G.A. New Sm-Nd and Rb-Sr (ID-TIMS) isotope data for apatite-phlogopite clinopyroxenites from the dunite "core" of the Konder Massif, Aldan Shield // Doklady Earth Sciences. 2012. Vol. 445. Part 2. P. 956-961.

El'yanov A.A., Andreev G.V. Magmatism and metallogeny of platform areas affected by multistage activization. Novosibirsk: Nauka Press. 1991. 168 p. (in Russian).

Gurovitch V.G., Zemlyanukhin V.N., Emel'yanenko E.P. et al., Geology, petrology and ore-forming potential of the Kondyor Massif. Moscow: Nauka Press. 1994. 176 p. (in Russian).

Knauf V.V. On the metrological background of mineralogical investigations // Zapiski Vsesoyuznogo Mineralogicheskogo Obshchestva. 1996. Vol. 125. P. 109-113 (in Russian).

Malitch K.N. Platinum-group elements in clinopyroxenite-dunite massifs of the Eastern Siberia (geochemistry, mineralogy, and genesis). St. Petersburg: Saint Petersburg Cartographic Factory VSEGEI Press. 1999. 296 p. (in Russian).

Malitch K.N., Belousova E.A., Griffin W.L. et al., Laurite and zircon from the Finero chromitites (Italy): new insights into evolution of the subcontinental mantle // Ore Geology Reviews. 2017. Vol. 90. P. 210-225.

Malitch K.N., Efimov A.A., Badanina I.Yu. The age of Kondyor massif dunites (Aldan Province, Russia): First U-Pb isotopic data // Doklady Earth Sci. 2012. Vol. 446. № 1. P. 1054-1058.

Malitch K.N., Melcher F., Mühlhans H. Palladium and gold mineralization in podiform chromitite at Kraubath, Austria // Mineralogy and Petrology. 2001. Vol. 73. P. 247-277.

Malitch K.N., Thalhammer O.A.R. Pt-Fe nuggets derived from clinopyroxenite-dunite massifs, Russia: a structural, compositional and osmium-isotope study // Canadian Mineralogist. 2002. Vol. 40. P. 395-418.

Nekrasov I.Ya., Lennikov A.M., Oktyabr'sky R.A. et al., Petrology and platinum potential of the ring alkaline-ultramafic complexes. Moscow: Nauka Press. 1994. 381 p. (in Russian).

Pearson N.J., Alard O., Griffin W.L. et al., In situ measurement of Re-Os isotopes in mantle sulfides by laser ablation multicollector-inductively coupled plasma mass spectrometry: Analytical methods and preliminary results // Geochimica et Cosmochimica Acta. 2002. Vol. 66. P. 1037-1050.

Pushkaryov Yu.D., Kostoyanov A.I., Orlova M.P., Bogomolov E.S. Peculiarities of Rb-Sr, Sm-Nd, Pb-Pb, Re-Os and K-Ar isotope systems in the Kondyor massif: mantle susbstratum, enriched in PGE // Regional'naya Geologiya i Metallogeniya. 2002. Vol. 16. P. 80-91 (in Russian).

Shukolyukov Yu.A, Yakubovich O.V., Kotov A.B. et al., New geochronometer for the direct isotopic dating of native platinum minerals (190Pt-4He method) // Petrology. 2012. Vol. 20. № 6. P. 491-505.

PERTOGENETIC REASONS OF DIVERSITIES OF PICRITES OF THE LESSER CAUCASUS AND TALISH

***Mamedov M.N.*[1], *Babayeva G.J.*[1], *Mansurov M.M.*[2], *Abbasov K.F.*[1],*Kerimov V.M.*[3]**

[1]*Institute of Geology and Geophysics of NASA*

[2]*Baku State University*

[3]*Azerbaijan State University of Oil and Industry*

Picrites unlike other magmatic rocks, characterize composition of initial mantle sources. In the turn, formation of the picrites depends on specific geodynamic conditions, which facilitate a high degree of melting of the mantle substance. The petrological differences of the picrites likely, are because of variations in the composition of the initial sources and the degree of the partial melting of that sources. Within the Lesser Caucasus, picrites have been found within the bajocian and bathonian volcanics of the Lok-Murovdagh structural-formational zone.

Macroscopically the rocks are in dark black color, where the grains of an olivine are distinguishable from the background. Furthermore, intrusion has a slightly hornfelized contact with surrounding volcanics. They occur in the layer form morphology within the bajocian volcanics of the Murovdagh anticlinorium. This outcrop in the thickness of 15-20 m stretches more than 40-50 m in the northwest direction.

The rocks of the intrusion are almost monotone and composed of olivine and olivine-pyroxene bearing porphyritic picrites. The most bigger and overriding grains are presented with bipyramidal olivine. These olivines are cut with loopy serpentines (chrysotile, antigorite, lizardite and etc.). Between the loops the relicts of the olivines of forsterite-chrysolite composition ($Fo_{8-14\%}$) have been preserved. Not infrequently, in the loops of the serpentines have been concentrated a sufficient amount of a chromite. Beside of them, in some occasions octahedral grains of the chromite form intergrown crystals with olivine. Orthopyroxenes are presented with sporadic, short prismatic grains with the composition of the bronzite (Fs_{12-18}). Clinopyroxenes in comparison with the orthopyroxenes, spread widely in the rock and are presented with the chromite bearing diopside.

In the total crystalline basis of the picrites occur small rounded grains of the olivine (Fo_{20}) and short prismatic segregations of the diopside-salite.

In the contact zone of the intrusion the olivine has been fully chloridized and in the most cases epidote is identified. These very picrites have been recorded within the Allahverdi and Lok-Aghdam anticlinoria.

Relatively younger, i.e. upper cretaceous picrites, picrodolerites and picrobasalts have been recorded in the santonian volcanics of the Gazakh trough of the Lok-Aghdam structural formational zone. Here, picrites and picrodolerites in the south-western side of the aforementioned trough form thin layer shaped veins, stocks and so forth.

Picrites and picrodolerites are also characterized by black color and are made up of porphyritic rocks. Phenocrysts are presented with hyalosiderite olivine (Fo_{40-48}), augite ($Wo_{41}En_{36}Fe_{23}$) and bitovnite plagioclase (An_{70-78}). Beside of them, sporadic square formed ferrochromites and titanomagnetites occur. In the content of the picrites the dominant part is phenocrysts of olivine and clynopyroxene. As picrites pass to picrodolerites the amount of the olivine and the clinopyroxene gradually decreases and the amount of a plagioclase increases noticeably.

In picrobasalts the major phenocrysts are also composed of olivine and clinopyroxene. In the intersertal and vitrophyric base of these rocks small phenocrysts of plagioclase and clinopyroxene have been recorded.

Subalkaline picrites, picrotephiretes and picroteshenites have been recorded within the santonian alkali and subalkali volcanics of the Khojavend trough of the Lok-Karabagh zone of the Lesser Caucasus. Here subalkali picrite as an inclusion (up to 3x5cm) has been detected in lava breccias of the tephrites. Inclusions of the subalkali picrites are distinguishable in the mass of dark grey tephrite. The structure of the subalkali picrite is also porphyritic and the bulk mass is holocrystalline. Phenocrysts consist of phlogopite, chrome diopside, olivine and chrome spinel. Phenocrysts of the chrome diopside and olivine presents equally, olivine constitutes 10% of the phenocrysts. Phlogopite presents not more than 4-6%. Holocrystalline bulk mass is composed of chrome diopside, in relatively less amount of phlogopite, In the picrodolerites the amount of the olivine and the phlogopite gradually decreases, whereas the amount of the chrome diopside increases. Picroteshenites in the form of a black belt are confined to the lower parts of the Tugh differential intrusion. One of the peculiarity of these subalkali picrites and their differentiates is that, they have abundance of chermak molecule ($CaAl_2SiO_6$=10-16%) in the clinopyroxenes and phlogopite occurs in the content. The normalized La/Yb ratio varies between 4.9-7.6.

Subalkali picrites have been recorded in the Talish mountains of the Elbrus zone.

Subalkali pircrites of the Talish Mountains are of the later Eocene and early Oligocene age. They are located within the flysch like tuffogenic sedimentary complex of the later Oligocene in the form of dike, small stocks and sometimes layer injections. Here, subalkali picrites as other analogues have black color. Where big clinopyroxene phenocrysts (up to 0.5x2.5 cm) are distinguishable from the background. Under a microscope a structure of these picrites is porphyritic, bulk mass is holocrystalline. Phenocrysts consist of olivine (Fo_{20-25}), clinopyroxene ($Wo_{44}En_{44}Fe_{12}$) in the equal quantity and in the relatively lesser quantity of phlogopite (2-4%) and chrome spinel (0.5-1%). In the bulk mass dominating part is small prisms of clinopyroxene. It is necessary to note that, unlike the clinopyroxenes of the subalkali picrites of Khojavend, here clinopyroxene is lesser abundant in chermak molecule ($CaAl_2SiO_6$=4-6%).

On the base of the obtained geologic-petrological as well as geochemical data of difference of the picrites, it is possible to note that, picrites of the Murovdagh and Allahverdi anticlinoria are characterized by the low concentration of the REE and the flat behavior of these elements. Furthermore, the normalized La/Yb ratio varies in the narrow range- from 0.9 to 1.3. All these prove that, picrites of noted structures are likely derivatives of the depleted mantle substance.

Subalkali picrites of the Khojavend trough of the Lesser Caucasus and Talish zone are noticeably enriched in light REE and depleted in heavy REE. Thereby, normalized La/Yb ratio increases. Furthermore, the total normalized quantity of the REE increase (4.2-7.4). So, it can be considered that, these picrites have melted from the metasomatically changed mantle.

Picrites and picrodolerites of the Kazagh trough of the Lesser Caucasus are relatively lesser enriched in light and heavy REE. Their total normalized content varies in wide range (from 7.1 to 8.2). Apparently, a highly heated picritic decreasing of the penetration of the faults in transitional magma chambers have undergone gravitational crystallization-differentiation. By the virtue of it, carriers and concentrators of the heavy REE such as olivine, pyroxenes and chrome spineliods settled in the bottom part of the transitional chambers. Light REE concentrated in the residual melting. Accordingly, the Kazakh trough differs from the other structures of the Lesser Caucasus and Talish in the spectrum of the REE propagation.

Thus, differences of the picrites of the Lesser Caucasus and Talish mountains are the results of differences in upper mantle substance, as well as the degree of their melting. Furthermore, an important value have the geological-geodynamical conditions of the melting of the picrites and their crystallization.

References

Леснов Ф.П. Редкоземельные элементы в ультраосновных и основных породах и в их минералах. Новосибирск: Гео. 2007, с.133-140.

Izokh A.E. et al. The Ureg Nuur Pt-bearing volcanoplutonic picrite-basalt association in the Mongolian Altay as evidence for a Cambrian-Ordovician Large Igneous Province // Russian Geology and Geophysics. 2010. Vol.51. Iss. 5 p.p.521-533.

HIGH PRESSURE TRANSITIONS IN THE SYSTEM MGAL2O4 – MGCR2O4 AT 10–24 GPA AND 1600°C

***Matrosova (Sirotkina) E.A.*[1], *Bobrov A.V.*[1,2], *Bindi L.*[3], *Irifune T.*[4]**

[1]*Vernadsky institute of Geochemistry and Analitycal Chemistry RAS, Moscow, Russia*
ekaterina.a.sirotkina@gmail.com;
[2]*Geological Faculty, Moscow State University, Moscow, Russia;*
[3]*Dipartimento di Scienze della Terra, Università di Firenze, Via La Pira 4, 50121 Florence, Italy*
[4]*Geodynamics Research Center, Ehime University, Matsuyama 790-8577, Japan.*

$MgCr_2O_4$ and $MgAl_2O_4$ are the most important end-members of chrome spinel inclusions in natural diamonds and mantle-derived peridotite (Sobolev, 1974). In addition, spinel and Cr-spinel are widespread in igneous and metamorphic rocks as accessory minerals, and are considered as an important indicator for petrogenesis (e.g., Sack, Ghiorso, 1991). Chromium-bearing spinels are characterized by the negative correlation between aluminium and chromium. The concentration of $MgCr_2O_4$ in chrome spinel from inclusions in diamonds and xenoliths of Grt-peridotite reaches 95 and 85 mol % (63–68 wt % and 57–63 wt % Cr_2O_3), respectively (Meyer, Boyd 1972; Sobolev 1974), whereas the content of Al_2O_3 does not exceed 4–8 wt %. Spinel with the lowest Cr content (25-38 wt% Cr_2O_3) is observed in the xenoliths of spinel peridotites from kimberlites and alkaline basalts (Gregoire et al., 2006 etc). Chromian spinels containing high-pressure minerals (e.g., diamond and coesite) were discovered in chromitites in the Luobusa ophiolite, Tibet (Yamamoto et al. 2009; Dobrzhinetskaya et al. 2009). The $MgCr_2O_4$ (Ishii et al., 2015) and $MgAl_2O_4$ (Irifune et al., 1991; Akaogi et al., 1999 etc) systems have been deeply studied experimentally. However, high-pressure and high-temperature phase relations in the $MgAl_2O_4$–$MgCr_2O_4$ join have not been studied yet. Our experiments were aimed on the study of phase relations, synthesis of post-spinel phases (with a calcium titanate- and calcium ferrite-type structures) and their solid solutions in the $MgAl_2O_4$–$MgCr_2O_4$ system at 10–24 GPa and 1600°C.

The experiments were performed using a 2000-t multi-anvil high-pressure apparatus at the Geodynamics Research Center, Ehime University (Japan). Tungsten carbide cubic anvils with 4.0/3.0 mm truncation edge length were applied as the second-stage anvils of the high-pressure apparatus. The pressure medium was a semi-sintered (Mg,Co)O octahedron of 10.0/8.0 mm in edge length. A tubular $LaCrO_3$ heater was inserted into the pressure medium. The temperature was measured using a $W_{97}Re_3$–$W_{75}Re_{25}$ thermocouple. The temperature measurement accuracy was ±10°C. Pressure was controlled to ±0.5 GPa (Irifune et al., 1991). Details of the experimental techniques were described by Sirotkina et al. (2015).

At 10–24 GPa and 1600°C we studied the full range of the starting materials in the $MgAl_2O_4$ (Sp)–$MgCr_2O_4$ (MChr) system in increments of 30 mol % MChr and 2 GPa, which allowed us to synthesize post-spinel phases with a wide compositional range. Depending on PT-parameters and starting composition, the main phases obtained in experiments were $Mg(Al,Cr)_2O_4$ with spinel-type structure (at 10–16 GPa), association of phase $Mg_2Cr_2O_5$ with modified ludwigite structure-type (mLd) and $(Cr,Al)_2O_3$ eskolaite/corundum and phase $Mg(Cr,Al)_2O_4$ with calcium titanate-type structure or

periclase (at 14–23 GPa), $Mg(Cr,Al)_2O_4$ with calcium titanate-type structure (at a pressure of >17 GPa) and phase $Mg(Al,Cr)_2O_4$ with calcium ferrite-type structure (at a pressure of >23 GPa).

Textural relationships in experimental samples are evident from BSE photomicrographs (Fig. 1). At 12 GPa, $Mg(Al,Cr)_2O_4$ spinel is stable in the middle part of the system. This mineral forms massive aggregates (Fig. 1a) with a size of individual grains up to 200 μm. Increase of pressure up to 15 GPa results in the formation of an association of $Mg_2(Al,Cr)_2O_5$ (mLd) and corundum (Cor) by the following reaction:

$$2Mg(Cr,Al)_2O_4(MChr/Sp)=Mg_2(Cr,Al)_2O_5(mLd)+(Cr,Al)_2O_3(Esk/Cor) \quad (1)$$

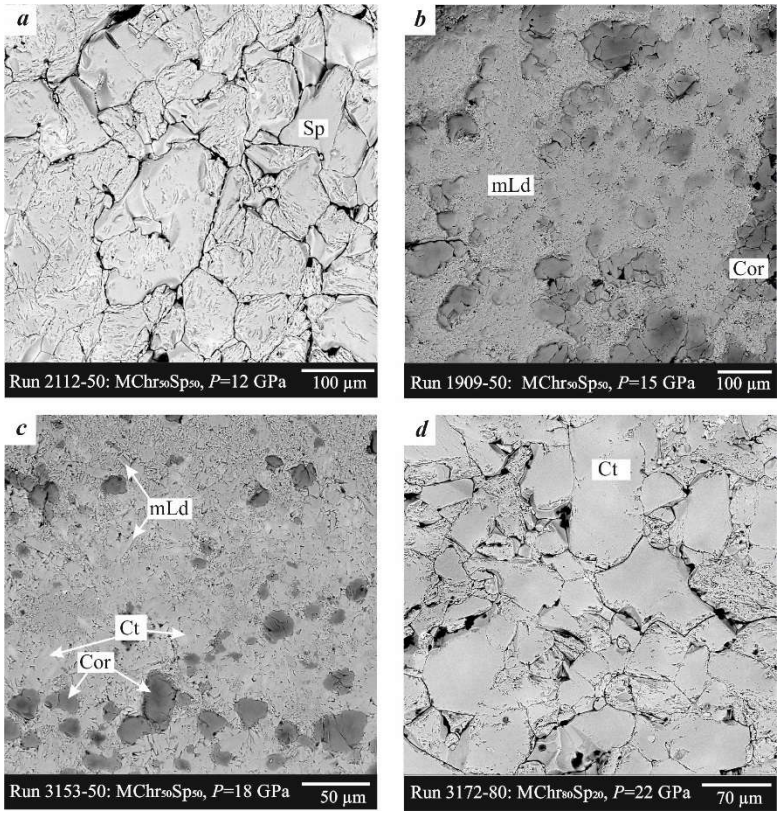

Fig. 1. BSE images of textural relationships in the $MgAl_2O_4$–$MgCr_2O_4$ system at 10–24 GPa.

The sample texture is formed by small elongated mLd crystals and relatively large euhedral Cor grains with size <100 μm (Fig. 1b). A paragenesis of $Mg(Cr,Al)_2O_4$ (Ct) with mLd and Cor appears at 18 GPa in the narrow range of starting compositions (40–60 mol % MChr) by the reaction (1). Decrease of chromium content in the bulk compositions (0–40 mol % MChr) results in the formation of an association of mLd, Cor and periclase (Per). Appearance of this association is controlled by the reaction: $MgO\ (Per)+(Al,Cr)_2O_3(Cor)=Mg(Al,Cr)_2O_4(Sp)$ (2).

The texture of the experimental sample is similar to that described previously and shown in Fig. 1c. The texture is formed by an aggregate of euhedral Cor crystals with grain size of >30 μm and relatively small crystals of Ct in the fine-grained mass of elongate mLd crystals with length up to 20 μm. The stability field of phase $Mg(Cr,Al)_2O_4$ (Ct) opens up at pressures of >17 GPa in the chromium-rich part of the system. The formation of Ct is controlled by the reaction (1). Ct forms large euhedral crystals with a grain size of up to 150 μm (Fig. 1d).

The most Cr-rich mantle assemblages include podiform chromitites in ophiolitic complexes, were formed through reaction between mantle peridotite and melt with subsequent magma/melt mixing at an uppermost mantle level (Arai, Yurimoto, 1994). Recently the data on the composition and relationships of Cr-bearing phases were involved for substantiation of the high-pressure origin of the Luobusa chromitite in the processes of deep recycling and upwelling mantle flow (Arai, 2013). The P-T parameters of the chromitite formation have been discussed by petrologists for a long time.

Yamamoto et al. (2009) suggested a UHP precursor with a Cf structure originally formed at a pressure of >12.5 GPa and then decomposed to low-pressure chromite containing silicate exsolutions.

Ishii et al. (2015) studied the simple MgCr2O4 system and suggested that absence of the phase assemblage (mLd+Esk) stable at 12–18 GPa provides evidence for the lower (<12 GPa) pressures of the origin. The new phase $Mg(Mg,Cr,Si)_2O_4$, which was synthesized by Bindi et al. (2015), is stable in a wide pressure range (12–18 GPa). The discovery of this phase contradicts the conclusion of (Yamamoto et al., 2009) and limits the highest pressure of the Luobusa chromitite formation to ~12 GPa, above which mCt is stable. However, as we can see, the authors considered systems without aluminium. Addition of Al to the starting material allows us to simulate the composition of podiform chromitites in ophiolitic complexes more accurately. In this relation, further experimental studies are required to evaluate the competitive reaction between Al and Cr to establish the structural features of post-spinel phases and P-T parameters of stability of these phases, as well as the limit entry of Cr to the $MgAl_2O_4$ – Cf and Al to $MgCr_2O_4$ – Ct.

This study was supported by the Russian Science Foundation (project no. 17-17-01169). Synthesis of the post-spinel phases was partly supported by the Foundation of the President of the Russian Federation (Grant No MK-1277.2017.5).

References

Akaogi M., Hamada Y., Suzuki T. Kobayashi M., Okada M. High pressure transitions in the system $MgAl_2O_4$–$CaAl_2O_4$: a new hexagonal aluminous phase with implication for the lower mantle. // Phys Earth Planet Inter. 1999. Vol. 115(1). P. 67-77.

Arai S. Conversion of low-pressure chromitites to ultrahigh-pressure chromitites by deep recycling: a good inference // Earth Planet Sci Lett. 2013. Vol. 379. P. 81-87.

Arai S., Yurimoto H. Podiform chromitites of the Tari-Misaka ultramafic complex, southwestern Japan, as mantle–melt interaction products. // Economic Geol. 1994. V. 89. P. 1279–1288.

Bindi L., Sirotkina E.A., Bobrov A.V., Irifune, T. Structural and chemical characterization of $Mg[(Cr,Mg)(Si,Mg)]O_4$, a new post-spinel phase with sixfold-coordinated silicon. // Am Mineral. 2015. Vol. 100(7). P. 1633-1636.

Dobrzhinetskaya L.F., Wirth R., Yang J., Hutcheon I.D., Weber P.K., Green H.W. High-pressure highly reduced nitrides and oxides from chromitite of a Tibetan ophiolite. // Proceedings of the National Academy of Sciences. 2009. Vol. 106(46). P. 19233-19238.

Gregoire M., Bell D.R., Le Roex A.P. Garnet lherzolithes from the Kaapraval Craton (South Africa): Trace element evidence for a metasomatic history. // J Petrol. 2006. Vol. 44. P. 629–657.

Irifune T., Fujino K., Ohtani E. A new high- pressure form of $MgAl_2O_4$. // Nature. 1991. Vol. 349. P. 409–411.

Ishii T., Kojitani H., Fujino K., Yusa H., Mori D., Inaguma Y., Matsushita Y., Yamaura K., Akaogi M. High-pressure high-temperature transitions in $MgCr_2O_4$ and crystal structures of new $Mg_2Cr_2O_5$ and post-spinel $MgCr_2O_4$ phases with implications for ultra-high pressure chromitites in ophiolites. // Am Mineral. 2015. Vol. 100. P. 59–65.

Meyer H.O.A., Boyd F.R. Composition and origin of crystalline inclusions in natural diamonds. // Geoch Cosmochim Acta. 1972. Vol. 59. P. 110-119.

Sack R.O., Ghiorso M.S. An internally consistent model for the thermodynamic properties of Fe−Mg-titanomagnetite-aluminate spinels. Contrib Mineral Petrol. 1991. Vol. 106(4). 474-505.

Sirotkina E.A., Bobrov A.V., Bindi L., Irifune T. Phase relations and formation of chromium-rich phases in the system $Mg_4Si_4O_{12}$–$Mg_3Cr_2Si_3O_{12}$ at 10–24 GPa and 1,600 °C // Contrib Mineral Petrol. 2015. Vol. 169:2. DOI: 10.1007/s00410-014-1097-0.

Sobolev N.V. Deep-seated inclusions in kimberlites and the problem of the Upper Mantle composition. Nauka. 1974. Vol. 183.

Yamamoto S., Komiya T., Hirose K., Maruyama S. Coesite and clinopyroxene exsolution lamellae in chromites: In-situ ultrahigh-pressure evidence from podiform chromitites in the Luobusa ophiolite, southern Tibet. // Lithos. 2009. V. 109. P. 314-322.

MAJOR AND TRACE ELEMENT COMPOSITION OF ROCK-FORMING MINERALS IN OLIVINE LEUCITITES FROM GAUSSBERG VOLCANO (WEST ANTARCTICA): IMPLICATIONS FOR PARENTAL MAGMA ORIGIN

***Migdisova N.A.*[1], *SushchevskayaN.M.*[1], *Portnyagin M.V.*[1,2], *Batanova V.G.*[1,3]**

[1]*Vernadsky Institute of Geochemistry and Analytical Chemistry of Russian Academy of Sciences, 119991, Kosygin str., 19, Moscow, Russian Federation, nat-mig@yandex.ru*

[2]*GEOMAR Helmholtz Centre for Ocean Research, Kiel, Germany*

[3]*Institut des Sciences de la Terre (ISTerre) Université Grenoble Alpes-CNRS Maison des Géosciences 1381 rue de la Piscine BP 53, 38041 Grenoble Cedex 9, France*

Separation of Antarctica from India and the opening of the Indian ocean began about 130 Ma under the influence of the Kergelen mantle plume. The plume influence is presently spread along the eastern edge of the Antarctica. The Gaussberg volcano is located on the eastern coast of the Princess Elizabeth Land (57° S, 89° E). The surface of the volcano is covered with well preserved pillow lavas (0.5 - 2 m in diameter) and with lava fragments encrusted with vitreous 3-5 cm thick glassy margins, which suggest subglacial eruptions. The rocks have olivine leucitite composition, K-Ar ages of 56 ± 5 ka and are considered to be the youngest known manifestations of lamproite magmatism on Earth (Tingey, 1983).

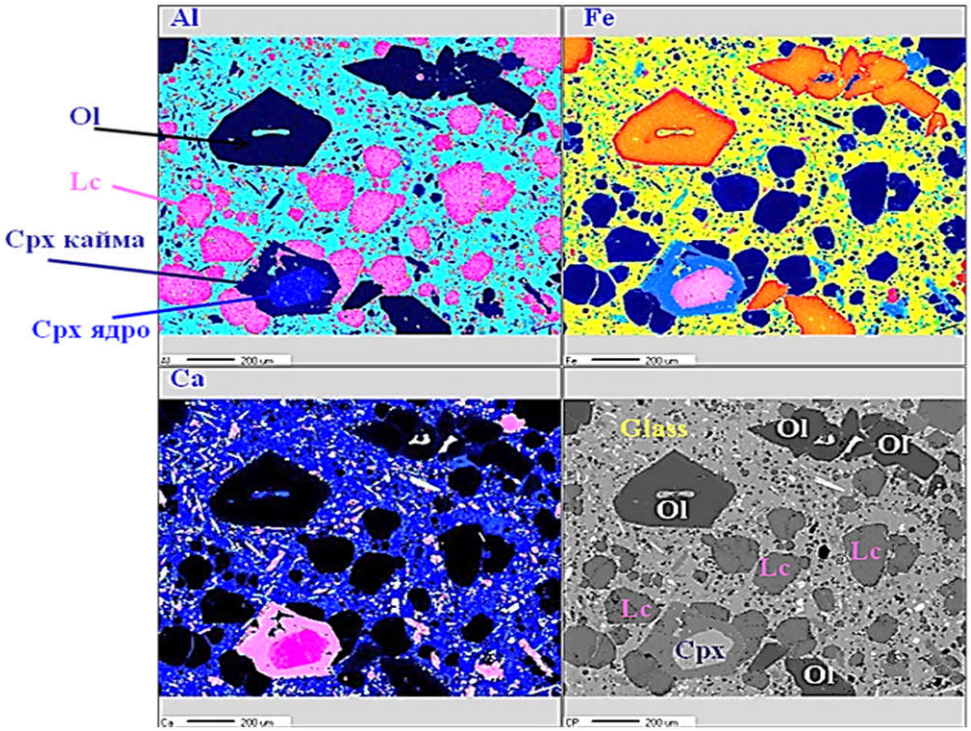

Fig. 1. Distribution of Al, Ca, Fe and BSE intensity in a fragment of typical Gaussberg lamproite.

The samples studied were fresh lava fragments. The rocks are vesicular. The amount of voids increases towards the pillow margins. Mineral assemblage consists of microphenocrysts of olivine (10%), leucite (20-40%) and clinopyroxene (5%) usually < 1 mm in size (Fig. 1). Rare crystals of apatite, ilmenite, phlogopite, titanium magnetite, zircon, orthopyroxene are also present. The groundmass (30-60%) consists of microliths of leucite, diopside, red-brown mica and amphibole in glassy matrix. The order of crystallization is: chromium spinel → olivine → clinopyroxene → leucite (Foley, 1985; Sushchevskaya et al., 2014). Gaussberg lamproites exhibit highly enriched in LREE, strongly fractionated spectra ($La_n/Yb_n = 80$, $Dy_n/Yb_n \approx 2.2$, $Sm_n/Nd_n = 0.4$). Characteristic features of the lamproites are also Zr, Hf, Ba and Pb maxima and K, Rb, U, Nb, Ta minima relative to REE of similar incompatibility in the PM-normalized patterns.

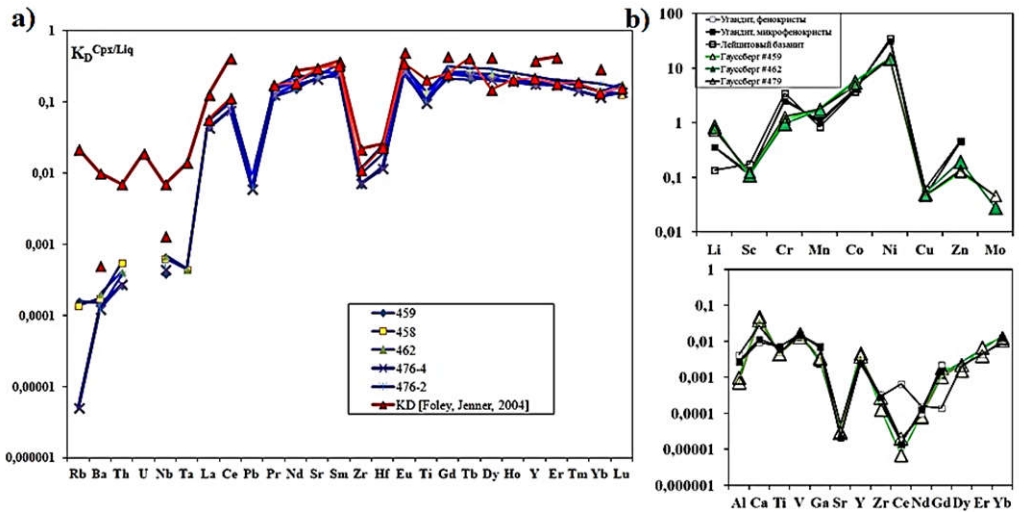

Fig. 2. Partition coefficients between clinopyroxene and melt (a) and olivine and melt (b).

Here we present new high precision data on the concentrations of major and trace elements in olivine, clinopyroxene and leucite phenocrysts from the Gaussberg olivine leucitites. Mineral analysis was performed using high precision techniques specially developed for the determination of very low concentrations of elements in mineral phases by the microprobe JEOL JXA 8230 at the ISTerre Université Grenoble Alpes (Batanova, 2015) and by LA-ICP-MS at the Institute for Geosciences at the Christian-Albrecht University (Kiel, Germany). La-ICP-MS analyses were conducted on a mass spectrometer Agilent 7500s combined with a system of laser ablation GeolasPro (Cogerent). The diameter of the laser beam was 60 microns. Other conditions of analysis and standardization were similar to those described in the paper (Sobolev et al., 2016).

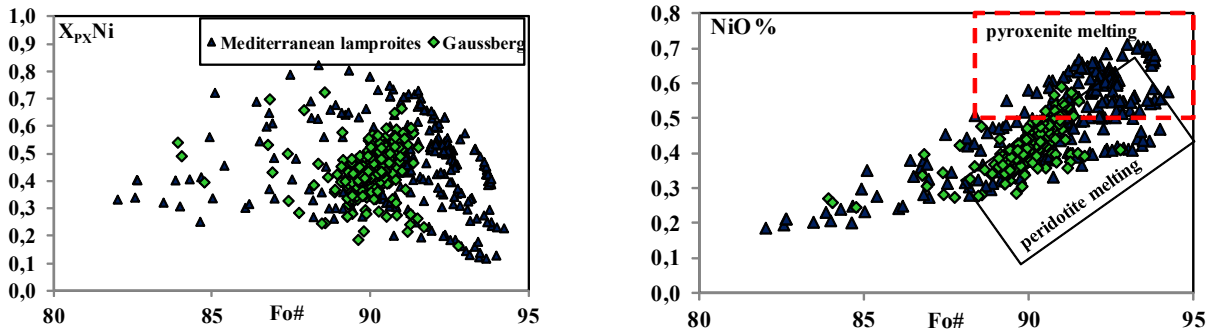

Figure 3. The rare element contents in Gaussberg olivine phenocrysts in comparison with Mediterranean belt olivine lamproites (Prelevic et al., 2013).

The major results are following:

1) The compositions of coexisting olivine and Cr-spinel (Coogan, 2014) suggest crystallization temperature 1180 – 1250 °C. Oxygen fugacity varied from the less oxidized fO_2 values (below the buffer MW) to more oxidized (NNO) during the melt evolution.

2) We estimated for the first time the partition coefficients of a number of trace elements between the main mineral phases and lamproitic melt. In particular, $D_{Cu}^{olivine/melt}$ = 0.02 and $D_{Zn}^{olivine/melt}$ = 0.76-0.81 have significant importance for the interpretation of the mantle source of primary lamproitic melts.

3) We propose that the source of Gaussberg lamproites was a mixture of pyroxenite of non-continental provenance and depleted mantle peridotite.

This work was supported by RNF grant №16-17-10139.

References

Tingey R.J., McDougall I., Gleadow A.J.W. The age and mode of formation of Gaussberg, Antarctica // Journal of the Geological Society of Australia. 1983. № 30. P.241-246.

Foley S.F. The oxidation state of lamproitic magmas // Min. Petr. Mitt. 1985. V. 34, p. 217-238.

Сущевская Н.М., Мигдисова Н.А., Антонов А.В., Крымский Р.Ш., Беляцкий Б.В., Кузьмин Д.В., Бычкова Я.В. Геохимические особенности лампроитовых лав четвертичного вулкана Гауссберг (Восточная Антарктида) - результат влияния мантийного плюма Кергелен // Геохимия. 2014. №12. С.1-21.

Batanova V., Sobolev A.V., Kuzmin D.V. Trace element analysis of olivine: High precision analytical method for JEOL JXA-8230 electron probe microanalyser // Chemical Geology 2015. V. 419. DOI: 10.1016/j.chemgeo.2015.10.042.

Coogan L.A., Saunders A.D., Wilson R.N. Aluminium-in-olivine thermometry of primitive basalts: Evidence of an anomalously hot mantle source for large igneous provences // Chemical Geology, 2014. V. 368, pp. 1-10.

Prelevic D., Jacob D.E., Foley S.F. Recycled continental crust is an essential ingredient of Mediterranean orogenic mantle lithosphere. Earth Planet. Sci. Lett., 362, p. 187-197, 2013.

KREEP-COMPONENT AS A RESULT OF THE DIFFERENTIATION OF BASALT MAGMA

Miklyaeva E.P., Bychkova Ya.V., Bychkov A.Yu.

Lomonosov Moscow State University, Moscow, Russia, yanab66@yandex.ru

KREEP-basalt is one of important characteristic features of lunar geology. A lot of samples, brought from the Moon by expedition of Apollon 11, 12, 15, 17 are characterize by the specific composition. These rocks are distinguished by a high content of such elements as K, rare earth elements and P. Genesis of these rocks is open to question, because they are not typical for Earth as a result of magma crystallization. Parent magma of these rocks must be very specific – enriched by incoherent elements.

The most informative objects to research processes of basalt magma fractionation on the Earth are layered intrusions. They have different composition and are characterized by different degree of crust contamination, but there differentiation is certainly a result of consistent crystallization during the cooling of magma chamber. Noritic layered intrusions can be considered as terrestrial analogues of the magmatic ocean of the Moon. Author for a long time research features of structure and composition of Kivakka layered intrusion (Northern Karelia). Average composition and sequence of its crystallization is the same as in Bushveld massif. Kivakka layered intrusion contain 4 types of rocks, which result the process of crystallization differentiation of basaltic magma. They form consistent layering from dunite to gabbronorite with thin layering, confined to change of cumulative paragenesis. In extreme differentiates of the top pegmatoid gabbronorites in the Upper zone a lot of lens appeared. They are characterized by high concentrations of REE, K, P (Table 1, Fig 1). Eu / Eu* is negative whereas in all norite and gabbro-norite it is positive dui to plagioclase (Fig 1).

Such parameters are typical for most of Upper zone granophyres in layered intrusions. It is not enougth information about all of them, but some of data are in the Table 1. Two samples of gabbro-norite, containing KREEP lenses, are placed in the upper positions of this table, and two samples of KREEP lunar norite are placed in the lower positions for comparison. It is important, that not all of these rocks are situated in the highest parts of massifs. For example in Dovyren intrusion the first appearance of granophyres is noted 400 m below the roof, in Tsipringa intrusion – 700 m below the roof.

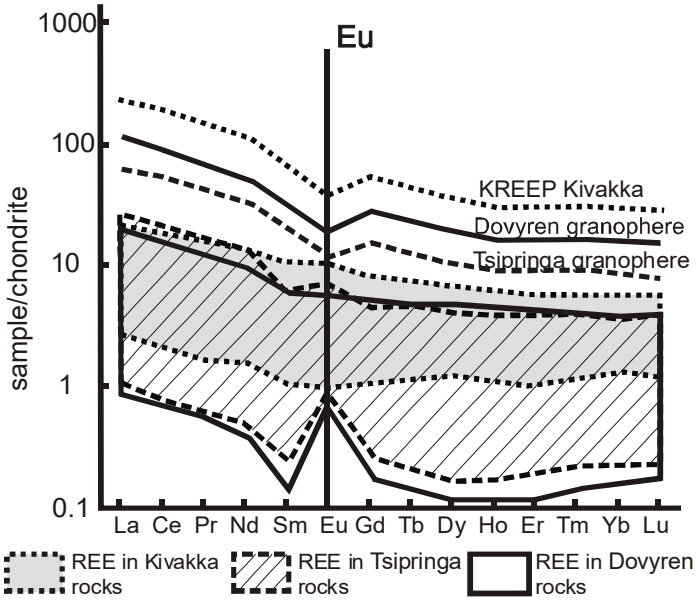

Fig. 1. Spider-diagram of REE in some intrusions, with position of KREEP-rocks

Table 1. Composition of granophyre, KREEP lenses from Kivakka intrusion and containing rocks of different layered intrusions.

Intrusion and type of rocks	SiO_2	Al_2O_3	TiO_2	MgO	FeO	MnO	CaO	Na_2O	**K_2O**	**P_2O_5**	sum
	w %	w %	w %	w %	w %	w %	w %	w %	**w %**	**w %**	w %
Kivakka gabbro-norite	50.53	13.40	0.42	11.89	10.02	0.18	9.63	2.00	0.29	0.05	98.41
Kivakka gabbro-norite	48.55	14.74	0.56	8.38	10.42	0.18	12.89	2.91	0.34	0.05	99.02
Kivakka KREEP lense	51.86	14.86	1.30	4.39	14.94	0.17	8.52	3.18	**0.75**	**0.15**	100.12
Kivakka KREEP lense	63.27	13.37	1.56	2.03	7.87	0.13	6.72	3.65	**0.80**	**0.54**	99.94
Dovyren granophyre	58.64	16.11	1.14	3.04	13.51	0.17	4.09	1.89	**2.50**	**0.10**	101.19
Tsipringa granophyre **	54.21	14.38	2.05	3.93	12.17	0.23	8.71	2.79	**0.65**	**0.88**	100.00
Tsipringa granophyre	49.42	14.45	1.82	6.21	15.36	0.23	7.83	3.45	**0.79**	**0.24**	99.81
Scaergaard granophyre ***	57.30	11.13	1.42	0.81	17.47	0.28	4.83	3.51	**1.83**	**0.35**	98.93
Scaergaard granophyre ***	58.81	12.02	1.26	0.72	15.56	0.21	5.03	3.87	**2.25**	**0.71**	100.44
Scaergaard granophyre ***	60.23	11.19	1.18	0.51	15.24	0.24	5.11	3.92	**1.94**	**0.27**	99.83
Duluth diorite****	49.30	12.20	3.43	4.90	13.80	0.21	9.10	2.75	**0.80**	**0.63**	97.12
Low-KREEP lunar Norite*	45.70	15.84	1.38	17.89	9.27	0.12	9.13	0.55	**0.22**	**0.22**	100.32
High-KREEP lunar Norite*	47.90	15.60	1.80	10.93	10.74	0.15	9.90	0.78	**0.52**	**0.60**	98.92

Wood et al. 1977, ** Semenov et al. 1995, *** Wager & Brown, 1968, **** Layered intrusions, 1996

The XRF analysis was carried out at the Laboratory for the Analysis of Mineral Substances of the IGEM RAS by A.Yakushev.

Diameter of KREEP lenses in Kivakka intrusion is 10-50 sm and they have no sharp boundaries with the host coarse-grained gabbronorite. These lenses are formed by quartz-orthoclase symplectite (Fig. 2a), apatite, Ti-magnetite, zircon, baddeleite (Fig. 2b), amphibole, phlogopite and even REE-minerals. Apatite, amphibole and phlogopite are characterized by high concentration of Cl. The same minerals are present in granophyre of Upper zones in layered intrusions and in lunar KREEP basalt.

Composition of apatite in Kivakka KREEP lenses is like lunar apatite (Lin et.al, 2012) and like apatite from Bushveld Upper zone (VanTongeren, 2012). As for REE concentration (Fig. 3) it is close to lunar and one of apatite generation from Bushveld (the second Bushveld apatite generation is characterized by the lack of Eu-anomaly). Apatite is characterized by high concentration of Cl –0.64-1.74% (Table 2). This phenomenon makes us think, that genesis of KREEP can be result of liquation. Such hypothesis was proposed to explain the apparent of two generation of apatite in the Upper zone of Bushveld.

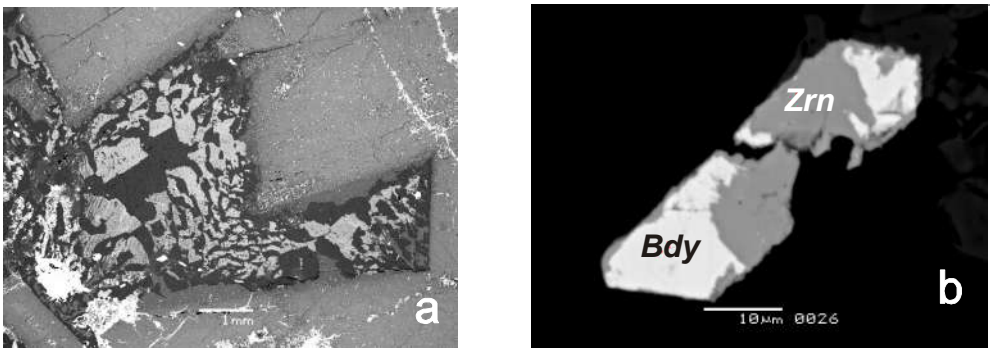

Fig. 2. Microphotographs of the minerals
from Kivakka KREEP-lenses.
a. symplectite, b. zircone with baddeleite

We conducted a series of experiments on melting of different rocks of Kivakka massif with water and NaCl at different conditions and proportion in IEM RAS under the direction of O.G Safonov. The first experiment of melting (T=1000ºC, P=2 kBar) different rocks of massif (90%) with NaCl (10%) in 6 samples, partial melting occurred, 1 melting was not achieved. The result of the second experiment of melting (T=1200 ºC, P=2.5 kBar) of mix gabbro-norite (90%) and NaCl (10%) with water (5, 10, 15 and 20%) was the formation of glass regardless of the mix-water ratio without any features of liquation.

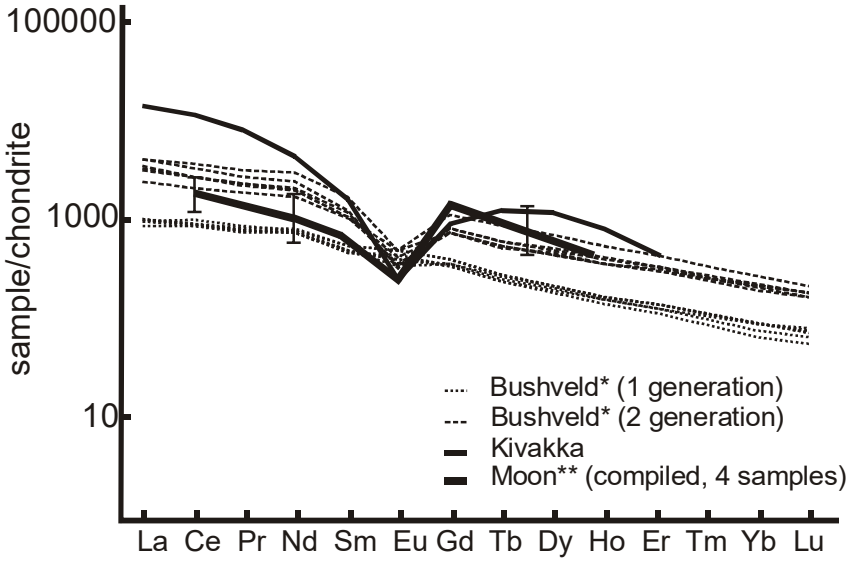

Fig.3. Spider-diagram of REE configuration inapatite from Kivakka and Bushveld (VanTongeren, 2012) layered intrusions and inapatite in lunar KREEP (Lin et.al, 2012)

In conclusion we can say that KREEP-component is not specific lunar feature. Such types of rocks appears in the most of the earth differentiated massifs and, apparently are the result of deep fractionation of basalt parent magma. Residual melt accumulated incoherent elements and was located in layeres (Bushveld, Duluth, Tsipringa, Dovyren) or in lenses (Kivakka, Scaergaard). While we do not know for sure geological structure of lunar objects, we can not pinpoint the location of KREEP rocks, but the similarity in many respects with the same terrestrial rocks makes as think, that their genesis is the same as on the Earth.

Table 2. Composition of Kivakka and lunar KREEP apatite.

	Kivakka KREEP apatite							Lunar apatite*			
	KVP 55-4	KVP 76-05	KVP 76-07	KVP 76-16	KVP 76-18	KVP 74-05	KVP 74-06	VHK KREEP		Matrix	
FeO		0.19	0.14	0.03	0.05	0.4	0.39	0.7	0.84	0.61	0.59
P_2O_5	42.08	41.06	41.09	40.98	41.34	40.62	38.84	41.2	41.9	41.9	40.6
CaO	54.18	54.39	54.1	54.27	54.37	53.75	51.83	54.8	54.7	53.9	53
SiO_2	0.31	0.34	0.33	0.41	0.36	0.4	2	0.49	0.51	0.49	1.57
Ce_2O_3		0.1	0.22	0.01	0.13	0.27	1.41	0.06	0.09	0.08	0.07
Cl	0.92	0.71	1.74	0.64	0.66	0.84	0.93	0.94	1.03	1.12	1.17
F	2.87	2.48	1.77	2.48	3.07	2.42	2.28	2.75	2.9	3.09	2.88
Total	100.36	99.54	99.75	99.2	100.28	99.19	99.13	99.79	100.85	99.75	99.18

*(Lin et.al, 2012)

This work was supported by Russian Science Foundation research project No 18-17-00170.

References

Hiroshi Wakita, J. C. Laul, R. A. Schmitt. Some thoughts on the origin of lunar ANT-KREEP and mare basalts // Geoc. J., 1975, Vol. 9, pp. 25-41.

John A. Wood. A Survey of Lunar Rock Types and Comparison of the Crusts of Earth and Moon // NASA Technical Reports Server (NTRS) 19780004984. 1977.

L.Wager and G.Brown. Layered igneous rocks. Edinburg and London. 1968. 552 p.

Layered intrusions. Ed. R.G.Cawthorn. Elsevier. Amsterdam. 1996. 531 p.

Lin Y. , Shen W. , Liu Y. , Xuc L., Hofmann B.A., Maob Q., Tang G.Q., Wua F., Li b X.H. Very high-K KREEP-rich clasts in the impact melt breccia of the lunar meteorite SaU 169: New constraints on the last residue of the Lunar Magma Ocean // Geoc. et Cosmoc. Acta. 2012. 85. P.19–40

Semenov V.S., Koptev-Dvornikov E.V., Berkovskii A.N., Kireev B.S., Pchelintseva N.F., Vasil'eva M.O. Layered troctolite-gabbro-norite Tsipringa intrusion, Northern Karelia: geologic structure and petrology // Petrology. 1995. Vol. 3. P. 645.

VanTongeren J.A. and Mathez E.A. Large-scale liquid immiscibility at the top of the Bushveld Complex, Sourth Africa // Geology, 2012. Vol.40. №6. P. 491-494.

SOME OBSERVATIONS ON SPILITIZED BASALTS OF THE WESTERN DECCAN TRAPS, INDIA

Naik A.[1], Sheth H.[1], Samant H.[2], D'Souza S.[2]

[1]Department of Earth Sciences, Indian Institute of Technology Bombay, Mumbai 400076, India (email: hcsheth@iitb.ac.in)

[2]Department of Geology, St. Xavier's College, Mumbai 400001, India

Spilites are altered basaltic rocks that contain sodic plagioclase (albite) and chlorite, instead of the calcic plagioclase (labradorite) and clinopyroxene (usually augite) typical of basalt. The conversion of calcic to sodic plagioclase requires a source for Na, which may be seawater or hydrothermal fluids, whereas the Ca released by basalt alteration forms minerals like epidote and calcite in the resultant spilite. Primary spilitic magmas have been proposed, a hypothesis not generally favoured, whereas at least two other hypotheses exist for spilites, namely, alteration of basalt by hydrothermal fluids or hot seawater, or low-grade burial metamorphism of basalt under a thick volcanic pile, with many proponents (see Amstutz, 1974, and references therein).

The Deccan Traps of India form a large (presently 500,000 km^2) flood basalt province, ~65 million years in age. The basalts are largely tholeiitic, especially those of the western and southwestern parts of the province next to the western Indian rifted margin. There is extensive spilitization of the lower part of this basaltic pile exposed in the Konkan Plain between the western Indian coastline and the Western Ghats escarpment (Sukheswala, 1974; Sethna and Javeri, 1999; *Fig. 1a-c*). The spilitized

basalts have a very distinctive appearance: they are characteristically spotted, with abundant, roughly circular, black or dark grey spots on a greenish or light grey background. The green-grey coloured rock is spilitized, whereas the black spots are parts of the basalt which have escaped spilitization (Sethna and Javeri, 1999). We note that presence of relict pristine spots of black basalt in a greenish spilitized matrix makes the notion of a primary spilitic lava implausible. The spotty character results from an incomplete reaction between the basalt and Na-rich fluids causing spilitization.

Some of these spilitized basalt occurrences are well-formed pillow lavas, as at the Bagwada quarry near Daman (Sethna and Javaeri, 1999; Ali, 2014; *Fig. 1a*), representing subaqueous counterparts of small-scale compound pahoehoe lava flows. The Bagwada occurrence is thus similar to the pillowed spilites of the Mumbai area, which formed in shallow marine conditions (Sukheswala, 1974; Vallance, 1974; Hellman, 1981, 1984). With such conditions, a ready source of the Na required for albitization is available.

However, most of the spilitized basalts along the Konkan Plain, over a distance of several hundred kilometers, are not pillowed, but are very thick eruptive units with no internal contacts (*Fig. 1b, c*). They nevertheless have the same spotted character as the Bagwada spilitized basalt pillows. It could be argued that these thick flow units (which are partly spilitized like the pillowed ones at Bagwada) may simply indicate the entry of high-eruption rate lava flows into a shallow sea, which again would provide a ready source of Na. We note here that the Bagwada pillows sit adjacent to a very thick flow unit, without a fault in between, and this may represent a thick flow unit coming to rest and feeding small pillows as breakouts at its terminus.

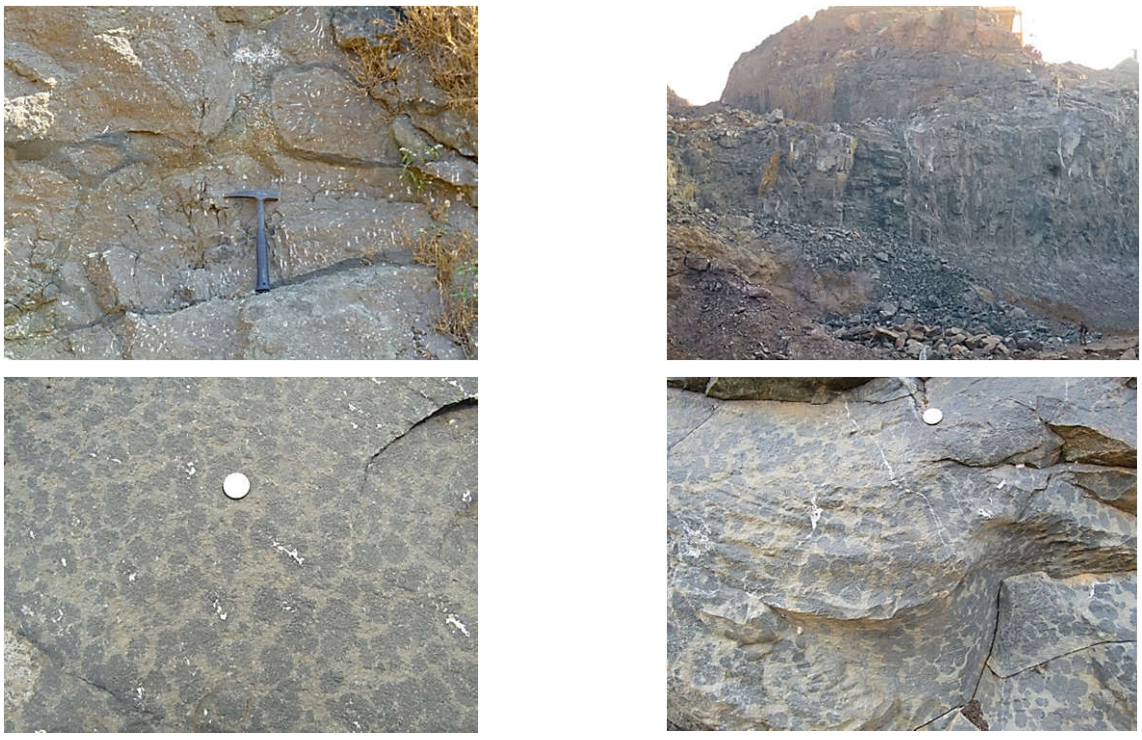

Fig. 1. (a) Spilitized basalt pillows at Bagwada, near Daman. The black spots are pristine, unaltered basalt. (b) A very thick spilitized basalt flow, without internal boundaries, at Dunetha quarry near Daman. The rocks are light green to grey and spotted throughout, like those shown in the following photos. In the centre of photo is a thick tholeiitic dyke. Person in lower right corner of photo is Berthold Ottens. (c) Typical spilitized basalt with spotty appearance in the Vasai area, near sea level. Coin diameter 2.5 cm. (d) Essentially identical spilitized basalt at 550 m in the Tungareshwar section, Vasai. Coin 2.5 cm wide.

While the above remains a possibility, we have found a spilitized basalt flow in the Tungareshwar section near Vasai (sample TNG 14, *Fig. 1d*), at 550 m above present mean sea level (A. Naik, Ph.D. thesis in preparation). The sea was never this high, and there is no indication of block-

faulting that may have brought this spilitized flow several hundred meters up from sea level. Moreover, the spilitized basalt flow is underlain and overlain by non-spilitized flows. Thus, low-grade burial metamorphism cannot explain the spilitization in only this flow, and in none of the other flows, especially the underlying flows.

We propose therefore that alteration processes specific to this flow, caused by hydrothermal fluids, produced this spilitized basalt. The hydrothermal solutions may have been derived from the flow itself, after advanced crystallization. Indeed, the common presence of natrolite among other zeolites common in flood basalts like those of Iceland and the Deccan Traps (Walker, 1960; Sukheswala et al., 1974; Avasia and Gandopadhyay, 1984; Ottens, 2003) indicates that the late hydrothermal solutions can contain significant amounts of Na. Alternatively, such solutions may have been supplied by intense intrusive activity in the Vasai region, seen in the numerous gabbroic plutons and innumerable dykes of varied compositions, mafic to felsic.

We agree that deep burial of flood basalts under a growing volcanic pile and associated low-grade metamorphism can produce spilites and spilitized basalts in general, and that this may well explain the low-lying spilitized basalts of the Konkan Plain (with a subaqueous, marine or lagoonal environment added for the Bagwada occurrence). As seen above, this process cannot explain the high-elevation occurrence of spilitized basalt which is identical in every way with the low-elevation spilitized basalts.

The “spilite problem” (Amstutz, 1974) has been all but forgotten in recent times but is an important topic in geology, requiring successful integration of datasets of field geology and volcanology, mineralogy, igneous and metamorphic petrology, and high- and low-temperature geochemistry. We point out that the western Deccan Traps is an excellent region to investigate the spilite problem.

References

Ali MDS. Geology, petrography and eruptive environment of spilitic lavas of the Daman area, southern Gujarat. 2014. M.Sc. dissertation, Indian Institute of Technology Bombay.

Amstutz G. C. Spilites and Spilitic Rocks. Berlin: Springer. 1974. 426 p.

Avasia R. K., Gandopadhyay M. Distribution of secondary minerals in the western Deccan Traps of Bombay-Baroda coastal tract, India. Ind Mineralogist, Sukheswala Vol. 1984, pp. 215–230.

Hellman P. L. The geochemistry and phase chemistry of the spilite-tholeiite, Bhoiwada section, Bombay Island, India. In: Subbarao, K. V., Sukheswala, R. N. (Eds.) Deccan Volcanism and Related Basalt Provinces in Other Parts of the World. 1981. Geological Society of India Memoir, Vol. 3, pp. 434–459.

Hellman P.L. The geochemistry and phase chemistry of a spilitic pillow from the Bhoiwada section, Bombay Island, India. Ind. Mineralogist, Sukheswala Vol. 1984, pp. 44–68.

Ottens B. Indian Zeolites and Related Species: Minerals of the Deccan Traps, India. Min. Rec. 2003 Vol. 34, pp. 4–82.

Sukheswala R. N. Gradation of tholeiitic Deccan basalt into spilite, Bombay, India. In: Amstutz G.C. (Ed.) Spilites and Spilitic Rocks. 1974. Berlin: Springer, pp. 229–250.

Sukheswala R. N., Avasia R. K., Gangopadhyay, M. Zeolites and associated secondary minerals in the Deccan Traps of western India. Min Mag. 1974 Vol. 39, pp. 658–671.

Sethna S. F., Javeri P. Geology and petrochemistry of Deccan spilitic basalts at and around Daman, India. J. Geol. Soc. Ind. 1999 Vol. 53, pp. 59–69.

Vallance, T. H. Spilitic degradation of a tholeiitic basalt. J. Petrol. 1974 Vol. 15, pp. 79–96.

Walker G. P. L. Zeolite zones and dyke distribution in relation to the structure of the basalts of eastern Iceland. J. Geol. 1960 Vol. 68 pp. 515–528.

ISOTOPE-GEOCHEMICAL MODELS OF MAGMOGENESIS AND EVOLUTION OF CARBONATITE COMPLEXES OF THE URALS FOLD BELT: RB-SR, SM-ND AND LU-HF ISOTOPE SYSTEMATICS

Nedosekova I.L.[1], Belyatsky B.V.[2]

*[1]Zavaritsky IGG UB RAS, Ekaterinburg, Russia (*correspondence: vladi49@yandex.ru)*

[2]Karpinsky Geological Institute, CIR, St.Petersburg, Russia

The isotope characteristics of the carbonatite complexes of the Urals and associated REE-Zr-Nb deposits are obtained. Using the Sm-Nd and Lu-Hf isotope systems for the Ilmeny-Vishnevogorsk carbonatite-miaskite complex (IVC), the substrate age was determined (T_{DM}: 700-850 Ma, T_{DMC}: 900-1200 Ma), crystallization age (428-417 Ma) and subsequent metamorphic transformations (380-250 m.y. ago). The depleted nature of the melting substrate for IVC magmas with the probable mixing of the depleted source with the lower crust and/or plume component is established: $^{87}Sr/^{86}Sr_{440}$= 0.70336–0.70380, ε_{Nd440} (+2.9…+5.8), ε_{Hf440} (+4.7…+11.4) (Nedosekova et al, 2010; Nedosekova et al, 2013; 2015; 2016).

The age of the protolith (T_{DM}: 900-1300 Ma), age of formation of ore (rare-metal) alkaline metasomatites and carbonatites (285-250 Ma) was determined for the Buldym carbonate-ultramafic complex (Nedosekova, 2012; Nedosekova et al, 2014). The isotope characteristics of the ultramafic and carbonatites of the Buldym massif correspond to moderately enriched mantle compositions of the EM1 type: $^{87}Sr/^{86}Sr_{440}$ = 0.70421–0.70470, ε_{Nd440} (+0.7…-2.8), and ε_{Hf440} (0…-2) (Nedosekova et al, 2013).

As a result of the overview of Sm-Nd and Lu-Hf isotope data, the Buldym carbonate-ultramafic complex has a slightly depleted character of protolith, which differs from the magma substrate of the Ilmeny-Vishnevogorsk carbonatite-miaskite complex by age and isotopic composition (share of depleted and enriched material in the mantle substrate) (Fig.1). Thus, for the miaskite-carbonatite complex (IVC), the model age (T_{DM}) of the protolith is 600-900 Ma (calculated from the one-stage model, which assumes the generation of magmas from the depleted mantle), and for the Buldym carbonatite-ultrabasic complex, the model age is 900-1300 Ma. The calculation of the protolith model age by a two-stage model, assuming a crustal source of magma generation (T_{DMC}), also shows the difference in ages of these complexes (T_{DMC}: 900-1250 Ma – IVC, T_{DMC}: 1000-1450 Ma – Buldym Complex). It should be noted that the model ages (T_{DMC} and T_{DM}) of the protoliths of IVC (900-1250 Ma) and of the Buldym (900-1300 Ma) complexes almost coincide.

These data are provoking to discuss two ulternative models of magmogeneration of the Ilmeny-Vishnevogorsk and Buldym complexes:

1) diversity in time of formation of the substrate of the Buldym (1300-900 Ma) and Ilmeny-Vishnevogorsk (900-600 Ma) complexes from mantle sources of different isotope composition, but initially of depleted substances (DM);

2) synchronous formation of the ptotolith of the Ilmeny-Vishnevogorsk (T_{DMC}: 900-1300 Ma) and Buldym (T_{DM}: 900-1300 Ma, T_{DMC}: 1200-1450 Ma) complexes, involving both mantle and crustal sources of substance, which may be associated with simultaneous magmogenesis at various depths. It is noteworthy that the time of substrate of Buldym complex formation corresponds to the Riphean stages of continental rift propagation (1450(?), 1385-1350 Ma – Mashak event), fixed by outpourings of alkaline basalts and riftogenic magmatism in the Riphean rocks of the Bashkir anticlinorium on Ufa branch of the Russian platform (Puchkov, 2010).

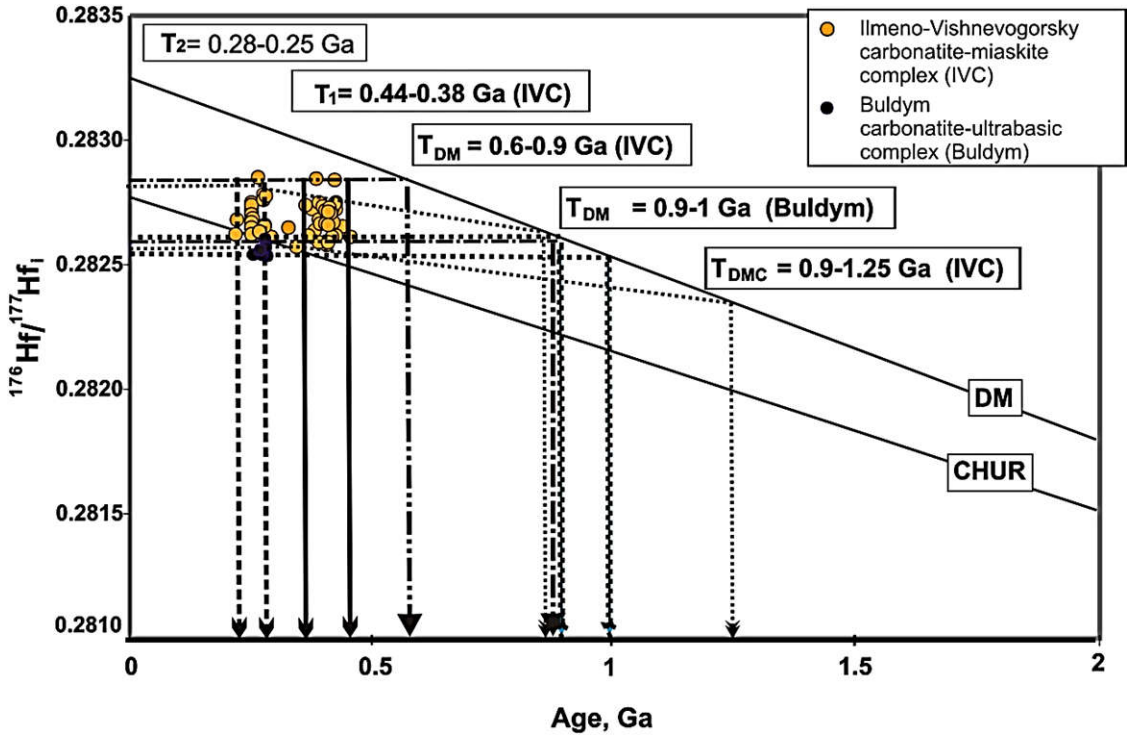

Fig. 1. Time of the model sources formation, stages of magma genesis and evolution of rare-metal carbonatite complexes of the Urals (Lu-Hf isotope systematics). Mantle reservoirs: DM (depleted mantle); CHUR (chondrite composition reservoir). T_{Dm} – the time of protolith formation from the depleted mantle, T_{Dmc} – the time of protolith formation according two-stage model of magma genesis from the crust source, T_1 – the time of alkaline-carbonatite magmas and rare-metal (Nb-Zr-REE) formation at the paleozoic stage of activity, T_2 – the time of rocks and ores of carbonatite complexes transformation on the stage of Uralian collision.

Summing up we conclude that isotope-geochemical models of magmogenesis and evolution of rare-metal carbonatite complexes of the Urals have been developed. The formation of the substrate occurred at various stages of tectono-magmatic activation – 1300-900 and 900-600 Ma; generation and intrusion of alkaline-carbonatite magmas – 440-380 Ma, which corresponds to the main stages of rifting of the Russian platform and paleocontinental part of the Urals. Isotopic models indicate the depleted character and heterogeneity of melting sources (DM and EM1 type), multi-stage magmatic and ore formation at the stage of Paleozoic activation, and the transformation of rocks and ores of carbonatite complexes at the stage of collision metamorphism (280-250 Ma).

Source of financial support (Project 17–05–00154).

References

Nedosekova I.L. The age and matter sources of the Ilmeny-Vishnevogorsk alkaline complex (S. Urals): geochemical and Rb-Sr, Sm-Nd, U-Pb and Lu-Hf isotopic data // Litosphera. 2012. № 5. P. 77-95 (in Russian).

Nedosekova I.L., Belousova E.A., Sharygin V.V. The substance sources for the Ilmeny-Vishnevogorsk complex based on Lu–Hf-isotopes in zircons // Doklady RAS. 2010. V. 435. № 2. P. 234-239 (in Russian).

Nedosekova I.L., Belousova E.A., and Belyatsky B.V. Hf Isotopes and Trace Elements as Indicators of Zircon Genesis in the Evolution of the Alkaline-Carbonatite Magmatic System (Il'meno-Vishnevogorskii Complex, Urals, Russia) // Doklady RAS, 2015. V. 461. № 5. P. 569-574 (in Russian).

Nedosekova I.L., Belousova E.A., and Belyatsky B.V. U-Pb-age и Lu-Hf isotopic systems of zircons of the Ilmeny-Vishnevogorsk complex, S. Urals // Litosphera. 2014. № 5. P. 19-32 (in Russian).

Nedosekova I.L., Belyatsky B.V., Belousova E.A. REE and hafnium isotope composition as an indicators of zircon genesis due to the alkaline-carbonatite magmatic system evolution (Russia) // Geology and geophysics. 2016. V.57. № 6. P. 1135-1154 (in Russian).

Nedosekova I.L., Belousova E.A., Sharygin V.V., Belyatsky B.V., Baynova T.B. Origin and evolution of the Il'meny-Vishnevogorsky carbonatites (Urals, Russia): insights from trace-elements compositions, Rb-Sr, Sm-Nd, U-Pb and Lu-Hf isotope data // Mineralogy and Petrology. 2013. V. 107. P. 101-123.

Puchkov V.N. Geology af the Urals and subUrals (actual questions of stratigraphy, tectonics, geodynamics and metallogeny). Ufa, DisainPoligrafServis. 2010. 280 p.

COMPARISON OF THE EFFECTIVENESS OF VARIOUS METHODS FOR THE PREPARATIO OF DIFFERENT TYPES OF ROCKS FOR ICP-MS ANALYSIS

Nikolaeva I. Yu., Bychkova Ya.V., Bychkov A.Yu.

Lomonosov Moscow State University, Moscow, Russia, yanab66@yandex.ru

Mass-spectrometry play the great rule in geochemistry research of rocks and minerals. It make possible to determine law concentrations of wide spectrum of trace elements. Rocks and minerals are characterized by complex matrix, containing macro components. It required series of sequential operations to desolve solid samples, using different reactives. Tree main methods are used for this task: 1. acidic decomposition with microwave, 2. fusion with carbonates, hydroxides or borates of alkali metals, followed by dissolution of the resulting smelt. Any one has advantages and disadvantages and can be used depending on the task.

While using acidic decomposition (Bychkova et al., 2016), authors were convinced that not all elements can be dissolved completely. Such elements as Zr, Hf, Nb, Ta in granite, andesite and granodiorite, B in all rocks and other became a real problem. To solve the problem of volatile elements like B, Se, As we tried to use method of sintering with soda. It became successful both for some volatile elements and for Zr, Hf, Nb, Ta in acid rocks. This method usually applies to decompose metal materials (Dolezhal et al., 1968). For it realization it is necessary to use platinum melting pots in high temperature muffle. Authors had modified method for rocks and used alundum pots. Proportions of sample (0.1 g) and soda are 1:3, sintering temperature 800ºC, time of sintering 2-2.5 hours. After sintering samples were dissolved in the mix of concentrated acids: 3.5 ml HNO_3:HF (10:1) and 0.5 HCl. Then solution was diluted to the volume of 50 ml.

It is necessary to emphasize that sintering method does not throw off silicate matrix. It creates additional matrix pressure in the process of measurement and Si imposes interference on ^{45}Sc, while we use quadrupole mass-spectrometers.

Important part of any methodical research is verification by certified samples. We used samples or rocks with different contrast composition – dunite (DTS-1b), basalt (BHVO-2), granodiorite (GSP-2), granite (SG-3), sienite (SY-2), kimberlite (GSO-8042-94) and bottom sediment (MODAS-2). Bottom sediments were tested also for the decomposition quality of the organic component. All samples were prepared for measurement by two methods – acidic decomposition and sintering with soda. Measurement was realized by mass-spectrometer of high resolution Element-2 in the laboratory of experimental geochemistry of MSU geological faculty. Before measurement all samples were diluted 100 times and supplemented by internal standard of In to control instrument fluctuations.

As a result of decomposition we can see, that not all samples were dissolved completely by acidic decomposition - a precipitate formed in the solutions. DTS-1b (dunite) is characterized by dark crystal residue, and MODAS-2 (bottom sediments) is characterized by dark suspension. It show, that acidic decomposition does not provide dissolution of chromite and organic component, while samples decomposited by sintering method showed visually complete dissolution.

Comparison of some important results of measurement is presented in table.

Table.1 Composition of some trace elements in reference material.

	BHVO-2			GSP-2			SY-2			GSO-8042-94		
	A.D.	S.D.	**Pref. Value**	A.D.	S.D.	**Pref. Value**	A.D.	S.D.	**Pref. Value**	A.D.	S.D.	**Pref. Value**
	mg/g	mg/g	**mg/g**	mg/g	mg/g	**mg/g**	mg/g	mg/g	**mg/g**	mg/g	mg/g	**mg/g**
Rb	8.8	9.1	**9.3**	242	237	**245**	220	216	**217**	24	27	**22**
Sr	391	396	**394**	245	236	**240**	280	274	**271**	825	915	**810**
Ba	129	134	**131**	1384	1333	**1340**	441	445	**460**	789	794	
La	15	15	**15**	182	183	**180**	69	68	**75**	103	108	
Ce	36	37	**38**	427	428	**410**	168	163	**175**	189	194	
Pr	5.1	5.2	**5.3**	54	54	**51**	20	20	**19**	19	20	
Nd	23	24	**24**	199	202	**200**	76	75	**73**	65	67	
Sm	5.5	5.7	**6.0**	24	24	**27**	15	15	**16**	9.1	9.4	
Eu	1.9	2.0	**2.0**	2.2	2.2	**2.3**	2.4	2.4	**2.4**	2.5	2.5	
Gd	5.5	5.6	**6.2**	15	15	**12**	16	15	**17**	9.5	6.0	
Tb	0.96	0.95	**0.94**	2.00	1.96	**1.09-1.54**	3.1	3.1	**2.5**	0.95	0.81	
Dy	5.2	5.2	**5.3**	5.6	5.7	**6.1**	20	20	**18**	3.0	3.0	
Ho	0.96	0.99	**0.99**	1	1	**1**	4.7	4.7	**3.8**	0.49	0.51	
Er	2.5	2.5	**2.5**	3.1	3.2	**2.2**	15	15	**12**	1.4	1.2	
Tm	0.30	0.31	**0.33**	0.21	0.24	**0.29**	2.5	2.5	**2.1**	0.14	0.14	
Yb	1.9	1.9	**2.0**	0.9	1.3	**1.6**	18	18	**17**	0.67	0.76	
Lu	0.25	0.26	**0.28**	0.14	0.20	**0.23**	2.9	2.8	**2.7**	0.13	0.07	
Pb	1.7	1.8	**1.7**	50	47	**42**	58	55	**85**	69	63	**68**
Th	1.2	1.2	**1.2**	104	106	**105**	353	354	**379**	10	14	
U	0.40	0.44	**0.41**	2.1	2.4	**2.4**	274	261	**284**	2.8	2.8	
Sc	32	32	**32**	6.0	6.3	**6.3**	6.9	7.0	**7.0**	11	11	
V	302	296	**318**	49	48	**52**	47	45	**50**	66	69	**70**
Y	24	24	**26**	23	25	**28**	123	122	**128**	12	13	
Zr	167	170	**171**	35	485	**550**	290	298	**280**	139	62	**140**
Nb	16	16	**18**	21	25	**27**	28	28	**29**	126	130	**110**
Hf	4.4	4.0	**4.5**	0.3	12	**14**	7.6	7.9	**7.7**	3.3	1.6	
Ta	1.1	1.0	**1.2**	0.6	0.8	**0.5 - 1**	1.6	1.6	**2.0**	6.1	4.7	

A.D. – acidic decomposition, S.D. – decomposition by sintering method, Pref.Value – preferred value (GeoRem).

Measured values showed relatively good consistency with preferred values for both methods. But some features must be discussed. Basalt (BHVO-2) and syenite (SY-2) showed the best results, and we can recommend both methods for decomposition.

Decomposition of granodiorite (GSP-2) by acidic method was not successful due to such elements as U, Sc, Y, Zr, Hf, Nb and Ta. They were not dissolute completely. The worst result was obtained for Zr and Hf, which measured concentrations were 10 times less than preferred values. Sintering method shows good result for all of these elements.

Test of kimberlite was complicated by insufficient quantity of preferred values, so we could test only 8 elements. This test shows that the best result can be obtained using acidic decomposition, while sintering method does not provide complete transfer of Zr to solution.

Results for dunite was unsatisfactory, because of very low concentrations of trace elements. Such of rocks can be prepared for measurement by sintering, because this method allows to dissolve a significant share of chromite, but dilution was too strong.

Test for granite turned out to be ambiguous. Most complete dissolution of Rb, Sr, Cs, Pb, V was achieved by acidic method, but for Zr, Hf, Ta sintering method was more successful.

As a conclusion we can recommend acidic decomposition for basalt, alkaline rocks and kimberlite, while decomposition by sintering method is more effective for andesitic, dioritic and acid rocks. Also it is good to decompose spinel and organic constituent.

Authors wish to thanks Dr. A.Kozlovsky for critical analysis of the results.

This work was supported by Russian Science Foundation research project No 18-17-00170.

References

Bychkova Ya V., Sinitsyn M.Yu, Petrenko D.B., Nikolaeva I.Yu, Bugaev I.A., Bychkov A.Yu. Method peculiarities of multielemental analysis of rocks with inductively-coupled plasma mass spectrometry // Moscow University Geology Bulletin. 2017. Vol. 72. № 1. pp. 56-62.

J.Dolezhal, P.Povodra, Zd.Shultcek. Methods of decomposition of rocks and minerals. Moscow. 1968. 274 p.

GeoRem. Geologocal and Environmental reference Materials. http://georem.mpch-mainz.gwdg.de/sample_query_pref.asp.

THE ORIGIN OF MAGNETITE-APATITE ROCKS OF MUSHGAI-KHUDAG COMPLEX (SOUTH MONGOLIA)

***Nikolenko A.M.*[1], *Doroshkevich A.G.*[1,2], *Chakrabarty A.*[3], *Ragozin A.L.*[1,4]**

[1]*VS Sobolev Institute of Geology and Mineralogy Siberian Branch Russian Academy of Sciences (SB RAS), pr. Akademika Koptyuga 3, 630090, Novosibirsk, Russia*

[2]*The Geological Institute of SB RAS, st. Sakhyanova 6a, 670047, Ulan-Ude, Russia*

[3]*Indian Institute of Science Education and Research (IISER) Tirupati, Department of Earth and Climate Science, Andhra Pradesh – 517507, India*

[4]*Novosibirsk State University, st. Pirogova 2, 630090, Novosibirsk, Russia*

The Mushgai-Khudag complex (in Russian, Mushugai-Khuduk) is a part of the Late Mesozoic Central Asian carbonatite province (Nikiforov and Yarmolyuk, 2004). This complex is located in the southern part of Mongolia in the Gobi desert. The complex hosts nephelinites, alkali feldspar trachytes, phonolites, which are crosscut by stocks and dykes of alkaline syenites, shonkinites and magnetite-apatite rocks, as well as numerous small fine-grained carbonatite dykes (Samoilov and Kovalenko, 1983). A very late-stage fluorite mineralization is widespread in the Mushgai-Khudag area. The single Rb-Sr isochron age of alkaline syenites: 139.9 ± 5.9 Ma (Baatar et al., 2013).

Apatite and magnetite-apatite rocks are exposed in two stocks 30 × 70 and 10 × 30 m in size within the alkaline syenite field. The former stock is called Apatite Hill. Very coarse-grained magnetite rocks (nearly monomineralic) comprise the central parts of the stock and gradually changes to magnetite-apatite (interstitial apatite), apatite - phlogopite and pure apatite towards the peripheral part of the stock. In the southern part of the Apatite Hill ~3 × 5 m zone of hydrothermally altered apatite and magnetite-apatite rocks have been found. The host alkaline syenites are characterized by the presence of apatite-magnetite schlieren of variable dimension. In schlieren, apatite fills interstitial spaces between magnetite grains. Sometimes apatite-phlogopite rims are observed at the contact with host alkaline syenites.

Magnetite-apatite rocks show variable degrees of hydrothermal alteration. The distinction between the unaltered, weakly altered to those with extensively hydrothermally altered variety can be made out even in the hand-specimen. The primary magmatic assemblages are represented by apatite, magnetite, ilmenite and phlogopite while the hydrothermal assemblages are characterized by goethite, phosphosiderite, monazite-Ce, celestite, rutile, quartz, fluellite, fluorite, barite, gypsum and pyrite. Modal proportions of apatite and magnetite, which constitute together about 90 % of the rock, varies considerably.

Compositionally, apatite corresponds to fluorapatite (F up to 1.6 wt.%). Apatite in unaltered rocks forms idiomorphic crystals ranging in size from a few mm to 10-15 cm in pegmatoidal areas and contains SiO_2 (up to 2.1 wt.%), SO_3 (up to 1.8 wt.%) and Na_2O (up to 0.8 wt.%), $LREE_2O_3$ (up to 4.5 wt.%). In contrast, apatite from the altered rocks are characterized by elevated contents of SiO_2 and REE_2O_3 and reaches up to 6.6 wt.% and 15.0 wt.% respectively. Magnetite forms isometric grains

from several mm to 10 cm in size. It contains ilmenite lamellae oriented in the [111] direction. Magnetite is often replaced by hematite along the edges and along the cracks. In the areas of the most intensive hydrothermal reworking magnetite is almost completely replaced by goethite. Phlogopite is observed as flakes up to 20 cm in size, usually in association with apatite.

Oxygen isotope composition of apatite from unaltered rocks is characterized by the $\delta^{18}O$ values from 5.1 ‰ to 5.6 ‰. Phlogopite has the $\delta^{18}O$ value of 7.3 ‰. The values are similar to those that are typical for the mantle-derived igneous rocks (Hoefs, 2008), including carbonatite (Demény et al., 2010 and others). The altered apatite shows heavier $\delta^{18}O_{SMOW}$ (6.0 to 7.5‰) than the unaltered one. The $\delta^{18}O$ change observed for altered apatite may be interpreted as the result of postmagmatic isotope exchange with the hydrothermal fluids. It is difficult to uniquely infer the nature of the fluids. They can be post-magmatic water-rich fluids or low-temperature crustal water as well as mixture of both.

The chondrite-normalized REE patterns for apatite from unaltered magnetite-apatite rocks are steep and relatively smooth, and show a slightly negative Eu anomaly with Eu*/Eu from 0.49 to 0.63 (Fig. 1). In contrast, apatite from hydrothermally altered magnetite-apatite rocks shows strong LREE enrichment without Eu anomaly. In comparison with apatite from magnetite-apatite rocks, apatite from shonkinites shows lower REE concentration and without an Eu anomaly. The chondrite-normalized REE plots of apatite from alkaline syenite are generally steep with a weak negative Eu anomaly, with Eu*/Eu from 0.37 to 0.53.

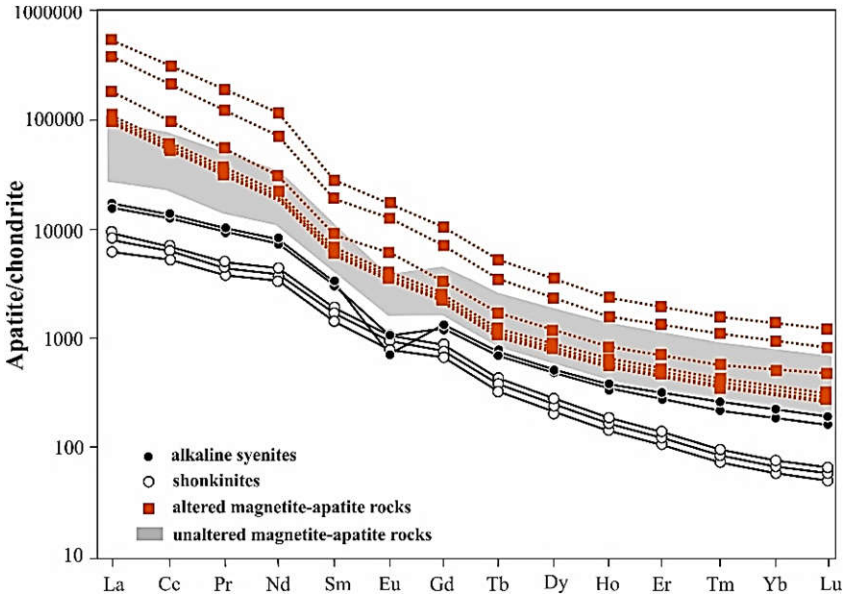

Fig. 1. Chondrite-normalized distribution of REE in apatites from shonkinites and alkaline syenites, unaltered and altered magnetite-apatite rocks. Normalizing values of chondrites are from Sun and McDonough (1989).

As demonstrated by the chondrite-normalized plots, the concentrations of ∑REE in apatite increase from shonkinites to alkaline syenites with a negative Eu anomaly. Such trend probably reflects fractional crystallization involving feldspar fractionation. The subsequent increase of ∑REE concentrations in apatite from magnetite-apatite rocks and the preservation of the negative Eu anomaly implies that the rocks are also a product of magmatic fractional crystallization of the parental alkaline silicate phosphorus-rich melt.

In our opinion, the formation of magnetite-apatite rocks can be probably related to the liquid immiscibility process. Separation of silicate and salt melts may have occurred at the time of alkaline syenite crystallization. This is supported by the presence of magnetite-apatite schlieren in host alkaline syenites and the appearance of Eu anomaly in apatites from magnetite-apatite rocks. Additional evidence is provided by practical absence of silicates from the magnetite-apatite rocks. Furthermore, Andreeva et al. (2003, 2007) observed silicate-salt liquid immiscibility in melt inclusions in minerals

from rocks of Mushgai-Khudag complex and recent experimental studies (Hou et al., 2018) demonstrated that the formation of iron oxide-apatite deposits could be explained by liquid immiscibility from silicate melt. On the other hand, some doubts arise from the fact that we did not observe the silicate-salt immiscibility in melt inclusions in apatite from the Mushgai-Khudag magnetite-apatite rocks.

The studies were supported by the research project of the Institute of Geology and Mineralogy SB RAS, No 0330-2016-0002.

References

Andreeva, I. A., Kovalenko, V. I. Magma compositions and genesis of the rocks of the Mushugai-Khuduk carbonatite-bearing alkaline complex (southern Mongolia): evidence from melt inclusions. Periodico di Mineralogia, 2003, 72, 95-105

Andreeva, I. A., Kovalenko, V. I., Naumov, V. B. Silicate-salt (sulfate) liquid immiscibility: a study of melt inclusions in minerals of the Mushugai-Khuduk carbonatite-bearing complex (southern Mongolia). Acta Petrologica Sinica, 2007, 23, 73-82

Baatar, M., Ochir, G., Kynicky, J., Iizumi, S., Comin-Chiaramonti, P. Some Notes on the Lugiin Gol, Mushgai Khudag and Bayan Khoshuu Alkaline Complexes, Southern Mongolia. International Journal of Geosciences, 2013, 4(08), 1200.

Demény, A., Kele, S., & Siklosy, Z. Empirical equations for the temperature dependence of calcite-water oxygen isotope fractionation from 10 to 70° C. Rapid Communications in Mass Spectrometry, 2010, 24(24), 3521-3526.

Hoefs, J. Stable isotope geochemistry. Springer Science & Business Media. 2008.

Hou, T., Charlier, B., Holtz, F., Veksler, I., Zhang, Z., Thomas, R., & Namur, O. Immiscible hydrous Fe–Ca–P melt and the origin of iron oxide-apatite ore deposits. Nature communications, 2018, 9(1), 1415.

Nikiforov, A. V., Yarmolyuk, V. V. Late Mesozoic central Asian carbonatite province. Geodynamic evolution of the lithosphere of the Central Asian mobile belt Irkutsk, 2004, 2, 47-49.

Samoilov V.S., Kovalenko V.I. Complexes of Alkaline Rocks and Carbonatites in South Mongolia (in Russian). 1983.

Sun, S. S., & McDonough, W. S. Chemical and isotopic systematics of oceanic basalts: implications for mantle composition and processes. Geological Society, London, Special Publications, 1989, 42(1), 313-345.

AL SUBSTITUTION MECHANISM IN ANHYDROUS BRIDGMANITE AS A FUNCTION OF AL CONTENT

Noda M.[1], Kakizawa S.[1], Inoue T.[1,2]

[1]Geodynamics Research Center, Ehime University, Matsuyama 790-8577, Ehime, Japan, m_noda@sci.ehime-u.ac.jp

[2]Department of Earth and Planetary System Science & Hiroshima Institute of Plate Convergence Region Research (HiPeR), Hiroshima University, Higashi-Hiroshima 739-8526, Hiroshima, Japan.

Bridgmanite (Brg, Mg-silicate perovskite) is the most abundant mineral in the lower mantle, and almost Al in lower mantle can be incorporated into Brg in anhydrous condition (e.g. Irifune, 1994). The Al substitution mechanism is supposed to be complicated, because there are two types of Al substitution mechanisms in anhydrous Brg, Tschermak and oxygen vacancy substitutions (e.g. Kojitani et al., 2007). However, the pure Tschermak and oxygen vacancy substitutions Brg has not been reported so far in low Al content, when we checked the previous reported compositions carefully (e.g. Irifune et al, 1996; Kubo and Akaogi, 2000). The previous studies have used powder samples as the starting materials, so we considered that the absorbed water may affect the results. We investigated Al substitution mechanism in Brg as a function of Al content in extremely anhydrous condition.

The high pressure synthesis experiments were conducted at 28 GPa and 1600-1700°C for 1hour using a Kawai-type multi-anvil apparatus. Four different Al content samples were prepared as the starting materials. Glass rods were used as the starting materials to eliminate the absorbed water on the sample surface. The chemical compositions of the starting materials were examined by SEM-EDS.

The recovered samples were identified by X-ray and neutron (in J-PARC) diffractions and SEM-EDS. Both the X-ray and neutron diffraction results showed that stishovite (SiO_2) and periclase (MgO) coexisted with Brg in our Tschermak and oxygen-vacancy substitution samples, respectively. However the chemical compositions of the synthesized Brg could not be measured by SEM-EDS because of the small grain size less than submicron. Therefore the chemical compositions were estimated from the result of Rietveld analysis of neutron diffraction conducted in J-PARC by subtracting the amount of the other phases. The results will be shown in the conference.

ULTRAMAFIC ALKALINE MAGMATISM OF THE SOUTHWESTERN PORTION OF THE SIBERIAN CRATON: RB-SR, AR-AR AND U-PB DATING, SR-ND-PB ISOTOPIC SYSTEMATICS

Nosova A.A.[1], Kargin A.V.[1], Chugaev A.V.[1], Sazonova L.V.[2], Dubinina E.O.[1], Lebedeva N.M.[1], Travin A.V.[3], Smirnova M.D.[2], Gareev B.I.[4], Batalin G.A.[4]

[1]Institute of Geology of Ore Deposits, Petrography, Mineralogy and Geochemistry, Moscow, Russia, nosova@igem.ru

[2]Lomonosov Moscow State University, Moscow, Russia, sazonovalv52@mail.ru

[3]Sobolev Institute of Geology and Mineralogy, Siberian Branch, Russian Academy of Sciences, Novosibirsk, Russia

[4]Institute of Geology and Petroleum Technologies, Kazan Federal University

The Phanerozoic ultramafic-alkaline magmatism of the Siberian Craton is represented mainly by Devonian and Mesozoic episodes of kimberlite and carbonate-rich ultramafic lamprophyres (UMLs) magmatism that pre- and post-date the Siberian Traps, respectively (e.g. Sun et al., 2014).

We present results of the Rb-Sr, Ar-Ar and U-Pb dating, Sr-Nd-Pb isotopic systematics and geochemical investigation of the Devonian pre-trap (*the Ilbokich occurrence*) and Triassic post-trap (*the Chadobets occurrence*) ULMs located in the southwestern portion of the Siberian Craton within the Irkineeva–Chadobets Trough (ICT). These data allow us to determination of the asthenospheric and lithospheric contribution to primary UML melts and compare pre-and post-Trap ULM magmatism within a single domain with thick lithosphere (150 km and more) and equally manifestations of the Siberian Trap magmatism.

The ICT is located in the southern sector of the Angara–Kotui intracontinental large-scale rift system evolved from Meso- to Neoproterozoic time and terminated its rift activity in the Cambrian. Some of the Angara–Kotui rift structures were reactivated at the Devonian time, when the oceanic plate subducted beneath the Siberian continent (Nikishin et al., 2002), that enabled the passage of small volume lamprophyre melts. The ICT includes the south-western periphery of the Tunguska flood-basalt province, which is outside the main Permian–Triassic linear rift structures of Siberia (Nikishin et al. 2002).

The Ilbokich area is located in the northern part of the ICT. UML dykes represented by aillikite and damtjernite have been found in the Neoproterozoic dolomite in borehole sections at depths of 2775–2833 m. *The Chadobets uplift* is located roughly 70 km to the southwest of the Ilbokich area. The Chadobets ultramafic-alkaline rocks are represented by carbonatites, kimberlites, aillikite, mela-aillikite, clinopyroxene-bearing aillikite and damtjernite with wide range of phlogopite, clinopyroxene, monticellite and nepheline contents. They have been found as dykes, sills, small intrusions and explosion pipes (Lapin, 2001).

The age of UMLs. We have previously dated the Ilbokich aillikite of 392 ± 2 Ma by Rb-Sr isochron method using phlogopite, carbonate and whole-rock samples (Kargin et al. 2016). A perovskite from the Ilbokich aillikite dyke was dating by U–Pb LA-ICP-MS during this study. We

yielded a $^{206}Pb/^{238}U$ age of 399.8 ± 3.8 Ma, which is similar to the previously published age. Chebotarev et al. (2017) previously determined the age of the Chadobets UMLs (alkali picrites)as 252 ± 12 Ma using U–Pb sensitive high-resolution ion microprobe analysis of perovskite samples. High uncertainties of the obtained age remained unclear a temporal position of Chadobets UMLs relatively to the Siberian Trap magmatism that has been occurred at 248-250 Ma (Reichow et al., 2008). We have undertaken to date of Chadobets aillikites using $^{39}Ar/^{40}Ar$ and Rb-Sr isochron methods. The phlogopite sample from the aillikite yielded an age spectrum with plateau defined by 95% of ^{39}Ar release with an age of 243.4 ± 3.1 Ma. The Rb-Sr data for the aillikites data for the aillikites, including the analysis of rock-minerals and whole-rock samples, defined two individual isochrones. For Chdb-32/87 sample the regression of the 3 points yields the age 240 ± 1 Ma (MSWD = 2.7) and $(^{87}Sr/^{86}Sr)_0$ = 0.70367 ± 2. Close age was obtained at Chdb-53/452.5 sample – 241 ± 1 Ma (3 points, MSWD = 1.1), but with another initial value of the $^{87}Sr/^{86}Sr$ ratio, equalled0.70294 ± 4. Our new precision age estimates indicate the post-trap position of Chadobets aillikites. This is supported by the presence of xenoliths derived from the Siberian Traps within Chadobets pipes (Lapin, 2001).

Major and trace element compositions. The UMLs from both occurrences show similar chemical composition that is typical for UMLs from worldwide occurrences. All aillikites and damtjernites show incompatible trace element enrichments that is more pronounced for Chadobets rocks. All rocks have broadly similar trace element primitive mantle normalized distributions. Differences occur as relative depletions at K, Sr and variable Zr–Hf anomaly for Chadobets rocks, depletion at Th, U and positive Zr–Hf anomaly for the Ilbokich aillikites. The Chadobets damtjernites have significantly elevated Cs and Rb concentrations. The high Ce/Pb (34-256) of the Chadobets UMLs precludes any contamination by continental crust.

Isotopic compositions. The initial Sr and Nd isotopic compositions of the Ilbokich UMLs fall in the narrow range $^{87}Sr/^{86}Sr_0$ 0.7032-0.7042 and εNd(T) 4.03-3.97. Chadobets UMLs have similar Sr isotopic signature with $^{87}Sr/^{86}Sr_0$ 0.7031-0.7043 and slightly more depleted Nd isotopic signature with εNd(T) 4.09-5.08. These ranges are similar to those of perovskites from Devonian and Mesozoic kimberlites and UMLs of the central and north parts of the Siberian craton (Sun et al., 2014).

The more obvious differences between the two aillikites groups are recognized in Pb–Pb isotopic space. The Chadobets UMLs have $^{206}Pb/^{204}Pb$ and $^{208}Pb/^{204}Pb$ ratios between 17.3 and18.6 and 34.8 and 37.5, respectively, with invariable$^{207}Pb/^{204}Pb$ ratios between 15.5 and 15.6, whereas the Ilbokich aillikites are characterized by $^{206}Pb/^{204}Pb$ close to 18.0 and $^{208}Pb/^{204}Pb$ of 38.0 with $^{207}Pb/^{204}Pb$ ratios around 15.6.

Oxygen isotopic composition of carbonate from both aillikite groups is characterised by highly variable $\delta^{18}O$ values from +12.1 up to +20.5 ‰ (SMOW). The isotopic composition of carbon ranging from $\delta^{13}C$ = -1.3 ‰ to -7.1‰ and shows enrichment in ^{13}C compared to primary mantle-derived carbonatites.

Crustal contamination. The Pb isotope ratios of Ilbokich aillikites tend toward values that indicate the involvement of materials that could be derived from upper continental crust. The Sr–Nd–Pb isotope ratios of the Ilbokich aillikites contradicts long-term geochemical enriched nature of the crustal contaminant. The oxygen and carbon isotopic composition of carbonates from Ilbokich aillikites and host Neoproterozoic dolomites (our data) indicates that the most likely this contaminant was a sedimentary carbonate rock. The geochemical and isotopic signature of Chadobets aillikites does not show obvious signs of crustal contamination.

Asthenospheric and SCLM contribution. The Sr-Nd-Pb isotope systematics and geochemical signature of the Siberian UMLs indicate two main mantle components, contributing to aillikitic magma compositions. The first component was derived from the convecting mantle. Presence of asthenospheric component evident in all UMLs, most distinctly in their unradiogenic$^{87}Sr/^{86}Sr$, and radiogenic $^{143}Nd/^{144}Nd$ isotopic composition. The Pb isotope ratios of aillikites follow the trend from OIB sources toward metasomatic mantle lithosphere. Geochemical difference between the pre-trap (Ilbokich) and post-trap (Chadobets) aillikites indicates the different origin of the subcontinental lithospheric mantle (SCLM) components, that had contributed to pre- and post-trap UMLs magmas. The Ilbokich UMLs have lower Ce/Pb, U/Pb, Nb/U and higher Rb/Sr, Ba/Nb ratios relatively the

Chadobets ones. These geochemical features link to phlogopite- and/or amphibole-rich metasomes within the lithospheric mantle (e.g. Prelevic et al., 2015). These metasomes could be formed during subduction when sediment-derived melts interacted with the overlying lithospheric mantle peridotite to yield hydrous, phlogopite-rich assemblages (Prelevic et al., 2015). The Pb-Pb isotopic ratios show the distinct contribution of the metasomatised SCLM to Chadobets UMLs. The Chadobets rocks have elevated Sm/Zr, Eu/Ti ratios and other geochemical features indicate the carbonate-rich composition of mantle metasomes.

We are grateful to A.V. Lapin and A.V. Postnikov for permission and assistance in UMLs sampling; V.S. Kamenetsky for U–Pb LA-ICP-MS study of perovskite from Ilbokich area. This study was supported by the Russian Foundation for Basic Research, project №18-05-00644A and by the Ministry of Education and Science of the Russian Federation contract No. 14.Y26.31.0029 in the framework of the Resolution No.220 of the Government of the Russian Federation.

References

Chebotarev D.A. et al. Geochronology of the Chuktukon carbonatite massif, Chadobets uplift (Krasnoyarsk Territory) // Russ Geol Geophys, 2017, Vol. 58, pp. 1222–1231.

Kargin A.V. et al. Devonian ultramafic lamprophyre in the Irkineeva–Chadobets trough in the southwest of the Siberian Platform: Age, composition, and implications for diamond potential prediction // Geol Ore Depos, 2016, Vol. 58, pp. 383–403.

Lapin A.V. Kimberlites of the Chadobets Uplift in relation with problem of formation–metallogenic analysis of platform alkaline ultrabasic magmatic rocks (In Russian) // Otechestvennaya Geol, 2001, Vol. 4, pp. 30–35.

Nikishin A.M. et al. Permo-Triassic intraplate magmatism and rifting in Eurasia: Implications for mantle plumes and mantle dynamics //Tectonophysics, 2002, Vol. 351, pp. 3–39.

Prelevic D.et al. Magmatic Response to Slab Tearing: Constraints from the Afyon Alkaline Volcanic Complex, Western Turkey // J Petrol, 2015, Vol. 56, pp. 527–562.

Sun J. et al. Repeated kimberlite magmatism beneath Yakutia and its relationship to Siberian flood volcanism: Insights from in situ U-Pb and Sr-Nd perovskite isotope analysis // Earth Planet Sci Lett, 2014, Vol. 404, pp. 283–295.

Reichow M.K. et al. The timing and extent of the eruption of the Siberian Traps large igneous province: Implications for the end-Permian environmental crisis // Earth Planet Sci Lett, 2009, Vol. 277, pp. 9–20.

FIRST REPORT OF METAMORPHIC DIAMOND FROM JAPAN: ITS OCCURRENCE AND MINERALOGICAL FEATURE

***Ohfuji H.*[1], Nishiyama T.[2], Fukuba K.[3]**

[1]*Ehime University, ohfuji@sci.ehime-u.ac.jp*

[2]*Kumamoto Univ.*

[3]*Ehime University*

Non-kimberlitic diamonds have been reported mostly from orogenic belts produced by continental collision such as in ultra-high pressure metamorphic rocks (e.g. Kokchetav, Kazakhstan) and in ophiolites (e.g. Tibet and Polar Urals, Russia). Recently, microdiamonds have been identified in Higo- and Nishisonogi metamorphic rocks in Kyusyu, Japan by micro-Raman spectroscopy (Nishiyama et al., 2014a; 2014b). In the former rock micro(nano?)-diamonds were found in fluid inclusions (negative crystals) in chromite crystals constituting chromitite contained in a serpentinite block, while in the latter rock they occur in a matrix of pelitic schist in a serpentinite mélange. In the both cases, a peak centered at 1330-1332 cm^{-1}, which is characteristic to diamond, was clearly observed in the Raman spectra collected from the surface of thin-sections which were carefully prepared by mechanical polishing using only carborundum (SiC) and alumina abrasives so that the samples are not contaminated by any extrinsic diamond sources. In this study, we conducted the direct

electron microscopic observation of those diamond and diamond-like carbon grains contained in the two metamorphic rocks.

We carefully prepared cross-sections from sample blocks by ion-milling using a JEOL cross-section polisher (CP) to avoid any potential contaminations during the sectioning process. The ion-polished surface was then coated with osmium and observed by FE-SEM equipped with EDS. Thin cross-sections foils were cut out from some target areas containing microdiamond grains by focused ion beam (FIB) for TEM observation. In the samples from the Higo metamorphic belt, diamond-like carbon grains were found exclusively inside negative crystals in chromite and show a spindle shape of < 1 μm. TEM analysis of the grains revealed that they consist of randomly aggregated nanocrystalline graphite of tens to hundreds nm and show no signs of the presence of diamond phases according to the selected-area electron diffraction and high-resolution imaging. These poorly crystalline graphite grains may be a pseudomorph after diamond produced by the retrogressive phase transition during ascending of the host rock.

On the other hand, in the pelitic schist from Nishisonogi (Nagasaki) metamorphic belt, diamond grains occur mostly in pore spaces (cavities) in the phengite and chlorite matrix and is always associated with carbonate (dolomite and magnesite) grains. The pelitic schist samples also contain graphite crystals with tubular shapes in the matrix and pyrite grains, but diamond was not found near those graphite crystals. TEM observation showed that individual diamond crystals are ~0.5 μm in size and show angular to octahedral (euhedral-like) shapes. Electron diffraction pattern collected from each crystal show single-crystal patterns which are reasonably explained by diamond reciprocal patterns. Raman thermometry of graphite in the host rock gives a metamorphic temperature of 450 °C, which is the lowest temperature condition for diamond formation in metamorphic rocks. If the Nishisonogi microdiamonds formed in the diamond stability field, the pressure condition will be at least 2.8 GPa, corresponding to the lawsonite eclogite facies. The formation of the microdiamond in such a relatively low pressure and temperature condition may be explained by the precipitation from a C-H-O fluid composed of neutral species such as CO_2, H_2O and CH_4 upon change in the oxygen fugacity (e.g. Frezzotti et al., 2014).

References

Frezzotti, M.L., Huizenga, J.M., Compagnoni, R., Selverstone, J. (2014) Diamond formation by carbon saturation in C-O-H fluids during cold subduction of oceanic lithosphere. Geochim. Cosmochim. Acta, 143, 68-86.

Nishiyama, T., Moribe, Y., Ishimaru, S., Arai, S., Mori, Y., Shigeno, M. (2014) Subduction origin for UHP chromitite from the Nishisonogi metamorphic rocks, Western Kyoshu, Japan. Japan Geosci. Union Meeting Abstract, SCG08-10.

Nishiyama, T., Shiosaki, D., Eguchi, H., Yoshiasa, A. (2014) Microdiamond-bearing UHP chromitite from the Higo Metamorphic Rocks, Central Kyushu, Japan. Japan Geosci. Union Meeting Abstract, SMP46-02.

MINERALOGY OF KOSVITES FROM KONDER MASSIF

***Osipov A.S.*, Antonov A.A., Perhurova V.A.**

Saint-Petersburg State University, Department of mineralogy, osipov.anst@yandex.ru

During the mineralogical study The Konder massif rocks, close attention was paid to the «ore» pyroxenites (kosvites), often located in contact with the bodies of agpaitic rocks, and containing in its composition the phases of noble metals. In the course of research the mineral composition of kosvites, the morphology and relationships of the individual phases, the peculiarities of their chemical composition were described.

The Konder massif is located in the Eastern part of the Aldan shield of the Siberian platform, in the basin of the river Mai, in the area between its left tributaries - the Omni and Maymakan. It is the alkaline-ultramafic ring zonal structure with a diameter of 7.5 km, folded with platinum-bearing dunites, clinopyroxenites and kosvites, which are cutted by the vein bodies of alkaline pegmatites.

Kosvite - is a variety of pyroxenite with sideronitic texture, where the main minerals are monoclinic pyroxene and magnetite. Kosvites are widespread in the central part of the massif within a stock of dunites. This rocks forms dike bodies whith capacity ranges from few centimeters to tens of meters, length - from 2 to 300 m, often cutted by the vein alkaline rocks. In the contact areas of kosvites and alkaline rocks there are widely developed hydrothermal-metasomatic transformations. Thus, among kosvites there are segregations and separated bodies of coarse-grained rocks of apatite-phlogopite-magnetite composition, with debatable genesis.

We studied several samples of kosvites, different in structure – dense fine-grained rocks, medium-grained rocks and coarse-grained loose rocks.

The main rock-forming minerals are diopside, phlogopite, magnetite (titanomagnetite) and apatite. As can be seen from fig. 1, kosvites have sideronitic texture – the grains of apatite and pyroxene, cemented with xenomorph mass of ore minerals, primarily titanomagnetite can be clearly highlighted.

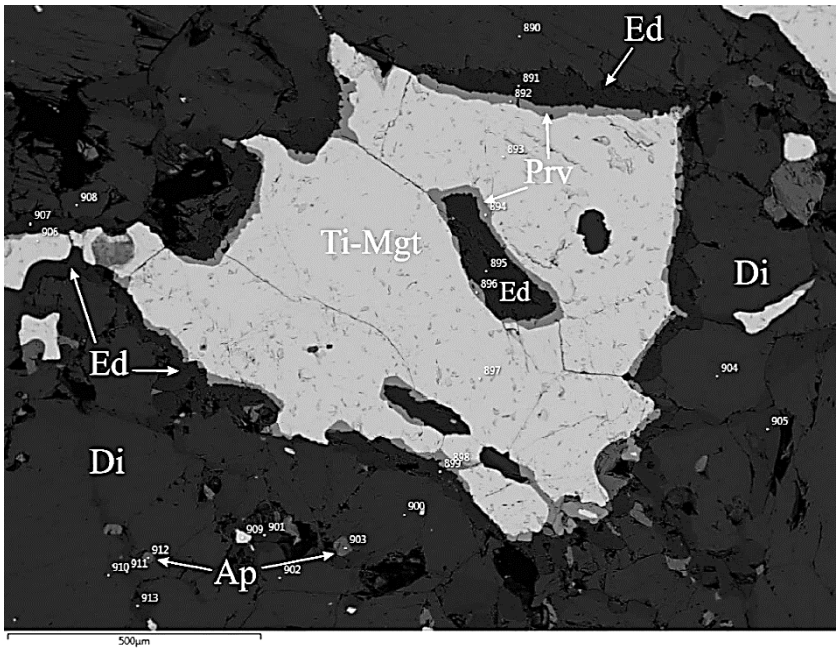

Fig. 1. Sideronitic texture of kosvites. Titanium-bearing magnetite (Ti-Mgt), diopside (Di), edenite (Ed), apatite (Ap) and perovskite (Prv) can be observed.

The secondary minerals are titanite, perovskite, amphibole, chlorite, ilmenite, chalcopyrite, pyrite and chalcocite. As accessory mineralization revealed xenotime, barite, pyrrhotite, pentlandite, minerals of noble metals – platinum, palladium, gold and silver.

Pyroxene in kosvites represented by diopside. It has a fairly constant composition. As admixtures there are a small amount of Fe (up to 0.25 wt.% FeO), Al (up to 0.14 wt.% Al_2O_3), Mn и Ti (up to 0.02 wt.% MnO and TiO_2). Diopside regularly bears the traces of secondary transformations – it substituted by amphibole (ferrous edenite), which, in turn, is replaced by clinochlore. Herewith significantly increases the content of Al (up to 0.58 wt.% Al_2O_3), Fe (up to 0.32 wt.% $FeO+Fe_2O_3$), Ti (up to 0.08 wt.% TiO_2). Appear admixtures of Na (up to 0.27 wt.% Na_2O) and K (up to 0.02 wt.% K_2O). Herewith, the contents of Ca, Mg and Si are reduced.

Apatite forms relatively large subidiomorph grains. It is characterized by the presence of admixture of Sr (up to 0.73 wt.% SrO), Fe (up to 0.54 wt.% FeO) and S (up to 0.58 wt.% SO_3). According to the composition of the anionic group, the mineral is an intermediate species between fluoride- and hydroxyl-apatite. In some grains it was also noted the presence of chlorine.

Phlogopite forms a large grains with pronounced cleavage, has a fairly constant chemical composition. From admixtures it is worth to note Ti (up to 3.05 wt.% TiO_2) and Na (up to 1.79 wt.% Na_2O).

Accessory mineralization is represented by inclusions of sulfides (chalcopyrite, pyrite, chalcocite), single grains of xenotime and small veins of barite. In addition, medium-sized couplings,

combined with an aggregate of magnetite, chalcopyrite and chalcocite, revealed in these rocks, are particularly interesting in a way it contains the minerals of noble metals – gold, silver and platinum. According to our observations, such couplings are the late formations and require further more detailed studying.

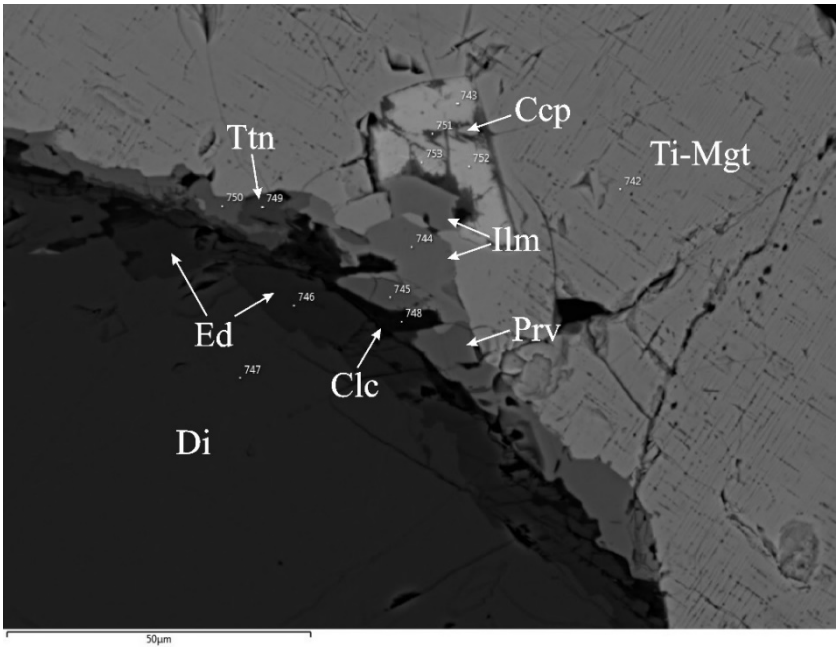

Fig. 2. Two trends of the postmagmatic transformations of kosvites: diopside (Di) → edenite (Ed) → Clinochlore (Clc) and titanium-bearing magnetite (Ti-Mgt) → ilmenite (Ilm) → perovskite (Prv) → titanite (Ttn).

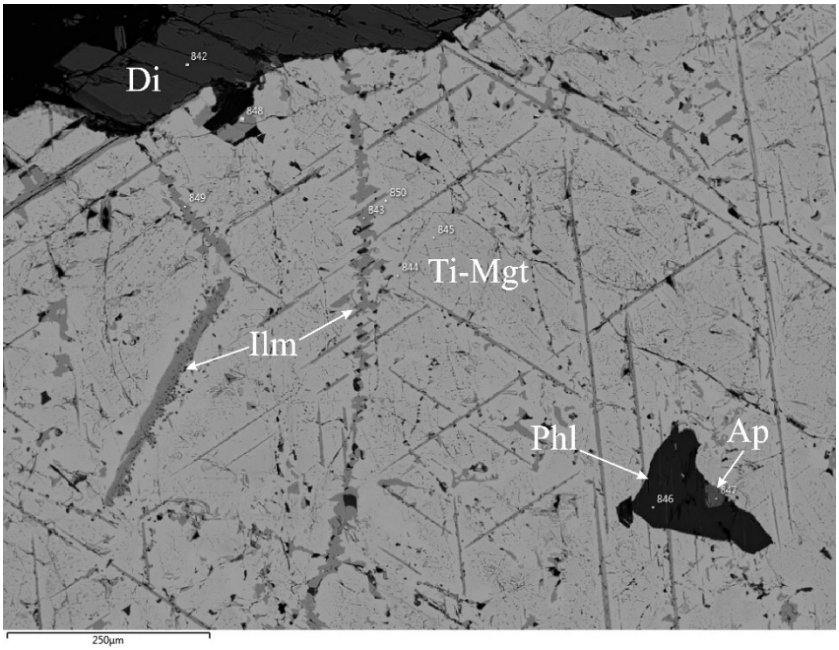

Fig. 3. The breakdown structure of titanium-bearing magnetite (Ti-Mgt), formed by ilmenite (Ilm). Also apatite (Ap), diopside (Di) and phlogopite (Phl) can be observed.

The partial pseudomorphoses and other signs of hydrothermal-metasomatic transformation of rocks are clearly shown at the micro level. Observations of the spatial-age relationships between the minerals in kosvites allow to identify the two trends of postmagmatic transformations (fig. 2). In the marginal parts of

grains of diopside evolving edenite, which subsequently replaced by clinochlore. In this sequence, the alumina content of minerals is increases. In the main ore mineral – titanomagnetite – observed the breakdown structure formed by ilmenite (Fig. 3). Ilmenite also forms edges around magnetite grains, and in some cases ilmenite is successively replaced by perovskite and titanite (Fig 1, 2).

In total, the data collected during this research suggests that the apatite-phlogopite-titanium magnetite segregations were formed as a result of post-magmatic transformations of kosvites.

Analytical work was completed at the Department of Mineralogy of the St. Petersburg state University and at the resource center "Geomodel" at hardware complex, including the electron microscope Hitachi S-3400N with analytical set-top boxes: analysis of diffraction of reflected electrons EBSD - AzTec HKL Channel 5 Advanced, quantitative energy-dispersive microanalysis EDX - AzTec Energy 350, wave dispersive quantitative analysis WDS - INCA 500 (Engineer-analysts - Nataly S. Vlasenko and Vladimir V. Shilovsky).

References

Булах А.Г. «Руководство и таблицы для расчета формул минералов»//142 с., М: «Недра», 1967

Гурович В.Г., Емельяненко Е.П., Землянухин В.Н., Каретников А.С., Квасов А.И., Лазаренков В.Г., Малич К.Н., Мочалов А.Г., Приходько В.С., Степашко А.А. «Геология, петрология и рудоносность Кондерского массива» Наука, Москва, 176 стр., 1994.

Кривовичев В.Г. «Минералогический словарь» // СПб.: Изд-во С.-Петерб. ун-та. — 556 с., 2009.

Некрасов И.Я., Ленников А.М., Октябрьский Р.А. и др. «Петрология и платиноносность кольцевых щелочно-ультраосновных комплексов» М.: Наука, 381 с., 1994а.

Whitney D.L., Evans B.W. «Abbreviations for names of rock-forming minerals» // American mineralogist, volume 95, pages 185-187, 2010.

SPECIFIC PERALKALINE HYDROTHERMAL FORMATION RELATED TO ORE-BEARING COMPLEX OF THE LOVOZERO MASSIF (KOLA PENINSULA, RUSSIA): MINERALOGY, ORIGIN, BEHAVIOR OF RARE ELEMENTS

Pekov I.V. [1,2]

[1]*Faculty of Geology, Moscow State University, Moscow, Russia*

[2]*Vernadsky Institute of Geochemistry and Analytical Chemistry, RAS, Moscow, Russia*

e-mail: igorpekov@mail.ru

The layered foyaite–urtite–lujavrite complex containing the richest loparite ores of the famous Lovozero alkaline massif (Kola peninsula, Russia) hosts numerous ussingite and/or natrolite veins with diverse and specific peralkaline (hyperagpaitic) mineralization. In particular, they are uncovered by underground mine workings at Mts. Karnasurt, Kedykverpakhk and Alluaiv. First data on minerals from these veins were published in 1970s by I.V. Bussen, E.M. Es'kova, A.P. Khomyakov, Yu.P. Men'shikov and their co-authors. Khomyakov (1995) briefly reported these veins as "type no. 3 of hyperagpaitic rock in the Lovozero massif". The author of the present paper systematically studies this object since 1992. The detailed descriptions of seven veins located at Mt. Kedykverpakhk were given in 2000 and they were considered as "hyperalkaline pegmatite veins and veinlets" (Pekov, 2000). Later, based on the extended material, the author essentially revised a view on their genesis: this vein complex belongs to "pure" hydrothermal formation and strongly differs in the genetic aspect from "true" hyperagpaitic pegmatites which also occur at the same area. These veins seem interesting not only in mineralogical aspect but also for geochemistry of rare elements, brightly demonstrating their behavior in peralkaline systems at the temperatures lower than 300ºC.

The vein complex includes several hundred (as minimum) veins and veinlets up to *ca*. 1 km long and from 1 to 15 (sporadically up to 25 cm) thick. The veins fill several systems of near-vertical

fractures and typically run in NW–SE or NNW–SSE directions. They crosscut the thin layer of loparite-rich malignite (so-called ore layer II-4) and covering foyaite or urtite and terminate 0.1–0.5 m under the malignite layer. Contacts between veins and host rocks are sharp. The metasomatic aureoles (10–20 cm thick) are observed in host rocks around the veins. The metasomatic alteration, at the first time, the replacement of a rock by natrolite, sodalite, villiaumite, and natisite, is especially intense in foyaite and malignite. The veins demonstrate bright signs of crystallization of minerals in open space, from selvages to axial part. It is possible to distinguish associations belonging to two main stages of mineral formation in the veins: I – minerals crystallized simultaneously with vein-forming ussingite and/or natrolite (the majority of minerals) and II – late, definitely low-temperature minerals crystallized in residual cavities, mainly in axial part of a vein.

The veins demonstrate various and original mineral composition: more than 70 mineral species are found there including 12 species first discovered in this vein complex. All minerals, except of some minor phases, contain Na as species-defining constituent and many of them are Na-rich: >15-20 wt.% Na_2O. We observe here a diversity of minerals of some lithophile rare elements (Li, Sr, *LREE*, Th, Nb) and so-called "saline" phases, including six silicates containing only sodium as a metal cation (natrosilite, revdite, makatite, kanemite, grumantite, and chesnokovite). These mineralogical features cause the similarity of the veins with cores of differentiated hyperagpaitic pegmatites typical for Lovozero. In both cases rare-element minerals are concentrated in outer parts of ussingite or natrolite bodies while "saline" phases occur in central zones. This similarity was a reason to unite these veins with pegmatites initially (Pekov, 2000).

However, the differences between these veins and pegmatites are essential. There are as follows. (1) Typical hyperagpaitic pegmatites do not fill fractures and their bodies have other shapes; cross-cutting of such pegmatites by the described veins was observed. (2) Unlike pegmatites, the veins do not contain nepheline and early generations of feldspars (microcline and albite there are only late and occur in very scarce amounts in cavities of ussingite) and alkali amphiboles; aegirine is a minor component. (3) The veins, unlike any Lovozero pegmatite, are extremely Zr-poor; only some crystals of lovozerite-group zirconosilicate kapustinite were found in these veins for our 25-years history of systematic studies. (4) Hypersodic specialization of the veins, including extremely high value of the Na:K ratio: $n \cdot 10^3$-10^4. (5) The presence of hyperagpaitic metasomatic aureoles around the veins that is uncommon for the majority of the Lovozero pegmatites. (6) The abundance of natisite, $Na_2TiOSiO_4$, in these aureoles and sporadically in veins; this titanosilicate is characteristic for the described vein complex but extremely rare in other mineral assemblages in Lovozero. (7) The veins contain much more OH- and, especially, H_2O-bearing minerals in comparison with the typical Lovozero pegmatites. (8) The difference in villiaumite, NaF, distribution: in pegmatites villiaumite mainly occurs in cores whereas in the vein complex its major amount is concentrated in aureoles surrounding veins. (9) The veins are Ca-depleted and typically demonstrate the ratio Sr:Ca > 1. (10) The veins contain much less organic (bituminous) substances compare to the majority of the Lovozero pegmatites.

The most substantiated genetic model presents a differentiated peralkaline pegmatite as a product of the fractional crystallization, in close system, of a fluid-rich melt that gradually transits to aqueous solution with temperature lowering (Kogarko, 1977; Khomyakov, 1995). Thus, the formation of such pegmatites includes two main stages: earlier, a pegmatitic *sensu stricto* stage and later, a hydrothermal stage. Our observations show that (1) the Lovozero differentiated pegmatites started to form before the appearance of the above-mention system of fractures and (2) the formation of hydrothermal ussingite/natrolite zone of such pegmatites is in general a result of crystallization in a geochemically close system.

Unlike pegmatites, the veins described there seem products of a geochemically open system, a result of the reaction of a Na-oversaturated fluid (solution) with host rocks. The appearance of this fluid is probably caused by the migration of mobile components (at the first time, H_2O, F and Na) to the zone with lower pressure, *i.e.*, a fracture. This fluid also alters the rocks surrounding fractures, including the dissolving of minerals containing Ti and rare elements. Processes of mobilization, transport and concentration of these constituents were local: rare elements and Ti were transported for distances not longer than 15–20 cm. Alkali feldspar of host rocks remains stable in these processes (it

is unaltered in the metasomatic aureoles) that seems a cause of strong depletion of the veins in potassium.

Uneven distribution of elements in the veins and surrounding metasomatic aureoles is obviously caused by their different mobility in this fluid (solution). Titanium minerals are mainly concentrated in selvages of the veins and the aureoles. Distribution of natisite is especially impressive: it is the main concentrator of Ti in aureoles sporadically forming up to 50 vol.% of a metasomatic near-vein rock. Selvages of some veins are enriched in lomonosovite, $Na_2Ti_2Si_2O_9 \cdot Na_3PO_4$, and vuonnemite, $Na_5TiNb_2Si_4O_{17}F \cdot 2Na_3PO_4$. The latter is typically "shifted" in comparison with the former to the axial part of a vein. Silicates and phosphate-silicates of *REE* and Th (steenstrupine – thorostenstrupine series and nordite group minerals, phosinaite, umbozerite) are concentrated near selvages while *REE* and Sr phosphates (belovite, vitusite) occur closer to the axial part of a vein. The distribution of Li minerals is as follows: tainiolite and neptunite-series members occur near selvages whereas Li-amphibole (potassic-ferri-leakeite) in the intermediate zone and the "saline" phosphate olympite in the axial zone.

The "facial" zonation is also genetically informative. Different mineral assemblages are related to areas in which a vein crosscuts different rocks which become a source of corresponding chemical constituents. *LREE*, Th, Ti and Nb silicates and phosphate-silicates (lomonosovite, vuonnemite, natisite, steenstrupine, nordite, *etc*.) as well as *LREE* and Sr phosphates (belovite, vitusite) mainly concentrate at the area where a vein crosscuts the layer of loparite malignite containing up to 25-30% loparite, (Na,*LREE*,Th,Sr)(Ti,Nb)O_3, and enriched by Sr-bearing fluorapatite, $(Ca,Sr)_5(PO_4)_3F$. Loparite and apatite are partially or completely dissolved in the metasomatic aureole surrounding a vein and the above-mentioned Na-rich minerals with *LREE*, Sr, Th, Ti and Nb crystallized instead of them inheriting these elements. Similar situated is observed for aluminosilicates: at the area in which a vein crosscuts a layer of loparite malignite, natrolite (Si:Al = 1.5 in atom proportions) is the main constituent of a vein whereas at the area where a vein crosscuts foyaite, a rock richer in silica compare to malignite, mainly ussingite, an aluminosilicate with Si:Al = 3, occurs. Typical Lovozero pegmatites do not demonstrate such features.

The abundance of natrolite, a zeolite stable at temperatures not higher than 300ºC and crystallized from aqueous solutions (Breck, 1974; Pekov et al., 2004), undoubtedly indicates the hydrothermal origin of the described veins. It should be specially noted that, unlike majority of peralkaline pegmatites (Khomyakov, 1995; Pekov, 2000), they preserve hyperagpaitic composition during all process of their evolution which spreads to very low temperatures. It is clearly demonstrated by the presence of significant amount of a highly hydrated Na silicate chesnokovite, $Na_2SiO_2(OH)_2 \cdot 8H_2O$ (Pekov et al., 2007), a phase stable under *ca*. 70ºC.

The absence of Zr phases and the distribution of Ti and Nb minerals in this vein complex allows to evaluate relative mobilities of these elements. The mobility increases in the sequence Zr → Ti → Nb.

It seems important that loparite is unstable in hyperagpaitic hydrothermal solutions even at low temperatures, < 300ºC, and easily alters to Ti, Nb and *LREE* silicates and, especially, phosphate-silicates. This fact indicates that the metasomatic origin of loparite in peralkaline rocks of the foyaite–urtite–lujavrite complex of the Lovozero massif seems improbable.

This study was supported by the Russian Foundation for Basic Research, grant 18-05-00332 in part of crystal chemistry of sodium silicates.

References

Breck D.W. Zeolites Molecular Sieves: Structure, Chemistry and Use. New York: John Wiley & Sons. 1974. 771 p.

Khomyakov A.P. Mineralogy of Hyperagpaitic Alkaline Rocks. Oxford: Clarendon Pr. 1995. 223 p.

Kogarko L.N. Problems of Genesis of Agpaitic Magmas. Moscow: Nauka Publishing. 1977. 294 p. (in Russian)

Pekov I.V. Lovozero Massif: History, Pegmatites, Minerals. Moscow: OP. 2000. 480 p.

Pekov I.V. et al. Zeolites of Alkaline Massifs. Moscow: Ecost. 2004. 168 p. (in Russian)

Pekov I.V. et al. Chesnokovite, $Na_2[SiO_2(OH)_2]\cdot 8H_2O$, the first natural sodium orthosilicate from the Lovozero alkaline pluton, Kola Peninsula, Russia: description and crystal structure of a new mineral species // Geol. Ore Dep. 2007. Vol. 49. No. 8, pp. 727-738.

CRYSTAL CHEMISTRY OF KAMENEVITE, A NEW MINERAL FROM THE KHIBINY ALKALINE COMPLEX, KOLA PENINSULA, RUSSIA

Pekov I.V.[1,2], Zubkova N.V.[1], Yapaskurt V.O.[1], Turchkova A.G.[1], Pushcharovsky D.Yu.[1]
[1]Faculty of Geology, Moscow State University, Moscow, Russia, igorpekov@mail.ru
[2]Vernadsky Institute of Geochemistry and Analytical Chemistry, RAS, Moscow, Russia

A new hydrous potassium titanosilicate, ideally $K_2TiSi_3O_9\bullet H_2O$, was found at the Oleniy Ruchey apatite mine, Mt. Suoluaiv, Khibiny, Kola Peninsula, Russia, and named in honour of the Russian geologist Dr. Evgeniy Arsenievich Kamenev (born 1934), an outstanding specialist in the geology of the Khibiny alkaline complex and its mineral deposits and one of the discoverers of the Oleniy Ruchey apatite deposit (1961). The new mineral was found in a K-rich peralkaline (hyperagpaitic) pegmatite together with pectolite, villiaumite, ershovite, shafranovskite, umbite, sidorenkite, djerfisherite, rasvumite, and Na-bearing neotocite. Kamenevite occurs as coarse lamellar, flattened on [010], crystals up to 0.02 x 0.1 x 0.3 mm, rectangular (Fig. 1) or irregular in shape. They form aggregates up to 0.7 mm across replacing lomonosovite and filling cracks in crystals of slightly etched lomonosovite.

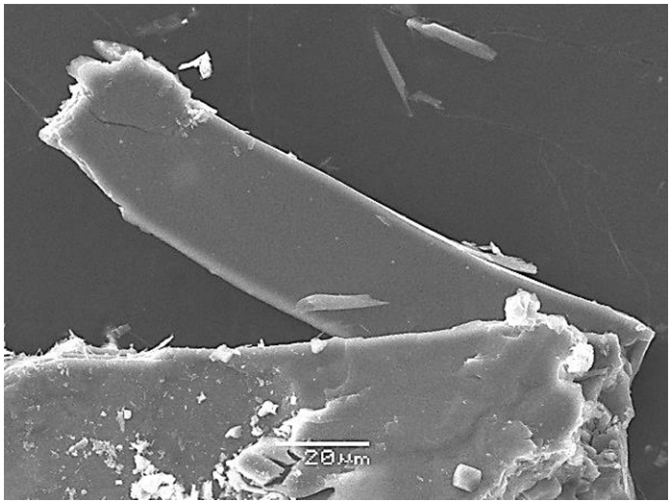

Fig. 1. Kamenevite crystal. SEM (SE) image.

The empirical formula of kamenevite (based on 10 O *apfu*, with 1 H_2O *pfu*) is $(K_{1.92}Na_{0.06}Ca_{0.01})_{\Sigma 1.99}(Ti_{0.94}Zr_{0.03}Fe_{0.02}Nb_{0.01})_{\Sigma 1.00}S_{3.01}O_9\bullet H_2O$.

The crystal structure of kamenevite was studied using the single-crystal XRD data (Xcalibur S CCD diffractometer, Mo$K\alpha$ radiation). The new mineral is orthorhombic, space group $P2_12_12_1$, a = 9.9166(4), b = 12.9561(5), c = 7.1374(3) Å, V = 917.02(6) Å^3, Z = 4. The structure was solved by direct methods and refined on the basis of 2201 independent reflections with $I > 2\sigma(I)$ to the final R = 0.0384. Hydrogen atoms of the water molecule were found in a difference Fourier map and refined in a semi-free way. Kamenevite is isostructural to umbite, $K_2ZrSi_3O_9\bullet H_2O$ (Ilyushin *et al*., 1981; Khomyakov *et al*., 1983; Ilyushin, 1993), with Ti instead of Zr and is a natural analogue of the well-known synthetic compound $K_2TiSi_3O_9\bullet H_2O$ which is in focus of studies in applied chemistry for last two decades because of its strong zeolitic properties (Lin *et al*., 1997; Bortun *et al*., 2000; Zou and Dadachov, 2000). The crystal structure of kamenevite (Fig. 2) is based on the heteropolyhedral framework built by $[Si_3O_9]^{\infty}$ wollastonite-type chains linked by isolated from each other Ti-centred octahedra. Each TiO_6 octahedron share all six oxygen vertices with SiO_4 tetrahedra. The

heteropolyhedral framework contains channels running along [001] in which extra-framework K^+ cations and H_2O molecules are located.

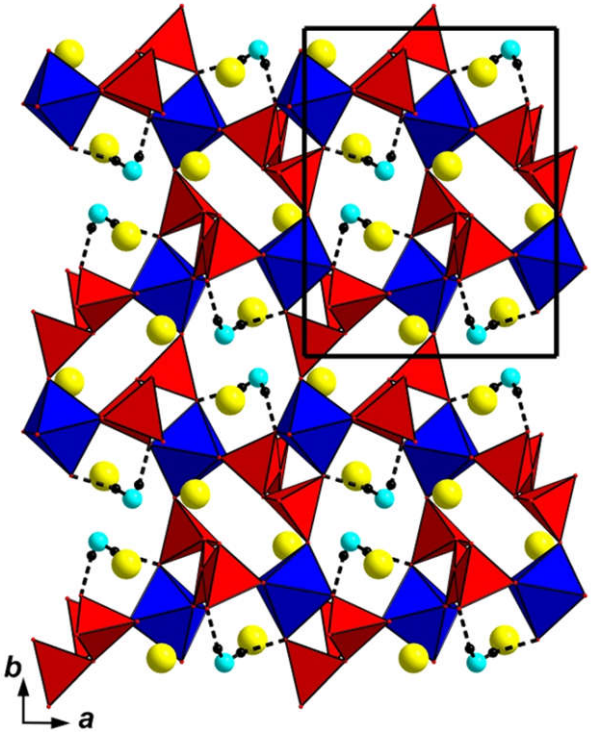

Fig. 2. The crystal structure of kamenevite in the *ab* projection. TiO_6 octahedra are dark grey, SiO_4 tetrahedra are grey, K atoms are large white circles, O atoms of H_2O molecules are medium light-grey circles and H atoms are small black circles. Hydrogen bonds are shown as dashed lines. The unit cell is outlined.

Kamenevite and umbite belong to the large family of natural microporous, zeolite-like silicates containing transition elements and large (alkali and/or earth-alkali) cations. Their synthetic analogues and crystallochemically related compounds are now under active studies or already in industrial use as ion exchangers, sorbents, catalysts, catalyst carriers or ion conductors. The most diversity of such minerals is formed in highly alkaline complexes, mainly in pegmatites and hydrothermal bodies related to the peralkaline, agpaitic rocks (Pekov and Chukanov, 2005). Kamenevite demonstrates rare for minerals example of a titanosilicate with a heteropolyhedral framework containing isolated from each other octahedra TiO_6. This structural feature is very common for microporous zirconosilicates but not for titano- and niobosilicates in which TiO_6 or NbO_6 octahedra usually form condensed motifs. This explains, *e.g.*, the rarity of titanium minerals of the eudialyte, lovozerite, benitoite and hilairite groups in comparison with their zirconium members, in spite of significant prevailing of Ti over Zr in alkaline rocks and in Earth's crust in general. Kamenevite contains minor admixture of Zr and is associated with umbite with Zr >> Ti. Thus, in spite of isotypism, these minerals do not form a continuous solid-solution series there.

This study was supported by the Russian Foundation for Basic Research, grant 18-05-00332 (in part of crystal structure determination).

References

Bortun A.I. et al., Synthesis, characterization, and ion exchange behaviour of a framework potassium titanium trisilicate $K_2TiSi_3O_9 \cdot H_2O$ and its protonated phases // Chem. Mat. 2000. Vol. 12. p. 294-305.

Ilyushin G.D. New data on crystal structure of umbite $K_2ZrSi_3O_9 \cdot H_2O$. Inorg. Mat. 1993. Vol. 27, p. 1128-1133.

Ilyushin G.D. et al., The crystal structure of a new natural modification of $K_2ZrSi_3O_9 \cdot H_2O$ // Dokl. Akad. Nauk SSSR. 1981. Vol. **257**, p. 608-610 (in rus.).

Khomyakov A.P. et al., Umbite and paraumbite, new potassium zirconosilicates from the Khibiny alkaline massif // ZVMO. 1983. Vol. 112. p. 462-469 (in rus.).
Lin Z. et al., Synthesis and structural characterization of microporous umbite, penkvilksite, and other titanosilicates // J. Phys. Chem. B. 1997. Vol. 101. p. 7114-7120.
Pekov I.V. and Chukanov N.V. Microporous framework silicate minerals with rare and transition elements: minerogenetic aspects// Rev. Min. Geochem., 2005, 57: Micro- and Mesoporous Mineral Phases, 145-171.
Zou X. and Dadachov M.S. $K_2TiSi_3O_9 \cdot H_2O$ // Acta Cryst. C. 2000. Vol. 56. p. 738-739.

ILMENITE FROM THE GRIB KIMBERLITE (ARKHANGELSK DIAMOND PROVINCE, RUSSIA): PETROGRAPHY, COMPOSITION AND GENESIS

***Peresetskaya E.V.*[1], *Kargin A.V.*[2], *Nosova A.A.*[2], *Sazonova L.V.*[1], *Lebedeva N.M.*[2]**
[1]*Lomonosov Moscow State University, Moscow, Russia*
[2]*Institute of Geology of Ore Deposits, Petrography, Mineralogy and Geochemistry, Moscow, Russia, kargin@igem.ru*

Magnesian ilmenite (picroilmenite) is a common indicator mineral of kimberlite magmatism. Its composition is used not only as an essential tool in prospecting of potentially diamondiferous kimberlite, but also as an instrument to study of metasomatic processes in the subcontinental lithospheric mantle (SCLM) as well as evolution of a kimberlite melt during its ascend and interaction with the SCLM (Golubkova et al., 2013; Castillo-Oliver et al., 2017). Here we provide new compositional data for picroilmenite from the Grib kimberlite (Arkhangelsk diamond province, Russia) and propose some genetic models.

The Grib kimberlite (376 ± 3 Ma, Larionova et al., 2016) is located in the north part of East-Europe Craton within Arkhangelsk diamond province. Based on geochemical and isotope systematics, kimberlite is classified as a Group-I kimberlite (review in Larionova et al., 2016). This kimberlite hosts a variety of mantle xenoliths including garnet-ilmenite peridotite and ilmenite-garnet-orthopyroxene xenoliths as well minerals of a megacrysts suit including picroilmenite.

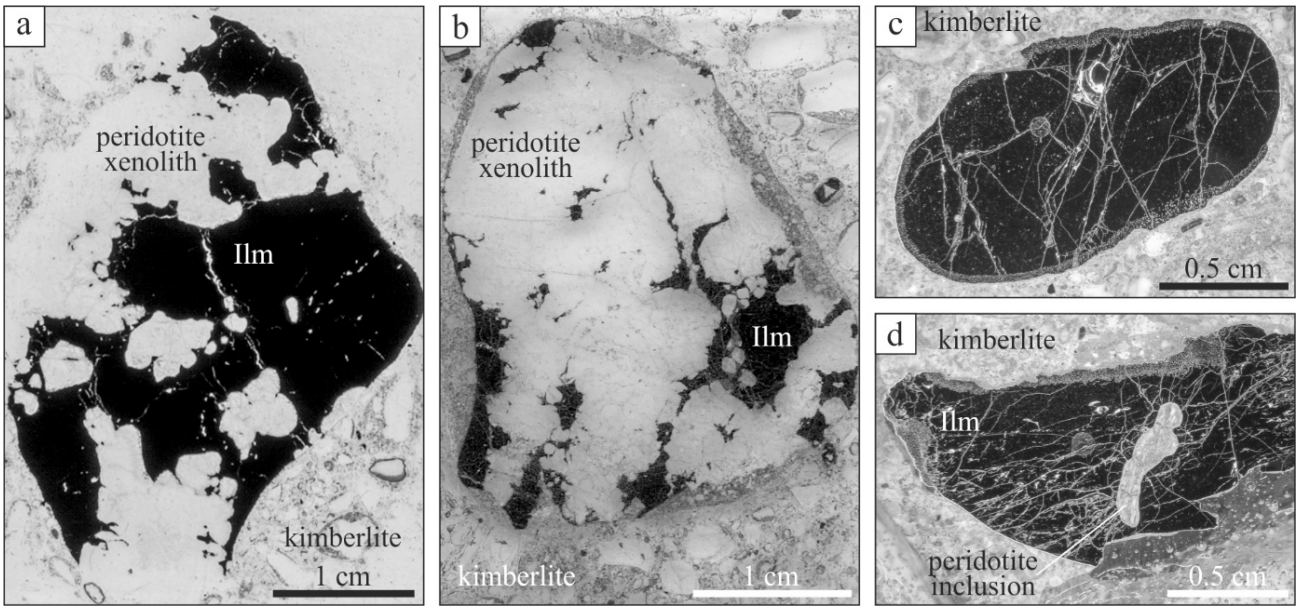

Fig. 1. A-b – thin section photographs of peridotite xenoliths with picroilmenite: a – picroilmenite forms small narrow bifurcated apophyses, b – fragments of peridotite cemented by picroilmenite; c-d – photographs of picroilmenite megacrysts: c – oval shaped megacrysts, d – angular megacryst with fragments of altered peridotite. Ilm – ilmenite.

Picroilmenite within garnet coarse peridotite xenoliths may constitute up to 70 vol.% of the rock. Silicate minerals of the peridotite association are entirely altered. Picroilmenite occurs as sinuous and elongated anhedral polycrystalline aggregates in the interstitial space between peridotite minerals and penetrates along their boundaries. Picroilmenite forms small narrow bifurcated apophyses in peridotite (Fig. 1a). Sometime, fragments of peridotite could be cemented by picroilmenite (Fig. 1b). In sheared peridotite picroilmenite forms rounded to anhedral shapes. Picroilmenite contains a significant amount of serpentized inclusions of different size and shapes that probably represented altered peridotite minerals. In some altered peridotite grains, we can see rounded drop-shaped flakes of ilmenite. Sometimes these drops grow together and form dumb-bell shape.

Megacrysts are relatively large individual nodules of the picroilmenite composition. They are often intensively fractured and usually form round to oval shapes (Fig. 1c) with diameters up to 4 cm. Less often, some megacrysts have angular or elongated grains. In contact with host kimberlite, megacryst grain boundaries are resorbed. Also frequently, megacrysts contain impalpable rounded inclusions of serpentized phases, or larger fragments of altered peridotites (Fig. 1d) reached 0.5 cm. Such inclusions testify that megacrysts are not independent formation and appear as a disintegrated part of ilmenite peridotite.

In garnet-orthopyroxene xenoliths where garnet has typical for megacrysts composition [high TiO_2 (up to 1.1 wt.%) and moderate CaO (4.1-5.0 wt.%) and Cr_2O_3 (2.6-3.4 wt.%) contents] ilmenite occurred in three typical forms: (1) as angular isometric or elongated grains in interstation between garnet and orthopyroxene (Fig. 2a); (2) as veins with width up to 4 mm (Fig. 2c); boundaries of these veins are cragged, hogbacked with multiple apophyses and garnet inclusions; (3) as round spherical drop shapes with diameters up to 200 μm (Fig. 2b) within garnet grains or serpentinized silicate phase. Sometimes these drops grow together. The fine-grained granoblastic texture of orthopyroxene-garnet xenoliths points at original rock recrystallization with equilibria metamorphic structures. Round and drop ilmenite shapes in big garnet grains as well as the occurrence of ilmenite veins may indicate crystallization ilmenite from a Fe-Ti-bearing melt. However, these drop-like shapes also could be formed after equilibrium ilmenite inclusions with garnet during metamorphic processes.

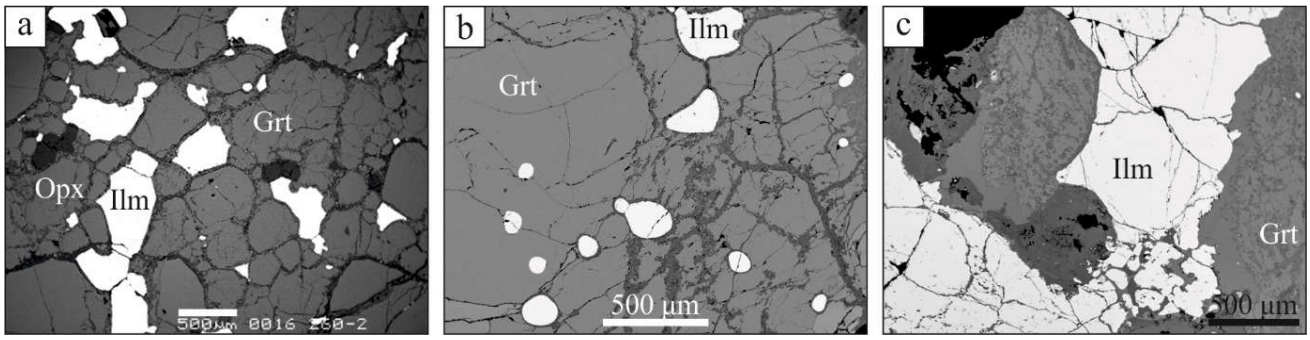

Fig. 2. BSE images of garnet-orthopyroxene xenoliths: a – isometric or elongated ilmenite (Ilm) grains in interstation between garnet (Grt) and orthopyroxene (Opx); b – ilmenite veins cut garnet (Grt); c – round spherical drop shapes of ilmenite (Ilm) in garnet (Grt).

The composition of ilmenite from peridotite xenoliths is characterised by variations in MgO (14.00-14.52 wt.%), Cr_2O_3 (1.26 - 2.20 wt.%) with range of FeO (19.97 - 25.26 wt.%) and Fe_2O_3 (2.25 - 9.45 wt.%), Nb_2O_5 (up to 0.06 wt.%), V_2O_3 (0.48-0.83 wt. %). At the contact with kimberlite the concentrations of MgO and Cr_2O_3 increase up to 14.91 wt.% and 2.60 wt.% respectively.

The ilmenite from garnet-orthopyroxene xenoliths has higher concentrations of MgO (13.94-15.50 wt.%) and Cr_2O_3 (2.08 - 3.06 wt.%) than ilmenite from peridotite xenoliths with decreasing of Fe_2O_3 (3.58 - 8.00 wt.%) and close contents of Nb_2O_5 (up to 0.05 wt.%), V_2O_3 (0.41 to 0.94 wt.%). In contact with garnet, the Cr_2O_3 contents increase, and MgO contents decrease.

The composition of megacrysts overlaps compositions of ilmenite from peridotite and garnet-orthopyroxene xenoliths that is consistent with their origin as disintegrated fragments of ilmenite

bearing mantle xenoliths: megacrysts' contents vary widely: MgO from 13.51 to 15.11 wt. %, Cr_2O_3 from 1.34 to 3.23 wt. %, FeO from 18.91 to 24.71 wt. %, Nb_2O_5 up to 0.11 wt.%.

According to Cr_2O_3-MgO concentrations, ilmenite compositions form two trends: (1) increase Cr_2O_3 with decrease MgO; (2) decrease MgO with decrease Cr_2O_3.

The first one is showed at contacts ilmenite with silicate phases, extra with garnet in peridotite and garnet-orthopyroxene xenoliths. In this case, the diffusion rebalancing in ilmenite contact with the garnet controlled the composition of ilmenite and determinate the wide varieties of Cr_2O_3 and MgO contents.

The second trend corresponds with "Haggerty parabolic curve" that could indicate fractional crystallisation during generation of normal- and low-Cr ilmenites or/and changing of the redox condition into more oxidative one.

The petrographical position of picroilmenite can indicate crystallisation from a Fe-Ti liquid. Such melt can form in the result of separation from a carbonate-silicate liquid with a Fe-Ti component (Litvin et al., 2018). The Fe-Ti melt penetrates into the rock partially breaks it and crystallise as veins. The Fe-Ti melt also takes some peridotite separating fragments with inclusion formation. Spherical drop shapes of picroilmenite in peridotite or within large garnet grains also can point at crystallisation from a melt. Experimental works at a temperature of 1000-1200^{0}C and a pressure of 6-7.5 kb confirm that aggregates of ilmenite and different silicates form in the result of crystallisation from the kimberlitic melt (Mitchell, 2004).

References

Castillo-Oliver M. et al. Use and misuse of Mg- and Mn-rich ilmenite in diamond exploration: A petrographic and trace element approach // Lithos. 2017. Vol. 292–293. pp. 348–363.

Haggerty S.E. The chemistry and genesis of opaque minerals in kimberlites // Physics and Chemistry of the Earth. 1975. Vol. 9. pp. 295–307.

Golubkova A.B. et al. Mg-ilmenite megacrysts from the Arkhangelsk kimberlites, Russia: Genesis and interaction with kimberlite melt and postkimberlite fluid // Geochemistry Int. 2013. Vol. 51. № 5. pp. 353–381.

Larionova Y.O. et al. Kimberlite Age in the Arkhangelsk Province, Russia: Isotopic Geochronologic Rb-Sr and $^{40}Ar/^{39}Ar$ and Mineralogical Data on Phlogopite // Petrology. 2016. Vol. 24. № 6. pp. 562–593.

Litvin Yu.A. et al., Interaction of Titanium Minerals and Their Melts with Diamond-Forming Media (Experiments at 7–8 GPa) // Geochemistry International, 2018, Vol. 56, No. 2, pp. 148–161.

Mitchell R.H. Experimental studies At 5–12 GPa of the Ondermatje hypabyssal kimberlite // Lithos, Vol. 76, Issues 1–4, September 2004, Pages 551-564.

Wyatt B.A. et al. Compositional classification of "kimberlitic" and "non-kimberlitic" ilmenite // Lithos. 2004. Vol. 77. № 1–4 SPEC. ISS. pp. 819–840.

EPIGENETIC COPPER MINERALS OF THE KONDYOR MASSIF

Perhurova V.A., Antonov A.A., Osipov A.S.

Saint-Petersburg State University, Saint-Petersburg, Russia (vikt.perhurova@gmail.com)

Kondyor massif is Russia's largest alluvial platinum asset. It is a perfect circular alkali-ultrabasic zonal intrusion about 7.5 kilometers in diameter. Host rocks are represented by Archaean metamorphic rocks and overburden terrigenous deposits of the upper Proterozoic complex. Most of the massif consists of dunites, which form an isometric stock body about 6.5 kilometers in diameter. Together with other ultrabasic rocks occupy an 90% area of the massif. Margin dunite core is composed of clinopyroxenites and melanocratic gabbro of normal alkaline condition with a capacity of 500 meters. Margin of intrusion at the periphery of the stock compose a dike-like kosvite bodies. They form a large field in the center of the array. This structure is cross-cutting by later (in relation to host rocks) different in size dykes and gangue bodies of alkaline rocks.

In channel fill deposits within the ring Kondyor massif meet regularly nonrounded fragments of oxide green copper rocks. The staff of the St. Petersburg state University took samples of such unit

during an expedition on the Kondyor massif in 2013. Mineral composition morphological and chemical characteristics of individual minerals was studied.

Green copper rock morphologically represent a continuum of bright blue-green color with lots of inclusions. In cavities (up to 2 cm), there are free-open textured powdery congeries of brown and light green colors. The rock also has a large number of lamelliferous congeries of mica and large inclusions of dark-brown isometric flake.

First approximation, it seems that the mass is a solid dense green mineral. But at the microscale level there is a heterogeneity and diversity of the mineral composition of the rock. The mineral inclusions are represented by diopside, amphibole (Ferri-katophorite), phlogopite and vermiculite. In many cases, these minerals similar to source minerals (Fig. 1 a). The matrix is composed of a fine crystalline congeries of malachite, brochantite, dioptase, chrysocolla and copper sulfides. Also visible on the germination of brochantite through the vermiculite aggregates on the cleavage planes (Fig. 1 b). This altered and heterogeneous mass of hypergene minerals has a transient chemical composition, which has not been fully diagnosed. X-ray diffraction analysis showed that the main mineral phase in the rock is malachite and brochantite. Among the inclusions in the mass, rare but large flakes of titano-magnetite and magnetite were installed.

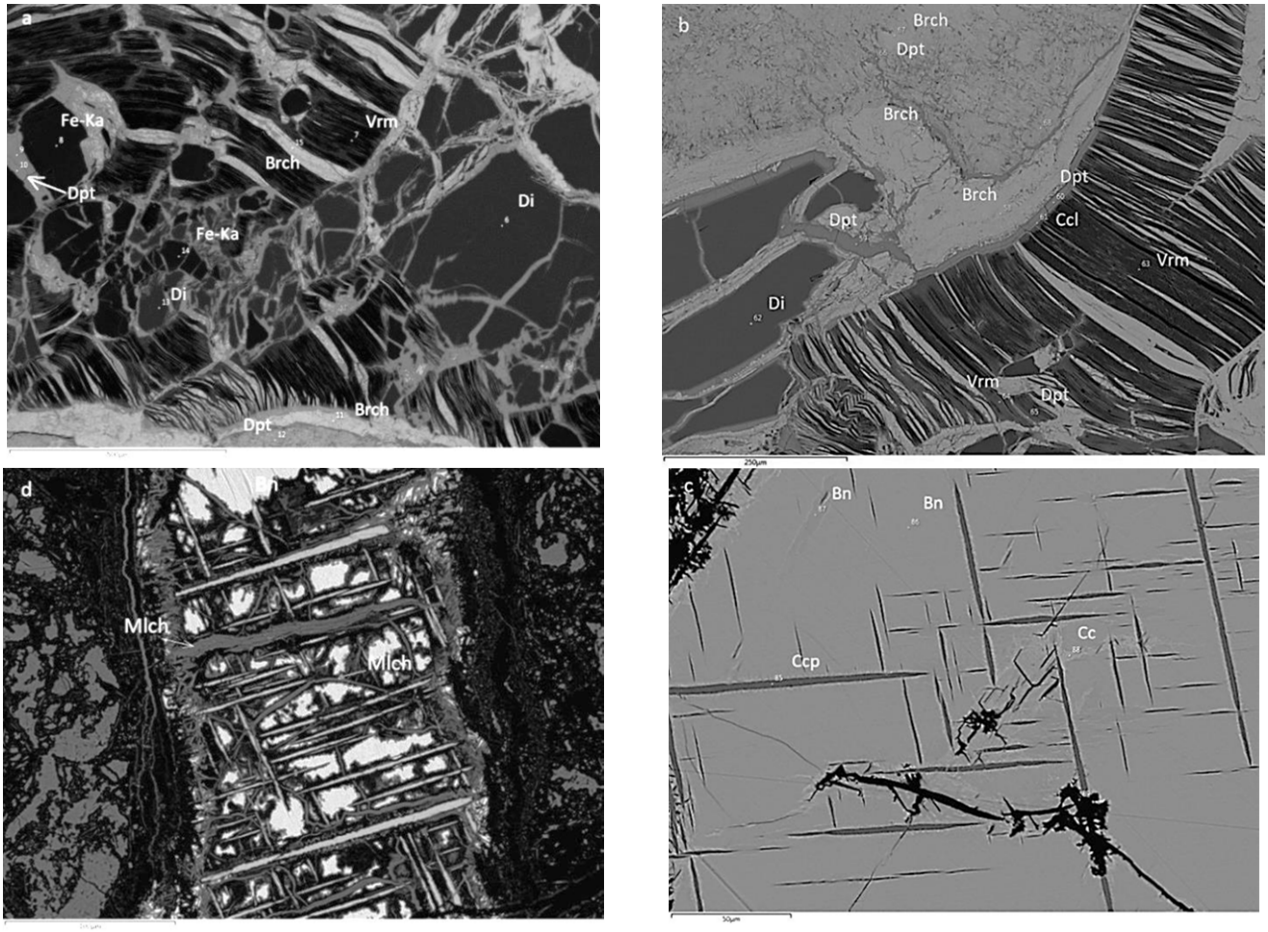

Fig. 1. Mineral assemblage and microprobe analysis points of rocks from the oxidation zone of the Kondyor massif.
Di – diopside; Dpt – dioptase; Fe-Ka – ferri-katophorite; Vrm – vermiculite; Brch – brochantite. Ccl – chrysocolla; Mlch – malachite; Ccp – chalcopyrite; Bn – bornite; Cc - chalcocite.

Diopside in the studied rocks contains sodium (up to 3 wt% Na_2O), aluminum and chrome (≈1 wt% Al_2O_3, Cr_2O_3) (table. 1). Amphibole according to the microprobe analysis diagnosed as ferri-katophorite (table. 2). Mica is represented by phlogopite and its hydrous analogy vermiculite (table. 2). All these minerals contain titanium adulteration ≈1 wt% TiO_2 in amphibole and up to 2 wt% TiO_2 in mica.

In the studied specimen rock observed a large number of sulphides: bornite, chalcopyrite, chalcocite. Sulfides are oxidized to varying degrees and replaced by hypergene formations: malachite and chrysocolla, which have the form of branching folium developed over the surface of the specimen (Fig.1 d). In some areas malachite replaces all copper-sulfide formations. In bornite there are naturally oriented growths of chalcopyrite (Fig. 1 c, d). Dispersive impregnation of native silver was recorded in sulfide clusters.

Table 1. Chemical composition of the diopside (wt %).

№	Na_2O	SiO_2	TiO_2	Al_2O_3	Cr_2O_3	MgO	CaO	FeO	MnO	Fe_2O_3	Total
1	2,51	54,30	-	0,71	1,04	13,66	21,08	1,63	0,29	5,30	100,53
2	2,51	54,30	-	0,71	1,04	13,66	21,08	1,63	0,29	5,30	100,53
3	2,48	54,64	-	0,63	1,22	13,57	20,75	2,79	0,27	4,06	100,41
4	2,70	54,15	0,36	0,60	1,15	13,51	20,77	1,33	0,23	5,79	100,58

Table 1.1. Conversion of chemical composition of diopside to formula coefficients (4 cation).

№	Na	Si	Ti	Al	Cr	Mg	Ca	Fe^{2+}	Mn	Fe^{3+}	O
1	0,18	1,98	-	0,03	0,04	0,75	0,82	0,05	0,00	0,16	6,00
2	0,18	1,99	-	0,03	0,03	0,74	0,83	0,05	0,01	0,15	6,00
3	0,18	2,00	-	0,03	0,04	0,74	0,81	0,09	0,01	0,11	6,00
4	0,19	1,99	0,01	0,03	0,03	0,74	0,82	0,04	0,01	0,16	6,00

Table 2. Chemical composition of the ferri-katophorite (wt %).

№	K_2O	Na2O	SiO_2	TiO_2	Al_2O_3	Cr_2O_3	MgO	CaO	FeO	MnO	Fe_2O_3	Total
5	0,88	6,21	52,46	0,89	4,49	1,01	18,89	8,20	6,37	0,32	0,19	99,92
6	1,01	6,07	52,29	1,27	4,72	1,02	18,53	7,95	6,13	0,27	0,55	99,81

Table 2.1. Conversion of chemical composition of ferri-katophorite to formula coefficients (16 cation).

№	K	Na	Si	Ti	Al	Cr	Mg	Ca	Fe^{2+}	Mn	Fe^{3+}	O
5	0,16	1,67	7,29	0,09	0,74	0,11	3,91	1,22	0,56	0,04	0,22	22,00
6	0,18	1,64	7,29	0,13	0,78	0,11	3,85	1,19	0,71	0,03	0,09	22,00

Table 3. Chemical composition of the mica and hydromica (wt %).

№	K_2O	Na2O	SiO_2	TiO_2	Al_2O_3	Cr_2O_3	MgO	CaO	FeO	MnO	Total
7	-	-	44,06	1,75	12,90	0,52	26,77	0,15	13,55	0,30	100,00
8	-	-	40,87	1,81	11,82	0,58	23,62	-	21,30	-	100,00
9	-	-	47,08	1,95	13,84	0,53	28,23	-	8,08	0,27	100,00
10	-	-	46,96	2,08	13,76	0,65	27,83	-	8,73	-	100,00
11	-	-	40,51	1,71	12,00	0,55	23,58	-	21,66	-	100,00
12	-	-	49,03	-	12,10	-	29,68	-	9,19	-	100,00
13	7,23	2,35	41,80	1,09	15,80	0,29	25,37	-	6,09	-	100,00
14	5,18	1,23	42,85	1,12	16,49	0,33	26,61	-	6,19	-	100,00

Table 3.1. Conversion of chemical composition of mica and hydromica to formula coefficients (22 oxygen).

№	K	Na	Si	Ti	Al	Cr	Mg	Ca	Fe^{2+}	Mn	O
7	-	-	2,92	0,09	1,01	0,03	2,65	0,01	0,75	0,02	10,00
8	-	-	2,83	0,09	0,96	0,03	2,43	-	1,23	0	10,00
9	-	-	3,02	0,09	1,05	0,03	2,7	-	0,43	0,01	10,00
10	-	-	3,02	0,1	1,04	0,03	2,67	-	0,47	0	10,00
11	-	-	2,81	0,09	0,98	0,03	2,44	-	1,26	0	10,00
12	-	-	3,15	-	0,92	-	2,84	-	0,49	0	10,00
13	0,62	0,31	2,82	0,05	1,25	-	2,55	-	0,34	0	10,00
14	0,44	0,16	2,83	0,06	1,29	0,02	2,62	-	0,34	0	10,00

The study of the morphology and chemical composition were performed in the thin sections and polished sections. Energy-dispersive microanalysis (resource center of SPBU "Geomodel", Hitachi S 3400); optical microscopy (department of mineralogy, St. Petersburg state University, Leica P450) and X-ray diffraction analysis was carried out (resource Center x-ray diffraction research methods, St. Petersburg state University, "MiniFlex II" Cu-Ka).

Data was obtained suggest that the substrate for the formation of the studied malachite-like rocks are kosvite and associated Apatite-titanomagnetite-phlogopite rocks. This is evidenced both by the similarity of the mineral composition of sourse minerals in «malachite» and features of the chemical composition of minerals. Also kosvite discovered chalcocite-chalcopyrite clusters containing gold-palladium-silver mineralization.

References

Gurovich V. G., Emelyanenko E. P., Zemlyanukhin V. N. Geology, petrology and ore mineral resources of the Konder massif. 1994. 11-15 p. (in Russian).

NOBLE METAL MINERALS IN CARBONATITES OF KOVDOR MASSIF

Petrov S.V., Martynova A.A., Shelukhina Y.S.
Institute of Earth Sciences, SPbSU, petrov64@gmail.com

The first founding of noble metal mineralization in the ores of Kovdor massif was done by B.V. Gavrilenko and co-authors. Native silver and akantite were diagnosed in the polished sections from the sulphide concentrate of apatite-magnetite-baddeleyite ores of Kovdor, in addition, they repeatedly noted the triple phases of the Pb-Sb-Sn composition. After these works, the focus was made on this concentrate when studying the mineralogy of precious metals in the ore of Kovdor. N.S. Rudashevsky and co-authors (1995, 2004) found more than two dozen phases in similar products, the main ones being isoferroplatinum, sperrylite, mertieite-II, moncheite, arsenopalladinite, atokite, isomertiite and others (table 1). Phases of native metals – gold, silver, and electrum – are defined in heavy fraction from crushed ores.

Similar results were obtained by E.V. Putintseva and co-authors (1997, 1999) in the study of the sulphide mineralization of Kovdor ores. PGE mineral grains are mainly irregular in shape with uneven edges, but often also have crystallographic shapes. Crystallographic shapes are common for isoferroplatinum (cubic crystals), sperrylite and, sometimes, mertieite-II. PGE minerals most often occur in monomineral grains, but there are also intergrowth of these minerals. The most often intergrowth are formed by moncheite and sperrylite, mertieite-II and sperrylite, rustenburgite and atokite with sperrylite and others (table 1). The compounds of platinum and palladium are diverse: along with the Au, Ag, Pt, and Fe alloys, the Pt and Pd sulphides are also found, as well as intermetallic compounds. The presence among the PGE minerals of both high- and low-temperature phases indicates the changes in conditions during the formation process of noble metals. The noble metal phases were separated from a combined ore sample, thus it is difficult to make the conclusion about the pattern of distribution of precious metal minerals by ore types of Kovdor deposit.

The predominant PGE mineral is moncheite, mainly its bismuth variety. Sperrylite is the second abundant mineral. Platinum minerals predominate over palladium. This probably reflects the essential contribution of the foscorites of I and III stages, characterized by Pt specialization, to the total mass of heterostatic-time PGE mineral formation. In addition, the predominance of platinum minerals over palladium minerals can be explained by inclusions in copper sulphides (chalcopyrite, bornite) in the form of an isomorphous impurity or submicroscopic impregnation (<1 μm). Indirectly, this is proved by an increased concentration of Pd in comparison with Pt in monomineral fractions of chalcopyrite and bornite. For chalcopyrite from ores of the Anomalous Zone: Pt - 2.5, Pd - 11.3, Au - 13.5 (ppm), for bornite: Pt - 6.2, Pd - 17.4, Au - 22.0 (ppm). The most common palladium mineral in ores of Kovdor deposit is mertieite-II.

Table 1. Noble metal minerals in ores of Kovdorsky massif.

Mineral	Formula (taking composition into account)	Rudashevsky, et al. (1995)	Putintseva, et al. (1999)	Our data, 2012	Our data, 2018
Native gold	Au	x	x	o	
Electrum	AuAg	x			o
Native silver	Ag	x	x	o	o
Native platinum	Pt	x	x		
Isoferroplatinum	Pt_3Fe	x	x		
Atokite	$(Pt,Pd)_3Sn$	x	x	o	
Rustenburgite	$(Pt,Pd)_3Sn$	x	x		
Zvyagintsevite	$(Pt,Pd)_3(Pb,Bi)$	x			
Paolovite	Pd_2Sn		x		
Plumbopalladinite	$Pd_3(Pb,Bi)_2$	x			
Arsenopalladinite	$(Pd,Pt)_8(As,Te,Pb,Sb,Sn)_3$	x			
Isomertieite	$(Pd,Pt)_{11}As_2(Sb,Te,Sn)_2$	x			
Insizwaite	$PtBi_2$		x		
Mertieite-I	$(Pd,Pt)_{11}(As,Sb,Sn)_4$	x			
Mertieite-II	$(Pt,Pd)_8(Sb,As,Sn)_3$	x	x	o	o
Sobolevskite	PdBi	x			
Sperrylite	$PtAs_2$	x	x	o	o
Stumpflite	Pt(Sb,Sn)		x	o	
Braggite	(Pt,Ni,Pd)S	x			
Cooperite	(Pt, Ni)S	x	x		
Erlichmannite	$(Os,Ru)S_2$				o
Hessite	Ag_2Te	x	x		
Stutzite	$Ag_{5-x}Te_3$			o	
Moncheite	$Pt(Te,Bi)_2$	x	x	o	o
Kotulskite	Pd(Te,Bi)			o	o
Argentopentlandite	$Ag(Fe,Ni)_8S_8$	x		o	
Acanthite	Ag_2S			o	o
Stromeyerite	CuAgS				
Lenaite	$(Ag,Cu)FeS_2$				o
Untitled	$(Pd,Ag)_2(Te,Pb,Sb,Sn)$	x			o
Untitled	$Pd_2(Sn,As)$		x		
Untitled	$Pd_2(Sn,Sb)$		x		

Notes: the main minerals are highlighted in bold. x – minerals from sulphide concentrate; o - minerals from heavy fractions and polished sections.

In the chemical composition of isoferroplatinum the only impurity elements are Cu and Pd. Moncheite almost always contain impurity of Bi (up to 28 wt.%). Sperrylite sometimes contain Sb (up to 1.5 wt.%), S (up to 0.9 wt.%) and Ni. Mertieite-II, in addition to the constant impurity of Sn and As, sporadically contains in significant concentrations of Pt. There are no end-members of the series Pt_3Sn-Pd_3Sn in the ores, only intermediate members Pd-rustenburgite and Pt-atokite were found. In addition to paolovite (Pd_2Sn), other minerals of Pd_2A composition are present in the ores of Kovdor, where A is Sn, Sb, Pb and As with different quantitative ratios of ligands, and palladium can be replaced by silver.

In further studies of the noble metal mineralization, the focus was on the ores of the Anomalous Zone. In the study of polished sections and heavy fractions from ores, the presence of PGE minerals in copper-bearing varieties of ores were found.

The most widely spread are silver minerals (fig. 1): native silver and the products of its change - acanthite, lenaite, stromeyerite, as well as hessite and stutzite (tab. 1). Among the PGE minerals sperrylite is most common; in one of the crystals epitaxial inclusion of erlichmanite is observed (fig. 2). All noble metal minerals are in association with bornite, chalcopyrite, galena, siegenite, wittichenite and hawleyite.

The list of noble metal minerals found in ores of Kovdor deposit by now is presented in table 1. A total of 32 mineral phases of various groups were established, of which 3 phases are not known before.

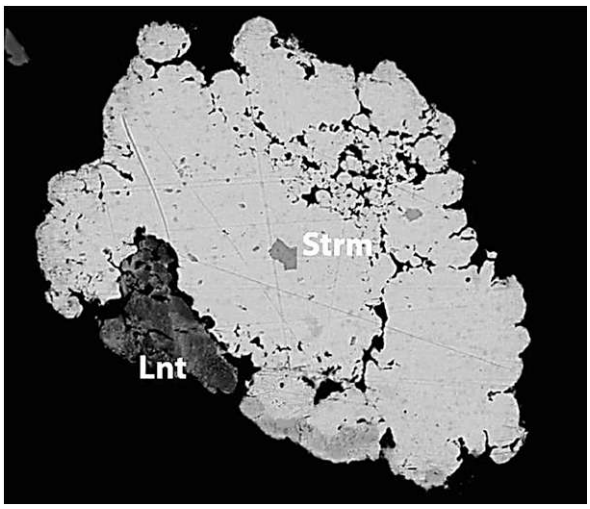

Fig. 1. Native silver grain (70 mkm) with inclusions of stromeyerite (Strm) and in intergrowth with lenaite (Lnt), BSE.

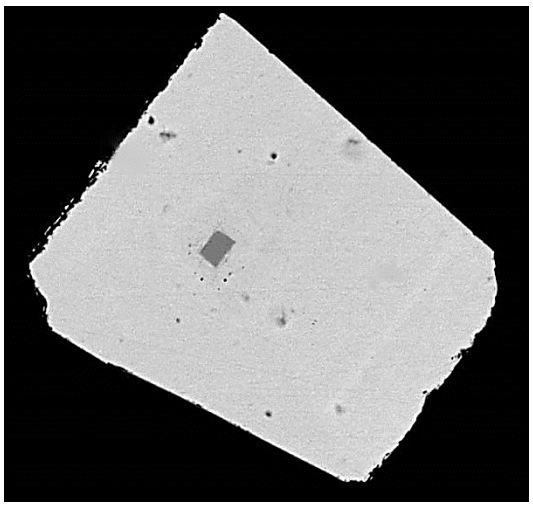

Fig. 2. Sperrylite crystal (60 mkm) with inclusion of erlichmannite, BSE.

References

Putintseva V.V. et al. Precious metals in products of processing of Kovdor deposite ores // Ore processing. 1997. № 5. P. 22-25

Putintseva V.V. et al. New data about precious metals mineralization of alkaline complexes of Karelian-Kola region // Materials of international conference «Carbonatites of Kola peninsula». SPbSU, 1999. P. 97-98.

Rudashevsky N.S. at al. Pt-metal and Au-Ag mineralization on ores and carbonatites of alkaline-ultrabasic complex (Kovdor massiv, Russia) // ZVMO. 1995. № 5. P. 1-15.

Rudashevsky N.S., et al. A review and comparison of PGE, noble-metal and sulphide mineralization in phoscorites and carbonatites from Kovdor and Phalaborwa n book: Phoscorites and carbonatites from Mantle to Mine: the Key Example of the Kola Alkaline Province, Edition: Mineralogical Society Series, 10, Chapter: 11, Publisher: Mineralogical Society, London., Editors: A.Zaitsev, F.Wall, 2004, pp.363-393.

MANTLE XENOLITHS OF THE NEW DIAMONDIFEROUS KIMBERLITE PIPE LUELE (ANGOLA): PARGENESES AND PARTICULARITIES OF THE MINERALS CHEMICAL COMPOSITION

***Pokhilenko L.N.*[1], *Afanasyev V.P.*[1], *Pervov V.A.*[2], *Korolyuk V.N.*[1], *Pokhilenko N.P.*[1,3]**

[1]*V.S. Sobolev Institute of Geology and Mineralogy, Siberian Branch, Russian Academy of Sciences, Novosibirsk, Russia, lu@igm.nsc.ru*

[2]*Departamento de Geologia, Sociedade Mineira de Catoca, República de Angola*

[3]*Novosibirsk State University, Novosibirsk, Russia*

The Luele kimberlite pipe (Angola) is the largest among the deposits discovered over the last 60 years. It is already explored down to 400 meters. 26 xenoliths extracted from it's core were carefully analyzed. Studied samples divided into the paragenetic groups one can see in the Table 1, where the main and accessory minerals are presented. The overwhelming majority of samples are phlogopitized; half - contains amphibole, the third part - ilmenite. Attention is drawn to the large amount of titanium-containing minerals and the admixture of niobium in these minerals (Fig. 1, b: Nb_2O_5 content (wt.%) in dark perovskite zones – 1.8, in white zones – 11, in zirconolite – 11). Crichtonite was found as an inclusion in clinopyroxine (Fig. 1, f). The exotic sulfides – shandite ($Pb_2Ni_3S_2$) and talcusite ($TlCuFe_{0.6}S_2$) (Fig. 1, d) – were detected at the same time like usuall sulfides of Ni, Fe, Cu. There was a vermicular zircon in one of the websterites (Fig. 1, e). The exsolution lamellae were observed in

some pyroxenes (Fig. 1, d). Secondary minerals of silicates and oxides are serpentine and magnetite (hematite) of a wide range of compositions, often with various impurities.

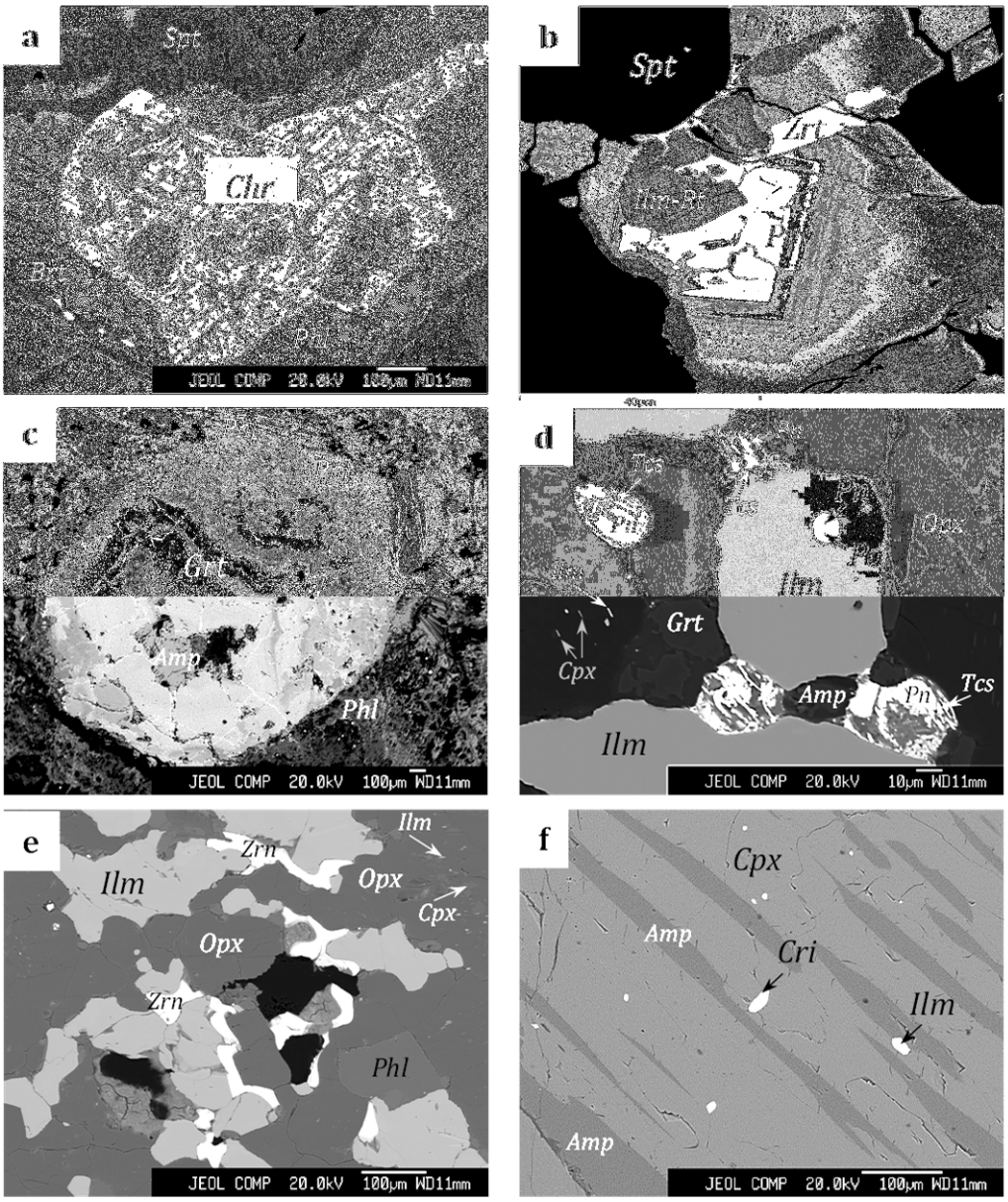

Fig. 1. Fragments of the mantle xenoliths from Luele pipe, regime BSE.
a – Lu-15: regular intergrowths of chromite (Chr) in phlogopie (Phl); b – Lu-44: zirconolite (Zrt) in zoning perovskite (Prv); c – Lu-37: extremely zoning garnet (Grt) with amphibole (Amp) inclusion; d – Lu-13: primary and secondary sulfides (pyrrhotite - Po, pentlandite - Pn, talcusite - Tcs); lamellae of clinopyroxene (Cpx) and ilmenite (Ilm) in ortoperoxene (Opx); e – Lu-13: vermicular zircon (Zrn) in Grt-Ilm-websterite; f – Lu-66: replacement of clinopyroxene by amphibole; crichtonite (Crt) and ilmenite inclusions in clinopyroxene.

The chemical composition of rock-forming minerals has some differences in comparison with similar minerals from the known diamondiferous pipes of Yakutia and South Africa. Garnets with a sharp and rare zoning are noted: 1) garnet of eclogite - chaotically spotted zoning of the whole grain on CaO-MgO-FeO (in wt.%: 4.8-8.6, 8.7-16, 14.8-21.5, correspondingly; see Fig. 1, c); 2) harzburgite garnet - strong heterogeneity of the edges with Al_2O_3-Cr_2O_3-FeO (in wt.%: 16.2-20.5, 2.4-9.9, 6.7-8.9, correspondingly). Olivine from chromite vherlites demonstrates strong spotted zoning (Mg# 86-92). Ilmenite from the olivine glimmerite has anomalously high TiO_2 (57.86 wt.%) and MgO (18.79 wt.%). Ilmenite inclusion in serpentinized olivine from garnet-harzburgite contained a significant admixture

of MnO (12.6 wt. %). On the whole, the compositions of the ilmenites of the studied parageneses show a good positive correlation between chromium and magnesium (R^2=0.45). Wherlite's chromite was found in the form of regular ingrowths with phlogopite (Fig. 1, a). The chromite, containing 54-63 wt.% of Cr_2O_3, practically did not detect in its composition Al_2O_3.

Table 1. Main and accessory minerals of the studied xenoliths from Luele pipe (Angola).

	Ilm-dun			Spl-dun		Chr-wherlite				harz	lherz		Ilm-websterite			Grt-pxt		eclogite						glimmerite		
Sample-Lu	12	31	44	39	51	1	15	30	40	41	36	7*	13**	66**	10	33	72	5	8	37	47	48	65	46$^+$	32$^+$	14
Ol	+	+	+	+	+	+	+	+	+	+	+	+													spt	
Grt										+	+	+	+	+		+	+	+	+	+	+	+	+			
Opx										+	+	+	+	+	+											
Cpx						+	+	+	+	inc/rel	+	+	+	+	+	+	+	+	+	+	+	+	+	+	+	
Chr/Spl				spl	spl	chr	chr	chr	chr																	
Ilm/Usp	ilm	ilm	ilm							inc			ilm	ilm	ilm				ilm				ilm		usp	
Amp								+		+	+		+	+		+	+	+	+	+	+			+		
Phl	+		+	+	inc	+	+	+	+	rim	+	+	+	+	+	+	+	+		+			+	+	+	+
Su			Pb,Ni									Ni	Fe,Ni Tl, Cu	Ni		Ni,Cu Co,Fe			Ni,Cu Co,Fe							
Cb (Ca,Sr)							Sr			Ca				Ca				Sr		Ca				Ca		
Rt/Prv/Ttn		prv	rt, prv								rt	rt				rt		ttn			rt, ttn	rt				
Mag/Gem	+		+						+			+			+	+	+		+		+			+	+	
Ap							+										+									+
Brt							+	+							+					+						
Zrn/Zrt			zrt										zrn													
Pct													inc													
Cri														inc												

Comments: 1) the mineral abbreviations from Whitney& Evans (2010); cri – crichtonite, su – sulphides, zrt – zirconolite; 2) * - deformed; ** - with Grt; $^+$ - with Cpx; 3) dun – dunite, harz – harzburgite, lherz – lherzolite, pxt – pyroxenite; 4) lam – lamella, inc – inclusion, rel – relict of a grain, rim – rim around garnet.

A distinctive feature of the investigated xenoliths can be considered their strong enrichment with alkalis, hydroxyl group, titanium, to a slightly lesser extent - calcium, zirconium, niobium, REE, thallium. Regular chromite-phlogopite ingrowths suggest the joint growth of these minerals, that is, the chromite of diamond association was formed under the conditions of the activity of the water-alkaline fluid. The zoning of many minerals speaks of abrupt changes in the conditions and environment of their formation. All this implies non-traditional scenarios for the formation of rocks block in the given section of the lithosphere.

The work was supported by grant 16-05-00811 of the Russian Foundation for Basic Researchers and was carried out as a part of the Project No 0330-2016-0006.

References

Whitney D.L., Evans B.W. (2010): Abbreviations for names of rock-forming minerals. American Mineralogist, 95, 185–187.

HETEROGENEITIES IN PERIDOTITES OF THE ANCIENT PLATFORM LITHOSPHERIC MANTLE BASE: TYPES AND ORIGIN

N.P. Pokhilenko[1,2], A.M. Agashev[1], L.N. Pokhilenko[1].

[1] VS Sobolev Institute of Geology and Mineralogy SB RAS, Novosibirsk, Russia.

[2] Novosibirsk State University, Novosibirsk, Russia

Corresponding email: chief@igm.nsc.ru

Xenoliths of the cratonic lithospheric mantle (CLM) in kimberlites carries unique information about structure, composition and evolution of the ancient cratonic lithosphere and provide a rock samples from the CLM vertical cross section from the Moho Boundary up to at least 300km. This material also carries information concerning the character and intensity of processes occurring in the CLM roots including zone of CLM – asthenosphere interaction and kimberlite melts generating zone. Of special importance are peridotite xenoliths formed at P-T conditions of the diamond stability field providing perhaps the only opportunity for direct study of composition and evolution of the most deep-seated part of the ancient CLM.

This paper includes results of complex study of peridotite xenoliths with different types of heterogeneities formed at conditions of the diamond stability field. These peridotites include:

1) extremely fresh xenoliths of sheared pyrope lherzolits of Udachnaya pipe representing zone of lithosphere-asthenosphere interaction. A combination of compositional, geochemical, isotopic and petrographic features shows that these most deep-seated rocks of the lithospheric mantle were intensely deformed under conditions of significant stress pressure in the base of lithosphere, and have a complex evolution of their chemical composition, including a stage of partial melting and at least two stages of metasomatic enrichment (Boyd et al., 1997; Agashev et al., 2013; Pokhilenko et al., 2015). A partial melting of the most enriched sheared pyrope lherzolites can be related with the primary kimberlite melt formation as well as formation of the kimberlite megacrysts suite;

2) xenoliths of ultradepleted harzburgites and dunites with clear signs of silicate type metasomatic treatment, and it was shown that sub-cratonic basaltic metasomatic fluids of the Siberian Platform re-fertilized previously depleted CLM peridotites. The intermediate stage of transformation of the ultradepleted harzburgites into the enriched in pyroxene peridotites have been found in a rare xenoliths from Udachnaya pipe (Pokhilenko et al., 1999, 2015; Howarh et al., 2014). Garnet grains in these xenoliths are zoned with the deep-purple core and red-orange rim. The core compositions belong to the subcalcic, Cr-rich pyropes, typical for extremely depleted harzburgites and dunites. Whereas, rim composition is corresponds to lherzolite and even to pyroxenite paragenesis. The Cr_2O_3 content drops from 11.8 wt% in the core to 1wt % in the rim and CaO content significantly increased from core to rim. The calculations of REE content in garnet crystallized from basaltic melt indicate that this process can account for the heavy REE contents in garnet rim, but contain a less of middle REE`s and significantly less of LREE`s. Therefore, the rims of the garnets not simply grow from the basic melt, but it formed by more complicated multistage process. It could be an interaction of existing Cr rich garnet with the sub-lithospheric basic melt as the combined composition of garnet core and that of calculated garnet are more similar to the rim composition, but still not account for LREE enrichment. The later metasomatic enrichment by kimberlite melt can add the necessary LREE`s to the rim (Pokhilenko et al., 2015);

3) rare polymict breccia xenoliths containing mixed fragments of CLM rocks and minerals from wide interval of depths and different associations. Four xenoliths of polymict breccia were found in South African pipes of Cretaceous age: Bultfontein and DeBeers (Lawless et al. 1979), and several xenoliths of this type were reported for the Siberian Udachnaya, Sytykanskaya and Noyabrskaya pipes, and South African Premier pipe (Pokhilenko, 2009; L.Pokhilenko et al., 2014). These xenoliths contain CLM material from wide interval of depths – beginning from zone of CLM – asthenosphere interaction corresponding to depth from near 270-250 km to 130-120 km for those from the Middle Paleozoic Udachnaya pipe (Siberian Platform) and Proterozoic Premier pipe (Kapvaal Craton)

(Pokhilenko, 2009), and from 140-130 km to 100-90 km from Mesozoic Noyabrskaya pipe (Siberian Platform) (L.Pokhilenko et al., 2015).

4) rare xenoliths of megacrystalline peridotites with clear sings of significantly different intensity of carbonatite type metasomatic treatment reported for Udachnaya pipe. This type of rock can contain garnets of different composition both in major (Ca, Mg, Fe, Cr) and rare elements (Pokhilenko et al., 1993; Shimizu et al., 1999) and sometimes even garnets of different parageneses: high-Cr low-Ca pyropes belonging to harzburgite-dunite paragenesis and high-Cr high-Ca garnets of wehrlite paragenesis coexisting with cpx.

All the CLM peridotite heterogeneities described above can be related with: a) processes of metasomatic treatment by basaltic melts of varying composition and sub lithospheric origin (types 1 and 2). This type of transformation of the Siberian Platform CLM peridotite composition – extremely intensive re-fertilization was related with a very high scale influence of the Siberian Permo-Triassic Super Plume melts, but in smaller scale this type of processes happened for the Siberian CLM peridotites several times before (Pearson et al., 1995); b) metasomatic treatment of carbonatite type (types 1 and 3). These carbonatite melts can be of different origin (Pokhilenko et al., 1991, 1993, 2015; Pearson et al., 1995), and the variability of ^{4}He in the these types of CLM peridotites may be related with participation in metasomatic processes enriched fluids from ancient subducted slabs added to proto-kimberlitic fluids-melts of initially nearly carbonatitic composition (Barry et al., 2015; Pokhilenko et al., 2015); c) dynamic processes related in space and time with processes of kimberlite formation (type 4), presenting a combination of plastic and fracture deformation of CLM peridotites with generation of proto-kimberlitic melts and initial stages of their movement to the Earth surface (Pokhilenko, 2009).

This study was supported by RFBR, Grant # 16-05-00811

References

Agashev A.M., Ionov D.A., Pokhilenko N.P., Golovin A.V., Cherepanova Y., Sharygin I.S. Metasomatism in lithospheric mantle roots: Constraints from whole-rock and mineral chemical composition of deformed peridotite xenoliths from kimberlite pipe Udachnaya// Lithos. 2013. Vols 160-161, pp. 201-215.

Barry P.H., Hilton D.R., Day J.M., Pernet-Fisher J.F., Howarth G.H., Magna T., Agashev A.M., Pokhilenko N.P., Pokhilenko L.N., Taylor L.A. Helium isotopic evidence for modification of the cratonic lithosphere during the Permo-Triassic Siberian flood basalt event// Lithos. 2015. Vols 216-217, pp.73-80.

Howarth G.H., Barry P.H., Pernet-Fisher J.F., Bazioti, I.P., Pokhilenko N.P., Pokhilenko L.N., Bodnar R.J., Taylor L.A., Agashev A.M. Superplume metasomatism: Evidence from Siberian mantle xenoliths// Lithos. 2014. Vols 184–187, pp. 209-224.

Pokhilenko N., Sobolev N., Kuligin, S., Shimizu N. Peculiarities of distribution of pyroxenite paragenesis garnets in Yakutian kimberlites and some aspects of the evolution of the Siberian craton lithospheric mantle// Proceedings of the **VIIth International Kimberlite Conference**. Red Roof Design, Cape Town, 1999. pp. 689-698.

Pokhilenko N. Polymict breccia xenoliths: Evidence for the complex character of kimberlite formation// Lithos. 2009. Vols 112, pp. 934-941.

Pokhilenko N.P., Sobolev N.V., Boyd F.R., Pearson D.G., Shimizu N. Megacrystalline pyrope peridotites in the lithosphere of the Siberian platform: mineralogy, geochemical peculiarities and the problem of their origin. Russ. Geol. Geophys. 1993. Vol. 34, pp. 56-67.

Pokhilenko L.N., Pokhilenko N.P., Afanasiev V.P. Polymict breccia xenolith from Noyabrskaya pipe (Yakutia) // 30th International Conference on **"Ore Potential of Alkaline, Kimberlite and Carbonatite Magmatism"** Abstract Book Akdeniz University-Antalya / UCTEA Chamber of Turkish Geological Engineers-Ankara, 2014. pp. 131-134.

Shimizu N., Pokhilenko N., Boyd F., Pearson D. Trace element characteristics of garnet dunites/harzburgites, host rocks for Siberian peridotitic diamonds// Proceedings of the **VIIth International Kimberlite Conference**, Red Roof Design. Cape Town, 1999. pp. 773-782.

FE IN THE EARTH'S CORE: NEW DATA AND NEW IDEAS

Pushcharovsky D.Yu.
Faculty of Geology, Lomonosov Moscow State University, Leninskie gory, Moscow, 119234 Russia, dmitp@geol.msu.ru

Iron is among the most abundant elements in the terrestrial planets. Pure iron likely accounts for 96 percent of the inner core's composition, along with nickel and possibly light elements. Consequently, the interest to this element and to its compounds at HP and HT is growing up. The crystal chemical analysis of Fe-minerals of geophysical interest, which are considered as the possible constituents of the Earth's core, is the aim of the review.

The origin and the metallic composition of the Earth's core is one of the outstanding unanswered questions in planetary science. The differentiation of the Earth into a metallic core and silicate mantle (Goldsmith, 1922) occurred during the accretion of the planet when the solar system was very young, less than 30 m. y., whereas the inner core was formed ~1 b. y. ago.

The composition of the Earth's core

The phase diagram of iron was discussed intensively during the past two decades by Andrault, Badro, Dubrovinsky, Saxena, Shen, and others. Five Fe-polymorphs, namely bcc (alpha, delta), fcc (gamma), hcp (epsilon) and dhcp (beta) were identified. Most recent experiments suggest that hcp-Fe is stable at inner core pressures and relatively low temperatures. However at pressure >200 GPa and at high temperatures over 5000 K a new (sixth) cubic bcc-Fe is more stable. This was confirmed theoretically by Belonoshko et al. (2017) and experimentally by Hrubiak et al. (2018). The bcc phase is stabilized at high temperatures by a diffusion mechanism. It is less dense, its atoms are more mobile and easier can be adjusted to the stress. Thus, at P 330 GPa the melting point of Fe is 6400 K.

Tao Wang et al. (2017) implied that the Earth's inner metallic core has double-layered structure. Assuming these ideas, a hcp-Fe can be attributed with outer inner core whereas bcc-Fe can be more typical for inner core.

Light elements in the core

The mean atomic mass in the core is approximately 49.3, compared to 55.85 for pure iron (Bazhanova et al., 2017). To explain these differences, we have to allow for approximately 10–20 mol.% of lighter elements. The possible candidates for the light elements are carbon, hydrogen, silicon, oxygen and sulfur (after Fei, Badro, Ohtani, Litasov, Shatskiy, Sakamaka et al.). S and C are considered as the most probable partners of Fe and Ni in the core. The mineralogically acceptable phases of these elements in the Earth's core are reviewed.

The crystal structure of Fe_7C_3: C-atoms are in the trigonal prisms formed by Fe. The interest to this compound was reinforced after the recent results of HP-study of dolomite (Dorfman et al., 2018). At T = 1500 – 2200°C and P 51 - 113 GPa the Mg-component of dolomite reacted with iron to form diamond, iron carbide (Fe_7C_3), and (Mg,Fe)O. Another Fe-carbide, cohenite, was identified as inclusions in the large gem-quality diamonds formed in the Earth's deep mantle. The C-atoms are located in the centers of 8-vertices polyhedra formed by Fe-atoms.

The crystal structures of four mineralogically possible sulfides in the lower mantle and core are considered: (i) Fe_7S (the presence of this compound is questionable); (ii) FeS (structure type of MnP, sp.gr. Pnma) is derivative of NiAs. In its condensed framework, the FeS_6 octahedra share the edges and the faces. The structure is stable to P>120 GPa and to T> 3000 K; (iii) Fe_3S_2, the likely component of the lower mantle. The condensed framework is formed by SFe_9 polyhedra; (iv) Fe_2S, the likely component of the inner core to P = 300 GPa. The dense framework is formed by SFe_{10} polyhedra.

New chemical reactions with Fe-minerals in the Earth's deep lower mantle and at the core–mantle boundary

The recent results of ultra-high pressure mineralogical studies provided the new data related with decomposition of Fe-rich Mg-wustite, dehydrogenation of goethite and its transformation to pyrite-like phases FeO_2 and FeOOH in the Earth's deep lower mantle. At the base of the mantle, the latter compound decomposes to $Fe_2O_3 + H_2O$. This process may cause incorporation of H into the outer core and the formation of FeH_x. This conclusion is of great interest: according the cosmochemical data H-abundance in the Universe is 0.06 mas % and consequently its content in the Earth's core is 10 000 more in respect to hydrosphere. Thus, the forms of hydrogen concentration in the core are a subject for discussion.

Similarly with hydrogen it was found that at the core's temperature and pressure the noble gas xenon will interact with iron (P=200 GPa, T= 1700°C) and nickel (P= 150 GPa, T= 1200°C) to form $XeFe_3$ and $XeNi_3$ (Stavrou et al., 2018). Both structures (sp. gr. Pmmn) are distictly different, despite their similarity with Cu_3Au structure type. They also exhibite that at extreme conditions electropositive at ambient pressure elements could gain electrons and form anions. These results are considered as a possible explanation of Xe depletion in Earth's atmosphere in respct to Xe-content in the carbonaceous chondrites.

The new model of the Earth's deep interior

According to seismic tomography maps for various depth levels and the data available on geophysical discontinuities, mineral composition, and phase transformations in the mantle, it is proposed that the latter can be subdivided into six geospheres. The cornerstone of the new concept lies in the recognition of middle mantle between 840 and 1700 km, which is separated from the upper and lower mantle by the boundary zones, 170 and 500 km thick, respectively. This idea, elaborated by Pushcharovsky & Pushcharovsky (2012), recently was confirmed by the study of iron partitioning between ferropericlase and bridgmanite in the Earth's lower mantle (Xu et al., 2017).

Within the new thermodynamic model of iron and aluminum chemistry for lower mantle conditions, the lower mantle has two regions. An upper region contains Fe^{3+}-rich bridgmanite with HS ferropericlase and metallic Fe. A lower region incorporates LS iron-rich ferropericlase coexisting with iron-depleted bridgmanite and almost no metallic Fe. The transition between both regions occurs at a depth of ~1600 km. Thus, further subdivision of the lower mantle is confirmed on macro- (geophysical, geological) and micro- (mineral physics, electronic state) levels.

This study was supported by the Russian Foundation for Basic Research: grant no. 18-05-00332.

References

Bazhanova Z.G., Roizen V.V., Oganov A.R. High-pressure behavior of the Fe–S system and composition of the Earth's inner core// Phys.-Usp. 2017. Vol. 60 pp.1025–1032.

Belonoshko A.B., Lukinov T., Fu J., Zhao J., Davis S., Simak S.I. Stabilization of body-centred cubic iron under inner-core conditions// Nature Geosci. 2017. Vol. 10 pp. 312–316.

Dorfman S.M., Badro J., Nabiei F., Prakapenka V.B., Cantoni M., Gillet Ph. Carbonate stability in the reduced lower mantle// Earth Planet. Sci. Lett. 2018. Vol. 489 pp. 84–91.

Hrubiak R., Meng Y., Shen G. Experimental evidence of a body centered cubic iron at the Earth's core condition// arXiv:1804.05109v1 [physics.geo-ph].

Pushcharovsky D.Yu., Pushcharovsky Yu.M. The mineralogy and the origin of deep geospheres: a Review// Earth-Sci. Rev. 2005. Vol. 113. Nos. 1–2 pp. 94–109.

Stavrou E., Yao Y., Goncharov A.F., Lobanov S.S., Zaug J.M., Liu H., Greenberg E., Prakapenka V.B. Synthesis of xenon and iron–nickel intermetallic compounds at Earth's core thermodynamic conditions// Phys. Rev. Lett. 2018. Vol. 120 pp. 096001-096001-6.

Wang T., Song X., Xia H.H. Equatorial anisotropy in the inner part of Earth's inner core from autocorrelation of earthquake coda// Nature Geosci. 2015. Vol. 8. No. 3 pp. 224–227.

Xu S., Lin J.-F., Morgan D. Iron partitioning between ferropericlase and bridgmanite in the Earth's lower mantle// J. Geophys. Res. Solid Earth. 2017. Vol. 122 pp. 1074–1087, doi:10.1002/2016JB013543.

BOHEMIAN MASSIF, CENTRAL EUROPE, TECTONIC BEHAVIOUR OF THE SOLIDIFIED ASTROBLEME AND THE RELATED DISTRIBUTION OF ORE DEPOSITS

Rajlich P.
Museum of Southern Bohemia, petr.rajlich@muzeumcb.cz

The Geomorphologic Circular structure in Central Europe is well visible on satellite imagery and plastic terrain map (Fig. 1). Known as the Czech massif, carries a series of traces of two billion years old impact multiring basin with a diameter of up to 600 km. Together with the pre-impact and the younger faults it appears inside and around the Bohemian massif in the gravity map based on EGM 08 data (Fig. 2).

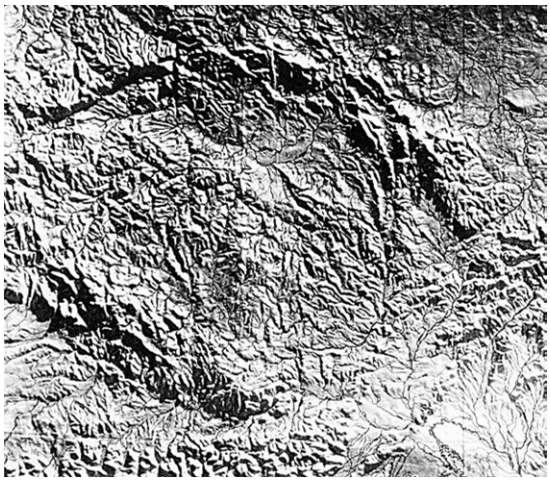

Fig. 1. NE illuminated plastic map of the Bohemian Massif.

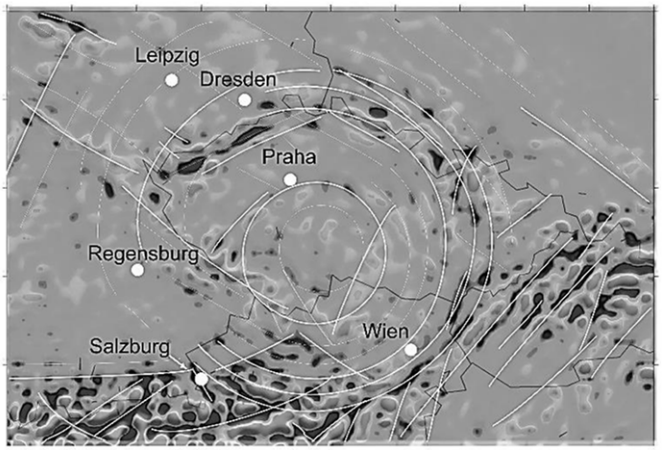

Fig. 2. EGM 08 gravity anomaly map of Middle Europe with ring structure and fault interpretation.

The ring structure is centered around a 60 km wide below the Moho boundary up to 5 km sunk hole in the earth mantle with the missing overburden of the lower crust (Fig. 3). The teared off fragments of serpentinites, garnet peridotites and lower crust rocks are mixed around the central recess into the crater megabreccia, which was strengthened at the end of the cratering through the penetration of aplite to pegmatitic veins. Components of the multiring structure are the NNE - SSW pre-crater faults splayed through impact like in a size-comparable meteoritic crater Chicxulub. The range of impact inner basin matches with the presence of shocked quartz, diamonds, graphitized oil traps and the Pseudotachylite brecciated veins. The estimated age of the unit is 2 billion years. The younger faults of Permian to Neogene age are mostly of NW – SE direction. (Fig. 4). Except in the Permian cut off Southwestern part the whole acted morphologically in the younger orogeneses as circular mountains around mantle depression and around the original contour of the anticipated inner crater basin.

The most significant deposits of polymetallic ore are concentrated on pre-impact NNE – SSW faults, at the edge of the central recess and on the NW edge of a solidified impact basin (Fig. 5). NW edge of the hardened inner basin as a place of main interaction with faults of the NW-SE is also the site of the largest occurrence of tin, tungsten, lithium, fluorite and uranium. Occurrences of Sn, W and lithium are the result of intrusion of younger – Permian porphyries to granites and the intrusion of accompanying pneumatolytic deep-seated fluids. From NW to SE penetrating faults stopped and splayed in the dense network on the edge of the solidified area and didn´t continue further inside (Fig. 6). The Permian porphyries and pneumatolytic solutions penetrated along these fractures carrying Sn, W, Li, P and F. A similar but less strong tectonic situation repeated in Senonian and in the upper Tertiary with fluorite deposition.

No significant mineralisation is bound to the large bodies of the granites torn from the transient cavity of the crater and to the extensive penetration of aplitic to pegmatitic veins from the closing stage of the cratering.

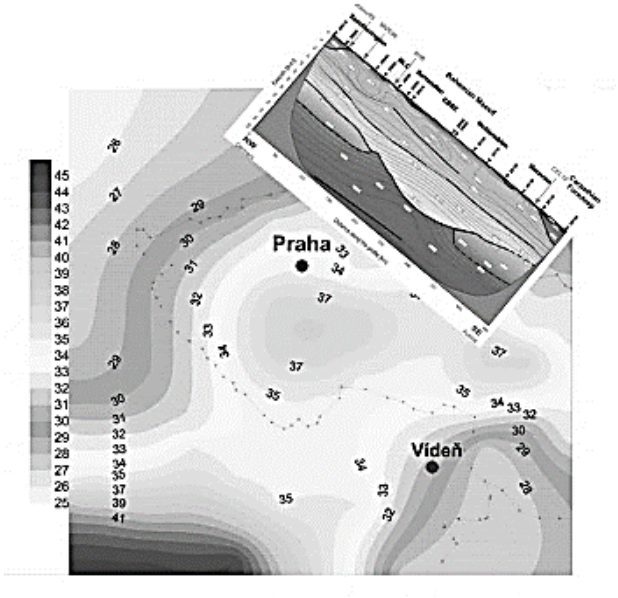

Fig. 3. Moho depth map and profile through Bohemian Massif (map data Beránek 1976, seismic profile Hrubcová et al. 2002).

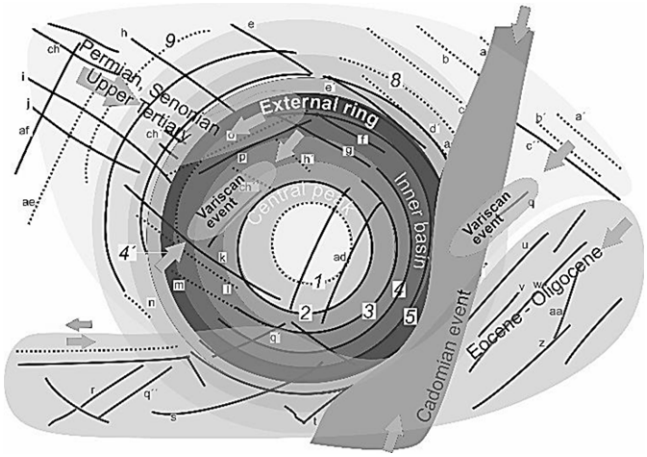

Fig. 4. Areas of the ring structures influenced by younger orogenies with the stress directions.

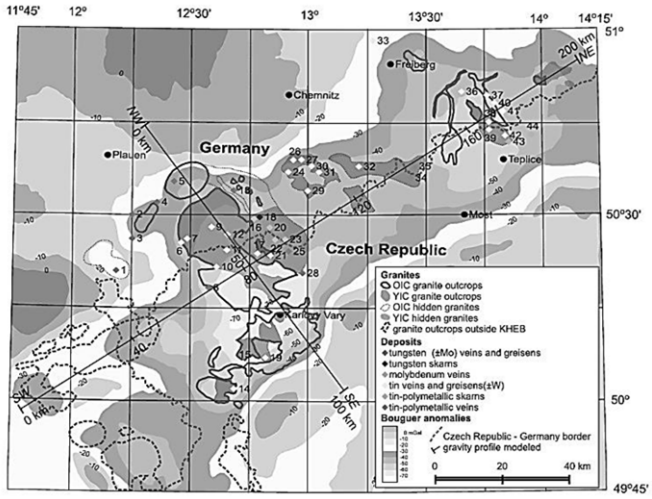

Fig. 5. Gravity map, granites and Sn, W mineralization of the NW edge of the hardened parth of the astrobleme.

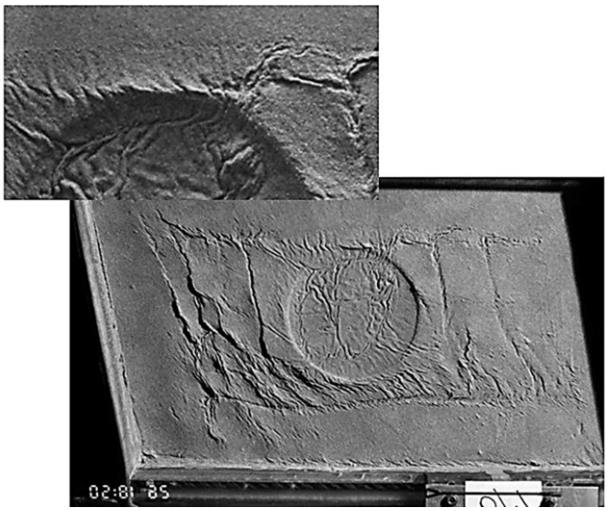

Fig. 6. Lihospheric size analog model of the hardened circular structer behaviour in reverse motion top to East with manifestation of fault on the structure rim.

With the time of increasing penetration of ore bearing fluids since the crater creation is probably the result of penetration and still deeper reactivation of the fractures by the action of the motion-inert hard disk crater breccia on the underlying mantle.

References

Rajlich P.: Czech Crater.- Jihočeské muzeum, Sbroník Jihočeského muzea v Českých Budějovicích, Přírodní vědy, 47, Supplementum, 114 p. ISBN 978-80-86260-80-8.

Rajlich P.: Space Event in Czech quartz (and in the Czech massif).- Petr Rajlich, GEOLOGIE, 166 p. ISBN 978-80-260-5678-2.

Štemprok M., Blecha V. Variscan Sn–W–Mo metallogeny in the gravity picture of the Krušné hory/Erzgebirge granite batholith (Central Europe)//Ore Geology Reviews 69 (2015) 285–300.

SECULAR VARIATIONS AT THE OBSERVATORIES MIKHNEVO AND BELSK

Riabova S.A.
Instiute of Geosphere Geodynamics, riabovasa@mail.ru

The largest part of the geomagnetic field is generated by the geodynamo in the Earth's liquid core (e.g., Chapman, Bartels, 1940; Kono, 2009; Rikitake, 2012). Other sources to the geomagnetic field include electrical currents in the ionosphere and magnetosphere (the external field), magnetized rocks in the lithosphere (crustal field), and induced electrical currents in the mantle and oceans (induced field). The core, crustal and induced field combined is called the internal field. The core field, also referred to as the main field, varies slowly in time, typically on secular time scales. Typical secular variation processes take time: from about a year for a geomagnetic jerk (Courtillot et al., 1978; Chulliat et al., 2010; Mandea et al., 2010) or the so-called rapid secular variation fluctuations (Olsen and Mandea, 2008; Mandea and Olsen, 2009), to several decades for convective core flows, torsional oscillations, waves and magnetic diffusion (see, e.g., Finlay et al., 2010) and several centuries between archeomagnetic jerks (Gallet et al., 2003).

The knowledge of this secular variation of Earth's magnetic field is a key tool for exploring the spatial and temporal characteristics of the geodynamo, for magnetic survey and for search for mineral deposits. The comparison of experimental values of geomagnetic observatories with the model ones allows estimating the reliability of the model fit and highlighting local anomalies of the Earth's crust or deviations from the smoothed regional / global data involved in the development of the model (e.g. Urrutia-Fucugauchi and Campos-Enríquez, 1993).

In present work, the data of the geomagnetic field registration at the mid-latitude observatories Mikhnevo (54.959º N 37.766º W) and Belsk (51.837º N, 20.792º W) for the period 2008 – 2016 are used.

The registration of geomagnetic variations at observatory Mikhnevo was carried out using magnetometer LEMI-018i, at observatory Belsk was carried out using a torsional quartz variometer. The theoretical estimate of the secular variation of the geomagnetic field and its derivative was made based on the International Geomagnetic Reference Field (IGRF) model of the 12th generation (Thebault et al., 2015). To determine secular variation as free as possible from annual and seasonal variations resulting from magnetospheric and ionospheric currents, including the resulting induction effects, first differences of the X, Y and Z monthly means at time t were calculated as the difference between those at time $t + 6$ months and $t - 6$ months. This has the implication that secular variation information is limited to 6 months before the last available main field observations.

The trend component for the northern horizontal component of the geomagnetic field decreases smoothly during the analyzed period and is characterized by slightly pronounced minima during equinox periods and maxima during solstices. In this case, the amplitude of the annual variation (the difference between summer-winter values) is of the order of 15 nT. The trend components of the eastern horizontal and vertical components, as well as the total geomagnetic field vector during nine years are practically linear, with a monotonous increase in the period from 2008 to 2016. The marked course of trend components during the analyzed period for the vertical and horizontal components of the geomagnetic field is due to their secular variations (e.g., Kono, 2009; Rikitake, 2012). In the period from 2008 to 2016, the secular variation of the geomagnetic field (long-term trend) was positive, which indicates an increase in the geomagnetic field in the analyzed period.

The comparison of the monthly averages of variations in the geomagnetic field and values calculated from using the IGRF model of the 12th generation shows a difference between the calculated and experimental values, while the course of the graphs of experimental values and theoretically calculated ones is similar. The similar results were obtained for the total vector F calculated from the experimental data. The difference between the calculated using the IGRF model values (main field) and experimental ones of the Earth's magnetic field at observatories Mikhnevo and Belsk mainly is due to the lithospheric component of the geomagnetic field. This confirms the coincidence of the value and sign of the difference between the calculated values from the experimental data and the calculated values of the total vector (-1267 nT at Mikhnevo and 362 nT at

Belsk) with the values of the anomalous magnetic field (less than 1000 nT at Mikhnevo and about 400 at Belsk.

The jerk is conceived as a sudden change in the slope of the secular variation (i.e. the first time derivative of the Earth's magnetic field), and generally occurs on a few month to a few year timescale. So the secular variation can be thought as a series of straightline segments separated by geomagnetic jerks. Geomagnetic jerks are most commonly defined as V or Λ shaped features in the secular variation although other characteristics forms can be identified. Jerks represent the most rapid observed internally generated magnetic features known and are associated with fast flows at the surface of the outer core (Finlay et al., 2016), although their generation source is not fully understood. Using quiet-time monthly mean geomagnetic *X, Y* and *Z* data from observatories Mikhnevo and Belsk, 2011 and 2014 geomagnetic jerk are identified. The evidence of the 2011 and 2014 geomagnetic jerks could be found in all field components at both observatories. The 2011 and 2014 jerks were previously identified in the research of variations in geomagnetic field components in the regions: South Atlantic-Africa, Europe and North-West Atlantic, and Australasia (Chulliat and Maus, 2014; Chulliat et al., 2015; Finlay et al., 2015; Kotzé, Korte, 2016), 2014 (Torta et al., 2015; Kotzé, 2017) with a slight discrepancy in time.

References

Chapman S., Bartels J. Geomagnetism. London: Oxford University Press. 1940. 601 p.

Chulliat A., Alken P., Maus S. Fast equatorial waves propagating at the top of the Earth's core// Geophysical Research Letters. 2015. Vol. 42. Iss. 19. pp. 3321-3329.

Chulliat A., Maus S. Geomagnetic secular acceleration, jerks, and a localized standing wave at the core surface from 2000 to 2010// Journal of Geophysical Research. 2014. V. 119. Iss. 3.pp. 1531-1543.

Chulliat A., Thebault E., Hulot G. Core field acceleration pulse as a common cause of the 2003 and 2007 geomagnetic jerks// Geophysical Research Letters. 2010. Vol. 119. Iss. 3. pp. 1531-1543.

Courtillot V., Ducruix J., Le Mouel J.-L. Sur une acceleration recente de la variation seculaire du champ magnetique terrestre// Comptes Rendus Hebdomadaires Des Seances De l'Academie Des Sciences. Serie D: Sciences Naturelles. 1978. Vol. 287. pp. 1095-1098.

Finlay C.C., Dumberry M., Chulliat A., Pais A., Short time-scale core dynamics: theory and observations// Space Science Reviews. 2010. Vol. 155. pp. 177-218.

Finlay C.C., M. Olsen N. Kotsiaros S., Gillet N., Tøffner-Clausen L. Short time-scale core dynamics: theory and observations// Earth, Planets and Space. 2016. Vol. 8. Iss. 112. https://doi.org/10.1186/s40623-016-0486-1.

Finlay C.C., Olsen N., Tøffner-Clausen L. DTU candidate field models for IGRF-12 and the CHAOS-5 geomagnetic field model// Earth Planets Space. 2015. Vol. 67. Iss. 114. https://doi.org/10.1186/s40623-015-0274-3.

Gallet Y., Genevey A., Courtillot V. On the possible occurrence of archeomagnetic jerks in the geomagnetic field over the past three millennia// Earth and Planetary Science Letters. 2003. Vol. 214. pp. 237-242.

Kono M. Geomagnetism. Treatise on Geophysics, Vol. 5. Amsterdam: Elsevier. 2009. 589 p.

Kotze P.B. The 2014 geomagnetic jerk as observed by southern African magnetic observatories// Earth, Planets and Space. 2017. Vol. 69. Iss. 17. https://doi.org/10.1186/s40623-017-0605-7.

Kotze P.B., Korte M. Morphology of the southern African geomagnetic field derived from observatory and repeat station survey observations: 2005−2014// Earth Planets Space. 2016. Vol. 68. Iss. 23. https://doi.org/10.1186/s40623-016-0403-7.

Mandea M., Holme R., Pais A., Pinheiro K., Jackson A., Verbanac G. Geomagnetic jerks: rapid core field variations and core dynamics// Space Science Reviews. 2010. Vol. 155. pp.147-175.

Mandea M., Olsen N. Geomagnetic and archeomagnetic jerks: where do we stand? // EOS of Transactions of American Geophysical Union. 2009. Vol. 90. Iss. 24. pp. 208-209.

Olsen N., Mandea M. Rapidly changing flows in the Earth's core // Nature Geoscience. 2008. Vol. 1. pp. 390-394.

Rikitake T. Electromagnetism and the Earth's interior. Amsterdam-London-New York: Elsevier. 2012. 320 p.

Thebault E., Finlay C.C., Beggan C.D. et al. International Geomagnetic Reference Field: the 12th generation// Earth, Planets and Space. 2015. Vol. 67. Iss. 79. https://doi.org/10.1186/s40623-015-0228-9.

Torta J.M., Pavón-Carrasco F.J., Marsal S., Finlay C. Evidence for a new geomagnetic jerk in 2014// Geophysical Research Letters. 2015. Vol. 42. Iss. 19. pp. 7933-7940.

Urrutia-Fucugauchi J., Campos-Enríquez J.O. Geomagnetic secular variation in Central Mexico since 1923 AD and comparison with 1945-1990 IGRF models// Journal of Geomagnetism and Geoelectricity. 1993. Vol. 45. pp. 243-249.

REE- FLUORITE MINERALIZATION WITHIN TAJNO CARBONATITE INTRUSION (NORTHERN POLAND) - A NEW INSIDE

***Ruszkowski M.*[1], *Wiszniewska J.*[2]**

[1]*Department of Geology, University of Warsaw,* ruszkowskimichal@wp.pl

[2]*Polish Geological Institute – National Research 4,* janina.wiszniewska@pgi.gov.pl

In NE Poland (NE of the Trans-European suture zone), the Proterozoic basement is covered by a thick Phanerozoic sedimentary pile. Geophysical prospecting and drilling operations have lead to the discovery of the 3 alkaline-carbonatite massifs intruding the basement: the small (~5 km2) Tajno massif and a much bigger (100 – 400 km2) Elk and Pisz bodies.

The Carboniferous sub-platform Tajno alkaline-carbonatite intrusion is located within a narrow alkaline magmatic belt, which trends E–W from SW Lithuania to NE Poland, along the southern border of the Mesoproterozoic A–type magmatic Mazury Complex. The Tajno pluto–volcanic massif comprises clinopyroxenite cumulates and syenites that are crosscut by carbonatite veins of variable thickness (Wiszniewska, 2017).

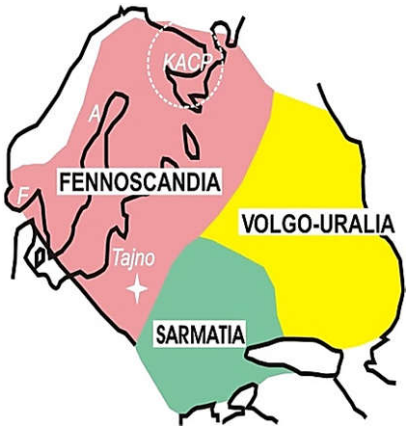

Fig. 1. Localization of Tajno massif in Poland and other occurrences of carbonatite intrussions in Fennoscandia (KACP: Kola Alkaline Carbonatite Province;A: Alnö massif, F: Fen massif adapted from Gee i Zeyen, 1996)

The Tajno massif (NE Poland) was discovered in the 50's by gravity method. It was drilled and studied during the early 60's and once more in the 80's. It is cover by the 600 m thick, Mesozoic to Cainozoic sedimentary rock sequences. Twelve boreholes, down to about 1300 m, allow to delineate the approximate extent of the massif that covers about 5 km². Tajno massif intruded the Proterozoic granites, gneisses and migmatites of the so-called Mazowsze unit south of the Mazury anorogenic magmatic complex of NE Poland that comprises the Suwalki anorthosite massif and related rocks (Wiszniewska, 2002). The crystalline basement of NE Poland belongs to the East European Craton (EEC) and more particularly to the Fennoscandian block (Fig. 1). The Tajno Massif is characterized by a great lithological and structural variability of alkaline rocks. The main, oldest plutonic rocks are fenitized ijolites, surrounded and intruded by microperthite syenite, malignite and nepheline syenite.

Petrography

Cumulate pyroxenite is playing the main role in the composition of the intrusion. Metasomatized pyroxenite were also formed due to alkaline metasomathosis. Dikes of variable composition e.g. melanephelinite, nephelinite, phonotephrite, tephriphonolite, phonolite, trachyte, and tinguaite are crosscutting the entire complex. The central part of this structure is built of pyroclastic and volcanic rocks of the chimney breccia, cemented by carbonatites. Three stages of carbonatite intrusions were distinguished in the Tajno massif (Dziedzic, Ryka, 1983; Ryka, 1992). Carbonatites of the first stage are brecciated and kept only as fragments in the chimney diatrema breccia. Carbonatites of the II stage are appearing most profusely and they are very heterogeneous. They contain titanite and amphibole and usually display in form of veins of a few centimetres into even 1,2 meter thickness or binders cementing blocks of pyroxenite. Many other rocks within the breccia pipe were subjected by metasomatosis. Carbonatite veins and breccia binder of the stage III are clearly post-kinematic. Most of carbonatites from the Tajno intrusion are calcio-carbonatite, containing mainly calcite and fluorspar (Fig. 2). In CL images calcite has a characteristic red-orange colour, partly with lighter or darker tint, originating from additives of Mn^{2+}. Ankerite, as a strongly ferruginous mineral isn't demonstrating the luminescence. Blue luminescence of strontianite in examined carbonatite is triggered with presence of Ce^{3+}, however purple luminescence colour of fluorspar is coming from Eu^{2+} that is typomorphic for carbonatite and mafic alkaline rocks. Observation in CL (Wiszniewska et al., 2010) helped to establish an sequence of crystallization carbonate phases in examined carbonatite (Fig. 3).

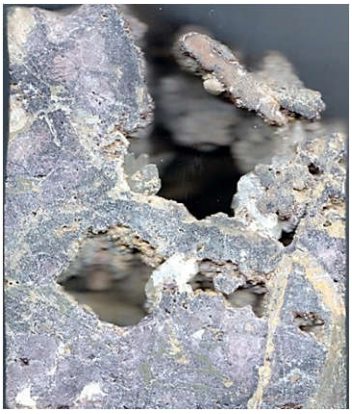

Fig. 2. High-resolution scan of a core fragment from Tajno. Well-visible caverns filled with carbonate mineralization and building up of the rock structure with the fluorite group minerals.

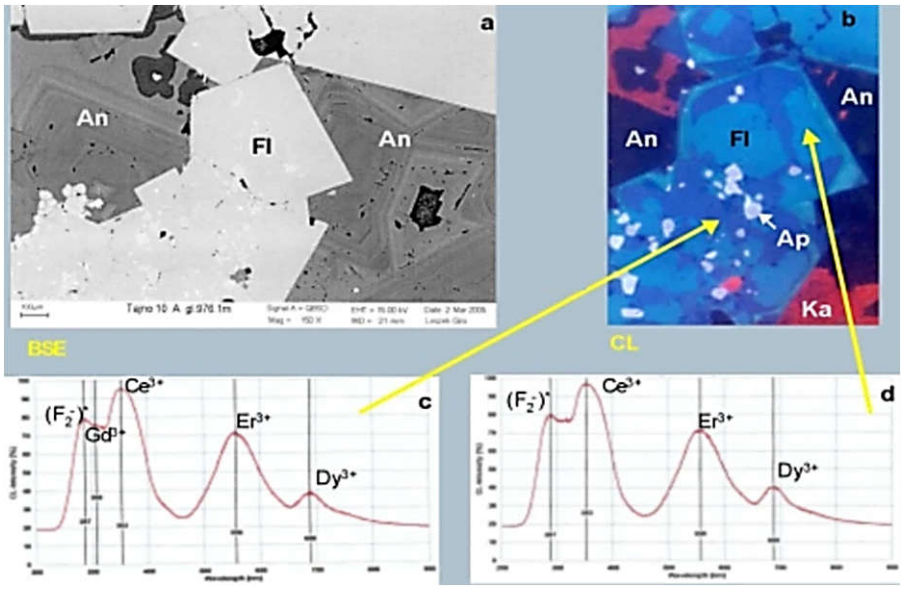

Fig. 3. a) BSE image showing zonning structure of ankerite due to changing of Fe content in mineral; b) CL image of fluorite (Fl) with blue colour of luminescence, red luminescence of calcite (Ka), grey apatite (Ap) and ankerite (An) without luminescence; c, d) CL spectra of fluorite indicating REE presence and internal defects of crystalographic structure.

Chondrite-normalised REE characteristics for alkaline rocks of the syenite, nepheline syenite and ijolite type and carbonatite of the Tajno intrusion are demonstrating a wide range for La from 70 to 4000 (x chondrite) with flat pattern for HREE. Typical syenite from T- 2 borehole have flat REE pattern, devoid of the anomaly, similarly to nepheline syenite from drilling T- 8, however they are a little bit poorer in the REE content from the middle of the graph e.g. Nd, Sm, Eu, Gd, Tb, Dy, but similar of HREE contents. The most interesting carbonatite minerals are REE-carriers minerals. The most popular carbonatite mineral after calcite and fluorspar in the Tajno Massif is burbankite with brightly yellow CL colours. Other REE minerals being found in Tajno massif it parisite, synchysite, bastneasite and carbocerianite. Bastneasite and synchysite in CL light have the intense orange colour, and exhibit the internal structure different from calcite (Wiszniewska, Sikorska, 2005). Rare-earth elements are being dispersed in early stages of the carbonatite activity, but in later stages are more concentrated and showing the affinity with the fluorine concentration in the melt. The average REE content for the Tajno complex, in terms of oxides, is estimated to be 0.33 wt.%. The rocks are very unusual by their low Nb (Ta) content. In Tajno, Ryka (1992b) has observed REE-rich carbonatites with total Re_2O_3 in the range 2 to 9 wt%.

Dating of the Massif

The latest measurements of U-Pb zircon SIMS and SHRIMP ages for the 3 alkaline intrusions: Tajno, Elk and Pisz, yield the same age, close to 360 Ma, which suggests that the emplacement was very similar with the KAP. Tajno is a differentiated pluto-volcanic complex in which the UAC (ultramafic-alkaline complex) trilogy has been found. The Elk intrusion appears as a ring-structure essentially made of various syenites (mostly foid-bearing) that are quite similar to those of Khibina and Lovozero. Pisz is a gabbro-syenite intrusion of 348 ±5,1 Ma. Initial (at 360 Ma) Sr (0.7037-0.7040) and Nd (+ 0.7 to +3.5) isotopic ratios point to a slightly-depleted time-integrated mantle source comparable to that of the KAP parental magma and close to the FOZO mantle reservoir which is a ubiquitous component in both the MORB and OIB mantle sources.

A few grains of pyrrhotite separated from the Tajno carbonatite (sample T10 – 1047m) have been analysed by the Re – Os method. The total Os content is very low (0.096 ppb); Re content is 17.06 ppb. This sulphide thus has a very high 187Re/188Os ratio of 2466 and is highly radiogenic (187Os/188Os = 14.56). It is thus a low level, highly radiogenic (LLHR) sulphide and a single isotopic analysis can provide a model age. Using a reasonable primitive initial Os isotopic ratio of 0.2, a model age is 348 ±2 Ma. This data suggested that these 3 intrusions form new Polish Alkaline Province (PAP) (Demiffe, et al., 2013) establishing an interesting occurrence of the widespread Upper Devonian alkaline and carbonatite magmatism related to rifting of the East European Craton.

The PAP is slightly younger (the age range is 345.5-348) than the KACP. Recent discussions show that the magmatic event at Kola was of relatively short duration similarly to new dated PAP.

References

Demaiffe D., Wiszniewska J., Krzeminska E., Williams I. S., Stein, H. Brassinnes S., Ohnenstetter D., Deloule E. A Hidden Alkaline and Carbonatite Province of Early Carboniferous Age in Northeast Poland: Zircon U-Pb and Pyrrhotite Re-Os Geochronology.// 2013, The Journal of Geology, vol. 121, p. 91–104.

Dziedzic A., Ryka W., Carbonatites in the Tajno Intrusion (NE Poland) //1983, Archiwum Mineralogiczne, XXXVIII vol.2 Warsaw 1, pp. 4-28.

Ryka, W. Ed, Geology of the Tajno massif (Northeastern Poland)// 1992a. Wyd. Geol. pp. 90.

Ryka, W. Geology of carbonatites. In Ryka W. ,(Ed) : Geology of the Tajno massif (Northeastern Poland) // 1992b. Wyd. Geol., Warszawa, pp. 43-77.

Wiszniewska J., Age and the genesis of Fe-Ti-V ores and related rocks in the Suwalki anorthosite massif (NE Poland)// 2002,Biuletyn, PIG, 401, pp. 96.

Wiszniewska J., Gonzalez-Alvarez I., Kusiak M., Petecki Z, Central European carbonatites under cover: insights for mineral exploration from the Tajno alkaline intrusions, NE Poland.//2017, Conference: Goldschmidt, Paris.

Wiszniewska J., Krzemińska E.,. Sikorska M. - CL images of REE-bearing minerals of the Tajno carbonatites, NE Poland. Alkaline Rocks.// 2010, Petrology, Mineralogy, Geochemistry, Conference dedicated to the memory of J.A. Morozewicz, Abstracts and excursion guide.- Kyiv, p.71-73.

ZIRCONIUM-HAFNIUM RIMS AROUND FE-TI OXIDES IN THE SUWALKI ANORTHOSITE MASSIF (NE POLAND) – A CASE STUDY

***Ruszkowski M.*[1], *Wiszniewska J.*[2], *Krzeminska E.*[2]**

[1]*Department of Geology, University of Warsaw, ruszkowskimichal@wp.pl*

[2]*Polish Geological Institute – National Research 4, Warsaw, janina.wiszniewska@pgi.gov.pl*

The ore mineralization in the Suwalki Anorthosite Massif (SAM) is located within the rocks belonging to the AMCG rock suite (anorthosite - mangerite - charnockite – granite rapakivi) in NE Poland. These rocks are covered by several hundredths meters thick sedimentary Phanerozoic rock sequences. The intrusive Mesoproterozoic SAM rocks are associated with the deep lineaments in the Earth's crust. The SAM occupies an area of 250 km^2 (Wiszniewska, 2002) and its central part is made up of massive anorthosites surrounded by ring of norites and gabronorites. In the southern part of SAM an ilmenite-magnetite rocks (ferrolites) with accompanying sulphide polymetallic mineralization (Fe-Cu-Ni-Co) have been discovered in early 60`s of the XX century. During 30 years of drilling surveys the three ore fields: Krzemianka, Udryn and Jeleniewo were documented. The ore bodies have a lenticular structures and are intersected with a network of granitoid and pegmatite veins. The main ore levels appear at a depth of 800 to 2,300 m below ground level. The main ore minerals are titanomagnetite, ilmenite and sulphides: pyrrhotite, pyrite, chalcopyrite and pentlandite. About 1.5 billion tons of Fe-Ti-V ores have been documented in this deposits. The ores contain approx. 28% Fe_2O_3, 7% TiO_2 and 0.3% V_2O_3, and 1-4% Fe-Cu-Co-Ni sulphides and other strategic elements (Wiszniewska, 2002).

SAM ores mineralization

The ore mineralization of SAM has a high variability of composition and forms. The dominant ore minerals in the massive ore zones are titanomagnetite with ilmenite. The sizes of magnetite grains vary between 1-8 mm. In the titanomagnetite grains, the dissolution of ilmenite lamellae occurs in three planes, ulvöspinel nets and spinel grains of hercynite - pleonaste composition, forming clusters, lenses and needle-like precipitations. The normal spinel (pleonaste) is the first of the products of admixtures in titanomagnetite. The physico-chemical condition changes during the evolution of the primary ore oxides influenced the distribution of trace elements in magnetite and ilmenite. Under high oxygen pressure (fO_2) condition, unstable vanadium carrier -ulvöspinel (ulvite), was transformed into metastable protoilmenite and ilmenite, but vanadium transferred into the magnetite structure (Speczik et al., 1988, Wiszniewska, J. 1998). The second, most abundant ore mineral is ilmenite. It constitutes an average about 10-15 vol. % of ilmenite-magnetite rocks. The greater part of the original ilmenite crystallized simultaneously with the titanomagnetite or formed during the decomposition of a solid solution of titanomagnetite (Speczik et al., 1988). Ilmenite grains reach a considerable size, even 0.5-1.0 cm, but on average they have 1-3 mm (J. Wiszniewska, 1993). Ilmenite is often accompanied by pleonaste and hercynite spinels. The incorporation of vanadium into the ilmenite structure was associated with a temperature drop in the system and the formation of lenticular hematite admixtures in ilmenite grains.

Zirconium-hafnium around the Fe-Ti oxides

Zirconium is a common chemical element in the Earth's crust and it constitutes about 0.0028% of its mass (Eichstaedt I. 1973). This situates it in 19th place in terms of spreading in the crust. Zirconium is commonly dispersed among other rock forming minerals and the most important Zr minerals are baddeleyite (ZrO_2) and zirconium ($ZrSiO_4$). It is also present in minerals containing titanium, niobium, tantalum and rare earth elements. The largest concentrations of Zr are mainly found in titanium minerals. The processes of chemical and metallurgical purification of titanium minerals such as rutile and ilmenite are also the sources of Zr.

Hafnium is always associated with Zr in its ores and minerals. Hf content usually oscillates between 1-3% within zirconium mineral, exceptionally exceeding even 5 vol. %. The average content of hafnium in the Earth's crust is estimated at 0.0025% (Eichstaedt I. 1973). However, it does not create an independent minerals. These elements have similar chemical features and properties and therefore it is extremely difficult to separate them. The convergence of the properties of Zr and Hf is so great that in the entire periodic table there are no other elements more similar of two of those (except for the lanthanides).

In mafic rocks, zirconium minerals are extremely rare and very fine grained. A valuable source of information about the evolution and age of the rocks contain large zirconium grains. Automorphic crystals and needle-like zirconium forms are well-known and widely described. Habitus of zirconium crystals is of genetic importance and after their recognition, it is possible to constrain what is the source rock of them.

A very rare phenomenon are elongated, marginal forms of zirconium appearing around titanium oxide minerals. Such zirconium forms has recently been described from several anorthosite, gabbroic and basaltic massifs in the world (Charlier B. at al., 2007, Morisset C.E., Scoates J.S., 2008).

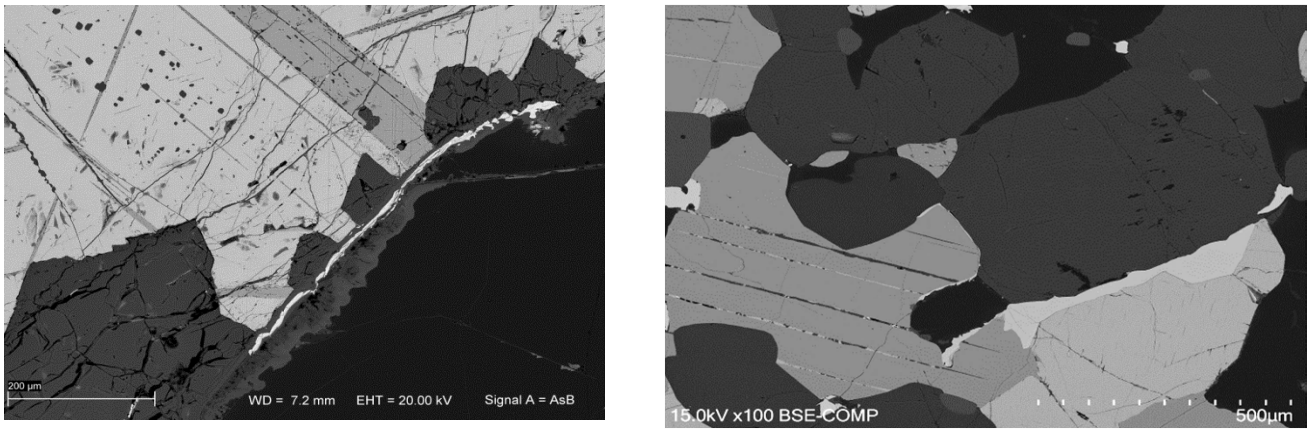

Fig. 1. BSE images of zirconium-hafnium rim of the ”blown candle flame” type.

Up till now, no such structures have been evidenced from the SAM. Thanks to applying a modern research methods of the nano-space (SEM-EDS and EPMA equipment at Warsaw University), narrow, irregular rims of unknown, heterogeneous mineral around Fe-Ti oxide minerals from SAM were recognized. The largest concentrations of such rims have been found in the rock samples of Jeleniewo, Jezioro Okragle, as well as from Krzemianka and Udryn. Examinations in nano-space revealed rims of zirconium-hafnium composition (Ruszkowski, Wiszniewska 2018). They are genetically connected with Fe-Ti oxides: ilmenite, hematite - ilmenite and titanomagnetite. In certain cases, the appearence of Cu-Fe sulphides associated with Fe-Ti oxides have been also surrounded by zirconium rims. The first most frequent group of zirconium structures reach 80 - 250 µm in length and 4 - 30 µm in width. They create narrow, but visible Fe-Ti oxide grain rims, even up to 70%. The second, sinus -like rims group is much more massive, clearly inhomogeneous. This rims reach about 150 µm length and 50 µm wide. The third group have the most spectacular forms making the so-called "blasted candle flame structures" (Fig. 1). They are bigger and more massive than others. Their width range from 20 to 45 µm. and length exceeds even 350 µm. The geochronological U-Pb dating have been carried out for the first time in the SHRIMP IIe Laboratory at the Polish Geological Institute in Warsaw. The age of Zr rim structures have yielded 1506 +/- 8 Ma with low content of U(29-58ppm) Th (12-62 ppm) and radiogenic Pb ((3-17 ppm) and Th/U (0.44 -0.75). The fourth group of zircon crystals are the most common in rocks. They are thin, (about 25 µm in diameter), isolated automorphic grains, dispersed between ore mineral crystals or among the gangue minerals. (Ruszkowski, Wiszniewska, 2018).

In the largest clusters of zirconium fractions and crystals belonging to the above mentioned groups, the chemical analyses by EDS and EPMA were performed, which showed large, local

enrichment of Hf (from 0.5 to 0.8% by weight) in zirconium structures. Maximum concentrations of Hf is richest in the third group. It is also worth mentioned that the heterogeneity of these forms and numerous longitudinal cracks. The boundaries of adjacent crystals are crushed and blurred. This suggests their involvement in later fluid inflow processes. A large variety of zirconium forms and variability of their chemical composition is part of the complex history of the transformation of the SAM mineralogy. (Ruszkowski, Wiszniewska, 2018).

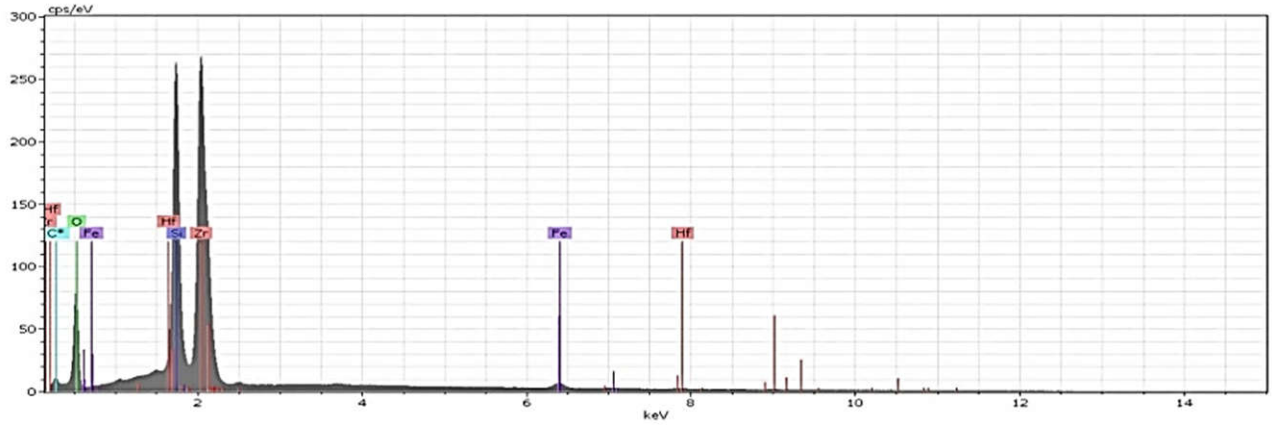

Fig. 2. EDS analysis graph of zirconium-hafnium rim of the ”blown candle flame” type.

The research was financed from NCN grant no. 2015/17/B/ST10/03540 and FUW 21/04/2017.

References

Charlier B. Skra.Ø., Korneliusen A., Duchesne J.C., Auwera J.V. Ilmenite composition in the Tellnes Fe-Ti deposit, SW Norway: fractional crystallization, postcumulus evolution and ilmenite zircon relation. //2007, Contrib Mineral. Petrol., 154: pp.119-134.

Morisset C.E., Scoates J.S., Origin of zircon rims around ilmenite in mafic plutonic rocks of Proterozoic anorthosite suites. //2008The Canadian Mineralogist, 46: pp.289 -304.

Eichstaedt I. Księga Pierwiastków.//1973Wyd. Wiedza Powszechna.

Ruszkowski, M. Wiszniewska. J. Initial recognition of zirconium-hafnium rims around ore minerals in the Fe-Ti-V deposits, Suwalki Anorthosite Massif (NE Poland). Wstępne rozpoznanie obwódek cyrkonowo-hafnowych wokół minerałów kruszcowych w złożach Fe-Ti-V w suwalskim masywie anortozytowym (północno-wschodnia Polska) // 2018, Przegląd Geologiczny vol.66 nr. 2.

SPECZIK S., WISZNIEWSKA J., DIEDEL R. Minerals, exssolution features and geochemistry of Fe-Ti ores of the Suwalki district (North-East Poland). // 1988, Mineralium Deposita, 23: 200-210.

Wiszniewska, J. Wiek i geneza rud Fe-Ti-V i skał towarzyszących w suwalskim masywie anortozytowym (północno-wschodnia Polska). // 2002, Biuletyn PIG. Nr 401. Pp.1-

Wiszniewska, J. Mineralogy of the Fe-Ti-V ores of the Suwalki Anorthoste Massif. In Geology of the Suwalki Anorthosite Massif, (Northeasten Poland)// 1998, Prace PIG CLXI, pp.137-151.

FORMATION OF ALKALINE MINERALIZATION IN ACID LEACHING ZONE OF PAUZHETKA HYDROTHERMAL SYSTEM (SOUTH KAMCHATKA)

***Rychagov S.N.*[1], *Sandimirova E.I.*[1], *Chernov M.S.*[2], *Sergeeva A.V.*[1]**

[1]*Institute of Volcanology and Seismology of FED RAS, Petropavlovsk-Kamchatsky, 683006, rychsn@kscnet.ru*

[2]*Geological faculty of M.V. Lomonosov State Moscow University*

The team of contributors explores various aspects of the formation of hydrothermal clays on thermal fields (t/f) of Kamchatka: chemical and mineral compositions, macro- and microstructure, physical and mechanical properties of clays were studied; the significance of the clay sequence as a

complex geochemical barrier in the structure of modern hydrothermal systems was demonstrated (Rychagov et al., 2009, 2012). By an example of East-Pauzhetka thermal field (EPTF), for the first time in the world scientific practice ever, zones with mineral ore associations were drilled at the base of clay strata (Rychagov et al., 2017). These data stimulated the continuation of drilling of wells in EPTF in order to study the deeper horizons of the base of the hydrothermal clay strata.

The stratum of EPTF hydrothermal clays has a zonal structure described in detail earlier (Feofilaktov et al., 2017). Additional wells at the base of the stratum opened argillized intensively fissured andesites and metasomatic breccias of andesites. Cement of brecciats as well as cracks and areas reaching a thickness of 20 cm are composed of silica minerals (opal, chalcedony, quartz), carbonates, smectites, chlorite-smectites, pyrite, iron oxide, etc. Analytical studies have identified a complex mineral composition.

The main matrix of altered andesites, as well as the material of veinlets and geodes were analyzed. Montmorillonite, quartz, zeolites, calcite and magnesia calcite, pyrite, clinochlore were identifed by IR spectroscopy and diffractometry. Lomonite, stilbite, heylandite, and clinoptilolite were detected in zeolites; predominantly calcium and Na-Ca medium- and high-silica zeolites occur. Two groups of minerals were distinguished by detailed electron microscope studies: 1) primary magmatic and metamorphic minerals; 2) hydrothermal-metasomatic minerals.

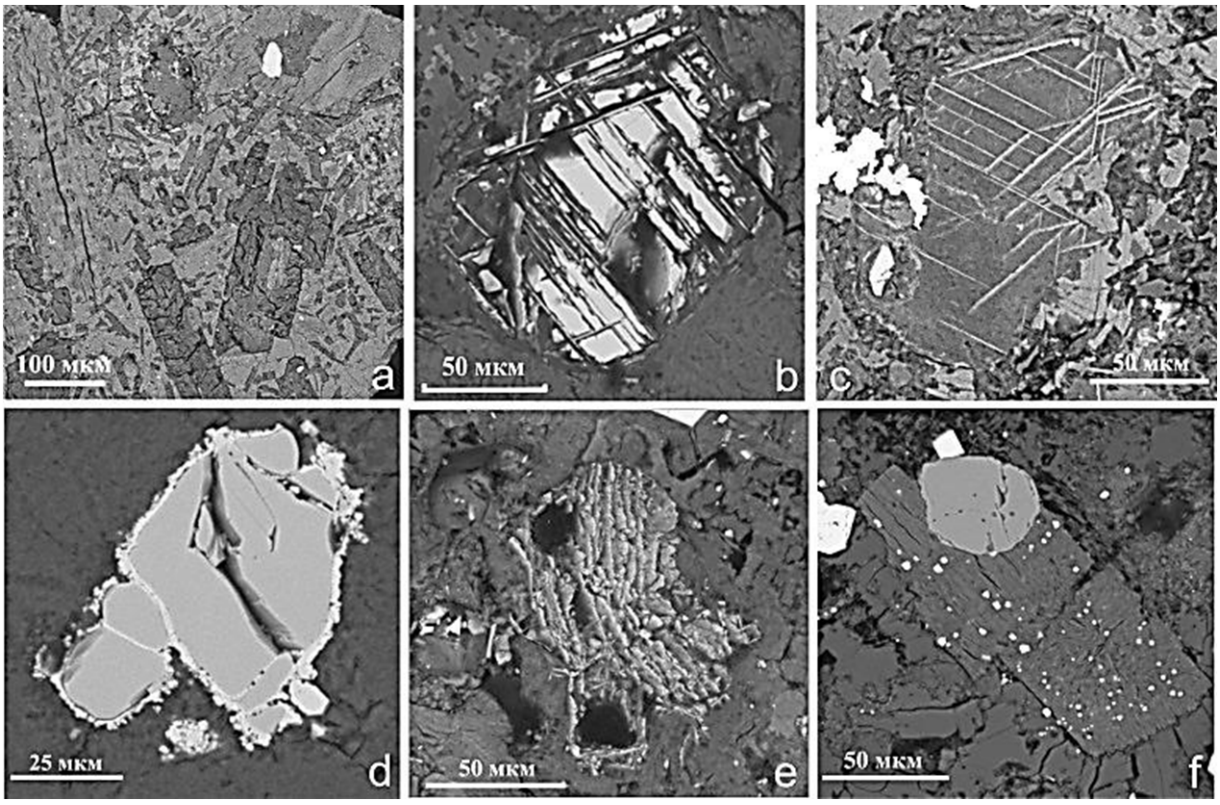

Fig. 1. Primary magmatic minerals and their alterations: a - pseudomorphic replacement of porphyritic phenocrysts and the main mass of andesites with smectites, chlorite-smectites, carbonates and zeolites; b - crystal of titanomagnetite with characteristic structures of decomposition of solid solution; c – pseudomorphs of titanosilicate and magnetite (light bands) in amphibole (?) with inclusions of apatite grains (white is pyrite); d – Fe-Cr-Ti-V-containing spinel with a pyrite rim; e – titanosilicate (substitution of titanomagnetite, other minerals, or pores) in a zeolite-chlorite bulk; f – replacement of porphyritic phenocrysts of dark-colored minerals (amphibole?) with chlorite and chlorite-smectite, round gray grains – fluorapatite, small light crystals – pyrite. The research was carried out in Institute of Volcanology and Seismology of FED RAS (V.M. Chubarov, analyst) using a scanning electron microscope (SEM) VEGA 3, equipped with an energy-dispersive spectrometer (EMF) X-MAX 80.

Primary magmatic minerals are common in the main matrix of rocks. These minerals are augite, plagioclases of andesine-labrador series, magnetite and titanomagnetite, Mn-containing ilmenite; grains of Mg-Al-Cr-containing spinel and rutile are traced. Pyrrhotite is in the form of small inclusions in pyrite. Titanium-zirconium minerals containing rare and rare earth elements (Sc, Nb, Hf, Y, Ce, Nd, Sm, Gd, Er, Th, U) were detected in ilmenite intergrowth and in the form of individual small grains (≥ 3 mm). Other phases of complex (variable) composition, for example, titanates and titanosilicates are traced (Fig. 1). We classify them as primarily magmatic with a certain degree of conventionality, since they can have a metamorphic origin. Probably, as a result of metamorphic alteration of Ti-containing minerals, silicon-titanium mixtures and sphene-containing inclusions of a number of metals are formed.

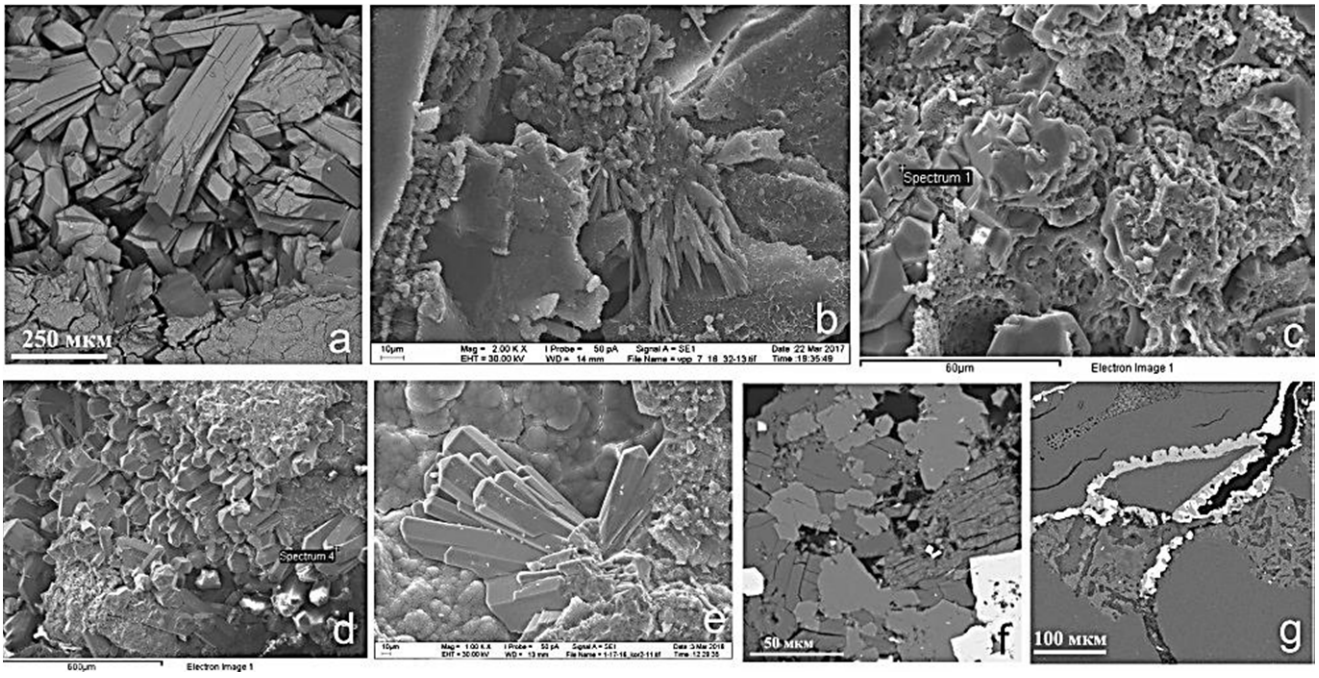

Fig. 2. Hydrothermal metasomatic minerals: a-stilbite-Ca, which fills the pores in the chlorite-smectite mass; b - radial-radiant aggregates of zeolite crystals (clinoptilolite?) in association with montmorillonite, opal and chlorite-smectites; c - calcite crystals in montmorillonite; d - crystals of apatite filling pores and cracks in the chlorite-smectite mass; e - radial fibrous aggregates of apatite crystals, walls of pores are covered with globular aggregates of opal-Fe-chlorite composition; f - formation of small crystals (leaves) of apatite along the aggregate of zeolite-potassium feldspar-pyrite-chlorite composition; g - performance of microcracks in hydrothermal clays with hydroxylapatite (gray) and pyrite (white). The researches was carried out in Institute of Volcanology and Seismology of FED RAS by means of SEM equipped with EDS X-MAX 80 (a, f, g); and at the Geological Faculty of Moscow State University with the help of SEM LEO 1450VP equipped with EDS INCA 300 (b, c, d, e).

Hydrothermal metasomatic minerals include zeolites, apatite, smectites, potassium feldspar, Mg-Fe-chlorites, cryptocrystalline quartz (chalcedony), opal, calcite, barite, gypsum, pyrite, marcasite, chalcopyrite, sphalerite. Zeolites are widely distributed: in the matrix of andesites, they form scattered small crystals and clusters of irregular shape, they replace plagioclases and cover voids with formation of geodes and large (up to 5-7 mm thick) veins. In addition to mono-mineral precipitates, zeolites with chalcedony, potassium feldspar, chlorite, calcite, pyrite (Fig. 2). Sometimes traces of crystal dissolution are noticeable, they are typically replaced with smectites and chalcedony, possibly with potassium feldspar. The zonation in the crystal structure of some zeolites, caused by the variations in Ba concentrations in the composition of the zones, is manifested. Three types of medium- and high-silicon zeolites were identified: heylandite-Ca, stilbite-Ca and lomontite; stilbite-Ca is the most

common. The wide occurrence of stilbite-Ca is probably due to the fact that high-silica zeolites are among the latest minerals that are formed when the P-T parameters of solutions are reduced (Kostov, 1971). Apatite is also one of the most common minerals. Two species that differ in chemical composition, morphology of crystals and (probably) origin were identified. Fluorapatite (as a rule, contains chlorine) forms barrel-shaped, spindle-like and oval grains up to 0.1 mm in size – often in place of leached pyroxene crystals or in fissured plagioclase crystals. Hydroxylapatite in the form of brushes of columnar crystals up to 0.05 mm in size lines pores and cracks, forms monomineral or pyrite-containing veinlets. Probably, fluorapatite is not only of late-magmatic or metamorphic origin, but also of hydrothermal-metasomatic origin. Hydroxylapatite reflects the current process of hydrothermal metasomatic transformation of andesites, the movement of solutions through cracks, and the formation of hydrothermal clays. Other widespread newly-formed andesite minerals of the clay stratum base are potassium feldspar, chlorites and chlorite-smectites, quartz and chalcedony, calcite (magnesian calcite), sulfides.

Thus, at the base of the hydrothermal clays of the East-Pauzhetka thermal field, fractured and brecciated andesites have been penetrated by core drilling wells. Porphyritic phenocrysts and the bulk of andesites are almost completely replaced by secondary minerals: smectites, medium- and high-silicon Ca-Na-zeolites, Ca-Mg-carbonates, opal, chalcedony, quartz, pyrite, etc. Zeolites, carbonates, silica minerals, apatite, chlorites, etc. fill cracks, voids and large ($\leq$ 20 cm of thickness) zones. Primary ore minerals are transformed into complex mixtures (for example, into titanosilicates) and are a source of rare and rare-earth elements. Complex mineral mixtures (chlorite-smectites, etc.) are largely formed under the influence of pore solutions. Pore solutions found in hydrothermal clays and mineralized zones have a hydrocarbonate (up to 1500 mg/l HCO_3^-) or hydrocarbonate sulfate (500-1600 mg/l SO_4^{2-}) composition. Ca^{2+} (200-300 mg/l), Mg^{2+} (100-260 mg/l) and Na^+ (110-195 mg/l) prevail in the cation composition, but the concentrations of K^+ (83-106 mg/l) and NH_4^+ (110- 155 mg/l) are also high. The total mineralization of pore solutions varies from 2.7 to 4.0 g/l. Mineralization, probably, was formed in several stages. At the present stage, active cation exchange between smectites and chlorites, zeolites-carbonates-potassium feldspar and other phases still continues. The data obtained indicate an alkaline environment of mineral formation in the rocks at the base of the hydrothermal clays of EPTF. Such a situation in the typical zone of acid leaching (argillization of rocks) can be created due to the acid-alkaline evolution of a water-salt fluid deep alkaline highly mineralized (metalliferous) hydrothermal solutions mix with meteoric waters. A similar model for the differentiation of acidic and alkaline fluid components is proposed for hydrothermal systems with vapour reservoirs (Zhatnuev, 2001). The Pauzhetka hydrothermal system is considered to be a water-dominating system, but EPTF is localized in the structure of the tectono-magmatic uplift of the Kambalny Range, and the thermal waters are probably formed under the influence of its magmatic foci (Structure …, 1993, Feofilaktov et al., 2017).

This work was supported by the RFBR (projects 16-05-00007 and 16-05-00971) and the Far East program (project 18-2-003). The research was carried out using the equipment obtained in the framework of the Moscow University Development Program.

References

Zhatnuev N.S. A Model for the evolution of acid-alkaline properties of fluid in hydrothermal systems with vapour reservoirs // Reports of the Academy of Sciences. 2001. Vol. 379. No. 2. pp. 241-246.

Kostov I. Minerology. Moscow: Mir, 1971. 584 p.

Rychagov S.N., Davletbayev R.G., Kovina O.V. Hydrothermal clays and pyrite of geothermal fields: significance of modern endogenic processes (South Kamchatka) in geochemistry // Volcanology and Seismology. 2009. No. 2. pp. 39-56.

Rychagov S.N., Sergeeva A.V., Chernov M.S. Mineral associations of the base of the clay strata as indicators of the fluid regime of the Pauzhetka hydrothermal system (Kamchatka) // Pacific Geology. 2017. Vol. 36. No. 6. pp. 90-106.

Rychagov S.N., Sokolov V.N., Chernov M.S. Hydrothermal clays of South Kamchatka's geothermal fields: a new approach and study results // Geochemistry. 2012. No. 4. pp. 378-392.

Structure of hydrothermal system. Moscow: Nauka, 1993. 298 p.

Feofilaktov S.O., Rychagov S.N., Bukatov Yu.Yu. et al. New data on the structure of the zone of discharge of fluids in the area of the Eastern Pauzhetka thermal field (South Kamchatka) // Volcanology and Seismology. 2017. No. 5. pp. 36-50.

MINERAL CHEMISTRY, GEOTHERMOBAROMETERY , GEOCHERONOLOGY, TECTONO – MAGMATISM AND MINERALIZATION IN BOROUJERD GRANITOID COMPLEX ,SANANDAJ – SIRJAN ZONE,WESTERN IRAN

Safari M.[1], Jahani M.[2], Abbasov N.[3]

[1]Department Of Geology, Payame Noor University, Tehran, Iran

[2]Department Of Geology, faculty of Earth Sciences, Shahid Chamran University Of Ahvaz, Iran, Geologist.Janjani@Gmail.Com

[3]Baku State University, Azerbaijan

Following the classical work of Alavi (1994), the Zagros orogen of Iran is divided, from southwest to northeast, into three tectono-stratigraphic zones, i.e., the Zagros fold and thrust belt, the Sanandaj-Sirjan zone or Zagros imbricate zone, and the Urumieh-Dokhtar mag-matic arc. The Sanandaj-Sirjan zone is ~1500 km long and ~150–200 km wide. The Borujerd complex is composed of granitic intrusions with wide range of late magmatic product including pegmatites and quartz veins, and a well- developed aureole in pelitic country rocks.The studied area includes the north east corner of the Khoramabad quadrangle and is an area of Mesozoic schists, intrusive igneous rocks and pegmatites (Fig 1). The oldest known exposed rocks are Precambrian, but the intrusives are emplaced into metasediments of early Mesozoic age. Regional metamorphism reached a peak in the greenschist facies, but subsequent thermal metamorphism has occurred locally, associated with granitoid emplacement. Intrusions include granite, granodiorite and quartz diorite. This intrusive activity culminated with the emplacement of the pegmatites which exhibit a north-west trend (Masoudi et al 2005). The goal of this study was to use Mineral chemistry, geothermobarometery, geocheronology, tectono – magmatism for mineralization study.

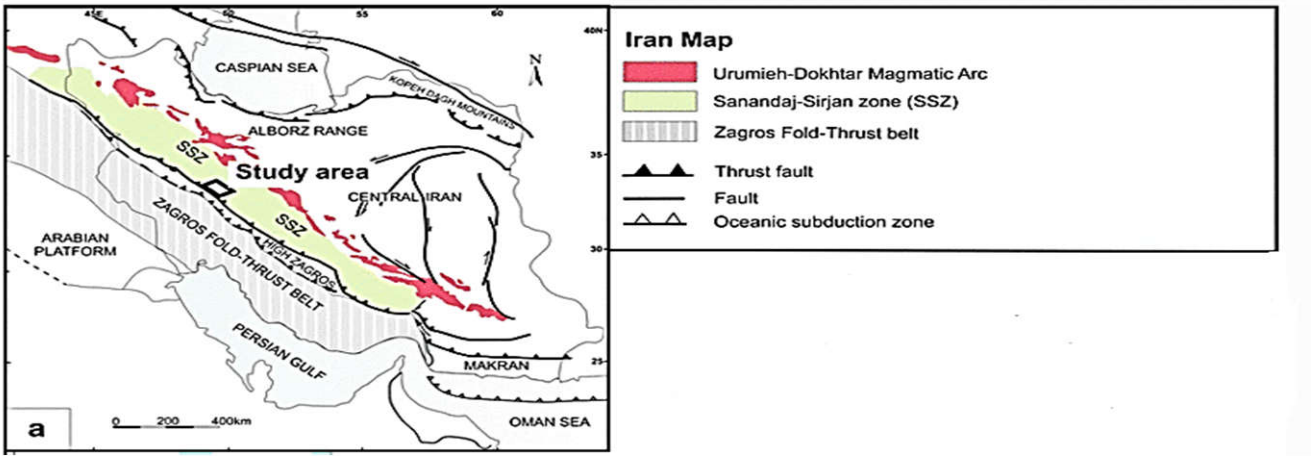

Fig 1. Geological Map Of Iran Zones (Shakerardakani et al 2018).

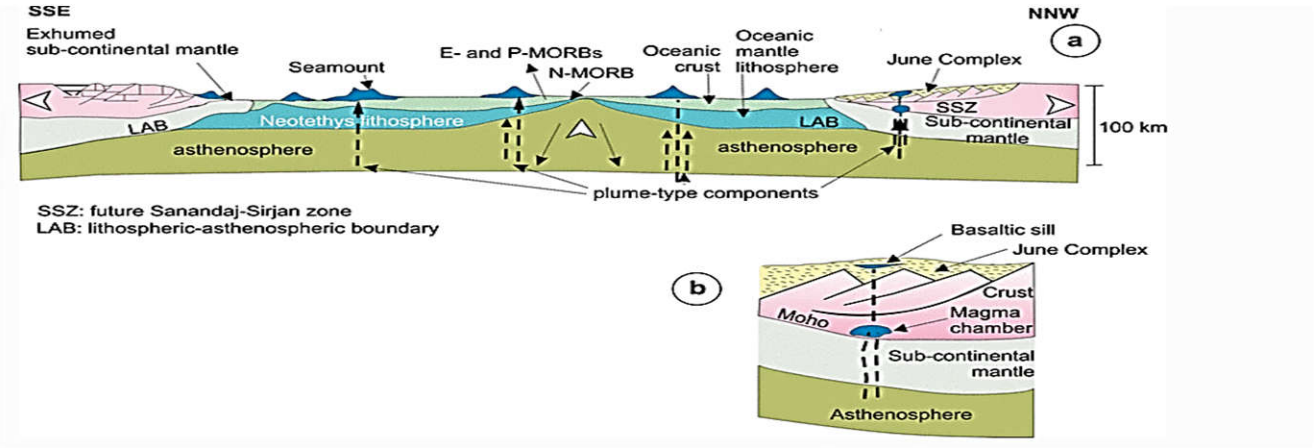

Fig 2. The continental crust of the SSZ has been thinned during Permian and Triassic times and the pressure estimates of clinopyroxene cores might indicate its crystallization in a lower crustal magma chamber (Fig. 13b) (Shakerardakani et al 2018).

For this study, 400 points of rock forming minerals by EMPA method have been analyzed by the CAmeCA SX-100 machine. The results are presented in this paper. The obtained results from the mineral chemistry in this study indicate that the studied amphiboles are calcic amphiboles, and in terms of chemical composition they can be called Magnesiohomblende (Fig 3 and 4) (Deer et al 1998).

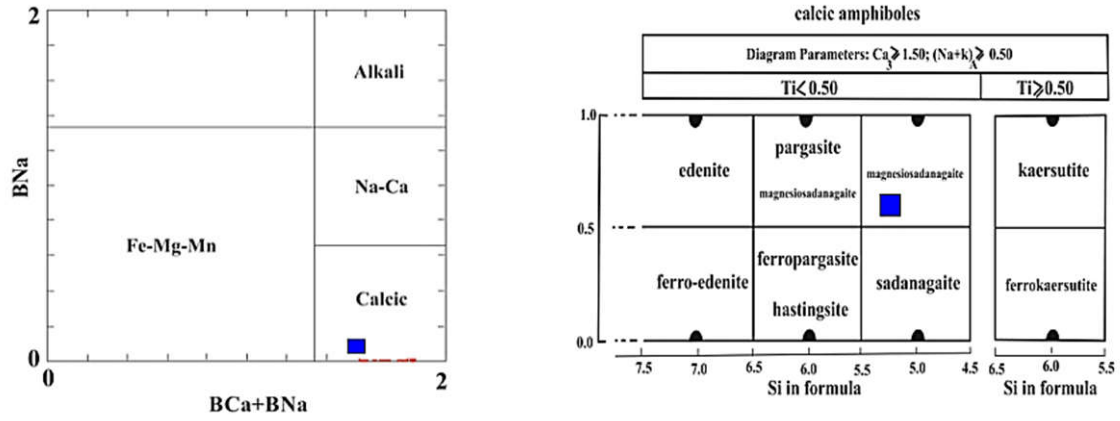

Fig 3 and 4. Amphiboles classification of based on (Rieder et al 1997).

Plagioclases are also orthoclase (Fig 5). The nature of magma constructing gabbroic rocks is the calc-alkaline (Fig 6.. In addition, due to the low Na_2o ratio it can be said, that tectonically these amphiboles are of S-Amph type and are related to the subduction zones (Fig 7 and 8). The results indicate that the chemical composition of biotite is not within the phlogopite range (Fig 9) and Due to the fact that Fe (Fe + Mn) ratio is greater than 0.33, it is not within the range of phlogopite. Most biotites located in the region coexist with Muscovite in the calc-alkaline igneous rocks (Fig 10). The study of biotite confirms their primary properties. In general, the Ti value in the studied biotite is not significant, but its predominant value is related to the nephleen sinites. Also, due to the ratio of Fetot ($Fe^{tot} + Mg^{+2}$) to Al^{Iv}, which is less than 0.6, it can be said that the oxygen fugacity was high. This indicates the nature of magma is Acidic. On the other hand, it can be said that the water level vary suitable for hornblende crystallization and mineralization. Different methods were used to perform thermobarometry, the best of which showed that the formation temperature of granitoid mass has been in the range of 768°C and a pressure of 3.6 Kb. For study of geothermobarometery used of (Holland and Blundy 1994) (Anderson and Smith 1996) and (Schmidt 1992) methods (Fig 13). The magma originated at a depth which is near the Moho discontinuity. According to this paper it can be said Ages between 170 Ma are related to subduction. Regarding the chemistry of halogens, it can be said that

due to the lack of Cl and its effective role in the transfer of metals, mineralization has not occurred and this factor is one of the most important reasons for the lack of fertility in theboroujerd granitoid complex. Regarding the chemistry of halogens, it can be said that due to the lack of Cl and its effective role in the transfer of mineralization metals, this is one of the most important reasons for the lack of fertility in the boroujerd granitoid complex.

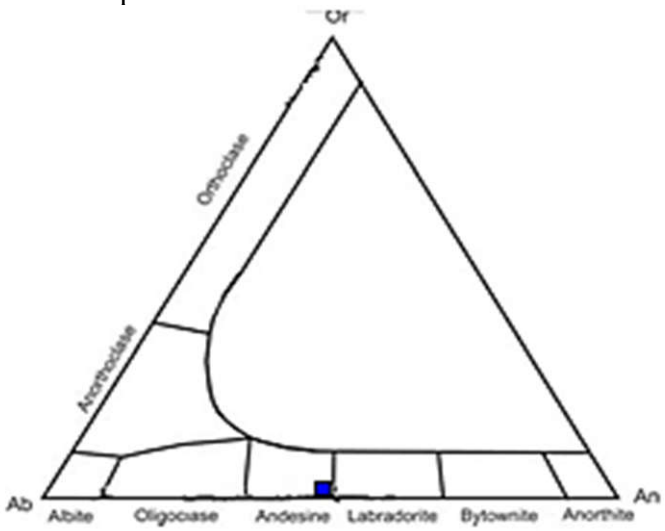

Fig 5: Plagioclases classification.

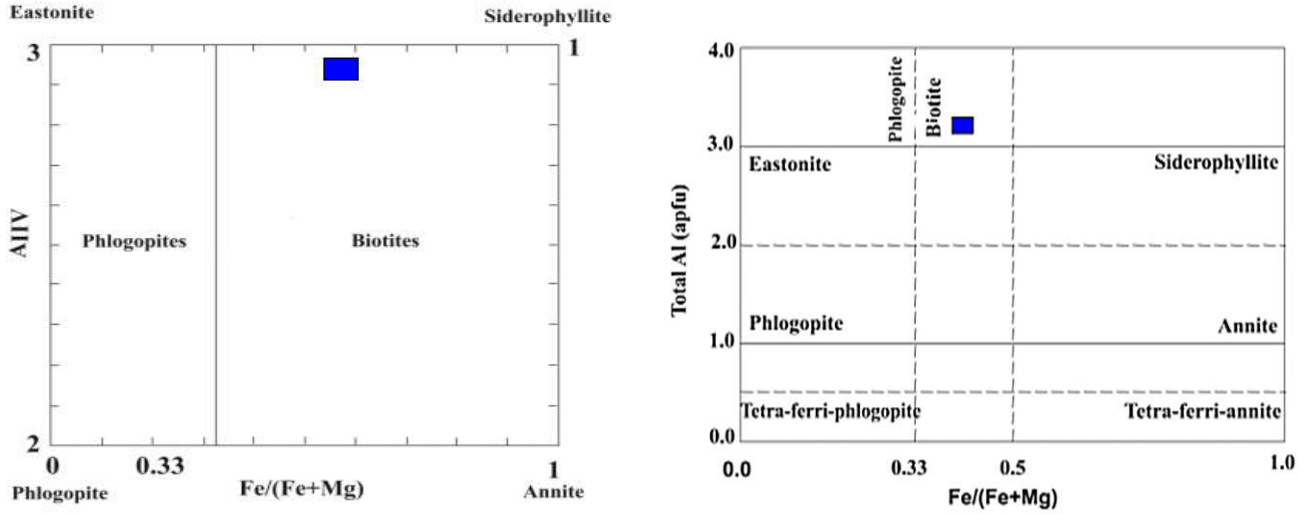

Fig. 9.Biotite classification of based on (Rieder et al 1998).

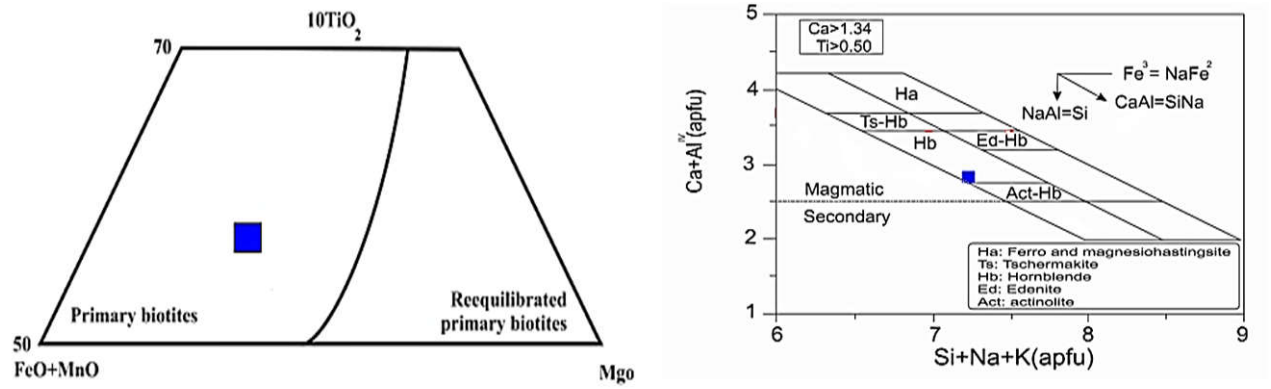

Fig. 5. Combination of biotites in grapg (Nachit 2005). Fig 5: Combination of Amphiboles in grapg.

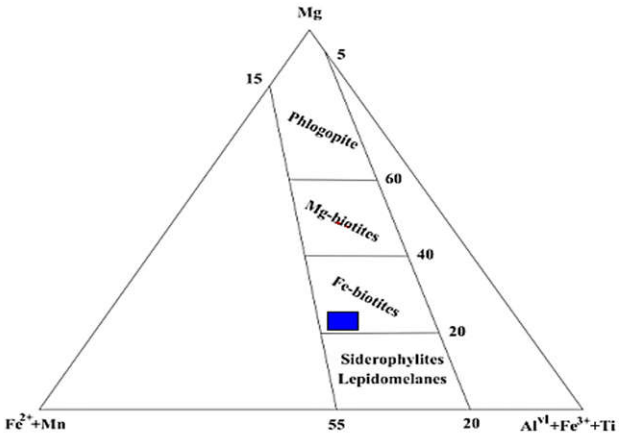

Fig. 10. Combination of biotites in grapg (Foster 1960).

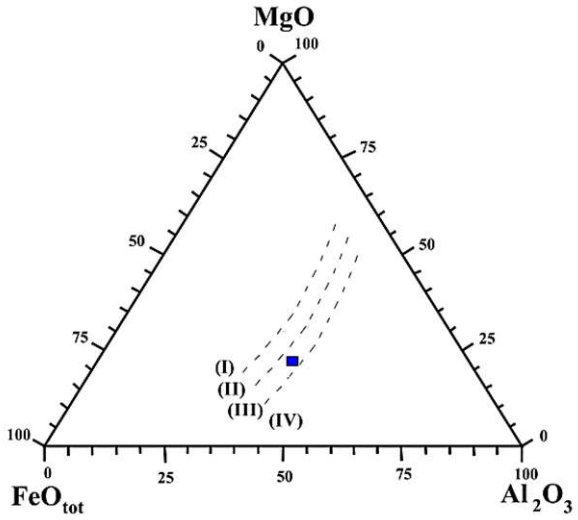

Fig. 8. Combination distribution of micas on the triple graph (Albuquerque, 1973) Al_2O_3-FeOtot-MgO.

Fig 11. Primary or secandary of Biotites.

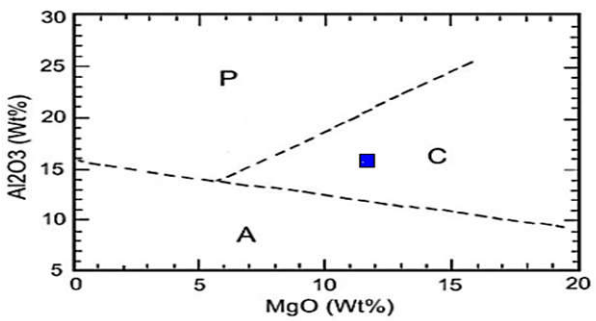

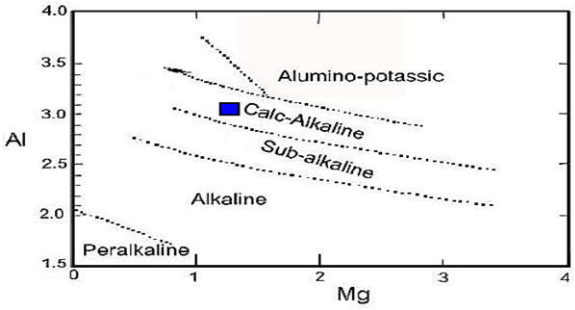

Fig 6. Tectonomagmatic setting based on biotites mineral chemistry.

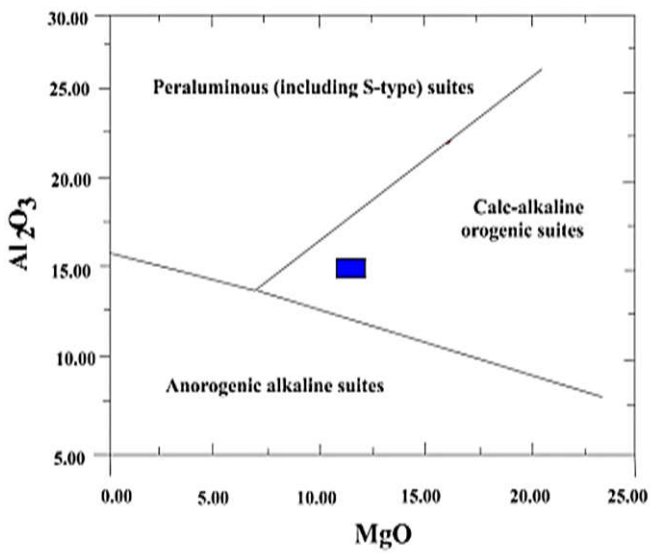

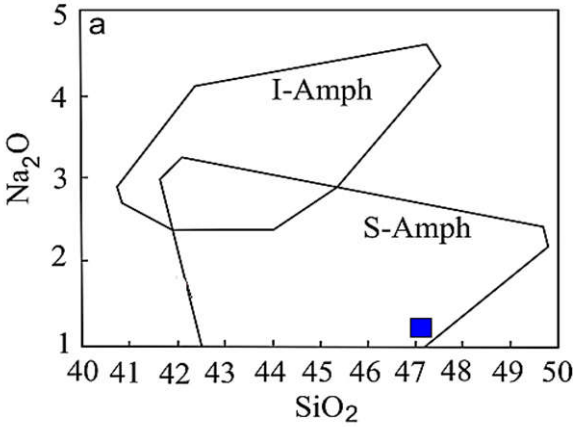

Fig 7 and 8. Tectonomagmatic setting based on amphiboles mineral chemistry.

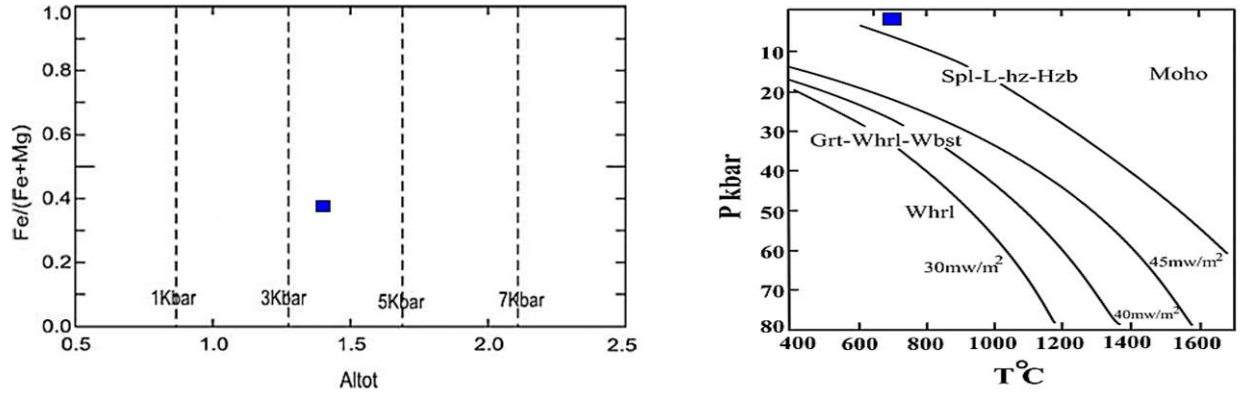

Fig. 13. Geothermobarometery graph for boroujerd granitoid complex.

References

Ahadnejad V, Valizadeh MV, Deevsalar R and Rezaei-Kahkhaei M, 2011. Age and geotectonic position of the Malayer granitoids: Im-plication for plutonism in the Sanandaj-Sirjan zone, W Iran. Neues Jahrbuch für Geologie und Paläontologie, Abhandlungen 261(1): 61–75.

Ahmadi-Khalaji A, Esmaeily D, Valizadeh MV and Rahimpour-Bonab H, 2007. Petrology and geochemistry of the granitoid complex of Boroujerd, Sanandaj-Sirjan zone, Western Iran. Journal of Asian Earth Sciences 29(5–6): 859–877, DOI 10.1016/j.jseaes.2006.06.005.

Alavi M, 1994. Tectonics of Zagros orogenic belt of Iran: New data and interpretation. Tectonophysics 229(3–4): 211–238, DOI 10.1016/0040-1951(94)90030-2.

Alirezaei S and Hassanzadeh J, 2012. Geochemistry and zircon geo-chronology of the Permian A-type Hasanrobat granite, Sanandaj-Sirjan belt: A new record of the Gondwana break-up in Iran. Lithos 151: 122–134, DOI 10.1016/j.lithos.2011.11.015.

RUTILE AS A CONCENTRATOR OF ANTIMONY IN FUMAROLIC EXHALATIONS OF THE TOLBACHIK VOLCANO (KAMCHATKA, RUSSIA)

***Sandalov F.D.*[1], *Pekov I.V.*[1,2], *Koshlyakova N.N.*[1], *Sidorov E.G.*[3]**

[1]*Faculty of Geology, Moscow State University, Moscow, Russia, fyodor.sandalov@yandex.ru*

[2]*Vernadsky Institute of Geochemistry and Analytical Chemistry, RAS, Moscow, Russia*

[3]*Institute of Volcanology and Seismology, Far Eastern Branch of the Russian Academy of Sciences, Petropavlovsk-Kamchatsky, Russia*

Rutile is a relatively common mineral in deposits of two active, hot fumaroles Yadovitaya and Arsenatnaya located at the summit of the Second scoria cone of the Northern Breakthrough of the Great Tolbachik Fissure Eruption, Tolbachik volcano (Kamchatka, Russia). Both Yadovitaya and Arsenatnaya are the brightest representatives of fumaroles belonging to the oxidizing type. The temperature of crystallization of rutile seems here not lower than 350-400°C (based on our measurements). In the chemical composition this fumarolic rutile is in general uncommon and differs from the same mineral from other geological formations. Samples chemically close to the end member TiO_2 were not found there. Typically, the Tolbachik fumarole rutile contains in total more than 12 wt.% admixtures, including chalcophile elements. Rutile turned out the major concentrator of antimony in the Tolbachik fumaroles and forms here a continuous isomorphous series with the isostructural mineral tripuhyite, $Fe^{3+}Sb^{5+}O_4$. The limits found for this series correspond to the following compositions: $(Ti_{1.834}Fe_{0.076}Sn_{0.056}Sb_{0.034})_{\sum 2.000}O_{3.962}$ [rutile with 88.8 wt.% TiO_2, 3.6 wt.% Fe_2O_3 and 3.7 wt.% Sb_2O_5 from Arsenatnaya] – $(Fe_{0.741}Sb_{0.714}Ti_{0.460}Sn_{0.064}Al_{0.017}Cr_{0.004})_{\sum 2.000}O_{3.976}$ [tripuhyite with 16.7 wt.% TiO_2, 26.9 wt.% Fe_2O_3 and 52.5 wt.% Sb_2O_5 from Yadovitaya]. Besides Sb and Fe, significant admixtures in the Tolbachik fumarole rutile (wt.%) are: MgO up to 0.1, ZnO up to 0.4, CuO up to 1.9, Al_2O_3 up to 1.9, Cr_2O_3 up to 2.1 and SnO_2 up to 11.8. The major substitution scheme in this solid-solution system is $Sb^{5+} + Fe^{3+} \rightarrow 2Ti^{4+}$ while others are $Sn^{4+} \rightarrow Ti^{4+}$, $2Sb^{5+} + M^{2+}$

$\rightarrow 3Ti^{4+}$ and, probably, $2M^{3+} + [vac]^0 \rightarrow 2Ti^{4+} + O^{2-}$ (M^{3+} = Fe, Al, and Cr, M^{2+} = Mg, Zn, and Cu and $[vac]^0$ = vacancy). It should be noted that no another mineral with Sb content >1 wt.% was found in the Tolbachik fumaroles. Parameters of tetragonal unit cell of the Fe- and Sb-enriched (5–8 wt.% Fe_2O_3 and 11–14 wt.% Sb_2O_5) rutile from Arsenatnaya calculated from powder X-ray diffraction data are: a = 4.608(1), c = 2.981(1) Å and V = 63.3(2) Å^3.

Solid solution between rutile and tripuhyite ("squawcreekite") was earlier reported for some endogene ore deposits characterized by strongly oxidizing conditions of mineral formation (Smith, Perseil, 1997; Cabella et al., 2003) while for the minerals from volcanic fumaroles there are first data.

This study was supported by the Russian Foundation for Basic Research, grant 18-05-00051.

References

Cabella R. et al. Squawcreekite-rutile solid solution from the Kajlidongri Mine (India) // Eur. J. Miner. 2003. Vol. 15, p. 427-433.

Smith, D.C., Perseil, E.-A. Sb-rich rutile in the manganese concentrations at St. Marcel-Praborna, Aosta Valley, Italy: petrology and crystal-chemistry // Miner. Mag. 1997. Vol. 61, p. 655-669.

ZONED LHERZOLITE-DUNITE XENOLITH FROM THE GRIB KIMBERLITE, ARKHANGELSK PROVINCE, RUSSIA: DIRECT EVIDENCE OF MANTLE METASOMATISM

Sazonova L.V.[1], Nosova A.A.[2], Kargin A.V.[2]

[1]Lomonosov Moscow State University, Moscow, Russia, sazonovalv52@mail.ru

[2]Institute of Geology of Ore Deposits, Petrography, Mineralogy and Geochemistry, Moscow, Russia, kargin@igem.ru

We have studied petrography and mineralogy of the mantle-derived zoned lherzolite-dunite xenolith from the Grib kimberlite, Arkhangelsk province, Russia and recognised several stages of mantle metasomatism. Zoned xenoliths are rare among xenolith brought to the surface by kimberlite melts and present the direct evidence of mantle metasomatism.

Petrography. The xenolith has elongated rounded shape, approximately 7 cm x 5 cm in size. The xenolith consists of two zones: (1) – 2-3 cm in width, presented serpentinised olivine (dunite zone) and (2) – 2-2.5 cm in width, consist of garnet (~15 vol.%), clinopyroxene (~25 vol.%), serpentinised olivine (~55 vol.%), and secondary association of phlogopite+Cr-spinel+amphibole (~5 vol.%) (lherzolite zone). The boundary between zones is sharp.

The dunite zone has medium-coarse granoblastic texture. According to relict textures and secondary minerals, the primary association of dunite includes olivine and minor garnet and orthopyroxene. In the most cases, olivine is entirely replaced by serpentine and magnesian chlorite, but sometimes the fresh olivine relicts have existed. Olivine grains have polygonal shapes with a triple junction at an angle of 120° that indicates recrystallisation and equilibrium of dunite minerals (Fig. 1a). This zone also contains phlogopite accumulations that usually occurs as a secondary phase during pseudomorphism of garnet.

The lherzolite zone has mosaic-porphyroblastic texture. Porphyroblasts are presented by garnet with size is 5-6 mm (Fig. 1a). The groundmass has fine-medium-grained texture and consists of garnet (2-3 mm), altered olivine (and orthopyroxene ?, 1-3 mm), clinopyroxene (up to 4 mm), and secondary mineral association of phlogopite, chromium spinel, rare amphibole that replaced garnet porphyroblasts. Sometimes the fragments of relictic granoblastic texture of dunite zone are presented (Fig. 1a). Clinopyroxene grains have an elongated, curved shape, and cutting contacts with olivine that indicates un-equilibrium texture of this lherzolite zone (Fig. 1b). In addition, clinopyroxene show signs of recrystallisation (Fig. 1b). The zoned composition of the studied xenolith couple with petrography indicate that this xenolith is the fragment of the melt infiltration channel.

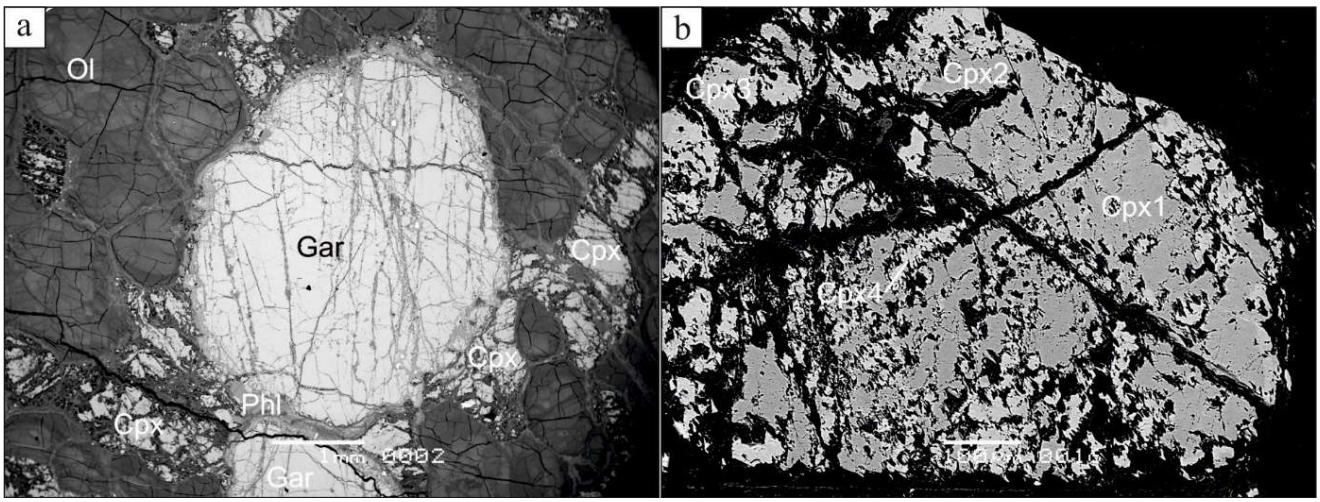

Fig. 1. BSE images of lherzolite-dunite xenolith: (a)– garnet porphyroblast with phlogopite rim, elongated clinopyroxene grains, polygonal shapes of olivine grains; (b) – zoned clinopyroxene grain with relict *Cpx1*, recrystallized *Cpx2-3* and secondary veinlet with *Cpx4*, lherzolite zone.

Mineral composition. *Olivine* had been studied as a large grain (2000x1000 μm) within the dunite zone. The composition of olivine is homogeneous in term of Fo content (92.53±0.03) with low concentrations of Al (16±5 ppm), Ca (76±12 ppm), Mn (687±25 ppm), and high Ni (2935±25 ppm) and Cr# value (0.87±0.05) that correspond with the composition of olivine from mantle peridotite xenoliths (e.g. Bussweiler et al., 2017). By Ti content (151±6 ppm) the studied olivine different from olivine from peridotite xenoliths within the Grib kimberlite and is close to high-Mg and high-Ti olivine macrocrysts within kimberlite (Sazonova et al., 2015).

Garnet is composed of pyrope with moderate contents of Cr_2O_3 (4.89±0.05 wt.%) and CaO (5.01±0.70 wt.%) and comparable with garnet from mantle lherzolite xenoliths (Grutter et al., 2004). The concentrations of Na_2O (0.12±0.05 wt.%) and TiO_2 (0.21±0.07 wt.%) are typical for low-Ti garnet within peridotite xenoliths from the Grib kimberlite (Kargin et al., 2016). Some garnet grains show zoning composition with an insignificant decrease of Ti and increase of Cr contents.

Clinopyroxene (Cpx) forms several generations of grains different by the petrographic position and composition. *Cpx3* occurs as small individual grains or forms outer zones within zoned grains and characterised by intensive fracturing. *Cpx1* forms relict parts of zoned grains (in general inner zones) without any deformations (Fig. 1b) and presents the earlist Cpx generation. *Cpx2* forms transitional zones between *Cpx1* and *Cpx3*.

Cpx4 and *Cpx5* have later origin and are associated with large late veinlets or dissolution channels in olivines wherein they associated with late phlogopite.

In general, the composition of *Cpx1-3* is typical for clinopyroxene from lherzolite xenoliths from kimberlite. *Cpx2* and *Cpx3* are characterised by enrichment in cosmochlore and jadeite components (8-12 and 10-15 mol % correspondingly). *Cpx3* has 4.07±0.30 wt.% Na_2O and 3.4±0.49 wt.% Cr_2O_3 with Mg# = 0.91. *Cpx2* has close to *Cpx3* composition with more significant variations, as well as a higher Mg # = 0.91-0.92. *Cpx1* shows higher Mg# values (0.94) with lower Na_2O (2.59±0.06 wt.%) and Cr_2O_3 (2.70±0.08 wt.%) contents (7-8 mol. % cosmochlore and 6-7 mol. % jadeite component) than *Cpx3*. *Cpx1* also has lower Al, Ti and higher Ca contents and Cr# values than *Cpx3* and *Cpx2*. The composition of *Cpx1* is comparable with the composition of clinopyroxene from garnet peridotite xenoliths and low-Ti and high-Cr megacrysts from the Grib kimberlite (Kargin et al., 2016; 2017). Na-rich *Cpx*3-2 is characterized by REE and other trace elements distribution similar to Cpx group 1 from the Grib kimberlite (Schukina et al., 2015), Cpx group A (Zinerna et al., 2013) and Cpx group IIa (Nimis et al., 2009) from Zagadochnaya kimberlite. Na- medium *Cpx1* has distinctly different trace elements distribution with strong enrichment in LREE and HREE fractionation similar to Cpx group 2 from Grib kimberlite (Schukina et al., 2015), Cpx group B, C (Zinerna et al., 2013) and Cpx group IIIa (Nimis et al., 2009) from Zagadochnaya kimberlite.

Cpx4 and *Cpx5* have moderate Mg# values (0.92), high Cr# values (0.5-0.8) and lower Na_2O (1.97±0.30 wt.%) content than *Cpx1-3*.

Phlogopite grains have a bivariate composition. Phlogopite pseudomorphed garnet grains has low Ti (0.39±0.05 wt.%) and Cr (1.00±0.17 wt.%) contents with high Mg# values (0.93-0.94) and correspond with the composition of phlogopite megacrysts and phlogopite from clinopyroxene-phlogopite and garnet-peridotite xenoliths (Kargin et al., 2017). Phlogopite within the late veinlets network associated with *Cpx4* and *Cpx5* has lower Mg# values (0.92-0.93), higher Ti (0.99±0.58 wt.%) and Cr (0.95±0.54 wt.%) concentrations. These phlogopites overlap by composition with phlogopite from kimberlite groundmass.

Amphibole that pseudomorphed clinopyroxene and garnet has pargasite composition.

P-T estimates. We obtained the T and P values for lherzolite mineral assemblage using a combination of the enstatite-in-clinopyroxene (En-in-Cpx) thermometer and Cr-in-Cpx barometer (Nimis and Taylor, 2000) with the modified protocol by (Ziberna et al., 2016). Cpx3 and Cpx2 show very close T and P values: T=737±30°C and P = 35±2.3 kbar. These PT values correspond with geotherm of 36 mW/m2 (Hasterok and Chapman, 2011). Cpx1 shows higher T values (780±30°C) and close P estimates (32±2.3 kbar). Late Cpx4 and Cpx5 show higher T values (800-820±30°C) and lower P estimates (25-28±2.3 kbar).

References

Bussweiler Y. et al. The aluminum-in-olivine thermometer for mantle peridotites - Experimental versus empirical calibration and potential applications // Lithos. 2017. Vol. 272-273. pp. 301-314.

Grütter H.S. et al. An updated classification scheme for mantle-derived garnet, for use by diamond explorers // Lithos. 2004. Vol. 77. № 1–4 SPEC. ISS. pp. 841–857.

Hasterok D. et al. Heat production and geotherms for the continental lithosphere // Earth and Planet. Sc. Let. 2011. Vol. 307(1–2), pp. 59–70.

Kargin A.V. et al. Composition of garnet and clinopyroxene in peridotite xenoliths from the Grib kimberlite pipe, Arkhangelsk diamond province, Russia: Evidence for mantle metasomatism associated with kimberlite melts // Lithos. 2016. Vol. 262, pp. 442–455.

Kargin A.V. et al. Cr-rich clinopyroxene megacrysts from the Grib kimberlite, Arkhangelsk province, Russia: Relation to clinopyroxene–phlogopite xenoliths and evidence for mantle metasomatism by kimberlite melts // Lithos. 2017. Vol. 292–293. pp. 34–48.

Nimis P. et al. Single clinopyroxene thermobarometry for garnet peridotites. Part I. Calibration and testing of a Cr-in-Cpx barometer and an enstatite-in-Cpx thermometer // Contrib. to Mineral. Petrol. 2000. Vol. 139. № 5. pp. 541–554.

Sazonova L.V. et al. Olivine from the Pionerskaya and V. Grib kimberlite pipes, Arkhangelsk diamond province, Russia: Types, composition, and origin // Petrology. 2015. Vol. 23. № 3. pp. 227–258.

Shchukina, E.V et al., Metasomatic processes in the lithospheric mantle beneath the V. Grib kimberlite pipe (Arkhangelsk diamondiferous province, Russia) // Russ. Geol. Geophys. 2015. Vol. 56, pp. 1663–1678.

Ziberna L. et al, Error sources in single-clinopyroxene thermobarometry and a mantle geotherm for the Novinka kimberlite, Yakutia //Am. Mineral. 2016. Vol. 101, pp. 2222–2232.

Ziberna L., et al, Metasomatic Processes in the Central Siberian Cratonic Mantle: Evidence from Garnet Xenocrysts from the Zagadochnaya Kimberlite // J. Petrol. 2013. Vol, 54, pp. 2379–2409.

THE COMPOSITIONAL EVOLUTION OF PYROXENES FROM THE EUDIALYTE LUJAVRITES COMPLEX OF THE LOVOZERO MASSIF, RUSSIA

Sedova A.M., Evdokimov M.D.

Department of Mineralogy, St. Petersburg State University, Saint-Petersburg, Russia, a.sedova@spbu.ru

The Lovozero massif is the largest known alkaline layered intrusion at present, and so questions of its formation remain highly relevant. During the formation of the massif (at the main magmatic stage) rocks of three intrusive phases were intruded. The compositions of the first two phases can be described by the classical scheme of single-phase formation of layered intrusives. It is however, assumed that the formation of the third phase occurred from a more differentiated portion of the melt, in a shallow intermediate chamber (Wager, Brown 1967, Korobeinikov, Laajoki, 1994). The third intrusive phase (eudialyte lujavrites complex) is composed mainly of eudialyte lujavrites, less foyaites and urtites. Recent mineralogical compositional studies of this phase are considered only in conjunction with other intrusive phases (Korobeinikov, Laayoki, 1994, Kogarko et al., 2006; Suk et al., 2009; Когарко, 2015). Our current work (Sedova, Evdokimov, 2018), fills a gap where the composition of pyroxenes in the eudialyte lujavrites complex were considered in detail. The clinopyroxenes of the eudialyte lujavrites complex are represented by aegirine, rarely - aegirine-augite with variations in content of Ti, Fe^{2+}, Al, Mg, Ca, Mn, Zr and Nb. Their composition is dependent upon the size and shape of the crystals, the composition of host rock, and upon the specific section from where the rocks were selected (valley of the Tulbnunuai river, the Kuftuay river at the foot of Mannepakh mountain, Anguendaschorr mountain, the Geologists pass, Kedykverpakh mountain). In our work (Sedova, Evdokimov, 2018) the evolution of pyroxenes was studied by way of the variational diversity of crystal zonation that was first applied. This made it possible to establish two different evolutionary trends of the chemical composition of pyroxenes (Fig. 1): General trend (low zirconium) pyroxenes and particular one (high zirconium).

Pyroxenes from the eudialyte lujavrites complex in the Lovozero massif have been found for the first time to have such high ZrO_2 (3.09 wt. %) content (Sedova, Evdokimov, 2018), although in these rocks zirconium containing phases (eudialyte) are widely distributed. Calculations of clinopyroxene compositions by end-member forms showed the possible presence of Zr-johansenite and Ti-Zr-aegirine end-members in them. The latter was found in other alkaline rocks (Andersen et al., 2016).

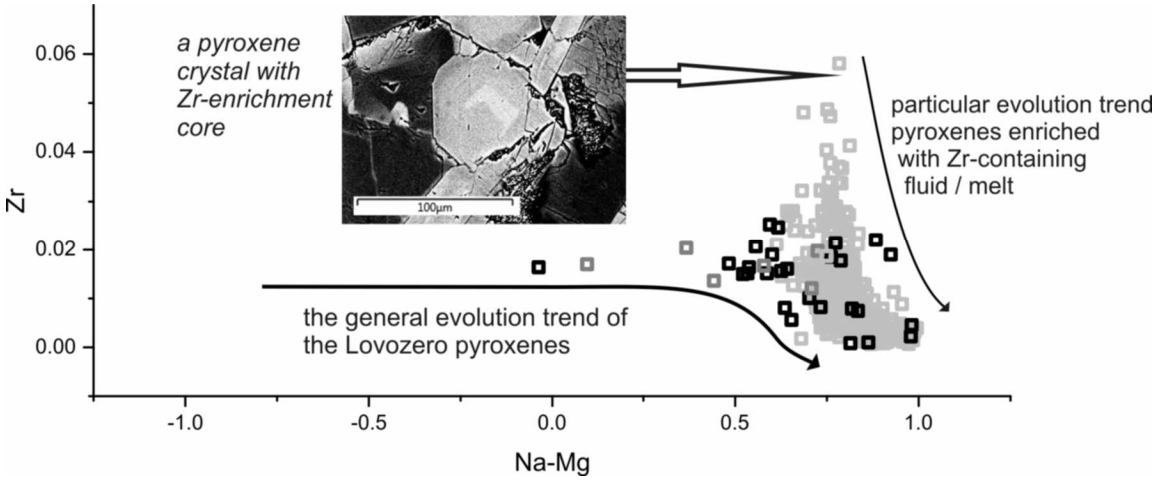

Fig. 1. Two branches showing the evolution of clinopyroxenes: based upon a Zr fractionation index (p.f.u.) from rocks of the eudialyte lujavrites complex from the Lovozero massif. Data are from Sedova and Evdokimov (2018); Kogarko et al. (2006); Когарко (2015); Suk et al. (2009).

The authors thank Dr. A.N. Zaitsev and Dr. N.V. Sorochtina for discussion of results, also thank to N.S. Vlasenko and Dr. V.V. Shilovsky from Resource Center "Geomodel" and Dr. Yapaskurt from the Moscow State University's CCU for qualitatively performed analizes.

References

Andersen T., Elburg M., Erambert M. The miaskitic-to-agpaitic transition in peralkaline nepheline syenite (white foyaite) from the Pilanesberg Complex, South Africa // Chemical Geology. 2016. Vol. 455. p. 166-181.

Kogarko L. N., Williams C. T. and Woolley A. R. Compositional evolution and cryptic variation in pyroxenes of the peralkaline Lovozero intrusion, Kola Peninsula, Russia // Mineralogical Magazine. 2006. Vol. 70(4). p. 347–359.

Korobeynikov A.N. and Laaioki K. Petrological aspects of the evolution of clinopyroxene composition in the intrusive rocks of the Lovozero alkaline massif // Geochemistry International. 1994. Vol. 31. p. 69-76.

Suk N.I., Kotelnikov A.R., Kovalsky A.M. Iron-magnesium minerals from differentiated rocks of Lovozersky alkaline massif // Geochemistry, Mineralogy and Petrology. Sofia. 2009. Vol. 47. p. 97-107.

Wager L.R., Brown G.M. Layered igneous rocks. Edinburg, Scotland, Oliver & Boyd. 1967. 588 p.

Когарко Л.Н. Фракционирование циркония в пироксенах щелочных магм // Геохимия 2015. Вып. 1. С. 3-11.

Седова А.М., Евдокимов М.Д. Характеристика химического состава и эволюция клинопироксенов комплекса эвдиалитовых луявритов Ловозерского щелочного массива// Вестник СПбГУ. Науки о Земле. 2018. Т.63. Вып.1. С. 69–102.

THE MINERALOGY OF THE EFFUSIVE SILICATE ROCKS FROM THE MOSONIK VOLCANO, NORTHERN TANZANIA

Sedova A.M.[1], Zaitsev A.N.[1,2], Spratt J.[2]

[1]Department of Mineralogy, St. Petersburg State University, Saint-Petersburg, Russia, a.sedova@spbu.ru

[2]Department of Core Research Laboratories, Natural History Museum, London, UK

The Mosonik volcano belongs to the Neogene-Resent volcanics of the Natron-Engaruka region of the East African Rift system. It is one of several stratovolcanoes located on the northeastern tip of the Gregory Rift Valley. Mosonik is attributed as having the earliest phase of eruptions in this province (Dawson, 2008) and is dated in the range 3.18-1.28 Ma (Isaac & Curtis, 1974; Dawson, 2008). In 1961, it was mapped by the Tanganyika Geological Survey (Guest et al., 1961), with published data (Paslick et al., 1996) on the composition of minerals from basanites, nephelinites and phonolites. According to the results of this study the compositions of melilite and nephelinite, Zaitsev et al. (2015) have indicated that the Mosonik volcano could be a potential source for the Upper Laetolil Footprint Tuff 7.

According to our data the main effusive rocks of Mosonic are various nephelinites and phonolites, quite often they contain xenoliths of plutonic rocks: melteigites, foyaites, ijolites, and rocks of the enclosing stratum (andesites). Carbonatites mostly occur as boulders of various sizes within creek deposits.

Among nephelinites there are nephelinites *s.s.*, phonolitic nephelinites, calcite-phonolite nephelinites and melilite nephelinites. Microphenocrysts are represented by nepheline (45-60%), pyroxenes of diopside-hedenbergite solid solution, in some cases with aegirine edging (15-30%), apatite (3-10%) and titanite (3-10%). Calcite content reaches 10% within the calcite varieties of nephelinites, sanidine up to 10% in phonolitic nephelinites, which are strongly altered. Melilite nephelinites are also characterized by the following coposition: melilite (20%), perovskite (5%), schorlomite (3%). In rare cases within the nephelinites there are microphenocrysts of nepheline.

Phonolites are represented by the following species: phonolites, sodalite phonolites and calcite phonolites. Phenocrysts are represented by nepheline (40-65%), pyroxenes of the diopside-hedenbergite series, rarely with aegirine edging (10-50%), sanidine (15-40%), Mg-Fe mica (0-5%), titanite (1-10%), and apatite (0-8%). In these rocks a large number of macrophenic crystals of nepheline, pyroxene, and often sanidine are observed.

The work is supported by Russian Foundation of Basic Research (grant 18-05-00835) and St. Petersburg State University (Geomodel Resource Center).

References

Dawson J. B. The Gregory Rift Valley and Neogene-Recent Volcanoes of Northern Tanzania. London. 2008. 112 pp.

Guest N. J., James, T. C Pickering R., and Dawson J. B. Angata salei. Geol. Surv. Tanganyika. Quarter degree sheet 39. 1961

Isaac, G. L. & Curtis, G. H. Age of the Acheulian industries from the Peninj Group, Tanzania // Nature. 1974. p.249.

Paslick, C., Halliday, A. N., Lange, R. A., James, D. & Dawson, J. B. Indirect crustal contamination: evidence from isotopic and chemical disequilibria in minerals from alkali basalts and nephelinites from northern Tanzania // Contributions to Mineralogy and Petrology. Vol. 125. 1996. 277–292.

Zaitsev A.N., Spratt J., Sharygin V.V., Wenzel T., Zaitseva O.A., Markl G. Mineralogy of the Laetolil Footprint Tuff: A comparison with possible volcanic sources from the Crater Highlands and Gregory Rift // Journal of African Earth Sciences. Vol. 111. 2015. pp. 214–221.

PETROLOGY AND CONDITIONS OF FORMATION OF THE MADIAPALA SYENITES, CENTRAL ZONE OF THE LIMPOPO COMPLEX, SOUTH AFRICA

***Selyutina N.E.*[1,2], *Safonov O.G.*[1,2]**

[1]*Lomonosov Moscow State University, Moscow, Russia, Nata-me98@mail.ru*

[2]*Korzhinskii Institute of Experimental Mineralogy RAS, Chernogolovka, Russia*

The Madiapala syenite body is located in the western part of the Central Zone (CZ) of the high-grade Limpopo Complex, South Africa. It is situated within the Alldays TTG gneisses with an age 2610 - 2640 Ma. According to the SHRIMP geochronological data using the ^{207}Pb / ^{206}Pb ratio in titanites, Rigby et al. (2011) reported an age of the syenites 2010.3 ± 4.5 Ma. This age corresponds to the period of the Paleoproterozoic tectono-thermal activity (D3/M3) in the CZ, which was characterized by a massive fluid influx along regional and local shear-zones. Using pseudosection method (THERMOCALC), Rigby et al. (2008) estimated 6 kbar and 770°C as peak P-T parameters for the syenites and interpreted them as conditions of metamorphism of pre-existing syenites during the Paleoproterozoic metamorphic stage. Different model for the formation of the syenites within the TTG gneisses is suggested by Safonov et al. (Safonov, Aranovich, 2014; Safonov et al., 2014) on the basis on experiments on the interaction of biotite-amphibole tonalite gneiss with H_2O-CO_2-(K, Na) Cl fluids at 750 and 800ºC and 5.5 kbar (Safonov et al., 2012, 2014). These experiments demonstrated that the leading factor for formation of the syenite assemblages after tonalite gneiss is an increase of potassium activity in a fluid (associated with the salt component of the fluid). Thus, the Madiapala syenites could be a product of the syenitization of the TTG gneisses under influence of saline H_2O-CO_2 fluids.

The earliest assemblage in the syenites is potassium feldspar + clinopyroxene + titanite ± apatite. In order to estimate the conditions for formation of this assemblage, we used the PERPLE_X (Connolly, 2005) software, version 6.7.7 for Windows, to construct the P-T pseudosections for the dry syenite system, for the hydrous system and for the system saturated with an aqueous-carbonic fluid. These graphs showed that the observed association occurs in the water-bearing system (Fig. 1).

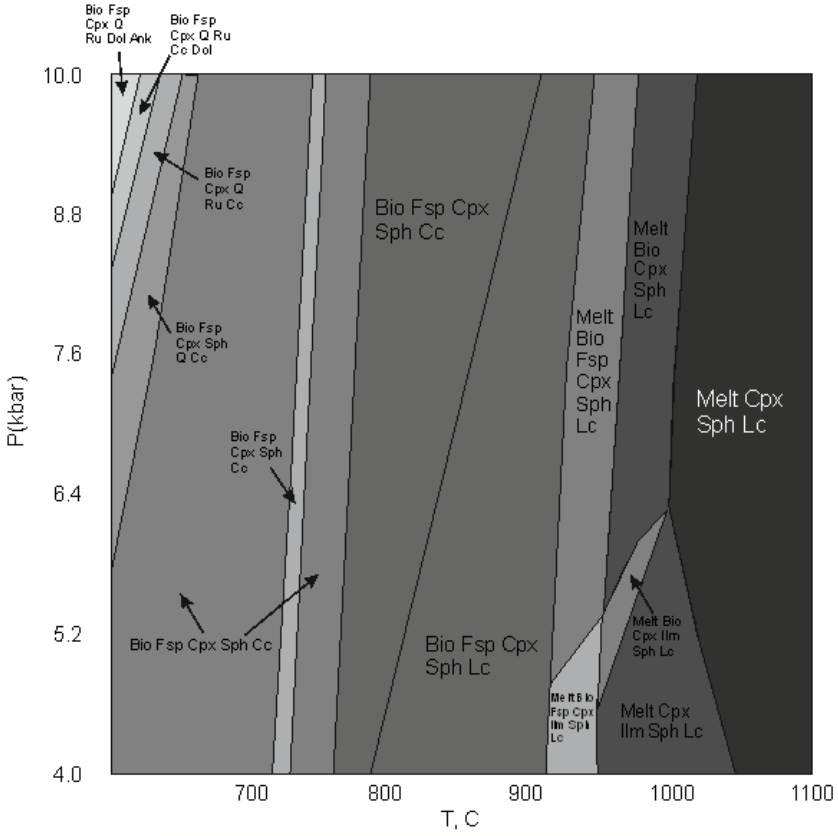

Fig. 1. P-T pseudosection for the syenite bulk composition in a system with a saturated H2O-CO2 fluid (mole fraction of CO2 is 0.5).

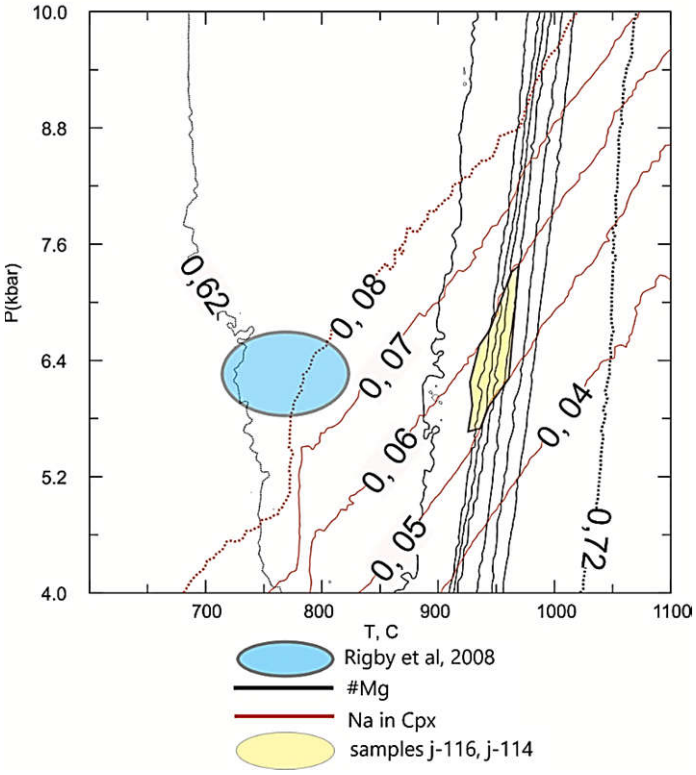

Fig. 2. Isopleths for Mg-number and Na content in clinopyroxene for the Madiapala syenites.

Following to the pseudosection, isopleths X_{Mg} = 0.64 – 0.67 и 0.05 – 0.06 a.p.f.u. Na in clinopyroxene, characteristic for the syenites, converge at temperatures 930-960ºC and pressures 5.6 - 7.4 kbar.

At similar pressure, the calculated temperatures are much higher than the temperatures estimated by Rigby et al. (2008) (Fig. 2) for amphibole-bearing metasomatic veins in the syenite body (6.4 ± 0.6 kbar, 770 ° C). We suggest that temperatures > 900 ° C correspond to crystallization of the primary

magmatic assemblage Cpx + Kfs + Sph ± Ap, whereas amphibole-bearing assemblages recorded the cooling of the syenite magma. Pseudosection in terms of lg(a_{H2O}) and lg(a_{K2O}) show that the Alldays gneiss can be transformed to the syenite via increase of the potassium activity at constant P and T.

Thus, the formation of the primary syenite assemblage occurred at pressures of about 6.4 kbar and temperatures of 950°C in the study of Alldays tonalite gneisses with a H_2O-CO_2-salt fluid, in which a potassium-salt component played an important role. The formation of amphibole-bearing assemblages, studied by Rigby et al. (2008), occurred during cooling of the syenite magma at the middle-crustal level 18-20 km.

References

Connolly J. A. D. Computation of phase equilibria by linear programming: a tool for geodynamic modeling and its application to subduction zone decarbonation // Earth and Planetary Science Letters. 2005. Vol. 236. Iss. 1-2 pp. 524-541.

Rigby M., Mouri H., Brandl G. PT conditions and the origin of quartzo-feldspathic veins in metasyenites from the Central Zone of the Limpopo Belt, South Africa // South African Journal of Geology. 2008. Vol. 111. Iss. 2-3 pp. 313-332.

Rigby M. J., Armstrong R. A. SHRIMP dating of titanite from metasyenites in the Central Zone of the Limpopo Belt, South Africa // Journal of African Earth Sciences. 2011. Vol. 59. Iss. 1 pp. 149-154.

Safonov O. G., Kovaleva, E. I., Kosova, S. A., Rajesh, H. M., Belyanin, G. A., Golunova, M. A., & Van Reenen D. D. Experimental and petrological constraints on local-scale interaction of biotite-amphibole gneiss with H_2O-CO_2-(K, Na) Cl fluids at middle-crustal conditions: Example from the Limpopo Complex, South Africa // Geoscience Frontiers. 2012. Vol. 3. Iss. 6 pp. 829-841.

Safonov O. G., Aranovich L. Y. Alkali control of high-grade metamorphism and granitization // Geoscience Frontiers. 2014. Vol. 5. Vol. 5 pp. 711-727.

Safonov O. G., Kosova S. A., Van Reenen D. D. Interaction of Biotite–Amphibole Gneiss with H_2O–CO_2–(K, Na) Cl Fluids at 550 MPa and 750 and 800° C: Experimental Study and Applications to Dehydration and Partial Melting in the Middle Crust // Journal of Petrology. 2014. Vol. 55. Iss. 12 pp. 2419-2456.

REGULARITIES IN THE LOCATION OF VOLCANOGENIC PYRITE-POLYMETALLIC DEPOSITS IN SIBERIA

Seravina T.V., Kuznetsov V.V.

Central Research Geological Prospecting Institute of Non-Ferrous and Precious Metals, Moscow, Russia, tanyaseravina@gmail.com

The most important factor in the formation of large reserves of pyrite ores is the connection with contrast or successively differentiated volcanogenic formations, the proximity of the ore source, the presence of structures that favored the accumulation and rapid burial of large ore bodies, and the long duration of ore formation processes against the background of the paleovolcanic regime (Dergachev, 2010; Kuznetsov, 2014). The most promising regions of the Russian Federation for the development of mineral resource base of polymetallic ores are: Rudnoaltay, Salair, Kyzyltashtyg and Priargun mineragenic zones. Polymetallic and pyrite-polymetallic deposits in volcanogenic associations (VHMS) and sedimentary rocks (SEDEX) have been identified within these zones. The pyrite-polymetallic deposits of the Rudnoaltay, Salair, Kyzyltashtyg and Priargun mineragenic zones are formed synchronously with volcanism.

The Rudnoaltay mineragenic zone includes Zyryanovsky, Leninogorsky, Zmeinogorsky, Rubtsovsky, Zolotushinsky and Priirtyshsky ore zones, which are confined to volcanogenic-sedimentary rocks. According to the composition, age and ratio of the volcanogenic and sedimentary components, these rocks are divided into two formations related to the potassium-sodium series and corresponding to two cycles of volcanism: the lower (ems-eifel-early givet) - successively

differentiated basalt-containing andesite-dacite-rhyolite calc-siliceous-terrigenous, and the upper (late givet-fran) - contrast basalt-rhyolite siliceous-terrigenous.

The mineralization of polymetallic and pyrite-polymetallic deposits of the Salair mineragenic zone (Pushtulimsky, Salairsky, Yelovsko-Kotorovsky and Ognevo-Romanovsky ore regions) is associated with two geological formations of the sodium series: the lower successively differentiated basalt-andesite-dacite-rhyolite and upper-contrast basalt-rhyolite . The deposits of these formations correspond to two cycles of volcanic activity in the region, as well as in the Rudnoaltai mineragenic zone (Seravina, 2017).

The ore-bearing Lower Cambrian (Riphean) volcanic rocks of the Kyzyltashtyg mineragenic zone belong to the contrast basalt-rhyolite formation (Distanov, 1977).

The Priargun mineragenic zone is divided into two subzones: actually, Priargunsky and Undino-Gazimursky, which have different metallogenic specialization. The Vend-Cambrian depressions are composed of carbonate-terrigenous rocks, to which are associated deposits of the Priargunsky type. They are inherited by volcano-tectonic depressions and volcanic depressions, composed of ore-bearing volcanogenic-terrigenous rocks, in which the deposits of Noyon-Tologoy type are localized. According to the model of pyrite-polymetallic deposits of the Noyon-Tologoy type ore-bearing formation is the medium-late Jurassic successively differentiated potassium-sodium (sodium) volcanogenic-siliceous terrigenous geological formation.

The analysis of the localization of the various objects of the Rudnoaltay, Salair, Kyzyltashtyg and Priargun mineragenic zones shows that the ore fields are confined to volcano-tectonic depressions. Their internal structure is complicated by small extrusive and lava domes; streams, associated with them small uncompensated basins, composed of intermediate, remote, often siliceous facies, corresponding to the deposits. The ratio of siliceous-terrigenous and volcanogenic rocks in its composition is determined on the one hand by the proximity of volcanic apparatuses (subvolcanic rocks - related to the vent's volcanic facies), and on the other by the nature and intensity of volcanic activity within the ore fields and deposits. Depressions that contain the deposits occupy over-dome, slope or supra-volcanic position, including on the sides of reef-building structures. There are stratified ore bodies, localized in the intermediate and remote facies of volcanism and the body, confined to extrusive and subvolcanic bodies of the vent facies. The position of the ore bodies of the deposits in the section is controlled by a thin alternation of volcanic and sedimentary rocks. Here they occupy a definite stratigraphic position, localizing among the primarily siliceous facies. This position of mineralization can be traced for many hundreds of meters, both in the fall and in the strike of the ore zones. Thus, the main ore bodies of the deposits are very compact, capturing a stratigraphic interval from 50 to 150 m, rarely 200 m.

The pyrite-polymetallic deposits, ore occurrences and mineralization points of the Rudnoaltay, Salair, Kyzyltashtyg and Priargun mineragenic zones are pyrite-polymetallic in mineral composition. They are represented by gold-silver-containing pyrites (barite) -polymetallic, copper-lead-zinc, copper-zinc-pyrite, copper-pyrite, sulfur-pyrite and quartz-carbonate-sulfide continuous massive, interspersed, veined ores. The main ore minerals are: pyrite, sphalerite, galena, arsenopyrite, chalcopyrite, boulangerite, jamsonite, tennantite, tetrahedrite; secondary - sulfosols of lead and silver, marcasite, chalcopyrite, burnonite; non-metallic: quartz, chlorite, dolomite, barite, talc and sericite.

Altered rocks in various quantities are present in all deposits and are represented by metasomatites of ore-bearing zones of hypogene leaching (quartz-sericite-chlorite) and precipitation (chlorite, sericite-chlorite). These and other metasomatites are products of acid leaching and sedimentation, belonging to the quartz-sericite formation. They are most clearly manifested in siltstones and tuffs of acidic composition. The intensity of manifestation and the morphology of the near-ore- altered rocks depends on the position of the deposits relative to the ore-supply channel. The host, near-ore-altered rocks and ores of most pyrite-polymetallic deposits are superposed with products of post-volcanic, dynamo-thermal and contact metamorphism with similar mineral complexes that change the appearance of ore fields and deposits. The most intensely metamorphosed zones correspond to the amphibole-hornfels facies of contact metamorphism, the others - muscovite-hornfels. Recrystallization of primary ore concentrations with the formation of aggregates with a predominance of granoblastic structures occurred during the recrystallization stage. Subsequently, partial or complete mobilization of ore matter took place with its subsequent redeposition.

References

Dergachev A.L. Evolution of volcanogenic pyrite formation in the history of the Earth. Moscow State University. 2010 262 p (in Russian).

Distanov E.G. Pyrite-polymetallic deposits of Siberia. Novosibirsk: Nauka. 1977. 350 p (in Russian).

Kuznetsov V.V., Kudryavtseva N.G., Galyamov A.L., Kuznetsova S.V., Seravina T.V., Geological and genetic basics of forecasting and searching of pyrite-polymetallic deposits of Rudnoaltay type // Domestic Geology, 2014, No. 2, p. 30-38 (in Russian).

Seravina T.V., Inyakin A.V., Kuznetsov V.V., Murzin O.V., Zayatdinov M.R., Konkina A.A., Kudryavtseva N.G., Features and conditions of accumulation of volcanogenic-sedimentary rocks of the Lower Cambrian (Salair Range) // Domestic Geology, 2017, No. 2, p. 22-30 (in Russian).

GEOCHEMICAL FEATURES OF THE MID-PALEOPROTEROZOIC TIKSHEOZERO ULTRAMAFITE-ALKALINE-CARBONATITE COMPLEX, NORTHERN KARELIA

***Sharkov E.V.*[1], *Chistyakov A.V.*[1], *Bogina M.M.*[1], *Shchiptsov V.V.*[2], *Belyatsky V.B.*[3], *Frolov P.V.*[2]**

[1]*Institute of Geology of Ore Deposits, Petrography, Mineralogy and Geochemistry RAS, Moscow, Russia, sharkov@jgem.ru*

[2]*Institute of Geology of the Karelian Scientific Center RAS, Petrozavodsk, Russia*

[3]*Federal State Budgetary Enterprise 'A.P. Karpinsky Russian Geological Research Institute, Saint-Petersburg, Russia*

The Tiksheozero ultramafic-alkaline-carbonatite complex in the Northern Karelia is one of the world's oldest (~2000 Ma: Corfu et al., 2011) intrusions of this type. The Tiksheozero complex together with the adjacent Elet'ozero syenite-gabbro complex (2086±30 Ma: Sharkov et al., 2015), belongs to the Mid-Paleoproterozoic Jatulian-Ludicovian large igneous province in the eastern Fennoscandian Shield (Sharkov, Bogina, 2006). However, as compared to the Elet'ozero complex, the Tiksheozero Complex consists mainly of clinopyroxenites, with significant role of carbonatites and foidolites, at relatively low content of Fe-Ti oxides. Nevertheless, available studies of the Tiksheozero complex were mainly focused on carbonatites completing the evolution of this complex (Shchiptsov et al., 2007; Ivashchenko, Golubev, 2011; Tichomirowa, 2006; Kuleshevich, 2016), whereas data on the main phases of the complex are practically absent. In order to fill this gap, we carried out the geochemical study of ultramafic and alkaline components of this complex.

The complex about 24 km^2 in area is hosted in Archean granite-gneisses and early Paleoproterozoic granites (Fig. 1). It is generally accepted that it was formed in several phases: (1) olivinites, clinopyroxenites; (2) foidolites and theralites, (3) nepheline syenites; and (4) carbonatites. Calcite carbonatites with apatite usually contain rare-metal (Zr, Nb, Ta) mineralization; dolomite-calcite carbonatites were found mainly in Vostochny block.

The ultramafic rocks of the first intrusive phase are low-Ti (TiO_2 – 0.41-0.78 wt %) high-Mg (#Mg – 80-86) rocks, which is determined by variable amount of diopside and olivine, as well as low content of Fe-Ti oxides. They are ascribed to the rocks of normal alkalinity (Na_2O+ K_2O up to 0.72 wt %). Rare ore clinopyroxenite contains up to 6.06 % TiO_2 and up to 45 wt % Fe_2O_3. Melilitolites are high-Ca ultramafic rocks with Mg# from 45 to 58. Foidolites are represented by alkaline Ne-Cpx rocks of the jacupirangite-melteigite-ijolite series with significant variations of alkalis: from a few percents in jacupirangite to 9% in melteigite; Mg# also shows significant variations from 45 to 67. The latest rocks of the Tiksheozero complex are mainly calcite low-Mg, low-Fe carbonatites as well as carbonate-silicate rocks, which show significant variations in composition and are enriched in Na_2O and Al_2O_3 relative to the rocks of the earlier phases.

Geochemical features of studied rocks are illustrated in Fig. 2. All the rocks are enriched in large-ion lithophile elements (LILE), while alkaline rocks are additionally enriched in HFSE. Chondrite-normalized REE patterns show variable fractionation. The rocks show increase in the total REE from clinopyroxenites through ijolite-melteigites and melilitolites, to carbonate-silicate rocks and

carbonatites. The lowest REE fractionation is observed in clinopyroxenites and the highest, in the carbonate-silicate rocks and carbonatites.

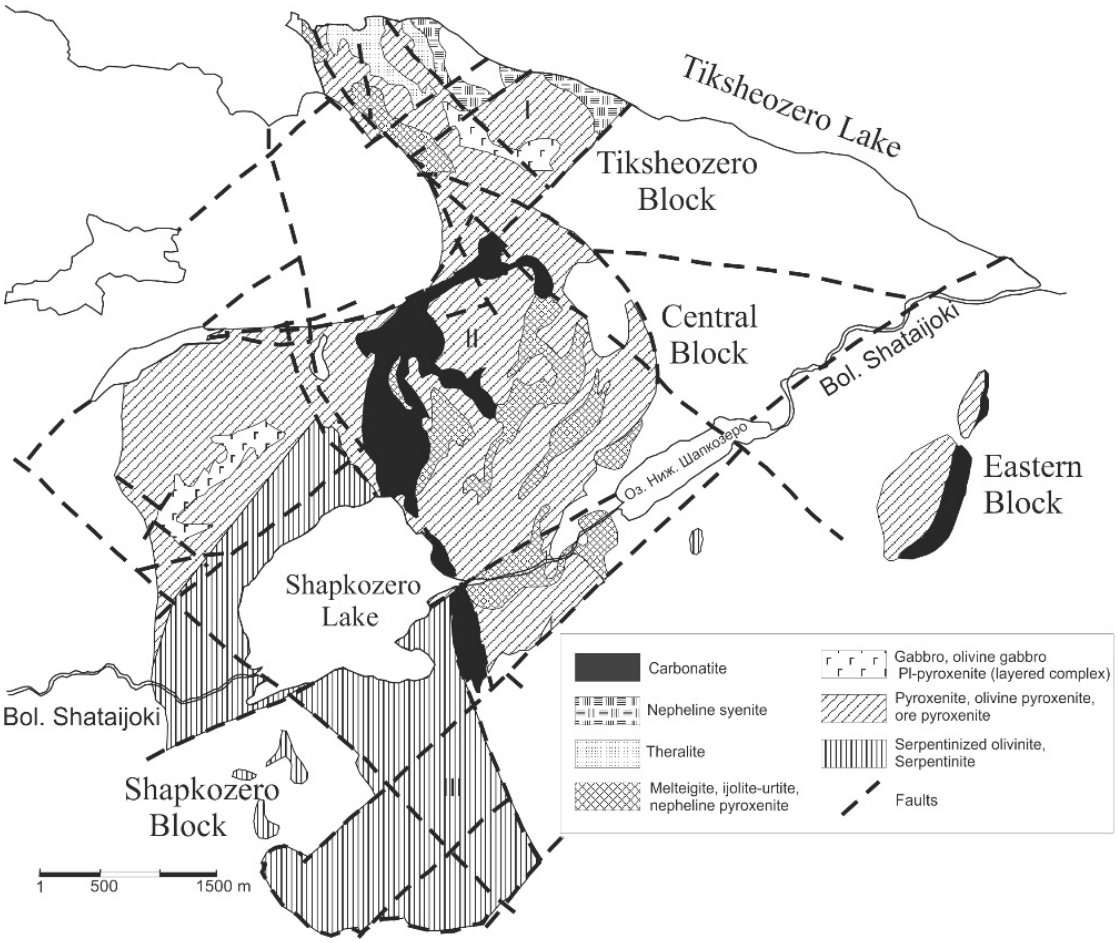

Fig. 1. Schematic geological map of Tiksheozero complex (after Kholodilov and Karpatenkov,1988; Shchiptsov et al., 2007; Ivashchenko, Golubev, 2011).

Clinopyroxenites and melteigite-urtites form complementary plots and, correspondingly, the clinopyroxenites can be considered as cumulus rocks formed through precipitation of clinopyroxene and olivine. It is noteworthy that ore clinopyroxenites has extremely high HFSE contents, and enriched in REE, especially LREE. Melilitolites with steep REE pattern were presumably formed from a distinct, deep-seated garnet-bearing source. Theralites also have highly fractionated REE pattern and could be considered as derivatives of melilitolite.

The typomorphic feature of all carbonatite rocks is the strongest negative Zr-Hf anomaly (Fig. 2). It is seen that the studied melilitolites and theralites also have well pronounced deep Zr-Hf anomaly, which suggests their relation with a carbonatite-metasomatic event. At the same time, the lack of Zr-Hf anomaly in the foidolites suggests their independent evolution, with no contribution from a carbonatite melt/fluid.

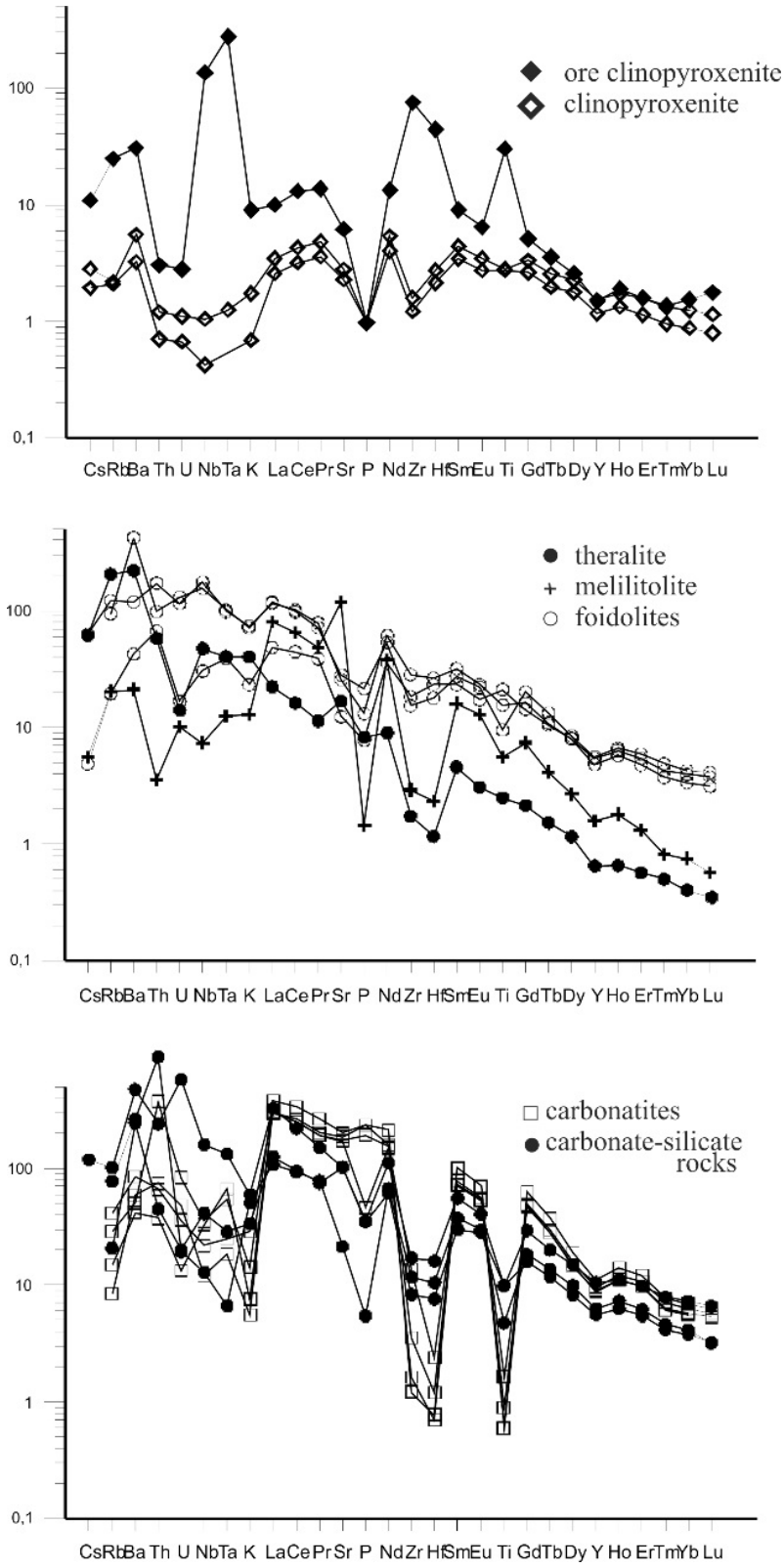

Fig. 2. PM-normalized spidergram of rocks of the Tiksheozero complex. Data on carbonatites after L.V. Kuleshevich (2011).

In this respect, this complex is similar to syenite-gabbro complexes (intrusive versions of basalt-trachyte suite) where syenites have no genetic relation with gabbros, and are separated by a Daly Gap. Study of mantle xenoliths in basalts and melt-pockets in them showed that primary melts of these suites (Fe-Ti basalts and trachytes, respectively) were generated in the same mantle plume head owing to adiabatic melting of the inner part of the head (basalts) and incongruent melting of its cooled margin

above zone of adiabatic melting under the influence of exolsved fluids (trachytes) (Sharkov, Bogatikov, 2017). In our case ultramafites and foidolites, on the one hand, and carbonatites and carbonate-silicate rocks, on the other hand, also have independent origin. Moreover, the study of mantle xenoliths in basalts of Spitsbergen and Cape Verde islands revealed the existence of carbonatite and carbonate- silicate melt-pockets in xenoliths of spinel lherzolites (Ionov et al., 1996). So, we suggest that the origin of carbonatite and carbonate-silicate melts was related to incongruent melting of cooled margins of mantle plume heads under the influence of carbonate mantle fluids related to the mantle plume material.

References

Corfu F. et al. U-Pb ID-TIMS age of the Tikshozero carbonatite: expression of the 2.0 Ga alkaline magmatism in Karelia, Russia // Cent. Eur. J. Geosci. 2011. V. 3. N 3. P. 302-308.

Ivashchenko V.I. and Golubev A. I. Gold and platinum of Karelia: genetic types of mineralization and prospects. Petrozavodsk: KNTS RAS, 2011, 369 p. (in Russian).

Ionov D.A. et al. Carbonate-bearing mantle peridotite xenoliths from Spitsbergen: phase relationships, mineral composition and trace-element residence // Contrib. Miner. Petrol. 1996. V. 125. # 4. P. 375-392.

Kuleshevich L.V. Rare-earth mineralization of the Tiksheozero-Elet'ozero alkaline complex (North Karelia) // Geology and Mineral resources of Karelia. Petrozavodsk: KNTS RAS. 2016. № 18. P. 71-87 (in Russian).

Sharkov E.V. et al. Genesis and Age of Zircon from Alkali and Mafic Rocks of the Elet'ozero Complex, North Karelia // Petrology. 2015. V. 23. No 3. P. 259-280.

Sharkov E.V., Bogatikov O.A. A Likely Reason for the Appearance of the Daly Gap in Magmatic Series of Large Igneous Provinces: Geological and Petrological Evidence // Doklady Earth Sci. 2017. V.472. Part 2. P. 231-236.

Sharkov E.V., Bogina M.M. Evolution of the Paleoproterozoic magmatism: geology, geochemistry, and isotopic constraints // Stratigr. Geol. Correl. 2006. Vol. 14. N 4. P. 345-367.

Shchiptsov V.V. et al. Geological, technological, and economic appriasal of the potential of carbonatite resources of the Tiksheozero intrusion (association of alkaline and carbonatite rocks) // Geology and Mineral resources of Karelia. Petrozavodsk: KNTS RAS. 2007. No.10. P. 159-170 (in Russian).

Tichomirowa M. et al. The mineral isotope composition of two Precambrian carbonatite complexes from the Kola Alkaline Province – Alteration versus primary magmatic signatures // Lithos. 2006. V. 91. P. 229–249.

CARBONATE INCLUSIONS IN MANTLE-DERIVED CR-PYROPES FROM THE CHOMPOLO LAMPROPHYRES, ALDAN SHIELD, SIBERIAN CRATON DERIVED

Sharygin I.S.[1], Nikolenko E.I.[1], Priimak V.V.[2], Lobov K.V.[1], Rezvukhin D.I.[1]

[1]Sobolev Institute of Geology and Mineralogy, Siberian Branch of Russian Academy of Sciences, Novosibirsk, Russia, isharygin@igm.nsc.ru, igor.sharygin@gmail.com

[2]Department of Geology and Geophysics, Novosibirsk State University, Novosibirsk, Russia

Here we present results of the micro-Raman spectroscopy, SEM-EDS and EPMA studies of carbonate-bearing mineral inclusions in mantle-derived xenocrysts of lherzolitic Cr-pyrope from the Aldan dike and Ogonyok pipe of the Chompolo field, Aldan shield of the Siberian craton. There are ten dikes, pipes and vein bodies within the Chompolo field. The magmatic rocks of the Chompolo field were previously interpreted as kimberlites, however, recent studies re-classified their as lamprophyres (Kornilova, 1997).

The chemistry of the studied garnets, namely their high Cr_2O_3 contents and Mg#, clearly points to their mantle origin (Sobolev et al., 1973; Schulze, 2003). The host garnets are Cr-rich (0.4-7.0 wt%) pyropes with Mg# = 73-85, Ca# = [100·Ca/(Ca+Mg+Fe+Mn)] = 10-17 and TiO_2 contents below 0.4 wt%. They belong to lherzolitic paragenesis in terms of CaO and Cr_2O_3 contents. The inclusions of

olivine, clinopyroxene and Cr-spinel in Cr-pyropes also suggest the mantle origin of the parent peridotites.

Among studied samples twelve garnet grains contain dolomite-bearing inclusions, ten – magnesite-bearing inclusions, and five – calcite-bearing inclusions. Cr-pyrope crystals enclose either single or multiple individual mineral inclusions. There are monomineralic and composite mineral inclusions (Fig. 1). Other minerals found along with carbonates within inclusions in the Chompolo garnets are olivine, clinopyroxene, Cr-spinel, phlogopite, amphibole, talc, rutile, Mg-ilmenite, minerals of the crichtonite group, apatite, baryte, graphite, and sulphides.

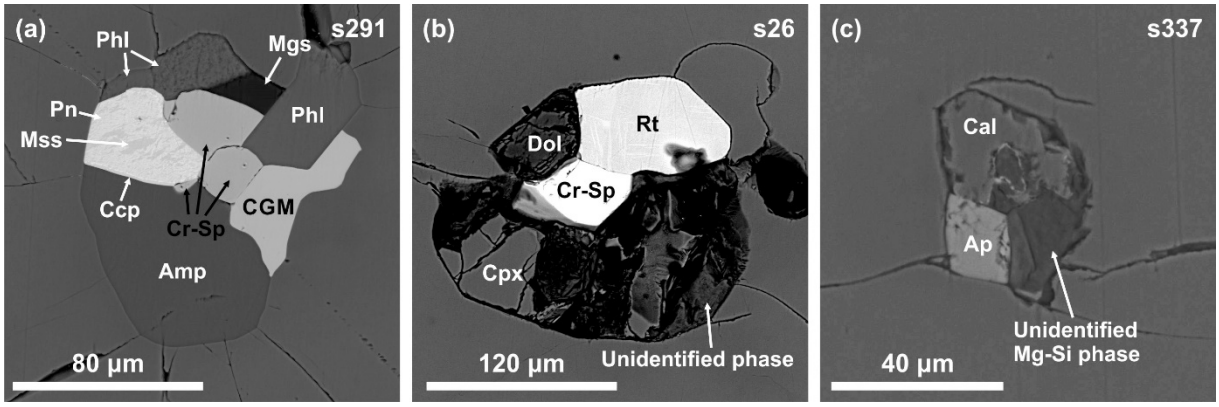

Fig. 1. Back-scattered electron images of carbonate-bearing inclusions in mantle-derived garnets from the Chompolo lamprophyres. Mgs – magnesite, Dol – dolomite, Cal – calcite, CGM – crichtonite-group mineral, Ap – apatite, Phl – phlogopite, Amp – amphibole, Rt – rutile, Cr-Sp – Cr-spinel, Cpx – clinopyroxene, Mss – monosulphide solid solution, Pn – pentlandite, Ccp – chalcopyrite.

Thermobarometric calculations applied to carbonate-bearing garnets yielded pressure range of 2.6-3.6 GPa and temperature interval of 680-920 °C; these values likely reflect the ambient PT-conditions during the residence of studied samples within the mantle. The residual pressure up to 2.1 GPa was inferred for graphite inclusions assuming pressure dependence of the graphite G-band upshift (Nikolenko et al., 2017).

Mantle metasomatism refers to the process of compositional and mineralogical changes of mantle rocks due to interaction with mantle fluids or melts. Several different metasomatic agents have been proposed, ranging from supercritical hydrous fluids to silicate and carbonate melts. There is a consensus that volatile-bearing minerals (mica, amphibole, and apatite) and titanium-rich minerals such as rutile and minerals of the crichtonite group are of metasomatic origin in mantle peridotites (Haggerty, 1991; Wang et al., 1999; Pearson et al., 2003; Konzett et al., 2013; Malkovets et al., 2016; Rezvukhin et al., 2016). We interpreted the shape, composition, and distribution of carbonate-bearing mineral inclusions in Chompolo garnets as evidence of their syngenetic origin with the host garnets. Therefore, studied mineral inclusion assemblages suggest an episode(s) of mantle metasomatism in the lithospheric mantle of the Siberian craton beneath the Aldan shield, contemporaneous with the formation of host Cr-pyrope crystals. The presence of carbonate and graphite within inclusions in Cr-pyropes indicates that metasomatic agent(s) was CO_2-rich melt (i.e., carbonate melt) or COH fluid.

This work was supported by the grants Nos. 16-35-60052 mol_a_dk and 15-05-04885 from the Russian Foundation for Basic Research and the RF state assignment project No. 0330-2016-0006.

References

Haggerty S.E. Oxide mineralogy of the upper mantle // Rev. Mineral. Geochem. 1991. Vol. 25. pp. 355-416.

Konzett J. et al. Two episodes of fluid migration in the Kaapvaal Craton lithospheric mantle associated with Cretaceous kimberlite activity: evidence from a harzburgite containing a unique assemblage of metasomatic zirconium-phases // Lithos. 2013. Vol. 182, pp. 165-184.

Kornilova V.P. Petrography and mineralogy of the calc-alkaline lamprophyres and eruptive breccias at the basin of Chompolo river // Otechestvennaya Geologiya. 1997 Vol. 9. pp. 6-9.

Malkovets V.G. et al. Cr-rich rutile: A powerful tool for diamond exploration // Lithos. 2016. Vol. 265. pp. 304-311.

Nikolenko E.I. et al. Graphite-bearing mineral assemblages in the mantle beneath Central Aldan superterrane of North Asian craton: combined confocal micro-Raman and electron microprobe characterization // J. Raman Spectrosc. 2017. Vol. 48. pp. 1597-1605.

Pearson D.G., Shirey S.B., Canil D. Mantle samples included in volcanic rocks: xenoliths and diamonds. In: Carlson RW, Holland HD, Turekian KK (eds) Treatise on Geochemistry, Vol 2: Geochemistry of the Mantle and Core. Elsevier, Amsterdam, 2003. pp. 171-275.

Rezvukhin D.I. et al. Inclusions of crichtonite-group minerals in Cr-pyropes from the Internatsionalnaya kimberlite pipe, Siberian Craton: Crystal chemistry, parageneses and relationships to mantle metasomatism // Lithos. 2018. Vol. 308-309. pp. 181-195.

Schulze D.J. A classification scheme for mantle-derived garnets in kimberlite: a tool for investigating the mantle and exploring for diamonds // Lithos. 2003. Vol. 71. pp. 195-213.

Smelov A.P., Timofeev V.F. The age of the North Asian Cratonic basement: an overview // Gondwana. Res. Vol. 12. pp. 279-288.

Sobolev N.V. et al. Chrome-rich garnets from the kimberlites of Yakutia and their parageneses // Contrib. Mineral. Petrol. 1973. Vol. 40. pp. 39-52.

Wang L. et al. Mineral inclusions in pyrope crystals from Garnet Ridge, Arizona, USA: implications for processes in the upper mantle // Contrib. Mineral. Petrol. 1999. Vol. 135. pp. 164-178.

FELDSPARS AND FELDSPATHOIDS FROM FUMAROLE SUBLIMATES OF THE TOLBACHIK VOLCANO (KAMCHATKA, RUSSIA)

***Shchipalkina N.V.*[1,2], *Pekov I.V.*[1,3], *Koshlyakova N.N.*[1], *Sidorov E.G.*[4]**

[1]*Faculty of Geology, Lomonosov Moscow State University, Moscow, Russia*

[2]*Shubnikov Institute of Crystallography and Photonics RAS, Moscow, Russia*

[3]*Vernadsky Institute of Geochemistry and Analytical Chemistry RAS, Moscow, Russia*

[4]*Institute of Volcanology and Seismology, Far Eastern Branch of RAS, Petropavlovsk-Kamchatsky, Russia*

The discovery of various tecto-aluminosilicates in sublimates of the active Arsenatnaya fumarole located at the Second scoria cone of the Northern Breakthrough of the Great Tolbachik Fissure Eruption (Tolbachik volcano, Kamchatka) was unexpected. They include different feldspars (potassic feldspar, anorthoclase, andesine, labrador, bytownite, anorthite, members of the series between celsian and alkali feldspars) and feldspathoids (kalsilite, nepheline, sodalite and haüyne) associated with hematite, tenorite, aphthitalite, langbeinite, anhydrite, metathénardite, sylvite, halite, diverse arsenates, *etc*.

Tecto-aluminosilicates occur here as white or colorless crystals up to 0.2 mm in size (Fig. 1) or form (feldspars) crusts up to 1 mm thick covered or replaced basalt scoria.

In general *chemical composition* of tecto-aluminosilicates from the Arsenatnaya fumarole and other geological formations is different. This fact is due to unusual conditions of crystallization at low (atmospheric) pressure and high temperatures involving volcanic gas, enriched not only by Na, K, S, Cl, F, and O but also As, Cu, Zn, Mo, W and other "ore" components, as a carrier.

The impurity of As_2O_5 is inherent for practically all silicates. Its content is (wt. %) up to 25.5 for potassic feldspar, up to 1.1 for K-Na feldspar, up to 1.4 for bytownite, up to 2.8 for kalsilite and nepheline, up to 1.6 for sodalite, and up to 2.5 for haüyne. As^{5+} substitutes Si in tetrahedral Al-Si-O frameworks of feldspars and feldspathoids.

Compositional variations of feldspars from the Arsenatnaya fumarole are shown in Fig. 2.

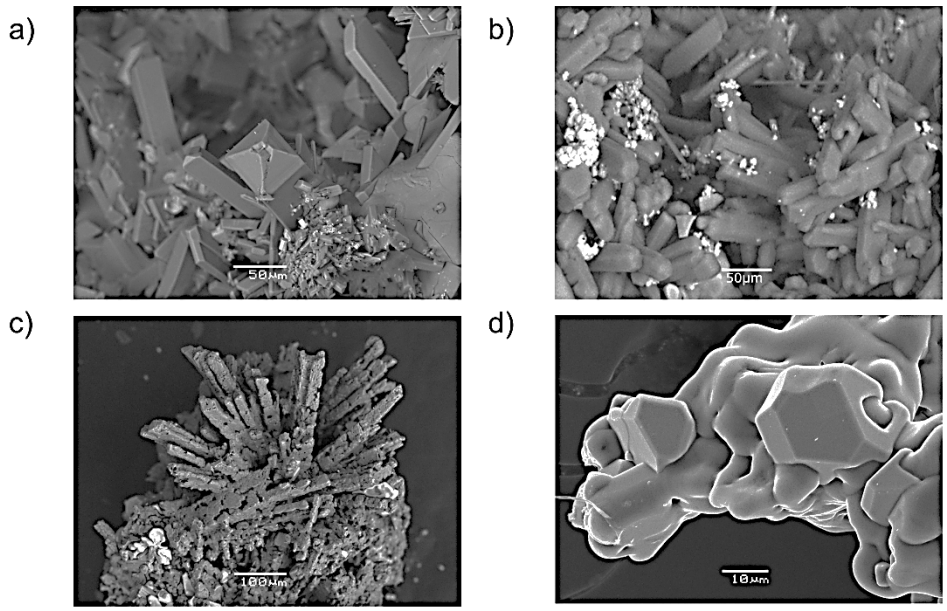

Fig. 1. Typical crystals and aggregates of potassic feldspar (a), kalsilite (b), sodalite (c) and haüyne (d). Backscattered-electron images (a – c) and secondary-electron image (d).

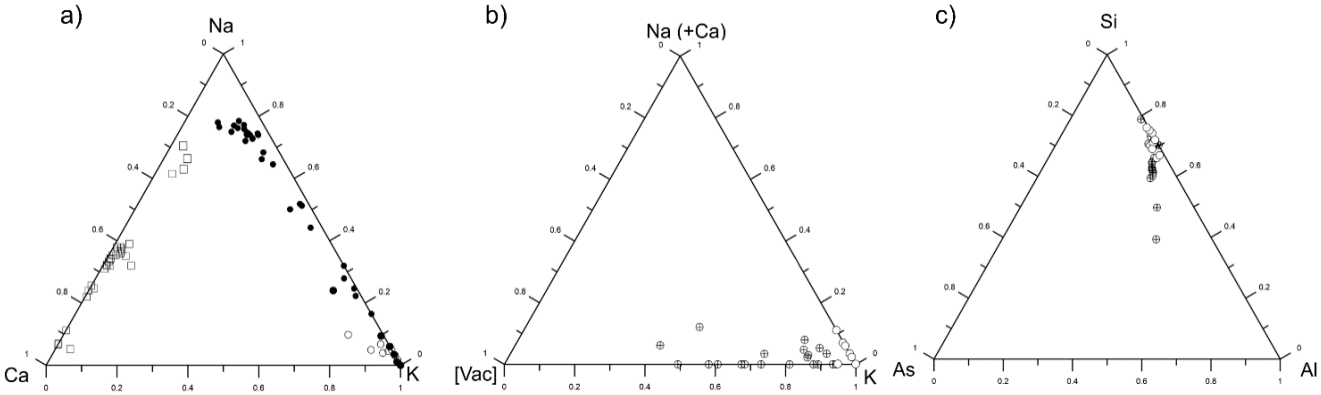

Fig. 2. Ratios of major extra-framework cations in *different feldspars* from the Arsenatnaya fumarole: (a): ○ – As – bearing potassic feldspar, ● – K–Na – feldspar, □ – plagioclase (from anorthite to andesine); ratio of extra-framework and framework components (including vacancy [Vac]) (b and c): in *potassic feldspar* - ○ and As-bearing potassic feldspar - ⊕.

There are two varieties of As-bearing potassic feldspar: (1) with ordinary feldspar stoichiometry and (2) with deficiency of extra-framework cations. The first group represents an isomorphous series $KAlSi_3O_8$ – KAl_2AsSiO_8 (idealized formula of filatovite) with the main substitution schemes $2Si^{4+} \leftrightarrow Al^{3+} + As^{5+}$ and $Al^{3+} + Si^{4+} \leftrightarrow Zn^{2+} + As^{5+}$ (the latter was suggested by Vergasova et al., 2004). In the second group the surplus of positive charge could be balanced by vacancies in the extra-framework sites: $[vac]^0 + As^{5+} \leftrightarrow K^+ + Si^{4+}$. Such feldspar was firstly reported by Koshlyakova et al. (2014) from the same locality.

Members of the celsian-anorthoclase series occur in deeper zones of the Arsenatnaya fumarole as tiny inclusions (less than 10 μm) in open-work aggregates of diopside and hematite. The representative empirical formulae of these minerals, based on 8 O atoms, are $(Na_{0.31}Ba_{0.28}K_{0.27}Sr_{0.12}Ca_{0.05})_{\sum 1.03}(Si_{2.50}Al_{1.47}Fe^{3+}_{0.02})_{\sum 3.99}O_8$ and $(Ba_{0.57}Sr_{0.17}K_{0.10}Na_{0.09}Ca_{0.06})_{\sum 0.99}(Si_{2.10}Al_{1.86}Fe^{3+}_{0.07})_{\sum 4.03}O_8$.

Haüyne and sodalite from the Arsenatnaya fumarole are characterized by wide variations of contents of both cations and anions extra-framework components (Fig. 3).

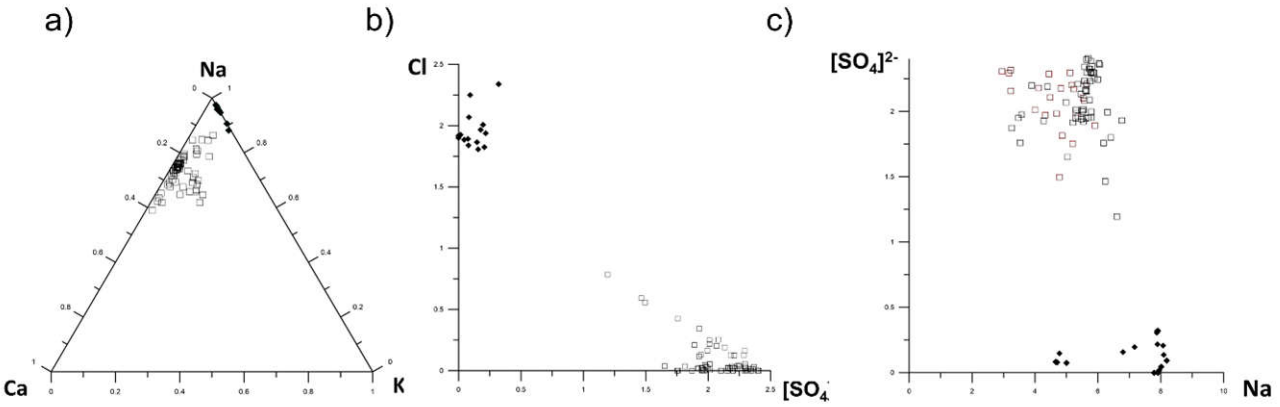

Fig. 3. Ratios of major extra-framework cations and anions in sodalite (black rhombs) and haüyne (blank squares) from the Arsenatnaya fumarole.

These variations could be described by the following major substitution scheme: $Na^+ + Cl^- \leftrightarrow Ca^{2-} + SO_4^{2-}$. In the haüyne part of the isomorphous series the continuous solid solution with the limits $Haü_{100}$ – $Haü_{63}$ was observed. Similar situation was reported for synthetic analogues of haüyne and sodalite by Van Peteghem and Burley (1963), but within the limits $Haü_{100}$ – $Haü_{75}$. Another interesting chemical feature of haüyne from Arsenatnaya is the presence of MoO_3 and WO_3 impurities, up to 4.2 and 1.7 wt.%, respectively. These components have not been reliably found in minerals of the sodalite-group yet. However, synthetic sodalite-type aluminates with extra-framework anions MoO_4^{2-} and WO_4^{2-} are known (Depmeier, 1999).

Powder and single-crystal X-ray diffraction studies of sodalite, haüyne, kalsilite and As-bearing potassic feldspar gave the following data. (1) Sodalite and Mo,W-free haüyne have the space group *P*-43*n* and unit-cell parameter *a* = 8.8793(3) and 8.882(4) Å, respectively. This space group confirms that Si and Al are ordered in the tetrahedral framework. The unit cell of a Mo,W- bearing haüyne corresponds to orthorhombic model: *a* = 12.87(4), *b* = 12.87(4), *c* = 9.11(3) Å. This mineral is suggested to be orthorhombic by analogy with so-called CAM compound (Depmeier, 1999). (2) Kalsilite possesses space group $P6_3$ with unit-cell parameters *a* = 5.1562(5), *c* = 8.6888(11) Å. Si and Al are ordered in the framework. According to (Carpenter, Cellai, 1996; Cellai et al. 1999), kalsilite with space group $P6_3$ crystallizes at $t > 500^oC$, while at the lower temperatures the modification with space group *P*-31*c* is stable. (3) As-bearing potassic feldspar is closer to orthoclase then other forms of $KAlSi_3O_8$ on the powder X-ray diffraction pattern. However, its unit-cell parameters, especially, α = 91.32(1) - 95.71(3)° and γ = 92.36(1) – 94.61(2)° differ from 90° and β = 108.2(2)° (for typical orthoclase β is close to 116°). Such differences could be due to a unit cell distortion caused by significant As^{5+} impurity.

This work was supported by the Russian Foundation for Basic Research, grants nos. 18-05-00332 (studies of kalsilite) and 18-05-00051 (studies of sodalite-group minerals).

References

Carpenter M.A. and Cellai D. Microstructures and high-temperature phase transitions in kalsilite//American Mineralogist. 1996. Vol. 81 pp.561–584.

Cellai D. et al. X-ray study of the trigonal—hexagonal phase transition in metamorphic kalsilite// American Mineralogist. 1999. Vol. 84 pp.1950–1955.

Depmeier W. Structural distortions and modulations in microporous materials// Molecular Sieves. 1999 Vol. 2 pp.113-137.

Koshlyakova et al. As-bearing potassium feldspar – the product of fumarolic exhalations and gas metasomatism on the Tolbachik volcano, Kamchatka, Russia// XXXI International Conference "The Potential of Alkaline, Kimberlite and Carbonatite Magmatism". 2014. pp.55-56.

Pekov I.V. et al. Fumarolic arsenates – a special type of arsenic mineralization// European Journal of Mineralogy. 2018. DOI: https://doi.org/10.1127/ejm/2018/0030-2718.

Van Peteghem J.K. and Burley B.J. Studies on solid solution between sodalite, nosean and hauyne// Canadian Mineralogist. 1963. Vol. 7 pp.808-813.

Vergasova L.P. et al. Filatovite, $K[Al,Zn)_2(As,Si)_2O_8$, a new mineral species from the Tolbachik volcano, Kamchatka peninsula, Russia// European Journal of Mineralogy. 2004. Vol. 16 pp.533-536.

INVESTMENT OPPORTUNITY FOR THE CHERNIGIVKA CARBONATITE DEPOSIT IN UKRAINE

Sheremet E.M., Kozar N.A., Setya L.D., Agarkova N.G.

M.P. Semenenko Institute of geochemistry, mineralogy and ore formation of the National Academy of sciences of Ukraine, Kyiv, Ukraine, evgsherem53@gmail.com, kozar.geolog@rumbler.ru, lasetaya@yandex.ru, nataagarkova@yandex.ru

The Chernigivka Carbonatite Massif (the West Azov Domain of the Ukrainian Shield) constitutes a part of the Chernigivka carbonatite zone [1]. Alkaline rocks and carbonatites are revealed by drilling down to 1,300 m depth. Carbonatites at the Chernigivka site attain a thickness of 400 to 450 m, and 9 major and a series of thin carbonatite bodies are delineated at the deposit. The thickness of ore bodies varies from 30–40 to 170 m. The ore productivity coefficient for fresh carbonatite is 0.96–1.00 and for the weathering crust is 0.7 to 1.0. According to the classification of reserves this deposit belongs to the 2nd group.

Ore bodies are represented by calcite, calcite-dolomite and dolomite carbonatites. Carbonatites contain apatite ores. The cutoff grade for P_2O_5 is 2.5 %, being 7.5 % at conditions of natural occurrence of carbonatites. The average concentration of P_2O_5 in carbonatites is 4.3 % and in the weathering crust it is 8 %.

The main accessory minerals in carbonatites are pyrochlore, fergusonite, columbite, baddeleyite, rutile, titanite, allanite, zircon, and monazite.

The main metallogenic characteristics of the Chernigivka carbonatite massif are as follows.

i) Carbonatites are highly enriched in REE (the average concentration is 0.15 %, the highest concentrations are 2-3 %) and moderately enriched in Nb (from 50 to 1,300 ppm, the average concentrations are 100–500 ppm) with low content of Zr (50–150 ppm, reaching in places 0.2 to 0.3 %) (Sheremet E.M. et al., 2017).

ii) The main Nb ore minerals in carbonatite are pyrochlore, Ce-fergusonite and columbite and REE ore minerals are monazite, apatite and to some degree allanite.

Carbonatites of the Chernigivka massif must be considered primarily as complex rare-metal apatite ores with average concentration of apatite around 10 %. Monazite of the Chernigivka carbonatites is also of interest as it is virtually thorium-free.

The Novopoltavka (the Chernigivka) carbonatite rare-metal apatite deposit is classified as large complex object. The average concentrations (%) are: P_2O_5 3–4; Nb_2O_5 0.06–0.30; Ta_2O_5 0.002–0.003; TR_2O_3 0.17–4.60 (Castor, 2008).

A feasibility study of final mining parameters is based on the following technical and economical indices: the integral capacity of two ore mines will be annually 13 MT of ore and 12.45 KT of P_2O_5. Concentration recovery of apatite is 78.8 % from the weathering crust and 80.0 % from the fresh ore. The quality of apatite concentrate is 37 %, in which case the resulting carbonate concentrate will be c. 3,960 KT, magnetite concentrate (66 % Fe and 0.07 % P) – 326 KT, and the rare-metal complex concentrate from rare-metal apatite ores together with their reserves will amount to 299.6 MT.

Calculated commercial reserves are as follows: weathered crust apatite ores + fresh carbonatite ores – 590 MT, of which P_2O_5 – 36.38 MT with the average concentration of 9.6 %, $\sum TR_2O_3$= 1.65 MT with the average concentration of 1.3 %; magnetite concentrate – 6.3 MT; rare-metal apatite ores – 413 MT, of which P_2O_5 – 15.845 MT with the average concentration of 9.1 %, $\sum TR_2O_3$ – 1.24 MT

with the average concentration of 0.36 %; Nb_2O_5 – 325 KT with the average concentration of 0.08 %; reserves related to apatite – $\sum TR_2O_3$ – 567 KT with the average concentration of 1.46 %; magnetite concentrate – 8.96 MT. In addition, reserves of Nb and Zr ores outside of apatite ores were estimated and comprise of: ZrO_2 – c. 220 KT with the average concentration of 0.5 %; Nb_2O_5 – c. 38 KT with the average concentration of 0.2 %.

A comparison of the Chernigivka carbonatite deposit with the Bayan Obo deposit in China shows that the Bayan Obo deposit has larger reserves reserves. The Bayan Obo expected reserves comprise of up to 1,500 MT of iron ore (35 % wt. Fe), 48 MT of REE (6 % wt. TR_2O_3) and 1 MT of Nb (0.13 % wt. Nb). The Bayan Obo Mine produced 55,300 tons of TR_2O_3 in 2005 accounting for 47 % of the total REE production of China and 45 % of that in the world (Castor, 2008). REE occur dominantly in monazite and bastnasite. The Bayan Obo ores are hosted by dolomite associated with apatite, fluorite, barite, albite, aegirine, aegirine–augite and altered phlogopite. They have very high content of REE (6 %) and extremely high LREE/HREE (LREE/HREE) ratios.

A comparison of the Chernigivka carbonatite deposit with the Mountain Pass deposit in North America also shows that the latter has larger reserves. The Mountain Pass Mine proved and probable ore reserves were estimated in 1987 and were 29 MT with average content 8.9 % of rare-earth oxides and 5 % of cutoff grade (Castor, 2008).

In any case, the Chernigivka deposit is a large enough deposit. Like other REE deposits in Ukraine (the Azov, Mazursvka, and Anadol deposits) it is not being mined yet. However, taken together they might be the main deposits for establishing the rare-earth industry in Ukraine.

References

Sheremet E.M. et al. Prospects of finding of deposits of a new type of rare-earth ores in the Azov Domain of the Ukrainian shield / E. M. Sheremet, S. G. Kryvdik, S. N. Strekozov; M. P. Semenenko Institute of geochemistry, mineralogy and ore formation of the National Academy of sciences of Ukraine, 2017. – 244 p.

Castor S.B. Rare earth deposits of North America // Resource Geology. – 2008. – N 58. – P. 337-347.

HIDDEN CARBON ROOTS OF ORE FORMING SYSTEMS

***Simakin A.G.*[1], *Salova T.P.*[1], *Nekrasov A.N.*[1], *Gabitov R.I.*[2], *Kubrakova I.V.*[3], *Korost D.*[4]**

[1]*Korzhinsky Institute of Experimental Mineralogy of the Russian Academy of Sciences, Chernogolovka, Russia, simakin@iem.ac.ru*

[2]*Department Geosciences at MSU, USA*

[3]*Vernadsky Institute of Geochemistry and Analytical Chemistry of the Russian Academy of Sciences, Moscow, Russia*

[4]*Lomonosov Moscow State University, Moscow, Russia*

Ore formation is a multi-step process, and more attention is usually paid to the culminate stages yielding the greatest economic concentrations. For example, in the formation of Au deposits of the formation of black shale, the fluid in the last stage contains water and dissolved salts, so that at their geochemical modeling various aspects of the CO_2-H_2O-NaCl system arise (Bortnikov et al., 2007). At the same time, the very process of the black shale formation (e.g., Sukhoi Log, East Siberia) caused the accumulation of a specific group of elements, including Au, Mo, V, Mn, Ba, Cr, Ni, Co (Chang et al., 2008), deposited at the bottom of the shallow see, presumably from the deep fluid. Siderophile metals, PGE and Au (Ni- PGE-Au) are associated in the Mo ores of Zunyi deposit, Tibet (Coveney and Nansheng, 1991). Such associations can be linked with the presence of the organometallic compounds in the root zone of the ore forming systems at the high pressure and temperature.

Many classes of organometallic compounds can exist in nature. At the high temperature the simplest compounds of carbon are stable such as CH_4, CO, COS, CH_4S_2. Currently we are working on the pi-complexes of the transitional d-elements and Au^+. Such complexes can form when pi-bonded carbon atoms present in the molecule structure. In the sequence CO, C_2H_4, C_2H_2, carbon monoxide

forms the strongest pi-bonds with metals and, therefore, carbonyls are the most stable compounds. At the ambient conditions (T=298 K, 1 bar) stable carbonyls are known for many elements: Ni, Co, Re, Cr, W, Mo, PGE. However, individual gaseous or liquid carbonyls for Pt and Au at atmospheric pressure are unknown. We study experimentally solubility of Au and Pt as carbonyls in the dry reduced carbonic fluid at P=2-3 kbar and T=900-1100ºC. We worked with dry fluid in Pt capsules in IHPV. As a source of CO-CO_2 fluid we used $FeCO_3$ or MgC_2O_4 thermally decomposed during the experiment. Oxygen fugacity was near Wu-Mt buffer (or CCO at these PT). It was found that platinum is well disolved in this fluid. We observe rediposited from the fluid Pt in the form of spirals with diameter less than micron, rodes, inclusions in the quenching aluminosilcate glassy spheres. Glass traps of the different compositions were used to catch dissolved in the fluid material at the end of experiment. Albite glass trap was closed on the early stage of experiments, silica glass traps remain open for fluid to the end of experiment. Pt concentrations in the traps from different runs and determined with various methods were in the range from 2 to 1500 ppm, that is fairly larger than 1.5 ppm we recorded previously (Simakin et al., 2016) . X-Ray tomography demonstrated that Pt within glass trap forms dispersed microparticles that can be missed with LA-ICP-MS analysis. Gold is dissolved in the reduced carbonic fluid as well. Au capsules walls were intensively erroded during experiments and holed for less than half hour. Gold concentrations in sodium-silica glass traps measured with LA-ICP-MS were highly variable in the range 0.2-100 ppm. Bulk chemical analysis of the welded silica glass trap yields 52 ppm of Au.

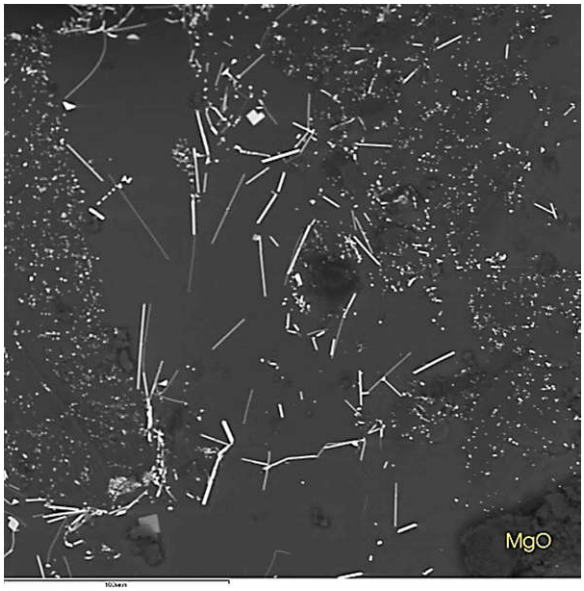

BSE image of platinum crystals deposited from the fluid along with alumino-silicate load on the surface of MgO resulted from Mg_2C_2O4 at quenching. Run conditions were P=200 MPa, T=950ºC, initial ratio CO/CO2=1.

How ordinary CO_2-H_2O fluid can be reduced to gain large concentrations of the active components: CO, COS, CH_4S? Reaction of CO_2-H_2O fluid with ultrabasic rocks rich in olivine results in the decreasing of the oxygen fugacity. At the studying of the skarns with blue diopside from Ioko-Dovyren intrusion (North Transbaikal Area) we estimated evolution of the fO_2 in the fluid. We found that during the decarbonatization reaction, the CO_2-rich fluid has a sufficiently high fO_2 (>NNO) to form VO^{2+} ion, providing a blue color to the diopside. After the interaction with olivine cumulate fluid is reduced to fO_2 = QFM-2. Fluid with at the starting X_{CO2}=0.5and X_{H2O}=0.5 in the equilibrium with FeS and olivine cumulate at P= 200 MPa and T=950ºC contains (Simakin et al., 2018): CO 10.4 mol.%, CH_4 - 3.1 mol.%, a H_2 4.4 mol.%, H_2S 0.48 mol.%, COS 0.08 mol.%, S_2=0.67 10^{-7} mol.%, SO_2 0.3 10^{-7} мол.%. An example of the activity of the reduced carbonic fluid in the uppermost mantle is presented in (Ishimaru and Arai, 2008). Authors reported olivine with NiO content up to 5 wt.% in the peridotite xenolith from Avacha volcano, Kamchatka. It is obvious that such a high nickel content can be achieved only by interacting with a fluid with a low sulfur content, otherwise (Ni, Fe)S is formed in association with olivine with a normal NiO content of about 0.4-0.6 wt.%. We find that pressure of the peridotite origin was about 0.9-1 GPa (our mono-amphibole geo-barometer estimate) corresponding to

the local MOHO. High solubility of Ni as $Ni(CO)_4$ at P=1 GPa was predicted in our paper (Simakin et al., 2016). Carbonyl decomposition can produce native Ni reported in the Avacha xenoliths.

This study was supported by RFBR grant № 18-05-00597.

References

Симакин А.Г., Кислов Е.В., Салова Т.П., Шапошникова О.Ю., Некрасов А.Н. Восстановленный углекислый флюид как фактор рудогенеза на примере аподоломитовых скарнов Йоко-Довыренского массива // Петрология, 2018 (в печати).

Bortnikov N.S., G.N. Gamyanin, O.V. Vikent'eva, V.Yu. Prokof'ev, V.A. Alpatov and A.G. Bakharev. Fluid Composition and Origin in the Hydrothermal System of the Nezhdaninsky Gold Deposit, Sakha (Yakutia), Russia // Geology of Ore Deposits, 2007. Vol. 49, pp. 87–128.

Chang Z., Large R.R, Maslennikov V. Sulfur isotopes in sediment-hosted orogenic gold deposits: Evidence for an early timing and a seawater sulfur source // Geology, 2008. Vol. 3, pp. 971–974.

Coveney R.M. and Nansheng C. Ni-Mo-PGE-Au-rich ores in Chinese black shales and speculations on possible analogues in the United States // Mineral. Deposita, 1991. Vol. 26, pp. 83-88.

Ishimaru S. and Arai S. Nickel enrichment in mantle olivine beneath a volcanic front // Contrib. Mineral. Petrol., 2008. Vol. 156, pp. 119–131.

Simakin A.G.,. Salova T.P, Gabitov R.I. and Isaenko S.I. Dry CO_2–CO fluid as an important potential deep Earth solvent // Geofluids, 2016. Vol. 16, pp. 1043–1057.

EXPERIMENTAL STUDY OF SUBSOLIDUS PARAGENESES OF ULTRAMAFIC LAMPROPHYRES OF THE IRKENEEVA-CHADOBETS TROUGH, SOUTHWESTERN SIBERIA AT 5 GPA

***Smirnova M.D.*[1], *Butvina V.G.*[2], *Safonov O.G.*[2]**

[1]*Institute of Geology of Ore Deposits, Petrography, Mineralogy and Geochemistry RAS (IGEM RAS), Moscow*

[2]*Korzhinskii Institute of Experimental Mineralogy (IEM) RAS, Chernogolovka, butvina@iem.ac.ru*

Occurrences of alkali non-diamondiferous ultramafic lamprhophyres, which recently were found on southwest edge of Siberian craton (Kargin et al., 2016), are very informative and may help us to understand origin mechanisms and evolutions of such rocks, so comprehensive study of this case are important. Especially, experimental works on nature samples might model the system, what have been done in this work.

The first results of experimental study of a natural sample of ailikites from the Irkeneeva-Chadobets trough are presented in this paper. This sample represented ultramafic lamprophyres occurrence – Ilbokich uplift, where the rocks form a dykes. According to classification scheme (Tappe et al.,2005), these rocks are classified as ailikites. They are characterized by a porphyritic an/or globular texture, are enriched in primary magmatic carbonates (up to 25 wt.% of bulk CO_2), show great variety of olivine xeno- and/or phenocrysts, and rare pyroxene phenocrysts. Groundmass is composed of carbonates, phlogopite, clinopyroxene, spinel, ilmenite, rutile, perovskite, Ti-garnet, and K-feldspar. Variety of mineral assemblages, their composition and morphology indicate multi-stage evolution of the rocks, which included early magmatic, late magmatic and autometasomatic stages.

Variety of minerals, their composition and morphology indicates multi-stage evolution, which can be distinguished to magmatic and late magmatic, on which many autometasomatic processes occurred. Studied rocks are volatile-rich and the late stage processes strongly influenced on the paragenesis, because of that determination of solidus minerals is difficult, but very important to understand mechanism of origin. According to monomineral olivine thermometer (De Hoog et al., 2010) and some published data on ailikites (Tappe et al., 2006), the ailikite-forming melts of the the Irkeneeva-Chadobets trough were, presumably, produced at pressure about 5 GPa and temperature range 1400-1200°C (Smirnova et al., 2017). Nevertheless, the source of these rocks is difficult to

reconstruct. Along with geochemical approaches, experimental reproduction of a sub-solidus and super-solidus assemblages for these rocks at high-pressure can help to solve this problem.

We present results of the experimental study on ailikite from the Ilbokich uplift at 5 GPa and 1150 – 1500°C. Least altered ailikite sample, which is devoid of visible macro- and phenocrysts samples, was taken for the experiments. The experiments were performed with the toroidal "anvil-with-hole" apparatus and were carried out using platinum capsules. Duration of each experiment was 10 hours, exclude experiment under 1500°C, that one has been done for 3 hours. Samples were analyzed with electron microprobe in Moscow State University (JEOL JSM-6480LV) and IGEM RAS (JEOL JXA-8200).

All run samples characterized by full melting of a starting material, relative homogeneity and main mineral association: clinohumite + garnet + clinopyroxene + ilmenite + perovskite. In all experiments there are holes in ground mass, they may be a results from crumbled out carbonate, this can be proofed by rare carbonate inclusions in clinopyroxenes.

Experiments up to 1500°C are similar, but under higher temperature (1500°C) olivine became stable in this system. But in all run the grains have mosaic zonation, pores can be observed and carbonate are extremely rare, when in starting sample it was one of main phase.

This experimental data show that the area of stability of Ti-clinohumite are wide in that type of rocks, which is consistent with literature date (Hermann at al., 2007). In natural samples usually observed altered phases, which is considered as olivine, but may be in late evolution of the magma crystalized clinohumite, not olivine additional research is needed to clarify this issue.

This work was supported by the Russian Foundation for Basic Research (grant 16-05-00266).

References

Chakhmouradian, A. R., and C. A. McCammon. "Schorlomite: a discussion of the crystal chemistry, formula, and inter-species boundaries." *Physics and Chemistry of Minerals* 32.4 (2005): 277-289.

De Hoog, J. C., L. Gall, D. H. Cornell (2010) Trace-element geochemistry of mantle olivine and application to mantle petrogenesis and geothermobarometry. Chemical Geology, Vol. 70, pp. 196-215.

Hermann, Jörg, et al. "OH-bearing planar defects in olivine produced by the breakdown of Ti-rich humite minerals from Dabie Shan (China)." *Contributions to Mineralogy and Petrology*153.4 (2007): 417-428.

Kargin, A. V., et al. "Devonian ultramafic lamprophyre in the Irkineeva–Chadobets trough in the southwest of the Siberian Platform: Age, composition, and implications for diamond potential prediction." Geology of Ore Deposits 58.5 (2016): 383-403.

Smirnova et al., 2017 "Phenocrysts and megacrysts of olivines from ultramafic lamprophyres of the Chadobets and Il'bokich uplifts, Southwestern Siberia" EGU General Assembly 2017.

Tappe, Sebastian, et al. "Integrating ultramafic lamprophyres into the IUGS classification of igneous rocks: rationale and implications." *Journal of Petrology* 46.9 (2005): 1893-1900.

Tappe, Sebastian, et al. "Genesis of ultramafic lamprophyres and carbonatites at Aillik Bay, Labrador: a consequence of incipient lithospheric thinning beneath the North Atlantic craton." *Journal of Petrology* 47.7 (2006): 1261-1315.

METALLOGENIC MINERALIZATION IN SERPENTINITES FROM THE NUI NUA MASSIF (SONG MA, NORTH VIETNAM)

Smoliński W.*[1], Natkaniec-Nowak L.[1], Khac G.N.[2], Xuan B.T.[2], Gunia P.[3], Dumanska-Słowik M.[1], Myszewski A.[1]

[1]Faculty of Geology, Geophysics and Environmental Protection, AGH-University of Science and Technology, Krakow 30-059, 30 Mickiewicz Av., Poland, e-mail: smolinski@agh.edu.pl

[2]Faculty of Geosciences and Geoengineering, Hanoi University of Mining and Geology, 18 Duc Thang Ward, North Tu Liem Dist, Ha Noi, Vietnam

[3]Faculty of Earth Sciences and Environmental Management, University of Wroclaw, Wroclaw 50-204, 9 Max Born Sq.

Song Ma Suture Zone is interpreted as a fragment of oceanic lithosphere situated between the Indochina and South China blocks (Hutchison, 1975; Findlay and Trinh, 1997). Serpentinized ultramafic rocks of the lowest part of an ophiolitic suite dated at Middle Cambrian, occur as small bodies at the Nui Nua, Hon Vang, Chieng Khuong and Bo Xinh regions. The biggest outcrop of serpentinites is exposed in Thanh Hoa Province called the Nui Nua Massif – Fig. 1.

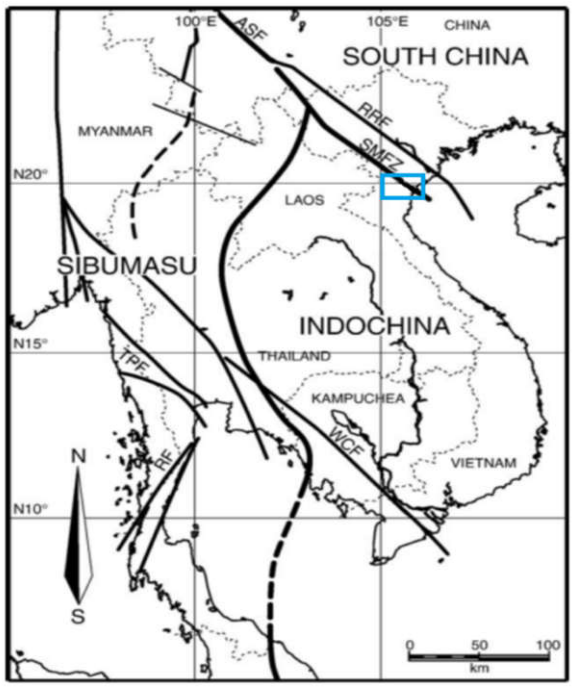

Fig. 1. Simplified structural sketch of Vietnam showing localization of Nui Nua Massif (blue square). The positions of main faults and continental blocks are marked according to Lepvrier et al., (2004). ASF: Ailao Shan Fault; RF: Ranong Fault; RRF: Red River Fault; SMSZ: Song Ma Suture Zone; TPF: Three Pagodas Fault; WCF: Wang Chao Fault (modified after Trung et al., 2006).

The Nui Nua Massif from Song Ma Suture Zone, is overlain by Triassic sedimentary rocks in the south and southwest, and covered with Quaternary sediments on north and north-east. The chromite-bearing serpentinized peridotites occur in the Nui Nua Massif, together with dunites, harzburgites, gabbros and diabases. The age of those rocks is considered as Cambrian and Ordovician (Chien, 1964; Vuong et al., 2006). All of primary silicates have been replaced by serpentine-group minerals or converted into actinolite-bearing and talc-actinolite schists (Son, 1975)

The preliminary mineralogical studies of serpentinites from Nui Nua Massif (Thanh Hoa Province) were conducted by Halpin et al. (2016) and Ngo et al. (2016) for recognizing the types of its metallogenic mineralization. Ours microscopic observations in transmitted light (Fig.2.) have indicated that serpentine minerals often occur in two forms: (1) small cell-shaped lizardite filling the whole rock background and (2) flattened and disturbed chrysotile veins. Sometimes, serpentinites contain small, sharp-edged and fragmented primary olivine and pyroxene (diallage) relics. Magnesiochromite and andradite often occur as sharp-edged, strongly cracked, irregular forms, rarely forming small aggregates.

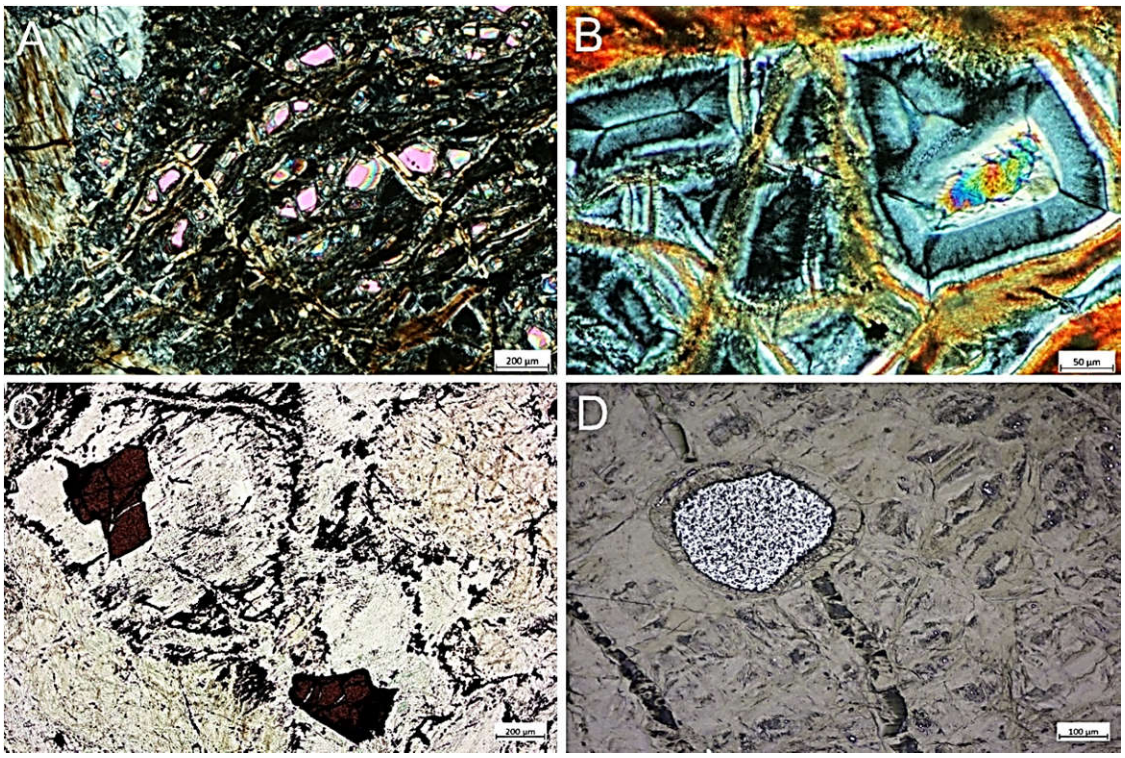

Fig. 2. A) The small sharp-edged relics of primary olivine surrounded by mesh-structure of serpentinite (transmitted light, NX). B) Cell-shaped banded lizardite (transmitted light, NX); C) The garnet-andradite grains including translucent brownish chromian spinels (transmitted light, NX); D) magnesiochromite grain in serpentine background (in reflected light).

The SEM-EDS observations have shown that magnesiochromites are main accessory component of those rocks. They form "grains" about 1 mm in size, which are randomly distributed within the rock mass. The Raman bands at 735 (A_{1g} mode), 689 (A_{1g} mode) and 546 cm^{-1} (F_{2g} mode) registered for magnesiochromite well correspond, with previously published data (e.g. Wang et al., 2002; Lenaz and Lughi, 2013; D'Ippolito et al., 2015).

Andradite found in these serpentinites most often forms large, oval-shaped, isometric grains up to 0.5 mm in diameter with characteristic rims composed of magnetite. Its Raman spectrum shows the most intensive peaks (see Mingsheng et al., 1994 at 875 cm^{-1} (A_{1g}), 516 (T_{2g}), 370 cm^{-1} (E_g) and 353 (E_g) cm^{-1}.

Magnetite occurs in two forms there: (1) narrow rims around magnesiochromites crystals and (2) small individual grains in the serpentinite background. Its presence is proved by three marker bands at 668 (A_{1g}) and 547 (T_{2g}) and 313 (E_g) cm^{-1} (de Faria et al., 1997; Hanesch, 2009). The accessory ilmenite was evidenced also by the strongest band at 696cm^{-1} (Wang et al., 2004).

This work was financially supported by the AGH University of Science and Technology research grant number 11.11.140.158 (Krakow, Poland) and University of Wroclaw research grant number 0401/0156/17 (Wroclaw, Poland).

References

Chien N.V. Nui Nua ultramafic massif. J. Geol. 1964. Vol. 31. pp.3–6 (in Vietnamese).

D'Ippolito V., Andreozzi G.B., Bersani D., Lottici P.P. Raman fingerprint of chromate, aluminate and ferrite spinels. J. Raman Spectrosc. 2015. Vol. 46. pp.1255–1264.

de Faria D.L.A., Venâncio Silva S., de Oliveira M.T. Raman microspectroscopy of some iron oxides and oxyhydroxides. J. Raman Spectrosc. 1997. Vol. 28. pp.873–878.

Findlay R.H., Trinh P.T. The structural setting of the Song Ma region, Vietnam and the Indochina-south China plate boundary problem. Gondwana Res. 1997. Vol. 1. pp.11–33.

Halpin J.A., Tran H.T., Lai C.K., Meffre S., Crawford A.J., Zaw K. U-Pb zircon geochronology and geochemistry from NE Vietnam: A “tectonically disputed” territory between the Indochina and South China blocks. Gondwana Res. 2016. Vol. 34 pp.254–273.

Hanesch M. Raman spectroscopy of iron oxides and (oxy)hydroxides at low laser power and possible applications in environmental magnetic studies. Geophys. J. Int. 2009. Vol. 177. pp. 941–948.

Hutchison C.S. Geological Society of America Bulletin Ophiolite in Southeast Asia. Geol. Soc. Am. Bull. 1975. Vol. 86. pp.797–806.

Lenaz D., Lughi V. Raman study of MgCr2O4-Fe2+Cr2O4 and MgCr2O4-MgFe23+O4 synthetic series: The effects of Fe2+ and Fe3+ on Raman shifts. Phys. Chem. Miner. 2013. Vol. 40. pp.491–498.

Lepvrier C., Maluski H., Van Tich V., Leyreloup A., Truong Thi P., Van Vuong N. The Early Triassic Indosinian orogeny in Vietnam (Truong Son Belt and Kontum Massif); implications for the geodynamic evolution of Indochina. Tectonophysics 2004. pp. 393.

Mingsheng P., Mao H.K., Dien L., Chao E.C.T. Raman spectroscopy of garnet-group minerals. Chinese J. Geochemistry. 1994. Vol. 13. pp.176–183.

Ngo T.X., Santosh M., Tran H.T., Pham H.T. Subduction initiation of Indochina and South China blocks: Insight from the forearc ophiolitic peridotites of the Song Ma Suture Zone in Vietnam. Geol. J. 2016. Vol. 51. pp.421–442.

Son, P. Report of the Geological Map of Son La at the Scale of 1:200,000 Geological Map (Hanoi). 46. Department of Geology of Vietnam. 1975. pp. 4–11 (in Vietnamese).

Trung N.M., Tsujimori T., Itaya T. Honvang serpentinite body of the Song Ma fault zone, Northern Vietnam: A remnant of oceanic lithosphere within the Indochina-South China suture. Gondwana Res. 2006. Vol. 9. pp.225–230.

Wang A., Kuebler K., Jolliff B.L., Haskin L.A. Raman Spectroscopy of Fe-Ti-Cr-Oxides, Case Study: Martian Meteorite EETA 79001. Am. Mineral. 2004. Vol. 89. pp.665–680.

Wang Z., Neill H.S.C.O., Lazor P., Saxena S.K. High pressure Raman spectroscopic study of spinel MgCr2O4. J. Phys. Chem. Solids. 2002. Vol. 63. pp.2057–2061.

RARE METAL MINERALIZATION OF PEGMATITES OF THE OTBOYNOE DEPOSIT

Sokolov S.V.

FSBI «VIMS», Moscow, Russia; vims-sokol@mail.ru

The Otboynoe deposit is part of the pegmatite field, which belongs to the Eastern Sayan rare-metal province. The research of rare-metal mineralization was conducted on the material technological ore sample, which was selected from representative on the mineral composition large pegmatite vein.

The structural-textural features, chemical and mineral composition of ore bearing pegmatites of this deposit were studied by complex methods: various optical microscopic, EPMA, XRD, and chemical analytical techniques.

The major rock-forming pegmatite minerals compose two associations: dominant quartz-microcline-albite and less commonly microcline-albite ones. Secondary mineral component − muscovite forms evenly distributed in a feldspathic matrix impregnation, or stands out together with quartz in the form of pocket concentrations.

Because the pegmatites are dominated by albite, they usually have inequigranular textures (mainly small- to medium-grained) and massive structures. The presence of coarse-crystalline microcline blocks in albite aggregate (from 10-15 cm to 30-40 cm) causes pegmatoid textures, and the development of quartz and microcline phenocrysts makes the rock porphyritic. Portions of the pegmatites with an uneven distribution microcline, quartz and muscovite in albite have taxitic structures.

The leading chemical components of the studied ore sample are SiO_2 (73,0%), Al_2O_3 (16,1%) and alkalis (7,51% Na_2O and 2,17% K_2O), which are the main constituents of the rock-forming feldspars and quartz (Table 1). According to the contents of the Ta_2O_5 (0,029 %) the sample is classed with high-grade, and its Nb_2O_5 concentration (0,017% %) is a

common-grade. Note that the sample contains elevated concentrations of Rb (0,17%), 3 ppm Th and 6 ppm U and, hence, is low radioactive.

The rare metal pegmatite mineralization of the Otboynoe deposit contains various elements and corresponding mineral-concentrators of Ta and Nb (niobo-tantalates), Be (beryl, bertrandite), Li (lepidolite, Li-muscovite), Rb (Rb-microcline, Rb-muscovite), Zr (zircon), and Sn (cassiterite).

Among the foregoing elements, the leading position belongs to Ta, which is the main valuable component in the most common niobo-tantalates of pegmatites: microlite $(NaCa)Ta_2O_6(F,OH)$, ixiolite $(MnSn)Ta_2O_8$, tantalite $Mn(TaNb)_2O_6$ and wodginite $MnSnTa_2O_8$. As a rule, they are closely related to albite and only in very rare cases inclusion of microlite and ixiolite were found in microcline, quartz and muskovite. The accompanying useful elements are Nb (the main mineral-concentrators are columbite $(FeMn)Nb_2O_6$ and niobotantalite $(MnFe)(TaNb)_2O_6$) and as well as Rb, which is enriched in microcline (Sokolov, Nechelyustov, 2017).

Table 1. Chemical composition of ore sample.

Component	Wt. %	Component	Wt. %
SiO_2	73,0	Nb_2O_5	0,017
TiO_2	0,019	Rb	0,17
Al_2O_3	16,1	Sn	0,0036
FeO	0,60	Zr	0,0016
MgO	0,14	Li	0,0021
MnO	0,022	Th	0,0003
CaO	0,23	U	0,0006
Na_2O	7,51	S_{total}	<0,10
K_2O	2,17	H_2O^+.	0,04
P_2O_5	0,14	LOI	0,34
Ta_2O_5	0,029	Total	100,63

Tantalum mineralization occurs in the pegmatites mostly in the form of disseminated micrometer-sized crystals and grains (mostly 5-110 μm, sometimes up to 240 μm), which are only rarely as large as 1-3,5 mm.

Based on its optical and morphological properties, the microlite is clearly distinguished from other niobo-tantalates: (1) it belongs to the cubic crystal system (and hence, is optically isotropic), while wodginite is monoclinic, and the rest are orthorhombic; (2) it constitutes suboctahedral crystals and rounded grains; (3) in thin sections, it is colorless or slightly colored brown and greenish tones. All other minerals of this group have a prismatic or tabular habit, and they are characterized by reddish-brown and brown colours, as seen by the naked eye and under a microscope, and have a distinct pleochroism; black colours are also typical for ixiolite and columbite-tantalites.

Evidently, many of the Ta-Nb-minerals have similar and even coinciding crystallographic and physical properties, and this makes it difficult to identify these minerals. This was done in thin sections under a microscope and by X-ray diffraction and electron-probe analyses.

Data on the chemical (elemental) composition of minerals were obtained on an JXA-8100 Superprobe microprobe equipped with an EDS Link Pentafet energy dispersive spectrometer, with proprietary INCA Software-400. Natural minerals of well-defined composition and synthetic compounds were used as the samples comparison. The analytical results are presented in Table 2, in which the mineral species are arranged in descending order of their contents in the pegmatites, that was determined from the frequency of occurrence in the microprobe specimens and, hence, the number of analyses. This assessment is generally consistent with XRD data on heavy fractions of small-volume specimens and with observations in thin sections.

Very closely similar chemical and geochemical properties of Ta and Nb predetermine their simultaneous presence in the same rare metal minerals. Moreover, Ta and Nb show crystal-chemical affinity with Sn, Ti, Fe, Mn, which are constantly, but in different amounts and proportions, found together with niobo-tantalates (see Table 2).

Table 2. Chemical composition of niobo-tantalates (average contents, wt. %).

Mineral	F	Na_2O	CaO	FeO	MnO	TiO_2	SnO_2	Nb_2O_5		Total
Microlite I (39)*	1,49	0,82	13,70	1,73	1,79	0,88	2,12	7,13	70,64	99,67[1)]
Microlite II (28)	0,33	0,68	8,80	1,52	1,36	1,18	5,59	6,99	63,00	90,05[2)]
Stannomicrolite (9)	1,00	0,70	7,10	2,19	4,05	1,13	13,15	6,71	59,81	95,42[3)]
Ixiolite I (26)	–	–	–	2,43	9,53	1,00	13,83	7,41	65,22	99,42
Tantalite (14)	–	–	–	3,55	12,11	0,45	1,36	16,08	66,44	99,99
Niobotantalite I (27)	–	–	0,69	4,08	11,05	0,60	0,34	29,24	53,55	99,55
Wodginite (6)			–	2,76	9,10	1,04	12,92	5,27	68,72	99,81
Columbite (3)	–	–	1,31	11,03	5,52	0,72	–	55,84	25,26	99,68

* Numerals in parentheses indicate the number of analyses.

Note. The total includes: [1)] $-O=F_2$ 0,63%, [2)] $-O=F_2$ 0,14% and 0,74% U_3O_8, [3)] $-O=F_2$ 0,42%.

The some phases analyzed on a microprobe were identified as microlite based on the presence of F, Na, and Ca and on a high content of Ta. The identification of the minerals of the columbite-tantalite series was done on the basis of elevated amounts of Mn or Fe, but especially of Nb in the absence (columbite) or a low content (tantalite and Nb-tantalite) Sn. Ixiolites and wodginites are different from microlites (except stannomicrolite) and especially from tantalites in bearing a higher content of Sn. Similar to microlites, they contain much less Nb than minerals of the columbite-tantalite series. Bearing similar Fe, Mn, Ti and Sn concentrations, ixiolite and wodginite were distinguished from one another based on the statistically determined Ta : Nb ratio, which was 8,8 for the ixiolite and 13,0 for the wodginite.

Microlite is present in the ore sample in two generations. The later generation (microlite II) differs from the earlier one (microlite I) deficit amount that arises as a result of reduced contents of elements in crystallochemical position *A* (F, Na, Ca) and Ta.

Microtite II replaces sometimes crystals/grains microlite I, but it forms mainly the external zones, stains and even complete pseudomorphs on ixiolites and wodginites and, as a consequence, enriched in Sn. According to Yu.A. Pyatenko (1966), pyrochlore group minerals (they are microlites with the formula $A_{2-x}B_2O_6X$ in our case) are secondary and metamict.

References

Pyatenko Yu.A. Pauling's second rule and pyrochlore group minerals // New data on minerals. Vol. 17. M.: Nauka, 1966. p. 119-123 (in Rus).

Sokolov S.V., Nechelyustov G.N. Contents and distribution of Rb in pegmatite minerals from the Otboynoe deposit // Proceedings of the 200th Anniversary Meeting of the Russian Mineralogical Society. Saint Petersburg. Russia. 2017. Vol. 2. P. 169-170 (in Rus).

REDUCED FLUID AT MAGMATIC TEMPERATURE AND ITS SOURCE (UITKOMST MASSIF, BUSHVELD)

***Solovova I.P.*[1], *Averin A.A.*[2], *Yudovskaya M.A.*[1,3]**

[1]*Institute of Geology of Ore Deposits, Petrography, Mineralogy, and Geochemistry, RAS, Moscow, (solovova@igem.ru),*

[2]*Frumkin Institute of Physical Chemistry and Electrochemistry (IPCE) RAS, Moscow, Russia)*

[3]*School of Geosciences, University of Witwatersrand, Wits 2050, South Afric*

The composition and genesis of primary Bushveld magmas are still disputable. The main difficulty in solution this problem is because the products of crystallization of the original magma are complicated by cumulative processes, contamination by crustal material, metasomatism, reactionary and secondary changes of rock. Based on the petrological study of the rocks of the complex, a number of researchers suggested that active participation of water-carbon CO_2- fluids in the evolution of magmas and the transformation of products of their primary crystallization. Our approach to the solution of these problems is based on the experimental investigation of inclusions in minerals. We

studied inclusions in cumulus olivine (Fo_{90-91}) from ultramafic rocks in the central part of the Uitkomst Complex, which is genetically related to the Bushveld Complex.

Rare primary melt inclusions are 30-50 □m in size and contain euhedral daughter phases dominated by olivine and orthopyroxene (Fig. 1a). In some cases, they are combined with spinel crystalline inclusions. During heating experiments, melting of daughter phases and appearance of melt and fluid were observed in these inclusions starting from 1010-1050°C. The complete homogenization of the inclusions was not reached even at 1430°C. The compositions of melts recalculated to equilibrium with the host olivine have 54-57 wt% SiO_2, up to 18 wt% MgO, less than 3.6 wt% CaO, and up to 5 wt% $Na_2O + K_2O$ ($Na_2O>K_2O$). Among the daughter minerals there are no phases responsible for such high concentrations of alkalis. However, some inclusions contain intergranular regions of glass with an alkali concentration above 8 wt.% (Fig. 1b).

It was also found that cumulus olivine contains inclusions of large (up to 300 □m) multimineral aggregates by irregular or round shape (type A1 and A2). The mineral association of aggregates A1 (Fig. 1c) is represented by olivine, orthopyroxene, amphibole, phlogopite, albite, glass and fluid (Fig. 1d), Fe-Ni-Cu-sulphides, and, sometimes, pectolite ($Ca_2NaH(SiO_3)_3$), carbonate and Fe-Ni-Cu metal alloy. In some cases, they are naturally-decrepitated (Fig. 1e) and contain small fractions of melt and fluid (Fig. 1f).

Together with inclusions of polyphase aggregates, there are monomineral inclusions surrounded by a rim of reactive glass (Fig. 1g). Inclusions of aggregates type A2, in addition to minerals in aggregates type A1, contains apatite with 6 wt% Cl, titanite, perovskite, rutile, ilmenite, sodalite, zeolite (natrolite) and carbonate (Figs. 1h, 1i). The mineral association of such inclusions does not correspond to the rocks of the complex, but is close to pegmatite hydrothermal formations at the late-magmatic stage Main Peridotite unit (Gauert et al., 2014).

The estimated total compositions of hermetic full-crystalline inclusions of aggregates A1 and A2 types (Table, columns 1 and 2) indicate their high magnesia and alkalinity at a H_2O content of 2 to 4 wt.%. With the exception of TiO_2 and CaO, they are close to the compositions of crystalline aggregates inclusions studied in spinel of the Merensky Reef (Table, column 3) (Li et al., 2005).

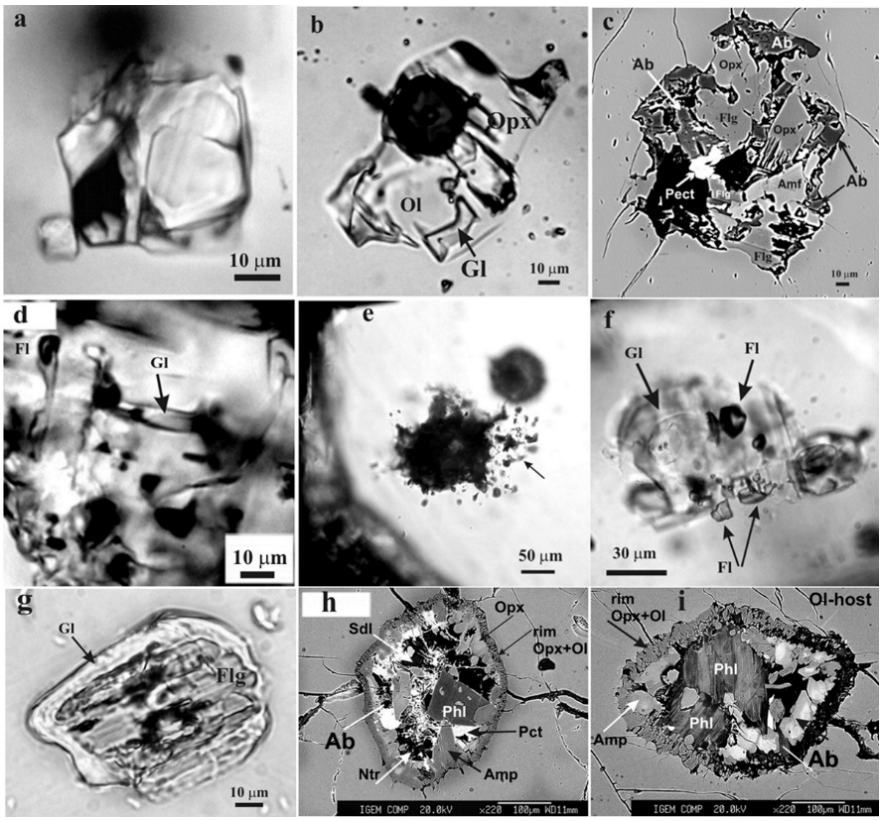

Fig. 1. Photomicrographs of the inclusions in cumulus olivine. (a)– primary melt inclusion; (b)– primary melt inclusion with intergranular glass; (c)– inclusion of polymineralic aggregate type A1; (d)– fragment of the polymineralic aggregate A1 with glass and fluid; (e-f)– naturally-decrepitated inclusions of the polymineralic aggregate, (f)– with glass and fluid; (g)– monomineral inclusion of phlogopite surrounded by the rim of the reactive melt; (h-i)– polymineralic aggregates type A2 with idiomorphic crystals of Opx, Amp and Flg.

Table. 1 Bulk composition of inclusions of polycrystalline aggregates A1 and A2 types, wt%.

	1	2	3		1	2	3
SiO_2	49.5	45.8	47.7	CaO	5.6	6.2	1.2
TiO_2	0.4	0.7	2.5	Na_2O	4.1	4.3	2.4
Al_2O_3	9.2	12.1	9.5	K_2O	1.4	3.3	1.5
FeO	4.3	3.5	4.4	H_2O	2.2	3.9	2.6
MgO	22.8	19.7	26.2	Summ	99.6	99.3	97.9

Fluid within partially-decrepitated polycrystalline aggregates and halo around them were studied by Raman spectroscopic method. The study showed that their main component is CH_4 (peaks of 2917 and 3020 cm^{-1}). N_2 (2330 cm^{-1}), H_2 (4155 cm^{-1}) and carbonate (CO_3^{2-} 1092 cm^{-1}) are present in a subordinate amount in the fluids (Fig. 2).

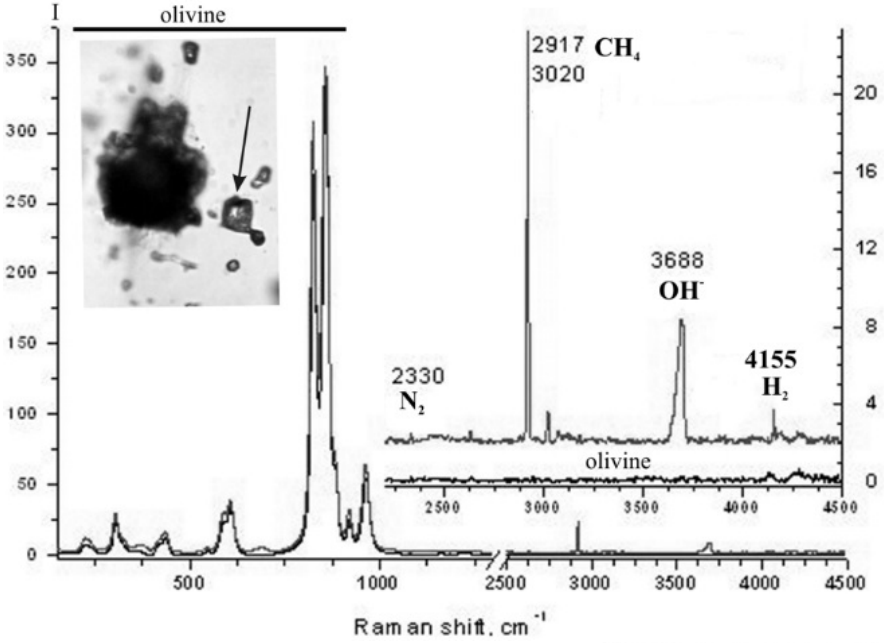

Fig. 2. Raman spectra of fluid in inclusions of partially-decrepitated polycrystalline aggregates containing CH_4, N_2, H_2 and H_2O. Arrow show studied inclusion.

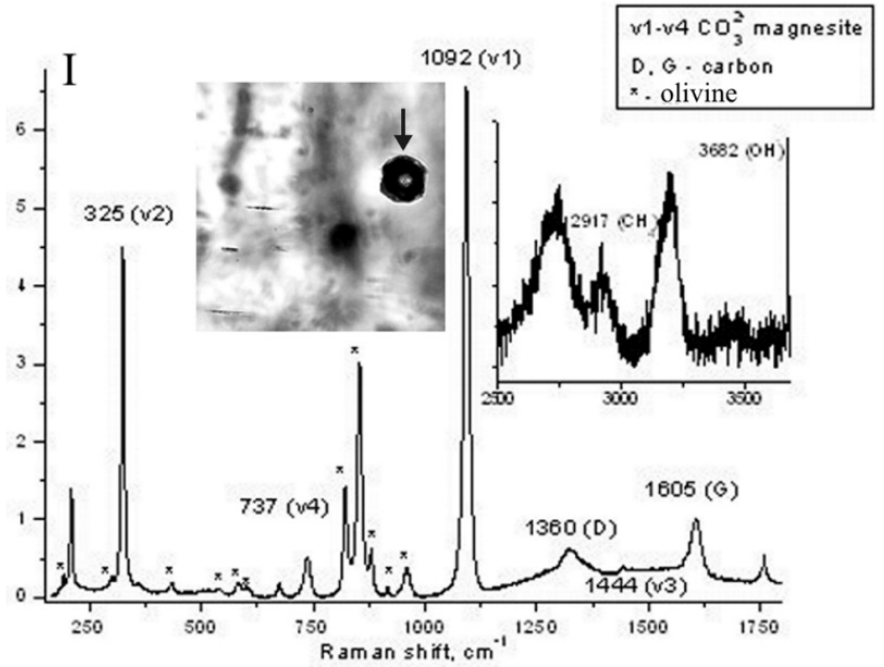

Fig. 3. Raman spectra of fluid inclusions in cumulus olivine containing CH_4, CO_3^{2-}, graphite (C) and H_2O. Arrow show studied inclusion.

Cumulus olivine containing primary melt inclusions is penetrated by subparallel chains of the smallest fluid inclusions (<1 μm). The SIMS analysis of olivine with such inclusions showed up to 4000 ppm H_2O and 25 ppm Na, and its IR absorption spectrum exhibits a band at 3700-3750 cm^{-1},

which is characteristic of water. In rare cases, these olivine crystals contain single fluid inclusions of negative form and up to 15 μm in size. Raman spectroscopic study showed that, in addition to CH_4 (peak 2917 cm^{-1}), they contain the OH^{-1} group of the structural water and carbonate (1444, 1092, 737 and 325 cm^{-1}) (Fig. 3). For these inclusions, a profile was made from the center to the edge. It is established that when moving from the center to the edges, carbon peaks appear (1360 (D) and 1605 (G) cm^{-1}), the intensity of which gradually increases. Consequently, graphite is deposited on the walls of methane-containing fluid inclusions. The ratio of the intensity of the peaks I(D)/I(G) close to 0.5 and corresponds to the dispersed modification of graphite.

Thus, the following was established. 1. High-magnesian composition of primary magmas is combined with an extremely high concentration of alkalis. 2. The presence of melted daughter phases and glass with a high content of alkalis in the primary inclusions. 3. Numerous polycrystalline inclusions of xenogenic aggregates in olivine, containing high-magnesian minerals and phases with volatile components. 4. Signs of melting and recrystallization of these phases (presence of glass and fluid phase). 5. Decrepitation of aggregates with separation of the melt enriched with fluids. 6. The reduced fluids typical for pegmatitic formations, up to the appearance of Fe-Ni-Cu metal alloy.

As a result of the study, it can be assumed that the cumulus olivine were affected by infiltration of volatile (reduced)-rich alkaline melt. This melt is separated from the partially melted xenoliths when it enters the hot magma (>1100°C). The captured xenoliths and impurities contributed to the formation of etching vesicles in olivine (Tingle et al., 1992). Etching and later healing of olivine crystals results to the compositionally variable inclusions to be trapped.

References

Gauert C. et al. Late-stage magmatic-hydrothermal mineral associations in the Ni-Cu-PGE sulphide-bearing (ultra-) basic Uitkomst Complex, South Africa // Abs. IMA14. 2014. pp. 74.

Li C. et al. Origin of phlogopite-orthopyroxene inclusions in chromites from the Merensky Reef of the Bushveld Complex, South Africa // Contrib. Mineral. Petrol. 2005. Vol. 150. pp. 119–130.

Tingle T. et al. Formation of fluid inclusions and etch tunnels in olivine at high pressure // Am. Miner. 1992. Vol. 77, p. 296-302.

COMPOSITION VARIATIONS OF RARE-METAL MINERALS FROM THE ELET'OZERO MASSIF ALKALINE PEGMATITES, NORTH KARELIA

Sorokhtina N.V.[1], Belyatsky B.V.[2], Kononkova N.N.[1], Antonov A.V.[2]

[1]Vernadsky Institute of Geochemistry, RAS, 119991 Kosygina str., 19, Moscow, Russia, nat_sor@rambler.ru

[2]Karpinsky Geological Institute (VSEGEI), CIR, Sredniy ave., 74, St-Petersburg, Russia

The Paleoproterozoic alkaline–mafic-ultramafic Elet'ozero massif occurs within the Karelian megablock in the eastern part of the Baltic Shield (Sharkov et al., 2015). The massif forms lopolite-like concentric zonal body and consists of a number of rock types (from older to younger): gabbro and pyroxenite (~ 90% of the area), diabase, spessartite, nepheline syenite and alkaline pegmatite (~ 10%). The rare-metal ore deposits are confined to alkaline nepheline syenite pegmatites, that are composed of plagioclase, nepheline and clinozoisite mainly, minor amphibole, pyroxene, micas, piemontite, ilmenite, titanite, magnetite, fluorapatite, calcite and others.

We have studied rare-metal accessory mineralizations from two pegmatite bodies: 702 and 706, one of which intruded gabbro in the central part of the massif and the other from the contact of the massif with granitoids. In the first case the rare-metal association is formed by pyrochlore group minerals, mongolite, allanite-(Ce) and zircon, in the latter one – by pyrochlore group minerals, columbite-(Fe), vigezzite, chevkinite-(Ce), allanite-(Ce), nioboaeschynite-(Ce), euxenite-(Y), fluorbritholite-(Ce), britholite-(Ce), monazite-(Ce), thorite and zircon.

Pyrochlore is a most common mineral of the rare-metal pegmatite association and often formed yellow and brown crystals without growth zoning. Fractured and marginal parts of the mineral are

replacement by pyrochlore of the later generations. Zircon, fluorapatite, albite, fluorite, Ca-, Sr- and REE carbonates, sulfides and barite inclusions are often found in the central parts.

In one sample, pegmatite 702, we observed pyrochlore replacement by allanite-(Ce) and mongolite along fracture zones and margins. Pyrochlore with black columbite-(Fe) crystals from pegmatite 706 was formed at the same time (Fig.), the later vigezzite replaced pyrochlore (Tabl. 1). Magnetite was found in this paragenesis also. During pegmatite formation hydrothermal CO_2-rich alkaline fluids were very active and columbite-(Fe) recrystallization was followed by that of vigezzite, according to possible reaction: $Fe^{2+}Nb_2O_6+CaCO_3 \rightarrow (Ca,Ce)(Nb,Ta,Ti)_2O_6 + Fe^{2+}Fe^{3+}{}_2O_4 + CO_2\uparrow$.

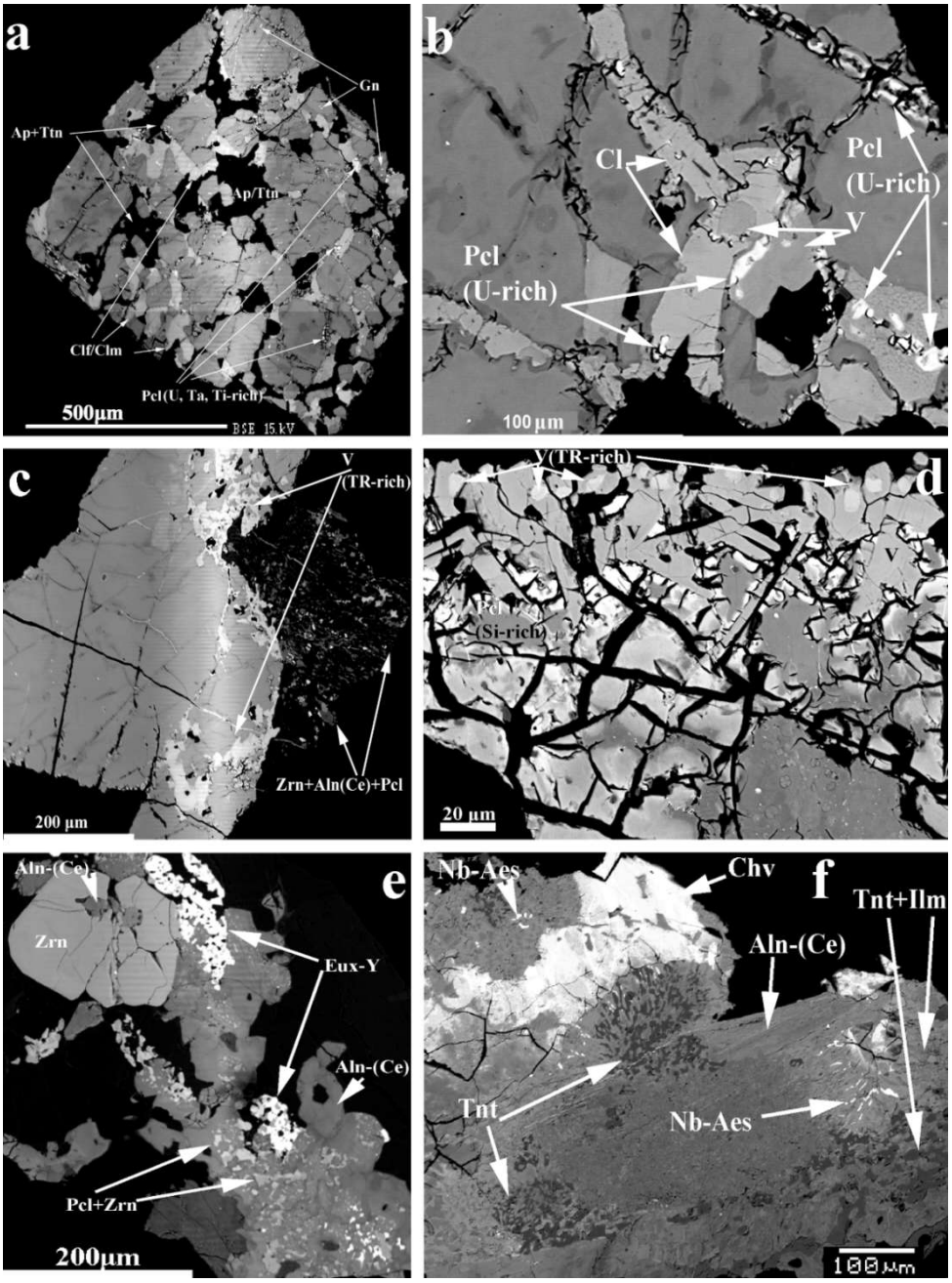

Fig. 1. Paragenesis and morphology of rare-metal minerals in pyrochlore (Pcl) grains (a-d) and groundmass of Elet'ozero pegmatites, BSE-images, Ap – apatite, Tnt – titanite, Ilm – ilmenite, Gn – galena, Clf – columbite-(Fe), Clm – columbite-(Mn), V – vigezzite, Zrn – zircon, Aln(Ce) – allanite-(Ce), Eux-Y – euxenite-(Y), Chv – chevkinite-(Ce), Nb-Aes – nioboaeschynite-(Ce).

Table 1. Averaged composition of niobium oxides intergrowing with pyrochlore, wt.%.

component	TR_2O_3	CaO	SrO	BaO	MnO	MgO	FeO	TiO_2	Nb_2O_5	Ta_2O_5	ThO_2	UO_2
Columbite-(Fe), n=14	0.38 (0.1-1.05)	0.8 (0.08-1.8)	tr	0.11 (tr-0.34)	8.17 (4.28-11.07)	0.08 (tr-0.14)	10.76 (8.25-15.95)	1.4 (0.77-3.15)	72.08 (69.24-74.32)	3.69 (1.26-4.68)	0.06 (tr-0.23)	tr
Vigezzite, n=18	0.65 (tr-3.24)	15.94 (5.34-16.48)	tr	0.06 (tr-0.26)	0.21 (0.08-0.71)	tr	0.29* (0.10-4.25)	1.11 (0.5-6.15)	75.81 (70.08-80.55)	2.45 (0.92-5.66)	0.24 (tr-1.07)	(1.45-1.92)
phase by vigezzite, n=5	0.42	1.21	0.11	0.55	0.18	tr	2.55*	7.84	72.04	5.73	0.08	3.21

* for Fe2O3

The chemical composition variations of different pyrochlore generation from both pegmatites are similar (Tabl. 2). The central zones of unaltered pyrochlore usually consist of hydroxy- or fluorcalciopyrochlore, the fractured cation-deficient zones and rims are hydro-, fluorkeno- or hydrokenopyrochlore (Christy, Atencio, 2013). The pyrochlore margins are Si enriched that is usual for mineral from alkaline rocks. The composition evolution trends of pyrochlore-group minerals are directed to decreasing of Ti, Nb, Ta, Ca, Na and accompanied by an increase of REE and Fe according to isomorphic substitution: $Ti^{4+} + Ca^{2+} \leftrightarrow (Nb,Ta)^{5+} + Na^{+}$; $(Nb,Ta)^{5+} \leftrightarrow Fe^{3+} + Ca^{2+}$; $(Th, U)^{4+} + Ta^{5+} \leftrightarrow Nb^{5+} + 2Ca^{2+}$; $2Ca^{2+} \leftrightarrow Na^{+} + REE^{3+}$. In some cases, intermediate altered zones contain different proportions of Nb and Ta (lower Nb/Ta) and enriched in Th. These differences may be connected with the last stages of alkaline melt evolution and influence of the post magmatic processes. The REE increase in last pyrochlore generations is supported by the abundance of REE-bearing minerals, mainly allanite-(Ce). The maximum of mineral diversity (allanite-(Ce), chevkinites-(Ce), nioboaeschynite-(Ce), euxenite-(Y) and other) found within the interstitial areas of pegmatites 706 (Fig.). Contemporaneous crystallization of Ce-rich and Y, Yb-rich minerals may indicate the existence of additional sources for their formation.

Chevkinite-(Ce) is the earliest REE phase in paragenesis, it occurs as a relict of corroded and zoning grains and is characterized by varying amounts of La/Ce, Si/Al, Nb, Th, Ca, Fe, and Ti (Fig., Tabl. 3). The next REE mineral is allanite-(Ce), which contains various proportions of REE and Fe. Subsequently, the lower-temperature hydrothermal alteration, chevkinite-(Ce) was changed to allanite-(Ce) with simultaneous crystallization of Nb-rich titanite (up to 6 wt.% Nb_2O_5) and ilmenite (Fig.). The fractionation of light and heavy REE begins in the process of successive crystallization of euxenite-(Y) and britholite group minerals, which are mainly concentrates of heavy REE in pegmatites.

The internal texture of rare-metal paragenesis and mineral chemistry indicates that the alkaline pegmatite-706 of the Elet'ozero massif from the contact zone with granite was formed during multiphase crystallization in an open system by mixing two different fluids: the first fluid enriched in Nb>Ta, Ti, Fe, Ca, LREE with the same geochemical signature as the main mineralization, and the second fluid enriched in Ti>Nb, Fe, Y, and HREE, with contrasting geochemical conditions. Secondary mineral paragenesis is formed at high activity of P, Y, HREE, Nb, Ti, Zr, and Th, which involves the mobilization of rare-metals by late hydrothermal peralkaline fluids, which are probably derived from an unknown source at a depth (may be related to granite), during late metallogenic stages. According to the composition of the rocks of the Elet'ozero massif, the final products of differentiation - alkaline pegmatites are enriched in Nb, Ta, Th, U, REE up to ore grade.

U-Pb SHRIMP-II zircon dating has shown that the time of the Elet'ozero gabbro intrusion was 2040-2010 Ma. Alkaline pegmatites were intruded about 1900 Ma that significantly disturbed the U-Pb isotopic system of gabbro zircons (Sharkov et al., 2015). The duration of the massif magmatic formation can be estimated only as 40-60 m.y. The rare-metal mineralization according to pyrochlore mineralogical and isotope-geochemical data was a polystage process complicated by secondary enrichment and recrystallization of ore deposits at 1740, 1680-1660 and 400 Ma.

Table 2. Averaged composition of pyrochlore-group minerals of Elet'ozero pegmatites, wt.%.

grain phase	weakly altered central zone		altered intermediate and rim zones		intermediate and rim zones enriched LREE		cation-deficiently rim zone		altered intermediate and rim zones with low Nb/Ta	
N	702 n=82	706 n=18	702 n=20	706 n=15	702 n=8	706 n=13	702 n=11	706 n=2	702 n=4	706 n=11
Y2O3	0.20 (tr-0.44)	0.14 (tr-0.53)	0.17 (0.1-0.41)	0.09 (tr -0.12)	0.45 (0.12-1.42)	0.81 (tr -3.01)	0.29 (0.08-0.63)	tr	0.07 (tr -0.13)	tr
La2O3	0.08 (tr-0.59)	0.08 (t -0.18)	0.05 (tr-0.1)	0.11 (tr-0.8)	0.68 (0.17-1.16)	0.59 (tr-3.49)	0.99 (0.07-5.04)	0.5	0.31 (0.06-0.78)	tr
Ce2O3	0.55 (tr-6.36)	0.29 (tr-0.69)	0.42 (0.1-0.77)	0.25 (tr-0.79)	3.79 (0.81-13.26)	1.93 (0.11-6.37)	1.28 (tr-5.48	0.35	0.74 (0.15-1.87)	0.18 (tr-0.41)
Pr2O3	0.12 (tr-0.47)	0.09 (tr-0.38)	0.13 (tr-0.29)	0.14 (tr-0.31)	0.23 (0.13-0.67)	0.28 (tr-0.49)	0.23 (tr-0.62)	tr	0.16 (tr-0.41)	0.06 (tr-0.21)
Nd2O3	0.12 (tr-0.76)	0.03 (tr-0.08)	0.10 (tr-0.49)	0.10 (tr-0.39	0.39 (0.09-0.77)	1.16 (0.3-3.33)	0.35 (tr-1.14)	tr	tr	tr
CaO	21.06 (18.69-22.53)	19.43 18.09-20.68	17.43 13.04-19.59	16.44 13.58-17.73	15.33 12.06-18.49	14.82 11.48-16.78	5.91 3.64-9.23	1.50	8.41 3.94-13.84	17.02 5.02-19.77
SrO	0.42 0.11-0..68	0.17 0.02-0.48	0.49 0.29-0.67	0.29 0.05-0.44	0.31 0.04-0.76	0.10 0.03-0.25	0.32 0.09-0.37	tr	0.46 0.13-0.63	0.23 0.05-0.57
BaO	0.17 0.05-0.73	0.11 0.02-0.33	0.41 0.06-1.64	0.12 0.04-0.29	0.22 0.09-0.51	0.06 0.06-0.16	2.43 1.23-5.27	0.53	1.80 1.24-2.73	0.17 0.04-0.44
MnO	0.14 0.03-0.46	0.52 0.35-0.85	0.28 0.01-0.46	0.44 0.3-0.66	0.25 0.05-1.45	0.23 0.02-0.43	0.33 0.12-0.7	0.12	0.32 0.05-0.43	0.47 0.16-0.94
Fe2O3	0.86 0.1-3.1	3.05 0.19-5.25	2.44 0.26-4.42	2.67 1.29-4.07	1.04 0.03-3.49	2.05 0.24-5.45	2.50 0.69-4.8	3.31	4.75 2.7-9.97	0.66 0.12-2.58
Na2O	0.99 0.3-2.52	0.48 0.47-1.02	0.30 0.1-0.85	0.22 0.12-0.46	1.02 0.05-2.29	0.13 0.07-0.3	0.06 0.01-0.12	0.10	0.18 0.1-0.51	1.05 0.05-1.61
ZrO2	0.18 0.05-1.26	tr	0.12 0.01-0.33	0.03 0.01-0.26	1.98 0.02-10.6	0.12 0.02-0.14	0.10 0.03-0.18	tr	0.15 0.06-0.28	tr
TiO2	6.69 5.63-7.91	5.88 4.89-6.69	6.48 5.91-7.01	5.68 4.94-6.52	7.02 5.41-11.86	4.67 2.01-6.76	6.55 5.08-7.63	7.28	7.00 6.58-7.67	11.16 9.44-13.81
Nb2O5	57.29 52.46-61.06	58.17 51.38-64.64	57.25 52.47-60.9	58.08 47.92-62.3	53.22 49.15-57.67	61.28 45.04-69.83	58.11 45.76-65.04	69.23	46.40 41.07-57.16	34.13 30.2-39.74
Ta2O5	4.20 2.28-5.31	3.78 1.69-5.26	4.24 1.58-5.4	4.41 2.25-5.43	3.89 1.78-5.24	3.48 1.05-6.09	4.86 3.65-6.21	6.13	16.16 7.66-24.47	16.43 13.06-21.18
ThO2	0.65 0.01-1.32	0.70 0.05-2.63	0.43 0.05-2.1	0.46 0.05-1.67	0.41 0.06-0.78	0.46 0.05-1.25	0.16 0.05-0.56	tr	0.11 0.01-0.17	0.27 0.04-0.83
UO2	1.49 0.26-3.61	1.02 0.05-2.03	1.41 0.22-3.24	1.15 0.05-1.93	1.24 0.63-2.51	0.59 0.05-1.66	1.24 0.28-2.67	1.87	1.99 0.69-4.73	11.16 6.98-17.64
Al2O3	0.04 0.02-0.18	0.15 0.04-0.48	0.19 0.05-1	0.42 0.11-0.65	0.24 0.02-0.82	0.71 0.01-0.72	0.39 0.06-1.1	0.5	0.75 0.06-2.8	0.07 0.01-0.31
SiO2	0.09 0.01-1.52	0.59 0.02-1.94	1.74 0.08-5.45	2.70 1.11-8.66	1.41 0.05-4.35	1.79 0.11-9.37	2.78 0.19-7.34	2.72	2.29 0.32-6.05	0.13 0.02-1.25
F	1.51 0.52-4.66	1.08 0.69-1.89	0.48 0.02-1.35	0.29 0.07-0.69	0.97 0.12-2.09	0.15 0.03-0.28	0.17 0.05-0.41	tr	0.24 0.03-0.59	1.29 0.97-1.47
Nb/Ta	14.24 10.39-26.20	17.25 11.03-34.98	15.21 10.6-36.82	13.80 10.94-21.84	15.71 10.28-27.61	22.09 10.59-42.90	12.07 9.96-13.82	11.25	3.65 1.82-5.58	2.13 1.43-3.04

Range of values; n – number of analysis, tr – below detection limit.

Table 3. Averaged composition of rare-earth minerals from later association of Elet'ozero pegmatite №706, wt.%.

mineral	Chevkinite-(Ce)		Allanite-(Ce)		Nioboaeschynite-(Ce)	Euxenite-(Y)	Fluorbritholite-(Ce)		Britholite-(Ce)	Monazite-(Ce)
Number of analyses	L, n=4	D, n=2	n=8	n=4*	n=4	n=10	range	n=10	n=1	n=5
Y2O3	0.37	0.70	-	-	1.47	26.48	3.77-6.05	4.60	10.05	0.08
La2O3	12.62	6.26	6.05	5.62	2.79	0.12	7.33-12.5	10.30	2.26	22.68
Ce2O3	27.21	20.51	10.8	13.78	12.40	0.47	21.75-29.49	26.61	13.80	28.28
Pr2O3	2.05	1.42	0.84	tr	1.97	0.10	2.26-11.79	8.42	2.26	1.44
Nd2O3	6.94	5.46	2.13	2.51	8.17	0.38	8.38-9.8	9.04	7.39	4.55
Sm2O3	0.79	1.33	0.45	tr	1.78	1.46	1.59-2.69	2.11	1.84	1.09
Gd2O3	0.37	0.55	0.21	tr	0.98	3.91	1.33-2.4	1.68	2.43	0.22
Dy2O3	-	tr	-	-	0.28	4.42	-	-	-	-
Er2O3	-	tr	-	-	0.32	2.95	-	-	-	-
Yb2O3	-	tr	-	-	0.20	2.66	-	-	-	-
CaO	1.13	3.56	13.1	11.54	3.94	1.82	3.77-19.38	11.24	10.26	0.32
MgO	0.12	0.00	tr	tr	tr	tr	tr	tr	tr	tr
MnO	0.84	0.36	0.77	0.62	tr	0.10	tr	tr	tr	tr
Fe2O3	10.90	6.06	14.3	15.13	4.11	0.77	0.5-4.58	1.20	3.01	0.00
PbO	0.15	0.18			0.13	0.20	0.1-0.3	0.13	0.27	0.79
TiO2	15.75	18.44	0.42	0.43	22.82	0.43	tr	tr	tr	tr
Nb2O5	0.61	6.03	0.07	0.36	22.88	45.25	tr	tr	tr	tr
Ta2O5	0.25	0.30	0.2	0.14	0.72	0.85	tr	tr	tr	tr
ThO2	0.81	2.94	0.12	0.15	9.39	3.63	1.17-3.08	2.24	tr	12.44
Al2O3	0.41	3.67	16.5	14.33	0.07	tr	tr-2.41	0.59	3.04	0.05
SiO2	18.80	15.77	32.9	31.03	1.06	tr	16.11-20.77	19.28	23.78	3.58
P2O5	tr	tr	-	-	-	-	0.91-9.91	3.45	0.31	24.09
F	tr	tr	tr	tr	tr	tr	0.9-2.91	1.94	0.58	0.61

*- for pegmatite №702. L, D - light and dark areas in BSE.

The Sm-Nd and U-Pb isotope systems of individual pyrochlore grains reflect the tectonothermal evolution of the massif, accompanied by structural and chemical changes in minerals including cation-ion exchange with postmagmatic fluids, recrystallization of pyrochlore accompanied by redistribution of components within the grain during its formation (closed geochemical system) or redistribution of components and exchange with surrounding minerals (open system).

The study was partly supported by state contract K41.2014.014 with Sevzapnedra.

References

Christy, A. G. and Atencio, D. Clarification of status of species in the pyrochlore supergroup. Mineralogical Magazine. 2013. 77. 13-20.

Sharkov E.V., Belyatsky B.V., Bogina M.M., Chistyakov A.V., Shchiptsov V.V., Antonov A.V., Lepekhina E.N. Genesis and age of zircon from alkali and mafic rocks of the Elet'ozero Complex, North Karelia. Petrology. 2015. 23 (3). 259–280.

IS THERE THE CR-SPINEL INCLUSIONS LINKAGE TO EMERALD GREEN COLOR IN MARIINSKOE (FORMER MALYSHEVO) DEPOSIT, THE MIDDLE URALS OF RUSSIA?

***Sorokina E.S.*[1], *Popov M.P.*[2], *Kononkova N.N.*[1], *Nikolaev A.G.*[3]**

[1]*Vernadsky Institute of Geochemistry and Analytical Chemistry (GEOKHI RAS), Kosygin st., 19, Moscow, elensorokina@mail.ru;*

[2]*Institute of Geology and Geochemistry, the Uralian branch RAS, st. Ak. Vonsovsky, 15, Yekaterinburg, popovm1@yandex.ru;*

[3]*Kazan (Volga region) Federal University, Kremlyovskaya st., 18, Kazan, anatolij-nikolaev@yandex.ru*

The Mariinskoe (former Malyshevskoe) emerald deposit is located in the northern part of metamorphic rocks within the Malyshevsky-Aulsky zones of mélange between two granite massifs: in 1.5 km from the contact of the Aduisky massif and in 0.5 km to the west of the Malyshevsky massif. In the southeast, at 15 km from the Mariinsky deposit, there is an ophiolite complex represented by the serpenitized ultrabasites of the Bazhenov complex of the dunite-harzburgite formation.

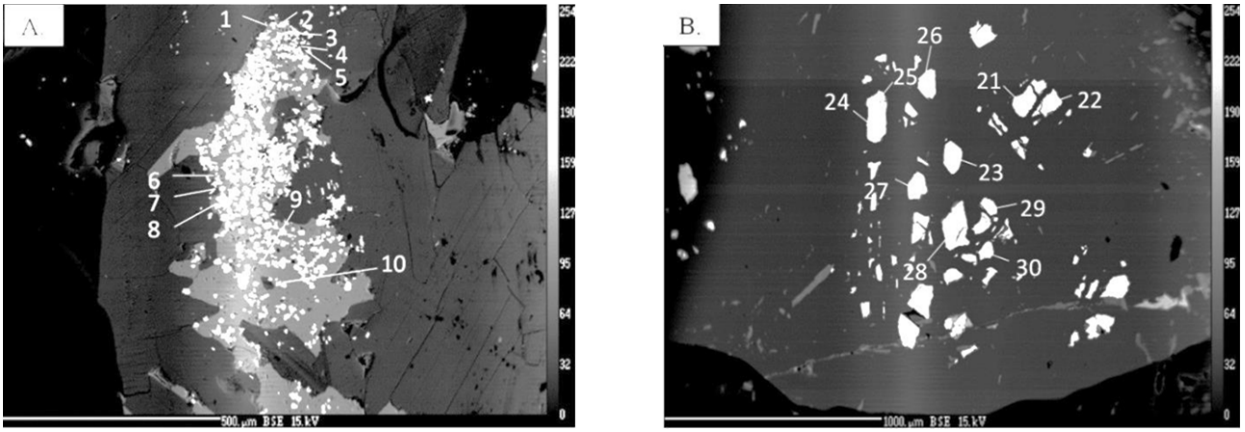

Fig. 1. BSE images of alumochromite within emerald (a) and green beryl (b). Numbers indicate the analyzed points in tables 1 and 2.

Table 1. Chemical composition of chromium spinel inclusion within emerald.

	1	2	3	4	5	6	7	8	9	10
Cr_2O_3	41.63	44.18	41.02	41.66	45.04	48.12	45.68	44.9	48.06	40.79
TiO2	0.07	0.11	0.15	0.1	0.12	-	-	0.47	bdl	0.13
CaO	0.7	0.66	0.87	0.77	0.55	0.39	1.26	1.25	0.96	1.18
Al_2O_3	17.98	16.34	18.19	18.4	14.99	13.25	14.64	13.27	13.29	18.01
MgO	0.51	0.44	0.49	0.41	0.37	0.42	0.45	0.47	0.31	0.5
FeO_{tot}	33.81	34.1	34.72	35.2	33.81	33.1	33.13	34.82	33.16	34.72
MnO	2.18	2.37	2.19	2.24	2.21	2.28	2.15	2.29	2.69	2.13
NiO	-	0.11	0.12	0.1	-	-	-	0.1	-	-
ZnO	1.74	1.75	1.65	1.75	1.41	1.34	1.53	1.47	1.17	1.83
V_2O_3	0.36	0.5	0.37	0.44	0.45	0.4	0.4	0.5	0.37	0.43
Total	99.29	100.71	99.82	101.15	99.11	99.52	99.37	99.6	100.23	99.87
	Recalculated on 4 O anions									
Cr	1.140	1.201	1.121	1.123	1.254	1.343	1.270	1.259	1.334	1.115
Ti	0.002	0.003	0.004	0.003	0.003	0.001	0.002	0.013	0.002	0.003
Ca	0.026	0.024	0.032	0.028	0.021	0.015	0.047	0.047	0.036	0.044
Al	0.734	0.662	0.741	0.740	0.622	0.551	0.607	0.554	0.550	0.734
Mg	0.026	0.023	0.025	0.021	0.019	0.022	0.024	0.025	0.016	0.026
Fe_{tot}	0.979	0.981	1.003	1.004	0.996	0.977	0.974	1.032	0.974	1.004
Mn	0.064	0.069	0.064	0.065	0.066	0.068	0.064	0.069	0.080	0.062
Ni	-	0.003	0.003	0.003	-	-	-	0.003	-	-
Zn	0.044	0.044	0.042	0.044	0.037	0.035	0.040	0.038	0.030	0.047
V	0.010	0.014	0.010	0.012	0.013	0.011	0.011	0.014	0.010	0.012

At the Mariinsky deposit, small chromite bodies are represented the by primary high-aluminous chromites. Chromite bodies are most often found in the micaceous metasomatites (close to emerald localization) on the contact with the chlorite-talc and antigorite zones. A special feature of these emerald crystals is a large number of different mineral inclusions significantly reducing the gem-quality. Beryls often show a.k.a. "eyes" - bright-green colored zones of the emerald located around the small inclusions of chromium spinels.

The chemical composition of chromium spinels measured by the electron micro-probe analysis (EMPA) is shown in tables 1 and 2. In the composition of chromium spinel inclusions in green beryl and emerald (Fig. 1), the contents of Cr_2O_3 is up to 51 wt.%, FeO_{tot} is up to 35 wt.%, Al_2O_3 is up to 24 wt.%, and the small values of ZnO is up to 4 wt.% were detected - a mineral alumochromite (Popov et al., 2018). Additionally, MnO content is up to 3 wt.%, MgO is about 1 wt.%, and V_2O_3 up to 0.5 wt.% were found.

Table 2. Chemical composition of chromium spinel inclusion within green beryl.

	21	22	23	24	25	26	27	28	29	30
Cr_2O_3	50.74	51.43	51.35	50.46	50.72	51.17	50.83	49.62	49.54	50.72
TiO2	0.15	-	-	-	-.	0.2	0.14	0.15	0.11	0.17
CaO	-	-	-	-	-	-	-	-	-	-
Al_2O_3	13.76	13.94	14.07	13.57	13.43	13.64	13.93	13.32	13.89	14.06
MgO	1.16	1.17	1.28	1.03	1.13	0.98	1.25	1.1	0.56	0.62
SiO_2	-	-	-	-	0.14	-	0.12	-	-	0.1
FeO_{tot}	29.84	29.72	29.57	29.89	30.35	30.23	29.22	29.62	28.4	28.11
MnO	1.35	1.35	1.46	1.47	1.44	1.49	1.3	1.28	2.41	2.39
NiO	-	-	-	-	-	-	-	-	-	-
ZnO	2.35	2.54	2.5	2.52	2.5	2.42	2.48	2.27	4.06	4.01
V_2O_3	0.29	0.28	0.2	0.26	0.17	0.19	0.22	0.24	0.21	0.27
Total	99.79	99.89	100.69	100.26	99.75	99.93	99.87	98.91	99.39	99.34
	Recalculated on 4 O anions									
Cr	1.394	1.392	1.399	1.409	1.394	1.397	1.401	1.411	1.379	1.373
Ti	0.004	0.002	0.001	0.002	0.002	0.005	0.004	0.004	0.003	0.004
Ca	-	-	-	-	-	-	-	-	-	-
Al	0.564	0.570	0.570	0.555	0.553	0.560	0.569	0.551	0.575	0.581
Mg	0.060	0.061	0.066	0.053	0.059	0.051	0.065	0.058	0.029	0.032
Si	-	-	-	-	0.005	-	0.004	-	-	0.004
Fe_{tot}	0.867	0.863	0.851	0.867	0.887	0.881	0.847	0.870	0.835	0.824
Mn	0.040	0.040	0.043	0.043	0.043	0.044	0.038	0.038	0.072	0.071
Ni	-	-	-	-	-	-	-	-	-	-
Zn	0.060	0.065	0.063	0.065	0.064	0.062	0.063	0.059	0.105	0.104
V	0.008	0.008	0.006	0.007	0.005	0.005	0.006	0.007	0.006	0.008

EMPA profile performed on beryl (emerald) with the steps of 10 μm (1-10 points) and 55 μm (11-20 points) in a close proximity to the alumochromite inclusion (p.1) toward the beryl edge (p. 20). The values are shown in a table 3. It is observed a regular decrease of the chromium content within a beryl in a close proximity to spinel inclusion toward the beryl edge from 1.5 wt.% to 1 wt.% (Popov et al., 2018). In addition, there is an insignificant decrease of iron concentration from 0.45 wt.% to 0.4 wt.% with the heterogeneous distribution of V_2O_3 content.

In Fig. 2, the absorption spectrum of Uralian beryl and emerald samples is shown. The spectrum was measured in a close proximity to the alumochromite inclusions previously analyzed by EMPA (see again Tables 1 and 2). A special feature of the absorption spectra is the presence of two broads bands in the visible range (at 416-435 nm and at 590-615 nm) linked to the Cr^{3+} ions replacing Al^{3+} ions in the octahedral positions of the beryl structure (Popov et al., 2018). A broad band with a maximum at 820 nm is linked to the Fe^{2+} ions replacing Al^{3+} ions in the octahedral positions. Narrow absorption bands at 1410 nm and at 1900 nm, and a broad band at around 2400-3000 nm are associated with the H_2O vibrations in the channels of the crystal and in fluid inclusions in beryl.

Table 3. Chemical profiles of green beryl (emerald) in a close proximity to alumochromite inclusion toward the beryl edge.

	Step is 10 μm									
No	1	2	3	4	5	6	7	8	9	10
Cr_2O_3	1.43	1.4	1.43	1.34	1.4	1.38	1.35	1.35	1.3	1.26
TiO2	-	-	-	-	-	-	-	-	-	-
CaO	-	-	-	-	-	-	-	-	-	-
Al_2O_3	13.48	13.64	13.47	13.49	13.33	13.47	13.25	13.52	13.38	13.45
MgO	2.27	2.38	2.28	2.35	2.38	2.34	2.33	2.3	2.27	2.27
SiO_2	64.97	64.74	64.51	64.53	64.59	64.74	64.55	64.93	64.36	64.46
FeO_{tot}	0.43	0.53	0.57	0.53	0.48	0.5	0.51	0.45	0.4	0.43
V_2O_3	0.03	0.08	-	0.1	-	0.06	-	0.07	0.04	0.02
MnO	-	-	-	-	-	-	-	-	-	
NiO	-	-	0.03	0.07	-	-	-	-	0.04	0.04
ZnO	0.12	0.26	0.01	0.07	-	-	0.07	0.05	0.02	0.04

Table 3 contd.

	Step is 55 μm									
No	11	12	13	14	15	16	17	18	19	20
Cr_2O_3	1.25	1.39	1.21	1.22	1.18	1.15	1.14	1.21	1.03	1.02
TiO2	-	-	-	-	-	-	-	-	-	-
CaO	-	-	-	-	-	-	-	-	-	-
Al_2O_3	13.37	13.64	13.31	13.39	13.48	13.43	13.37	13.43	13.71	13.63
MgO	2.16	2.27	2.34	2.36	2.19	2.29	2.19	2.32	2.21	2.27
SiO_2	64.64	64.84	64.56	64.76	64.77	64.72	64.35	65.01	65.00	64.81
FeO_{tot}	0.42	0.34	0.41	0.45	0.37	0.37	0.45	0.47	0.44	0.48
V_2O_3	0.05	-	0.09	0.06	0.07	-	0.02	0.01	-	-
MnO	0.05	0.03	0.06	0.05	0.01	0.04	-	0.01	0.01	-
NiO	-	0.03	-	-	-	0.03	-	0.04	0.05	-
ZnO	-	-	-	-	-	-	-	0.02	-	-

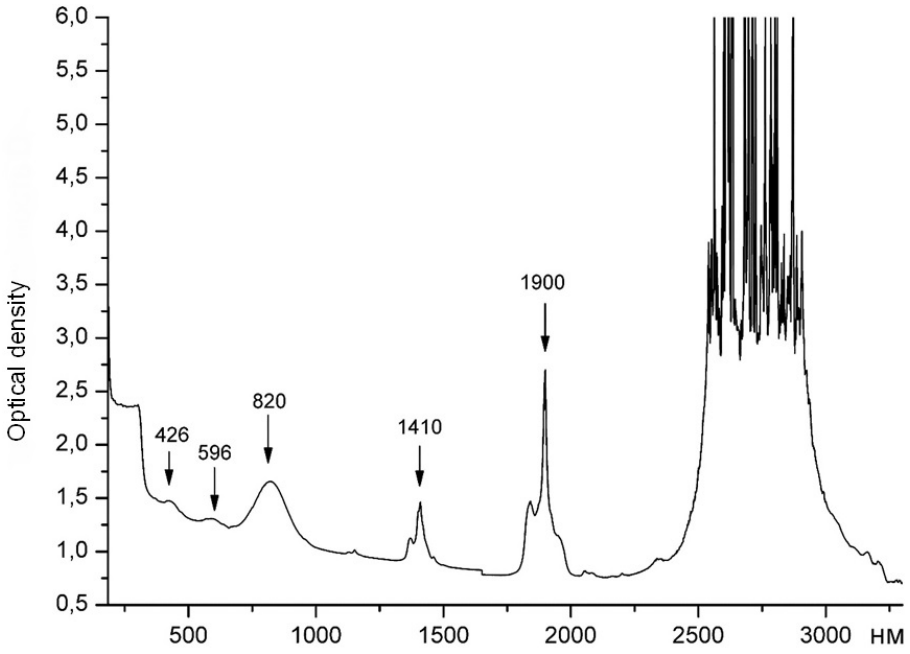

Fig. 2. The absorption spectrum of emerald measured in a close proximity to alumochromite inclusion.

Further research is required for better understanding of alumochromite inclusions influence to the emerald color from Mariinskoe deposits, Middle Urals of Russia.

References

Popov M.P., Sorokina E.S., Konokova N.N., Nikolaev A.G., Karampelas S. New data on the genetic linkage of beryl and chrysoberyl chromophores from Izumrudnye Kopi of Urals with chromium spinels of the Bazhenov ophiolite complex // Doklady Earth Sciences. 2018 (submitted).

ORIGIN OF CORUNDUM (BLUE SAPPHIRE) SYENITE PEGMATITES IN ILMENOGORSKY COMPLEX, SOUTH URALS OF RUSSIA: EVIDENCE FROM RB-SR ISOTOPIC STUDY

***Sorokina E.S.*[1], *Rassomakhin M.A.*[2], *Nikandrov S.N.*[2], *Orlova A.V.*[1], *Kostitsyn Yu.A.*[1]**

[1]Vernadsky Institute of Geochemistry and Analytical Chemistry RAS (GEOKHI RAS), Kosygin st., 19, Moscow, elensorokina@mail.ru

[2]Ilmen State Reserve, Chelyabinsk region, Miass

Corundum α-Al_2O_3 is a typical mineral of many igneous and metamorphic rocks. However, its variety blue sapphire colored by Fe^{3+} and / or Fe^{2+}/Ti^{4+} ions occurs only in several host rock types enriched in alumina and depleted in silica. Meanwhile, the production of gem-quality sapphires is concentrated mainly in the placers of debatable origin (Sorokina et al. 2016, 2017). Therefore, a study of blue sapphire origin found *in situ* within the host rocks may potentially provide useful information for the a better understanding of the petrogenesis for those corundums from the secondary placer occurrences.

At the Ilmen Mountains located in the South Urals of Russia, blue-colored corundum megacrysts sized up to 6 cm in length are found *in situ* within syenite pegmatites in mines 298, 299, 311, and 349. Their geochemical features and solid inclusions are closely similar to those found in placer deposits of Thailand and Northern Laos (Sorokina et al. 2016, 2017). Pegmatite veins hosting a mineral belonging to the exo-contact area of the main intrusive body of miaskites (a variety of nepheline syenite) called Ilmenogorsky massif. SHRIMP U-Pb dating of zircon from different syenites of the Ilmenogorsky massif yielded the ages ca. 450 and ca. 245 Ma. The first age is most likely associated with the crystallization of the magma, and the second age reflects a later stage of metamorphism (Rusin et al. 2006).

6 samples were collected for Rb-Sr isotopic study from mines 298, 299, and 349 of corundum syenite pegmatites (2 samples from each mine). For samples from mines 299 and 349, $(^{87}Sr/^{86}Sr)_0$ recalculated on 245 Ma is about 0.7062, while, this ratio is about 0.7141 – 0.7144 for samples from mine 298. The $(^{87}Sr/^{86}Sr)_0$ ratios of corundum syenite pegmatites from mines 299 and 349 refer the measured isotopic ratio likely to the crustal material and are closely similar to those of miaskites by Kramm et al. (1983). Meanwhile, the $(^{87}Sr/^{86}Sr)_0$ ratio of corundum syenite pegmatites from mine 298 is higher at 0.7141 – 0.7144 than those from mines 299 and 349, however also linked likely to the formation of rocks in the crustal conditions.

This study was supported by the Foundation of the President of the Russian Federation (projects no. MK-4459.2018.5).

References

Sorokina E.S., et al. Multiphase fluid inclusions in blue sapphires from the Ilmen Mountains, Southern Urals//Gems. Gemol. 2016. Vol. 52. Pp. 209 – 211;

Sorokina E.S. Blue sapphire megacrysts in syenite pegmatites from Ilmen Mountains, South Urals, Russia: New mineralogical data//Can. Mineral. 2017. Vol. 55. Pp. 823 – 843;

Rusin A.I., et al. Geology of Ilmen Mountains: situation and problems//Geology and mineralogy Ilmenogorsky complex: the situation and problems. Russian Academy of Sciences, Miass: Ural branch, Russia. 2006. Pp. 3–19 (in Russian);

Kramm U., et al. Origin of the Ilmenogorsk-Vishnevogorsk Nepheline Syenites, Urals, USSR, and Their Time of Emplacement during the History of the Ural Fold Belt: A Rb-Sr Study//J. Geol. 1983. Vol. 91. No. 4. Pp. 427-435.

RB-SR ISOTOPY OF NEWLY DISCOVERED CORUNDUM (SAPPHIRE)-SPINEL-CHLORITE-MUSCOVITE ROCK WITHIN META-ULTRAMAFITES OF ILMEN MOUNTAINS, SOUTH URALS OF RUSSIA

***Sorokina E.S.*[1], *Rassomakhin M.A.*[2], *Nikandrov S.N.*[2], *Orlova A.V.*[1], *Kostitsyn Yu.A.*[1]**

[1]*Vernadsky Institute of Geochemistry and Analytical Chemistry RAS (GEOKHI RAS), Kosygin st., 19, Moscow, elensorokina@mail.ru*

[2]*Ilmen State Reserve, Chelyabinsk region, Miass*

Corundum in the Ilmenogorsky alkaline complex is a common mineral. Widely known and most studied corundum associates with the syenite pegmatites of a complex (Sorokina et al. 2016, 2017). In 2003, the micaceous association of corundum within the meta-ultramafic rocks was discovered on the territory of the Ilmen State Reserve between the lakes Bolshoy Tatkul and Bolshoe Miassovo during the examination of the drainage ditches by S.N. Nikandrov (an employee of the Ilmen State Reserve). This area is composed of rocks of the Kyshtym stratum included in the Saitovsky series. The series consists of meta-terrigenous quartzite-schist rocks with included bodies of the mafic-ultramafic association. The age of these formations reflects the complex evolution of the series: ~1.3 Ga (relict terrigenous zircon); 462.9 ± 3.4 up to 421.7 ± 3.9 Ma - stage of metamorphic evolution (Krasnobaev et al. 2009), ca. 324 Ma and ca. 245 Ma – the stages of collision deformations (Rusin et al. 2006).

The host rocks sized the first tens of meters are composed of practically mono-mineral coarse-grained (up to 4-5 cm) enstatite meta-ultramafites with minor olivine and clinopyroxene, and replaced by the talc and chrysotile-asbestos (Sorokina et al. 2018). The corundums (blue sapphires) surrounded by a spinel-ganite corona embedded in the muscovite-chlorite matrix.

4 samples of corundum (sapphire)-spinel-chlorite-muscovite rock were collected for Rb-Sr analyses. $(^{87}Sr/^{86}Sr)_0$ ratios recalculated on ca. 245 Ma varied from 0.7088 to 0.7106, which is likely due to the formations of metasomatic rocks in crustal conditions.

This study was supported by the Foundation of the President of the Russian Federation (projects no. MK-4459.2018.5).

References

Krasnobaev A.A., et al. Zirconology of metamorphites of the Kyshtym-Arakulian strata of the Sysert-Ilmenogorsky complex//Proceedings of Zavaritsky Institute of Geology and Geochemistry (Trudy Instituta geologii i geokhimii im. akademika A.N. Zavaritskogo). 2009. Vol. 156. Pp. 264 – 268 (in Russian);

Rusin A.I., et al. Geology of Ilmen Mountains: situation and problems//Geology and mineralogy Ilmenogorsky complex: the situation and problems. Russian Academy of Sciences, Miass: Ural branch, Russia, 2006. Pp. 3–19 (in Russian);

Sorokina E.S., et al. Multiphase fluid inclusions in blue sapphires from the Ilmen Mountains, southern Urals//Gems Gemol. 2016. Vol. 52. Is. 2. Pp. 209–211;

Sorokina E.S., et al. Blue sapphire megacrysts in syenite pegmatites from Ilmen Mountains, South Urals (Russia): New mineralogical data//Can. Mineral. 2017. Vol. 55. Pp. 823-843;

Sorokina E.S., et al. Geochemistry of new blue corundum (sapphire) occurrence in Ilmen Mountains, South Urals of Russia: clues to “metamorphic” sapphire petrogenesis in placer deposits// Proccedings of EGU General Assembly. Vienna, 8 – 13 April 2018. Vol. 20. EGU2018-7338-1, 2018.

CHANGES OF MATTER PHASE STATE AND MINERAL SPECIES OF INTRUSIVE FORMATIONS OF DASHKESAN ORE AREA OF THE LESSER CAUCASUS

Suleymanli R.Dj.[1], Yuzbashova U.A.[2]
[1]Dashkesan mountain-ore production
[2]Baku State University, Ulyam2017@mail.ru

Long-term dynamics accompanying formation of intrusives showed that morphology of thermal field isotherms depends upon the form of initial intrusive under the conditions of isotropic host medium. Composing of vertical and horizontal thermal flows caused appearing of isotherms horizontal orientation in flat roof of massif. Conditions of stable temperatures formed in anomalous local areas and kept for a long period of time. Entirely of Earth Crust and Earth surface evolution underwent the complete rethink in mobilist terms. In this case it turned out that all processes described by plates tectonics occurred in more complicated form that it was supposed before. However, these amends untouched the main idea of this conception. Exception was magmatism occurring inside the plates which is typical for collision zone and it was considered to be inner monolithic. A noticeable leap can be observed on all these collision borders of the Lesser Caucasian in changing the velocity of seismic waves distribution (Akhmadov , 1965) which shows appropriate change of matter phase state and also change of one mineral species by other species according to depth (Alekseev, Alekseev, 2017).

Dashkesan ore region with such major deposits as iron ore, cobalt, alunite, barite, magnesium, alunite-pyrophillite, kaolinite, secondary quarzites, mable and other ore and non-ore mineral resources plays an increasingly important role in economy of Azerbaijan Republic. Ore mining is also highly developed here. Geological structure of ore region consists of volcanogenic, volcanogenic-sedimentary, intrusive and metamorphic rocks of the Middle and the Upper Jurassic. The older rocks are of the Upper Bajocian, they form the lower part of Kamargaya mountain northern slope nearby Sharukar village, here they are overlapped by agglomerate lavas, then horizon of yellow tuff sandstones of the Lower Bathonian. Then appear tuff conglomerates, tuff breccias and tuff sandstones of the Upper Bathonian, they are covered by thin horizon of argillites and sandstones of Callovian alternating by thick horizons of Oxfordian carbonaceous rocks, higher is alunite thickness covering the yellow tuffites of Kimmeridgian.

Intrusive massives outcrops within Dashkesan ore region, they are invaded by successive stages. Each stage is connected with mineralization and possesses its own dyke series or groups of intrusive rocks. Here heterochronous dykes may have a close petrographic composition in many cases. According to it study of intrusive massives and their dyke rocks should be conducted along with detailed petrographic and geochemical research and also with thorough chrystallochemical definition of rockforming minerals of intrusive rocks and dykes in order to reconstruct the history of their formation. Intrusive formations play an essential role in geological structure of Dashkesan ore region. Here more than 60 outcrops of intrusive bodies of stock types are registered here and also strata and cross-cutting apophyse taking the area of 30 sq.km jointly with 400 dykes. It is a part of thick polyfacial and polyphase intrusive complex. Intrusives of Dashkesan region is of great interest inasmuch as mineralization of this region is genetically connected with these intrusives. Though they were thoroughly studied by many researchers at different times but at present there is no a concrete idea on some issues of this problem.

The ages was a detatable issue for a long time: K.N.Paffengoltz considered Dashkesan intrusive to be of the Upper Eocene, Sh.A.Azizbekov – the Upper Cretaceous, V.N.Kotlyar suspected Pre-Cenomanian, V.Y.Khain suggested Pre-Cenomanian-Post-Upper Jurassic. R.N.Abdullayev, G.I.Kerimov and M.A.Gashkai referred intrusive to the Lower Cretaceous (Akhmadov , 1965, Report on geological.., 1962). This conclusion can be linked with M.A.Gashkai's data of absolute age. Definition of aplite age from Dashkesan intrusive taken from Bayansar area shows this age is within interval 100-150 mln. yrs and this corresponds to the Lower Cretaceous. Represented data allows to presume the Lower Cretaceous age of Dashkesan intrusive complex (Report on geological.., 1962). This complex intrusive cuts all complex of Middle and Upper Jurassic rocks. For a long time all researchers considered this intrusive to be paleofacial but monophasic. For the first time

K.N.Pafengoltz considered mapped area to be monophasic intrusive. The same idea belongs to Sh.A.Azizbekov and D.M.Akhmedov (Akhmadov , 1965). However, according to M.A.Qashkai's observations (Report on geological.., 1962) intrusive is polyfacial and polyphasic as well, and eruption of Dashkesan intrusive occurred from the same magmatic focus during Neocomian folded movements which caused four phases of intrusion: I phase-gabbroids, II phase-granitoids, III phase-granoaplites and IV phase-diabases (dykes).

First phase of intrusive activity is characterized by intrusion of main composition magma. Some intrusive massives of the first phase are found in area of vil. Kazakholchular mountain Pirsultan, vil.Rudnik and in other places. Morphologically they are cross-cutting bodies of stock types accompanying by apophyses of the same composition with not large area up to several hundred of square metres. The main mass of intruded material is located in the central part of area where intrusive remnants dissected by the late intrusions remained as some massives in valley of Koshkarchai river (nearby vil. Rudnik and in valley of Mollagasanlysu brook). The rocks of the first phase are represented by gabbro, orthoclase gabbrodiorites, quartz-orthoclase gabbro-norites, gabbro-syenites, augite-diopside diorites, etc. Hornblend-pyroxene quartz containing syenite-diorites and pyroxene-hornblend adamellite are found in some parts of intrusive of Pirsultan mountain. But generally these rocks are not typical for the first phase of intrusion.

Intrusion of the second phase intrusion according to facial composition and to morphology is more complicated. Magma composition is medium acid. Besides the major intrusive which takes more than 25 sq.km there are a lot of apophyses outcropped in area with several square metres up to several thousand square metres. Rocks composition of all outcrops vary within a wide range from adamellites to gabbro, gabbro-norites and gabbro-diabases. In this case the main mass of rocks is represented by adamellites, granodiorites, banatites, diorite-syenites and syenite-diorites, and in marginal parts of the main intrusive, in endocontacts and apophyses prevail medium and the main differences such as: syenite-diorites, diorites, gabbro-diorites, gabbro-diorites, gabbro-norites and gabbro. They outcrop in area nearby vil. Mollagasanly, mountain Ziyaratdag and mountain Pirsultan. The features of hybrid origin are typical for the rocks of the second phase intrusion. Rocks diversity is much more than in rocks of the first phase, and this is connected with high assimilation capability of magma providing the second phase intrusion and due to wide range of magma by volatile components.

Relationship between rocks of the first and second phases of intrusive can be easily established. Moreover, well-defined boundary of intrusive is observed between rocks of the first and second phases in some areas, for example village Mollagasanly and towards north of last village's cemetery apophyses of second phase intrusive are found and here gabbroids of the first phase are host rocks for them. Moreover, in near-contact area of second phase intrusive xenoliths gabbro of the first phase are found. All these facts undoubtedly prove that second phase intrusive formed when intrusive of the first phase had already consolidated. However, similarity of rocks of the first and second intrusion, availability of transition between them and similar hybrid differences and also a big likeness of rocks on microelements composition allow to consider that these intrusions are represented by independent phases of intrusions, but due to closeness of time the process of magma differentiation wasn't able to differentiate rocks composition. Probably it's more accurate to talk about subphases but not phases.

The third phase of intrusion in Dashkesan intrusive complex can be vividly observed and magma intrusion is characterized by more acid composition. The rocks are represented by vein leucocratic differences: plagioclasites, diorite-aplites, syenite-aplites, granite-aplites, aplites and plagioaplites. Body consists of usual small veins and veinlets of irregular shape, injections as fissure intrusions with thickness tens of meters and extension more than one kilometer. Morphologically more complicated bodies are also found, but a general configuration of the latter and correlation with host rocks point out that chambers with magma of third phase intrusion are of fracture pattern. The smaller ones among these intrusive – veinlets and small veins are mainly distributed in rocks of the first and second phases. They are commonly found. The larger bodies lean towards area nearby village Mollagasanly and towards east. Here several larger bodies and a great amount of small granoaplite veins can be observed in creek valley and on watershed with ravine Bayansary. It is characteristic that intrusion of the third phase, except for insignificant number of small veinlets, nowhere goes beyond

rocks development of the first and second phases. Scarnification is observed on joints in rocks of the second and third phases. Dykes belonging to the fourth phase of intrusion have a wider areal extent. About 400 dykes with extension 1,5-2,0 km are observed in area. Most of dykes are represented by rocks of the main composition – diabases and diabase porphyrites. Sulphoarsenide mineralization of cobalt is genetically connected with them. Here are dykes of gabbro-porphyrites, andesite porphyrites diorite porphyrites.

Extention of dykes is different but four directions prevail: NE 30-40°, NE 70-80°, NW 275-295°, NW 310-320°. Typical hydrothermal changes are observed in near-by selvages parts of dykes. Scarn and postscarn processes also appear in contacts by forming of garnet, epidote and other minerals. Most of dykes are represented by rocks of the main composition and only some ones by quartz-containing differences. Changes of composition are found in some dykes on vertical, in more hypsometric high parts they consist of rocks of middle and even acid composition but in deep erosion strippings – there are diabases and gabbro-porphyrites. This case doesn't permit to determine dykes according to rocks composition. All these rocks of dykes more or less are metamorphized – hornfelsed, epidotized, chloritized, sometimes – skarnificated and even substituted by magnetites. The recent fact defining age relationship between dykes and hydrothermal mineralization is of great interest. Age correlation between dykes and intrusions of the first and second phases defines easily. In area of mountain Pirsultan and village Kazakhyolchular dykes cross the rocks of the first phase. In area of village Mollagasanly dykes cross rocks of the first phase and transfer to rocks of the second phase. Therefore, dykes are not older than second phase.

To define age relationship between third phase rocks and dykes is not easy at all. According to field observations it has been found that only in one place-ravine at distance of 1 km towards NE of village edge Akhmadly dyke of aplite is cut by dyke of diabase. All dykes are just of the same-age formations. Among them are intercross dykes represented by conjugated fractures filled with rocks of one injection and also cross ones when one dyke "cuts" the other with contact effect and is younger in comparison with it. However, it is not a ground for separation dyke complex into several independent phases (7). It only shows that tectonic movements caused formation of wiggle joints and magma injection had a pulsing nature, whereas tectonic regime remained stable during all process of fissure intrusions formations. Taking into account the movement of magma flow formation of ore-forming porphyry intrusions of final phase occurred against the background of uplift of large rocks blocks, host granitoid plutons and was accompanied by their erosion. Transportation of melting to hypabyssal zone carried out on magmatic waters – fracture channels of different origin. Calculations of melting movement in channel taking into account magma crystallization on channel walls and reduction of carrying capacity show how hypabyssal body with volume of hundreds cubic kilometers could be formed from transported magma. Magma transition to the Upper horizons of crust and in this case unavoidable partial crystallization of meltings as a result of cooling and loss of fluids provide development of drain structures. Zone of deep fluid subflow formed on the base of hypabyssal intrusive. As a result of it magmatogene hydrothermal system formed which developed during melting crystallization. This predetermined significantly the place of ore cluster formation and loss of hydrothermal flow not less than 10.7 g/sm^2 which was necessary for formation of industrial concentrations of large iron-ore metals of Dashkesan type. Therefore, among dykes of fourth phase intrusion are different age formations though they formed in one phase of intrusion equivalent to other phases of complex Dashkesan intrusive. Facial transitions can be observed within all phase formations and also proper veins and apophyses. Under influence of this complex intrusive on host rocks of Dashkesan ore region the following deposits formed: contact-metasomatic skarn-magnetite deposits, hydrothermal cobalt, hydrothermal-metasomatic alunite and pyrophyllite deposits.

References

Akhmadov D.M. Some issues of genesis of iron-ore deposits in Dashkesan ore region. Geology of ore deposits. Moscow 1965 №6 p.91-95

Alekseev V.I., Alekseev I.V. Strategic metals in complexes of subalkaline rare-metal granites and metasomatites from the Russian sector of Asia-Pacific geodynamic zone. Proceedings of XXXIV

International Conference. “Magmatism of the Earth and related strategic metal deposits” Miass, 4-9 August 2017/Editors V.A.Zaitsev and V.N. Ermolaeva.-M: Geokhi ras, 2017, p. 6-9.

Report on geological-prospecting works for iron and cobalt ores in Dashkesan ore region. V. I, Baku, 1962.

EVOLUTION OF THE JURASSIC PLUME MAGMATISM WITHIN AHLMANNRYGGEN PROVINCE (QUEEN MAUD LAND, EAST ANTARCTICA)

***Sushchevskaya N.M.*[1], *Belyatsky B.V.*[2], *Tkacheva D.A.*[3], *Batanova V.G.*[1,4]**

[1]*Vernadsky Institute of Geochemistry, RAS, Moscow, Russia, nadyas@geokhi.ru*

[2]*Karpinsky Geological Institute (VSEGEI) St.Petersburg, Russia*

[3]*VNIIOkeangeologia, St.Petersburg, Russia; 4ISTerre Grenoble, France*

Jurassic magmatism formed under the influence of a huge Karoo plume around ~ 184-178 Ma and covered large areas in the provinces of the Karoo in South Africa, Ferrar and Queen Maud Land (QML) in Antarctica (e.g., Riley et al., 2005; Belyatsky et al., 2002). Within the eastern Antarctica, Jurassic magmatism is distributed over an area of about 145 000 km^2 and includes extended dikes and small intrusions of mafic composition, as well as rare alkaline and acid dikes. We have studied the dolerites from the Ahlmannryggen massif, where high-magnesian basalts were previously found. The basalt outcrops are confined to the margin of the supposed Grunehogna Craton, which has an Archean granite-gneissic basement with an age of about 3.0 Ga, covered by a metamorphosed sedimentary-volcanogenic sequences, in which mafic dikes were intruded about 1.0-0.8 Ga. High-Fe magnesian mafics are developed as dike complexes in the Ahlmannryggen Mountains (Fig. 1).

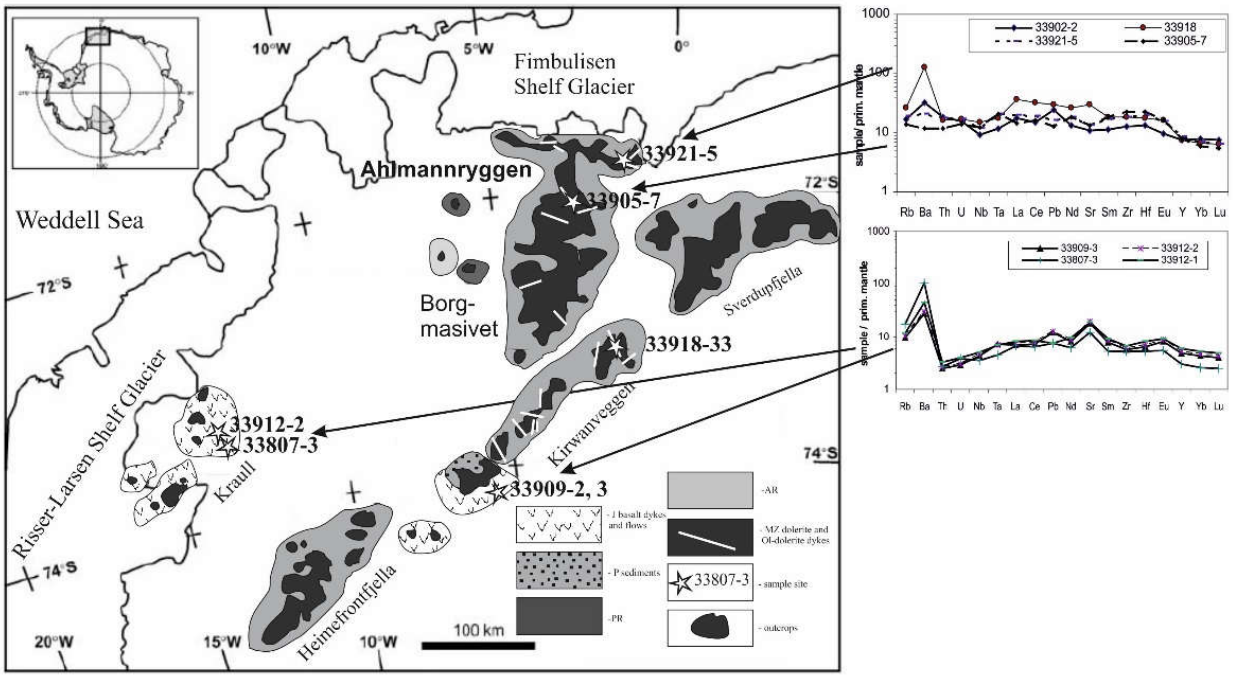

Fig. 1. Queen Maud Land map with 33 Russian Antarctic Expedition sampling sites and the character of dolerite enrichment with reference to primitive mantle.

Basalts of similar composition are noted also south of the Vestfjella Mountains, where they are represented by ferro-picrites, the source of which was the depleted upper mantle (Heinonen et al., 2010; Luttinen, Furnes, 2000). The composition of orthopyroxene, which along with olivine was liquidus phase, from two samples of dolerites (33921-7, 333905-7) consisting of 40-60% of plagioclase, orthopyroxene (about 20%), clinopyroxene (about 10%) and ore minerals, has been

analyzed. Olivine (about 1-3%) forms small rounded grains, sometimes, aggregation of grains in the matrix. In some cases, olivine is assumed only based on the morphological form of grains and secondary products of the whole-altered crystals (33905-7). The matrix, often altered, consists of plagioclase, titanomagnetite and olivine microphenocrysts. A grain of high-Mg and high-Ni olivine, indicating its possible origin from melts of a pyroxenite mantle source (Sobolev et al., 2009), has been found in sample 33921-7.

According to the content of the main components (averaged: SiO_2-49.4, TiO_2-3, MgO-11, Al_2O_3-10.5, FeO-13.2, Na_2O-1.65, K_2O-0.35%), the dolerite samples studied are close to the high-magnesian group of high-Ti Karoo province basalts, which is less common within the QML. A fairly flat spectrum of normalized lithophile elements is characteristic for the samples studied, with relative enrichment of the more incompatible elements relatively more compatible $(La/Yb)_n$= 6.3-4.9; $(Th/Nb)_n$ = 1.2-1.17; $(Zr/Y)_n$= 4.8-6.2, that may indicate the presence of garnet in the source of melts.

The isotope characteristics of magnesian dolerites distinguish the lower values of the lead primary isotope ratios (recalculated for the supposed time of melt intrusion - 180 m.y. ago): $^{206}Pb/^{204}Pb$: 17.33 - 17.37, $^{207}Pb/^{204}Pb$: 15.37 - 15.52, $^{208}Pb/^{204}Pb$: 37.40 - 37.79 and moderately elevated values of Nd ($^{143}Nd/^{144}Nd$: 0.51249-0.51259) and Sr isotope ratios ($^{87}Sr/^{86}Sr$: 0.7049 - 0.7063), which can be taken as a first approximation for the isotope composition of the enriched mantle source of these magmas (Fig. 2).

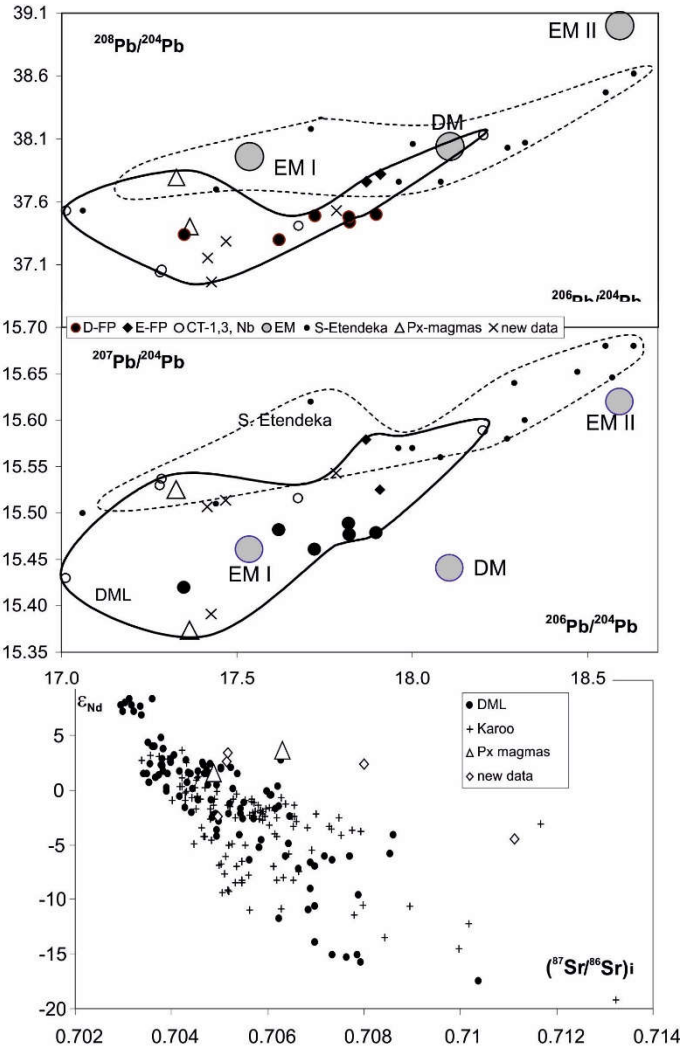

Fig. 2. Isotope signatures of pyroxenite-derived magmas in comparison with variations of isotope ratios plume-related magmas of the southern Etendeka and Karoo-Maud provinces.

A comparison of the isotope characteristics of QML magmas and those located northward in the Etendeka province (southern Africa) associated with the younger Tristan plume (130 Ma) showed that the Antarctic magmas as a whole differ in the less radiogenic Pb isotope composition. The admixture of the enriched EM-II source, typical for the southern Etendeka melts, is also manifested in the QML magmas, but to a lesser extent. This source presumably corresponds to the Gondwana enriched lithospheric mantle (Melankholina, Sushchevskaya, 2018). Another source similar to EM-I is more typical for QML magmas. It is manifested in the high-magnesian Fe-magmas of the Ahlmannryggen massif and corresponds to the mantle source of the pyroxenite composition, which was formed by mixing of the substances with a reduced long-term ratio of the U/Pb (low-mu) and increased Sm/Nd and Rb/Sr, with respect to the typically depleted mantle source, and the plume component, correspondingly. At the same time, the increased values of $^{87}Sr/^{86}Sr$ ratio may indicate the mantle source originally enriched with lithophile elements (and, primarily, rubidium) or the substantial admixture of crustal material in the melts studied as well. However, the increase of this ratio cannot be ruled out as a result of secondary transformation of the dolerite matrix, since to some extent, such changes have been seen in the studied samples (e.g. secondary amphiboles over orthopyroxene and olivine, partial plagioclase saussuritization, chlorite appearance etc.).The pyroxenite mantle component itself is characterized by a moderately depleted (or slightly enriched) composition of lithophile elements with ε_{Nd} varying in the range from +1.6 to +3.6, the ratio of $^{238}U/^{204}Pb$ - 7.7 and Sr isotope composition - $^{87}Sr/^{86}Sr$ about 0.7049. The model age of such a component, based on the composition of the dolerite Sm-Nd isotope system, may be as early as Archean - 2.65-2.3 Ga, if it is assumed the formation of this component occurred during separation from a depleted mantle reservoir with DMM characteristics. If a two-stage model used for Sm-Nd isotopic system formation, then the time of the protolith separation with Sm/Nd 0.17-0.20 from the mantle depleted peridotite was about 700 m.y. ago, and additional fractionation of rare-earth elements with increasing $f_{Sm/Nd}$ from -0.5 up to -0.03…-0.04 as a result of interaction of protolith melts with mantle peridotite and formation of pyroxenite melt occurred 180 m.y. ago. The supposed protolith should have a ratio Rb/Sr higher than the depleted mantle - not less than 0.17-0.2, and a reduced U/Pb ratio of 8.9 (*vs* 9.7) with respect to the one-stage model of Pb isotope system evolution (Stacey-Kramers model). The mafic (oceanic) crust or mafic eclogite possesses the most similar to these geochemical features, which simultaneously has features of a source depleted by lithophile elements and certain enrichment by some elements (for example, rubidium) due to the sedimentary component. Based on this, the most plausible is the correlation of the protolith of the studied dolerites with the material of the mafic eclogite formed 700-800 m.y. ago and transformed into pyroxenite melt 180 m.y. ago by interaction with mantle peridotite due to the subduction of the paleoceanic crust.

Model simulation showed that the recycled crustal material contained in the ascending plume would melt at a depth of 150-170 km, forming melts of the andesite composition, which, upon interaction with the peridotite substrate, form a reaction pyroxenite (Sobolev et al., 2009). With further ascent at depths of 150-120 km, this pyroxenite will melt with the formation of melts of pyroxenite composition. Peridotite melting only begins at a depth of 100 km. It is the well developed and thick lithosphere in the path of the rising plume that results in the melting of the reaction pyroxenite. The resulting melts can reach the surface under specific conditions, when the lithosphere is prone to early destruction. The resulting low-Ti magnesian melts of the Ahlmannryggen and Vestfjella massifs reach the surface near the marginal parts of the older Zimbabwe-Kaapvaal craton, reworked during the Proterozoic Rodinia supercontinent disintegration and the formation of the Queen Maud Land mobile belt, which is the continuation of the Natal orogenic belt in the South Africa (Jacobs et al., 1993).

The results of the pyroxenite melting experiments at pressures of 20-25 kbar showed the existence of melts close in composition to the samples we studied (Lambart et al., 2013). Such melts are characterized by a low MgO content of about 10% (in the studied – averaged 11%). The possibility of reaching the terrestrial surface by these melts is extremely low, since they react with peridotites, through which they uprise to the surface and become more magnesian. Compared with peridotite melts, the melts - derivatives of the pyroxenite source are insignificantly enriched by incompatible elements. These melts must be a relatively low-SiO_2 and high-FeO, as well as have a high CaO/Al_2O_3

ratio, but is not the case in our case, probably because of the great heterogeneity of the eclogite giving rise to pyroxenite as the mantle diapir ascent. The isotopic composition of the samples studied can reflect the composition of the pyroxenite source of the ancient oceanic lithosphere (EMI), which was subducted along the ancient subduction zone (Luttinen, 2018). Probably the unique finding of pyroxenitic high-Fe magnesian melts confined to the high-Ti trap region of the Karoo (central Karoo and northern part of the QML) is due to they mark the central part of the plume and correspond to the earliest eruptions. With the evolution of the plume, over time, the admixture of pyroxenites in the mantle wedge decreases and the melts acquire the characteristics of the melting lithospheric mantle, which is reflected in the isotope signatures of the melts by increasing the share of the EMII enriched component.

The work was suppoted by RSF grant 16-17-10139.

References

Belyatsky B.V., Prasolov E.M., Sushchevskaya N.M. et al. Особенности isotopic composition of Antarctic Jurassic magmas (Queen Maud Land)// Doklady Earth Sciences. 2002. Vol. 386, N4 pp.529-532.

Heinonen J.S., Carlson R.W., Luttinen A.V. Isotopic (Sr, Nd, Pb, and Os) composition of highly magnesian dikes of Vestfjella, western Dronning Maud Land, Antarctica: A key to the origins of the Jurassic Karoo large igneous province?// Chemical Geology. 2010. Vol. 277 pp.227–244.

Jacobs J., Thomas R.J., Weber K. Accretion and indentation tectonics at the southern edge of the Kaapvaal Craton during the Kibaran (Grenville) Orogeny// Geology. 1993. Vol. 21(3) pp. 203–206.

Lambart S., Laporte D., Schiano P. Markers of pyroxenite contribution in the major-element compositions of oceanic basalts: Review of the experimental constraints//Lithos. 2013. Vol. 160-161 pp.14-36.

Luttinen A.V. Bilateral geochemical asymmetry in the Karoo large igneous province// Scientific Reports. 2018. Vol. 8: 5223. doi: :10.1038/s41598-018-23661-3

Luttinen A.V., Furnes H. Flood basalts of Vestfjella: Jurassic magmatism across an Archaean-Proterozoic lithospheric boundary in Dronning Maud Land, Antarctica// Journal of Petrology. 2000. Vol. 41 pp.1271-1305.

Melankholina E.N., Sushchevskaya N.M. Tectono-magmatic evolution of South Atlantic continental margins and oceanic opening// Geotektonica. 2018. N2 pp. 20-41.

Riley T.R., Leat P.T., Curtis M.L. et al. Early–Middle Jurassic dolerite dykes from Western Dronning Maud Land (Antarctica): A. Identifying Mantle Sources in the Karoo Large Igneous Province// Journal of Petrology. 2005. Vol. 46, N7 pp.1489–1524.

Sobolev A.V., Krivolutskaya N.A., Kuzmin D.V. Petrology of parental melts and mantle sources of Siberia trap province magmas// Petrology. 2009. Vol. 17, N3 pp.276-310.

PETROLOGY AND REE MINERAL CHEMISTRY OF THE CHADEGAN METABASITES (SANANDAJ-SIRJAN ZONE, IRAN): EVIDENCE FOR ECLOGITE-FACIES METAMORPHISM DURING NEOTETHYAN SUBDUCTION

Tabatabaei S.M.M.*, *Akbari K.

Department of Geology, Faculty of Sciences, University of Isfahan, Hezarjerib Ave Postal Code: 81746–73441, Isfahan, Iran, tabataba@sci.ui.ac.ir, Tabatabalimp@ gmail.com

The metabasites of Chadegan are a part of Sanandaj-Sirjan Zone including eclogite, garnet amphibolite and amphibolite. These rocks formed during the subduction of the Neo-Tethys ocean crust under the Iranian plate that resulted in a progressive regional dynamothermal metamorphism under high pressure-medium temperature of eclogite and amphibolites facies condition and then was exhumed during the continental collision between the Afro-Arabian continent and the Iranian microcontinent. In the metabasite rocks, with typical MORB composition, garnet preserved a compositional zoning formed during metamorphism. The magnesium (X_{Mg}) gradually increases from

core to rim, while the manganese (X_{Mn}) decreases towards the rim. Chondrite-normalized REE patterns for these garnets exhibit core-to-rim increases in LREEs. The chondrite-normalized REE patterns of garnets, amphiboles and pyroxenes display positive trend from LREEs to HREEs (especially in garnet), which suggest the role of these minerals as the major controller of HREE distribution. The geochemical features show that the studied eclogite and associated rocks have a MORB origin, and probably formed in a deep-seated subduction channel environment. The geothermometry estimation yields average pressure of ~22 kbar and temperature of 470-520ºC for eclogite formation. The thermobarometry results for amphibolite facies gave T=650-700 ºC and P≈10-11 kbar.

The study area is located about 100 km west of Isfahan, 50 km northeast of Zagros main thrust, near Chadegan region. This metamorphic and deformed zone is part of Sanandaj-Sirjan Zone, which underwent complex magmatic, metamorphic, tectonic and deformation events. The metamorphic rocks in this area consist of various metapelites and metabasites.

The deformed rocks found in this region are small units of mylonitized granite. In the study area, metabasite rocks including amphibolite, eclogite and green schists are widely represented. The most important metapelites are composed of different types of schists. Field investigations, petrography and mineral chemistry show that basic rocks and their coexisting units have undergone an important high pressure metamorphism event to the grade of eclogite facies.

High pressure metamorphic rocks are important features in geophysics and geochemistry models and play a significant role in recreating geodynamic models related to convergent plate margin especially in thrusted and folded belts (e.g., Karabinos, 1988; Kurz & Froitzhiem, 2002). Based on absolute geochronological studies of white micas in the study eclogites, the age of the eclogite metamorphism peak, equal to subduction time, is assumed to be 190 million years, which corresponds to Early Jurassic (Davoudian et al., 2010). The age of metapelites from mentioned area in the above- is Jurassic (about 175 million years ago) as the same in Shemshak, Badamu and Hojedk formations (Geological Survey and exploration, 2006).

Since eclogites in the study area represent the first high-pressure metamorphism event in the Sanandaj-Sirjan Zone and are close to Zagros main thrust, the petrogenesis and mineral and REE chemistry studies of these rocks, together with other metabasites, are considerably useful to discover the geotectonic problems and metamorphism of this zone.

Conclusion

1. Metabasites of the study area including eclogite, garnet amphibolite and amphibolites shows MORB features and are the remnants of the Neo-Tethyan oceanic crust that was subducted beneath the Iranian lithospheric plate and uplifted to the surface after eclogitization and amphibolitization.

2. XMn gradually decreases from core to rim and XMg gradually increases toward the rim. Prograde evolution is inferred from garnet with bell-shaped Mn and bowl-shaped Mg profiles. These pieces of evidence indicate a clockwise P–T path. Concentration of LREEs is higher in rims of garnets in the amphibolite than in their cores, while the concentration of HREEs in core is higher than in rims, which can be attributed to the presence of high Ca content in the core.

3. The garnets composition in the eclogites shows that these rocks fit with the III-type. These eclogites related to subduction zones.

4. The results of thermobarometric calculations indicate a peak metamorphism in which eclogite formed at temperatures of 470-520ºC and an average pressure of ~22 kbar. An amphibolite facies overprint occurred at pressures of 7–11 kbar and temperatures of 650–700ºC. Eclogite formation pressure conditions can be correlated with the lithostatic overburden, and then these rocks must have been buried to depths of at least 70–75 km, corresponding to a geothermal gradient of ~7–8°C/km.

5. The geochemical features of trace elements show that the metabasites of the studied area have a tholeitic origin, like MORBs. Negative Nb anomaly in EMORB-normalized trace element patterns suggests a suprasubduction zone influence. Chondrite-normalized REE patterns of amphibole, garnet and pyroxene show enrichments in HREEs and MREEs relative to LREEs. Therefore, these minerals (specifically garnets) are the major controllers of HREE distribution.

6. Significant proportion of the eclogites and related HP-UHP rocks found in young orogens (such as metabasites of the studied area) formed by continent-continent collision are due to their

exhumation in a subduction channel, subsequent capture between the colliding plates, and further, but much slower exhumation in an exhumation channel with subhorizontal mass flow.

7. The studied area is located about 50 km to the northeast of the Main Zagros Reverse Fault, which is the assumed suture zone between the Arabian plate and Eurasia. This high-pressure metamorphism indicates the presence of subduction zone complexes or continental collision zones. Because of their MORB nature, the eclogites from this area represent relics of the Neo-Tethys oceanic plate, which was subducted under the Iranian microcontinent (as a part of Eurasia). Discovery of the eclogite-facies rocks with oceanic origin in Chadegan region supports the theory of subduction in the Zagros suture zone.

References

Davoudian, A.R. Mineral chemistry and crystallization of granitoid body bordering the river, the shear zone North of Shahrekord, with Special Reference to the presence of magmatic epidote.// Journal of Crystallography and Mineralogy of Iran. 2010. 3: 497-515.

Ghasemi, A., Hajihoseini, A., Hoseini, M. Geological Map of Chadegan.// Geological Survey and exploration. 2006. Scale 1:100,000

Karabinos, P. Heat transfer and fault geometry in the Taconian thrust belt, western New England, in Mitra, G., and Wojtal, S.F., eds., geometries and Mechanism of Thrusting, with Special Reference to the Appalachians.// geological Society of America Special Paper. 1988. 222: pp.35-45.

Kurz, W., Froitzheim, N. The exhumation of eclogite - facies metamorphic rocks - a review of models confronted with examples from the Alps.// International Geology Review. 2002. 44: 702-743.

DARREH SARY METAPELITES THE KEY OF SANANDAJ-SIRJAN ZONE TECTONIC SETTING, IRAN

Tabatabaei S.M.M., Hemmati O., Nadimi A., Fahim M.

Department of Geology, Faculty of Sciences, University of Isfahan, Hezarjerib Ave Postal Code: 81746–73441, Isfahan, Iran, tabataba@sci.ui.ac.ir, Tabatabalimp@ gmail.com

The Sanandaj-Srjan Zone (SSZ) is well known because of its metamorphic rocks and is between Zagros fold and thrust belt zone and Uromieh - Dokhtar Magmatic Arc (UDMA). Tectonic setting of this zone is an ambiguous until now. The Dareh Sary metapelites outcropped at the Northwest of Isfahan city and are in the middle of SSZ. At previous these rocks have been studied by some researchers like (Karimi, 2012, Karimi and Tabatabaei Manesh, 2016). Provenance of metasediments can be useful in identifying the tectonic setting of area (Gerdes and Zeh, 2006, Payne et al., 2006). Alterations obviously may significantly have important effects on the mobility of some elements in metamorphic rocks such as Si, Na, K, Ca and Rb (Spandlera et al., 2004). Hence, we consider relatively immobile elements such as the REE, HFSE, Zr, Sc and Th (Taylor and McLennan, 1985, Bhatia and Crook, 1986). So we use the Darreh Sary metapelites to identify SSZ tectonic setting.

Table 1 contains some chemical composition of Darreh Sary metapelites. Fig. 1-a shows the structural zones of Iran (Torabi and hemmati, 2011, slightly modified) and fig. 1-b demonstrate the Dareh Sary simplified geological map (Golpayegan geological map, 1992). According to the petrographical studies, metapelites of Dareh sary categorized in five category, include: slate, phyllite, quartz-muscovite-biotite schist, muscovite-biotite-garnet schist and quartz-staurolite-biotite schist.

These rocks originated from a wide area because their compositions are like UCC (REEs normalized patterns plotted data at (Fig. 2 a)). So these rocks can represent the SSZ average composition. For identifying provenance of these metapelites, the present data were plotted in the figure 2 b and c. which use La-Th-Sc, Th-Sc-Zr/10 (Bhatia and Crock, 1986), in these two figures the data plotted on the CIA (Continental Island Arc) restrict which indicate the provenance of Dareh Sary

Table 1. Trace elements composition of Dareh Sary metamorphic rocks (in ppm).

Method	ICP-MS									
Sample	Darreh Sary									
	DS-28 (Slate)	DS-29 (Slate)	DS-37 (Phyllite)	DS -40 (Phyllite)	DS -42 (Qz-Ms-Bt Schist)	DS -43 (Qz-Ms-Bt Schist)	DS -47 (Ms-Bt-Grt Schist)	DS -48 (Ms-Bt-Grt Schist)	DS -50 (Qz-St-Bt Schist)	DS -53 (Qz-St-Bt Schist)
Sc	22.75	36.95	35.69	15.05	31.80	20.17	16.93	22.73	10.87	13.63
Th	12.00	13.00	14.20	6.05	5.10	11.30	6.70	13.60	9.00	10.40
Zr	146.00	144.00	146.00	164.00	149.00	139.00	129.00	185.00	180.00	137.00
La	36.13	27.32	29.10	24.20	25.90	45.50	20.80	35.30	31.70	35.20
Ce	71.40	53.40	58.00	41.30	53.70	91.70	37.70	71.60	66.30	68.20
Pr	8.81	6.28	7.64	5.75	6.72	11.50	4.61	9.09	8.21	8.20
Nd	34.10	23.70	28.50	22.40	27.30	47.00	17.90	36.50	33.80	31.70
Sm	6.42	4.72	5.40	4.50	5.10	10.70	3.60	7.50	7.10	6.10
Eu	1.41	1.15	1.92	1.49	1.53	3.44	1.27	1.95	1.58	1.15
Gd	5.71	4.75	4.93	4.31	4.80	11.90	3.97	6.97	6.25	4.95
Tb	0.86	0.84	0.78	0.66	0.73	1.96	0.76	1.19	1.00	0.83
Dy	5.27	5.33	4.66	3.76	4.35	11.20	5.12	7.43	5.85	5.07
Ho	1.03	1.09	0.91	0.75	0.99	2.13	1.03	1.50	1.16	0.97
Er	3.04	3.12	2.69	2.32	2.72	5.78	2.90	4.22	3.63	2.82
Tm	0.46	0.43	0.37	0.39	0.39	0.78	0.42	0.57	0.51	0.40
Yb	2.81	2.61	2.60	2.40	2.70	4.30	2.80	3.70	3.30	2.80
Lu	0.48	0.37	0.46	0.35	0.45	0.64	0.41	0.51	0.51	0.38

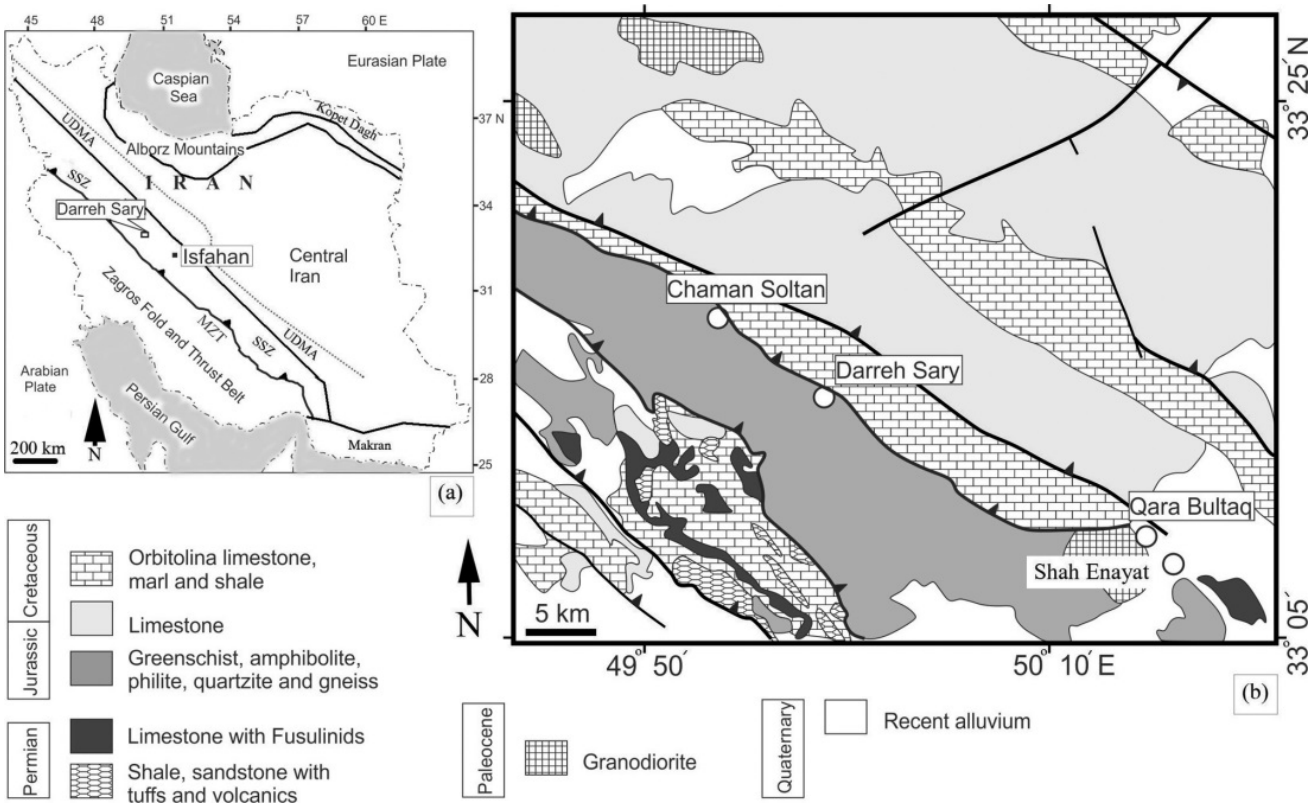

Fig. 1. a) Structural map of Iran (MZT = Main Zagros Thrust) (after Torabi and Hemmati 2011, slightly modified). b) the Dareh Sary area geological map (after Golpayegan geological map 1992, slightly modified).

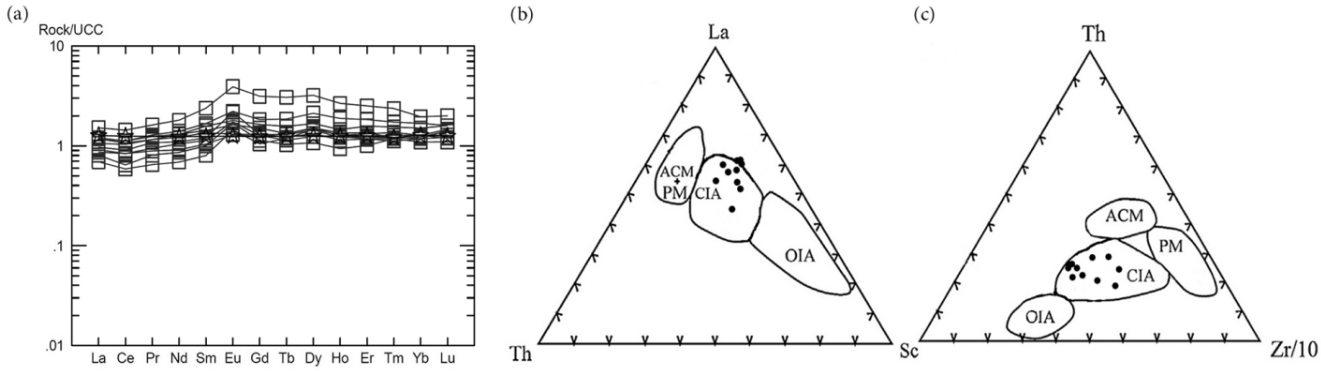

Fig. 2. a) Rock/UCC REE patterns (UCC data is after Taylor and McLennan, 1985 and the PAAS data is after McLennan et al., 1990), b & c triangular trace element diagrams of La-Th-Sc and Th-Sc-Zr/10 (Bhatia and Crock 1986) for Darreh Sary metapelites.

metapelites are CIA. The previous studies considered the SSZ as a part of Iranian microcontinent and Eurasia plate (Ghasemi and Talbot, 2005; Mohajjel et al., 2003, Numan, 2001, Mohajjel and Fergusson, 2000), now we can say that SSZ can be considered as a separated microcontinent in Iran and Eurasia.

References

Bhatia, M.R., Crook, K.A. Trace elements characteristics of graywackes and tec-tonic setting discrimination of sedimentary basins.// Contribution to Mineralogy and Petrology. 1986. Vol. 92 No. 2 pp. 181–193.

Gerdes, A., Zeh, A. Combined U–Pb and Hf isotope LA-(MC-) ICP-MS analyses of detrital zircons: Comparison with SHRIMP and new constraints for the provenance and age of an Armorican metasediment in Central Germany.// Earth and Planetary Science Letters. 2006. Vol. 249 No. 2 pp. 47–61.

Ghasemi, A., Talbot, C.J. A New Tectonic Scenario for the Sanandaj_Sirjan Zone (Iran).// J. Asian Earth Sci. 2005. Vol. 26 No. 1 pp. 683–693.

Karimi, S., Petrology of metamorphic rocks in Northern Sanandaj– Sirjan Zone (Muteh - Aligudarz). Ph. D Thesis: University of Isfahan. 2012. 178p (In Persian).

Karimi, S., Tabatabaei Manesh, S.M. Textural relations, P-T path, polymetamorphism and also geodynamic significance of metamorphic rocks of the Aligudarz-Khonsar region, Sanandaj-Sirjan zone, Iran.// Petrology. 2016. Vol. 24 No. 3 pp. 100-115.

Mohajjel, M., Fergusson, C.L. Dextral transpression in Late Cretaceous continental collision, Sanandaj – Sirjan Zone, western Iran.// Journal of Structural Geology. 2000. Vol. 22 No. 1 pp. 1125-1139.

Mohajjel, M., Fergusson, C.L., Sahandi, M.R. Cretaceous, Tertiary Continental Collision, Sanandaj_Sirjan Zone, Western Iran.// Journal Asian Earth Science. 2003. Vol. 21 No. 3 pp. 397–412.

Payne, J.L., Barovich, K.M., Hand, M. Provenance of metasedimentary rocks in the northern Gawler Craton, Australia: Implications for Palaeoproterozoic reconstructions.// Precambrian Research. 2006. Vol. 148 No. 4 pp. 275–291.

Spandlera, C., Hermann, J., Arculusa, R., Mavrogenes, J. Geochemical heterogeneity and element mobility in deeply subducted oceanic crust; insights from high-pressure mafic rocks from New Caledonia.// Chemical Geology. 2004. Vol. 206 No. 1 pp. 21– 42.

Taylor, S.R., McLennan, S.M. The Continental Crust: Its Composition and Evo-lution, London: Oxford. Blackwell. 1985. 327 p.

Torabi, G., Hemmati, O. Alkaline basalt from the central Iran, a mark of previously subducted paleo-tethys oceanic crust.// Petrology. 2011. Vol. 19 No. 7 pp. 690–704.

INTERPHASE PARTITIONING OF MINOR ELEMENTS IN THE DEEP TRANSITION ZONE AND UPPERMOST LOWER MANTLE: EXPERIMENTAL AND NATURAL DATA

***Tamarova A.P.*[1], *Bobrov A.V.*[1,2,3], *Sirotkina E.A.*[2], *Bindi L.*[4,5], *Irifune T.*[6]**

[1]*Department of Petrology, Geological Faculty, Moscow State University,*
[2]*Vernadsky Insitute of Geochemistry and Analytical Chemistry RAS, Moscow, Russia*
[3]*Institute of Experimental Mineralogy RAS, Chernogolovka, Russia*
[4]*Dipartimento di Scienze della Terra, Università di Firenze, Via La Pira 4, I-50121 Firenze, Italy,*
[5]*CNR, Istituto di Geoscienze e Georisorse, sezione di Firenze, Via La Pira 4, I-50121 Firenze, Italy,*
[6]*Geodynamic Research Center, Matsuyama University, Japan, dragon.of.rainbow@yandex.ru*

High-pressure phase equilibrium experiments have shown that ferropericlase, $MgSiO_3$ and $CaSiO_3$ perovskites are main phases of the lower mantle. Recently it was shown, that trace and rare-earth elements in the lower mantle preferably distributed to calcium perovskite in relation to bridgmanite and ferropericlase (Corgne et al., 2003). Calcium perovskite is often enriched in LREEs, whereas bridgmanite is depleted in them (Kaminsky, 2012). Most of minor elements are incompatible in bridgmanite; only Si, Mg, Sc, Zr, Lu and Hf are consistently compatible. Partition coefficients of REEs in bridgmanite increase from La (D_{La} = 0.01) to Lu (D_{Lu} up to ~1.5) (Liebske et al., 2005).

Experiments at 1100-2400°C and 21-24 GPa were performed using a 2000 ton multi-anvil press installed at the Ehime University (Matsuyama, Japan). Starting compositions were represented by the model pyrolite (Ringwood, 1991). As agents of partial melting were used: (1) H_2O in the composition of brucite $Mg(OH)_2$ (2 wt % H_2O), (2) mixture of carbonates (10 and 15 wt % of carbonate mixture). The carbonate composition was multicomponent: $CaCO_3$, $MgCO_3$, $FeCO_3$, Na_2CO_3, and corresponded to the carbonatite end-member of the carbonate–silicate matter of primary inclusions in natural diamonds (Schrauder, Navon, 1994). In each starting composition, a trace-element mixture was added in a weight ratio of 1/99.

Several assemblages were obtained in experimental samples. Crystallization sequences in carbonate-silicate system agrees with the other experimental data: fPer+L; L+fPer+Brd+CaPrv; fPer+Brd+ CaPrv+Carb (Fig.1). The samples produced in the hydrous system consisted of L+fPer; L+fPer+Brd+CaPrv; fPer+Brd+CaPrv (Fig. 1). Ferropericlase always appears to on liquidus of all systems studied, which is consistent with predominance of ferropericlase as inclusions in diamonds and its wide compositional range. In the carbonate-silicate system, partial melting occurs at ≥1700°C. In the hydrous system, partial melting is observed at ≥1900°C. Our experiments substantiate the mechanisms of isomorphism in the bridgmanite: $Mg^{2+}_A + Si^{4+}_B = Al^{3+}_A + Al^{3+}_B$ and $2Si^{4+}_B + O^{2-}_O = 2Al^{3+}_B + V_O$ (Akaogi, 2007) with prevalence of the second scheme.

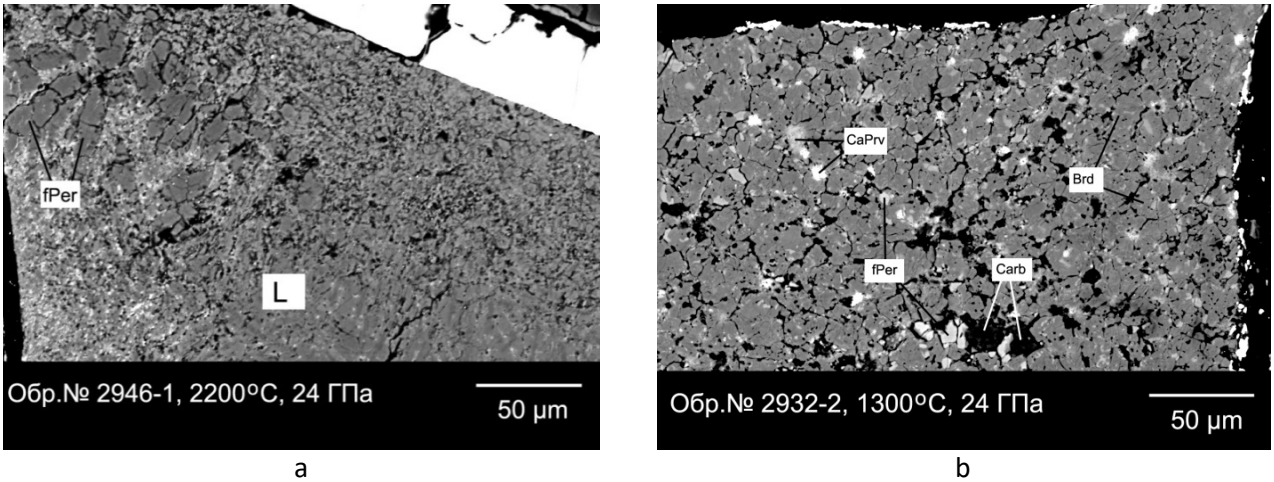

a b

Fig. 1. Parageneses corresponding to temperatures 2200 and 1300°C. Starting composition: a – Pyrolite + H_2O (2 wt %) + mixture of minor elements (1 wt %); b – Pyrolite + carbonate mixture (15 wt %) + mixture of minor elements (1 wt %).

It is shown that bridgmanite and ferropericlase are depleted in LREEs (Fig. 2). For calcium perovskite, on the contrary, we observe enrichment in LREEs and depletion in HREEs. Partition coefficients (CaPrv/L) of REEs in calcium perovskite decrease with temperature. The Onuma diagram, based on lattice strain model, shows that only Al, Cr are compatible for bridgmanite. The peak of the curve for trivalent elements is found at relatively low aluminum content, while larger REEs are on the wing of the parabola, demonstrating a monotonous decrease in the partitioning coefficients from HREEs to LREEs (Fig. 3). Pyrolite with carbonate is characterized by an increase in the partitioning coefficients for LREEs. The results obtained indicate that under the conditions of the Earth's lower mantle, trace and rare-earth elements may be accumulated not only in the $CaSiO_3$ perovskite (Ringwood et al., 1988), but in ferropericlase and bridgmanite as well.

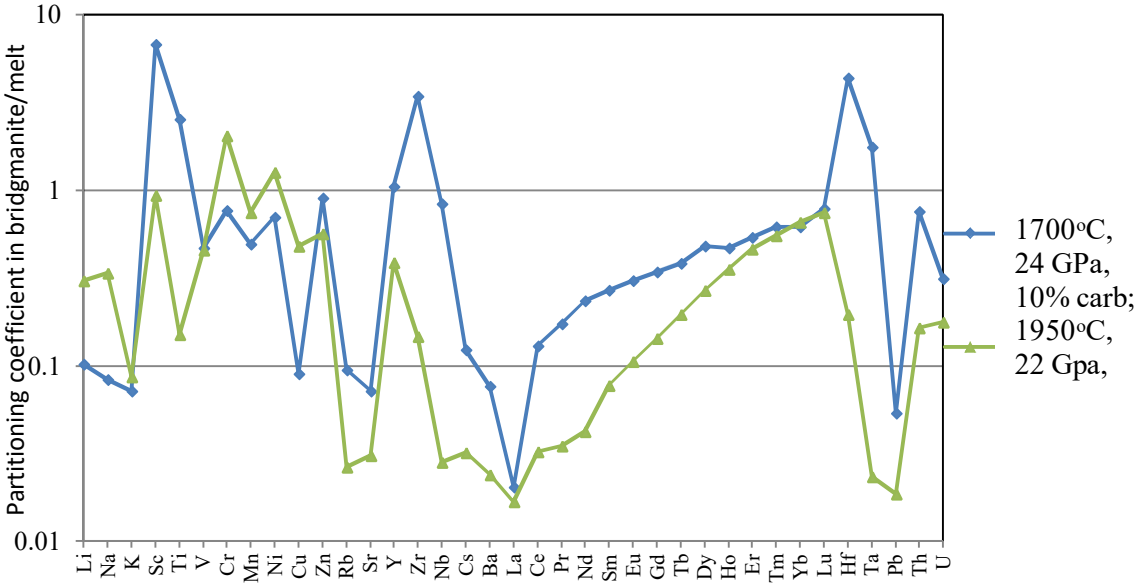

Fig. 2. Partitioning coefficients of minor elements in the bridgmanite/melt system.

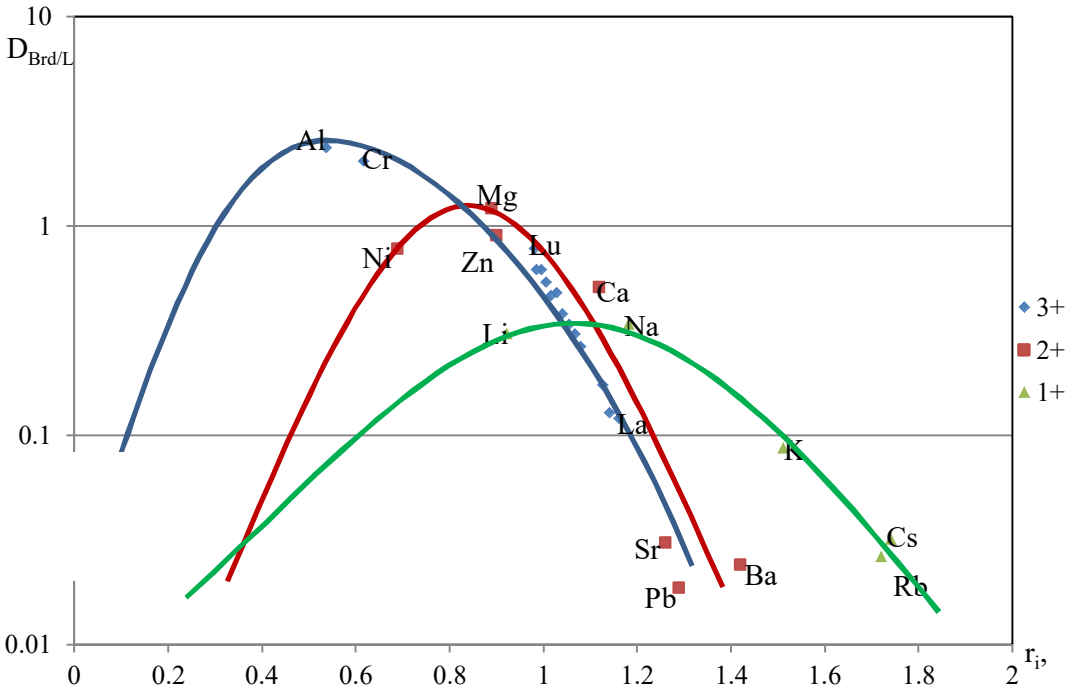

Fig. 3. Partitioning coefficients for monovalent, divalent and trivalent cations in bridgmanite/melt system. Experimental conditions: 1950 ° C, 22 GPa.

This study was supported by the Russian Science Foundation, project no. 17-17-01169.

References

Akaogi M. Phase transitions of minerals in the transition zone and upper part of the lower mantle // Special Papers-Geological Society Of America. – 2007. – Vol. 421. – p. 1.

Andrault D. Properties of lower mantle Al-(Mg, Fe) SiO~ 3 perovskite // Special Papers-Geological Society Of America. – 2007. – Vol. 421. – p. 15.

Corgne A., Allan N. L., Wood B. J. Atomistic simulations of trace element incorporation into the large site of MgSiO3 and CaSiO3 perovskites // Physics of the Earth and Planetary Interiors. – 2003. – Vol. 139. – №. 1-2. – p. 113-127.

Kaminsky F. Mineralogy of the lower mantle: A review of 'super-deep'mineral inclusions in diamond // Earth-Science Reviews. – 2012. – Vol. 110. – №. 1-4. – p. 127-147.

Liebske C. et al. Compositional effects on element partitioning between Mg-silicate perovskite and silicate melts // Contributions to Mineralogy and Petrology. – 2005. – Vol. 149. – №. 1. – p. 113-128.

Ringwood A. E. Phase transformations and their bearing on the constitution and dynamics of the mantle // Geochimica et Cosmochimica Acta. – 1991. – Vol. 55. – №. 8. – p. 2083-2110.

Schrauder M., Navon O. Hydrous and carbonatitic mantle fluids in fibrous diamonds from Jwaneng, Botswana // Geochimica et Cosmochimica Acta. – 1994. – Vol. 58. – №. 2. – p. 761-771.

VARIOUS ALKALINITY OF THE MAGMAS WITHIN A SINGLE VOLCANIC CENTER: THE RESULTS OF MELT INCLUSION STUDY IN MINERALS FROM ICHINSKY AND SHIVELUCH VOLCANOES, KAMCHATKA

***Tolstykh M.L.*[1], *Babansky A.D.*[2]**

[1]*Vernadsky Institute of geochemistry and analytical chemistry RAS, Moscow, Russia,* mashtol@mail.ru

[2]*Institute of Geology of Ore Deposits, Petrography, Mineralogy, and Geochemistry RAS, Moscow, Russia*

The search for a source of alkaline components in island-arc magmas has a long history. Often, partial melting of the mantle material (for example, mélange diapirs) is considered as the cause of the enrichment of island-arc volcanics by LIL elements and K (Cruz-Uribe, 2018). The study of melt inclusions in minerals from volcanic rocks with various silica and alkali contents will give additional information for solving this problem. We studied melt inclusions in minerals from lava and tephra of monogenetic cones and stratovolcanoes of the largest volcanic centers in Kamchatka – Shiveluch and Ichinsky volcanoes.

Shiveluch is located at the north-eastern part of Kamchatka at the triple junction between Kurile-Kamchatka and Aleutian island arcs. It is the biggest active andesitic volcanic center in Kamchatka. Its products are mainly represented by Mg Pl-Amf middle-K andesites ($SiO_2 \leq 55\%$). At the same time, in some Holocene soil-pyroclastic covers at the foot of this volcano two stratums of basic tephra horizons were identified, deposited 7500 and 3600 ^{14}C years BP (Volynets et al., 1997; Ponomareva et al., 2007, Churikova, 2010). High-Mg Ol basalts (tephra '7500') erupted from a small cone situated near Baidarny river (Churikova, 2010). High-Mg high-K Ol-Pl-Px basalts (tephra '3500') resulted from several sub-synchronous eruptions of the hidden monogenetic centers located in the SW part of Shiveluch massif by deposition area and size distribution of this basic ash and lapilli (Pevzner, 2011).

Ichinsky volcanic massif is located in the Sredinny Range of Kamchatka – the largest volcanic structure of the peninsula. Ichinsky is the biggest volcano in the Sredinny Range. It is a complex polygenetic volcano of Somma-Vesuvius type. Holocene deposits of the volcano are represented mainly by tephra, sometimes by andesite-dacitic middle-K lava flows. It is surrounded by a large monogenetic volcanic field, produced in Holocene two volumnious eruptions of Southern and Northern Cherpouk; lavas of these centers (Ol-Pl basaltic andesites and Pl andesites, respectively) formed spatial lava fields and are dated 6500 ^{14}C years BP. Indeed, only Southern Cherpuk can be considered a monogenic cone, and Northern Cherpuk has a direct relation to eruptions in the central volcano (Volynets et al., 2018).

We studied melt inclusions in different minerals of the rocks with contrast composition: 1) In Ol of basic tephra about 7500 ^{14}C years BP (Shiveluch massif); 2) In Px and Pl of basic lapilli formed during 4600-3600 ^{14}C years BP interval (Shiveluch massif); 3) In different minerals of andesitic tephra younger than 4000 ^{14}C years iBP (Shiveluch); 4) In Ol of the initial and final stages of the monogenetic eruption at Ichnisky massif (South Cherpouk, 6500 ^{14}C years BP); 5) In different minerals of dacitic tephra of the summit crater of Ichinsky volcano (6500 and 4200 ^{14}C years BP).

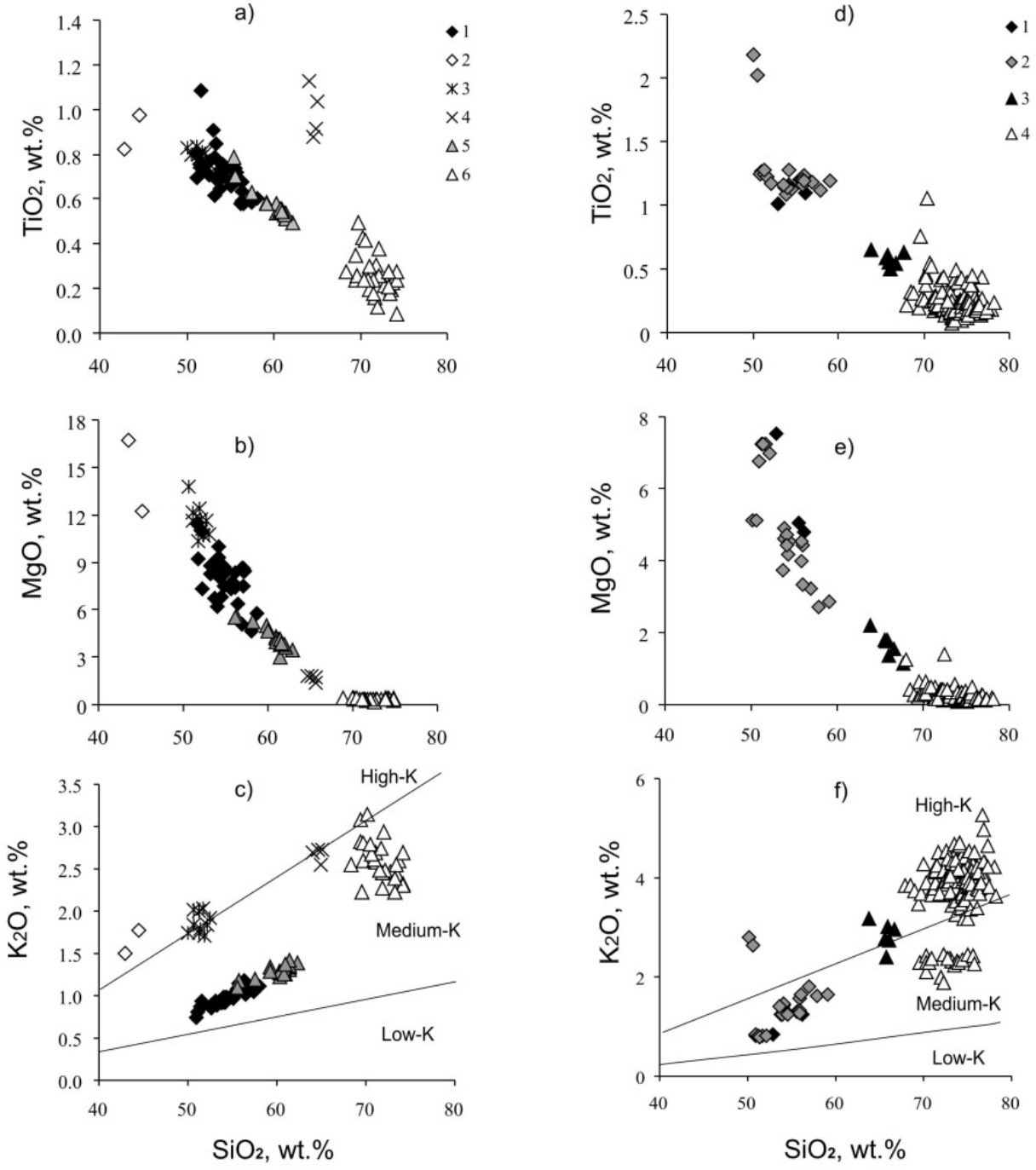

Fig. 1. Harker diagrams for Shiveluch volcanic massif melts (a-c) and Ichnisky volcanic massif melts (d-f). Legend: a-c 1, 3, 5 – whole rocks; 2, 4, 6 – melts of the monogenetic centers and polygenetic central volcano; d-f 1-3 – whole rocks, 2,4 – melts of the monogenic center and central volcano

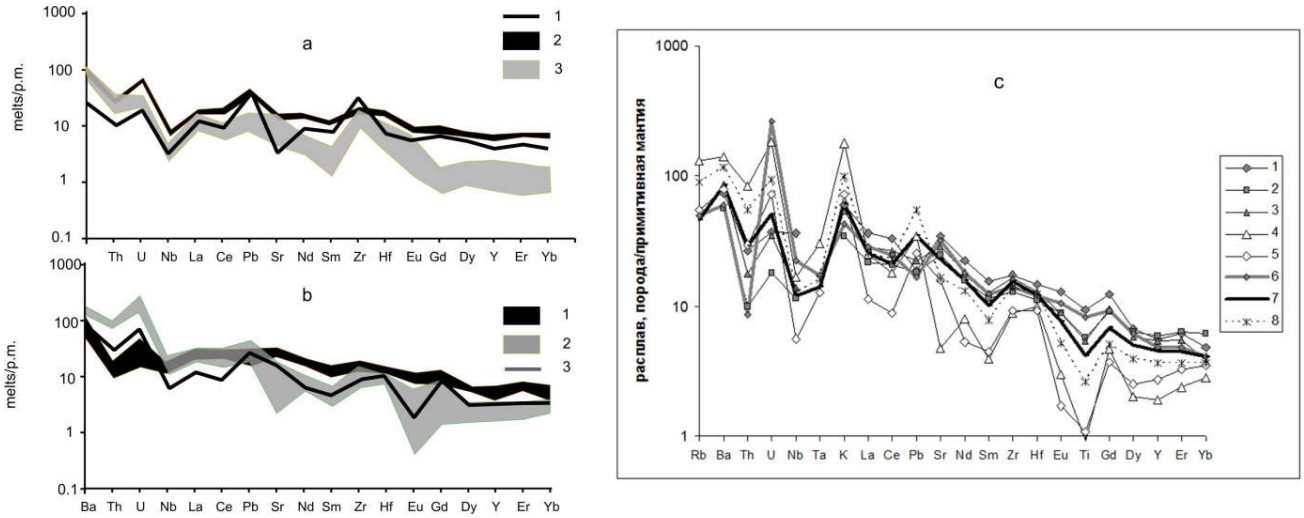

Fig. 2. Primitive mantle-normalized diagrams of trace element distribution in volcanic rocks. of (a) and Ichinsky (b) massifs. Legend: a - Shiveluch, 1, 2 – melts of monogenetic centers; 3 – melts of the polygenetic volcano; b – Ichinsky, 1 - melts of monogenetic center, 2, 3 - melts of the polygenetic volcano; c – Ichinsky, 1-3 – melts of monogenic center, 4,5 – melts of central volcano, 6,7 – rocks of monogenic center, 8 – rock of central volcano. Composition of primitive mantle after Sun and McDonough (1989).

A large amount of data on melt inclusions of Shiveluch and Ichinskiy centers is presented in (Tolstykh et al., 2015, Tolstykh et al., 2018). For comparison, data on the composition of melt inclusions in olivine were used (Volynets, 2006).

Rokcs and melts of monogenetic and polygenetic edifices have very different composition in both cases (both in SiO_2 and alkaline and femic components, fig. 1, 2). It is significant that in most cases the rocks are different from melts, with the exception of the Southern Cherpouk center (fig. 1d). For Shiveluch volcano high alkalinity characterizes one of the mafic centers (rocks and melts). High potassium is typical for silicic rocks and melts of Ichinskiy volcano. The concentrations of the main elements in the melts and rocks of these volcanoes form a complicated trend, which can be interpreted in terms of 1) genetic variation of melt sources, 2) combination of magmatic mixing, and, possibly, fractionation.

Trace elements distribution diagrams show melts characteristics even more clear (fig. 2). Basic melts in both cases are enriched by MREE and HREE and depleted incoherent elements poorer with respect to more differentiated magmas. The distribution diagrams of rare elements demonstrate complex relationships of their contents in contrast rocks and melts. Thus, increased alkalinity can characterize individual types of whole rocks and melts within a single volcanic center, but not a center as a whole. In case of basic alkaline rocks of Sheveluch the increased alkalinity can reflect compositions of the source and fluid. In case of Ichinsky volcano K-enrichment of acid magmas can demonstrate both the effect of fractionation, and the peculiarities of the processes of mixing and contamination.

This work is performed in accordance with research theme № 0137-2016-005 GEOKHI RAS, financial support by RFBR grants # 17-05-00112, #18-05-00224a.

References

Churikova T., Gordeychik B., Belousov F., Babanskiy A. Finding the center of the basic eruption on the Shiveluch volcano. Materials of the Conference, dedicated to the 75th anniversary of the Kamchatka volcanological station. 2010. pp. 96-100. (in Russian)

Cruz-Uribe A.M., Marschall H.R., Gaetani G., Le. Roux V. Generation of alkaline magmas in subduction zones by partial melting of mélange diapirs—An experimental study. Geology. 2018. V. 46. N. 4, pp. 343-346.

Pevzner M.M., Babansky A.D. Episode 4600-3100 14C of basaltic activity in andezitic Shiveluch Volcano, Kamchatka. 2011. 7th Biennual Workshop on JKASP: Mitigating Risk Through International Volcano, Earthquake, and Tsunami Scien. pp. 262-263.

Ponomareva V.V., Kyle P.R., Pevzner M.M., Sulerzhitsky L.D., Hartman M. Holocene eruptive history of Shiveluch volcano. Kamchatka Peninsula. In: "Volcanism and Subduction: The Kamchatka Region", AGUGMS, 2007. V. 172. pp. 263-282

Sun S.S., McDonough W.F. Chemical and isotopic systematics of oceanic basalts; implications for mantle composition and processes // Saunders, A.D., Norry, M.J. (eds) Magmatism in the ocean basins. Geological Society Special Publications. 1989. V.42. pp. 313-345.

Tolstykh M.L., Naumov V.B., Kononkova N.N., Pevzner M.M., Babanskiy A.D. Types of parental melts of pyroclastic rocks of various structural-age complexes of the Shiveluch volcanic massif, Kamchatka: evidence from inclusions in minerals. Petrology. 2015. V. 23. pp. 480-517.

Tolstykh M.L., Pevzner M.M., Naumov V.B., Babanskiy A.D. Characteristics of melts formed tephra of Pleistocene-Holocene eruptions of the Ichinsky volcano (Kamchatka), according to the study of melt inclusions. Geochemistry. 2018. In press.

Volynets A. Pleistocene-Holocene volcanism of the Sredinny Range of Kamchatka: composition of volcanic rocks and geodynamic model. Dissertation. 2006. MSU. 145 p. (in Russian)

Volynets O.N., Ponomareva V.V., Babanskiy A.D. Magnesian basalts in Shiveluch andesitic volcano. Petrology. 1997. V.2009. N 5. pp. 206-211 (in Russian)

SPECIFIC REE DISTRIBUTION IN ROCKS (KOSYU DEPOSIT, MIDDLE TIMAN)

Udoratina O.V., Nikulova N.Yu., Burtsev I.N.

Institute of geology, Komi SC UB RAS, Syktyvkar, udoratina@geo.komisc.ru

Kosyu rare-metal rare-earth deposit is located in the western part of Middle Timan within Chetlas uplift. The ore field is composed of metasedimentary Upper Riphean units of the Chelas series and intruding intrusive units of the Late Riphean-Vendian complex of Chetlas complex, represented by carbonatites and alkaline picrites. Rare-earth rare-metal mineralization is genetically associated with magmatites and associated structures of this complex. The carbonatites are represented by a bunch in the valley of the Kosyu river, the alkaline picrites – by steeply dipping (70-90^0) dikes stretching up to 5 km long, and small bunches controlled by tectonic dislocations of the northeastern strike. Kosyu ore field was formed as a result of hydrothermal-metasomatic transformations of both sedimentary-metamorphic rocks and alkaline picrites. Metasomatites with rare-metal rare-earth ore specialization are represented by fenites, phlogopite mica, goethite-feldspar rocks and quartz veins with goethite-hematite.

We received new geochemical data on the ore field-composing rocks – phenitized metasandstones, aleurolite, metasomatite on metapsamite and picritic breccia. We determined the content of rare and rare-earth elements by ICP-MS (Agilent 7700x, analyst D. V. Kuzmin) at Geonauka Center of Institute of geology Komi SC UB RAS, as well as in VSEGEI Centre, Saint Petersburg.

Breccia of alkaline picrites (sample 3052/3, the center of the ore zone) is characterized by a brecciated structure, a massive texture, and consists of debris, up to 3.0 cm of size, cemented by a fine-grained olivine-pyroxene matrix, actually picrites consisting of aegirine, alkaline amphiboles, pyroxenes, biotite, calcite and apatite and xenoliths of host rocks (quartzite and quartzite sandstones).

Aleurolite (about 340/2, 1.5 m from the ore zone), characterized by a layered aleuritic structure and a massive texture, is composed of slightly corroded clastic grains of quartz and feldspar of aleuritic and fine-sandy dimension, immersed in the basal sericite-chlorite cement pigmented with iron hydroxides. According to the results of the standard recalculation of the chemical analysis (Table 1), the aleurolite contains (vol.%): quartz ~ 35, muscovite ~ 32, potassium feldspar ~ 10, acid (No. 12) plagioclase ~ 9.0, chlorite ~ 8, hematite ~ 4, ilmenite ~ 0.8 and leucoxene ~ 0.5.

Aegirine metasomatite on metapsymite substrate (sample 340/4, in the fracture zone) is a greenish-bluish fine-grained rock cut by numerous quartz veins, under a microscope against the background of relicts of the original detrital rock, revealing a nematolepidoblastic structure and a massive texture. The rocks are composed of aegirine, edenite, feldspar, quartz (authigenic and allotigenic), muscovite and alkaline amphibole. According to the results of the standard recalculation, the main rock-forming minerals (vol.%) are: quartz (43), alkaline hornblende (26), aegirine (17), potassium feldspar (10) and glaucophane (4).

Fine-grained feldspar-quartz meta-sandstones (samples KO 1/15, KO 2/15, KO 4/15, KS 1/15) are characterized by a granoblastic structure, a massive texture and composed of quartz and feldspar grains with different degree of rounding. The cement is regenerative quartz and porous quartz-chlorite-sericite and brownish-brown colomorphic. The sandstones are similar by the composition and, according to the results of the standard recalculation, contain (vol.%): quartz 73-93, potassium feldspar 1-8, sour (No. 10) plagioclase 1-8, chlorite 1-5, muscovite 2-3, hematite 0.5-2.0, ilmenite 0.3-0.5.

By MgO content, the picritic breccia and aegirine metasomatite are classified, according to the classification by Ya. E. Yudovich and M.P. Ketris (2000), to pseudosiallites, and the aleurolite and sandstones have compositions typical of sedimentary rocks poorly affected by metasomatic processes. The increased alkalinity and hydrolysicity of aleurolite, as compared to sandstones, seem to be conditioned by allotigenic mica in its composition. The contents of rare-earth, rare and scattered elements in the rocks differ by two orders. The aegirine metasomatite from the ore-bearing zone is characterized by maximal REE content ~5946 g/t, the minimal values (~73 g/t) are found in slightly altered sandstones of sample KO 2/15 at the periphery of the ore field.

The REE spectra, normalized to primitive chondrite, have a slight slope, characteristic of metaterrigenous rocks, which are not associated with volcanism. The spectra of sandstones (Fig. 1, sample KO 1/15, KO 2/15, KO 4/15, KC 1/15) are similar. Their structure, typical of sedimentary rocks, is characterized by the predominance of light REE over heavy (LREE/HREE 3.48-4.27), almost horizontal interval of the spectrum of heavy rare earths and a clear europium minimum. The only difference between the REE spectrum of the picritic breccia is the absence of a europium minimum. Such a REE distribution spectrum of picritic breccia seems to be an exception and to be conditioned by the influence of xenoliths of host rocks in the breccia.

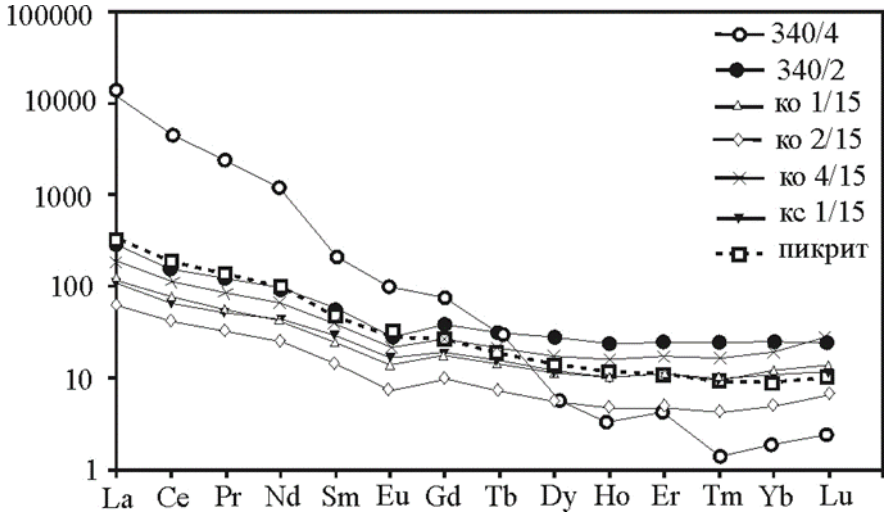

Fig. 1. Chondrite-normalized spectra of REE distribution in the rocks of Kosyu ore field.

In the REE composition of aegirine metasomatite the light rare earths predominate over heavy ones and there is practically no europium anomaly. The formation of metasomatic rocks, as a result of the interaction of alkaline solutions with the original unaltered sandstones of host rocks and crystallization of albite and potassium feldspar, resulted in enrichment by light lanthanides and their concentration in rare-earth minerals. LREE mineral-concentrator is monazite.

The quantitative index of REE amount depends on the position of sampling point with respect to the ore zone and reflects the degree of influence of the metasomatic processes particularly represented by the change of the sodium and potassium feldspars ratio. The samples of sandstones, studied by us, are practically not affected by metasomatic processes and keep the allothigenous amount of REE. The sandstone with a minimum K_2O content is characterized by the lowest value of the REE sum (sample KO 2/15). Also minimum contents of low-mobile Sc, Zr and Hf are determined there, the largest quantities of which are present in the metasomatite.

All studied rocks are impoverished by europium. The value of Eu/Eu* ratios in the picritic breccia is 0.85, slightly below threshold 0.9, suggesting the rocks formed from mantle material. The values of this index in aleurolite (0.59) and sandstones (0.63-0.65) correspond to normal values for these types of sedimentary rocks. The metasomatite is characterized by abnormally high content of light rare earths and is substantially depleted in heavy rare earths and U. La/Sc and Th/Sc ratios in aleurolites and sandstones are close to PAAS and largely determined by the initial compositions of psammites in which, based on Lan/Ybn value in interval 9.73-12.03, the prevalence of products of erosion of the upper continental crust is diagnosed.

The picritic breccia is marked by lack of europium anomaly and V, Cr, Co concentration characteristic of basic rocks. The sharp differences in the compositions of the described above rocks and metasomatites, expressed in the number and ratio of rare earth elements and rare elements, reflect the intensity and direction of metasomatic processes. The practically hurricane content of light rare earths is conditioned by a specific nature of the fluid, a bright diagnostic feature of its chemical composition is the significant predominance of sodium over potassium.

The received data allow concluding that the sandstone of Visinga formation, containing rare-metal rare-earth mineralization. formed in the shallow marine environment of continental margin during the period of absence of magmatic activity, due to erosion and resedimentation of an ancient platform and acid magmatic rocks of, probably, subplatform riftogenic complexes. The differences in the quantitative content of REE in the studied metapsammites are mainly resulted from their initial composition - content of allothigenous minerals-REE concentrators, correlated with the total initial alkalinity of the rocks and granulometric features of the deposits. The influence of basic volcanites and alkaline fracture-vein objects on the change of the composition of the rocks of Visinga formation is conditioned by the permeability of metapsamites. The criteria for diagnosing metasomatic transformations are a sharp predominance of sodium over potassium and increasing light REE content, together with decreasing heavy REE. LREE/HREE ratio is a quantitative measure of the metasomatic change.

State task № ГР АААА-А17-117121270035-0.

PETROLOGY AND GEOCHEMISTRY OF PODIFORM CHROMITE IN EASTERN PART OF VAN-TURKEY

Üner T.[1], Aksoy İ.[2]

[1]Department of Geological Engineering, Van Yüzüncü Yıl University 65500,Van, Turkey
[2]Department of Geological Engineering, Dumlupinar University, 43050 Kütahya, Turkey
(irem.arat@dpu.du.tr)

In this study, origin of chromite and dolerite dikes in the eastern part of Van region was investigated by field observations, microscopic studies and chemical analyses. The ultramafic rocks in the region are tectonites and harzburgite is the dominant lithological unit. Dunite crops around out less than harzburgite. It appears as an envelope chromite deposit if it exists. Basic dikes widespreadly observed in the study area and pyroxenite dikes crosscut these units. Chromites are disseminated, spotted, layered and massive in character and present a serie from harzburgites to massive chromite in the sequence of disseminated-spotted and massive chromite.

In this study, the whole rock major oxides, trace elements and mineral chemistry of ultramafic blocks (Harzburgite, Dunite and chromitite) in the Yüksekova complex are investigated to determine

the formation mechanism of ultramafic bodies (Eastern Turkey-Van Region). The whole rock Al_2O_3, CaO, FeO_t and MgO contents (%wt) of all ultramafic blocks indicates that depletion in these elements. Cr# (chromian number) of spinels and chromitites bodies and Fo components of olivine support with much higher degrees of depletion in the podiform chromite bodies. Diabase dikes usually accompany to chromites. Presence of intense chromite deposits in the Eastern Van region, high chromium contents of chromites, diabase dikes occurrences accompanying to chromites, being subduction related origin of dolerite dikes show that podiform chromites of the region formed in a island-arc environment by rock-melt interaction.

REE AND TRACE ELEMENT DISTRIBUTIONS OF FE-AL LATERITES ORIGINATED FROM YONCAYOLU METAMORPHICS, KAHRAMANMARAŞ (SE,TURKEY)

Unluer A.T., Budakoglu M., Kırıkoğlu S., Doner Z., Kocatürk H., Kumral M.
Istanbul Technical University, Department of Geological Engineering, 34469, Istanbul, Turkey, unluera@itu.edu.tr

The Carboniferous-Permian Yoncayolu Metamorphic rocks are considered to be the lower units of the, Keban-Malatya Metamorphic group. These rocks are can be described as gneisses, amphibolitschists, calchists, intercalated with metavolcanics, marbles and quartzites. The weathering products (bauxite nodules and terra rossa) of the Yoncayolu metamorphics are common in Northern parts of Kahramanmaraş area. Both Bauxite nodules and terra rossa enriched in iron (up to 80% Fe_2O_3) and aluminum (up to 52% Al_2O_3) due to the presence of goethite, hematite and diaspore minerals. Presence of high REE (100-500 ppm) indicates that the laterites are assembling the geochemical remarks of the metamorphic origin. On the other hand Pb (up to 0,15 PbO %), Zn (up to 0,35 %) and As (up to 0,11 %) also enriched in both Terra Rossa and bauxite nodules, due to the hydrothermal activities circulating trough metamorphic units. These hydrothermal activities are thought to be originated from the volcanic and plutonic activities during the Cretaceous period.

Financial support of this study is provided by The Scientific and Technological Research Council of Turkey. Project Number: 114Y646.

INITIAL SUBALKALINE MAGMATISM OF THE NEOARCHAEAN ALKALINE PROVINCE OF THE KEIVY STRUCTURE

Vetrin V.R. [1,2]
[1]*GI KSC RAS, 184209 Apatity, Murmansk region, 14 Fersman Str.*
[2]*IMGRE, 121357 Moscow, 15 Veresaev Str., vetrin@geoksc.apatity.ru*

The Earth's most ancient alkaline and subalkaline rocks with high potassium content occur in the Pilbara Craton, Western Australia. However, in many cratons on the Earth the first geologically important shows of alkaline magmatism are dated 2.5-2.7 Ga. The Kola Peninsula is one of such regions. In its central part, there is a 2500 km^2-long Neoarchaean alkaline province composed of alkaline granites, alkaline and nepheline syenites. Along with alkaline rocks, the province contains those of subalkaline composition.

Rocks of the Neoarchaean latite-monzonite-granite association (ALMG) preserved as xenoliths and remnants in plagiomicrocline granites in the SW part of the Keivy structure in the central Kola Peninsula. Products of subvolcanic, hypabyssal and mesoabyssal depth facies are obtained among the association rocks. The U–Pb datings of zircon from them showed 2674±6 Ma and reflect the time of the rock crystallization. The rocks of the near-surface and hypabyssal facies typically have sharply zoned plagioclase crystals. They are submerged into the fine-grain basis of granophyre or micropegmatite structure. Potassium feldspars with high Na content represented by orthoclase. Amphiboles and biotites have high concentrations of titanium, and magnetite content of up to 4 %. Porphyry-like granites of mesoabyssal facies include weakly zoned crystals of plagioclase and a

microcline with low Na content. They are characterized by a more leucocratic composition, biotite and amphiboles with of low titanium content and almost no magnetite.

Metavolcanics are chemically medium and high silicic rocks of normal (andesibasalts, andesites) and dominating subalkaline series (latites, quartz latites, trachyriodacites). The rocks contain 5.1-8.2 wt. % of alkali with the K_2O/Na_2O ratio from 0.7 to 1.2. On a diagram at coordinates $SiO_2 – K_2O$ the rocks are within the area of highly potassic magmatic products. Peculiar features of the metavolcanic composition are increased concentrations of titanium, phosphorus, alkali and iron. With low contents of alumina and magnesium, it determines generally high Fe/Fe+Mg ratio (F= 69–92) and high agpaitic coefficient (0.52-0.89). The rocks of hypabyssal facies, as well as porphyry-like granites of mesoabyssal depth facies preserve all peculiar features of the metavolcanic composition, i.e. increased concentrations of iron, potassium (3.1-4.5% and 3.7-5.2 % respectively), high content of Fe/Fe+Mg ratio (F= 75-83 and 75-97) and agpaitic coefficient (0.77-0.92 and 0.72-0.87). Rocks of all the depth facies have increased concentrations of highly charged and rare earth elements, i.e. Zr, Hf, Ta, Y, La, Ce, Nb. On diagrams at coordinates "SiO_2 – oxide, wt.%" rocks of ALMG produce a uniform evolutionary trend from andesite-basalts to leucogranites and subalkaline granites with overlapping contents of rocks from different depths. As the rocks become more silicic, their general iron content and agpaitic coefficient grow, while the number of their normative plagioclase decreases. The same trend is observed as the content of alkali and most rare elements (Rb, Ba, Zr, Nb, Th, U, Y, REE (except Eu) increases and concentrations of TiO_2, ΣFe, MnO, MgO, CaO, P_2O_5, Sr and iron group elements decrease. The distribution of REE is moderately fractionated with a distinct europium minimum (0.67-0.47). The above features of the rock composition may be explained by genesis of the volcanic-plutonic formation during the fraction crystallization of melts with restite produced. The latter mainly consists in pyroxene, amphibole, magnetite, titanite and apatite.

The studied quartz latites and quartz monzonites contain 9.1–13.5 ppm Sm and 47.9–69.2 ppm Nd. It is 60–90 and 105–150 times higher than contents of these elements in chondrite C1. The ratio $^{147}Sm/^{144}Nd$ is 0.11–0.12 and corresponds with its average crustal value (0.118±0.017). The value of the measured $^{143}Nd/^{144}Nd$ ratio in rocks is 0.511061–0.511365. The values of model age are within a narrow range of 3.14 to 3.21 Ga, with $\varepsilon Nd_{(2670)}$ of 2.2 to -1.3. These data indicate the Mesoarchaean age of the protolith and the presence of both crustal, and mantle matter in the composition of the association rocks. On diagrams at coordinates $^{147}Sm/^{144}Nd – ^{143}Nd/^{144}Nd$ minerals and their hosting rocks have isochron dependencies dated as 1817±72 and 1510±51 Ma. The obtained datings are considerably low than the age of the rocks dated with the U-Pb method using zircon (~2.67 Ga). Within the margin of identification errors, they are close to the ages of the Proterozoic metamorphism and metasomatism within the Keivy structure (1.95–1.5 Ga) and the palaeorifting Imandra-Varzuga structure south from it. The value of the Sm/Nd ratio in the studied rocks slightly varies (0.18–0.19). The isochron dependencies with lower figures of the defined age were probably due to redistribution of Sm and Nd isotopes between ancient and new minerals of the rock formed in the Proterozoic metamorphism.

The isotope composition of Hf is studied in zircon from samples of quartz latite and quartz monzonite. The two-stage model age of zircon $T_{Hf}(DM)$ is 3.05–3.39 Ga. It is close to the age $T_{Nd}(DM)$ of country rocks, which may be due to the syngenetic nature of the rock and zircon. Initial ratios $^{176}Hf/^{177}Hf$ are within the range of 0.280950–0.281069, and points of zircon composition plot a field on the evolution trend of the chondrite uniform reservoir (CHUR, Fig. 1). They are within the fields of compositions of zircon from gneisses of the Kola Superdeep Borehole, eclogites of the southern Kola Peninsula and are mainly within the field of compositions of the Neoarchaean zircon crystals from xenoliths of garnet granulites from the lower crust. According to isotope-geochemical data on all studied zircons and country rocks, the basic composition of protoliths is presumed.

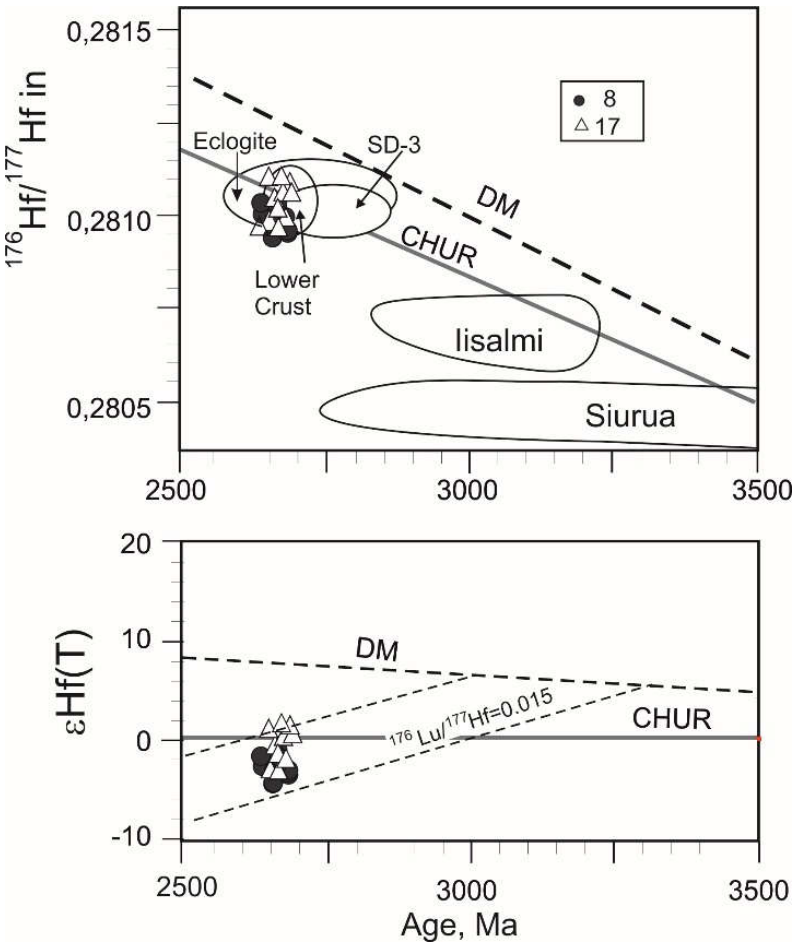

Fig. 1. Diagram of zircon composition "T, Ma – $^{176}Hf/^{177}Hf_{initial}$" and "T, Ma – εHf_{in}". Iisalmi, Siurua- areas of composition of zircon from the most ancient complexes of the NE Baltic Shield. SD-3- plagiogneisses of the Kola Superdeep Borehole. Eclogite – eclogites from the southern part of the Kola Peninsula. Lower crust – the area of composition of zircon from xenoliths of the lower crust of the region.

Considering the value εHf(T), points of composition of zircon are within the field of the crust development with $^{176}Lu/^{177}Hf$= 0.015 and ages of 3.0–3.3 Ga. It admits the initial melts to have formed mostly using the matter left in the crust for a long time. At the same time, positive values εHf(T) were defined for some zircon crystals from quartz monzonite, which indicates a possible impact of the mantle source in their petrogenesis.

Initial magmas of the association are presumed to have formed from melting of metasomatically altered basic rocks, when the lower crust was intruded by basic melts. They are initial for rocks of the dyke complex and gabbrolabradorite massifs. On diagrams at coordinates SiO_2-Mg#, SiO_2-K_2O, SiO_2-Na_2O points of the formation rocks composition are within the fields of partial melts, which were produced in melting of medium- to high-potassium rocks of basalt composition.

The U- Pb age of alkaline granites that spatially associate with ALMG is similar, but their time of formation is later, according to geological data. Compared to ALMG, alkaline granites have higher concentration of SiO_2, alkali (K_2O/Na_2O= 1.1–1.4), higher iron content (F= 84–98%), agpaitic value (0.86–1.2), and lower concentration of TiO_2, MgO, ΣFe, Al_2O_3 (Batieva, 1976). It might be determined by higher differentiation of their initial melts in comparison with ALMG. The alkaline granites are believed to have occurred from initial melts that are compositionally close to ALMG and formed under higher differentiation within the source.

The author is grateful to E.A. Belousova (Macquarie University, Sydney, Australia) and A.A. Kremenetsky (IMGRE, Moscow) for analyzing isotope composition of hafnium in zircon. The research is carried out under support of RFBR (grants 17-35-50002, 16-05-00026a) and state Contract № 13/17-1.

References

Batieva I.D. Petrology of alkaline granitoids of the Kola Peninsula. L.: Nauka. 1976. 224 p. (In Russian).

GEOCHEMICAL FEATURES OF KAMTHAI CARBONATITE COMPLEX, BARMER DISTRICT, RAJASTHAN, INDIA

Vladykin N.V.[1], Chosh P.[2]

[1]Institute of Geochemistry CO PAH. Irkutsk, Russia, vlad@igc.irk.ru

[2]Institute of Science, Bangalore

Kamthai carbonatite complex is located in Barmer district, Rajasthan,in south-west India, not far from the border with Pakistan (fig. 1). Age of the massif is (65±2 Ma) [S.K. Bhushan, 2015]. The outcrop of carbonatite complex region is insufficient. Country rocks of the complex are presented by lavas of riolite and sandstones of the Lower Cretaceous. Carbonatite complex comprises of ultrabasic alkaline rocks - ijolite-nephelinite, nepheline syenite, phonolite and carbonatite. Ijolite-nephelinites are the earliest rocks and are cut by dykes and bunches of carbonatites. Nepheline syenites form dykes of different sizes.

According to composition of carbonates and rare-earth minerals, three types of rocks are detached.

The first type is calcite carbonatites with c bastnaesite-synchysite-ancylite form dyke bodies with typical intergrowth of calcite and rear earth minerals (fig. 2). Rear earth carbonates are located in interstitions of large calcite aggregates. Calcite aggregates consist of small rounded grains of calcite, size up to 1 mm. Carbonatites of that type are main ores of this deposit, with concentrations of TR2O3 15-20%. There are also other minerals in these rocks: barite, cerianite, albite and microcline.

The second type is ankerite-calcite carbonatites, in which the main rear earth mineral is carbocernaite-(Ce), Sr-bearing calcite with lesser strontianite and abundant celestine carbocernaite-(Ce) commonly intergrown with bastnaesite-(La) and daqingshanite-(Ce), bastnaesite-(Ce). There is an interesting fact of crystallization of three rare earth fluorine-carbonates - bastnaesite, synchysite and parisite in these carbonatites.

The third type of carbonatites is presented by small veins of pink calcite with low concentrations of rare earth elements. Veins of carbonatites of the third type cut carbonatites of the first and the second types.

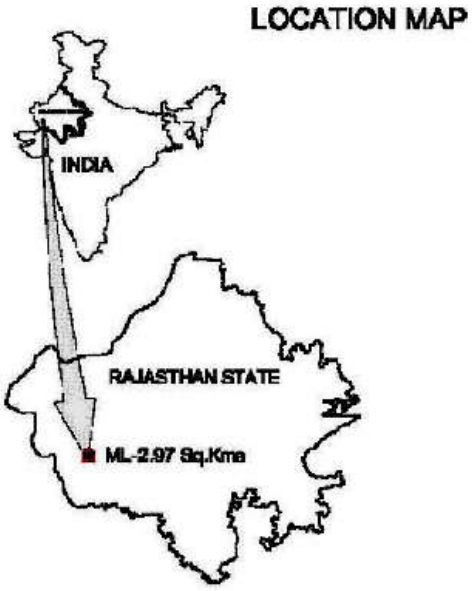

Fig. 1 Geographical position of the Kamthai massif.

Fig. 2. Typical intergrowth of calcite (white) with rare earth minerals (gray) in carbonatite of the first type.

Spider-diagrams of rare elements of different rocks of the carbonatite complex are shown in fig. 3. Clearly-defined negative anomalies of Nb, Ta, Zr, Hf, and Ti and less-defined Pb negative anomaly, are typical for carbonatites of the first type. Carbonatites of the second type have configurations of

anomalies similar to those of the first type, but they are not as clearly-defined. Carbonatites of the third type are characterized by lower concentrations of all elements, but configurations of diagram lines are similar to those of the second type, with less-defined anomalies. Spider-diagrams of all silicate rocks of the complex are similar and differ markedly from spider-diagrams of carbonatites. Seamless transitions from one element to another are typical for them; there are almost no well-defined positive and negative anomalies.

REE spectra of all rocks of the complex, normalized to chondrite, are shown in fig. 4. They are identical for all rocks, have similar line slants and have no fractionation of Eu. All these factors give evidence of their genetic relations. High concentrations of Nb are typical for silicate rocks of the complex.

Concentrations of Nb in nephelinites are 200-250 ppm, in nepheline syenites are 320-390 ppm, in phonolites are 150-200 ppm; in carbonatites concentrations of Nb are below 50 ppm.

According to a depth of formation, carbonatite complex belongs to a near-surface feature. All rocks are mainly having fine grained and microgranular texture. Flow structures are clear-cut in phonolites and nephelinites. According to previous researchers [S.K. Bhushan, 2015] carbonatites have magmatic genesis and we have the same opinion. Carbonatites of Kamthai clearly differ from carbonatites of Tamil-Nadu, South India [Vladykin et al., 2008].

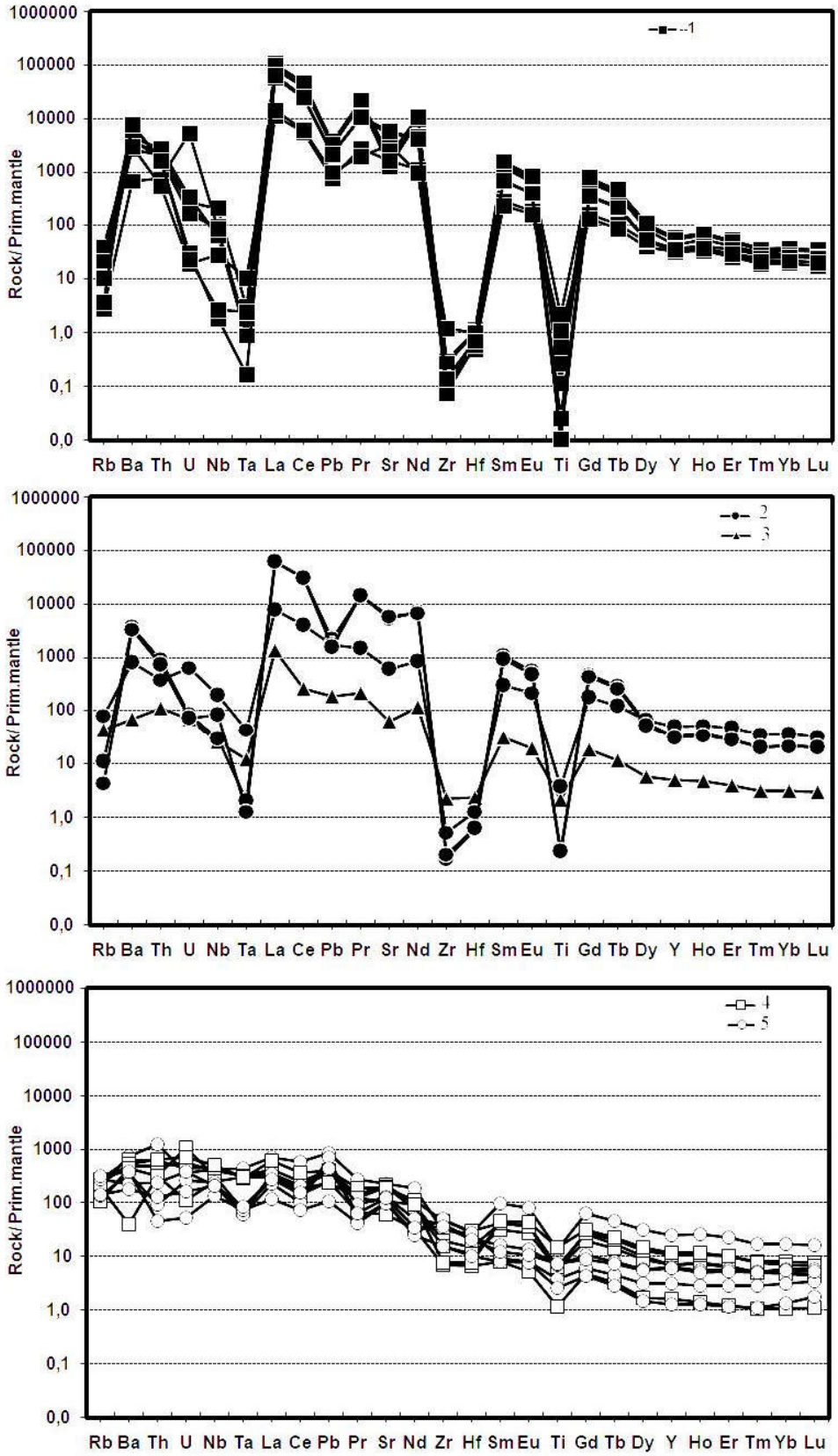

Fig. 3 Spider-diagram of rocks of the Kamthai massif.

Legend: 1 - calcite carbonatites with bastnaesite (type I); 2 - ankerite carbonatite with carbocernaite (type II); 3 - late calcite carbonatites; 4 - ijolites and nephelinites; 5 - phonolites and nepheline syenites.

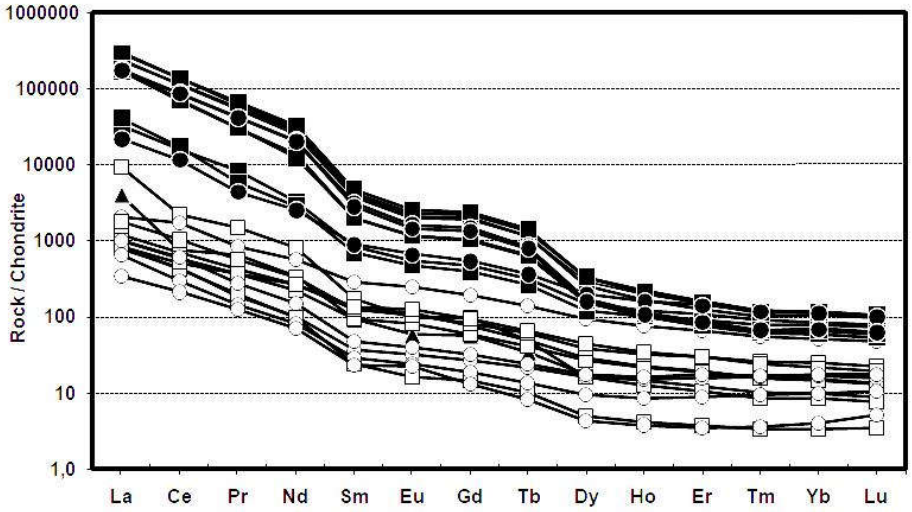

Fig. 4. REE spectra of rocks of the Kamthai massif. Legend: see fig. 3.

The work was supported by the Russian Foundation for Basic Research (grant 17-55-45028).

References

Bhushan S. K. Geology of the Kamthai Rare Earth Deposit //Journal geological society of India Vol.85, May 2015, pp.537-546.

Vladykin N.V., Viladkar S.G., Miyazaki T. and Ram Mohan V. Geochemistry of benstonite and associated carbonatites of Sevathur, Jogipatti and Samalpatti, Tamil Nadu, South India and Murun Massif, Siberia // Journal of the Geological Society of India, 2008, V. 72, № 3 p. 312-324.

SHANDITE IN VEIN OF SERPENTINE AND PHLOGOPITE FROM GARNET LHERZOLITE THE KIMBERLITE PIPE OF MIR

***Vorobei S.S.*[1,2], *Garanin V.K.*[1]**

[1]*Faculty of Geology, Moscow State University, Moscow, Russia*

[2]*Vernadsky Institute of Geochemistry and Analytical Chemistry, RAS, Moscow, Russia*

vgaranin@mail.ru, Patesonchic77@mail.ru

Shandite (Fig. 1) was first found in Nickel Reward Mine, Trial Harbour district, West Coast municipality, Tasmania, Australia. Named by Paul Ramdohr in 1950 for petrologist, Samuel James Shand [October 29, 1882 Edinburgh, Scotland - April 11, 1957 Boughty Ferry, near Dundee, Scotland], professor at University of Stellenbosch, South Africa, later chair of petrography at Columbia University, New York (www.mindat.org). Shandite was originally identified and named by Ramdohr (1950), who observed it in serpentinized ultramafic rocks at Trial Harbor, Tasmania, where it occurs with heazlewoodite and the Ni-Fe alloy awaruile (awaruite has been looked for but not found in the Isua sample). Ramdohr characterized this "shandite" optically and by X-ray methods, and suggested that it represents the Pb-analogue to the NiBi sulfide parkerite, $Ni_3Bi_2S_2$ (Robert F.Dymek, 1987).

The rare sulfide mineral shandite, $Ni_3Pb_2S_2$, has been identified in a metadunite from the Isua Supracrustal Belt, West Greenland (Robert F.Dymek, 1987). The shandite is found in serpeutinized "metadunite" where it forms a delicate rim on composite grains of heazlewoodite-pentlandite.

The most abundant sulfide is the Ni-rich phase heazlewoodite, whose composition is close to stoichiometric Ni3S2. The composition of the main elements of the literature (Robert F. Dymek, 1987)

heazlewoodite (weight %) Ni (72.7), Fe (0.1), S (26.47); pentlandite Fe (3.38), Co (52.65), Ni (11.58), Pb (0.26), S (32.35); shandite Ni (28.4), Pb (61.64), S (9.58).

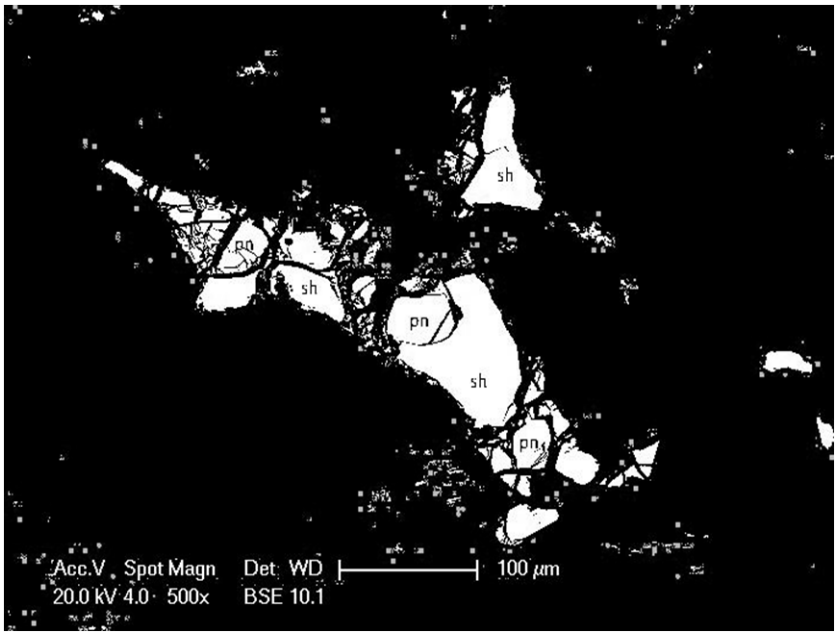

Fig. 1. Shandite $Ni_3Pb_2S_2$, Pentlandite (Fe, Ni)$_9$ S_8, Lizardite $Mg_3(Si_2O_5)(OH)_4$. Nickel Reward Mine, Trial Harbour district, West Coast municipality, Tasmania, Australia (www.mindat.org).

The studied sample occur from the Mir kimberlite pipe and represents a xenolith of garnet lherzolite. The main minerals of the rock are garnet (40-45 %), orthopyroxene (5-10%), clinopyroxene (20-25%) and olivine (15-20%). In the intervals of the garnet and clinopyroxene, amphibole is observed. In kelyphite rims in granate noted phlogopite and Ca-Al-Si-phase. The our xenolith from garnet lherzolite of the Mir kimberlite pipe including in vein phlogopite-serpentine-pentlandite-heazlewoodite and thin rim overgrow shandite (fig.2). The composition of atomic (%) pentlandite Fe (32.04), Ni (35.17), S (32.34); heazlewoodite Ni (74.1), Fe (1.83), S (25.95); shandite Ni (26.54-28), Pb (63.22-65.63), S (9.6-10.07), Cl (1.48).

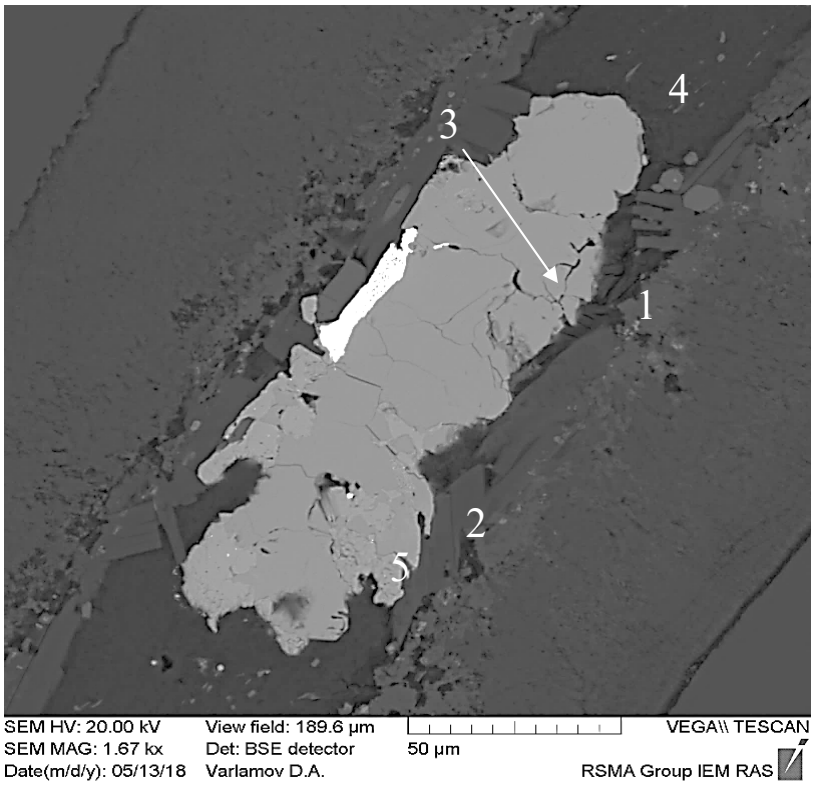

Fig. 2. The xenolith from garnet lherzolite Mir kimberlite pipe. 1 – pentlandite, 2 – heazlewoodite, 3 – shandite, 4 – phlogopite, 5 – serpentine.

It should be noted that scientists have studied synthetic parkerite and shandite (W.S Bnower, H.S. Parker and R.S. Roth). A study of parkerite, shandite, and other materials of similar chemical nature was therefore initiated in order to further determine the crystallographic nature of these phases and their chemical and physical properties (W.S Bnower, H.S. Parker and R.S. Roth).

The discovery of shandite is very rare in the kimberlite pipes of Yakutia. In the works there are studies of this mineral and its synthetic production.

Express my gratitude for the work and conduct of electron-probe microanalysis D. A. Varlamov.

References

W.S Bnower, H.S. Parker and R.S. Roth, Reexamination of synthetic parkerite and shandite, American mineralogist, vol.59, pp. 296-301, 1974.

Robert F.Dymek. Shandite, $Ni_3Pb_2S_2$ in a serpentinized metadunite from the Isua superacrustal belt, west Greenland, Canadian Mineralogist, Vol.25, pp.245-249, 1987.

www.mindat.org.

THE INCLUSION OF YIMENGITE IN GARNET LHERZOLITE FROM THE OBNAZHENNAYA KIMBERLITE PIPE.

***Vorobei S.S.*, Garanin V.K.**

Faculty of Geology, Moscow State University, Moscow, Russia,
Patesonchic77@mail.ru, vgaranin@mail.ru

Including xenolith of metasomatically altered garnet lherzolite (O-125) from the Obnazhennaya kimberlite pipe (Fig. 1). The potential new mineral species belonging to this group have been identified: yimengite Al-dominant analogue (Fig. 2). Yimengite $K(Cr, Ti, Mg, Fe, Al)_{12}O_{19}$, that is a rare mineral of group of magnetplumbite $PbFe_{12}O_{19}$ (Haggerty, 1991) with the general formula $AM_{12}O_{19}$.

Yimengite was first discovered in kimberlite dykes in Shandong province, China (Dong et al., 1983) in association with olivine, pyrope, magnesia chromite, phlogopite, ilmenite, chromium-diopside, apatite, zircon, moissonite. As a product of changes in xenocrystals of magnesia chromite, yimengite is detected in a heavy concentrate from kimberlite sill in the Guaniamo region, Venezuela (Nixon, Condliffe, 1989). According to the compositional characteristics of chromite, which develops yimengite, belong to the association of diamondiferous garnet harzburgites (Nixon, Condliffe, 1989). Discovered yimengite inclusions in diamonds (Sobolev et al., 1988; Bulanova et al., 2004), where it is also associated with the typomorphic minerals harzburgite association: chromite, chromium subcalcic garnet, enstatite.

The studied xenolith of garnet lherzolite, consisting of garnet (30-35 %), orthopyroxene (15-35 %), clinopyroxene (10-30 %), olivine (10-20 %) and alumochrome (5%).The composition of yimengite from xenoliths Obnazhennaya kimberlite pipe have specific composition, differing higher content Al_2O_3 (of 19.82-of 22.68 wt.%) and reduced Cr_2O_3 (29,18-31,93 wt.%) relative yimengite from listed objects. So yimengite from kimberlite dykes in China contains 1,30-1,61 wt.% Al_2O_3 and 36,94-of 37.06 wt.% Cr_2O_3 (Dong et al., 1983), from kimberlite sills of Venezuela - 3,61-3,95 wt.% Al_2O_3 and 39,08-to 39.37 wt.% Cr_2O_3 (Nixon, Condliffe, 1989).

In polymineral inclusions in chrome spinel from garnet lherzolite the Obnazhennaya kimberlite pipe yimengite forms a plate of the selection in length from 0.18 to 0.5 mm. Selection the heterogeneous composition of some sites is characterized by the ratio Al:Cr close to 1:1, other –Al>Cr. The chemical composition of the detected inclusions yimengite allow us to consider it as a potentially new mineral species, which is the Al-analogue of yimengite.

The composition of the mathiasite corresponds to formula $(K_{0,68}Ca_{0,24}Ba_{0,08}Sr_{0,06})(Ti_{14.01}Cr_{2,60}Mg_{1,88}Fe_{1,64}Al_{0,82}Mn_{0,05})O_{38}$. Phlogopite include impurities of TiO_2 (1,34 wt.%) and Cr_2O_3 (up to 1.45 wt.%). The composition of rutile: TiO_2 (99,44 wt.%), Cr_2O_3 (0.24 wt.%), FeO (0.21 wt.%).

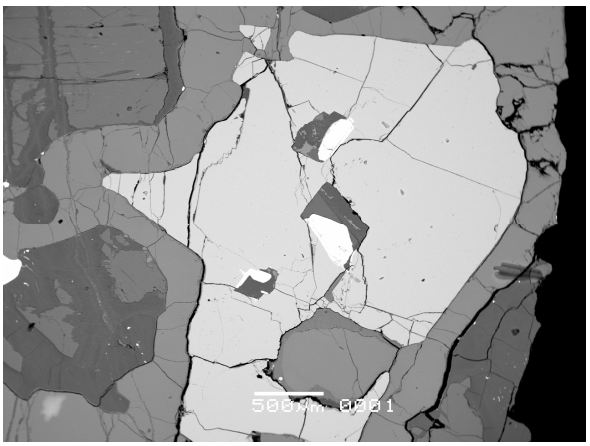

Fig. 1. Polymineral inclusion in chrome spinel. Sample (O-125), Obnazhennaya kimberlite pipe.

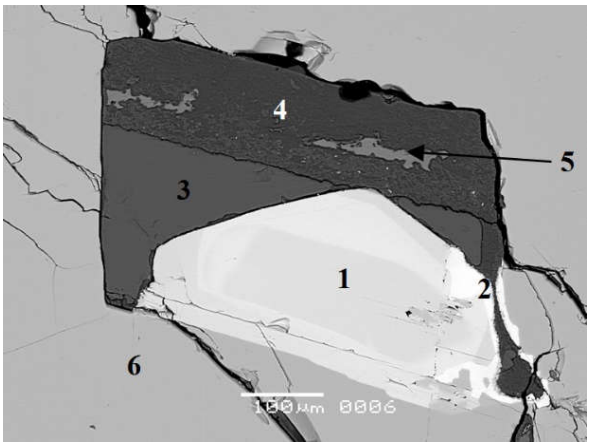

Fig. 2. Inclusions containing yimengite Al analogue (1), mathiasite (2), dolomite (3), serpentine (4), calcite (5) in Cr-Al-spinel (6). Garnet lherzolite the Obnazhennaya kimberlite pipe. BSE image.

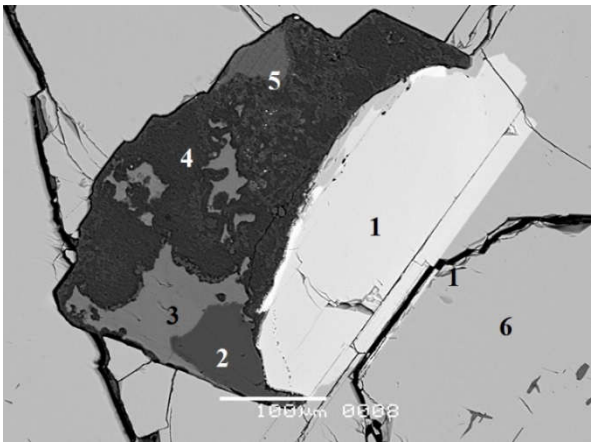

Fig. 3. Polymineral inclusions containing yimengite (1), dolomite (2), calcite (3), serpentine (4) and phlogopite (5) in Cr-Al-spinel (6). Garnet lherzolite the Obnazhennaya kimberlite pipe. BSE image.

Studies of the detected K-Al-Ti-Cr-containing phase by KR - spectroscopy confirmed its belonging to the minerals of the magnetoplumbite group. The formation of yimengite and mathiasite presumably associated with metasomatic changes in mantle alumochrome conditions under the influence of fluid enriched in Ti and K.

References

Bulanova G.P, Muchemwa D.G., Pearson B.J., Griffin S.P., Kelley S., Klemme C.B. Syngenetic inclusion of yimengite in diamond from Sese kimberlite (Zimbabwe) - evidence for metasomatic conditions of growth// Lithos. 2004. V. 77. P. 181-192.

Dong Z., Zhou J., Lu Q., Peng Z. Yimengite, $K(Cr,Ti,Fe,Mg)_{12}O_{19}$, a new mineral from China // KexueTongbao, Bull. Sci. 1983.№15. 932– 936 (in Chinese).

Haggerty, S.E., 1991. Oxide mineralogy of the upper mantle. In: Lindsley, D.H. (Ed.), Oxide Minerals: Petrologic and Magnetic Significance. Reviews in Mineralogy, vol. 25, pp. 355– 416.

Nixon P.H. and Condliffe E. Yimengite of K-Ti metasomatic origin in kimberlitic rocks from Venezuela // Mineralogical Magazine. 1989. Vol. 53.P. 305-309.

Sobolev, N.V., Yefimova, E.S., Kaminsky, F.V., Lavrentiev, Y.G., Usova, L.V., 1988. Titanate of complex composition and phlogopite in the diamond stability field. In: Sobolev, N.V. (Ed.), Composition and Processes of Deep Seated Zones of Continental Lithosphere. Nauka, Novosibirsk, pp. 185–186.

NEW PETROLOGY DATA OF NELSONITE DIKES FROM THE SUWALKI ANORTHOSITE MASSIF (NE POLAND)

***Wiszniewska J.*[1], *Ruszkowski M.*[2]**

[1]*Polish Geological Institute-National Research Institute, janina.wiszniewska@pgi.gov.pl*

[2]*Warsaw University, Department of Geology, michalruszkowski@student.uw.edu.pl*

The ore bearing apatite rocks with variable but low contents of silicate minerals called *nelsonites* have been found in several localities in the world and are usually related to the Proterozoic anorthosite suite (Darling, Florence 1995, Kolker, 1982, Dymek, Owens, 2001, Charlier et al. 2015,Duchesne, J.C. Liégeois, 2015) The name *nelsonite* have been used for the first time by Watson and Taber (1913) for ilmenite-apatite rocks from Nelson County in Virginia State, USA. This rare magmatic rocks form usually a very fine grained dikes or veins between dioritic and anorthosito-noritic complexes and they are composed of ilmenite, magnetite, magnetite-sulphide, rutile and even biotite with main opaque mineral – apatite (Kolker,1982, Darling, Florence,1995). First nelsonites were discovered in Poland within a western margin of the Suwalki Anorthosite Massif (SAM) in Łopuchowo IG-1 borehole, northeastern corner of the country (Krzeminski at al. 1988). They form nine zones of irregular veins between diorites gabbronorites and anorthosites in the depth interval of 2100-2300m. A main minerals of nelsonite veins are: fluoroapatite (50-70 vol.%), magnetite (5-20 vol.%),ilmenite (2-5 vol.%), pyrrhotite (2-10 vol.%),pyrite (1-2 vol.%), allanite and anhydrite. Some other ore minerals occur in traces as exsolutions in bigger host minerals, The nelsonite rocks from SAM are enriched in REE (5500 ppm). More detailed study reveals presence of Ce,Nd-rabdophane, Ce,Nd-allanite and REE-enriched apatite (Wiszniewska, 1997). Melt inclusions in apatite are filled by pyroxene, apatite, calcite, plagioclase, biotite, halite, sylvite, ore mineral plus aqueous solutions and gas contraction bubble. At 880ºC two melts (silicate and phosphate) were observed in the inclusions, which neither homogenized nor changed their proportions up to 1080ºC. This evidences the formation of nelsonite from an immiscible, two-phase melt. (Kozlowski, Wiszniewska, 2002, 2003).

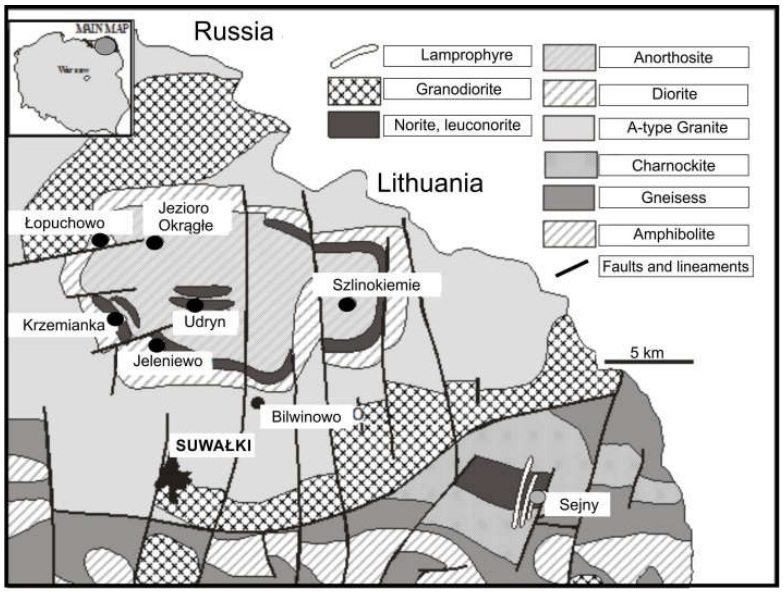

Fig. 1. Geological map of the (SAM) with indication of main Fe-Ti-V ore deposits. Łopuchowo IG-1 borehole contains nelsonite dikes. (Wiszniewska, 2002).

New petrological and SEM analyses on nelsonites from Łopuchowo borehole in nano-space brought new quality of the research. Several new mineralogical discoveries allow to distinguish a final stage of mineralization that was enriched in REE and PGE elements.

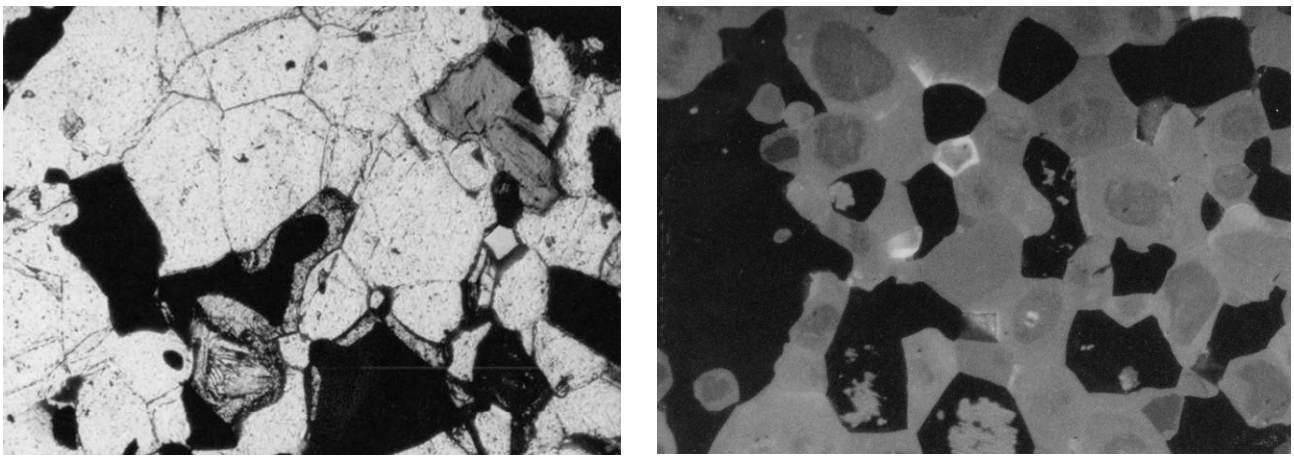

Fig. 2. Ore-apatite nelsonite TL and CL images with automorphic grains of zoned apatite, ore oxides, Fe-Cu-Co sulphides and REE minerals as rims and single minerals.

Methods

Analyses of main rock-forming minerals were carried out on thin sections from Łopuchowo IG-1 borehole with a Cameca SX–100 electron-probe microanalyzer at Polish Geological Institute of Warsaw. An acceleration voltage of 20 kV and a beam current of 15 nA were used. Observations and photographs of the samples were made by means of a scanning electron microscope FE-SIGMA VP (Carl Zeiss Microscopy GmbH) coupled with EDS spectrometers (Quantax XFlash 3 | 10, Bruker Nano GmbH). Small fragments of the samples were attached to the aluminum table with carbon tape. The samples were covered with a 20 nm layer of carbon or gold using a vacuum sputter dryer (Quorum 150T ES). The analyses were carried out at an aperture of 60 μm and an acceleration voltage of 10 keV. The intensity of the beam was 2.5 nA. The working distance of the sample from the column of SEM was depended on the height of the sample and selected so as to reach about 8 mm.

Results

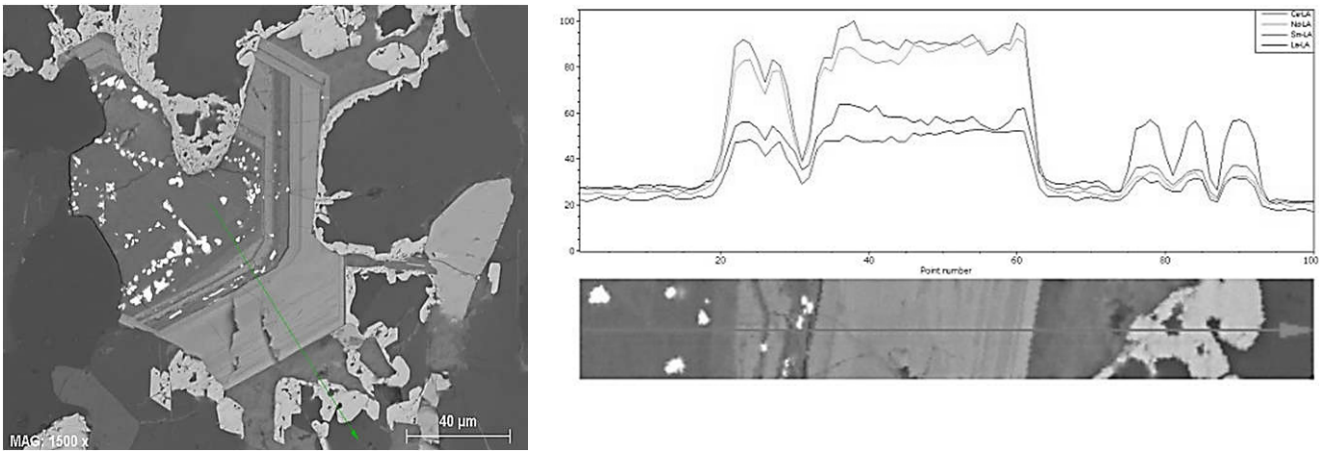

Fig. 3. BSE image of nelsonite REE minerals surrounded by apatite crystals and sulfide rims. Detection line of EDS is showing high content of Ce, La and Nd within rims of allanite.

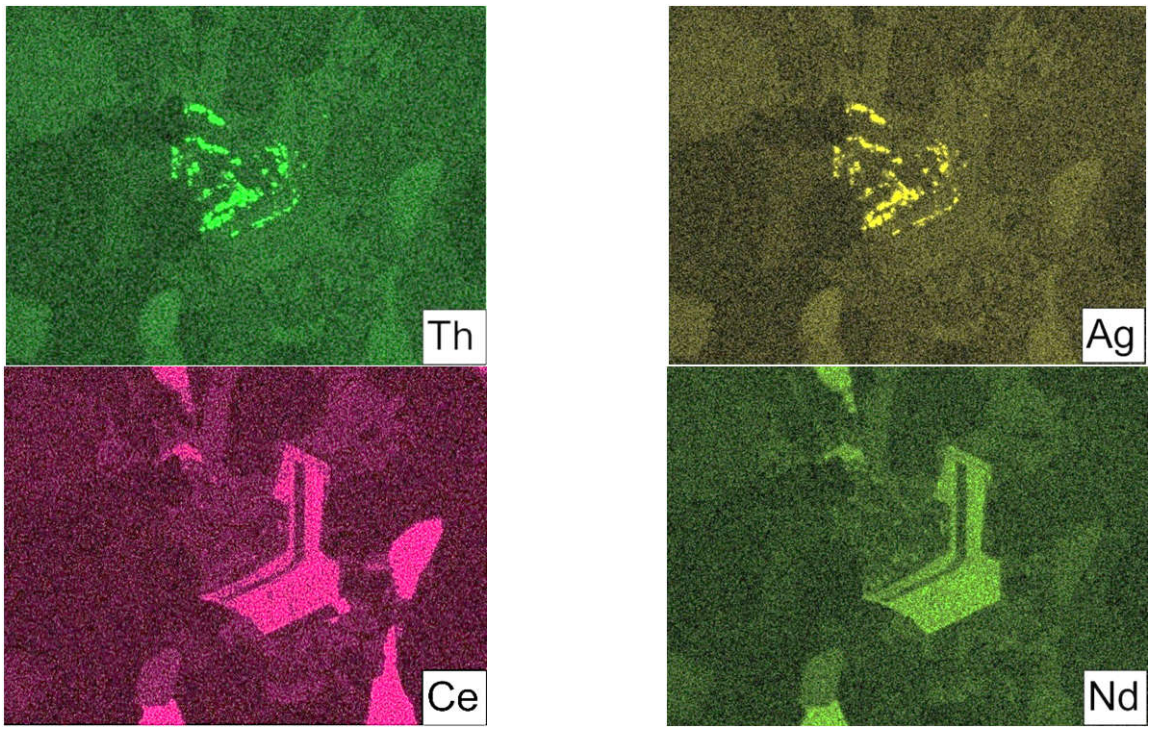

Fig. 3. Mapping images of Fig.2 area. Th and Ag distribution is visible inside the mineral structure. Enrichment of Ce and Nd concentrate in rims and separate REE minerals.

A former studies by Kozlowski, Wiszniewska, (2003) have shown that the concentrations of REE in apatites of nelsonite veins: La, Ce, Nd, with the typical flat or slightly increasing plotting line, indicated a relatively advanced stage of the magma differentiation (Fig. 4). High content of sulphides, that differs Suwalki nelsonites from other occurrences in the world and might have suggested that sulphur acted as one of the fluxing agents in the immiscibility process (Duchesne 1999). Homogenization temperature of melt inclusions in apatite (890-870°C), distinctly indicated that nelsonites formed at the final magmatic stage mainly from melt, which probably gradually and smoothly altered to a very saline high-temperature aqueous solution and subsequently to moderate-saline medium-temperature aqueous solution. The solutions produced the latest outer rims of the apatite grains (690-550 °C).

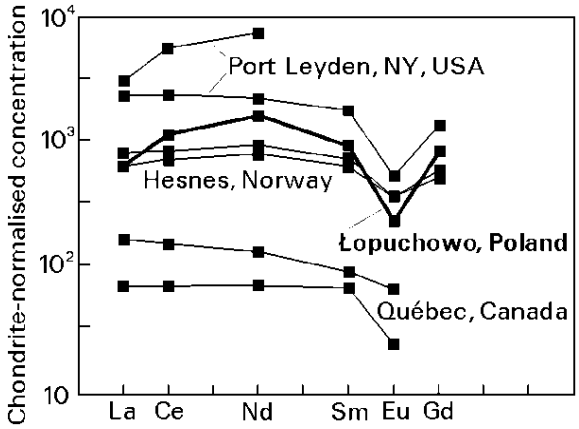

Fig. 4. Rare-earth-element contents in the Suwalki nelsonite compared to the *REE* characteristics of seve-ral world nelsonites.

A new measurements by SEM –EDS mapping method help to discover the distribution of La, Ce, Nd content in late stage REE minerals and fluoroapatite (franckolite) of nelsonite dikes. The occurrences of Th, Ag, Zr, Bi elements have been detected. Application of new equipment available at

Nano-Lab at Geology Dept. at Warsaw University has given an opportunity to study once more former samples of interesting rock material as nelsonites, jotunites and others. We were able to distinguish a new stage of final mineralization of the SAM, which was enriched in REE, Zr and PGE minerals in filaments and outer rims of earlier formed minerals.

Conclusions

The study reports the distribution of main, trace, REE and PGE elements in nelsonites in order to better constrain the origin of Fe-Ti-P-rich rocks. We conclude that: SAM nelsonites have been formed from melt consisting two immiscible phases: silicate one and phosphate one with carbonate admixture with the proportion of these two melts , close to 1:1 ratio(cf. Kozlowski, Wiszniewska, 2002, 2003).This studies in late 90-ties (Wiszniewska J., Kozlowski, 1999) of melt inclusions in apatites from the SAM nelsonites yielded the first evidence of crystallization of nelsonite from phosphate melt immiscible with silicate melt. A late-stage of SAM evolution, with final influxes of nelsonite and (parental for anorthosite) jotunite dikes have shown a distinct enrichment in REE, Zr, and PGE elements as a product of residual magma.

This work was supported by NCN project 2015/17/B/ST10/03540 and project Nr.21April 2017 awarded by the Foundation of the University of Warsaw.

References

Charlier B., Namur O., Bolle O., Latypov R., Duchesne J-C. Fe-Ti-V-P ore deposits associated with Proterozoic massif-type anorthosites and related rocks.// 2015.Earth-Science Reviews. Vol. 141, pp. 56-81

Darling R. S., Florence F. P., Apatite light rare earth element chemistry of the Port Leyden Nelsonite, Adirondack Highlands, New York: implications for the origin of Nelsonite in anorthosite suite rocks//1995. Economic Geology, 90(4):964-968

Duchesne, J.C., Fe-Ti deposits in Rogaland anorthosites (south Norway) geochemical chracteristics and problem of interpretation. //1999. Mineralium Deposita. 34, 182-198.

Duchesne, J.C. Liégeois, J.P. The origin of nelsonite and high–Zr ferrodiorite associated with Proterozoic anorthosite // 2015. Ore Geol. Rev., 71, pp. 40-56

Dymek, R.F., Owens, B.E. Petrogenesis of apatite-rich rocks (nelsonites and oxide-apatite gabbronorites) associated with massif anorthosites// 2001. Econ. Geol. 96, 797–815

Kolker A. Mineralogy and geochemistry of Fe–Ti oxides and apatite (nelsonite) deposits and evaluation of the liquid immiscibility hypothesis// 1982. Econ. Geol., 77, pp. 1146-1158

Kozłowski A., Wiszniewska J. Phosphate and Silicate inclusions in apatite and pyroxene from the Precambrian nelsonites and jotunites of NE Poland// 2002. Arch. Min., T. LIV, 2001-2002, pp.5-21

Kozlowski A., Wiszniewska J. The nelsonite problem: the origin by melt immiscibility//2003. NGU Spec. Publ., vol. 9, p. 35-37

Krzemiński L., Tyda R., Wiszniewska J. Mineralogic and geochemical study of ore–bearing apatite rocks (nelsonites) from the Suwałki Massif (NE Poland)// 1988. *Mineral. Polon*., 19, 2, 35–55.

Philpotts, A.R. Origin of certain iron–titanium oxide and apatite rocks//1967. Econ. Geol., 62, pp. 303-315

Watson T.L., Taber S. Geology of titanium and apatite deposits of Virginia.// 1913. *Virginia Geol. Surv. Bull*. 3–A, 308.

Wiszniewska J. Suwalki nelsonites – new mineralogical and geochemical data. (in Polish) // 1997, Geol. Review, vol.45, nr 9, pp. 883-892

Wiszniewska J., Kozlowski A. Fluid inclusions in ore-apatites from the Suwalki anorthosite, Poland.// 1999. Mineral Deposits: Processes to Processing. Stanley et al (eds) Vol.1. pp.115-121

DEVELOPMENTS OF DIAMOND ANVILS FOR THE STUDY OF HIGH-PRESSURE MINERAL PHYSICS

Yagi T.[1,2], Sakai T.[2], Irifune T.[2]
[1]Geochemical Research Center, The University of Tokyo, yagi@eqchem.s.u-tokyo.ac.jp
[2]Geodynamic Research Center, Ehime University

Diamond anvil cell (DAC) is now the most powerful tool to study the minerals expected to exist in the very deep part of the Earth. When it was invented in the middle of 20th century, however, no one expected that it will become a major tool to study the Earth's interior because, 1. samples were too small, 2. pressure values were uncertain, 3. pressure range was quite limited, and 4. high temperature experiment was difficult. Numerous efforts were made since then by many people and as a result the amount of information we can obtain by DAC experiments have increased enormously. In this report I am going to make a brief summary of such developments and report our recent works to extend the pressure range beyond the limit of conventional DAC.

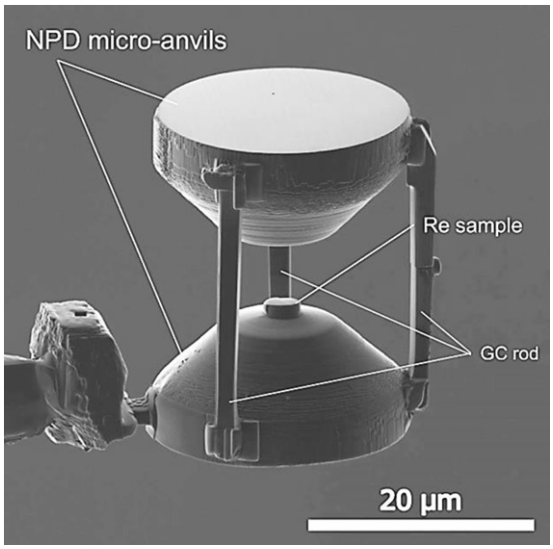

Fig. 1. An example of the micro-anvil system fabricated from nano polycrystalline diamond. This entire set up is compressed in a small sample chamber of conventional DAC.

In early days DAC experiments were limited at room temperature but after the invention of laser heating technique (Ming & Bassett, 1974) it became possible to heat the samples high enough to simulate the conditions of the Earth's deep interior. Extension of the pressure range beyond mega bar (Mao et al., 1978) made it possible to study the behavior of silicates in the lower mantle conditions (eg. Liu, 1974; Tsuchida & Yagi, 1989). However all these experiments were made by directly squeezing powder sample, heat it to high enough temperature, and examine recovered samples by X-ray diffraction at ambient condition. The situation has changed dramatically when synchrotron X-ray was combined with a laser-heated DAC. Very thin and bright X-ray beam produced at the synchrotron radiation facilities made it possible to obtain the diffraction patterns only from the heated region of the sample and high-pressure and high-temperature *in situ* X-ray measurements became routine. Another big advancement was made by using Transmission Electron Microscopy (TEM) and Focused Ion Beam (FIB) to analyze the samples recovered after the high P-T experiments using DAC. Sample size in DAC is very small; above 50 GPa it is typically about 30 μm in diameter and less than 10 μm in thickness. Moreover, very large temperature gradient exists in this tiny sample. In order to extract precise information from such sample, it is essentially important to use the analytical technique with high spatial resolution and magnification, and TEM is an ideal tool for such purpose. Use of FIB made it possible to pick up very tiny part of the sample from the desired location for the analysis of TEM. Because of these techniques, we can now get fruitful information for the behavior of various minerals up to the condition of the Earth's deep lower mantle.

FIB became a powerful tool for other purposes as well. We have been trying to extend the attainable pressures beyond the limit of conventional DAC, which is around 400 GPa, by adopting the FIB for machining very small size of diamond anvils. Figure 1 is an example of the micron-size diamond anvils used in our recent works (Sakai, Yagi, et al., 2015, 2018). It is made of nano polycrystalline diamond (NPD) and this entire assembly is compressed in the small sample chamber of conventional DAC. Although this "double-stage diamond anvil" is a promising technique to achieve pressures above 500 GPa, there are many experimental difficulties. The detail will be described in the lecture.

References

Ming L. & Bassett W. B., Laser heating in the diamond anvil press up to 2000°C sustained and 3000°C pulsed at pressures up to 260 kilobars, *Rev. Sci. Instruments* **45**, 1115 (1974).

Mao H. K. *et al*., High-Pressure Physics: Sustained Static Generation of 1.36 to 1.72 Megabars, *Science* **200**, 1145-1147 (1978).

Liu L. G., Silicate perovskite from phase transformations of pyrope-garnet at high pressure and temperature, *Geophys. Res. Lett*. **1**, 277-280 (1974).

Tsuchida T. & Yagi T., A new, post-stishovite high pressure polymorph of silica, *Nature*, 340, 217-220 (1989).

Sakai T., Yagi T. *et al*., High-pressure generation using double stage micro-paired diamond anvils shaped by FIB. *Rev. Sci. Instr*uments **86**, 033905 (2015).

Skai T., Yag T. *et al*., High pressure generation using double-stage diamond anvil technique: problems and equations of state of rhenium, *High Pressure Research* **38**, 107-119 (2018).

ORIGIN OF LITHIUM AND FORMATION PROCESS OF LITHIUM DEPOSITS IN THE SALT LAKES OF QAIDAM BASIN, CHINA

***Yu J.Q.*[1,2], *Zhang L.*[1,2], *Gao C.L.*[1,2], *Cheng A.Y.*[1,2], *Hong R.C.*[1,2,3]**

[1]*Key Laboratory of Comprehensive and Highly Efficient Utilization of Salt Lake Resources, Qinghai Institute of Salt Lakes, Chinese Academy of Sciences, Xining 810008, China, junqyu@isl.ac.cn*

[2]*Qinghai Provincial Key Laboratory of Geology and Environment of Salt Lakes, Qinghai Institute of Salt Lakes, Chinese Academy of Sciences, Xining 810008, China*

[3]*University of Chinese Academy of Sciences, Beijing 100049, China*

The great importance of lithium resource in the salt lakes of Qaidam Basin was not fully recognized until it became a strategic factor in electric car production. Nearly 80% of the brine lithium found in China was contained in the four salt lakes: Bieletan (BLT), DongTaijinaier (TD), XiTaijinaier (XT) and Yiliping (YLP), with a total lithium reserve of 2.3 million tonnes. In the past decade studies on exploiting the lithium deposits have emphasized on extraction methods and manufacturing technology. However, lacking sufficient knowledge on the origin of lithium, the mode of formation and distribution pattern of the Li-brine deposits has partitially led the problem of a serious loss of lithium resource in the processes of using Li and K coexisting brines for the large-scale potash production (Yu et al, 2018).

Qaidam Basin is a hyperarid basin located on the northern Tibet-Qinghai Plateau (Fig. 1). About one quarter of the basinal area is covered by salt flats and saline lakes. H-N River, the largest river draining into the Qaidam Basin, transports ~748.8 t dissolved lithium per year from the catchment in the Kunlun mountains into the terminal salt lakes in the basin (Fig. 2). Long-term evaporative concentration of the Li-bearing waters has resulted in the formation of the lithium brine deposits in the Qaidam Basin (Yu et al, 2013; Zhan et al, 2010).

The origin of lithium in salt lakes is usually associated with alteration and weathering of volcanic rocks, such as the Salar of Uyuni, Bolivia, where the extensive outcrops of felsic volcanics occur around the salar (Tibaldi et al, 2009; Risacher and Fritz, 2009). In the watershed of the four salt lakes, however, only limited intermediate-felsic volcanic outcrops occur in the upper reaches of the Hongshui

River (H-river) valley with the altitude of >4600 m above sea level, about 350 km away from the four salt lakes of Qaidam Basin.

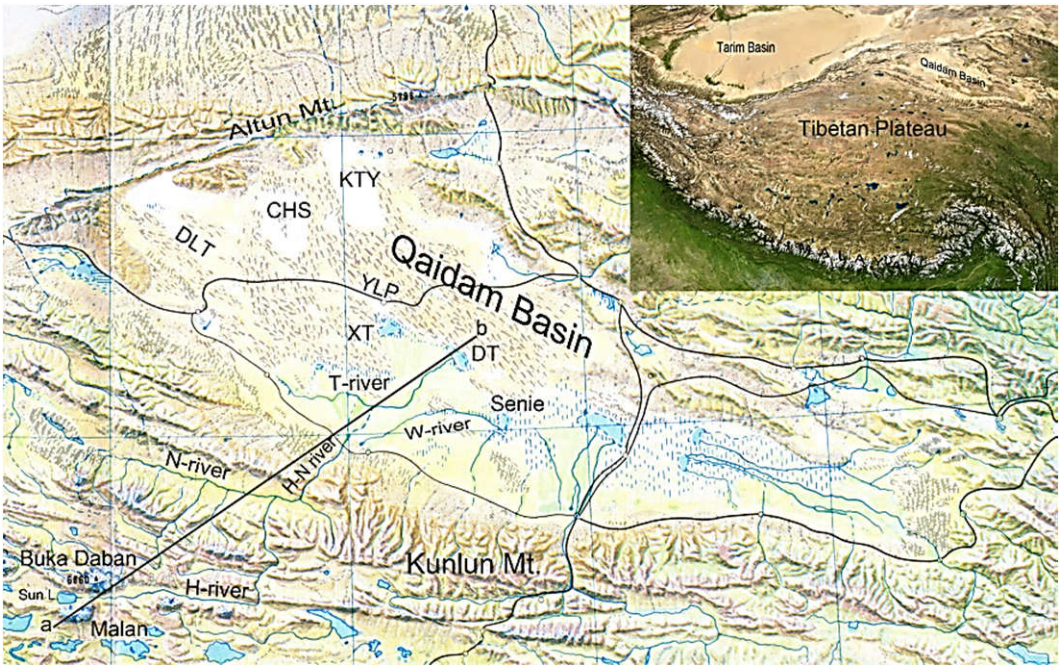

Fig. 1. Qaidam Basin is the largest inland drainage basin of the Tibetan Plateau. H-N river is the largest river draining from Kunlun mountains and transports ~748.8 t dissolved lithium per year into the Qaidam Basin.

Fig. 2. BLT, DT, XT and YLP are the terminal salt lakes of the H-N River.

Our recent investigation found that a hydrothermal field (Fig. 3) with ~150 hot-spring vents occur at around the location where two active faults converge. Li^{+} (96 mg/L) and As^{3+} (46 mg/L) concentrations of the hot-spring waters are unusually high, suggesting that the hydrothermal activities are associated with magmatic heat source. The input of the large amounts of Li-rich waters has

resulted in the H-river water rich in Li^+ (up to 8.5 mg/L). Neotectonic constraint of the Kunlun Fault system on the hydrothermal activities is evidenced by the rupture zone of the 2001 M_s 8.1 earthquake, which crossed the hydrothermal field with aligned hot spring vents over a length of ~1.5 km. The active Kunlun Fault may enhance hydrothermal activities. Such geologic, hydrogeochemical and geomorphic conditions ensure a long-term, distal supply of dissolved lithium for terminal salt lakes in the Qaidam Basin.

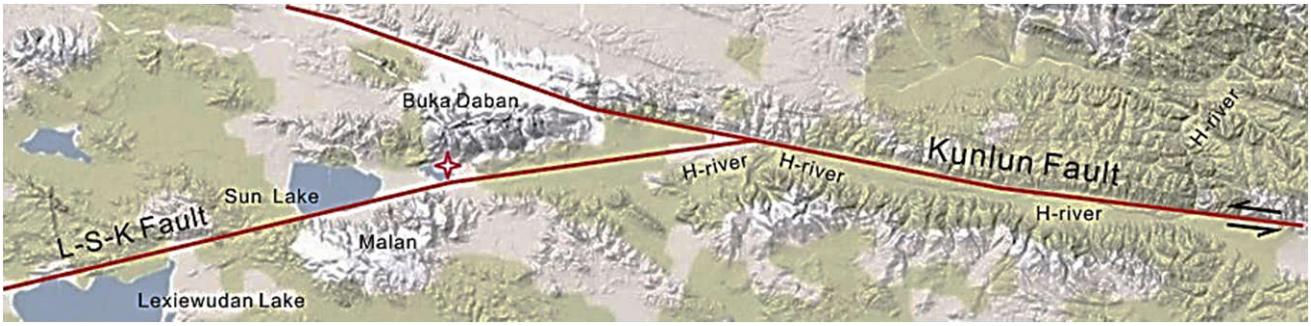

Fig. 3. Red cross-star indicates the location of a hydrothermal field with 150 hot-spring vents, which constantly discharge Li-rich water into H-river.

The existence of a magma chamber is central to any explanation of a geothermal origin for the lithium. One possibility causing the hot-spring water to be so concentrated in Li, As, and B is its close association with magmatic solution (White, 1957). Another possibility is due to the reaction of natural hot waters with volcanic rocks as long as appropriate temperatures and sufficient reaction times are satisfied (Ellis and Mahon, 1964). Both of these mechanisms for deriving the lithium in thermal waters require a convecting magma heat source: the former involves addition of Li-rich solutions from the magma, and the latter requires only heat transfer to allow leaching of lithium from lithium-rich volcanic rocks. The available data is insufficient to date to firmly determinate whether the Li in these hot springs was derived from alteration of the volcanic rocks or from magmatic differentiation at depth. Further investigation may shed more light on the interesting issue.

This research was funded by National Natural Science Foundation of China (NSFC-Qinghai Province joint grant No. U1407206; NSFC grant Nos. 41471013 and 41171171).

References

Ellis AJ, Mahon WAJ. Natural hydrothermal systems and experimental hot-water/rock interactions// *Geochim Cosmochim Ac* 1964. Vol. 28 pp.1323-1357.

Risacher F, Fritz B. Origin of salts and brine evolution of Bolivian and Chilean salars// *Aquat Geochem* 2009. Vol.15 pp.123-157.

Tibaldi A., Corazzato C., Rovida A. Miocene-Quaternary structural evolution of the Uyuni-Atacama region, Andes of Chile and Bolivia// *Tectonophysics* 2009. Vol. 471 pp. 114-135.

White DE. Thermal waters of volcanic origin// *Bull Geol Soc Am* 1957 Vol. 68 pp. 1637-1658.

Yu JQ., Hong R., Gao C., Cheng A., Zhang L. Lithium brine deposits in Qaidam Basin: Constraints on formation processes and distribution pattern// *J. Salt Lake Res*. 2018. Vol. 26 pp. 7-14.

Yu JQ., Gao C., Cheng A., Liu Y., Zhang L, He X. Geomorphic, hydroclimatic and hydrothermal controls on the formation of lithium brine deposits in the Qaidam Basin, northern Tibetan Plateau, China// *Ore Geol. Rev*. 2013. Vol. 50 pp. 171-183.

Zhan D., Yu JQ., Gao C., Zhang L. Hydrogeochemical conditions and lithium brine formation in the four salt lakes of Qaidam Basin// *J. Lake Sci.* 2010. Vol. 22 pp.783-792.

PYROXENE COMPOSITIONS OF KONTAY INTRUSION (POLAR SIBERIA).

Zaitsev V.A. ***Anosova M.O.***
Vernadsky Institute of Geochemistry and Analytical Chemistry RAS, Moscow, Russia
Va_zaitsev@inbox.ru, anosova@geokhi.ru

Siberian Large Igneous Province for a long time it has been in the focus of research of many scientific groups. The main attention to the of tholeiitic basalts of Noril'sk-Talnakh region and the Putorana plateau. Less attention has been placed on the suite of more alkaline rocks that are best exposed in the Maymecha and Kotuy River basins. Intrusive complexes of nearby east Maymecha-Kotuy province and Yakutian kimberlites located to the east also were intensively studied.

Relatively new object in this province is Kontay intrusion, found near the north-west border of Maimecha-Kotuy area (Lopatin, Kalashnik 2004).

Age of intrusion is controversial: wall-rock data define a poor Rb-Sr isochron which corresponds to an Early Paleozoic age of 483 ± 66 Ma, but no coeval have ever been found within a distance at least 500 km from it, and this intrusion is thus the only known component of the Early Paleozoic magmatic complex (Zaitsev et al., 2018). The alternative interpretation, that Rb-Sr isotope system reflect mixing the materials of sources at the Permian–Triassic boundary also problematic because no geochemical and mineralogical evidences of such mixing was found. We try to use of pyroxene as an indicator of magmatic differentiation in the Kontay intrusion to distinct these two possibilities.

A laser ablation system UP-213 (New Wave) attached to inductively coupled plasma-mass spectrometer Element-XR was used to measure microelements in clinopyroxene. Laser pulse frequency of 4 Hz and beam diameter of 30 μm were used for the analyses. Data reduction was performed with Glitter software program.

Intrusion is fully overlaid by Jurassic and Cretaceous marine and continental sediments and Quaternary glacial and fluvio-glacial sediments. All available material of intrusion is from single drill core. Intrusion is build up of three zones. In spite of significant differences in the composition of the rocks, the mineralogy of the rocks, trace-element composition and the typochemical traits of their minerals indicate that these rocks belong to a single layered series.

- **lower zone** (below 1100 m) consists of layered sequence with alternation of leucocratic and melanocratic layers of biotite- and ortopyroxene-bearing gabbro with pseudomorphoses after olivine. Often biotite corroded clinopyroxene. Accessory minerals: titanomagnetite, apatite.

Two group of clinopyroxene compositions, both are low-alumina diopside-hedenbergite exist in these part of intrusion. The first is relatively rich in titanium (0.9-1.2% TiO_2) and alumina (2-2.5% Al_2O_3) clinopyroxene, with Mg/(Mg+Fe)=0.44-0.50 containing 0.2–0.3 wt % MnO, and 0.3– 0.35 wt % Na2O. The second group of clinopyroxene compositions poorer in titanium (0.2-0.6% TiO_2) and alumina (0.5-1.4% Al_2O_3)**,** and little bit rieacer in manganese(0.3–0.4 wt % MnO), and sodium (0.32–0.4 wt % Na_2O). These rocks also contain orthopyroxene, fresh or partly or completely replaced by secondary minerals. Optopyroxee contain 1.5-1.9% CaO, 0.26-0.4 % TiO_2, 0.5-0.6% Al_2O_3 и 0.5-0.9% MnO, Mg# 70-73%.

- **middle zone** (1100-700m) consists of biotite- and K-feldspar bearing gabbro and monzonotes. Accessory minerals: zoned titanomagnetite-magnetite, ilmenite, apatite. Interstitial space often contain micrographical structures. Biotite corroded clinopyroxene and form interstitial crystals. Sometime, ilmenite in titanomagetite dissolution structures is replaced by secondary minerals, including biotite.

The composition of the clinopyroxene is analogous to that of the low-Ti clinopyroxene variety in the lower zone (0.1–0.7 wt % TiO_2, 0.5–1.5 wt % Al_2O_3, and 0.29–0.36 wt % Na_2O) and is noted for lower Mg# and a higher Mn concentration (0.6–0.9 wt % MnO).

- **upper zone** (700-214 m) consists of petrographically monotone quartz-monzonites and granosyenites with porphyrytic structures. Phenocrysts of plagioclase, magnetite, clinopyroxene and biotite (the last two minerals often fully replaced). The composition of the clinopyroxene is analogous to that in the middle zone and the low-Ti clinopyroxene variety in the lower zone. The mineral contains 0.5–0.7 wt % TiO2, 1.2–1.4 wt %Al_2O_3, 0.25– 0.4 wt %Na_2O, its Mg# is even lower (58–65%), and its Mn concentration is higher (0.7–0.8 w%).

Fe and Mg distribution between clinopyroxene and orthopyroxene in the lower zone of intrusion show temperature range from 750° to 1050°C by (Saxena et al., 1986) geothermometer. The pyroxene quadrilateral geothermometry (Lindsley, Andersen 1983) suggests equilibration temperatures from 700°C and up to 1100°C, focusing near 900°C. (fig 1). Calcium content in orthopyroxene correspond to the 1000-1100° C. We think that the last temperature correspond to the magmatic crystallization and the clinopyroxene composition correspond to overprinting process resulting in Ca enrichment in enrichment with calcium due to magnesium and iron dinning, because a generalization of the experimental data on the diffusion coefficients of elements in the diopside (Cherniak, Liang, 2012) showed that diffusion coefficients of Fe and Ca approximately one order of magnitude lower than Mg, and diffusion coefficient Ca being less dependent on temperature, so that at a temperature of less than 1000 ° C, Ca is a more mobile element than Fe.

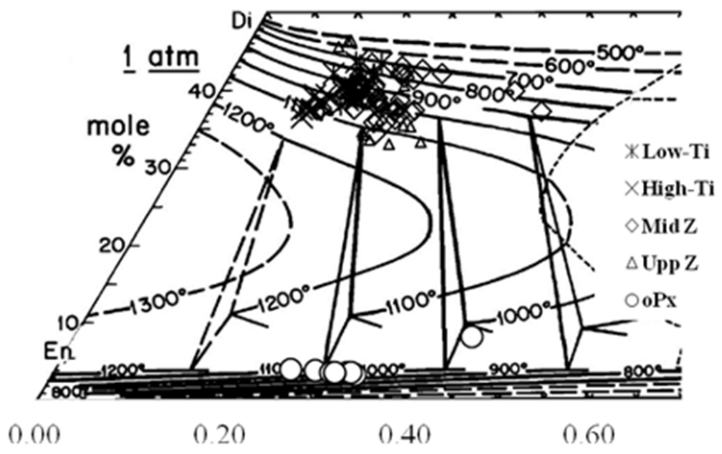

Fig.1 Quadrilateral components of Kontay pyroxenes. Di = diopside, He = hedenbergite, En = enstatite, Fs = ferrosilite. $Fe^{2+}$and $Fe^{3+}$are estimated from charge balancing the cations. Calculation of quadrilateral components is after Lindsley (1983). Experimental tie-lines between coexisting pyroxenes and isotherms are contoured at 100°C intervals between 700° and 1200°C at the low pressure (<2 Kbar) after Lindsley (1983).

The obtained REE data are demonstrated on the fig. 2. Chondrite-normalized rare earth element (REE) spectra for clinopyroxene generations are similar is shape but clearly differ by the concentration level and Eu/Eu* ratio (low-Ti clinopyroxene are richer in REE than high-Ti and show more significant Eu-minimum). REE patterns of low-Ti clinopyroxene from lower, medium and upper zones of intrusion are similar both in shape and in concentration level.

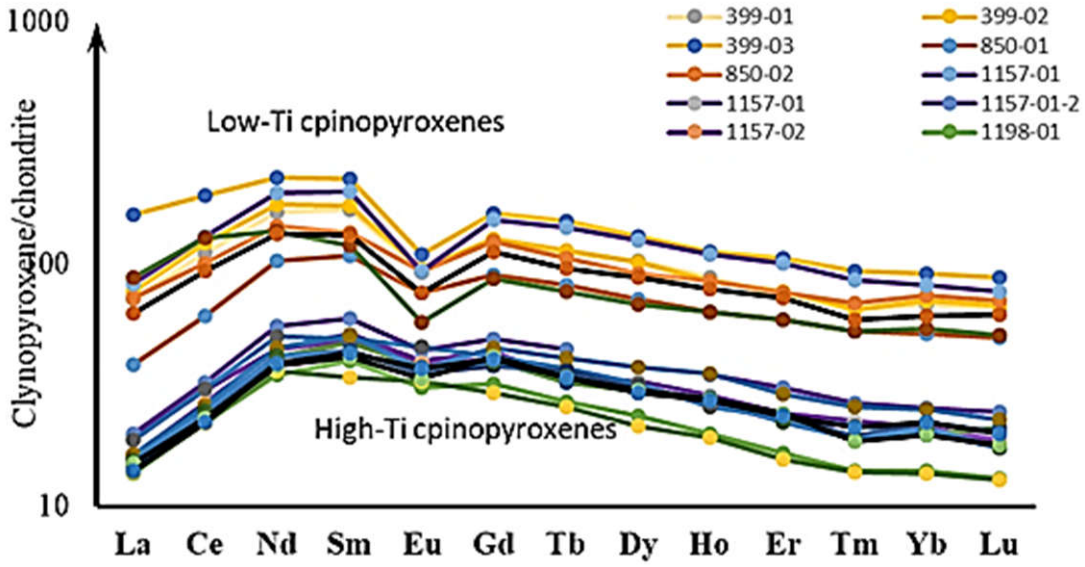

Fig. 2. Chondrite -normalized rare-earth element patterns of the clinopyroxenes.

We use partition coefficients CPx/Melt, calculated by the Wood and Blundy (1997) model for estimation of REE concentrations in the melt of Kontay intrusion. The observed variations in clinopyroxene composition practically do not affect in the estimation of partition coefficients. The rare-earth elements patterns in a melt equilibrium with high-titanium pyroxenes is close (but not exactly correspond) to the distribution of rare-earth elements in the rocks of the lower part of the Kotay intrusion (fig. 3). REE spectra of the melts, in equilibrium with low-Ti clinopyroxenes from the lower zone of intrusion and clinopyroxenes from the middle and upper parts of intrusion are differ from the wall-rock REE patterns of Kontay intrusion by the strong europium anomaly that does not appear in the whole-rock spectra and is characterized by a much higher La / Sm and lower Lu/Sm ratios.

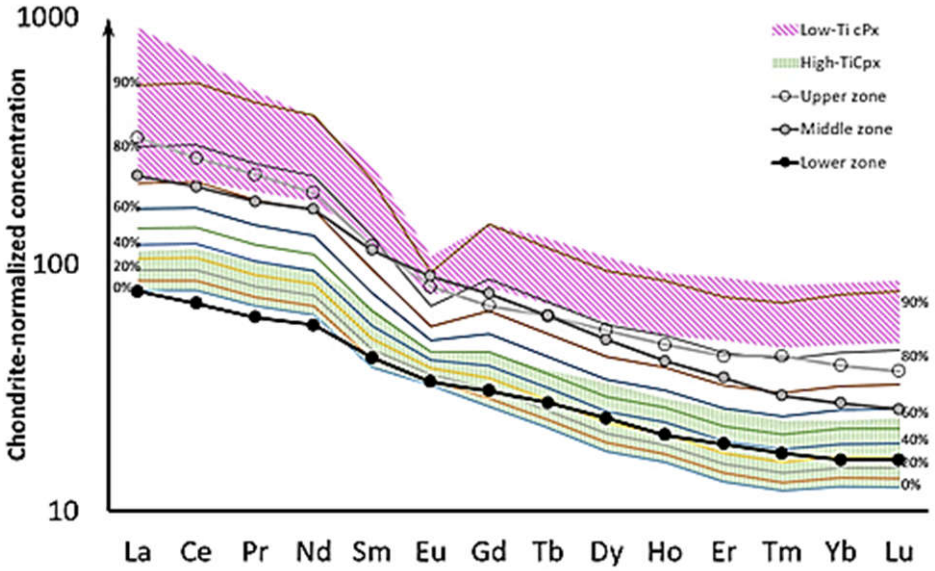

Fig. 3. Chondrite-normalized rare-earth element patterns of the melts in equilibrium with clinopyroxenes. Thick lines with large circles show the average composition of the lower (solid circles), middle (gray circles), and upper (open circles) zones of the intrusion. Thin lines show result of fractionation of clinopyroxene-plagioclase- magnetite association.

Fig. 3 also shows the results of the fraction crystallization modeling of clinopyroxene-plagioclase- magnetite association from the starting melt composition corresponding the equilibrium with the poorest in REE clinopyroxene. Partition coefficients between plagioclase and melt for REE excepting Eu were estimated using the Excel spreadsheet (Sun, Liang 2017). Partition coefficient fpr Eu was estimated as the average of coefficients available at GERM database.

The spectra of high-titanium melts well-correspond to the 0-40% of fractionation, and spectra of melts in equilibrium with low-Ti clinopyroxene and with clinopyroxene from the middle and upper parts of intrusion well-correspond to the 80-90% of fractionation. But the absence of compositions corresponding to the average levels of fractionation can not be obscured if it is allowed that the evolution of the melt occurred in situ. The composition gap may be explained by increasing of REE partition coefficients in a result of temperature decrement between high-titanium and low-titanium pyroxene crystallization. It can be assumed, for example, that the high-Ti pyroxene was crystallized in the chamber at a lower hypsometric level and brought into the volume of the Kontay intrusion in the form of suspended crystals.

It can be assumed that the emplacement of the Kontay intrusions of the magma occurred in two stages from the same source: first, less differentiated magma was introduced, from which crystallization of the first generation of clinopyroxene, the first generation of plagioclase, clinopyroxene occurred. After that, the evolution of magma in the source occurred faster than in the volume of the Kontay intrusion. As a result, the second portion of magma, introduced into the volume of the Kontay intrusion, was more differentiated than the interstitial melt existing in it.

The partial financial support was provided by the Russian Sciense Foundation (№ 15-17-30019)

References

Lindsley D.H. Andersen D.J. A two-pyroxene thermometer// Journal of Geophysical Research, Vol. 88, Suppl., p. A887 - A906.

Lindsley DH (1983) Pyroxene thermometry. Am Mineral 68:477–493

Lopatin G.G. and Kalashnik N.N. (2004) The new source of platinum-group metals in Maymecha-Kotuy province. In: Mineral recourses of Taimyr autonomy district and they perspectives. Materials of science-practical conference 25-28 October 2004, Sankt-Pererburg

Saxena S.K., Sykes J. Eriksson G. Phase Equilibria in the Pyroxene Quadrilateral//Journal of Petrology, Vol.27, Iss. 4, Pages 843–852

Sun C., Graff M., Liang Y. Trace element partitioning between plagioclase and silicate melt: The importance of temperature and plagioclase composition, with implications for terrestrial and lunar magmatism.// Geochimica et Cosmochimica Acta. 2017 Vol. 206, pp. 273-295

Wood BJ, Blundy JD (1997) "A predictive model for rare earth element partitioning between clinopyroxene and anhydrous silicate melt" Contributions to Mineralogy and Petrology, 129: 166-181

Zaitsev V. A., Elizarov D.V., Bychkova Ya.V., Senin V.G., Bayanova T.B. (2017) The first data about geochemistry and age of Kontay intrusion, Polar Siberia *Geochemistry international,* 2018, Vol. 56, Iss. 3, pp 211–225.

POSSIBLE WAY OF EUDIALYTE EXTRACTION PROCESS BY NITRIC ACID DECOMPOSITION AND SORPTION RECOVERY OF RARE AND RARE EARTH METALS FROM NITRATE SOLUTIONS

Zaitsev V.A., Gruzdeva A.N., Gromyak I.N., Khamizov R. Kh.

Vernadsky Institute of Geochemistry and Analytical Chemistry of the Russian Academy of Sciences (GEOKHI RAS), Moscow, Russia

Va_zaitsev@inbox.ru, alexgruzdeva@yandex.ru

Eudialyte group minerals are widely spread in agpaitic rocks zirconosilicates with various contents of substitution elements. Due to significant content of zirconium and valuable heavy rare earth elements eudialyte is belonged to be a perspective industrial mineral for several deposits, including (the Khibina, and Lovozero Complex (Russia), the Ilimaussaq Complex (Greenland), Norra Karr (Sweden), etc.).

No extraction process is known on an industrial scale, but several technologies of rare-metal separation from this concentrate were recently proposed. Most of developed processes are limited or do not explain the prevention of a silica gel formation. This gel contain connects a noticeable part of zirconium.

The thermodynamic calculations for sulfate acid-eudialite system allow to assume that during process of acid decomposition of eudialyte some part of zirconium besieges in the form of zircon [Litvinova, 2015].

In this regard is of interest to consider boundary conditions of formation of zircon stability. These boundary conditions are defined by balance between the dissolved zirconium forms, acid, water and silicon dioxide.

Equilibrium between zircon, nitric acid, silica and aqueous zirconium solution may be represented by equation:

$$\Sigma(ZrOx(NO3)y4-2x-y) + SiO2+H2O \leftrightarrow ZrSiO4 + HNO3$$

The factors that influence this equilibrium are total zirconium concentration, nitric acid concentration, nitrogen ion concentration, pressure and temperature. Actually, in case of eudialyte decomposition by nitric acid independent parameters are starting nitric acid concentration, eudialyte/acid ratio and temperature. Influence of these parameters was studied by thermodynamic modelling, using Gibbs program (Shvarov, 1999) in system H2O-HNO3-Na4Ca2ZrSi6O18 (simplified eudialite composition) in atmospheric pressure. Thermodynamic properties for amorphous silica were taken from (Helgeson, 1978).

Results of thermodynamic modeling are summarized in fig. 1. Calculations show that the stability of zircon increases with increasing temperature and a decrease in the initial liquid / solid ratio and the initial concentration of acid. Total zirconium concentration in the solution produced by reaction of eudialyte with nitric acid is increase by increasing of starting eudialyte/acid ratio up to saturation by zircon. After that, addition of eudialyte result in sharp decrement of zirconium concentration. For preventing zircon formation, one have to provide the significant acid excess. This circumstancing result in the second problem: for effective separation of metals in nitrate solutions, as a rule, it is required to get rid of excessive acidity.

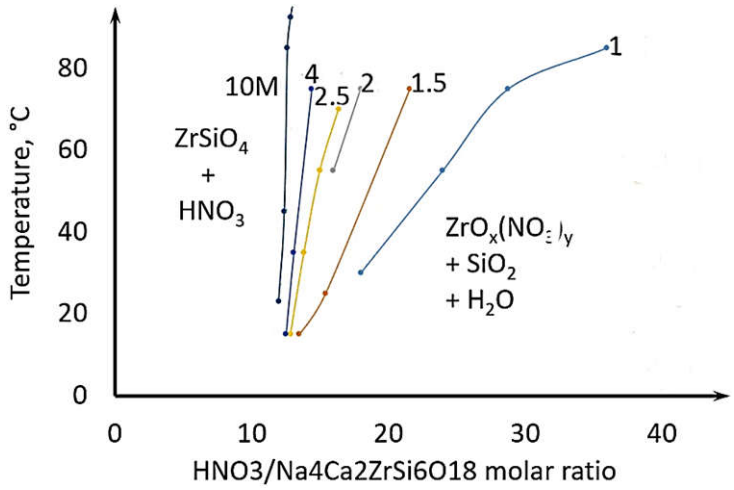

Fig. 1. Calculated position of zircon saturation line in equilibrium with acid nitritic zirconium solution and amorph silica for products of eudialie decomposition by nitric acid with starting concentration from 1 to 10 mol/L.

Method of Acid Retardation (AR) is an effective way for processing concentrated electrolyte solutions and is based on the separation of aqueous mixtures of strong acids and their salts on an anion exchanger in the same anionic form (Hatch et al., 1963). No auxiliary reagents other than water are required in such a process.

The main drawbacks of the method are the degradation of concentration profiles due to longitudinal dispersion of components of the liquid phase in a sorbent bed and the long duration the filtration cycles, connected to the displacement of water and the stock solution from the interspace volume of sorption bed at different stages of the AR-process. In GEOKHI RAS, a modified AR-method was developed in which the interspace volume in the column is filled with a special organic liquid immiscible with water and the aqueous solution being treated (Khamizov et al., 2012). The possibility of separating rare and rare earth metals in nitric acid solutions by this method was studied for systems with two liquid phases compared to a standard variant without organics.

The AR-process was tested using: a) a solution formed by the HNO_3 decomposition of eudialite concentrate from Lovosero massif (Russia) and, b) model solutions of metal nitrates, prepared from concentrated HNO_3 (65%), nitrates of Al, Fe, Y, Ca, Sr, La, Ce and zirconyl nitrate.

AR experiments were carried out by pumping separate solutions (upwards) and displacing agent (downwards) at a flow rate 1 $BV \cdot h^{-1}$ and at room temperature through columns with 30 ml (for experiments with real solutions) or 155 ml (for model solutions) resin beds. In the experiments for systems with two liquid phases decanol or dodecane were used to fill the interspace volume and all solutions were passed upwards. Regeneration was performed by water.

Strong base anion exchanger AV-17 (Russia) in the nitrate form first washed with water was used as a sorbent. For pumping the solutions a peristaltic pump BQ50-1J (Longerpump, China) was used. The metal ions concentrations solutions was determined using ICP-AES with an ICAP 9000 Thermo-Jarrell Ash (USA). The hydrogen ions concentration was controlled by pH-meter “Expert-pH” (Russia). with accuracy in the range of pH 0 - 14 ±0.02.

Fig. 2 demonstrates examples of break-through concentration curves for separation of rare and rare earth metals solution, formed by the HNO_3 decomposition of eudialite concentrate.

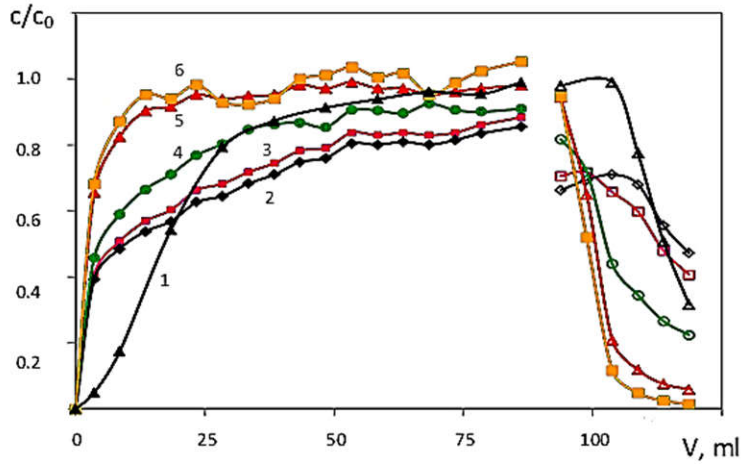

Fig. 2. Break-through concentration curves for separation of nitric acid (1) and nitrates of La (2), Ce (3), Nd (4), Y (5) and Zr (6) in the Acid Retardation process with a system with two liquid phases. The solid symbols correspond to the retardation stage, open symbols to the acid displacement stage.

At the acid retarding stage, on passing the initial solution through a column, the majority of cations, including Na, Ca, Sr, Fe, Mn, Ti, Zr and Y pass through the chromatographic bed without delay as part of neutral or sub-acid salt solutions. Nitrates of rare earths are found to behave differently from other metals, Ce and La sorption is much stronger, and their concentration fronts are wider. The behaviour of Nd is intermediate between these two groups. At the desorption stage on passing deionized water, Ce, and in particular, La, move simultaneously with acid and substantially later than the other metals.

The observed phenomena of REM behavior is found for the first time in the process of separating mixed nitric acid and salt solutions by AR.

Fig. 3 demonstrate of break-through concentration curves of separation of rare and rare earth metals with model nitric acid solutions for systems with two liquid phases (B) compared to a standard variant without organics (A).

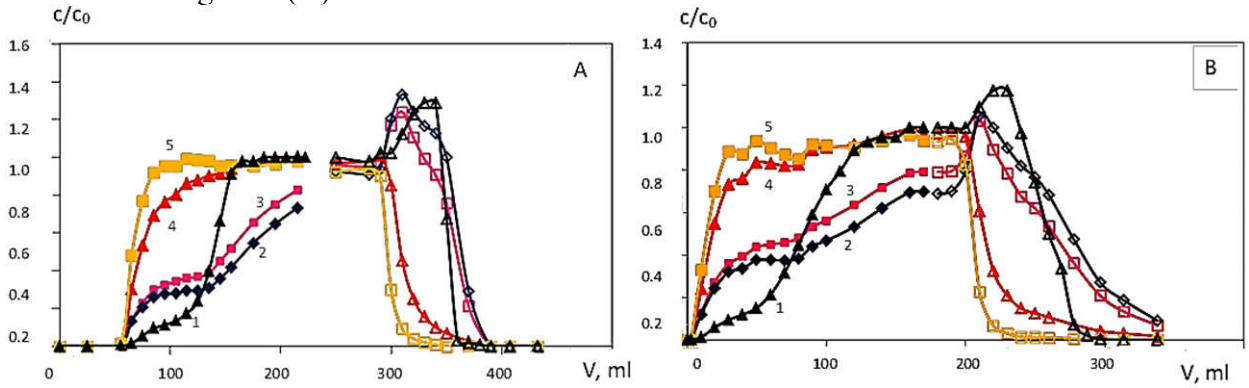

Fig. 3. Break-through concentration curves of nitric acid (1) and nitrates of La (2), Ce (3), Y (4) and Zr (5) for separation of model solution by the Acid Retardation process without organic liquid phase (A) and in the system with two liquid phases (B). The solid symbols correspond to the retardation stage, open symbols to the acid displacement stage.

It is seen that in spite of similarity of the behaviour of components the output curves of the acid in the experiment with two liquid phases have increased slopes. We suppose that the reason for this is an increase in the linear flow rate of a separated solution in this variation of the AR process.

The feature of the components separation in the nitrate system, in contrast to their behavior for example in a phosphate system (Khamizov et al., 2015) in that concentration of salt components, especially REM, in the acid retarding stage is not observed. This fact is connected with their partial separation from the acid, which is likely to be explained by the formation of strong anionic metal

complexes of nitric acid. On the other hand the formation of nitrate complexes makes it possible the separation of REM into two groups.

At the desorption stage on passing deionized water, acid is eluted to a high degree and a well defined peak of concentrated Ce, and in particular, La, move simultaneously with the acid and substantially later than the other metals.

Reported results show that method of Acid Retardation for nitric acid solutions containing rare and rare earth metals allows neutral or sub-acid solutions of metal nitrates (including Y and Zr) to be obtained in the acid retarding stage, and a concentrated fraction of acid cleared of metals, but enriched with La and Ce in the regeneration step.

The possibility of separating rare metals in nitric acid solutions by the AR method on a strong base anion exchanger (AV-17) in the nitrate form is experimentally demonstrated for systems with two liquid phases and compared to a standard variant without organics. It is shown that AR can be highly efficient for treating acidic multicomponent solutions in both cases. The advantage of the process of separation in column with two liquid phases is the short duration of the operating cycle, as well as no need for large amounts of recycled solutions. The observed difference in the behavior of rare-earth elements can be used for their preliminary separation at an early stage of the hydrometallurgical redistribution process.

References

Hatch M.J., Dillon J.A., Acid Retardation. Simple Physical Method for Separation of Strong Acids from Their Salts, Ind. Eng. Chem. Process Des. Dev, **2**, 253-263. (1963)

Helgeson, H.C., Delany, J.M., Nesbitt, H.W., and Bird, D.K. Summary and critique ofthe thermodynamic properties of rock-forming minerals// Amer.J.Sci., 1978v. 278-A, p. 229p.

Khamizov R.Kh., Krachak A.N., Gruzdeva A.N. et al, A method for the recovery of rare earth elements from the wet process phosphoric acid, RF Patent 2544731 (2015)

Khamizov R.Kh., Krachak A.N., Khamizov S.Kh., Separation of ionic mixtures in sorption columns with two liquid phases, in. Proceed. of the IEX 2012, The International Ion Exchange Conference/ ed. M. Cox, Queen's College, Cambridge, 2012, p.71-72

Litvinova T.E. Rare earth metal preparation from low-grade stock// Sci doctors degrees thesis 2015 (in russian).

Shvarov Yu.V. Algorithmization of the Numeric Equilibrium Modeling of Dynamic Geochemical Processes// Geochemistry International, vol. 37, No. 6, pp. 571-576

COMPARATIVE GEOLOGY AND GEOCHEMISTRY OF SEDIMENTARY ROCK-HOSTED GOLD AND ANTIMONY DEPOSITS OF YOUJIANG BASIN, SOUTH CHINA

***Zhaanbaeva A.*[1,2,3], *Ruizhong H.*[1,2], *Huang Y.*[1,2]**

[1]*State Key Laboratory of Ore Deposit Geochemistry, Institute of Geochemistry, Chinese Academy of Sciences, Guiyang 550081, China*

[2]*University of Chinese Academy of Sciences*

[3]*Institute of Geology, National Academy of Sciences of Kyrgyzstan, orogeny.geo@mail.ru, aizat@mail.gyig.ac.cn*

The Youjiang basin is the southwestern margin of giant Yangtze Craton and is located between Yunnan-Guizhou-Guanxi provinces, South China. It bounded by the deep-seated Mile-Shizong, Shuicheng-Ziyun-Bama and Red River regional faults which are major tectonic features of the basin (Cai and Zhang, 2009; Yang et al., 2012). The basin is an important region of South China low-temperature metallogenic domain and includes Au-As-Sb-Tl-Hg hydrothermal deposits. These multi-type deposits characterized by the low temperature (typically below 200-250°C), shallow depth and commonly hosted by sedimentary rocks from Cambrian to Triassic age (Hu et al., 2002; 2017).

China is the largest antimony producer in the world and supply with more than 92% of all the finished antimony products. The giant Muli, Qinglong, Dushan, Maxiong and other antimony deposits

(occurrences) are located in Youjiang basin. They mostly characterized as low-temperature vein-type deposits and are part of the world's most important Western Pacific Sb ore belt (Wu Jiada, 1993; Hu et al., 1996).

The special relationship between the vein-type antimony and sedimentary rock-hosted disseminated gold deposits in the basin is obvious. Gold deposits of Youjiang basin quoted as the classic examples of world-class "Carlin-type Au deposits". With more than 200 gold deposits and occurrences and 800 t of gold reserves (Hu et al., 2017), the Youjiang basin becomes the second largest Carlin-type gold mineralized area after Nevada.

It is a fact that Sb is the main ore mineral in antimony and commonly occurring mineral in most Carlin-type gold deposits of Youjiang basin. For example, large ore bodies with the Sb mineralization found in Carlin-type Badu and Getang deposits. Moreover, the results of previous works show high gold content of stibnite in Banqi Au deposit and abundant stibnite concentration on Hengxian Au deposit of the basin (Peters et al., 2007, Li and Peters, 1998). Therefore, clarification of the genetic relationship between the sedimentary rock-hosted Au and Sb deposits of Youjiang basin is a key point of this study.

Hydrothermal processes responsible for ore deposition vary between different deposit-types and can significantly fractionate trace elements in hydrothermal systems between the vapour, liquid and solid phase (Cline et al., 2005; Goldfarb et al., 2005; Seedorff et al., 2005; Simmons et al., 2005). The hydrothermal transport of Ag, Au, Cu, Pb, and Te is very sensitive to boiling, which due to metal deposition, sharply reduces the concentrations of metals in the aqueous phase. Boiling is an effective agent of ore deposition, and explains the formation of ores in low-intermediate sulfidation epithermal vein deposits, it also accounts for the proximal to distal zonation of hydrothermal alteration (Buchanan, 1981; Simmons et al., 2005). By contrast As, Mn, Mo, Ni, Sb, Tl, and Zn are much less sensitive to boiling. This second group of metals can thus continue to disperse upward and outward through the boiling zone in the aqueous phase, where deposition by additional processes, including cooling and mixing (Spycher and Reed, 1989), produce shallow-level metal anomalies that are useful for epithermal exploration (Simmons et al., 2005).

Valuable data can be gleaned from geochemical and isotopic studies of antimony ore mineral stibnite (Sb_2S_3), which can be a potentially important tool to understand ore genesis and ore source processes. In this regard, here we report the trace element, S and Pb isotopic compositions of stibnite from gold and antimony deposits of Youjiang basin.

Our study based on the results of inductively coupled plasma mass spectrometry (ICP-MS), demonstrated wide range of values with considerable intersystem variability. To distinguish the various types of Sb mineralisation, Cu, Pb, Zn, Ag, As, Bi have proven most diagnostic. The differences between the high and low values of As, Cu, and Pb range >1,000 times, the differences between the high and low values of Bi, Zn, Se range >100 times, and the differences between the high and low values of Ag, Te range <10 times. According to the element concentration in Sb, deposits can be divided into high, average and low enriched groups.

The Badu Carlin-type gold deposit introduce the first group and high in As, Cu, Pb, Ag, Zn, and contain invisible, few ppm of Au in stibnite, however, SEM analysis detected no free gold. According to Li Peirong et al., 2014, the ore forming fluids of the Badu homogenized at temperatures ranging from 335 to 337^{0}C that creates favorable condition for ore mineralization with the enriched element concentration, compare to other deposits, where the homogenization temperature is lower. Yata and Maxiong deposits are represent the second group, with the average content of As-Cu-Pb-Zn; although Yata known as a Carlin-type gold deposit and Maxiong as a Sb deposit, there is no big difference in element concentration. Qinlong and Muli deposits are introduced as a giant Sb deposits and show very low concentration of Cu, Pb, Zn, Ag, As, Tl, Bi and Se compare to previous deposits and introduce the last type.

The $\delta^{34}S$ isotopic composition of stibnite from the Au and Sb deposits show a broad variation, ranging from -14 to +19 analogously. Such large variations exclude the possibility that the S derived from a magmatic source (Ohmoto, 1986). It can be suggested that these variabilities possibly indicate the sedimentary source of sulphur, introduced by hydrothermal fluids. The Pb isotopic composition of

stibnite represents a narrow range, $^{206}Pb/^{204}Pb$=18.72-18.46, $^{207}Pb/^{204}Pb$=15.78-15.69, $^{208}Pb/^{204}Pb$=39.12-38.79, characterizing the same upper crustal source of lead for different deposits.

The results of this work show resembling source of S and Pb but obvious As-Cu-Pb-Zn-Bi-Ag-Se elements difference in Sb between the deposits. Based on this data, geological relationship, results of a large number of previous works and taking into account the boiling effect, we assume that Sb deposits possibly occurred as a distal manifestations and possibly later stage of the same hydrothermal system that caused the gold deposits formation in the basin.

References

Cai, J.X., Zhang, K.J., 2009. A new model for the Indochina and South China collision during the Late Permian to the Middle Triassic. Tectonophysics 469, 35-45.

Hu R.Z., Su W.C., Bi X.W., Tu G.Z., Hofstra A.H., 2002. Geology and geochemistry of Carlin-type gold deposits in China. Mineralium Deposita 37, 378-392.

Hu R.Z., Fu S.L., Huang Y., Zhou M.F., Fu S.H., Zhao C.H., Wang Y., Bi X.W., Xiao J., 2017. The giant South China Mesozoic low-temperature metallogenic domain: Reviews and a new geodynamic model. Journal of Asian Earth Silences 137, 9-34.

Hu X., Murao S., Shi M., Li B., 1996. Classification and Distribution of Antimony Deposits in China. Risource Geology 46, 287-297.

Kalinin Yu. A., Naumov E.A., Kovalev K.R., 2015. Spatial-temporal and genetic relationships between gold and antimony mineralization at gold-sulfide deposits of the Ob-Zaisan folded zone. Geology of ore deposits 57, 179-194.

Li P., Pang B., Wang B., Li Y., Zhou Y., LV J., Ma J., 2014. Fluid Inclusions and Rare Earth Elements of the Badu Gold Deposit, Guangxi, China: Implications for Mineralization. Acta Geologica Sinica (English Edition) 88, 1118-1119.

Murao S., Sie S.H., Hu X., Suter G.F., 1999. Contrasting distribution of trace elements between representative antimony deposits in southern China. Nuclear Instruments and Method in Physics Research B 150, 502-509.

Ohmoto, H., 1986. Stable isotopes in high temperature geological process. Reviews in Mineralogy & Geochemistry, Mineral Society of America16, 491-559.

Simmons, S.F., White, N.C., and John, D., 2005, Geological characteristics of epithermal precious and base metal deposits: Economic Geology 100th Anniversary Volume, p. 485–522.

Simmons S., Brown K., Tutolo B., 2016. Hydrothermal Transport of Ag, Au, Cu, Pb, Te, Zn, and Other Metals and Metalloids in New Zealand Geothermal Systems: Spatial Patterns, Fluid-Mineral Equilibria, and Implications for Epithermal Mineralization. Economic Geology 111, 589-618.

Spycher, N.F., and Reed, M.H., 1989, Evolution of a Broadlands-type epithermal ore fluid along alternative P-T paths: Implications for the transport and deposition of base, precious and volatile metals. Economic Geology 84, 328–359.

Su W.C., Heinrich C.A., Pettke T., Zhang X.C., Hu R.Z., Xia B., 2009. Sediment-hosted gold deposits in Guizhou, China: Products of wall-rock sulfidation by deep crustal fluids. Economic Geology 104, 73-93.

Wang Z.P., Xia Y., Song X.Y., Liu J.Z., Yang C.F., Yan B.W., 2013. Study on the evolution of ore-formation fluids for Au-Sb ore deposits and the mechanism of Au-Sb paragenesis and differentiation in the southwestern part of Guizhou Province, China. Chinese Journal of Geochemistry 32, 56-68.

Wu Jiada, 1993. Antimony vein deposits of China. Ore Geology Reviews 8, 213-232.

INCLUSIONS OF SiO_2 IN SUBLITHOSPHERIC DIAMONDS

Zedgenizov D. [1,2]***, Kagi H.*** [3]

[1] *Institute of geology and mineralogy SB RAS, Koptyuga Ave. 3, Novosibirsk 630090, Russia*

[2] *Novosibirsk State University, Pirogova St. 2, Novosibirsk 630090, Russia*

[3]*Geochemical Research Center, Graduate School of Science, The University of Tokyo, Hongo 7-3-1, Tokyo 113-0033, Japan*

zed@igm.nsc.ru

Diamonds provide a unique opportunity to study parts of the mantle that remain inaccessible by any other samplings. The SiO_2 is not characteristic for peridotitic rocks in the upper mantle, but it occurs there only as phase (quartz or coesite) of metabasic (eclogitic) association. These phases may rarely be found in mantle xenoliths but commonly as syngenetic inclusion in natural diamonds. In the present study we have analyzed inclusions of SiO_2 phases in sublithospheric diamonds from alluvial placers of Juina Province (Brasil) to identify residual strains and possible phase transitions. These data are used to discuss the fate of SiO_2 phase in deeply subducted metabasic environments.

Micro-Raman measurements on an intact inclusion of remnant vibrational band shifts give a maximum confining pressure ~3.5 GPa. In many cases the SiO_2 inclusions in diamonds from Juina Province form assemblages with typical inclusions of superdeep metabasic minerals: Maj–Gt, CaSi–Pv, and CaTiSi–Pv. Such assemblages suggest that the SiO_2 phases were possibly trapped as stishovite at a pressure of more than 8-10 GPa. The inclusions in most diamonds consist only of SiO_2, with no significant admixtures. The SiO_2 phase in some inclusions coexists with microblocks of the Al_2SiO_5 phase. The latter might be a result of the retrograde decomposition of previously trapped Al-stishovite. Note that the Al content of stishovite is known to increase with pressure and Al-stishovite is a potential water "container" in lower-mantle rocks of metabasic affinity (Litasov et al., 2007).

No reliable evidences for the presence of stishovite have been reported at present time. Considerable strain which is observed by EBSD and Raman spectroscopy for some inclusions of the SiO_2 and combined SiO_2 + Al_2SiO_5 phases in diamonds from Juina Province suggests that they were formed in the sublithospheric mantle, in metabasic substrates (Kaminsky, 2012; Litvin, 2014), and these phases were initially trapped as stishovite or Al-stishovite.

References:

Kaminsky, F.V. (2012). Earth Scences Reviews 110 (1–4), 127–147.

Litasov, K.D., Kagi, H., Shatskiy, A., Ohtani, E., Lakshtanov, D.L., Bass, J.D., Ito, E. (2007). Earth and Planetary Science Letters. 262 (3-4), 620–634.

Litvin, Yu.A. (2014). Doklady Earth Sciences 455 (1), 274-278.

REE AND ACTINIDES REMOBILIZATION IN LATE- AND POST-MAGMATIC PRODUCTS OF ALKALI GRANITE MAGMATISM, KEIVY, KOLA PENINSULA, RUSSIA

Zozulya D.R.[1]***, Macdonald R.***[2,3]***, Bagiński B.***[2]***, Lyalina L.M.***[1]

[1]*Geological Institute, Kola Science Centre RAS, 184209 Apatity, Russia*

[2]*Institute of Geochemistry, Mineralogy and Petrology, University of Warsaw, 02-089 Warsaw, Poland*

[3]*Environment Centre, Lancaster University, Lancaster LA1 4YQ, UK*

The Keivy alkali granite complex consists of 2.67-2.65 Ga aegirine-arfvedsonite granites (six sheet-like massifs of a few hundred meters thick and a total exposure area of ca. 2500 km^2), aegirine-augite-lepidomelane-ferrohastingsite syenogranites that occur at the margins of some massifs, and lepidomelane-ferrohastingsite syenite dykes that intrude the TTG basement of the Central Kola terrane (NE Fennoscandian shield). Numerous Zr-Y-REE-Nb ore occurrences and deposits are associated with different lithologies and were formed by various petrogenetic processes. In this work the main focus is the study of rare-metal rich mineralized granites, quartzolites and metasomatic rocks, formed at late- to post-magmatic stages. The bulk rock chondrite-normalised REE patterns for the above mentioned

lithologies have the V-shape form characteristic of hydrothermal environments. The question arises as to the nature of the fluids, which may remobilize and transport the REE and actinides.

Mineralized granite forms bodies up to 1.5 x 4 km at the surface and are confined to apical parts of the alkali granite massifs. The rocks are silica-rich (up to 40-50 vol. % of quartz) and enriched in Zr (700-21000 ppm, average 4700 ppm), Y (100-3900 ppm, average 550 ppm), Nb (40-400 ppm, average 180 ppm), REE (1000-1800 ppm, average 1300 ppm), Th (20-150 ppm), U (5-23 ppm). The main REE- and actinide-bearing minerals are chevkinite-(Ce), bastnäsite-(Ce), allanite-(Ce), fergusonite-(Y), monazite-(Ce), britholite-(Y), thorite, xenotime-(Y), apatite and pyrochlore groups minerals. Rare-metal minerals bear the features of hydrothermal origin (chain-like distribution of porous and metamict zircon, bud-shaped aggregates of zircon, alteration rims on anhedral chevkinite and britholite, the presence of REE-rich carbonate phases).

Quartzolites occur at the apical parts of alkali granite intrusions where they are hosted by both the granites and adjoining gneisses. Most quartzolite bodies vary from 0.5 to 1.5 m across. They are inequigranular, taxitic rocks, ranging from fine-grained to pegmatitic. A distinguishing feature is the very low content of feldspar (<10 vol.%). Quartz contents range from 50-90 vol.%. The primary mafic rock-forming mineral is aegirine or arfvedsonite; occasionally they are present in equal amounts. Magnetite and ilmenite also frequently occur as rock-forming minerals but in lesser amounts. Sporadic large annite laths occur in some bodies. The significant amount of fluorite and other F- and OH-bearing minerals indicates active involvement of fluids in the formation of the quartzolites. The whole rock may contain up to 30000-40000 ppm REE, 14000 ppm Nb, 6.5 wt % ZrO_2, 2.5 wt % Y_2O_3.

The rare-metal mineralization in the Keivy quartzolites is volumetrically significant (up to 20-30 vol.%) and variable in composition. Zircon is the typomorphic mineral of the ore assemblages. Other rare-metal minerals are irregularly distributed (from a few grams to tens of kilograms per ton of rock) and are represented by aeschynite-(Y), chevkinite-(Ce), fergusonite-(Y), britholite-group minerals, yttrialite-(Y), thorite, monazite-(Ce), xenotime-(Y) and bastnäsite-(Ce). Fluorbritholite-(Y), ytttrialite-(Y), fergusonite-(Y) and chevkinite-(Ce) are normally the main REE carriers and their overall content may reach 15-18 vol.%.

The rare-metal minerals in quartzolite tend to form aggregates embedded in a quartz matrix. The minerals clearly are broadly coeval. Mutual contacts between the phases are sharp and occasionally one phase forms inclusions in another, such as zircon in monazite and fergusonite in chevkinite. The only minerals with a firmly established sequence of crystallization are the yttrialite-(Y) and later fluorbritholite-(Y). The radially arranged cracks cutting through the quartz from the fergusonite-(Y) aggregates are probably a result of a volume increase associated with the radiation-induced amorphisation of the actinide-bearing mineral. The cracks are up to 10 μm wide and are filled with material ranging from homogeneous and bright to a patchy mix of BSE darker and lighter components.

Chevkinite-(Ce) has relatively high ThO_2 (2.1 wt%) and Nb_2O_5 (1.1 wt%) contents. Uranium levels are negligible. There is a loss of LREE, Fe and Si during alteration. In contrast, there was enrichment in Ti (maximum total Ti = 5.4 apfu), Nb, Th and Al. Chondrite-normalized patterns of the unaltered chevkinite-(Ce) show strong LREE enrichment while the altered phase shows positive Ce anomalies.

Fergusonite-(Y) is LREE-depleted and extremely HREE+Y-enriched. There are significant positive Eu anomalies, Eu/Eu* 1.6-2.4 and a persistent negative anomaly at Yb. Thorium, U, Ca and Fe are generally present at levels <0.1 apfu. The material filling the expansion cracks in quartz from fergusonite-(Y) are dominated by Nb, U, Pb and REE, with lesser amounts of Th, Si and Fe. Two main types can be distinguished: the first is rich in U (up to 35 wt% UO_2), the second in REE (≤25 wt% REE_2O_3). Abundances of PbO are up to 27 wt%, whereas ThO_2 levels are <0.7 wt%, with one exception (6 wt%). Silicon and Fe are highest in the REE-rich type. Chlorine levels are low (≤0.18 wt%) and F levels are below detection. Chondrite-normalised REE patterns are rather flat, with $[La/Yb]_{CN}$ varying from 1.5-4.3, and with strong Ce enrichment relative to the other LREE (Ce/Ce* 1.0-5.6). Analytical totals are low (75-90 wt%). The nature of the vein-filling material is uncertain. Compositionally it has some similarities to altered members of the pyrochlore supergroup but it may

not be crystalline. The veins do, however, provide evidence of fluid mobility during or after the alteration of the fergusonite-(Y).

Fluorbritholite-(Y) and yttrialite-(Y) have a sinusoidal chondrite-normalized REE pattern with a prevalence of HREE over LREE. Both minerals have negative anomalies of Pr and Nd, but fluorbritholite-(Y) is different in its higher content of LREE and distinct positive Ce anomaly. Variations of Y/Dy and La/Nd_n in fluorbritholite-(Y) and yttrialite-(Y) demonstrate that both minerals crystallized from CO_2-poor or CO_2-absent fluid. At the same time the H_2O/F ratio in the fluid was significantly higher during crystallization of yttrialite-(Y) than in fluorbritholite-(Y). Fractionation of actinides is possible during fluid evolution as yttrialite-(Y) contains extremely high ThO_2 (12.5 – 15.5 wt%), whereas the thorium content in fluorbritholite-(Y) is negligible.

Metasomatic rocks are confined to a linear tectonic zone at the contact between the Keivy terrane and the Central Kola composite terrane. The zone strikes in a SE-NW direction for ca. 12 km and has an outcrop width varying from 200 to 1500 m. A few hundred alkali granite and aplite veins are confined to this zone and are concordant with the faults. The length of the veins is 50-500 m, with thicknesses of 3-50 m. The granites intruded and metasomatically altered a range of rocks in the Keivy complex, namely, gabbro-anorthosites, gabbro-amphibolites and gneisses.

Metasomatic alteration of gabbro-anorthosite due to intrusion of the granite veins ranges from unaltered rocks to more intensively altered types as follows; massive gabbro-anorthosite – plagioamphibolite – amphibole-biotite metasomatite – mineralized garnet-biotite metasomatite – mineralized biotite-albite metasomatite with quartz – (epidotic metasomatite). Rare-metal mineralization is confined to small linear and lensoid bodies, nodules and pods 0.5-2 m in size. The rock is characterized by extremely high REE (85000 ppm), Y (42000 ppm), Nb (62000 ppm), Zr (67000 ppm), Th (17000 ppm), U (7700 ppm). Rare-metal mineralization is represented by thorite, chevkinite-(Ce), ferriallanite-(Ce) and allanite-(Ce), zircon, monazite, fergusonite-(Y), samarskite-(Y), aeschynite-(Y), pyrochlore, Nb-bearing titanite and rutile, ilmenite, magnetite, cassiterite, REE-carbonates, uraninite and gadolinite-group minerals. It is assumed that rare-metal minerals crystallized under medium- to low-temperature conditions as the earliest rare-metal mineral phase - zircon - is of hydrothermal origin (porous, numerous mineral inclusions, high content of Y, REE, Hf).

The sequence of events involving the major and minor rare-metal minerals is: (1) crystallization of chevkinite-(Ce) and included thorite and zircon; (2) fluid-driven replacement of chevkinite-(Ce) by ferriallanite-(Ce), alteration of zircon, with formation of some thorite, uraninite and Nb,Ti-oxides; (3) patchy replacement of ferriallanite-(Ce) by ilmenite + titanite ± magnetite, further growth of thorite; (4) formation of fingers of gadolinite-(Ce) in ferriallanite zone, followed by hingganite-(Ce) and thorite; (5) ferriallanite-(Ce) zone mantled by allanite-(Ce) zone containing samarskite; (6) all zones cut by veins (and rarer patches) of quartz and REE-carbonate. A simplified description of the replacement of chevkinite-(Ce) by ferriallanite-(Ce) is chevkinite-(Ce) + Ca + Al → ferriallanite-(Ce) + LREE + Fe + Si +Nb + Ti + Th. Some of the Th released entered secondary thorite and part of the Ti, Nb and REE entered fergusonite-(Y). Simultaneously, there was alteration of the zircon, and formation of minor thorite, uraninite and galena, using Th, U and Pb released by the alteration. Through continued interaction with the fluids, the ferriallanite-(Ce) was replaced by allanite-(Ce), with further uptake of Ca and Al and further release of Fe. The more highly altered allanite-(Ce) has much lower $[La/Y]_{CN}$ values (7–44) than the main trend compositions (66–1560), indicating selective removal of LREE and replacement by HREE during alteration. The Ca and Al in these reactions were possibly supplied by fluids involved in the epidotic metasomatism of the host rock. In some parts of the pod, fingers of gadolinite-(Ce) penetrated into the ferriallanite-(Ce) zone, followed by hingganite-(Ce), with loss of REE, Fe and the creation of vacancies in the structure. The patchy replacement of ferriallanite-(Ce) by titanite (and minor ilmenite) resulted in significant release of REE and Si, which contributed to the late-stage veins, and rarer patches, of quartz and REE-carbonates. The sequences of crystallization and composition of rare-metal minerals indicate that metasomatites formed under the influence of alkaline, F-bearing fluids with high activities of CO_2, Si, Ca and Al at some stages.

The partial financial support was provided by the Russian Foundation for Basic Research (№ 16-05-00427) and Russian Government grant (0231-2015-0009).

COMPARATIVE CRYSTAL CHEMISTRY OF MINERALS BELONGING TO THE SYSTEM $A_3M_6O_2(AsO_4)_4$ (A = K, Na, Ca; M = Cu^{2+}, Al, Fe^{3+}) FROM ALKALI-RICH FUMAROLIC EXHALATIONS OF THE TOLBACHIK VOLCANO (KAMCHATKA, RUSSIA)

***Zubkova N.V.*[1], *Pekov I.V.*[1,2], *Ksenofontov D.A.*[1], *Agakhanov A.A.*[3], *Turchkova A.G.*[1], *Vigasina M.F.*[1], *Pushcharovsky D.Yu.*[1], *Sidorov E.G.*[4]**

[1]*Faculty of Geology, Moscow State University, Moscow, Russia*

e-mail: n.v.zubkova@gmail.com

[2]*Vernadsky Institute of Geochemistry and Analytical Chemistry, RAS, Moscow, Russia*

[3]*Fersman Mineralogical Museum, RAS, Moscow*

[4]*Institute of Volcanology and Seismology, Far Eastern Branch of the Russian Academy of Sciences, Petropavlovsk-Kamchatsky, Russia*

Four new arsenate minerals shchurovskyite, $K_2CaCu_6O_2(AsO_4)_4$, dmisokolovite, $K_3Cu_5AlO_2(AsO_4)_4$ (Pekov et al., 2015), and recently discovered by us edtollite, $K_2NaCu_5Fe^{3+}O_2(AsO_4)_4$, and alumoedtollite, $K_2NaCu_5AlO_2(AsO_4)_4$, occur in close association with each other in exhalations of the active Arsenatnaya fumarole at the Second scoria cone of the Northern Breakthrough of the Great Tolbachik Fissure Eruption, Tolbachik volcano, Kamchatka, Russia. This assemblage is characterized by the presence of many sublimate minerals enriched by K and/or Na: aphthitalite, langbeinite, sylvite, halite, potassic feldspar, sodalite, numerous sulfates and arsenates with both chalcophile and alkali metals, *etc*. In perticular, four described minerals contain species-defining alkaline cations.

Edtollite and alumoedtollite are isostructural and represent a novel structure type while shchurovskyite and dmisokolovite are closely related in the topology of main building units and demonstrate two new structure types. All these minerals are characterized by the same stoichiometry and the same ratios between large *A* (K, Na, Ca) and medium-size *M* (Cu^{2+}, Fe^{3+}, Al) metal cations. Their general formula can be written as $A_3M_6O_2(AsO_4)_4$ in which *A* = K, Na, Ca and *M* = Cu^{2+}, Al, Fe^{3+}. However, the structural difference between edtollites and related to one another shchurovskyite and dmisokolovite is significant. Edtollites differ from shchurovskyite and dmisokolovite in atomic arrangement that causes strong differences in unit-cell dimensions and powder X-ray diffraction patterns. Edtollite and alumoedtollite are triclinic, space group *P*-1. Unit-cell parameters (edtollite/alumoedtollite) are: *a* 5.1168(6)/5.0904(11), *b* 9.1241(12)/9.0778(14), *c* 9.6979(14)/9.6658(2) Å, α 110.117(13)/110.334(17), β 102.454(12)/102.461(19), γ 92.852(11)/92.788(15)º, *V* 411.32(9)/404.88(14) Å^3 and *Z* = 1 for both. Shchurovskyite and dmisokolovite are monoclinic, space groups *C*2 and *C*2/*c*, respectively. Unit-cell parameters (shchurovskyite/dmisokolovite) are: *a* 17.2856(9)/17.0848(12), *b* 5.6705(4)/5.7188(4), *c* 8.5734(6)/16.5332(12) Å, β 92.953(6)/91.716(6)º, *V* 839.24(9)/1614.7(2) Å^3 and *Z* 2/4. The crystal structures of edtollite and alumoedtollite (Fig. 1a) are based on the heteropolyhedral pseudo-framework consisting of the columns built by Cu-centred distorted octahedra and square pyramids, distorted octahedra MO_6 (*M* = Fe^{3+}, Al^{3+}, Cu^{2+}) and isolated AsO_4 tetrahedra with K^+ and Na^+ located in wide and narrow channels of the pseudo-framework, respectively. The structures of shchurovskyite and dmisokolovite (Fig. 1b,c) are also based on the heteropolyhedral pseudo-framework but with significantly different topology comparing with edtollites: the main structural unit of their pseudo-frameworks is the layer formed by the Cu- and Al-centred polyhedra (dmisokolovite) or by Cu-centred polyhedra (shchurovskyite). They differ from one another in the orientation of Cu-centred polyhedra in the adjacent layers that causes the doubling of the unit-cell parameter *c* of dmisokolovite in comparison with shchurovskyite while the role of AsO_4 tetrahedra in both structures is the same and large cations have close arrangement: K cations are located in wide channels of the quasi-framework in both while narrow channels are occupied by (K,Na) in dmisokolovite and by Ca in shchurovskyite.

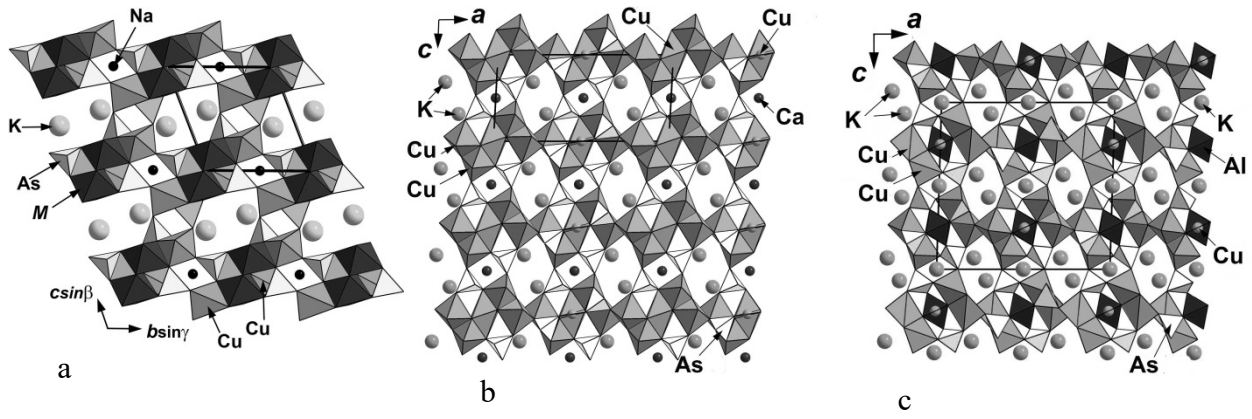

Fig. 1. The crystal structures of edtollites (*a*), shchurovskyite (*b*) and dmisokolovite (*c*). The unit cells are outlined.

The structure features strongly influence to physical properties: shchurovskyite and dmisokolovite are transparent green minerals with vitreous lustre while edtollite is brown-black and alumoedtollite is bronze-coloured, both with semi-metallic lustre.

The structures of all four minerals could also be described in terms of anion-centred (oxocentred) tetrahedra (Krivovichev *et al.*, 2013). The motifs of anion-centred tetrahedra in the structures of edtollites and the pair shchurovskyite – dmisokolovite differ significantly. In edtollites the chains $[O_2Cu_2M_2]^{\infty}$ built by edge-sharing OCu_2M_2 tetrahedra are defined while in shchurovskyite and dmisokolovite the motif of oxocentred tetrahedra is represented by isolated from each other dimers, $[O_2Cu_6]$ and $[O_2AlCu_5]$, respectively (Pekov et al., 2015).

This study was supported by the Russian Foundation for Basic Research, grant 17-05-00179.

References

Krivovichev S.V. et al., Anion-centered tetrahedra in inorganic compounds // Chem. Rev. 2013. Vol. 113. p. 6459-6535.

Pekov I.V. et al., New arsenate minerals from the Arsenatnaya fumarole, Tolbachik volcano, Kamchatka, Russia. IV. Shchurovskyite, $K_2CaCu_6O_2(AsO_4)_4$, and dmisokolovite, $K_3Cu_5AlO_2(AsO_4)_4$ // Min. Mag. 2015. Vol. 79. p. 1737-1753.

Научное издание

«Магматизм Земли и связанные с ним месторождения стратегических металлов»

Материалы XXXV Международной конференции, 3-7 сентября 2018

Москва, издательство «ГЕОХИ РАН», 2018

На английском языке

Scientific edition

«Alkaline Magmatism of the Earth and related strategic metal deposits»

Proceedings of XXXV International conference, 3-7 September 2018

Moscow, “GEOKHI RAS”, 2018

Editor-in-chief Academician L.N. Kogarko.

Editors: V.N. Ermolaeva, V.A. Zaitsev.
Art editor V.A. Zaitsev

Typesetting: V.I.Vernadsky Institute of Geochemistry and Analytical Chemistry of RAS (GEOKHI RAS)

Signed to print 14.08.2018 Format of 60x84/8
Offset paper. Headset "Times." Conv. pr. sh. 41.62.
Pressrun 120 copies. Order № 18-1

Printing: V.I.Vernadsky Institute of Geochemistry and Analytical Chemistry of RAS (GEOKHI RAS)
Kosygin Street, 19, 119991, Moscow, Russian Federation.